# Fluid-Mineral-$CO_2$ Interactions During Geological Storage of Carbon Dioxide

Andrew David Kilpatrick

Submitted in accordance with the requirements for the degree of
Doctor of Philosophy

The University of Leeds
School of Earth and Environment

September, 2014

The candidate confirms that the work submitted is his/her own and that appropriate credit has been given where reference has been made to the work of others.

This copy has been supplied on the understanding that it is copyright material and that no quotation from the thesis may be published without proper acknowledgement.

The right of Andrew David Kilpatrick to be identified as Author of this work has been asserted by him in accordance with the Copyright, Designs and Patents Act 1988.

© 2014 The University of Leeds and Andrew David Kilpatrick

## Acknowledgements

Thanks, first of all, go to my primary supervisor Bruce Yardley for all of his support and unending positivity throughout the project. Great thanks also go to Jörgen Rosenqvist and Chris Rochelle for their inexhaustible patience in educating me on all manner of geochemical, laboratory and experimental issues and helping me to avoid any major lab disasters.

Thanks to all of the lab-managers and technicians who have helped me with various pieces of work, including Lesley Neve, Linda Forbes, Andy Connelly, Tony Windross and David Banks at the University of Leeds and Bob Knight at the University of Hull. Special thanks go to Sam Allshorn who ran a tight lab for the majority of my stay at Leeds, despite constant interference from students and supervisors and was always on hand with friendly advice and assistance when needed.

Thanks to my other colleagues at the British Geological Survey, particularly Keith Bateman, Gemma Purser, Lauren Selby and Toni Milodowski for innumerable pieces of assistance, support and constructive chats.

The retention of my sanity was made possible only through the support and friendship of the surprising number of people who could tolerate my natural Scottish grumpiness; special mention must be made of Hannah Bentham, Fran Entwistle, Julia Crummy, Meg Galsworthy, Tom Long and David Tupman, without whom the last few years would have been immeasurably less enjoyable. Much love and thanks also go out to my office-mates for the provision of the odd moment of levity, your tolerance of my mess and for stealing various pieces of food which I was definitely saving for later.

The “Dumfries Crew” has not seen much of me over the last year or so and require special thanks for still making me feel at home when amongst them, despite me missing various 30$^{th}$ Birthdays, stag-dos and other celebrations. Cheers guys, look forward to seeing more of you…

Many thanks to Mum, Kate, Simon, Sam and Lala for always being there for me and for your love, tolerance, encouragement, support and advice over the years.

HUGE thanks to Fiona. I know the last couple of years have been (almost) as hard on you as they have on me and I couldn’t have hoped for a more supportive partner. I love you.

Finally, special thoughts and thanks go out to Dad. Wish you were here.

## Abstract

In order utilise geological carbon dioxide storage (GCS) at an industrial scale predictions of reservoir scale behaviour, both chemical and physical must be made. In order to ground-truth the geochemical data underlying such predictions, laboratory experiments at temperatures and $CO_2$ pressures relevant to GCS are essential.

Mineral dissolution rate, $CO_2$ solubility and pH data has been collected from batch experiments carried out on quartz, K-feldspar, albite, calcite, dolomite and Sherwood Sandstone materials. These experiments were designed to assess the influence of a variety of factors on dissolution rates: changes in grain size from 125µm - 180µm to 500µm - 600µm; changes in fluid composition from deionised water to 1.36M NaCl solution; changes in $CO_2$ pressure from 4 bar to 31 bar; changes in temperature from 22°C to 70°C. Experiments carried out on the Sherwood Sandstone material also included work on consolidated rock, rather than the powder used in other experiments.

Calculated dissolution rates for silicates were found to agree well with values calculated from literature-sourced dissolution equations and the USGS-produced general rate equation (USGS 2004) was found to be suitable for predicting these rates. Calculated dissolution rates for the carbonate minerals was found to be strongly retarded due to transport effects, with literature-sourced equations significantly over-predicting dissolution rates.

Dissolution of the sandstone material was found to be dominated by K-feldspar and dolomite dissolution, rates of which compare favourably with those obtained from the single mineral experiments. A significant increase in porosity was observed in the core flow-through experiment, associated with dolomite dissolution.

Several experiments were carried out using a Hele-Shaw cell in order to visualise the formation and migration of density plumes which form as $CO_2$ dissolved into unsaturated fluids. Introduction of NaCl and decreases in permeability were found to significantly retard migration of $CO_2$ saturated fluid, while minor heterogeneities in the cells served to focus and accelerate plume movement. Modelling work suggests that predictive models currently underestimate the rapidity of formation and migration of these plumes.

# Table of Contents

**Acknowledgements** ..... **3**

**Abstract** ..... **4**

**Table of Contents** ..... **5**

**List of Tables** ..... **10**

**List of Figures** ..... **11**

**Chapter 1 Background and Introduction** ..... **19**

1.1 Introduction ..... 19

1.1.1 GCS Background ..... 19

1.1.2 Physical Processes Accompanying Geological Carbon Storage ..... 22

1.1.3 Geochemical Mechanisms in GCS ..... 25

1.1.4 Geochemical Modelling of GCS ..... 30

1.2 Objectives and Aims ..... 32

**Chapter 2 Theoretical Background and Literature Review** ..... **34**

2.1 Geochemical Reactions During GCS: Theory and Experiment ..... 34

2.1.1 Experimental Background ..... 34

2.1.1.1 Flow-Through Experiments ..... 35

2.1.1.2 Batch Experiments ..... 37

2.1.1.3 Surface Area ..... 38

2.1.2 $CO_2$ Solubility and pH ..... 40

2.1.3 Silicate Dissolution ..... 43

2.1.3.1 Quartz Dissolution ..... 43

2.1.3.2 Feldspar Dissolution ..... 45

2.1.4 Carbonate Dissolution ..... 49

2.1.4.1 Calcite Dissolution ..... 49

2.1.4.2 Dolomite Dissolution ..... 53

2.2 Density Driven Flow in CCS ..... 60

2.3 The Sherwood Sandstone ..... 63

**Chapter 3 Dissolution Experiments Methodology** ..... **64**

3.1 Sample Preparation and Description ..... 64

3.1.1 Quartz Sample ..... 67

3.1.2 K-Feldspar Sample ..... 68

3.1.3 Albite Sample ..... 70

3.1.4 Calcite Sample ..... 72
3.1.5 Dolomite Sample ..... 73
3.1.6 Sandstone Sample ..... 74
3.2 Batch Experiments ..... 76
3.2.1 Gas System ..... 77
3.2.2 $CO_2$ Solubility ..... 78
3.2.3 Mineral Dissolution Experiments ..... 79
3.3 Core Experiments ..... 82
3.4 Data Treatment and Modelling ..... 84
3.4.1 Data Treatment and Dissolution Rate Calculations ..... 84
3.4.2 PHREEQC Modelling ..... 94
3.4.3 Errors and Uncertainties ..... 109
**Chapter 4 Mineral Dissolution Experiments ..... 112**
4.1 Silicate Minerals ..... 112
4.1.1 Quartz ..... 112
4.1.1.1 pH and $CO_2$ Solubility ..... 112
4.1.1.2 Dissolution Behaviour: General Observations ..... 116
4.1.1.3 Dissolution Behaviour: Fluid Composition ..... 117
4.1.1.4 Dissolution Behaviour: $pCO_2$ (4bar, 31bar) and temperature (22°C, 70°C) ..... 120
4.1.1.5 Quartz Dissolution Rates ..... 122
4.1.1.6 Quartz Experiments Overview and Discussion ..... 126
4.1.2 K-Feldspar ..... 128
4.1.2.1 pH and $CO_2$ Solubility ..... 129
4.1.2.2 Dissolution Behaviour: General Observations ..... 133
4.1.2.3 Dissolution Behaviour: Grain Size Effects ..... 137
4.1.2.4 Dissolution Behaviour: Effect of Fluid Composition ..... 140
4.1.2.5 Dissolution Behaviour: Effects of $pCO_2$ (4bar, 31bar) and Temperature (22°C, 70°C) ..... 143
4.1.2.6 K-Feldspar Dissolution Rates ..... 147
4.1.2.7 K-feldspar Experiments Overview and Discussion ..... 150
4.1.3 Albite ..... 155
4.1.3.1 pH and $CO_2$ Solubility ..... 155
4.1.3.2 Dissolution Behaviour: General Observations ..... 159

4.1.3.3 Dissolution Behaviour: Grain Size Effects .....161
4.1.3.4 Dissolution Behaviour: Effect of Fluid Composition.....165
4.1.3.5 Dissolution Behaviour: Effect of Elevated $pCO_2$ (4bar, 31bar) and Temperature (22°C, 70°C).....168
4.1.3.6 Albite Dissolution Rates.....174
4.1.3.7 Albite Dissolution Experiments Overview and Discussion .....177
4.2 Carbonate Minerals.....179
4.2.1 Calcite.....179
4.2.1.1 pH and $CO_2$ Solubility.....179
4.2.1.2 Dissolution Behaviour: General Observations .....184
4.2.1.3 Dissolution Behaviour: Grain Size .....185
4.2.1.4 Dissolution Behaviour: Fluid Composition .....187
4.2.1.5 Dissolution Behaviour: $pCO_2$ (4bar, 31bar) and temperature (22°C, 70°C) .....190
4.2.1.6 Calcite Dissolution Rates.....194
4.2.1.7 Calcite Experiments Overview and Discussion....200
4.2.2 Dolomite.....205
4.2.2.1 pH and $CO_2$ Solubility.....205
4.2.2.2 Dissolution Behaviour: general Observations.....209
4.2.2.3 Dissolution Behaviour: Grain Size .....211
4.2.2.4 Dissolution Behaviour: Fluid Composition .....214
4.2.2.5 Dissolution Behaviour: $pCO_2$ (4bar, 31bar) and temperature (22°C, 70°C) .....217
4.2.2.6 Dolomite Dissolution Rates.....223
4.2.2.7 Dolomite Experiments Overview and Discussion .....228
**Chapter 5 Sherwood Sandstone Dissolution Experiments Results ....231**
5.1 Powder Batch Experiments.....232
5.1.1 pH and $CO_2$ Solubility .....232
5.1.2 Dissolution Behaviour: Effects of Grain Size.....235
5.1.3 Dissolution Behaviour: Effects of Fluid Salinity .....241
5.1.4 Dissolution Behaviour: Effects of $pCO_2$ and Temperature .....247
5.1.5 Sherwood Sandstone Dissolution Rates.....258

5.1.6 Sherwood Sandstone Batch Experiments: Overview and Discussion ..... 271
5.2 Consolidated Sandstone Experiments ..... 275
5.2.1 Chemical Results ..... 277
5.2.2 Core Observations ..... 282
5.2.3 Flow-through Modelling ..... 288
5.2.4 Dissolution Rates ..... 291
5.2.5 Intact Experiments: Overview and Discussion ..... 293
**Chapter 6 Hele-Shaw Cell Experiments ..... 296**
6.1 Introduction and Methodology ..... 296
6.2 Initial Experiments ..... 300
6.3 pH Gradient Experiment ..... 305
6.4 Conclusions ..... 317
**Chapter 7 Synthesis: Applying Laboratory Derived Results to GCS .. 319**
7.1 Kicking Off: $CO_2$ solubility and pH ..... 319
7.2 The Long Haul: Mineral Interactions ..... 324
7.2.1 Mineral Dissolution and Precipitation ..... 324
7.2.2 From Single Minerals to Whole Rock Reservoirs ..... 331
7.3 Meanwhile…: The Effect of Density Plumes on GCS ..... 336
**Chapter 8 Conclusions and Future Work ..... 338**
**Bibliography ..... 342**
**Appendix A: Fluid Chemistry Data ..... 351**
A.1 Quartz Fluid Chemistry Data ..... 352
A.2 K-Feldspar Fluid Chemistry Data ..... 356
A.3 Plagioclase Fluid Chemistry Data ..... 363
A.4 Calcite Fluid Chemistry Data ..... 369
A.5 Dolomite Fluid Chemistry Data ..... 379
A.6 Sandstone Fluid Chemistry Data ..... 386
**Appendix B Selected Modelling Outputs ..... 400**
B.1 pH Calculations ..... 400
B.1.1 Quartz Experiments ..... 401
B.1.2 K-Feldspar Experiments ..... 403
B.1.3 Albite Experiments ..... 408
B.1.4 Calcite Experiments ..... 412
B.1.5 Dolomite Experiments ..... 415

B.1.6 Sandstone Experiments .....419
B.2 Kinetic Model Outputs .....423
B.2.1 Experiment 141 .....424
B.2.2 Experiment 142 .....425
B.2.3 Experiment 144 .....426
B.2.4 Experiment 146 .....427
B.2.5 Experiment 147 .....428
B.2.6 Experiment 148 .....429
B.2.7 Experiment 149 .....430

# List of Tables

**Table 1.1.1: Estimated storage potential of geological reservoirs..... 20**

**Table 3.1.1: Sample sources and sampling locations..... 64**

**Table 3.1.2: BET analysis results..... 65**

**Table 3.1.3: Formation fluid analysis from Cleethorpes borehole..... 66**

**Table 3.2.1: Summary of mineral and whole-rock dissolution experiments..... 80**

**Table 3.3.1: Core details..... 82**

**Table 3.4.1: Example of base data used in dissolution rate calculations..... 89**

**Table 3.4.2: Example of data used in rate calculation plots, for experiment 171..... 90**

**Table 3.4.3: Final calculated rates for various times..... 93**

**Table 4.1.1: Summary of experimental conditions for Quartz batch experiments..... 112**

**Table 4.1.3: Summary of K-feldspar experiments..... 128**

**Table 4.1.4: Calculated and measured pH and $CO_2$ content of final samples and at equilibrium..... 131**

**Table 4.1.5: Summary of albite dissolution experimental conditions..... 155**

**Figure 4.1.6: Calculated and measured pH and $CO_2$ contents of final samples and at equilibrium..... 157**

**Table 4.2.1: Summary of experimental conditions for Calcite batch experiments..... 179**

**Table 4.2.2: Summary of pH and $CO_2$ solubility measurements and calculations for Calcite batch experiments..... 181**

**Table 4.2.3: Calculated values of n (reaction order) and α (rate constant) with respect to $C/C_s$..... 199**

**Table 4.2.5: Summary of pH and CO2 solubility data for dolomite experiments..... 206**

**Table 5.1.1: Summary of experiments carried out on Sherwood Sandstone material..... 231**

**Figure 5.1.2: Summary of pH and $CO_2$ solubility data for sandstone powder experiments..... 233**

**Table 5.2.1: Summary of consolidated sandstone experiments..... 275**

**Table 6.2.1: Summary of original Hele-Shaw Cell experiments..... 302**

# List of Figures

**Figure 1.1.1: Variation in CO2 solubility with (a) Pressure and Temperature and (b) Salinity .....25**

**Figure 1.1.2: Dependence on CO2 trapping mechanisms on pH and divalent ion concentration .....27**

**Figure 3.1.1: SEM Image of quartz grain .....67**

**Figure 3.1.2: SEM Image of K-feldspar grain .....68**

**Figure 3.1.3: SEM Image of K-feldspar grain .....69**

**Figure 3.1.4: SEM Image of K-feldspar grain .....69**

**Figure 3.1.5: SEM Image of albite grain .....70**

**Figure 3.1.6: SEM Image of albite grains .....71**

**Figure 3.1.7: SEM Image of albite grain .....71**

**Figure 3.1.8: SEM Image of calcite grain .....72**

**Figure 3.1.9: SEM Image of dolomite grain.....73**

**Figure 3.1.10: SEM Image of illite bridge between grains .....75**

**Figure 3.1.11: SEM Image of pitted feldspar grain .....75**

**Figure 3.2.1: Schematic of laboratory set-up .....77**

**Figure 3.3.1: Setup for core flow-through experiment.....83**

**Figure 3.4.1: Plot of log(time) vs. log(K-feldspar concentration) for experiment 171. In this case K-feldspar concentration has been estimated using dissolved Si concentrations (See Table 2.1.2).....91**

**Figure 3.4.2: Plot of volume corrected time vs. feldspar concentration .....92**

**Figure 3.4.3: Plot of K-feldspar affinity (estimated from analysed concentrations) vs. calculated dissolution rate for experiment 171.....92**

**Figure 4.1.1: Calculated and measured pH values for experiment 121.....115**

**Figure 4.1.3: Quartz Saturation Indices for experiments 121 and 124.....116**

**Figure 4.1.4: Si release from experiments 121 (NaCl) and 125 (DI) .....117**

**Figure 4.1.5: Si release from experiments 124 (NaCl) and 126 (DI) .....118**

**Figure 4.1.6: Calculated quartz dissolution rates and quartz affinities for experiments 121, 125 and 126 .....118**

**Figure 4.1.7: Si release from experiments 121 (4 bar, 22°C) and 124 (31 bar, 70°C).....120**

**Figure 4.1.8: Si release from experiments 125 (4 bar, 22°C) and 126 (31 bar, 70°C) ..... 121**

**Figure 4.1.9: Calculated quartz dissolution rates for experiment 121 ..... 123**

**Figure 4.1.10: Calculated quartz dissolution rates for experiment 124 ..... 123**

**Figure 4.1.11: Calculated quartz dissolution rates for experiment 125 ..... 124**

**Figure 4.1.12: Calculated quartz dissolution rates for experiment 125 ..... 124**

**Figure 4.1.13: Calculated pH from analysed sample compositions for experiments 111 and 112 ..... 132**

**Figure 4.1.14: Elemental concentrations for experiment 172 ..... 135**

**Figure 4.1.15: Calculated saturation indices for samples from experiment 172 ..... 135**

**Figure 4.1.16: Calculated saturation indices for samples from experiment 111 ..... 136**

**Figures 4.1.17 – 4.1.20: Comparative charts of (from top left, moving clockwise) Si, K, Al and Ca concentrations for experiments 171 (125µm - 180µm) and 172 (500µm - 600µm) ..... 138**

**Figures 4.1.21: Calculated K-feldspar dissolution rates based on Si release for experiments 171 and 172 ..... 139**

**Figures 4.1.22 – 4.1.25: Comparative charts of (from top left, moving clockwise) Si, K, Al and Ca concentrations for experiments 171 (1.36M NaCl) and 173 (Deionised Water) ..... 141**

**Figures 4.1.26: Calculated K-feldspar dissolution rates for experiments 171 and 173 ..... 142**

**Figures 4.1.27 – 4.1.30: Comparative charts of (from top left, moving clockwise) Si, K, Al and Ca concentrations for experiments 171 (4 bar $pCO_2$, 22°C) and 176 (31 bar $pCO_2$, 70°C) ..... 144**

**Figures 4.1.31 – 4.1.34: Comparative charts of (from top left, moving clockwise) Si, K, Al and Ca concentrations for experiments 175 (4 bar $pCO_2$, 70°C) and 171 (4 bar $pCO_2$, 22°C) ..... 145**

**Figures 4.1.35: Calculated K-feldspar dissolution rates and affinity for experiments 171 and 176 ..... 146**

**Figures 4.1.36: Calculated K-feldspar dissolution rates and affinity for experiments 173 and 175 ..... 146**

**Figures 4.1.37 – 4.1.40: Calculated K-feldspar dissolution rates based on Si release and BET surface area, plotted together with various calculated predictions for (from top left moving clockwise) experiments 111, 112, 113 and 171 .....148**

**Figures 4.1.41 – 4.1.44: Calculated K-feldspar dissolution rates based on Si release and BET surface area, plotted together with various calculated predictions for (from top left moving clockwise) experiments 172, 173, 175 and 176 .....149**

**Figure 4.1.45: Calculated pH of samples from experiment 181 .....158**

**Figure 4.1.46: Elemental concentrations for samples from experiment 184.....160**

**Figures 4.1.47 – 4.1.50: Comparative charts of (from top left, moving clockwise) K, Al, Ca and Si concentrations for experiments 122 (125µm - 180µm) and 181 (500µm - 600µm).....162**

**Figures 4.1.55: Calculated albite dissolution rates and affinities for experiments 122 and 181 .....164**

**Figures 4.1.56: Calculated albite dissolution rates and affinities for experiments 184 and 182 .....164**

**Figures 4.1.57 – 4.1.60: Comparative charts of (from top left, moving clockwise) Al, Si, Ca and K concentrations for experiments 184 (NaCl) and 185 (DI).....166**

**Figures 4.1.61: Calculated albite dissolution rates and affinities for experiments 184 and 185 .....167**

**Figures 4.1.62 – 4.1.65: Comparative charts of (from top left, moving clockwise) Al, Si, Ca and K concentrations for experiments 122 (4bar, 22°C) and 184 (31bar, 70°C).....169**

**Figures 4.1.66 – 4.1.69: Comparative charts of (from top left, moving clockwise) Al, Si, Ca and K concentrations for experiments 181 (4bar, 22°C) and 182 (31bar, 70°C).....170**

**Figures 4.1.70 – 4.1.73: Comparative charts of (from top left, moving clockwise) Al, Si, Ca and K concentrations for experiments 185 (31bar, 70°C) and 183 (4bar, 70°C).....171**

**Figures 4.1.76: Calculated albite dissolution rates and affinities for experiments 185 and 183 .....173**

**Figures 4.1.77 – 4.1.80: Calculated Albite dissolution rates based on Si release and BET surface area, plotted together with various calculated predictions for (from top left moving clockwise) experiments 122, 123, 181 and 182 .....175**

**Figures 4.1.81 – 4.1.83: Calculated Albite dissolution rates based on Si release and BET surface area, plotted together with various calculated predictions for (from top left moving clockwise) experiments 183, 184 and 185 .....176**

**Figure 4.2.1: Calculated pH for samples from experiment 103.....182**

**Figure 4.2.2: Measured Ca concentrations for experiment 103 ..... 184**

**Figure 4.2.3: Comparative chart of Ca concentrations for experiments 191 (125µm - 180µm) and 103 (500µm - 600µm)..... 185**

**Figure 4.2.4: Calculated calcite dissolution rates and affinities for experiments 103 and 191..... 186**

**Figure 4.2.5: Comparative chart of Ca concentrations for experiments 191 (NaCl) and 193 (DI) ..... 187**

**Figure 4.2.6: Comparative chart of Ca concentrations for experiments 192 (NaCl) and 195 (DI) ..... 188**

**Figure 4.2.7: Calculated calcite dissolution rates and affinities for experiments 191 and 193..... 188**

**Figure 4.2.8: Calculated calcite dissolution rates and affinities for experiments 192 and 195..... 189**

**Figure 4.2.9: Comparative chart of Ca concentrations for experiments 191 (4 bar, 22°C) and 192 (31 bar, 70°C) ..... 190**

**Figure 4.2.10: Comparative chart of Ca concentrations for experiments 193 (4 bar, 22°C) and 195 (31 bar, 70°C) ..... 191**

**Figure 4.2.11: Calculated calcite dissolution rates and affinities for experiments 191 and 192..... 191**

**Figure 4.2.12: Calculated calcite dissolution rates and affinities for experiments 193 and 195..... 192**

**Figures 4.2.13 – 4.2.16: Calculated calcite dissolution rates and affinities for experiments (clockwise from top left) 103, 196, 193 and 195..... 195**

**Figures 4.2.17 – 4.2.18: Calculated calcite dissolution rates and affinities for experiments 192 (left) and 191 (right) ..... 196**

**Figure 4.2.19: Plot of log Rate vs. log(1-C/Cs) for all experimental data from calcite dissolution experiments..... 198**

**Figure 4.2.20: Plot of experimental rate divided by rate calculated from Equation 4.2.1, vs. Ca concentration..... 203**

**Table 4.2.4: Experimental conditions for dolomite dissolution experiments..... 205**

**Figure 4.2.21: Summary of pH data for experiment 132..... 207**

**Figure 4.2.22: Ca and Mg concentrations, corrected for bulk mineral stoichiometry for experiment 131 ..... 209**

**Figure 4.2.23: SEM photograph of precipitate on a dolomite grain retrieved from experiment 134..... 210**

**Figure 4.2.24: Comparative chart showing Ca release for experiments 131 (125-180µm) and 132 (500-600µm) ..... 211**

**Figure 4.2.25: Comparative chart showing Ca release for experiments 134 (125-180µm) and 135 (500-600µm) ..... 212**

**Figure 4.2.26: Calculated dolomite dissolution rates and affinities for experiments 131 (125-180μm) and 132 (500-600μm) .....212**

**Figure 4.2.27: Calculated dolomite dissolution rates and affinities for experiments 134 (125-180μm) and 135 (500-600μm) .....213**

**Figure 4.2.28: Comparative chart showing Ca release for experiments 131 (NaCl) and 133 (deionised water).....214**

**Figure 4.2.29: Comparative chart showing Ca release for experiments 143 (NaCl) and 134 (deionised water).....215**

**Figure 4.2.30: Calculated dolomite dissolution rates and affinities for experiments 131 (NaCl) and 133 (DI) .....215**

**Figure 4.2.31: Calculated dolomite dissolution rates and affinities for experiments 143 (NaCl) and 134 (DI) .....216**

**Figure 4.2.32: Comparative chart showing Ca release for experiments 133 (low P/T) and 134 (high P/T) .....217**

**Figure 4.2.33: Comparative chart showing Ca release for experiments 131 (low P/T) and 143 (high P/T) .....218**

**Figure 4.2.34: Calculated dolomite dissolution rates and affinities for experiments 133 (low P/T) and 134 (high P/T) .....218**

**Figure 4.2.35: Calculated dolomite dissolution rates and affinities for experiments 131 (low P/T) and 143 (high P/T) .....219**

**Figure 4.2.36: Comparative chart showing Ca release for experiments 136 (control) and 131 (low P/T) .....220**

**Figure 4.2.37: Comparative chart showing Ca release for experiments 136 (control) and 143 (high P/T).....220**

**Figure 4.2.38: Calculated dolomite dissolution rates and affinities for experiments 136 (control) and 131 (low P/T) .....221**

**Figure 4.2.39: Calculated dolomite dissolution rates and affinities for experiments 136 (control) and 143 (high P/T).....221**

**Figure 4.2.44 - 4.2.46: Calculated dolomite dissolution rates and affinities for experiments (clockwise from top left) 135, 136 and 143 .....226**

**Figure 5.1.1: Calculated pH for samples from experiment 142 .....234**

**Figures 5.1.2 – 5.1.5: Comparative charts showing (clockwise from top left) Al, Si, Ca and K release for experiments 141 (125-180μm) and 142 (500-600μm) .....236**

**Figure 5.1.6: Comparative chart showing Mg release for experiments 141 (125-180μm) and 142 (500-600μm) .....237**

**Figures 5.1.7 – 5.1.10: Comparative charts showing (clockwise from top left) K, Al, Si, and Ca release for experiments 147 (125-180μm) and 148 (500-600μm) .....238**

**Figure 5.1.11: Comparative chart showing Mg release for experiments 147 (125-180µm) and 148 (500-600µm) ..... 239**

**Figures 5.1.12 – 5.1.13: Calculated dolomite and K-feldspar dissolution rates for experiments 141 (125-180µm) and 142 (500-600µm) ..... 240**

**Figures 5.1.16 – 5.1.19: Comparative charts showing (clockwise from top left) Al, Si, K and Ca release for experiments 148 (NaCl) and 147 (DI) ..... 242**

**Figure 5.1.20: Comparative chart showing Mg release for experiments 148 (NaCl) and 147 (DI) ..... 243**

**Figures 5.1.21 – 5.1.24: Comparative charts showing (clockwise from top left) Al, Si, Ca and K release for experiments 144 (DI) and 141 (NaCl) ..... 244**

**Figure 5.1.25: Comparative chart showing Mg release for experiments 144 (DI) and 141 (NaCl) ..... 245**

**Figures 5.1.26 – 5.1.27: Calculated dolomite and K-feldspar dissolution rates for experiments 148 (DI) and 147 (NaCl) ..... 246**

**Figures 5.1.30 – 5.1.33: Comparative charts showing (clockwise from top left) Al, Si, Ca and K release for experiments 141 (4bar, 22°C) and 147 (31bar, 70°C) ..... 248**

**Figure 5.1.34: Comparative chart showing Mg release for experiments 141 (4bar, 22°C) and 147 (31bar, 70°C) ..... 249**

**Figures 5.1.35 – 5.1.438: Comparative charts showing (clockwise from top left) K, Al, Ca and Si release for experiments 144 (4bar, 22°C) and 148 (31bar, 70°C) ..... 250**

**Figure 5.1.39: Comparative chart showing Mg release for experiments 144 (4bar, 22°C) and 148 (31bar, 70°C) ..... 251**

**Figures 5.1.40 – 5.1.43: Comparative charts showing (clockwise from top left) K, Al, Ca and Si release for experiments 141 (4bar, 22°C) and 149 (4bar, 70°C) ..... 252**

**Figure 5.1.44: Comparative chart showing Mg release for experiments 141 (4bar, 22°C) and 149 (4bar, 70°C) ..... 253**

**Figures 5.1.45 – 5.1.48: Comparative charts showing (clockwise from top left) Al, Si, Ca and K release for experiments 149 (4bar, 70°C) and 147 (31bar, 70°C) ..... 254**

**Figure 5.1.49: Comparative chart showing Mg release for experiments 149 (4bar, 70°C) and 147 (31bar, 70°C) ..... 255**

**Figures 5.1.50 – 5.1.51: Calculated dolomite and K-feldspar dissolution rates for experiments 144 (DI) and 141 (NaCl) ..... 256**

**Figures 5.1.52 – 5.1.53: Calculated dolomite and K-feldspar dissolution rates for experiments 144 (DI) and 141 (NaCl) ..... 256**

**Figures 5.1.58 – 5.1.61: Calculated elemental release rates for experiments 141, 142, 144 and 146.....259**

**Figures 5.1.62 – 5.1.64: Calculated elemental release rates for experiments 147, 148 and 149.....260**

**Figures 5.1.65 – 5.1.66: Calculated dolomite and K-feldspar dissolution rates for experiment 141 .....262**

**Figures 5.1.67 – 5.1.68: Calculated dolomite and K-feldspar dissolution rates for experiment 142 .....262**

**Figures 5.1.69 – 5.1.70: Calculated dolomite and K-feldspar dissolution rates for experiment 146. .....263**

**Figures 5.1.71 – 5.1.72: Calculated dolomite and K-feldspar dissolution rates for experiment 147. .....263**

**Figures 5.1.73 – 5.1.74: Calculated dolomite and K-feldspar dissolution rates for experiment 144. .....264**

**Figures 5.1.75 – 5.1.76: Calculated dolomite and K-feldspar dissolution rates for experiment 148 .....264**

**Figure 5.1.77: Calculated dolomite dissolution rates for experiment 149.....265**

**Figures 5.1.78 – 5.1.80: Modelled elemental concentrations plotted against measured concentrations for Experiment 141.....268**

**Figure 5.1.81: Modelled Si and Al concentrations plotted against measured concentrations for Experiment 141, with Illite removed from model composition. .....269**

**Figure 5.2.1: Sherwood Sandstone chip used in experiment SC2 .....276**

**Figures 5.2.2 – 5.2.3: K (left) and Al (right) concentrations for samples from consolidated sandstone experiments.....278**

**Figures 5.2.4 – 5.2.5: Ca (left) and Mg (right) concentrations for samples from consolidated sandstone experiments.....279**

**Figure 5.2.6 & 5.2.7: SEM images of SCORE Inlet (Left) and STATIC Inlet (Right).....283**

**Figures 5.2.8 & 5.2.9: SEM images of SCORE outlet (Left) and STATIC outlet (Right).....284**

**Figures 5.2.10 & 5.2.11: SEM images of Heavily dissolved dolomite grain from SCORE in secondary electron (left) and backscatter (right) modes .....285**

**Figures 5.2.12 - 5.2.15: NMR measurements for both SCORE and STATIC cores, before and after reaction .....287**

**Figures 5.2.16 - 5.2.19: Modelled and measured elemental concentrations for SCORE.....289**

**Figures 5.2.20 - 5.2.22: Modelled and measured Mg concentrations, pH and dissolved $CO_2$ content for SCORE.....290**

**Figures 5.2.23 - 5.2.24: Calculated dolomite and K-feldspar dissolution rates for consolidated sandstone experiments and powder experiment 147 ..... 292**

**Figure 6.1.1: Processed images of Hele-Shaw cell experiments from the published work of: LEFT- Neufeld et al (2010); MIDDLE- Kneafsey & Pruess (2011); RIGHT- Faisal et al (2013) . 296**

**Figure 6.1.2: Original Hele-Shaw cell design ..... 298**

**Figure 6.1.3: Revised, openable Hele-Shaw cell design ..... 299**

**Figure 6.2.1: Run 1 at 0.5 hours (left) and 2 hours (right) ..... 303**

**Figure 6.2.2: Run 2 at 0.5 hours (left) and 2 hours (right) ..... 303**

**Figure 6.2.3: Run 3 at 0.5 hours (left) and 2 hours (right) ..... 303**

**Figure 6.2.4: Run 4 at 0.5 hours (left) and 2 hours (right) ..... 303**

**Figure 6.2.5: Run 5 at 24 hours (left) and one week (right) ..... 304**

**Figure 6.2.6: Run 6 at 0.5 hours (left) and 1 hour (right) ..... 304**

**Figure 6.2.7: Run 7 at 0.5 hours (left) and 1 hour (right) ..... 304**

**Figures 6.3.1 – 6.3.6: Photographs from pH gradient experiment taken at 10 minutes (top left), 30 minutes (top centre), 2 hours (top right), 5 hours (bottom left), 12 hours (bottom centre) and 16 hours (bottom right). ..... 307**

**Figure 6.3.7 – 6.3.13: Processed 10 minute image showing various pH ranges ..... 308**

**Figure 6.3.14 – 6.3.20: Processed 30 minute image showing various pH ranges ..... 309**

**Figure 6.3.21 – 6.3.27: Processed 2 hour image showing various pH ranges ..... 310**

**Figures 6.3.28 – 6.3.34: Processed 5 hour image showing various pH ranges ..... 311**

**Figures 6.3.35 – 6.3.41: Processed 12 hour image showing various pH ranges ..... 312**

**Figure 6.3.42 – 6.3.48: Processed 16 hour image showing various pH ranges ..... 313**

**Figure 6.3.49: Image of the model grid used to simulate the pH gradient experiment ..... 314**

**Figure 6.3.50 – 6.3.59: Processed 12 hour image showing various pH ranges (top) and corresponding model images (bottom) ..... 316**

# Chapter 1 Background and Introduction

## 1.1 Introduction

The focus of this thesis is relatively broad, but it has the overall aim of illuminating some of the issues relating to Carbon Capture in Storage (CCS). Specifically, the work presented here-in deals with various geochemical aspects of Geological Carbon Storage (GCS). Geochemical and physical processes affecting GCS and their interplay, will occur at a variety of temporal and physical scales, meaning that at the industrial scale, such systems may be very complex. The processes of interest include dissolution of $CO_2$ into pore water, migration of $CO_2$ rich water and the enhancement of mineral dissolution caused by $CO_2$ rich fluids. The following chapter provides some background on GCS and these processes.

### 1.1.1 GCS Background

It is now widely accepted that the increasing levels of greenhouse gases emitted to the atmosphere from anthropogenic sources over the last few decades are a major contributor to global warming. Carbon dioxide ($CO_2$) is the largest anthropogenically sourced contributor to warming and as such there is considerable interest in the development of technologies and strategies designed to reduce the levels of carbon dioxide emitted to the atmosphere. While renewable energy technologies provide the most clear cut way of ultimately reducing $CO_2$ emissions, industrial scale deployment of these technologies remains limited, due, at least in part, to the significant investment required to make the switch and also due to the unpredictability of renewable sources such as wind and solar power. Hence technologies which act to reduce $CO_2$ emissions, while retaining an overall reliance on fossil fuels are seen in some quarters as a useful “stop-gap” technology.

One such technology currently favoured as an option for reducing $CO_2$ emissions is CCS. CCS involves the capture of $CO_2$, most likely from point sources, such as power stations and other industrial plant, followed by transportation to a secure site where the gas can be sequestered or stored for a significant period of time. Storage could be in geological media, in oceans, or as stable mineral phases (mineral carbonation) (IPCC 2005). Storage within geological media is the most attractive option at the current

time, due to energy penalties associated with carbonation and the potential political and environmental issues associated with ocean storage.

Potential geological sites for $CO_2$ storage include salt caverns, un-mineable coal seams, depleted and disused oil reservoirs and deep saline aquifers (Bachu 2002; Gale 2004). Storage in salt caverns and coal seams are both emerging technologies, and due to energy costs and potential environmental drawbacks are unlikely to be implemented in the very near future. Depleted and disused oil reservoirs are immediately attractive as storage sites, since much of the industrial architecture required for the implementation of storage is already in place at these sites (pipeline networks, injection/monitoring wells etc.). Additionally, storage of $CO_2$ in conjunction with Enhanced Oil Recovery (EOR) can yield economic as well as environmental benefits making this option more attractive to the energy industry. However, storage arising directly from EOR operations is unlikely to amount to more than a fraction of current $CO_2$ emissions and, in the long-term, depleted and disused oil reservoirs are unlikely to have the capacity required for significant storage (Saylor & Zerai 2004). By far the highest storage capacity is in deep saline aquifers, with potential capacity of these formations estimated at between 1000 $GtCO_2$ and 100000 $GtCO_2$ (IPCC 2005).Table 1 shows the estimated storage potential of three different reservoir types. The lower of these estimates are based purely on volumetric trapping of $CO_2$ as a free-phase, while the higher estimates attempt to account for more complex processes such as dissolution and mineral trapping. As can be seen there is wide variation in capacity estimates, due to the various processes accounted for in the different estimates.

| **Geological Reservoir Type** | **Lower estimate of storage capacity ($GtCO_2$)** | **Upper estimate of storage capacity ($GtCO_2$)** |
|---|---|---|
| ***Oil and gas fields*** | *675* | *900* |
| ***Un-mineable coal seams*** | *3-15* | *200* |
| ***Deep saline formations*** | *1000* | *~$10^4$* |

**Table 1.1.1**: Estimated storage potential of geological reservoirs (IPCC 2005)

To reduce injection costs, limit $CO_2$ buoyancy and maximize the mass of $CO_2$ that can be stored in a given pore volume, $CO_2$ is likely to be injected as a supercritical fluid (Bachu 2002), in this state $CO_2$ fills the available volume as a gas would, but has a density varying from 200 kg/$m^3$ to 900kg/$m^3$ dependant on temperature and pressure (Saylor & Zerai 2004). The critical point for $CO_2$ is at 31.1$^oC$ and 7.38 MPa, corresponding to a depth of around 800m and hence potential storage sites are likely to lie a depths greater than 800m-1000m, although at lower temperatures storage of $CO_2$ as a liquid phase would be possible at considerably shallower depths.

### 1.1.2 Physical Processes Accompanying Geological Carbon Storage

The ultimate aim of GCS must be to trap injected carbon dioxide in the target reservoir, for significant (>1000 years) periods of time. While $CO_2$ may be trapped successfully as a free-phase, dissolution of $CO_2$ into formation waters is desirable in terms of storage security: dissolved $CO_2$ will be more limited in terms of potential migration and maximisation of dissolution will likewise maximise the storage potential of the target reservoir. Dissolution of $CO_2$ into formation brines, while driven by chemical processes, will be rate limited by the contact area between the injected $CO_2$ and the brine saturated area of the aquifer itself. This variable will be controlled by physical processes, such as the migration of the $CO_2$ plume through the aquifer, aquifer geometry, heterogeneity and flow properties. It is, therefore, important to understand the dominant physical processes likely to occur in a $CO_2$ storage setting.

Following injection of supercritical $CO_2$ into a reservoir, a number of physical processes will act to displace and trap the fluid. Displacement mechanisms will act on a number of scales within the reservoir. At the pore scale molecular diffusion and dispersion dominate. Near to the injection site mixing between the supercritical fluid and water will occur. On the larger, reservoir scale, buoyancy/density effects will dominate, caused by the low density of supercritical $CO_2$ relative to brine/water, as well as viscous fingering caused by its higher mobility (Bachu et al. 1994). The natural pressure gradient of the reservoir may also act upon the $CO_2$ plume, though in deep aquifers, where groundwater movement is very slow this is likely to be a relatively long term process (Gunter et al. 2004). Slow groundwater movement may be considered beneficial in that low migration potential will limit the risk of leakage in areas distal from, and less well characterised than, the injection area, but it may also retard the dissolution potential of the injected mass.

During the initial injection phase of a storage programme injected $CO_2$ will displace brine (which can be considered the wetting phase in such systems) around the well, forming a plume. Due to its relatively low density compared to brine the $CO_2$ will migrate upward, until vertical migration is halted by a cap-rock or other feature with a capillary entry pressure such that the $CO_2$ pressure is not great enough permeate it. At this point the plume will spread laterally (Oloruntobi & LaForce 2009) and assuming the cap-rock is laterally

extensive and retains its integrity across the storage site, we may assume at this point that the $CO_2$ is “structurally” trapped.

However, since the implementation of GCS technology is relatively recent and the detailed characterisation of such deep reservoirs can be difficult there has been concern over the potential of cap-rocks to leak. Leakage may occur by a failure in cap-rock integrity, either following chemical attack by the injected $CO_2$, or by structural failure caused by pressure changes in the underlying aquifer during the injection phase, or by leakage through pre-existing wells (Juanes et al. 2006) (a particular concern in depleted oil and gas fields). Therefore it is desirable to prevent the $CO_2$ plume from ever reaching the cap-rock, hence limiting the reliance on its integrity to provide the main trapping mechanism (Kumar et al. 2004).

The primary mechanism proposed for preventing contact between the injected $CO_2$ and the cap-rock is residual or capillary trapping. As already noted, during injection formation brine is displaced by non-wetting $CO_2$, this process is known as *drainage*. After injection has ceased and as the plume migrates upward, brine will displace the migrating $CO_2$ at the trailing edge of the plume, either by natural groundwater movement or by brine injection specifically for this purpose (Al Mansoori et al. 2009), this process is known as *imbibition*. This mechanism leads to isolation, or *snap off* of $CO_2$ from the trailing edge of the plume, effectively creating a trail of immobilised pockets of $CO_2$ trapped in the pore-space (Juanes et al. 2006). This process is responsible for the relative permeability hysteresis between the drainage and imbibition of brine by $CO_2$. Taking residual trapping into account when designing or modelling $CO_2$ injection schemes is important in terms of the behaviour and ultimate fate of a $CO_2$ plume and is recognised as an area worthy of further study (Kumar et al. 2004).

Numerous factors affect the trapping of $CO_2$ as a residual phase. These include relative permeability and which depends on interfacial tension, itself a function of pressure, temperature and salinity, and capillary pressure, which varies with pore throat size. More experimental data is needed to improve understanding of these processes in relation to $CO_2$ storage (Bachu & Bennion 2008). Additionally, there is a limited understanding of how aquifer heterogeneities will affect the residual trapping of $CO_2$. Previous experimental work (Oloruntobi & LaForce 2009), suggests that trapping is a function of heterogeneity, with high permeability pathways increasing the mobility and hence decreasing the residual trapping of $CO_2$. Likewise low

permeability layers which retard the movement of $CO_2$ may help to increase residual trapping.

The final physical process to be summarised in this section is convection. Brine which is saturated with $CO_2$ is around 1-3% denser than unsaturated brine. Hence, as the buoyant $CO_2$ dissolves into the surrounding brine, a density instability will be created, allowing saturated brine to sink and be replaced by fresh, unsaturated fluid. It has been argued that this may be the mechanism which dominates long term dissolution of $CO_2$ from a migrating plume, since it is believed to operate on timescales orders of magnitude faster than that of diffusion, which some consider to be the rate limiting step in $CO_2$ dissolution (Ennis-King & Paterson 2005).

### 1.1.3 Geochemical Mechanisms in GCS

Following injection of $CO_2$ into a target reservoir, supercritical $CO_2$ may be physically immobilised or may migrate, displacing formation fluid under its own buoyancy, or being carried by the local groundwater flow. During this phase of storage a number of interlinked chemical interactions will begin to act to bring the system to chemical equilibrium. The possible interactions are myriad and their exact nature will tend to be highly site specific (dependant on factors such as specific aquifer mineralogy and brine chemistry); they may continue for thousands of years before full equilibrium is reached (Baines & Worden 2004). However it is recognised that there are a number of basic geochemical processes which may act in the short to medium term to trap $CO_2$ as a relatively stable phase. The following section will provide a description of these mechanisms and highlight their potential importance in the geological storage of $CO_2$.

The initial interaction is the dissolution of supercritical $CO_2$ into the formation fluid. The extent of dissolution of a supercritical $CO_2$ plume will be partially controlled by fluid-rock interactions, but initially at least the solubility of $CO_2$ in formation brine will be controlled primarily by local pressure, temperature and salinity (Rochelle et al. 2004). Figure 1 demonstrates the dependence of $CO_2$ solubility on these parameters.

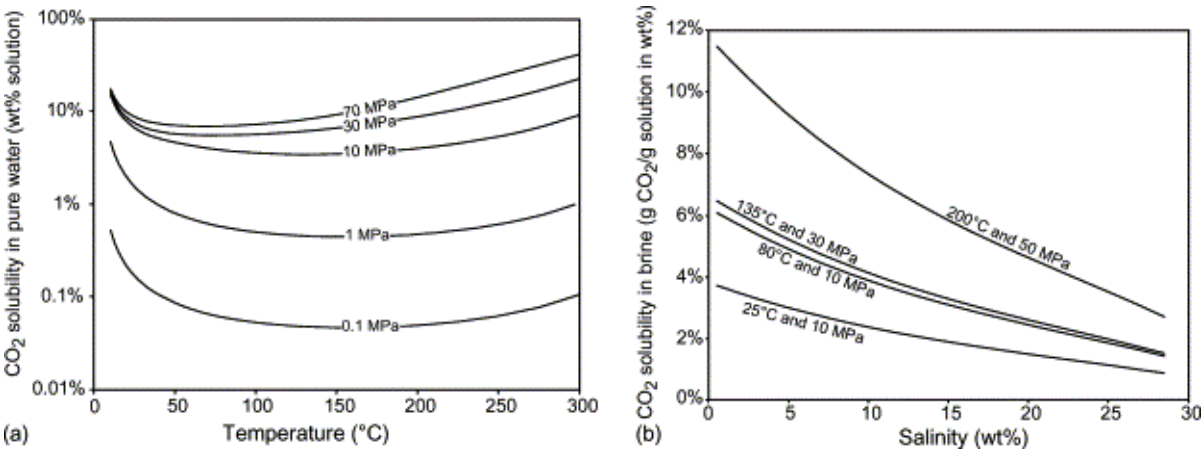


Figure 1.1.1: Variation in CO2 solubility with (a) Pressure and Temperature and (b) Salinity (reproduced from Bachu & Adams 2003)

Note that at the pressures and temperatures of interest (around $80^0$C and 8 MPa) increasing salinity acts to reduce $CO_2$ solubility (due to a salting out effect) and likewise increasing temperature decreases $CO_2$ solubility. Nevertheless dissolution of $CO_2$ into brines takes place rapidly at both laboratory and field scales (Rochelle et al. 2004), but the extent to which it

will act to dissolve the $CO_2$ plume will depend on the surface contact area relative to the volume of $CO_2$. The process will slow as concentration gradients emerge around the plume as formation water becomes saturated with dissolved $CO_2$.

Equation 1.1.1 describes the dissolution of gaseous (or supercritical) $CO_2$ into water:

$$CO_{2(g)} \Leftrightarrow CO_{2(aq)} + H_2O \Leftrightarrow H_2CO_{3(aq)} \qquad (1.1.1)$$

Here dissolved $CO_2$ exists in equilibrium with relatively weak carbonic acid by reaction with the formation water. Assuming a static and unreactive system, dissolution of free-phase $CO_2$ is unlikely to occur after pore-fluid saturation (around 5-10 wgt.% of solution at the pressures and temperatures of interest). Additionally in its dissolved state $CO_2$ has the potential to degas from formation water if there is a drop in pressure, which may raise issues of storage security in some systems. In order to drive the dissolution of further $CO_2$ and to store it in a more secure form dissolved $CO_2$ must either be moved away from the free-phase plume, allowing contact with fresh unsaturated fluid or the dissolved $CO_2$ must be removed chemically. Movement of $CO_2$ saturated fluid away from the free-phase plume may occur by natural or induced groundwater flow, by diffusion (which is likely to be very slow) or by convection (as detailed in Section 2.2). Alternatively dissolution of $CO_2$ into formation fluid may be driven by chemical effects, as detailed in the following paragraphs.

Dissolved $CO_2$ will dissociate to form dissolved ionic species as illustrated by equations 1.1.2 and 1.1.3:

$$H_2CO_3^* \Leftrightarrow HCO_3^- + H^+ \qquad (1.1.2)$$

$$HCO_3^- \Leftrightarrow CO_3^{2-} + H^+ \qquad (1.1.3)$$

This dissociation is controlled by pH (Gunter et al. 2004) as illustrated by Figure 1.1.2. As can be seen the initial dissociation of dissolved $CO_2$ releases acidity (Equation 1.1.2), thus if there is a large supply of free-phase $CO_2$ available for dissolution that the system will be maintained at a relatively low pH and the majority of dissolved $CO_2$ will remain as bicarbonate species.

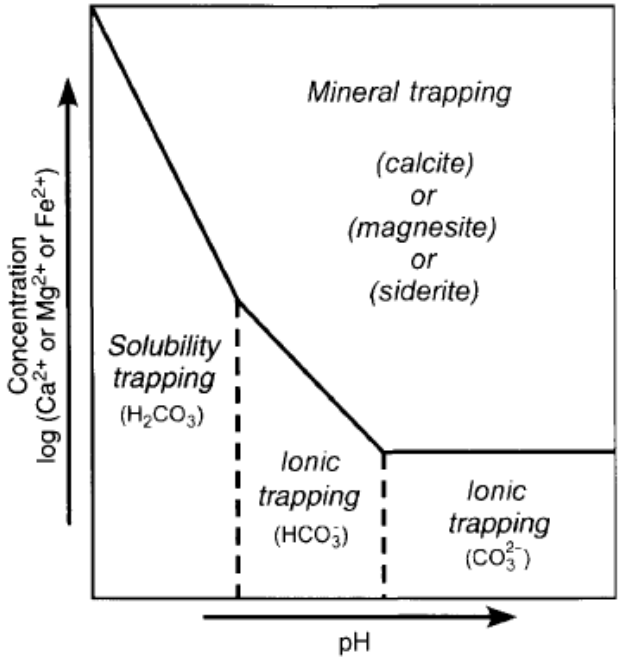


**Figure 1.1.2**: Dependence on CO2 trapping mechanisms on pH and divalent ion concentration (reproduced from Gunter et al. 2004).

From equations 1.1.1 - 1.1.3, further dissolution of $CO_2$ may occur if these reactions are pushed to the right, by neutralisation of the acidity or by removal of carbonate species through mineral-fluid interactions. Initial reactions are likely to involve relatively rapid lowering of acidity by carbonate dissolution or ion exchange, whereby accessible cations held on mineral surfaces, such as clays, are exchanged for hydrogen ions in solution. While the availability of the cations may be limited in many rocks, this can provide a rapid process for the neutralisation of acidity. Additionally the cations released may include Ca, Mg and/or Fe ions, which may interact with bicarbonate in the formation fluid, causing carbonate mineral precipitation, as illustrated in general form by equation 1.1.4:

$$HCO_3^- + M_{(aq)}^{2+} \Leftrightarrow M^{(II)}CO_3 + H_{(aq)}^+ \qquad (1.1.4)$$

Here, the carbonate precipitate may be, for example, calcite ($CaCO_3$), magnesite ($MgCO_3$) or siderite ($FeCO_3$) depending on the cations supplied (Rochelle et al. 2004).

Further interactions of dissolved $CO_2$ with aquifer minerals involve the breakdown of aluminosilicate minerals, and may be similar, in some respects, to mineral weathering reactions at the Earth's surface. A general form for these reactions is illustrated by equation 1.1.5 (Baines & Worden 2004):

$$CO_2 + H_2O + M^{(II)}Al_xSi_yO_z \rightarrow Al - si\ mineral + M^{(II)}CO_3 \qquad (1.1.5)$$

Depending on aquifer mineralogy, they might include: reaction of anorthite to calcite and kaolinite; reaction of albite to Na-smectite, bicarbonate and quartz; and, in the presence of an NaCl brine, the reaction of K-feldspar to dawsonite and quartz (Rochelle et al. 2004).

The products of these reactions have been observed during laboratory scale experiments carried out under GCS conditions, as well as in systems which have contained $CO_2$ for geological time-scales (Rochelle et al. 2004; Baines & Worden 2004). Examples include both formation of clays and carbonates and the dissolution of feldspars. More poorly constrained are the actual rates of these reactions in the context of an anthropogenic storage system and more experimental data is required to define the kinetics of multi-mineral systems. Also, while models used in simulation of $CO_2$ storage are now capable of taking into account processes such as ion exchange which acts as a buffer for pH, more experimental data is required to better constrain these processes (Michael et al. 2009). Since the dissolution and/or fixation of $CO_2$ is desirable in terms maximising storage security and volume it is important to further understand these reactions in the context of industrial scale storage systems.

In recent years much work has been done on the modelling of $CO_2$ solubility in NaCl solutions at a range of temperatures, pressures and salinities (Duan R. 2003; Portier & Rochelle 2005; Spycher & Pruess 2005) and increasing attention has been given to dissolution at conditions relative to $CO_2$ storage. However, these models often principally involve only $CO_2$ and brine, with no mineral interactions. Where mineral phases are included they are often only single, pure mineral phases, rather than the mixed, complex mineral assemblages one would find in a natural reservoir. Additionally, kinetic data for these mineral phases are often extrapolated from experiments carried out at pressures and temperatures outside the range of interest for GCS, and using unrealistic fluid:rock ratios. Application of such models to natural systems has shown that they often do not reproduce the long-term geochemical effects of storage (Baines & Worden 2004).

Additionally, it is clear that there is a discrepancy between laboratory-derived rates and those estimated in the field, which are typically slower by about half an order of magnitude. This is likely due to a number of factors including simplifying assumptions made about the available surface area and the fact that much data used in predictive modelling is extrapolated from high pH or

single mineral experiments. Due to the relative scarcity of field data, it is important to understand the factors affecting lab derived reaction rates, the controls on such rates, and how they might best be applied to more realistic situations/environments.

### 1.1.4 Geochemical Modelling of GCS

Predictive modelling is an important tool for the design and application of geological storage of $CO_2$. This section will outline some of the areas where predictive modelling has been applied, as well as some of the shortcomings and knowledge gaps which might be addressed to improve it.

Due to the nature of GCS there are a large number of uncertainties involved in the design of such schemes. Since storage will be at depths greater than 800m there will often be a lack of detailed data on geological structure, heterogeneities, mineralogy and brine chemistry. Hence predictive modelling, of chemistry and flow processes is integral to $CO_2$ disposal schemes, not only at the design stage, but throughout a schemes lifetime. Monitoring data can be fed back into models, hence refining them and reciprocally data from these models can be fed back into the engineering and sampling aspects of the scheme.

Initial modelling approaches involved standalone modelling of geochemical batch experiments, using codes such as PHREEQC, or of hydrodynamic processes, often using codes previously utilised by the petroleum industry, such as ECLIPSE or the TOUGH family of codes (Gaus et al. 2007). However, due to the complex feedback mechanisms between chemical reactions and flow processes (for example the dissolution of $CO_2$ from its supercritical state, or the effects of mineral dissolution and precipitation on formation porosity) it has become common practice to utilise fully coupled reactive transport models. These numerical simulations couple multi-fluid flow with reactive chemistry (Xu et al. 2010). The primary code currently used for modelling of $CO_2$ storage schemes for research purposes is TOUGHREACT, part of the TOUGH2 family of codes.

While lack of detailed data on deep storage sites necessitates considerable simplification of storage systems when modelled, predictive modelling is particularly useful for quantitative risk assessment of potential leakage and the long-term integrity of cap-rocks (Gaus et al. 2007; Celia & Nordbotten 2009); estimating storage capacity factors for sites (Xu et al. 2003); evaluating impacts of near-well chemical reactions (e.g. precipitation and dissolution of aquifer minerals) on injectivity or well integrity; for validation of laboratory and small scale field experiments (Gaus et al. 2007).

Current shortcomings of modelling approaches to $CO_2$ storage include the frequent absence of good data on the mineralogy (primary and secondary) of the storage sites, which can have a large influence on the predicted

reactions. Kinetic data is also sparse, particularly for precipitation rates (which are widely, but incorrectly, assumed to be equal to dissolution rates) for major minerals and actual reaction mechanisms (at which sites on mineral surfaces do reactions occur etc.) are also poorly understood (Gaus et al. 2007; Michael et al. 2009). Other shortcomings include the lack of data on the effects of co-injectant impurity gases and neglect of any reactions between the dry $CO_2$ and host minerals (Gaus et al. 2007).

## 1.2 Objectives and Aims

While a significant body of work has built up around CCS over the past 20 years, there are significant knowledge gaps in current understanding of the reactions and mechanisms which will act to safely store and trap carbon dioxide during and after injection. It is vital to understand these processes in order to assure the integrity of storage reservoirs over long periods of time (100s-1000s of years). In cases where laboratory and computer (modelling) based work are applied to “real-life”, large scale industrial projects such as CCS, such assurances are even more important, due to issues surrounding public safety and acceptance. Those implementing CCS projects must demonstrate long term reservoir integrity, not only to their own satisfaction, but to that of government and the public.

While geochemists have been studying the weathering of various carbonate and aluminosilicate minerals for many decades, until recently few studies have investigated the rates and mechanisms of dissolution under elevated (>1 bar) $pCO_2$, as would be appropriate for a storage setting. Additionally, many such experiments are carried out in flow-through reactors, where fluid composition and pH are maintained at “far from equilibrium” conditions. While such experiments provide valuable data on “steady-state” reaction rates at far from equilibrium conditions, their results will not generally provide data on the effect of precipitation reactions, non-stoichiometry or evolution of fluid composition, all of which may be important in many natural systems, including a carbon dioxide storage setting. Results from single mineral experiments are applied to “whole rock” natural systems, sometimes without due consideration to the nature of the experimental set-up and the resulting applicability of the results to the system in question.

The objectives of this work are, therefor:

a. To build up an experimentally consistent geochemical dataset pertinent to reactions between common sandstone minerals, $CO_2$ and brine. This will include $CO_2$ solubility in various systems, reactions and reaction rates.

b. To assess the applicability of laboratory results to CCS. Specific questions include: How do batch experiments on powders compare to experiments on consolidated materials and whole rocks? Can single mineral experiments be used to

predict the behaviour of whole rock reservoirs? Do models adequately predict these behaviours?

c. To assess how laboratory derived results might best be applied to actual reservoirs: how important are transport controls? How large an impact will discrepancies in laboratory derived dissolution rates actually have in predicting reservoir response?

# Chapter 2
# Theoretical Background and Literature Review

## 2.1 Geochemical Reactions During GCS: Theory and Experiment

### 2.1.1 Experimental Background

The design of experimental systems used to study mineral dissolution processes can vary widely, depending on the specific objectives of the work. However, such experiments generally fall into two broad categories:

a. Flow-through experiments, where systems are maintained at a particular distance from equilibrium via a constant flow of fresh fluid over the mineral surface. These experiments may be broadly termed as being at a “constant distance from equilibrium”;
b. Closed (“batch type”) experiments, where fluid is not replaced and hence evolves constantly with time as minerals and/or gas dissolves and equilibrium is allowed to be approached. These experiments may be broadly termed as “approaching equilibrium”.

Data used for modelling GCS and in comparative studies of mineral dissolution can come from a broad range of sources and hence experimental conditions, so it is important that the experimental setup used to gather the data is understood so that it may be correctly applied. The following section will provide a brief overview of common experimental set-ups used in mineral dissolution experiments.

#### 2.1.1.1 Flow-Through Experiments

Flow through experiments , in the context of GCS and mineral dissolution experiments, may be broadly divided into two categories: plug-flow experiments through a whole rock core or packed bed of minerals and mixed flow-through/fluidised bed reactors. In both cases the input fluid composition is generally kept constant, such that effluent from the experiment should reach a steady-state composition, allowing a relatively straight-forward measurement of dissolution rates.

Reactor fluid is preconditioned to meet the specific requirements of the experiment (in the case of studies aimed at GCS this commonly involves equilibrating fluid with $CO_2$) and is then passed through the reactor vessel.

A mixed flow-through reactor, in its simplest form, may consist of a stirred batch vessel with fluid inlet and outlet. The more complex fluidised bed reactor set-up is maintained at a specific turbulence whereby mineral grains are suspended, hence ensuring maximisation of mineral surface to fluid contact. In both cases the advantage of such systems is that they can maintain the fluid at a specific chemical affinity with respect to the mineral or rock in the reactor. Since the fluid is well mixed, all fluid in the reactor may be considered homogenous and diffusion limited dissolution, which may arise in closed systems, can be avoided (Dove & Crerar 1990; Carroll & Knauss 2005). Hence such experiments are very useful for studying systems (reaction rates) at far from equilibrium conditions, without having to worry about precipitation effects which will arise as a system evolves in closed reaction systems.

Plug-flow reactors are commonly used for the study of reactions within rock cores and are similar in design to the mixed-flow reactor in that a preconditioned fluid is passed through a core (or a packed bed of minerals), however unlike in the mixed-flow systems the objective of these experiments is often to allow fluid to evolve along the length of the reactor. Flow rates may be very low and in-situ mixing not generally possible. This gives rise to a more complex “evolving” system than seen in the mixed-flow reactors, but is more representative of a natural system, where precipitation and dissolution effects may be important.

For both mixed-flow and plug-flow set-ups, experiments may be carried out at elevated pressures and temperatures, though such conditions are more

difficult to achieve than in more “traditional” close batch experiments. In the case of experiments focused on GCS, it is necessary to exert at back-pressure, such that fluid in the system is maintained at a relatively constant pressure, preventing degassing of $CO_2$ due to pressure drops (Kaszuba et al. 2013). A description of such a set-up, used in this work, can be found in Section 3.3.

#### 2.1.1.2 Batch Experiments

In contrast to the flow-through experiments described above, batch reactors are closed or semi-closed systems where the system is allowed to evolve toward equilibrium. Fluid and mineral are placed in a sealed reactor, often open only to a gas atmosphere. In the case of the batch experiments presented in this work, the system is open to a constant $CO_2$ pressure. Samples are removed are regular intervals and hence the evolution of the system can be monitored. Although generally much simpler in design than the flow-through experiments described above, closed or semi-closed batch experiments have the advantage of more closely mimicking natural systems in allowing fluid evolution and precipitation reactions, which would not be observable in flow-through experiments (Fu et al. 2009; Lu et al. 2013).

Results from flow-through experiments therefor may be said to represent far-from equilibrium end member (assuming the use of a relatively high flow-rate), where dissolution rates will be at their maximum due to low chemical affinity and high surface area/high energy sites. Results from batch experiments on the other hand will reproduce the variation of rate as a system evolves toward equilibrium and will include complexities such backward reaction and precipitation effects. Flow-through reactors therefor provide the best way of studying forward reactions at far from equilibrium conditions, but are obviously not designed to mimic natural systems, which may be better studied through use of closed batch reactors.

The ability of batch reactor experiments to record precipitation effects may also be seen as a disadvantage, since such effects will necessarily have an impact on observed dissolution rates, making careful assessment of fluid chemistry vital in such systems in order that these effects may be accounted for (Kaszuba et al. 2013). Additionally, since the fluid:rock ratio is constantly evolving throughout the experiment as fluid samples are removed, corrections must be made to chemistry data collected from such systems to account for their changing volume, before accurate calculations of dissolution rates may be carried out (see section 3.4.1).

#### 2.1.1.3 Surface Area

A topic which has been (and continues to be) the subject of considerable debate with regards to mineral dissolution experiments is that of mineral surface area. Since reactions rates are generally normalised to available surface area, the method used to estimate surface area and the effect of changing surface area during an experiment, can have significant impact on the results of dissolution studies. The approach taken to accounting for surface area in an experiment can vary the final calculated dissolution rate by several orders of magnitude and it has been proposed that miscalculation of available surface area may account for a large part of the discrepancy between observed weathering rates in the field and those measured in the laboratory (White & Brantley 2003).

Surface areas used in dissolution studies are generally based either on "Brunauer-Emmett-Teller" (BET) measurements or on a geometric estimate. BET measurements are essentially a measure of the volume of gas (generally nitrogen, krypton or argon) which may be adsorbed onto material. As such it may be expected that such measurements should provide an accurate measurement of the actual reactive surface area of a given sample, however it is debateable whether or not the surface area that a gas "sees" is necessarily the same surface area that a fluid would contact: gas molecules are small and will permeate a sample more readily than a fluid and the effects of surface tension and capillary pressures are obviously lessened compared to those experienced by a viscous fluid. Hence in a closely packed mineral sample, many surfaces and pore-throats which may permit entry for a gas are not necessarily going to be accessible by a fluid, so that BET measurements may be considered to represent an upper limit of surface area. Additionally, BET surface areas are dependent on the size of the molecule used and so may vary from method to method (M.E. Hodson 2006).

Geometric estimates of surface area, on the other hand, can vary from a relatively simple geometry (packed spheres for example) for mineral grains to more complex relations involving surface roughness or grain size distribution (Hodson et al. 1998). At their most simplistic level geometric areas may represent a minimum surface area available for reaction. Additional terms may be introduced to account to factors such as surface roughness, which will raise the estimated surface areas toward the theoretical maximum represented by BET measurements. Geometric

measurements may also be refined through careful analysis of grain images under the microscope, which will provide a more accurate shape factor and assessment of factors such as surface roughness and stepping (Velbel & Losiak 2008).

The issues inherent in assessing actual reactive surface area are obviously compounded when moving from relatively simple systems of packed grains to natural systems, where variation in grain-size, porosity, permeability and degree of weathering are much larger. Here the theoretical maximum of BET measurements is evidently not appropriate: the movement of fluids and contact with minerals in these systems is hugely complex and surface area is never likely to reach the theoretical maximum. While BET measurements may be appropriate for well mixed systems in the laboratory, where grains surfaces are relatively fresh and clean (in fluidised bed reactors for example), it may well be the case that in the majority of batch and plug-flow reactors and in natural systems, simplified geometric area estimates may provide more realistic estimates of area available for reaction.

The importance of surface area becomes even more apparent if one considers changes in surface area during a dissolution experiment. During dissolution sample surface area will generally increase, as etch pits and steps are developed on mineral surfaces and this will lead to an overestimation in dissolution rate if sample surface area is assumed to be constant and is only measured prior to reaction. Surface area has been seen to increase 5-7 times over the course of mineral dissolution experiments (Stillings & Brantley 1995; Gautier et al. 2001) which, if left unaccounted for, would lead to a proportional increase in calculated dissolution rate. The majority of published data on mineral dissolution does not account for this effect, implying an overestimate of the majority of published dissolution rates.

While there is, presumably, a “correct” value for the surface area available for reaction of any given sample, it would be very difficult, if not impossible, to measure accurately and this value in any-case will vary constantly as reactions progress. Hence it is perhaps more important that workers seek constancy in their approach to surface area measurements and that when using multiple sets of data in comparative or modelling work, the original approach to surface area is checked and, where appropriate, modified to ensure consistency.

### 2.1.2 $CO_2$ Solubility and pH

The solubility of carbon dioxide under reservoir conditions is obviously of great importance, not only will $CO_2$ solubility influence the overall storage capacity of a reservoir, but where free-phase $CO_2$ is dissolving into the reservoir brine it will have a major effect on local pH.

Gaseous or supercritical $CO_2$ will initially dissolve to form an aqueous $CO_2$ phase following the reactions detailed in Section 1.1.3, which are reprinted here for reference:

$$CO_{2(g)} + H_2O \Leftrightarrow CO_{2(aq)} + H_2O \quad (2.1.1)$$

$$CO_{2(aq)} + H_2O \Leftrightarrow H_2CO_3^{\circ} \quad (2.1.2)$$

$$H_2CO_3^{\circ} \Leftrightarrow HCO_3^- + H^+ \quad (2.1.3)$$

$$HCO_3^- \Leftrightarrow CO_3^{2-} + 2H^+ \quad (2.1.4)$$

The initial hydration of aqueous $CO_2$ (Reaction 2.1.2) is relatively slow, while the dissociation of carbonic acid (Reaction 2.1.3) is very rapid (Dreybrodt et al. 1996). Indeed the rate constant for the backward reaction of carbonic acid to $CO_{2(aq)}$ and water is much higher than the forward reaction and the vast majority (>99%) of dissolved $CO_2$ exists as dissolved gas rather than carbonic acid (Van Eldik & Palmer 1982), hence the convention of using $H_2CO_3^{\circ}$ to indicate the sum of carbonic acid and aqueous $CO_2$ rather than one or the other.

In mineral free systems the direction and extent of the reactions outlined above will be dictated by the pressure, temperature and salinity of the system.

Where minerals are present, any reaction that consumes $H^+$ or bicarbonate (for example ion exchange with mineral surfaces, or the formation of metal carbonates with ions liberated from the mineral surface), will drive further dissolution of $CO_2$ into the formation brine.

Generally, the dissolution of $CO_2$ into formation water will be very rapid, at least in well mixed systems (Rochelle et al. 2004). Certainly the reactions involved are considerably faster than the rate of most mineral dissolution reactions, hence the assumption of equilibrium between $CO_2$ and formation fluid in many modelling calculations and considered over the time scales of GCS, or even most mineral dissolution experiments, this approach is probably valid for most situations.

Despite the relative rapidity of these reactions, it has been proposed that due to the rapid dissolution kinetics of some carbonate minerals (particularly calcite), in systems where these minerals dominate, dissolution of $CO_2$ may become rate limiting, even in well mixed environments (Dreybrodt et al. 1996). However, in general, it may be expected that physical supply of fresh, unsaturated brine will be the rate limiting factor in dissolution of free-phase $CO_2$.

The dissociation of weak carbonic acid (Equation 2.1.3) will release $H^+$ into solution and hence lower pH. In mineral free systems, equilibrium pH may be as low as pH 3 depending on the pressure and temperature conditions. Where minerals are present, rapid response to the drop in pH is likely to come initially from carbonate minerals, by for example dissolution of calcite:

$$CaCO_3 + H^+ \leftrightarrow Ca^{2+} + HCO_3^- \quad (2.1.5)$$

Which will consume hydrogen ions producing $Ca^{2+}$ and bicarbonate ions. While pH will also be likely low enough to attack silicate minerals, these reactions will generally be slower than those involving carbonates but silicate dissolution will still be an important process in providing metal ions to solution, which may, in the long term, allow precipitation of carbonate minerals. For example, feldspars, a common reservoir mineral, may break down to kaolinite, releasing $Ca^{2+}$ and which may be used in calcite precipitation:

$$CaAl_2Si_2O_8 + CO_{2(aq)} + 2H_2O \Rightarrow CaCO_3 + Al_2Si_2O_5(OH)_4 \quad (2.1.6)$$

Another commonly cited example is the breakdown of feldspar in the formation of dawsonite:

$$NaAlSi_3O_8 + CO_2 + H_2O \leftrightarrow NaAlCO_3(OH)_2 + 3SiO_2 \quad (2.1.7)$$

Although it should be noted that dawsonite is rarely identified in experimental work and often only appears in trace amounts in naturally $CO_2$ rich reservoirs (Wilkinson et al. 2009). Ion exchange, where hydrogen ions substitute for metal ions on mineral surfaces may also be an relatively rapid and important buffer of pH following $CO_2$ injection.

Due to increasing interest in $CO_2$ sequestration, a number of standalone models have been developed in recent years to predict $CO_2$ solubility over a wide range of pressure and temperature conditions. Recently produced models include those produced by Akinfiev & Diamond (2010)

and Duan et al. (2006) both of which were created to provide accurate predictions of solubility in brines based on available experimental data. Results from both of these models will be compared to results from the general geochemical modelling code PHREEQC3 and new experimental data in later sections (Chapters 4 & 5).

### 2.1.3 Silicate Dissolution

The following sections will present some brief background on the dissolution of selected silicate minerals at relatively low pH: with emphasis on the typical pH expected in a $CO_2$ saturated fluid. The selected minerals are quartz and feldspars (with particular focus on K-feldspar and albite), given that these are the dominant silicates present in the Sherwood Sandstone, the material focused on in this study (see Section 3.1.6).

#### 2.1.3.1 Quartz Dissolution

Quartz dissolution has been the subject of numerous studies over the last few decades, particularly in the area of hydrothermal energy systems, due to their relatively high reactivity in neutral-basic environments (Tester et al. 1994). While quartz has a relatively low reactivity in most other systems (compared to feldspars or carbonate minerals), it's inclusion in studies of geological sequestration of $CO_2$ is important, given that it will make up a large proportion the bulk matrix of any sandstone reservoir; nevertheless the slow dissolution rate of quartz at conditions relevant to GCS likely means that aqueous silica concentrations in solution will be, in large part, dictated by other silicate minerals.

Congruent hydrolysis of quartz to form silicic acid can be described by:

$$SiO_2 + 2H_2O_{(aq)} \Leftrightarrow H_4SiO_{4(aq)} \quad (2.1.8)$$

Or, alternatively:

$$SiO_2 + 2H_2O_{(aq)} \Leftrightarrow Si(OH)_{4(aq)} \quad (2.1.9)$$

Tester et al. (1994) suggested a general rate equation for quartz dissolution of the form:

$$r_{net} = \frac{dm_{H_4SiO_4}}{dt} = k_f \frac{A_s}{M_w}\left(1 - \frac{m_{H_4SiO_4}}{m^{sat}_{H_4SiO_4}}\right) \quad (2.1.10)$$

Where $A_s$ is the surface area ($m^2$), $M_w$ the mass of water (kg) in the system and $k_f$ the forward rate constant. Within transition state theory the forward rate constant will be dependent on the concentrations of the species ≡Si-O-Si≡ at the mineral surface (Tester et al. 1994). This surface bound species will form an activated complex when attacked by, for example, a hydroxide ion, which will in turn decompose, forming $H_4SiO_{4(aq)}$ (Dove, 1999).

Tester et al (1994) carried out dissolution experiments on quartz under a variety of different experimental conditions: using unagitated batch bottles, a flow-through packed bed reactor, a stirred autoclave, a rocking autoclave and a spinning basket. They found that at low temperatures a great deal of time was required to reach “steady-state” dissolution conditions: 400 days at 25°C, 70 days at 50°C. Correlating their results with other studies, they found good agreement between rate constants, derived both from BET and geometric surface areas, except at low (25°C) temperatures, where they assumed that steady state conditions took longer to reach for experiments where surface treatment was inadequate.

Contrary to the behaviour of various other silicate minerals, it has been observed that increasing concentrations of electrolytes in solution tend to increase the dissolution rate of quartz and to affect its solubility (Dove & Crerar 1990; Newton & Manning 2000; Shmulovich et al. 2006). Dove & Crerar (1990) investigated this effect, finding that NaCl had the largest effect of the salts used in the study, increasing the dissolution rate by 1.5 orders of magnitude over a 0.05M to 0.15M range in concentration. They hypothesised that the increase in dissolution rate observed may have been due to an increase in quartz solubility (hence an increase in chemical affinity) or by effects of cations in solution on the mineral surface itself; i.e. the rate is enhanced by adsorption of, for example, $Na^+$ (Brady & Walther 1990; Dove & Crerar 1990), by modifying the electrostatic characteristics of the dissolving fluid (Dove, 1999).

In terms of pH, changes in pH have found to have a major effect on quartz dissolution rates (Worley 1994; Brady & Walther 1990). For example, Brady & Walther (1990) found that increasing the pH from 4 to 11increased the observed quartz dissolution rate by over an order of magnitude at 25°C. Hence, at the relatively low pH that may be expected in many GCS settings, we may expect quartz dissolution rates to be depressed relative to studies conducted at neutral to basic pH. It is assumed that this depression in reaction rate due to lowering of pH is the main effect of introducing $CO_2$, since studies of quartz dissolution under $pCO_2$ have generally only been conducted at elevated pressures and temperatures (Newton & Manning 2000; Shmulovich et al. 2006), more appropriate to to deep crustal conditions.

### 2.1.3.2 Feldspar Dissolution

Feldspars have been a major focus of geochemical study for many decades, being the single most abundant mineral group on the earth (Oelkers & Schott 1995). Due to their importance in weathering cycles, studies of feldspar dissolution under low $pCO_2$ (<1 bar) have been fairly common. Only recently however, have studies been undertaken observing feldspar dissolution under the elevated $pCO_2$ and temperature conditions applicable to GCS. Additionally, as for many other minerals, the majority of feldspar dissolution studies involve flow-through systems, i.e. measurements of apparent steady state dissolution maintained at constant distance from equilibrium conditions, where precipitation reactions are not allowed to proceed (Lu et al. 2013). Moreover the majority of dissolution experiments conducted on feldspars have been for simple, single phase feldspars rather than the complex, mixed phase feldspars more commonly found in nature (Plunder et al. 2012, Fu et al. 2009). While this has enabled workers to better understand the mechanisms of and controls on feldspar dissolution it represents a significant knowledge gap when it comes to the modelling and explanation of behaviours of natural systems.

The following section will detail some of the commonly expected reactions and behaviours exhibited by feldspars in aqueous systems

Albite hydrolysis consumes $H^+$ and releases $SiO_2$ and $Na^+$, forming kaolinite:

$$NaAlSi_3O_8 + H^+ + 0.5H_2O = 0.5Al_2Si_2O_5(OH)_4 + Na^+ + 2SiO_2(aq) \quad (2.1.11)$$

Under acidic conditions, boehmite may be an early secondary precipitate:

$$NaAlSi_3O_8 + H^+ = AlO(OH) + Na^+ + 3SiO_2(aq) \quad (2.1.12)$$

Which in turn may be converted to kaolinite, through consumption of aqueous silica:

$$AlO(OH) + 0.5H_2O + SiO_2(aq) = 0.5Al_2Si_2O_5(OH)_4 \quad (2.1.13)$$

Though this conversion can be sluggish, even at elevated pressures and temperatures (Fu et al. 2009). Under more neutral conditions illite may also be a reaction product (Lu et al. 2013).

The dissolution of K-feldspar consumes $H^+$ and releases $K^+$ and silica into solution, forming muscovite and may be described by:

$$3KAlSi_3O_8 + 2H^+ = KAl_3O_{10}(OH)_2 + 2K^+ + 6SiO_2(aq) \quad (2.1.14)$$

Again, at low pH boehmite may be an early secondary precipitate (Fu et al. 2009):

$$KAlSi_3O_8 + H^+ = AlO(OH) + K^+ + 3SiO_2(aq) \quad (2.1.15)$$

Under acidic conditions, dissolution of anorthite consumes $H^+$ and releases $Ca^{2+}$, $Al^{3+}$ and silica:

$$CaAl_2Si_2O_8 + 8H^+ = Ca^{2+} + 2Al^{3+} + 2SiO_2(aq) + 4H_2O \quad (2.1.16)$$

Where concentrations of $K^+$ are relatively high (for example in systems where albite and K-feldspar are both present) conversion of albite to K-feldspar may occur (Fu et al. 2009), such that:

$$NaAlSi_3O_8 + K^+ = KAlSi_3O_8 + Na^+ \quad (2.1.17)$$

Helgeson et al. (1984) published a review and analysis of available data on feldspar hydrolysis. At the time three main hypotheses were prevalent to explain results from feldspar hydrolysis experiments: diffusion through an armour of surface precipitate, limiting dissolution or dissolution rate limited by reactions at the mineral/solution boundary or limiting of dissolution by diffusion through a non-stoichiometric layer leached on the feldspar surface. At the time, Helgeson et al. proposed that only the surface reaction hypothesis was consistent with detailed inspection of the feldspar surface.

The initial step in feldspar dissolution involves the reversible exchange of $H_3O^+/H^+$ with $K^+$, $Na^+$ and/or $Ca^{2+}$ on the feldspar surface. This process may significantly affect early solution compositions and will create an activated complex on the feldspar surface, the decomposition of which will limit overall feldspar hydrolysis as long as reaction at this surface is faster than diffusional transport from unaltered feldspar surfaces to the liquid-mineral interface (Helgeson et al. 1984; Busenberg & Clemency 1976).

Incongruent feldspar dissolution has been noted in numerous experimental studies and is usually attributed to either precipitation of secondary minerals (in closed system batch experiments) and/or preferential leaching of components from the feldspar surface (both batch and steady state, flow-through reactors) (Helgeson et al., 1984; Fu et al., 2009; Alekseyev, Medvedeva, Prisyagina, Meshalkin, & Balabin, 1997) .

Several studies have noted that the logarithm of alkali-feldspar steady state dissolution rates varies linearly with the logarithm of aqueous Al concentration and this has been interpreted as the result of rate control by an

Al depleted, silica rich surface complex formed by exchange between $H^+$ and $Al^{+3}$. (Oelkers & Schott 1995).

It has been widely noted that feldspar dissolution tends to progress at selective sites on the feldspar surface, the progress of which eventually leads to etch pits (Helgeson et al. 1984). Where albite and K-feldspar are both present, it has also been noted that albite dissolves preferentially (Fu et al. 2009). However, more recent work (Brantley & Stillings 1996) suggests that complex feldspars dissolve stoichiometrically after long (>2000 hours) periods of dissolution.

Exchange of $Na^+$, $Ca^{2+}$ or $K^+$ from the feldspar surface for ions (for example $H^+$ in acidic conditions) already in solution is a common early reaction in feldspar experiments. These reactions create leached layers on the feldspar surface and also have the effect of increasing the number of Al-O-Si and Si-O-Si bonds, which are in turn susceptible to hydrolysis (Alekseyev et al. 1997). Gautier et al. (1994) proposed that alkali feldspar hydrolysis consists of rapid exchange of $H^+$ with surface alkali (or in the case of anorthite, $Ca^{2+}$) ions, followed by an exchange reaction between three $H^+$ and one $Al^{3+}$ in the mineral structure, resulting in the breaking of Al-O bonds and the formation of silica rich surface complexes. The final stage of dissolution in this model is the breaking of Si-O bonds by hydrolysis, releasing the Si rich complex. Within this model rates of alkali feldspar dissolution are proportional to $H^+$ activity and the concentration of the Si rich surface complex and hence $Al^{3+}$ activity in solution. In contrast the dissolution rate of anorthite rich feldspars (>An70) will be largely independent of $Al^{3+}$ since in the case of anorthite, which has an Al/Si ratio of one, the $Al^{3+}/3H^+$ exchange step leads to complete detachment of the Si tetrahedra. Hence the final step of alkali feldspar dissolution – the breaking of the Si-O bonds, is not required for anorthite hydrolysis.

Feldspar dissolution rates tend to be relatively slow even at high temperatures, but the acidification of brine during sequestration and their relative abundance in potential sandstone reservoirs means that their reactivity will be of importance during geological sequestration of $CO_2$ (Fu et al. 2009).

Experiments conducted in NaCl bearing solutions indicate that, unlike quartz where dissolution rates are enhanced, feldspar dissolution is inhibited by the presence of $Na^+$, likely due to competition for surface sites between $H^+$ and $Na^+$ (Stillings & Brantley 1995). The presence of $CO_2$ on the other hand has

been found to enhance feldspar dissolution (Berg & Banwart 2000). Whether $CO_2$ has a direct effect on dissolution through formation of carbonate complexes on the mineral surface is a matter of debate, but it is generally assumed that the major effect comes from indirect acidification of the reacting fluid (Lu et al. 2013).

While for dolomite it was found that the majority of experiments looking at dissolution were conducted in steady-state flow through apparatus (see Section 2.1.4), where conditions were maintained at far from equilibrium, in the case of feldspar, perhaps because of the relative amount of work that has gone into their study, there are a large number of closed system batch experiments, similar to the sort presented here (e.g. Fu et al., 2009; Lagache, 1976). However, finding experimental results at conditions close to the ones used in this study has proved more problematic: $CO_2$ pressures involved are generally much lower or much higher than the ones used in this work. Similarly many of the experiments presented in the literature have been undertaken at relatively high temperatures (>100°C), partially because of the generally sluggish nature of feldspar dissolution. Similarly experiments have generally been conducted in low (<0.1M NaCl) salinity brines or deionised water, making direct comparisons between the results from this work and others difficult.

### 2.1.4 Carbonate Dissolution

#### 2.1.4.1 Calcite Dissolution

The dissolution of calcite in the system $H_2O$-$CO_2$-$CaCO_3$ is an important process in many natural systems, such as the dissolution of limestone in karst formation, (Svensson & Dreybrodt 1992) and as such has received a good deal of attention over the years.

Early work on calcite dissolution suggested that it is controlled by three parallel reactions (Plummer, Wigley, Parkhurst, & Wigley, 1978):

$$CaCO_3 + H^+ \Leftrightarrow Ca^{2+} + HCO_3^- \quad (2.1.18)$$

$$CaCO_3 + H_2CO_3^\circ \Leftrightarrow Ca^{2+} + 2HCO_3^- \quad (2.1.19)$$

$$CaCO_3 + H_2O \Leftrightarrow Ca^{2+} + HCO_3^- + OH^- \quad (2.1.20)$$

Where the final reaction may also be expressed as:

$$CaCO_3 \Leftrightarrow Ca^{2+} + CO_3^- \quad (2.1.21)$$

It has long been recognised that at low pH (<4) transport has a strong control on calcite dissolution and at higher pH (>4) dissolution is primarily controlled by surface reactions (L. Plummer et al. 1978). Early experiments also recognised that due to the relatively fast dissolution rate of calcite (compared to many silicate minerals for example), dissolution of calcite could outstrip the hydration and transport of gaseous $CO_2$, such that pH is lower than expected for a given constant $pCO_2$ and will rise more quickly. These effects should however be negligible at $pCO_2$>0.05 bar (Zaihua & Dreybodt 2001).

Plummer et al. (1978) carried out a series of free drift and stat experiments at a variety of $pCO_2$ and pH. Their interpretation of the results indicated that dissolution could be divided into three regions: a linear log-rate vs. pH region, where the dissolution rate was directly proportional to hydrogen ion activity, a region of decreasing pH dependence and a region of rapid reduction in rate with increasing pH, where the backward reaction becomes more important. The boundaries between these regions were observed to change with $pCO_2$ (shifting to higher pH as $pCO_2$ decreased). At a $pCO_2$ of around 1bar the middle region was found to extend from approximately pH 3.5 to pH 5.5, covering the pH observed in the experiments presented here.

Dissolution rate was also found to proportional to stirring rate, with a stronger correlation at low pH. At pH>5, stirring rate was found to have little effect.

In regions one and two, dissolution was found to be described by an equation of the form:

$$R = k_1 a_{H^+} + k_2 a_{H_2CO_3^*} + k_3 \quad (2.1.22)$$

In region one, the two terms on the right hand side of this equation are small, while in region two all of the terms are significant. In region three (high pH), the rate was found to be described by:

$$R = k_1 a_{H^+} + k_2 a_{H_2CO_3^*} + k_3 aH_2O - k_4 a_{Ca^{2+}} a_{HCO_3^-} \quad (2.1.23)$$

Experimentally derived values and temperature dependence of $k_1$, $k_2$, $k_3$ and $k_4$ are given in Plummer et al. (1978).

They found the rate at constant $pCO_2$ and temperature is described by

$$R = k_1 a_{H^+} + k_2 a_{H_2CO_3^*} + k_3 aH_2O - k_4 a_{Ca^{2+}} a_{HCO_3^-} \quad (2.1.24)$$

The forward rate is dependent on hydrogen ion transport and heterogeneous reactions, while the backward rate constant ($k_4$) is a function of $pCO_2$ and temperature. The forward rate mechanisms suggest the three controlling reactions shown above.

They explain the reaction mechanism in terms of the “adsorption layer heterogeneous reaction model”, whereby an adsorption layer is assumed between the solid surface and the hydrodynamic boundary layer, where species are loosely bound. It is assumed that reaction 2.1.18 is relatively fast, while 2.1.19 and 2.1.20 are relatively slow, which explains the dissolution rate dependence on $H^+$ transport at low pH. If 2.1.19 and 2.1.20 are sufficiently slow then the supply of $H_2CO_3$* and $H_2O$ across the boundary layer should ensure that activities across this region are equal for these species, while $a_{H+}$ will not be equal between the boundary layer and the solid surface.

The total forward rate at any pH, $pCO_2$ and $aH_2O$ is given by:

$$Rf = k_1 a_{H^+} + k_2 K_H P_{CO_2} + k_3 aH_2O \quad (2.1.25)$$

Where $K_H$ is the Henry’s law constant for $CO_2$ and k1 etc. given by….

$$logk_1 = 0.198 - \frac{444}{T} \quad (2.1.26)$$

$$logk_2 = 2.84 - \frac{2177}{T} \quad (2.1.27)$$

$$logk_3 = -5.86 - \frac{317}{T}\ (5°C - 25°C) \quad (2.1.28)$$

$$logk_3 = -1.10 - \frac{1737}{T}\ (25°C - 48°C) \quad (2.1.29)$$

Hydrogen ion attack is the dominant forward reaction at low pH and at higher pH the forward rate becomes increasingly independent of pH as carbonic acid attack and hydration become more important.

In 1989 Chou et al. published a comparative study on the kinetics and dissolution of various carbonate minerals, including calcite. They noted that carbonate minerals had been extensively studied and their dissolution rates generally expressed as a function of the degree of mineral under-saturation raised to a fractional power, but that at low pH rates were noted to be a function of the transport mechanisms between bulk solution and the mineral surface (see above). They carried out a series of experiments using fluidised reactor beds (flow-through) in order to minimise any transport effects. Even with this experimental set-up they found that transport effects had an influence on dissolution at very low (<4) pH. Their findings for calcite agreed with the work of Plummer: that the dissolution rate is proportional to $aH^+$ at low pH and constant in the neutral range, while at high pH the rate decreases as the backward reaction becomes more dominant (>pH8). They found that at pH > 8, the rate of precipitation (the backward reaction) increased almost linearly with pH. However they found that the backward rate fitting to their results was best described by:

$$R = k_b a_{Ca^{2+}} a_{CO_3^{2-}} \quad (2.1.30)$$

Such that the equation for the net dissolution rate becomes:

$$R = k_1 a_{H^+} k_2 a_{H_2CO_3^*} + k_3 a_{H_2O} - k_b a_{Ca^{2+}} a_{CO_3^{2-}} \quad (2.1.31)$$

They also noted the discrepancy between values for $k_1$ calculated from fluidised reactor bed experiments and single crystal experiments: the value of $k_1$ from Plummer et al. (1982) is considerably lower than that achieved in the reactor bed experiments of Chou et al. (1989). They attributed this discrepancy to a mixed control, where transport and surface reactions are both rate limiting in experiments where dissolution rates are high and stirring is low (the single crystal experiment).

Although calcite is not a major constituent of the Sherwood Sandstone material used in this study, it is often considered an important mineral in

studies of geological sequestration of $CO_2$. Because of its relatively high reactivity, calcite, where present, may act to rapidly buffer the pH of acidified pore-waters following dissolution of free-phase $CO_2$. Likewise, rapid dissolution of calcite cement may dramatically increase porosity near injection wells, while, conversely, where $Ca^{2+}$ rich pore waters are transported away from free-phase $CO_2$ calcite may well reprecipitate as pH is buffered, causing an overall reduction in porosity. For these reasons, several experiments were carried out on calcite, along with the Sherwood Sandstone related materials, the results of which are described in Chapter 5.

#### 2.1.4.2 Dolomite Dissolution

Dolomite is a common mineral in many sandstone reservoirs around the world and is a constituent of the Sherwood Sandstone Group in the UK, occurring as pore-filling cements, generally comprising <5% of the bulk rock (Burley 1984). Pure, stoichiometric dolomite has the formula $CaMg(CO_3)_2$ though some Fe or Mn replacement of Mg within dolomites is not uncommon.

The overall dissolution of dolomite in a solution under $pCO_2$ may be expressed as:

$$CaMg(CO_3)_2 + 2CO_2 + 2H_2O \Leftrightarrow Ca^{2+} + Mg^{2+} + 4HCO_3^- \quad (2.1.32)$$

While the thermodynamics and kinetics of calcite dissolution have been closely studied over the previous few decades, dolomite dissolution, in contrast, has received relatively little attention until more recently. Thermodynamic data for dolomite can be difficult to derive experimentally relative to calcite, due to dolomites relatively slow dissolution rate, its two component nature ($MgCO_3$ and $CaCO_3$) and complexities in the effects of composition and ordering (Morse & Arvidson 2002; Sherman & Barak 2000). Additionally, relatively few studies of dolomite dissolution kinetics have been made, particularly at elevated $pCO_2$, temperature and salinity (Pokrovsky et al. 2005).

Experimentally derived values for the solubility product of dolomite:

$$pK = -\log(Ca^{2+})\,(Mg^{2+})(CO_3^{2-})^2 \quad (2.1.33)$$

cover a large range, perhaps reflecting the problems associated with inconsistent ordering and composition between dolomite samples. Solubility products quoted in the literature range from log(-16) to log(-19) (Sherman & Barak 2000), though a generally accepted value and the one used in the PHREEQC.dat database is log(17.09), as derived by Hemingway & Robie (1994) by calorimetry. Further work has confirmed that this value reflects the solubility of many dolomites (Sherman & Barak 2000). However, due to the range in apparent solubility and the relatively slow nature of dolomite dissolution, it has been pointed out that “extreme caution” should be exercised in regards to referencing dolomite “saturation” during experiments (Busenberg & Plummer 1982).

As mentioned above, until recently there were relatively few studies of dolomite dissolution kinetics. One of the most influential and comprehensive studies of dolomite dissolution rates was that of Busenberg & Plummer (1982). They aimed to measure dissolution rates at “far from equilibrium”, using a spinning disc set-up, before varying the solution composition in the direction of equilibrium, not only to derive rate equations but also to confirm the solubility product of dolomite. They found that none of their experiments closely approached equilibrium, as marked by the $pK_{dolomite}$ of Hemingway and Robie, but they did derive an equation to model and explain the mechanics behind dolomite dissolution at far from equilibrium conditions:

$$R = k_1 a_{H^+}^n + k_2 a_{H_2CO_3^*}^p + k_3 a_{H_2O}^p - k_4 a_{HCO_3^-} \qquad (2.1.34)$$

Where $k_1$, $k_2$ and $k_3$ are forward rate constants and $k_4$ is a backward rate constant. They found that the exponents n and p were 0.5 for temperatures below 45$^o$C, but that the exponent n, of the hydrogen ion dependence increased at higher temperatures. They proposed that the following four parallel reactions could account for the net dissolution of dolomite:

$$CaMg(CO_3)_2 + 2H^+ \rightarrow Ca^{2+} + Mg^{2+} + 2HCO_3^- \qquad (2.1.35)$$

$$CaMg(CO_3)_2 + 2H_2CO_3^* \rightarrow Ca^{2+} + Mg^{2+} + 4HCO_3^- \qquad (2.1.36)$$

$$CaMg(CO_3)_2 + 2H_2O \rightarrow Ca^{2+} + Mg^{2+} + 2HCO_3^- + 2OH^- \qquad (2.1.37)$$

$$Ca^{2+} + Mg^{2+} + 2HCO_3^- \rightarrow CaCO_{3(s)} + MgCO_{3(s)} + 2H^+ \qquad (2.1.38)$$

Reaction 2.1.35 is associated with $k_1$ in equation 2.1.34, reaction 2.1.36 with $k_2$, reaction 2.1.37 with $k_3$ and reaction 2.1.38 (the backward reaction) with $k_4$. The authors point out that reaction 7 does not account for all the possible backward reaction mechanisms.

During their experiments, Busenberg and Plummer found that if untreated samples were used the dolomite surface became enriched in $MgCO_3$ at early times suggesting faster dissolution of the $CaCO_3$ component, hence equations 2.1.35 – 2.1.38 can be rewritten as consecutive parallel reactions, where the denominators *s*, *bk* and *a* indicate solid phase, activity in the bulk solution and charged surface sites respectively :

$$CaMg(CO_3)_{2(s)} + H_{(bk)}^+ \rightarrow MgCO_{3(s)} + Ca_{(a)}^{2+} + HCO_{3(a)}^- \qquad (2.1.39\_1)$$

$$MgCO_{3(s)} + H_{(bk)}^+ \rightarrow Mg_{(a)}^{2+} + HCO_{3(a)}^- \qquad (2.1.39\_2)$$

$$CaMg(CO_3)_{2(s)} + H_2CO^*_{3(bk)} \rightarrow MgCO_{3(s)} + Ca^{2+}_{(a)} + 2HCO^-_{3(a)} \quad (2.1.40\_1)$$

$$MgCO_{3(s)} + H_2CO^*_{3(bk)} \rightarrow Mg^{2+}_{(a)} + 2HCO^-_{3(a)} \quad (2.1.40\_2)$$

$$CaMg(CO_3)_{2(s)} + H_2O_{(bk)} \rightarrow MgCO_{3(s)} + Ca^{2+}_{(a)} + HCO^-_{3(a)} + OH^-_{(a)} \quad (2.1.41\_1)$$

$$MgCO_{3(s)} + H_2O_{(bk)} \rightarrow Mg^{2+}_{(a)} + HCO^-_{3(a)} + OH^-_{(a)} \quad (2.1.41\_2)$$

Where the initial reactions releasing $Ca^{2+}$ into solution are much faster than the following release of $Mg^{2+}$. It was found that as dissolution proceeded, near stoichiometric concentrations of Ca and Mg were eventually obtained.

Hence the Busenberg and Plummer model describes a system where each of the forward reactions has varying control over the system dependent on pH and $pCO_2$. At low pH (<6) and with a $pCO_2$ close to zero the dissolution rate is largely dependent on the hydrogen activity (the first term in equation 2.1.34). As $pCO_2$, and hence $H_2CO^*_3$ is increased the second term has more control over dissolution rate. At higher pH and when $pCO_2$ again approaches zero the third (hydration) term becomes important. The difference between the observed dissolution and that predicted by these terms is assumed to be largely dependent on $HCO^-_3$ adsorption onto positively charged sites on the dolomite surface (the final term in equation 2.1.34). The relatively rapid release of $Ca^{2+}$ followed by more sluggish $Mg^{2+}$ release allows reactions 2.1.35 – 2.1.36 to be broken down into three parallel sets of consecutive reactions. This accounts for the reaction order of 0.5 applied to Equation 2.1.34 at temperatures below 45$^o$C (since each consecutive reaction is essentially a “half-reaction”) and may also provide an explanation of the relatively sluggish dissolution of dolomite compared to that of calcite: dissolution is rate limited by the breakdown of the $MgCO_3$ component, while the $CaCO_3$ component is dissolved relatively quickly.

The temperature dependence of the rate constants ($k_1$-$k_4$ in Equation 2.1.34) was found to be described by:

$$logk_i = a\left(\frac{1}{T}\right) + b \quad (2.1.42)$$

Where T is the temperature in $^o$K and a and b are constants dependent on the dolomite composition.

Dissolved Mg and Ca concentrations were found to have little effect on observed rates. Similarly no dependence on stirring rate was found (at

45$^{o}$C), suggesting that dissolution at these conditions is largely surface (as opposed to transport) controlled.

The above “macroscopic” model for dolomite dissolution remains largely intact today although increasingly dissolution is being described in terms of more complex surface speciation models (Pokrovsky et al. 2005) which better account for the complex interaction between the dolomite surface and the adjacent diffusion boundary layer. More recent work which has modified or added to the above model is detailed below.

In 1985 Herman and White (Herman & White 1985) published results from a series of spinning disc experiments, designed to inspect the effect of fluid dynamics on dolomite dissolution. They found that there was some dependence of dissolution rate on spinning rate and hence some transport control. Rate was observed to increase with increased spinning rate. The effect of spinning rate was found to lessen dramatically as saturation increased and with decreasing temperature. Nevertheless, calculated rates and activation energies were similar to those observed by Busenberg and Plummer. They also observed, in agreement with the work of Busenberg and Plummer, that dissolution rate became very small even at relatively high undersaturations (at a saturation index of around -2). Based on the final rates they observed, it was calculated that the system would take at least 1 or 2 years to reach saturation.

In 1989 Chou et al (Chou et al. 1989) published details of a series of experiments looking at the effect of pH and $pCO_2$ on carbonate dissolution, using fluidised reactor beds rather than the spinning disc method. They hypothesised that two situations might arise leading to misrepresentation of dissolution rate in dolomites: at low $pCO_2$ and low pH the bulk solution may become oversaturated with respect to $CO_2$ leading to underestimation of the dissolution rate. Conversely at high $pCO_2$ $CO_2$ dissolution may be rate limiting and the solution could become undersaturated with respect to $CO_2$ leading to a more rapid increase in pH and an overestimation in dissolution rate. They found that there was good agreement between their results and those of Busenberg and Plummer at high pH, but observed that at pH<7 their results indicated faster rates than those predicted by Busenberg and Plummer. They found that the reaction order (exponents n and p in equation 2.1.34) that best fitted their data was 0.75, as opposed to 0.5 as obersved by Busenberg and Plummer at 25$^{o}$C. They argued, contrary to Busenberg and Plummer, that successive reactions (Eqns. 2.1.35 – 2.1.37) would not lead to

a reaction order of <1 and that the reaction order is better explained by uptake of $H^+$ at the dolomite surface and hence dependent on surface protonation and electrostatic interference of the surface. The authors proposed a revision of the Busenberg and Plummer model: assuming that reaction shown by Equation 2.1.39_1 is rapid and can be considered as being close to equilibrium then:

$$CaMg(CO_3)_2 + H^+ \Leftrightarrow MgCO_3 + Ca^{2+} + HCO_3^- \qquad (2.1.43)$$

With

$$K = \frac{a_{Ca^{2+}}\, a_{HCO_3^-}\, x_{MgCO_3}}{a_{H^+}} \qquad (2.1.44)$$

Where $x_{MgCO_3}$ is the activity of $MgCO_3$ at the dolomite surface. Assuming ideal behaviour of the surface species the rate is controlled by the reaction shown by Equation 2.1.41 and

$$R_f = k a_{H^+} x_{MgCO_3} \qquad (2.1.45)$$

The activity of $MgCO_3$ is fixed by:

$$x_{MgCO_3} = \frac{K a_{H^+}}{a_{Ca^{2+}}} a_{HCO_3^-} \qquad (2.1.46)$$

And the forward rate is given by:

$$R_f = k a_{H^+}{}^2 / a_{Ca^{2+}}\, a_{HCO_3^-} \qquad (2.1.47)$$

Sherman & Barak (2000) published the results from a series of experiments studying dolomite dissolution using powdered samples in batch experiments, mixed by orbital shaker, in an effort to refine the solubility product of dolomite and to test the revised dissolution model proposed by Chou et al (equation 16). They found that congruent dissolution of dolomite occurred in solutions with initial $pIAP_{dolomite}$>17 and that this dissolution fitted the revised model proposed by Chou et al well. Analysis of the equilibrium data suggested a $pK_{dolomite}$ for the samples used of between 17.0 and 17.4, a good agreement with the value of 17.09 proposed by Robie (1994).

Zaihua & Dreybodt (2001) looked at the kinetics and rate limiting mechanisms of dolomite dissolution, using spinning disc experiments at far from equilibrium conditions. They found that their results fitted Busenberg and Plummer's original model well at "high" $pCO_2$ (>0.05bar) but that at low $pCO_2$ the presence of a diffusion boundary layer between the dolomite surface and bulk fluid and the relatively slow conversion of $CO_2$ to

bicarbonate will limit the rate of mineral dissolution (Zaihua & Dreybodt 2001).

Further rotating disc experiments by Martinez & White (1999) and Gautelier et al. (1999) produced rates in agreement with previous studies and further confirmed that dissolution rates in acidic solutions are largely controlled by $H^+$ activity at the mineral surface, rather than Mg, Ca or carbonate concentrations.

Finally Pokrovsky et al have published a number of papers over recent years detailing dolomite surface speciation and dissolution kinetics (Pokrovsky et al. 1999; Pokrovsky et al. 2005; Pokrovsky et al. 2009). Using surface charge measurements at various pH, $pCO_2$ and ionic strength the authors proposed a surface complexation model to describe dolomite dissolution. This model predicts that at pH<4 the protonated species $>CO_3H^o$ dominates speciation of surface carbonate groups and that as pH increases deprotonation of the surface sites occurs and $CO_3^-$ becomes the dominant species. At pH>8 $MeOH_2^+$ surface species are replaced by $MeCO_3^-$. As observed by Busenberg and Plummer at pH<6 dolomite dissolution is enhanced by $H^+$. Since, at pH<8, metal sites are present as fully protonated $MeOH_2^+$ species, this rate enhancement must be caused by protonation of $< CO_3^-$ sites (Gautelier et al. 2007).

Pokrovsky et. al. also carried out various spinning disc and powder experiments to investigate dolomite dissolution kinetics. Like previous authors they found a moderate transport control on dolomite dissolution, reflected in increasing rates as stirring rate was increased. Also like previous authors they observed that final solutions were strongly undersaturated (IAP/K < 0.2) with respect to carbonate solid phases, that Ca and Mg concentrations had little effect on rate and that at low pH (2<pH<5) dissolution exhibited a complex dependence on pH. The effect of NaCl concentrations was found to be weak, with a slight increase in rate from $2.10^{-5}$M to 0.03M and no further changes in rate at NaCl concentrations up to 1M. Increasing $pCO_2$ was also found to increase dissolution rate as $pCO_2$ was raised from 0 atm to 10 atm, but was found to have no further effect for pressures up to 50atm. The results were modelled assuming that at low pH (i.e. under elevated $pCO_2$) dissolution was proportional to $aH^+$ according to the surface speciation model described above and this approach provided good agreement with experimental results. These studies serve to highlight

the importance of pH in controlling dissolution rate, over other factors such as $pCO_2$ or salinity.

## 2.2 Density Driven Flow in CCS

Dissolution of free-phase $CO_2$ into reservoir brines will results in an increase in density of the formation fluid. This increase is relatively minor (up to 2-3%), but can have a significant effect on the fluid dynamics of the system . The layering of denser, saturated fluid above unsaturated brines will create an instability which can lead to the onset of density driven convection, whereby the denser, saturated fluid moves down through the aquifer, while fresh unsaturated brine rises to take its place. While such dynamics may be relatively slow in a natural aquifer, this process could have large impacts on $CO_2$ storage schemes as in many situations, particularly in sluggish systems, with low natural groundwater flow, it represents a process which may greatly enhance the volumes of carbon dioxide trapped in solution. Solution trapping offers a more secure storage option than storage as a free-phase plume.

Interest in density driven flow as a process in CCS has increased over previous years, largely for the reasons outlined above and a number of relatively recent studies have been published dealing with the modelling and mathematics of density driven flow and convective instabilities. There remains, however, little experimental data with which to calibrate and check such models. One method that has been used to generate such data utilises the Hele-Shaw Cell (Neufeld & Huppert 2009; Kneafsey & Pruess 2011).

A Hele-Shaw cell simply consists of two parallel surfaces, with a narrow gap between. When the ratio between the gap width (h) and the radial dimension of the cell (r) becomes sufficiently small ($h/r \ll 1$) then flow within the cell becomes mathematically analogous to Darcy-like flow in a porous media, with an intrinsic permeability given by:

$$k = \frac{b^2}{12} \quad (2.2.1)$$

Where k is intrinsic permeability and h is the gap width.

Hence the Hele-Shaw cell is a very useful and versatile tool for visualising two-dimensional flow in porous media. A small number of researchers have worked on visualising the instabilities generated by dissolution of $CO_2$ into unsaturated fluid using this method in recent years.

Notable examples of recent work are published in Neufeld et al. (2010) and Kneafsey & Pruess (2011). Neufeld et al. simulated the dissolution of $CO_2$ into brine using a mixture of methanol and ethylene-glycol (MEG), which

alone is less dense than water, but mixes with water to create a denser solution. Hence a layer of MEG was added above water and the two allowed to mix to create an approximation of $CO_2$ saturated brine. Their results suggested the following conceptual model: a diffuse boundary layer at the fluid:$CO_2$ interface where instabilities due to the density difference lead to creation of $CO_2$ saturated fingers, which move laterally and coalesce before descent. Below the interface, the coalesced plumes descend at a rate dependent on the density contrast between the $CO_2$ rich downwelling material and the fresher upwelling material. Diffusion between the downwelling and upwelling material will act to lower the density contrast. Upon reaching the boundary interface, upwelling material will move laterally, creating the mixing regions where the main plume bodies form. Applying their results to an idealised site, the authors estimated that “convective dissolution” might account for 20 kg $m^{-2}$ $yr^{-1}$ $CO_2$.

The work presented in Kneafsey & Pruess (2010) presents a more realistic simulation of density driven flow, in that it utilises actual $CO_2$ rather than the MEG mixture used by Neufeld et al. They took advantage of the fact that the pH of water will drop from around 5.6 in equilibrium with atmospheric carbon dioxide to around 3.9 in equilibrium with one atmosphere of $CO_2$ and visualised saturation of water by carbon dioxide using a pH indicator. In this case the indicator used was bromocresol green, that changes from blue to yellow as pH moves from 5.4 to 3.8. $CO_2$ was introduced simply through a tube at the top of the cell: since $CO_2$ is denser that air it was supposed that air would be displaced from the gap at the top of the cell, leaving a pure $CO_2$ atmosphere.

They found that small scale fingers formed within the first 12 minutes and these (as in the work presented by Neufeld et al.) rapidly coalesced into larger downwelling plumes. They also found the “cell-wide convection” initiated relatively early. The modelling of their experiments did not recreate the cell wide convection seen in the cells. They also found that the fingers recorded in the experimental system were broader and fewer than those observed with modelling and over time the models produced fewer new fingers than were observed in the experimental work. However they did find that finger lengths were comparable at any given time and that fingers formed on similar time-scales in both modelled and experimental systems. They suggested that thermal convection may have been responsible for the rapid onset of large-scale convection in their experiments, while shear at the fluid surface where $CO_2$ was being introduced and small inconsistencies in

fluid distribution where the plates were not exactly parallel may have been responsible for other differences between models and experimental results. An additional disadvantage of their experimental approach was the generally low quality of the images, which had to undergo considerable processing to enhance the contrast between the low and high pH regions.

Work carried out as part of this thesis has aimed to improve on the experimental designs summarised above. In addition to investigating the behaviour of the plumes created by $CO_2$ dissolution, the experiments carried out in this work have aimed to design an experimental system where relatively small changes in pH (and hence $CO_2$ content) can be monitored easily, with the resultant images requiring relatively little enhancement in order to distinguish between areas of varying pH. This work is presented in detail in Chapter 6 of this thesis.

## 2.3 The Sherwood Sandstone

The focus of this work is on the likely behaviour of “Sherwood Sandstone Type” rock were it to be used to store $CO_2$. To this end several experiments have been carried out on samples from the Sherwood Sandstone itself, as well as using its constituent minerals in single mineral experiments.

The Sherwood Sandstone is a major UK aquifer and while it represents a considerable source of potable groundwater, its extent is such that, in deeper areas and offshore, much of the formation water present is highly saline and unpotable. This, together with its relatively high porosity and permeability make it an ideal target for GCS in the UK and Ireland (British Geological Survey 2006). It is buried at depths suitable for GCS in various locations, including Somerset, Cheshire, Yorkshire and Ulster and is sealed in these locations by the Mercia Mudstone Group.

The Sherwood Sandstone Group itself comprises a series of continental red-beds, comprising largely of quartz, K-feldspar, with some secondary dolomite, clays (typically illite and smectite) and hematite (Burley 1984).

# Chapter 3
# Dissolution Experiments Methodology

## 3.1 Sample Preparation and Description

A number of mineral samples and a peridotite and a sandstone were used in this study to investigate:

a) Carbon dioxide solubility in mineral-fluid systems;
b) Fluid pH in fluid-mineral systems under $pCO_2$;
c) mineral dissolution rates and fluid-mineral reactions under $pCO_2$.

Mineral samples were chosen largely to reflect the composition of the Sherwood Sandstone, while the peridotite, olivine and calcite were included in the study due to their relative reactivity with $CO_2$ saturated fluids.

Sample sources and sample locations are presented in Table 3.1.1.

| Sample | Description | Source | Sampling Location |
|---|---|---|---|
| ***Quartz*** | Milky quartz | http://www.geologysuperstore.com/ | India |
| ***Plagioclase Feldspar*** | | http://www.geologysuperstore.com/ | Euje, Southern Norway |
| ***Dolomite*** | Carboniferous | http://www.geologysuperstore.com/ | Great Orme, North Wales, UK |
| ***Peridotite*** | | http://www.geologysuperstore.com/ | Finland |
| ***Olivine*** | | http://www.geologysuperstore.com/ | Åheim, Central Norway |
| ***Calcite*** | Carboniferous | University of Leeds collection | County Clare, Ireland |
| ***Illite*** | Cambrian | Clay Minerals Society | Silver Hill, Montana, USA |
| ***KFeldspar*** | Pegmatite | - | Norway |
| ***Sandstone*** | Sherwood Sandstone | British Geological Society core store | Cleethorpes, UK |

**Table 3.1.1**: Sample sources and sampling locations

Samples were crushed using a clean mechanical jaw crusher and sieved with steel sieves to obtain 125-180µm and 500-600µm size fractions. Mineral samples were hand-picked to remove obvious impurities. The powdered samples were then washed in acetone in an ultrasonic bath to remove fine

particles. Samples were rinsed in deionised water until the supernatant ran clear, before being oven dried at 70$^{o}$C.

Where sufficient powder was available, samples were analysed for multi-point $N_2$ BET surface area before reaction, on a Micrometrics Gemini V BET at the University of Leeds. Samples were loaded into glass tubes, degassed under $N_2$ at 70$^{o}$C for 12-20 hours and weighed prior to measurement of nitrogen adsorption at liquid $N_2$ temperatures. The results and associated standard deviations are presented in Table 3-2. Geometric surface areas presented were calculated assuming cubic grains with no fractal properties using the formula:

$$SA = a \times \rho^{-1} \times r^{(d-3)} \quad (3.1.1)$$

Where SA is the surface area in $m^2/g$, a is a geometric parameter (6 for cubes), ρ is the solid density in $g/m^3$, r is the average grain radius in m and d is another geometric parameter (2 for Euclidean solids).

| Sample | Grain Size, μm | No. of Measurements | Average Value, $m^2/g$ | Standard Deviation (%) | Estimated Geometric Surface Area |
|---|---|---|---|---|---|
| ***Dolomite*** | 125-180 | 5 | 0.989 | 0.039 (4%) | 0.047 |
| ***Dolomite*** | 500-600 | 3 | 0.855 | 0.005 (1%) | 0.018 |
| ***Quartz*** | 125-180 | 7 | 0.044 | 0.001 (2%) | 0.047 |
| ***Quartz*** | 500-600 | 12 | 0.017 | 0.002 (12%) | 0.018 |
| ***Sandstone*** | 125-180 | 4 | 1.168 | 0.020 (2%) | 0.047 |
| ***Sandstone*** | 500-600 | 2 | 1.649 | 0.014 (1%) | 0.018 |
| ***Peridotite*** | 125-180 | 4 | 0.217 | 0.001 (1%) | - |
| ***Plagioclase Feldspar*** | 125-180 | 9 | 0.153 | 0.007 (5%) | 0.047 |
| ***Plagioclase Feldspar*** | 500-600 | 5 | 0.065 | 0.002 (3%) | 0.018 |
| ***Alkali Feldspar*** | 125-180 | 2 | 0.129 | 0.004 (3%) | 0.047 |
| ***Alkali Feldspar*** | 500-600 | 3 | 0.092 | 0.005 (5%) | 0.018 |
| ***Olivine*** | 125-180 | 6 | 0.556 | 0.020 (4%) | - |

**Table 3.1.2**: BET analysis results

The majority of experiments were carried out using either deionised water or a 1.36M sodium chloride solution. The sodium chloride solution was prepared by dissolving 79.5g of Alfa Aesar, ACS sodium chloride (min. 99.0% purity) in 1L milliQ deionised water. The brine's ionic strength was chosen to reflect the ionic strength of the formation fluid analysed from the Cleethorpes borehole where the Sherwood Sandstone core was drilled (British Geological Survey 1985). The brine analysis was provided by the BGS along with the core samples and the analysis results are presented in Table 3.1.3. Some of the initial $CO_2$ solubility experiments were carried out in a synthetic brine designed to more closely match the formation fluid. This solution contained 1.24M NaCl, 0.06M KCl and 0.05M $CaCl_2$. This brine was not used for any of the mineral dissolution experiments or for later $CO_2$ solubility experiments, as it was considered to make the fluid chemistry overly complex for the purposes of this study.

| Analyte | Concentration, mol/l |
|---|---|
| ***Na*** | 1.24 |
| ***K*** | 0.06 |
| ***Ca*** | 0.05 |
| ***Cl*** | 1.23 |

**Table 3.1.3**: Formation fluid analysis from Cleethorpes borehole

### 3.1.1 Quartz Sample

The quartz used in this study is fairly unremarkable. The sample used appeared, under SEM investigation, to be free of any other phases. Grain surfaces following preparation were largely clean and free of weathering features, though small-scale pitting was fairly common (Figure 3.1.1).

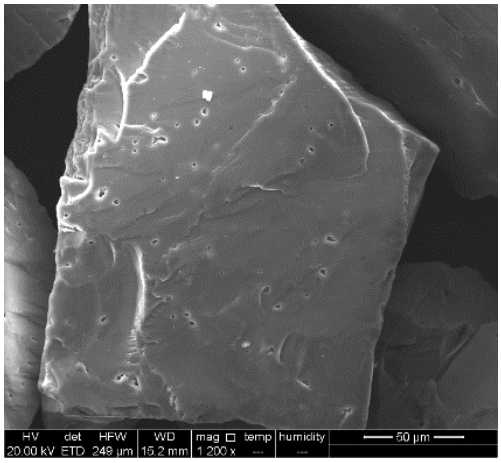


**Figure 3.1.1**: SEM Image of quartz grain, showing some minor pitting

### 3.1.2 K-Feldspar Sample

The first feldspar used in this study was nominally a K-feldspar, though it contained significant (~15 wgt. %) albite. The albite present, in turn, was a 96:4 molar solid solution of albite:anorthite, hence containing significant calcium. For the purposes of modelling, this solid solution was considered as two separate phases, rather than a solid solution. The formula of the bulk solid, as calculated from microprobe data, was found to be:

$$(K_{0.76}, Na_{0.23}, Ca_{0.01})\ Al_{1.02}\ Si_{2.99}\ O_8 \qquad (3.1.2)$$

The K-feldspar component is described by:

$$(K_{0.93}, Na_{0.06}, Ca_{0.00})\ Al_{1.00}\ Si_{2.96}\ O_8 \qquad (3.1.3)$$

And the albite:anorthite solid solution described by:

$$(K_{0.00}, Na_{1.01}, Ca_{0.04})\ Al_{1.09}\ Si_{3.08}\ O_8 \qquad (3.1.4)$$

Despite the fact that this is a “complex” feldspar, it will be referred to as K-feldspar for the remainder of this work.

The albite appears within the bulk K-feldspar material largely as perthitic “lenses” within the bulk material (Figure 3.1.2).

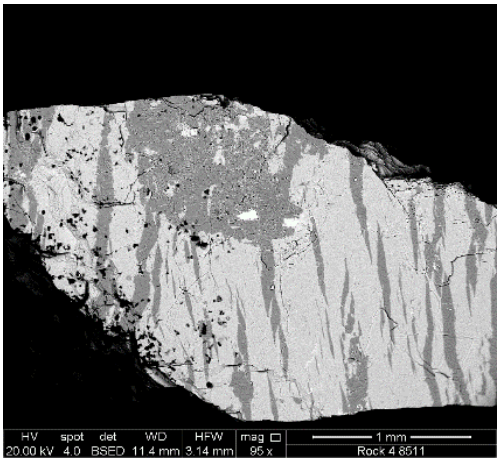


**Figure 3.1.2**: SEM Image of K-feldspar grain, showing albite “lenses”

While the sample appeared largely pure under SEM observation, some patches of secondary quartz were found (Figure 3.1.3). As for the quartz sample, the K-feldspar surface was found to be relatively clean and free of fines following treatment. However pitting and general signs of “weathering” were more apparent than for the quartz sample (Figure 3.1.4).

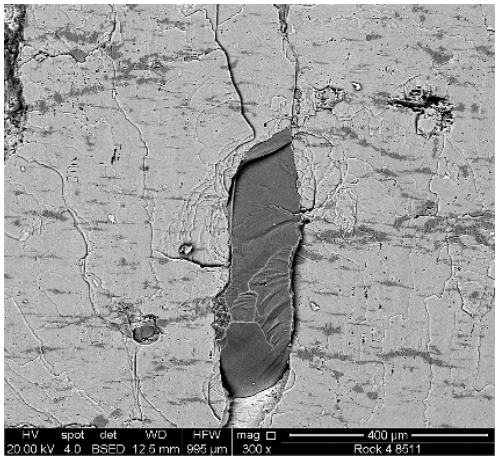


**Figure 3.1.3**: SEM Image of K-feldspar grain, showing quartz growth (centre)

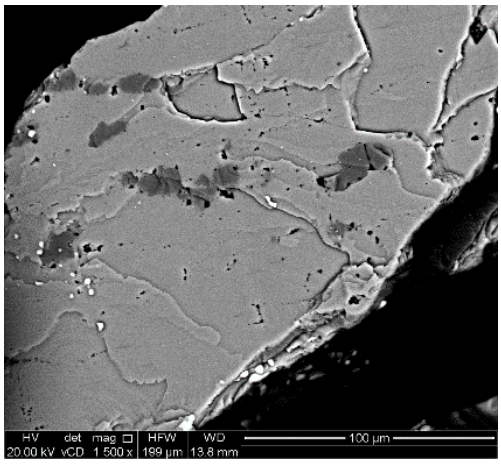


**Figure 3.1.4**: SEM Image of K-feldspar grain showing numerous, minor, pits

### 3.1.3 Albite Sample

As for the K-feldspar described above, the plagioclase detailed here is a “complex” feldspar, but for the purposes of the work presented here will be referred to as “albite”.

The albite sample used contained significant K-feldspar (~15 wgt. %). The formula of the bulk solid, as calculated from microprobe analysis, is given by:

$$(Na_{0.90}, Ca_{0.03}, K_{0.09})\ Al_{1.03}\ Si_{2.96}\ O_8 \qquad (3.1.5)$$

The albite component is described by:

$$(K_{0.01}, Na_{0.98}, Ca_{0.03})\ Al_{1.04}\ Si_{2.98}\ O_8 \qquad (3.1.6)$$

And the K-feldspar component by:

$$(K_{0.93}, Na_{0.03})\ Al_{0.96}\ Si_{2.84}\ O_8 \qquad (3.1.7)$$

The K-feldspar component occurs as streaks and lenses within the albite (Figure 3.1.5).

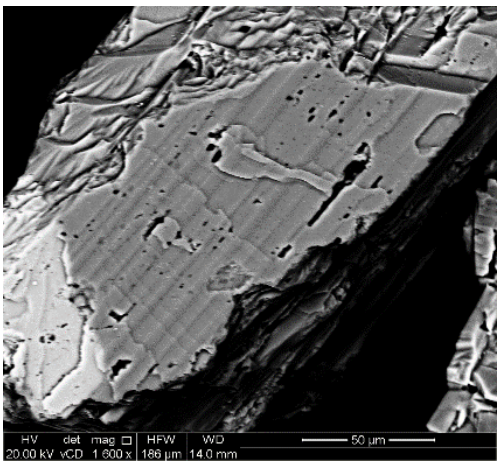


**Figure 3.1.5**: SEM Image of albite grain with (lighter) K-feldspar intergrowth

While largely pure, the bulk sample also contains occasional quartz grains (Figure 3.1.6). The sample also shows considerable pitting and stepping (Figure 3.1.7).

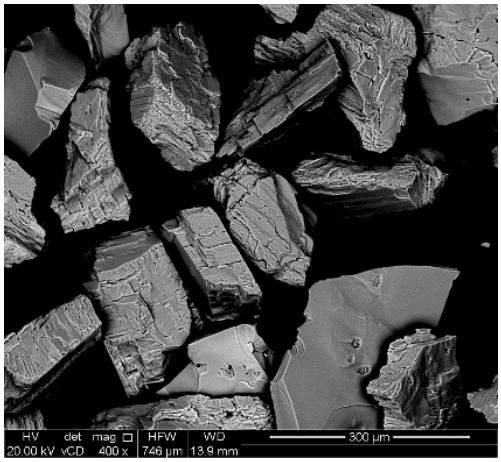


**Figure 3.1.6**: SEM Image of albite grains with two (bottom right and top left) quartz grains

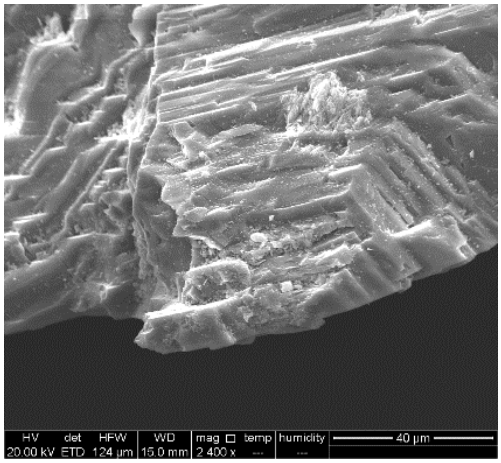


**Figure 3.1.7**: SEM Image of albite grain showing considerable stepping

### 3.1.4 Calcite Sample

Compiled EDS data, taken during SEM observations of the calcite, indicate that the sample is largely compositionally pure $CaCO_3$, with some trace Al. Following treatment, grain surfaces were observed to be largely clean, with very occasional and minor pitting (Figure 3.1.8).

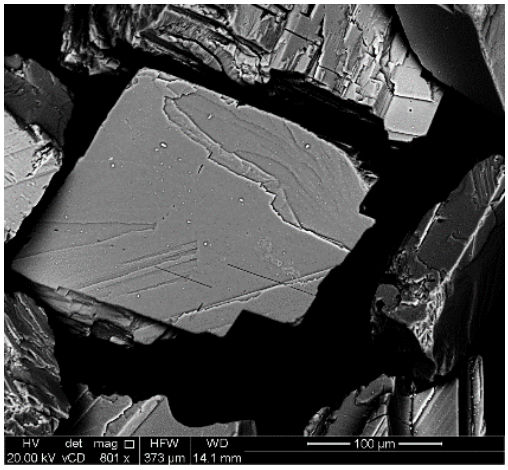


**Figure 3.1.8**: SEM Image of calcite grain

### 3.1.5 Dolomite Sample

Microprobe investigation of the dolomite sample found it to be slightly deficient in Ca relative to Mg and with some minor Fe and Mn. The average formula describing the bulk sample as calculated from these results is:

$$(Ca_{0.95}, Mg_{1.03}, Fe_{0.02})\ (CO_3)_2 \qquad (3.1.8)$$

Some rare calcite grains were also found within the sample during SEM observations, but otherwise the sample seemed largely pure. The sample, following preparation, showed considerable small scale pitting and stepping in places (Figure 3.1.9).

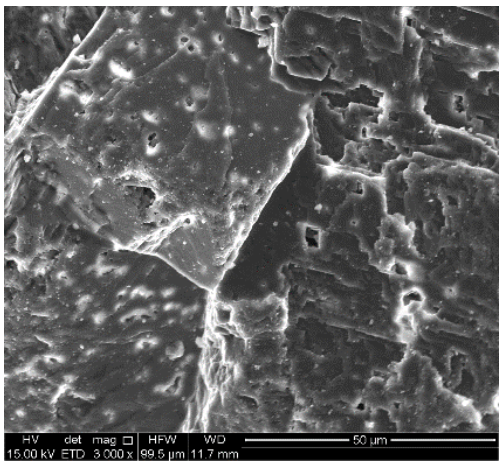


**Figure 3.1.9**: SEM Image of dolomite grain, showing considerable pitting

### 3.1.6 Sandstone Sample

Samples of the Sherwood Sandstone were provided by the British Geological Survey and were sampled from a core collected from a geothermal exploration well drilled in Cleethorpes, South Humberside. 0.5m of core was sampled, from 1319.3m – 1319.8m depth. Subsamples were then powdered for use in batch experiments and cored for use in experiments looking at consolidated material.

The sample was a medium red and purplish brown, medium sandstone, the core section sampled from was massive and moderately friable. The whole core section recovered (18.33m) has mean porosity of 23.6%, mean permeabilities of 2166 mD (arithmetic), 1657 mD (geometric) and mean transmissivities of 39.4 Dm (arithmetic), 30.4 Dm (geometric) (from 37 samples, data provided by the British Geological Survey).

SEM observations showed the sample to consist largely of quartz and K-feldspar. Dolomite and some fibrous Illite were also observed. Quantitative XRD analysis for the bulk samples was not available, hence bulk composition has been estimated from two samples taken from the same borehole at similar depth, analysed by the British Geological Survey. The composition from these results (neglecting porosity) is: 63% quartz, 23% K-feldspar, 4% albite, 6% dolomite and 3% Illite. This composition is used for any modelling described in the following sections, where a bulk composition is required, unless otherwise stated.

The dolomite is present both as discrete grains and as secondary cement between grains.

Illite, where present in the samples, is present as fibrous bridges (Figure 3.1.10). Also present are some patches of sylvite, presumably precipitated from the drilling fluid. These patches of sylvite and illite appeared to be largely removed during the treatment of grains prior to reaction.

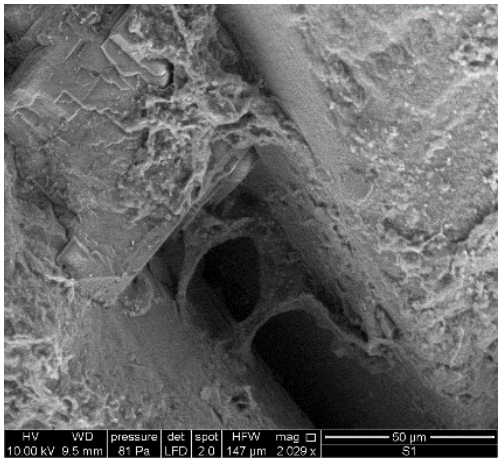


**Figure 3.1.10**: SEM Image of illite bridge between grains

The feldspar and dolomite grains present are often heavily pitted (Figure 3.1.11).

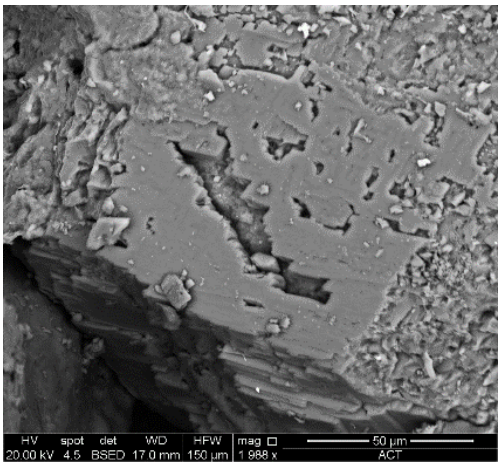


**Figure 3.1.11**: SEM Image of pitted feldspar grain

A variety of minor phases were also found to present within the sample, including iron oxides and gypsum.

## 3.2 Batch Experiments

Batch experiments were carried out using the prepared solids and fluids described above, to investigate mineral dissolution, fluid pH and $CO_2$ solubility in various systems. All experiments were carried out at either room temperature (22°C±1°C) or 70$^{o}$C and under a $pCO_2$ of either 4bar or 31bar (absolute). Low pressure (4bar $pCO_2$) experiments were carried out in 120ml Savillex perfluoroalkoxy (PFA) digestion vessels. High pressure (31bar $pCO_2$) experiments were carried out in 200ml high pressure/temperature Parr (type 4766) stainless steel (type 316) vessels, fitted with teflon liners. A schematic illustration of the laboratory set-up is shown in Figure 3.2.1.

### 3.2.1 Gas System

A gas system was constructed, using two gas regulators, allowing low and high pressure experiments to run in parallel. 50bar CP (99.995% purity) grade $CO_2$ cylinders were used for all experiments. Gas lines were run into a 115L oven monitored at 70$^{o}$C for the high temperature experiments. The gas line was fitted with two ESI USB pressure transducers (GS 4200 ESI Technology Lt., UK), a 0-100bar transducer for the high pressure line and a 0-16bar transducer for the low pressure line, which provided continuous monitoring and recording of pressure and temperature within the gas line during the experiments. The gas line was flushed with $CO_2$ and transducers zeroed (to an absolute pressure of 1 bar, gauge pressure of 0 bar) prior to use.

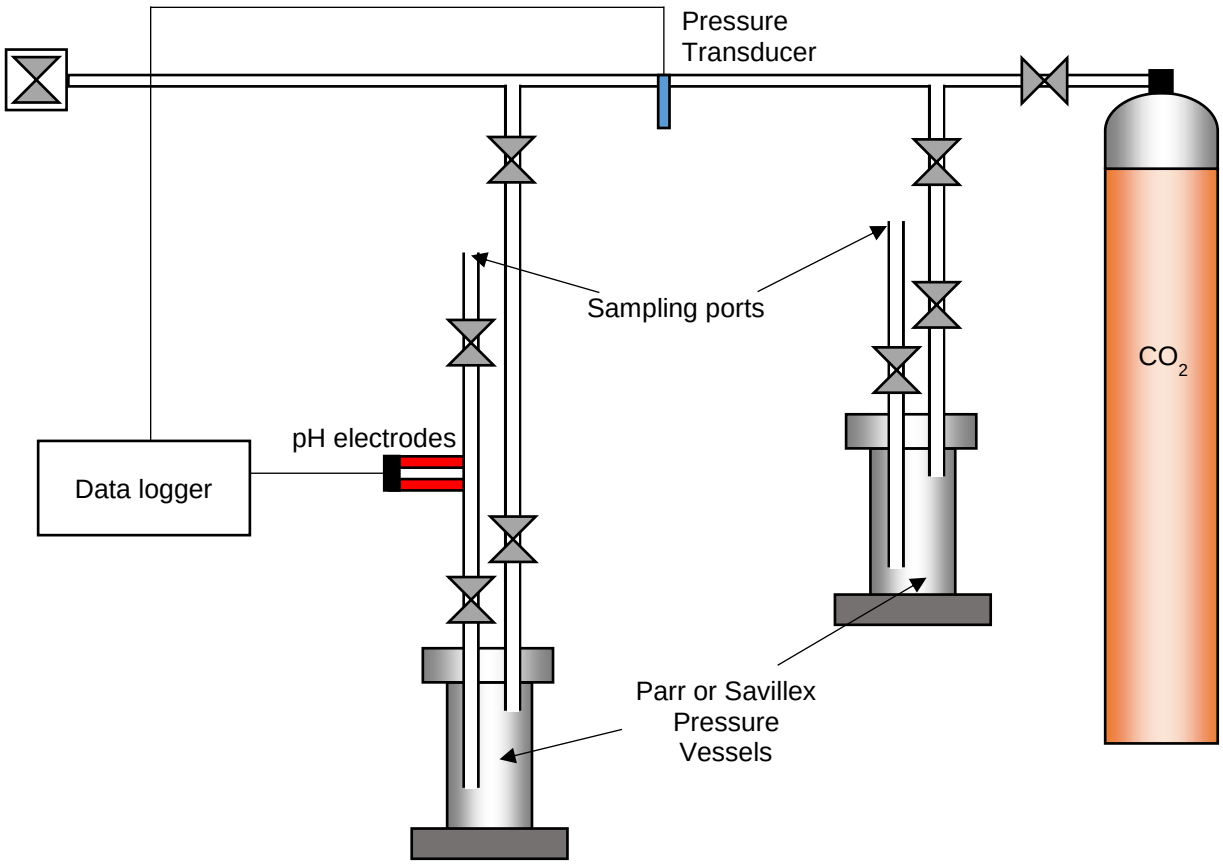


**Figure 3.2.1**: Schematic of laboratory set-up

### 3.2.2 $CO_2$ Solubility

A number of experiments were carried out to investigate carbon dioxide solubility, in both pure fluids (brine or deionised water) and mineral suspensions at, or approaching, equilibrium. For pure fluid experiments, vessels were partially filled with fluid and fitted with Teflon coated magnetic stirring beads. All solubility experiments were stirred vigorously, using a magnetic stirrer. All vessels were fitted with dip-tubes with 2µm PEEK filters Vessels were connected to the $CO_2$ line and the headspace flushed for several minutes with $CO_2$. For mineral suspension experiments, around 5g of powdered solid was added to the vessel before proceeding as for the pure fluid experiments. For mineral-fluid experiments, the suspensions were left for several days to equilibrate before addition of $CO_2$.

Following addition of $CO_2$, experiments were left to allow $CO_2$ saturation for periods of several hours to several days depending on the experiment. Following $CO_2$ saturation, vessels were connected to a sampling assembly constructed from stainless steel and PEEK tubing. The assembly was flushed with several millilitres of sample and then samples were allowed to bleed into polypropylene syringes prefilled with 4-8mls of 1M Titrinorm NaOH. The NaOH had previously been stored under a 1bar argon (zero grade) atmosphere. Slow bleeding of the fluid allowed sampling with minimum (< 0.05bar) reduction of the pressure of the system (hence preventing excessive degassing of $CO_2$). The NaOH absorbed the $CO_2$, retaining it in solution after removal from the pressurised system. During low pressure experiments the sampling assembly included a set of Unisense type pH500/ref100 electrodes, connected to a high-impedance voltmeter, allowing measurement of fluid pH at in-situ temperatures and pressures. pH was recorded when the reading was stable, generally after one hour of low flow past the pH electrodes.

The carbon dioxide content of the sample was determined by titration against 0.50M HCl (prepared from 1.00M Titrinorm VWR HCl), using a PC-titrate, Man-Tech auto-titrator. Three equivalence points were determined: for $OH^-$ ($V_1$), $CO_3^{2-}$ ($V_2$) and $HCO_3^-$ ($V_3$), and the carbon dioxide content of the sample was calculated from the average of ($V_3$-$V_2$) and ($V_2$-$V_1$). The titrator was calibrated with pH 4 and pH 7 buffers before use.

### 3.2.3 Mineral Dissolution Experiments

The prepared solid samples and fluids were also used to investigate mineral and whole-rock dissolution kinetics under $pCO_2$. Solids samples and fluids (as described previously) were added to vessels, at a fluid:rock weight ratio of 100:5. A list of kinetic experiments and associated conditions is presented in Table 3.2.1.

Dissolution experiments were not stirred magnetically, in order to prevent further breakdown of the powders and generation of extra surface area. Room temperature experiments were placed on a shaking table, set to 100 rpm, while 70$^{o}$C experiments were agitated manually two or three times daily.

Vessels were fitted with dip tubes, but not with filters, due to breakdown and blockage of the filters during long-term experiments. As for the solubility experiments, suspensions were left to equilibrate for a few days prior to $CO_2$ flushing and sealing. Due to leakage from vessels and $CO_2$ dissolution over time, vessels remained connected to the gas line for the duration of the experiments.

| Mineral | Grainsize fraction, µm | Solution | Pressure (absolute) | Temperature | Duration, hours | Mixing method |
|---|---|---|---|---|---|---|
| Potassium Feldspar | >500 | DI | 4 | 22°C | 677 | Stirred |
| Potassium Feldspar | >500 | DI | 4 | 22°C | 677 | Shaken |
| Potassium Feldspar | >500 | DI | 4 | 22°C | 677 | Unstirred |
| Quartz | 125-180 | 1.36M NaCl | 4 | 22°C | 623 | Swirled |
| Plagioclase Feldspar | 125-180 | 1.36M NaCl | 4 | 22°C | 623 | Swirled |
| Plagioclase Feldspar | 125-180 | 1.36M NaCl | 31 | 70°C | 166 | Swirled |
| Quartz | 125-180 | 1.36M NaCl | 31 | 70°C | 701 | Swirled |
| Dolomite | 125-180 | 1.36M NaCl | 4 | 22°C | 557 | Swirled |
| Dolomite | 500-600 | 1.36M NaCl | 4 | 22°C | 557 | Swirled |
| Dolomite | 125-180 | DI | 4 | 22°C | 531 | Shaken |
| Alk. Feldspar | 125-180 | DI | 4 | 22°C | 531 | Shaken |
| Quartz | 125-180 | DI | 4 | 22°C | 531 | Shaken |
| Dolomite | 125-180 | DI | 31 | 70°C | 581 | Swirled |
| Dolomite | 500-600 | DI | 31 | 70°C | 487 | Swirled |
| Quartz | 125-180 | DI | 31 | 70°C | 581 | Swirled |
| Sherwood Sandstone | 125-180 | 1.36M NaCl | 4 | 22°C | 1083 | Shaken |
| Sherwood Sandstone | 500-600 | 1.36M NaCl | 4 | 22°C | 1083 | Shaken |
| Dolomite | 125-180 | 1.36M NaCl | 31 | 70°C | 525 | Swirled |
| Olivine | 125-180 | 1.36M NaCl | 31 | 70°C | 525 | Swirled |
| Peridotite | 125-180 | 1.36M NaCl | 4 | 22°C | 341 | Shaken |
| Sandstone | 500-600 | 1.36M NaCl | 31 | 70°C | 701 | Shaken |
| Sandstone | 125-180 | 1.36M NaCl | 31 | 70°C | 556 | Shaken |
| Alk. Feldspar | 125-180 | 1.36M NaCl | 4 | 22°C | 794 | Shaken |
| Alk. Feldspar | 500-600 | 1.36M NaCl | 4 | 22°C | 794 | Shaken |
| Sherwood Sandstone | 125-180 | DI | 4 | 22°C | 794 | Shaken |
| Alk. Feldspar | 250-500 | DI | 31 | 70°C | 1559 | Swirled |
| Illite | 125-180 | 1.36M NaCl | 4 | 22°C | | Shaken |
| Plag | 500-600 | 1.36M NaCl | 4 | 22°C | | Shaken |
| Calcite | 125-180 | 1.36M NaCl | 4 | 22°C | | Shaken |
| Alk. Feldspar | 125-180 | 1.36M NaCl | 31 | 70°C | | Swirled |
| Plag | 500-600 | 1.36M NaCl | 31 | 70°C | | Swirled |
| Calcite | 125-180 | 1.36M NaCl | 31 | 70°C | | Swirled |
| Illite | 125-180 | DI | 4 | 22°C | | Shaken |
| Calcite | 125-180 | DI | 4 | 22°C | | Shaken |
| Illite | 500-600 | 1.36M NaCl | 4 | 22°C | | Shaken |
| Calcite | 500-600 | 1.36M NaCl | 4 | 22°C | | Shaken |
| Calcite | 125-180 | DI | 31 | 70°C | | Swirled |
| Sherwood Sandstone | 125-180 | DI | 31 | 70°C | | Swirled |
| Sherwood Sandstone | 125-180 | 1.36M NaCl | 4 | 70°C | | Swirled |
| dolomite | 125-180 | 1.36M NaCl | 4 | 70°C | | Swirled |

**Table 3.2.1**: Summary of mineral and whole-rock dissolution experiments

Experiments were generally run for between 500 and 1000 hours. Sampling for cation analysis was carried out throughout the experiment. Sampling assemblies were constructed from acid washed, stainless steel and PEEK tubing and HiP needle valves. Prior to sampling the sample lines were flushed with 1-2ml of sample. 0.5-1.5ml samples were then bled into pre-weighed sterile polypropylene syringes and filtered, using Minisart, sterile, 0.2µm filters into pre-weighed acid washed sample tubes, with 4ml 0.015M $HNO_3$ preservative. Preservative was prepared by adding 69% AnalaR NORMAPUR $HNO_3$ to milliQ deionised water and had a pH<2.5. Fluid volumes removed from the experiments and dilution factors were calculated using weights of filled syringes and sample tubes. Samples were sealed using para-film and stored away from direct light at room temperature until analysis.

Samples were taken from the experiments immediately before and after addition of $CO_2$. Experiments were then sampled at increasing intervals, three times a day initially, falling to 2 times a day, etc., as the experiment proceeded and reaction rates decreased. One duplicate sample was taken on or about every tenth sample, from a total of 20-40 samples per experiment. At the end of the experiments, samples were taken for measurement of dissolved $CO_2$ content and pH measurements made as described for the $CO_2$ solubility experiments above.

After final experimental samples had been taken, as much of the remaining fluid as possible was rapidly expelled from the vessel, to minimise the formation of precipitates during depressurisation. Reacted solids were roughly halved, one half left un-rinsed and the other gently rinsed in milliQ water. All samples were oven dried at 70$^{o}$C.

Samples taken during the experiment were sent to an external laboratory (University of Portsmouth, Dr. Gary Fones; Actlabs, Canada; University of Hull, Robert Knight) for cation analysis. Samples were further diluted 15x before analysis on an Agilent 7500ce ICP-MS. In addition to the in-house quality control (QC) samples, standards, blanks and references were prepared prior to dispatch of samples using the materials and methods utilised in the experiments (i.e. 1.36M NaCl, 0.015M $HNO_3$ etc.) as an added check on result quality. Additional checks on results were carried out for a limited number of samples using the in-house ion-chromatograph (University of Leeds, Dr. Sam Allshorn) for Mg, Ca and K analysis and UV spectroscopy for Al and Si.

## 3.3 Core Experiments

In addition to the batch experiments on powdered samples, experiments were also performed on cores cut from the Sherwood Sandstone. Cylindrical cores were cut from the same length of original sandstone core as was used to obtain the powdered samples. Three cores were cut and their porosity measured using a nitrogen porosimeter. NMR scans and permeability measurements were also performed on the cores prior to the experiments. Core details are presented in Table 3.3.1.

| Core | Length, mm | Breadth, mm | Porosity, % | Pore Volume, ml | Permeability, mD | Gas permeability, mD |
|---|---|---|---|---|---|---|
| 1 | 40.87 | 37.22 | 23.33 | 10.37 | - | - |
| 2 | 39.19 | 37.27 | 24.30 | 10.39 | 1334 | 1471 |
| 3 | 39.59 | 37.25 | 23.86 | 10.29 | 1013 | 1472 |

**Table 3.3.1**: Core details, error on permeability measurements is ±200mD

Core 3 was used for a static experiment, where the core was flooded with 1.36M NaCl brine, saturated with $CO_2$ at 30bar before being sealed and left in in an oven at 70$^{o}$C. Core 2 was used in a flow through experiment, again using 1.36M NaCl brine, saturated with $CO_2$ at 30bar and carried out at 70$^{o}$C.

The NaCl brine was prepared as for previous experiments and was saturated with $CO_2$ under 31bar (absolute) $pCO_2$ using an Isco high pressure syringe pump (TYPE) in a 2000ml stainless steel pressure vessel. The fluid was left under $pCO_2$ at 70$^{o}$C for several days to allow for complete $CO_2$ saturation.

The two experimental cores were fitted into core-holders and placed under a confining pressure of circa 50bar. For the “static” experiment, air from Core 3 was removed using a vacuum pump, before flooding with the $CO_2$ saturated brine, again using the Isco syringe pump. Brine was then flowed through the core at 2ml/minute for several minutes. The downstream end of the core was then sealed and the pump run at a constant pressure of 31bar(absolute) until flow was ceased. It was assumed that at this point the core was fully saturated with $CO_2$ saturated brine. The upstream end of the core-holder was then sealed and the core-holder detached from the pump. The core was then placed in an oven at a constant 70$^{o}$C.

The setup for the flow-through experiment using Core 2 is shown in Figure 3.3.1. A back-pressure cylinder, under 31bar $pCO_2$ was connected to the

brine filled pressure vessel. Both vessels remained in the oven. The 200ml Isco pump was regularly topped up with $CO_2$ saturated brine from the pressure vessel. Flow rate during filling was kept low (<5ml/min) to minimise degassing of $CO_2$. The core was initially vacuumed using a vacuum pump, before flooding with brine at 31bar. Following saturation the downstream end of the core was opened to the back pressure, via a sampling assembly. A constant flow-rate of 0.05ml/min was set. The brine was kept at 70$^{o}$C while in the pump using heated water from a water-bath/pump assembly, which was pumped round the Isco pump heating jacket. The length of piping carrying the brine from the outside of the oven to the core was kept as long as possible using coiled tubing, in order to keep the brine at temperature. All tubing was constructed from stainless steel or PEEK. Pressure transducers were placed at the upstream and downstream ends of the core-holder.

The sampling assembly was constructed from three 3-way valves, to allow sampling without depressurisation of the system. Flow could be bypassed around a sealed section of the assembly to allow sampling 1-2ml of fluid, before re-establishing the original flow-path. Samples were taken at a similar frequency and were filtered and preserved as for the mineral dissolution experiments described above.

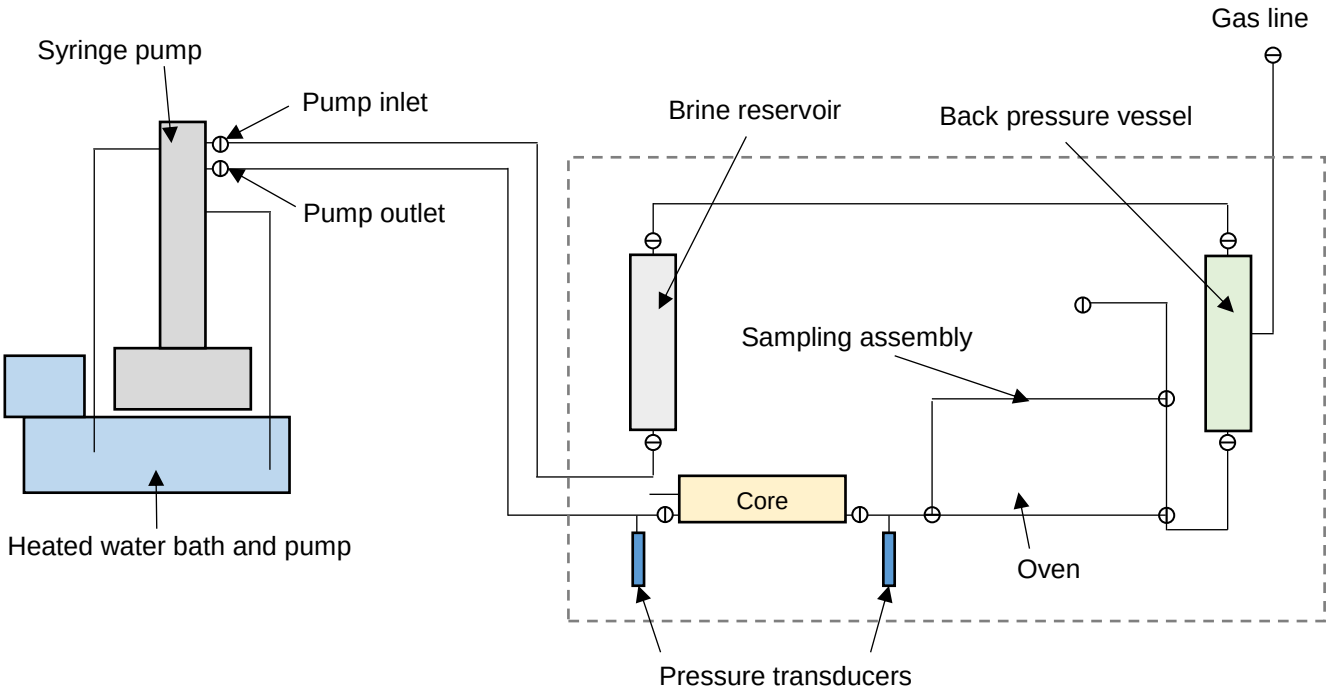


**Figure 3.3.1**: Setup for core flow-through experiment

## 3.4 Data Treatment and Modelling

### 3.4.1 Data Treatment and Dissolution Rate Calculations

The following section details the data treatment used on analysed fluid concentration for the mineral and sandstone dissolution experiments, the results of which are covered in Chapters 4 & 5. This section includes a full example of the data treatment used to calculate dissolution rate for a K-feldspar dissolution experiment (experiment 171), carried out at 4 bar $pCO_2$, 22°C, using 125-180µm fraction and 1.36M NaCl solution.

Sample solutions were analysed for major cations using ICP-MS. This initial "raw" data was corrected for matrix background concentrations and laboratory dilution before further treatment and analysis. Matrix blanks were prepared for analysis using the experimental starting fluids and the acid solution used to dilute experimental samples. The blanks were analysed along with the experimental samples. Resulting concentrations were subtracted from those measured in experimental samples.

All aliquots removed from the experiments were weighed before and after dilution, using a five point balance. Dilutions were made using 0.015M $HNO_3$ solution, from a stock made from 69% AnalaR analytical reagent and deionised water. Solution weights were used to calculate equivalent solution volumes based on the measured densities of both the experimental matrix (either deionised water or 1.36M NaCl) and the diluting fluid (0.015M $HNO_3$). These solution volumes were used to calculate the laboratory dilution factor for each sample. Hence the initial steps in data treatment were the removal of background concentrations as measured in the matrix blanks and application of calculated dilution factors to analysed concentrations to produce the original concentration of the sample as it was removed from the experimental vessel.

Dissolution experiments were carried out in closed batch reactors, with aliquots of solution removed regularly for cation analysis. Hence the reactor cannot be considered constant volume and a correction must be made to either measured concentrations or the sampling time to allow accurate measurements of dissolution rate to be made. In this case the sampling times ($t_i$) were corrected such that the corrected time ($t_i$*) represents the theoretical time at which the measured concentration in the sample would be reached in a system of constant volume. The correction was made using the formula from Choo et al. (2006):

$$t_i^* = t_{i-1}^* + \frac{V_0}{V_{i-1}\Delta t_i} \quad (3.4.1)$$

Where i is the ith sample, $V_0$ is the volume in the reactor at the point immediately before time zero, when the vessels were flushed and sealed and Δt is the sampling interval.

The two steps outlined above; calculation of pre-dilution concentrations, including a density factor and background correction and the calculation of volume constant sampling times, provided the base data used for the final mineral dissolution rate calculations. An example of this base data is provided in Table 3.4.1, using a sample of data from experiment 171.

Before rate calculations were carried out, duplicates and major outliers and results below detection were removed and major analyte concentrations (i.e. Ca and Mg for dolomite, Si for quartz) were corrected for mineral stoichiometry. Chemical formulae for the minerals used were calculated using microprobe data and the procedure outlined in Deer et al. 1992. Average bulk mineral formulae calculated for each mineral are given in Section 3.1. The stoichiometrically corrected concentrations were then used to give approximate “mineral” concentrations in solution. For example “dolomite concentration” was assumed to be the sum of the stoichiometrically corrected calcium and magnesium concentrations divided by two: one mole of calcium or magnesium is assumed to equate to one mole of dissolved dolomite. Measured concentrations at the first sampling point (t-1, prior to introduction of $pCO_2$) were subtracted from concentrations at all sampling points, such that t-1 represents a zero point.

Plots of log(C*) vs. log(t*) were constructed, where C* represents the dissolved mineral concentration, corrected as above. Example data and corresponding plot are given in Table 3.4.2 and Figure 3.4.1. Assuming a constant dissolution mechanism, controlled by the activity of dissolved species, such data will plot as a straight line, of the form:

$$\log_{10}[\mathrm{C}^*] = q \log_{10} t^* + \log_{10} k' \quad (3.4.2)$$

Solving this equation for C* yields:

$$[\mathrm{C}^*] = k' t^{*q} \quad (3.4.3)$$

Hence the mineral release rate r, at any given corrected time t*, is given by:

$$r = \frac{\partial[\mathrm{C}^*]}{\partial t} = q k' t^{*(q-1)} \quad (3.4.4)$$

And the specific mineral dissolution rate, R, is given by:

$$R = \frac{\partial[\mathrm{C}^*]}{\partial t} \times \frac{V_0}{A} \quad (3.4.5)$$

Where $V_0$ is the fluid volume in the reactor immediately prior to sample t0 and A is the mineral surface area in the experiment.

In the example data shown below (Figure 3.4.1), from the plot of log(C*) vs. log(t*), the value of q in the above equation (3.4.3) is 0.291 and the value of k' is 1.9E-7 (i.e. $10^{-6.74}$). Inputting these numbers into equation 3.4.3 and solving for various times yields a smoothed concentration vs. time curve, which can be compared to analysed concentrations in order to assess the fit. An example of this is given in Figure 3.4.2. As can be seen, the use of this method smooths out small scale variations in concentration and removes the effect of outliers, which if included in traditional point to point calculations of dissolution rate may produce erroneous results.

Final dissolution rates presented in this thesis were calculated using equation 3.4.5 and mineral surface areas as measured using BET (see Section 2.1.1.3). The final rates calculated using the sample data below are shown in Table 3.4.3.

The advantage of this method over the more traditional method of direct rate calculations from concentration/time data points is that it allows the calculation of instantaneous rates for any given time, rather than an average rate between samples, for data where concentration vs. time is non-linear. Assuming a good fit and no change in reaction mechanism, such plots also allow for accurate predictions for rates beyond the experiment end time (e.g. Oelkers, Schott, & Devidal, 2001).

There were a number of experiments where log(C*) vs. log(t*) did not plot as a straight line, but "kinked" at some point into the experiment, indicating precipitation of a solid phase or a change in dissolution mechanism. For such data two straight lines were fitted, for early and late time data. This essentially leads to two sets of values for q and k' in equation 3.4.3, which are switched depending on which period of time is being focused on.

Rates were calculated for both $N_2$ BET measured surface area and for calculated geometric surface area. Geometric surface areas were calculated using the formula:

$$A = a' \rho^{-1} r^{(d-3)} \quad (3.4.6)$$

Where a' is a geometric parameter (6 for a cube, 3 for a sphere), ρ is the mineral density (in g/m$^3$ taken from mindat.com), r is the average grain radius (m) and d is a constant (2 for Euclidean solids with no fractal properties). However, unless otherwise stated, rates quoted in the text have been derived using measured BET surface areas.

Rates calculated for the experiments presented here have been plotted against mineral affinity and compared to various literature derived rate equations.

Where mineral affinities have been used, these have been generated using analytical data, rather than from the smoothing approach described above. For example, K-feldspar affinity can be calculated using the equation:

$$A = RT \times \ln\left(\frac{K_{K-Feldspar}}{(a_{K^+} \times a_{Al(OH)_4^-} \times a^3_{H_4SiO_4})}\right) \quad (3.4.7)$$

Where $K_{K\text{-feldspar}}$ is the equilibrium constant for K-feldspar at the experimental conditions, R is the gas constant, T is the temperature in Kelvin, and $a_{K^+}$, $a_{Al(OH)_4^-}$ and $a^3_{H_4SiO_4}$ are the activities of the appropriate ions in solution. Activities were calculated by generating an input file of analysed concentrations for PHREEQC, which then performs the appropriate speciation calculations at experimental pressures and temperatures. This procedure has been used to generate affinity vs. rate plots as exampled in Figure 3.4.3.

Specific equations are explained in the appropriate sections, however all experimental mineral rates have been compared to the general rate equation published in the USGS' 'A compilation of rate parameters of water-mineral interaction kinetics for application to geochemical modelling' (USGS 2004). The equation is reproduced below:

$$\frac{dm}{dt} = -SA\begin{bmatrix} \left(k^{298.15K}_{acid} e^{\frac{-E_{acid}}{R}\left(\frac{1}{T}-\frac{1}{298.15K}\right)} a^{n_1}_{H^+}(1-\Omega^{P_1})^{q_1}\right) \\ +\left(k^{298.15K}_{neutral} e^{\frac{-E_{neutral}}{R}\left(\frac{1}{T}-\frac{1}{298.15K}\right)} (1-\Omega^{P_2})^{q_2}\right) \\ +\left(k^{298.15K}_{base} e^{\frac{-E_{base}}{R}\left(\frac{1}{T}-\frac{1}{298.15K}\right)} a^{n_3}_{H^+}(1-\Omega^{P_3})^{q_3}\right) \end{bmatrix} \quad (3.4.8)$$

Where SA is the surface area in m$^2$, $k_x$ represent the rate constants at acid, neutral and base conditions, $a_{H+}$ is hydrogen ion activity, $E_x$ represent the activation energies of the appropriate reactions, T is the temperature in Kelvin, R is the gas constant, Ω is the mineral saturation index and n, p and q are empirical parameters, given in the text for individual minerals.

This equation is (intentionally) similar in form the equations utilised by many reactive transport models. The equation used by TOUGHREACT to calculate mineral dissolution rates for example is:

$$k = k_{25}^{nu} exp\left[-\frac{E_a^{nu}}{R}\left(\frac{1}{T} - \frac{1}{298.15}\right)\right] + k_{25}^{nu} exp\left[-\frac{E_a^{nu}}{R}\left(\frac{1}{T} - \frac{1}{298.15}\right)\right] a_H^{n_H} + k_{25}^{nu} exp\left[-\frac{E_a^{nu}}{R}\left(\frac{1}{T} - \frac{1}{298.15}\right)\right] a_{OH}^{n_{OH}} \quad (3.4.9)$$

Where the sub/super-scripts *nu*, *H* and *OH* indicate neutral, acid and base mechanisms respectively.

Predicted rates calculated using this equation therefor, are similar to those which might be produced by a standard reactive transport modelling package used to investigate GCS and provides a useful comparison to “raw” laboratory derived rates.

| | | | | | Elemental concentrations, corrected for dilution and with matrix background removed | | | |
|---|---|---|---|---|---|---|---|---|
| **Sample** | **Hours from start** | **Fluid Volume in Vessel** | **Interval, hours** | **Volume Constant Time, hours/l** | **Al, mol/l** | **Si, mol/l** | **K, mol/l** | **Ca, mol/l** |
| **171t-1** | | 98.47 | | 0.00 | *9.34E-07* | *7.05E-06* | *0.00E+00* | *9.58E-05* |
| **171t0** | 0.02 | 95.07 | 0.02 | 0.02 | *1.21E-06* | *8.85E-06* | *0.00E+00* | *2.11E-04* |
| **171t1** | 1.53 | 92.11 | 1.52 | 1.59 | *4.54E-06* | *1.43E-05* | *6.15E-06* | *1.08E-04* |
| **171t2** | 3.57 | 89.65 | 2.03 | 3.76 | *1.43E-05* | *2.16E-05* | *0.00E+00* | *8.94E-05* |
| **171t3** | 5.40 | 86.57 | 1.83 | 5.78 | *1.13E-05* | *7.96E-05* | *3.87E-05* | *9.80E-05* |
| **171t4** | 22.70 | 84.43 | 17.30 | 25.45 | *2.77E-05* | *1.75E-05* | *0.00E+00* | *9.48E-05* |
| **171t5** | 25.87 | 82.32 | 3.17 | 29.15 | *2.72E-05* | *2.34E-05* | *0.00E+00* | *8.87E-05* |
| **171t6** | 30.20 | 79.92 | 4.33 | 34.33 | *2.91E-05* | *3.10E-05* | *0.00E+00* | *8.73E-05* |
| **171t6D** | 30.20 | 78.95 | 0.00 | 34.33 | *3.01E-05* | *2.89E-05* | *0.00E+00* | *1.02E-04* |
| **171t7** | 45.45 | 76.11 | 15.25 | 53.35 | *3.20E-05* | *2.08E-05* | *3.20E-06* | *9.38E-05* |
| **171t8** | 50.07 | 74.20 | 4.62 | 59.32 | *3.33E-05* | *2.75E-05* | *0.00E+00* | *8.51E-05* |
| **171t9** | 53.28 | 71.61 | 3.22 | 63.59 | *3.45E-05* | *3.63E-05* | *5.91E-07* | *8.53E-05* |
| **171t10** | 67.78 | 69.48 | 14.50 | 83.53 | *3.46E-05* | *2.57E-05* | *4.64E-08* | *9.67E-05* |

**Table 3.4**.1: Example of base data used in dissolution rate calculations, from K-feldspar experiment 171

| Sample | VCT, hours | VCT, seconds | log(VCT) | Dissolved K-Feldspar, mol/l (C*) | log(C*) |
|---|---|---|---|---|---|
| **171t-1** | 0.00 | 0.00E+00 | - | - | - |
| **171t0** | 0.02 | 6.00E+01 | 1.78 | 6.00E-07 | -6.22 |
| **171t1** | 1.59 | 5.72E+03 | 3.76 | 2.41E-06 | -5.62 |
| **171t2** | 3.76 | 1.35E+04 | 4.13 | - | - |
| **171t3** | 5.78 | 2.08E+04 | 4.32 | - | - |
| **171t4** | 25.45 | 9.16E+04 | 4.96 | 3.49E-06 | -5.46 |
| **171t5** | 29.15 | 1.05E+05 | 5.02 | 5.48E-06 | -5.26 |
| **171t6** | 34.33 | 1.24E+05 | 5.09 | 8.01E-06 | -5.10 |
| **171t6D** | 34.33 | 1.24E+05 | 5.09 | - | - |
| **171t7** | 53.35 | 1.92E+05 | 5.28 | 4.61E-06 | -5.34 |
| **171t8** | 59.32 | 2.14E+05 | 5.33 | 6.85E-06 | -5.16 |
| **171t9** | 63.59 | 2.29E+05 | 5.36 | 9.79E-06 | -5.01 |
| **171t10** | 83.53 | 3.01E+05 | 5.48 | 6.23E-06 | -5.21 |

**Table 3.4**.2: Example of data used in rate calculation plots, for experiment 171. In this case dissolved K-feldspar has been estimated from Si concentrations. Measured Si concentrations were corrected for Si stoichiometry in the mineral (as measured by microprobe), in this case by dividing them by 2.99. This yields an estimate of the dissolved K-feldspar concentration (C*).

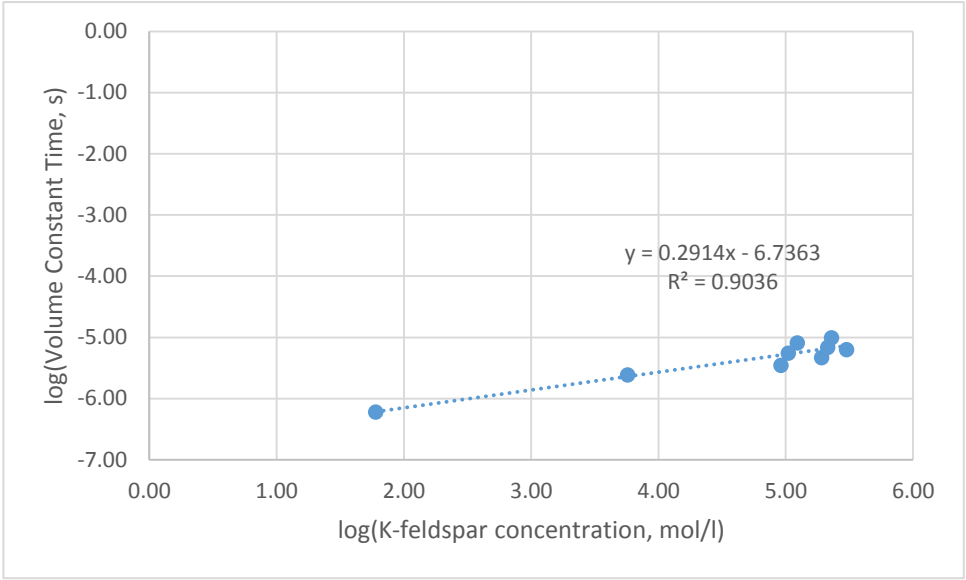


**Figure 3.4.1**: Plot of log(time) vs. log(K-feldspar concentration) for experiment 171. In this case K-feldspar concentration has been estimated using dissolved Si concentrations (See Table 2.1.2)

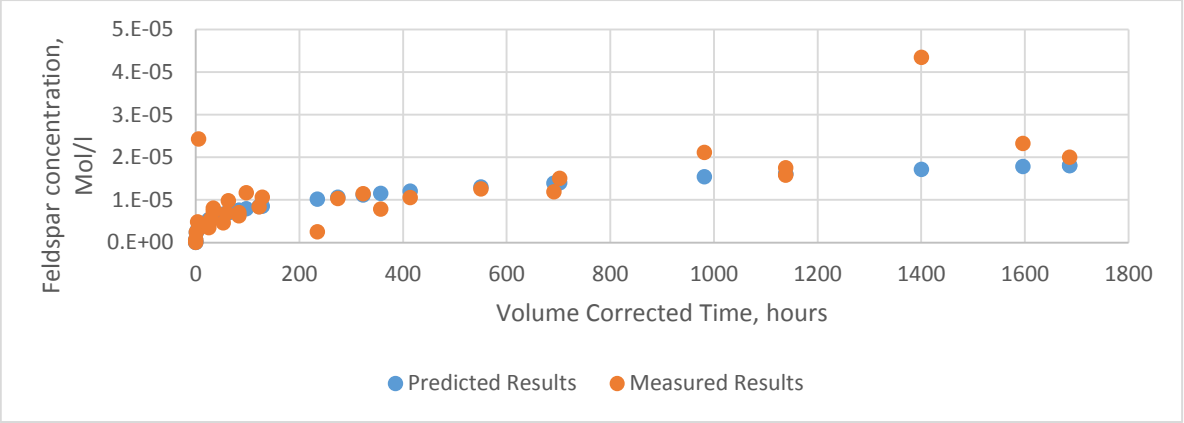


**Figure 3.4.2**: Plot of volume corrected time vs. feldspar concentration (based on Si values), using both analysed values and those predicted using equation 2.1.50 for experiment 171

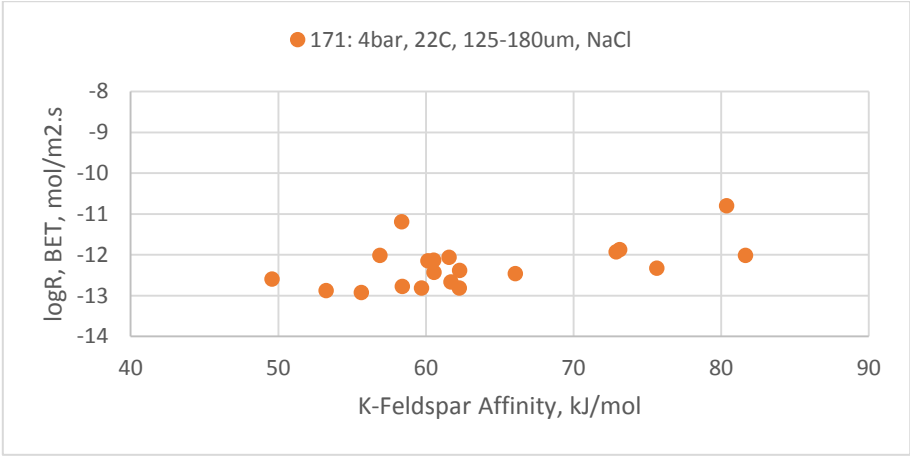


**Figure 3.4**.3: Plot of K-feldspar affinity (estimated from analysed concentrations) vs. calculated dissolution rate for experiment 171

| VCT (Hrs) | Calculated Rate (mol/m2/s) | log(Rate) |
|---|---|---|
| 0.02 | 4E-10 | -9.40 |
| 1.59 | 1.59E-11 | -10.80 |
| 3.76 | 8.62E-12 | -11.06 |
| 5.78 | 6.36E-12 | -11.20 |
| 25.45 | 2.23E-12 | -11.65 |
| 29.15 | 2.02E-12 | -11.69 |
| 34.33 | 1.8E-12 | -11.74 |
| 34.33 | 1.8E-12 | -11.74 |
| 53.35 | 1.32E-12 | -11.88 |
| 59.32 | 1.22E-12 | -11.91 |
| 63.59 | 1.16E-12 | -11.93 |
| 83.53 | 9.6E-13 | -12.02 |
| 83.53 | 9.6E-13 | -12.02 |
| 98.06 | 8.57E-13 | -12.07 |
| 122.41 | 7.32E-13 | -12.14 |
| 128.93 | 7.06E-13 | -12.15 |
| 234.90 | 4.61E-13 | -12.34 |
| 274.27 | 4.14E-13 | -12.38 |
| 323.44 | 3.68E-13 | -12.43 |
| 357.35 | 3.43E-13 | -12.46 |
| 414.49 | 3.09E-13 | -12.51 |
| 550.46 | 2.53E-13 | -12.60 |
| 691.33 | 2.15E-13 | -12.67 |
| 703.00 | 2.12E-13 | -12.67 |

**Table 3.4**.3: Final calculated rates for various times using the data and procedure outlined above. These rates were produced using BET surface area.

### 3.4.2 PHREEQC Modelling

The modelling package PHREEQC has been used extensively in this work for a variety of purposes. Modelling generally fell into two broad categories:

Equilibrium modelling of experimental systems, to generate theoretical $CO_2$ solubility and pH data with which to compare experimental results and;

Modelling of experimental samples in order to assess mineral saturations and compare measured $CO_2$ content and pH to predicted results.

In terms of “equilibrium” modelling, each experimental system described in this work was modelled three times.

Each experiment was first modelled as a pure fluid system, with no mineral included, but at experimental temperatures and pressures. The output from these models is assumed to describe how the experimental systems should appear, in a chemical sense, following addition of experimental $pCO_2$, but without any fluid-mineral interaction. An example input is given below:

```
DATABASE C:\phreeqc\database\PHREEQC.dat
SOLUTION 1
              temp      22 #Experimental Temperature, celsius
              pH        7
              pe        4
  redox     pe
              units     mol/kgw
              Na                  1.36 #Starting fluid composition, moles/litre
              Cl                  1.36
          -water    0.10 # kg water in system
GAS_PHASE 1
            -fixed_pressure
            -pressure 4 #Experimental Pressure, bar (absolute)
            -volume 1
             -temperature 22
             CO2(g)    4

End
```

Here a constant fixed $CO_2$ pressure is reacted with the pure starting fluid. Since there is a reaction occurring (dissolution of $CO_2$), PHREEQC will calculate the resultant fluid composition, including the dissolved $CO_2$ concentration, speciation and pH.

Secondly, experimental systems were modelled assuming fluid-mineral equilibrium, but with only an atmospheric $pCO_2$, assumed to be equivalent to a $CO_2$ partial pressure of 0.00036 bar. An example input is given below:

```
DATABASE C:\phreeqc\database\PHREEQC.dat
SOLUTION 1
   temp      22 #Experimental temperature, celsius
   pH        7
   pe        4
   redox     pe
   units     mol/kgw
   -water    0.110004805 #kg water in experiment
 Na 1.36 #Initial fluid composition, moles/litre
 Cl 1.36

EQUILIBRIUM_PHASES 1
Calcite 0 0.050046658 #Moles calcite in experiment

GAS_PHASE 1
   -fixed_pressure
   -pressure 0.00036 #Atmospheric pCO2, bar
   -volume 1
   -temperature 22
   CO2(g)    0.00036
end
```

In this case the weight of calcite in the experiment has been converted to the equivalent moles of pure phase for the model input: around 5g of calcite were present in the experiment, equivalent to around 0.05 moles of the pure phase. The mineral is allowed to dissolve, under atmospheric $pCO_2$, to equilibrium. The solubility of the mineral is dictated by the equilibrium constant for the dissolution reaction as expressed in the PHREEQC database. In this case, using PHREEQC.dat, the dissolution reaction for calcite is expressed as:

$$CaCO3 = CO3-2 + Ca+2$$

With an associated equilibrium constant (log k) of -8.48 at 25°C. This equilibrium constant will vary with temperature, many silicate minerals, for example, will become more soluble with increasing temperature. This variation is generally accounted for by PHREEQC through use of an analytical expression, of the form

$$log\_k = 0.5 + (A * T) + (B / T) + (C * log10(T)) + (D / T^2) + (E * T^2)$$

Where A, B, C, D and E are constants, generally calculated by non-linear regression of empirical data and T is the temperature in Kelvin. Where the constants for this expression have not been calculated, PHREEQC will calculate mineral solubility using the more general Van't Hoff's equation:

$\log K_T = \log K_{298} + \Delta H_r / (2.303 * 8.314e\text{-}3) * (1 / 298 - 1 / T)$

Where $\Delta H_r$ is the reaction enthalpy in kJ/mol.

In the modelling used in this thesis, calcite, dolomite and quartz were all represented as pure phases. The K-feldspar and plagioclase however, consisting of more than one phase, could not be represented in this manner. Using microprobe data, model representations of these minerals were calculated. The K-feldspar used in the experiments, was found to contain the equivalent of approximately 0.84 moles of K-feldspar, to 0.15 moles of albite to 0.01 moles of anorthite. Thus the equilibrium phases used in the above input for the K-feldspar experiments looked as below:

```
EQUILIBRIUM_PHASES 1
k-feldspar 0 0.015159309 #Equivalent moles of pure K-feldspar in experiment
albite 0 0.002769025 #Equivalent moles of pure Albite in experiment
anorthite 0 0.000203311 #Equivalent moles of pure Anorthite in experiment
```

Likewise the bulk plagioclase used in the experiments was found to be equivalent to 0.85 moles of albite to 0.15 moles of K-feldspar. Thus the equilibrium phase inputs looked thus:

```
EQUILIBRIUM_PHASES 1
Albite 0 0.016179273 #Equivalent moles of pure albite in experiment
k-feldspar 0 0.002682081#Equivalent moles of pure albite in experiment
```

It should be noted that anorthite did not exist as a distinct phase in the K-feldspar samples. However the albitic component contained notable calcium. Since PHREEQC generally deals only with pure phases, this was best represented as a "mix" of albite and anorthite, together with the majority K-feldspar. The sandstone sample used in the experiments was initially modelled straightforwardly using the composition described in Section 3.1.6: 63% quartz, 23% K-feldspar, 4% albite, 6% dolomite and 3% Illite, for example:

```
EQUILIBRIUM_PHASES 1
Quartz 0 0.052707132 #Equivalent moles of quartz in experiment
k-feldspar 0 0.004116411 #Equivalent moles of K-feldspar in experiment
Albite 0 0.000895404 #Equivalent moles of Albite in experiment
Dolomite 0 0.001725899 #Equivalent moles of dolomite in experiment
Illite 0 0.000351492 Equivalent moles of illite in experiment
```

Although some modelling runs omitted the Illite, as explained in Chapter 5.

The final equilibrium modelling runs were carried out as per the previous example, but with a $pCO_2$ equal to that used in the experiments, for example:

```
DATABASE C:\phreeqc\database\PHREEQC.dat
SOLUTION 1
   temp      22 #Experimental temperature, celsius
   pH        7
   pe        4
   redox     pe
   units     mol/kgw
   -water    0.110004805 #kg water in experiment
 Na 1.36 #Initial fluid composition, moles/litre
 Cl 1.36

EQUILIBRIUM_PHASES 1
Calcite 0 0.050046658 #Moles calcite in experiment

GAS_PHASE 1
   -fixed_pressure
   -pressure 4 #Experimental pCO2, bar (absolute)
   -volume 1
   -temperature 22
   CO2(g)    4
end
```

The aim of these runs was to investigate the theoretical equilibrium chemistry of the experiments, i.e. should the experiments run long enough, the fluid chemistry should be approximated by the results of these runs. Where minerals are included as “equilibrium phases” in the above runs, they will dissolve until the fluid is saturated with respect to the mineral in question (assuming enough mineral is present). This does not necessarily mean that

the system is at equilibrium, since as one mineral dissolves, another may be able to precipitate. Potential precipitates were identified based on the output mineral saturations as calculated by PHREEQC. Using the PHREEQC.dat database no additional mineral phases become saturated during the model runs for calcite, dolomite or quartz. However, model runs that included feldspar (those for the K-feldspar, plagioclase and sandstone experiments) indicate that at feldspar saturation, the systems are oversaturated with respect to Ca-montmorillonite, gibbsite, k-mica, quartz and kaolinite. Therefor a true equilibrium model would include these minerals as equilibrium phases, allowing them to precipitate from solution. However, inclusion of these phases as precipitates in the models was found to lead to complete dissolution of the original feldspar phases, components of which are re-precipitated as quartz and K-mica. This also results in rise in the predicted pH of the final fluids (by around 1-2 pH units). Such models clearly do not mimic the results of the experiments presented here: while some minor pitting of the feldspar was observed, large scale dissolution was not a feature of the, relatively short term, runs presented here. Evidently these inconsistencies are due to the fact that while PHREEQC assumes instant equilibration in the above models, experiments are likely to be kinetically limited, either due to the dissolution rate of the primary phases or precipitation rate of the secondary phases.

Experimental results presented here, in terms of pH, fluid composition and $CO_2$ solubility tend to fit the results of models run as detailed above, without the inclusion of secondary phases, much more closely than those where secondary phases are included. Hence the model “equilibrium” values for pH and $CO_2$ solubility presented in the remainder of this thesis represent the values expected of a fluid saturated with respect to the primary mineral of interest, rather than full equilibrium. A more rigorous modelling approach might include precipitation rates for the phases in question, but given such rates are notoriously difficult to measure with accuracy, such an approach would have come with an additional layer of problems and was outwith the scope of this project. In the case of the results presented here comparison with a model assuming primary mineral saturation and limited precipitation seems justified and useful, given the available results.

The final type of modelling carried out using PHREEQC was of the measured fluid chemistry of samples. This was designed to allow assessment of mineral saturation indices and speciation at the sampling points during the experiments. Analyte data was input as molar concentrations following the

initial data corrections for dilution, density etc. as described in Section 3.4.1, along with volume of fluid remaining in the experimental vessel at the sampling point and the experimental temperature and $pCO_2$. Little other data manipulation was required for the model inputs, other than for the sodium and chloride concentrations which were not directly measured. Chloride was assumed to have zero concentration in the deionised water experiments and a concentration of 1.36M in the brine based experiments. Sodium concentrations were more difficult to estimate, given the sodium present in the feldspars used. For the K-feldspar experiments, estimates were made of the K:Na ratio observed during experiments carried out by Jorgen Rosenqvist at the British Geological Survey, under similar conditions and using the same material, but with measurements of Na in solution. A polynomial was fitted to a curve of K/Na and used to extrapolate an estimate of Na concentration for given concentrations of K. No such data was available for the plagioclase experiments, hence in the case of these experiments an estimate of Na in solution was made based on Si concentrations and assuming that Na was release stoichiometrically with Si.

Evidently such estimates are subject to large uncertainties. These will have little impact on the brine experiments where sodium concentrations are already far in excess of anything likely to be released through mineral dissolution, but will have more impact on the results of models of the deionised water experiments. Charge balance output from PHREEQC suggests that the error on solution charge (calculated as 100 * (sum of cations – sum of anions) / (sum of cations + sum of anions)) for the deionised water samples from the feldspar experiments is as high as 20 - 30% for some of the solution inputs. These estimates are however necessary in order to allow such models to converge and produce a realistic solution. In hindsight a more satisfactory solution may have been to allow PHREEQC to add Na to achieve perfect charge balance, though this appears to make little difference to the outputs of interest (saturation indices, pH etc.) presented here.

An example input for a sample taken from a K-feldspar experiment is presented below:

```
DATABASE C:\phreeqc\database\phreeqc.dat

Selected_output #Selected output to be written to output file, including saturation indices, species required for affinity calculations etc
```

```
  -file       171.prn
  -state false
  -solution false
  -reaction false
  -simulation false
  -time false
  -step false
  -distance false
  -pe false
  -pH
  -alkalinity
  -totals   C(4) Al Ca Si K
  -saturation_indices          Al(OH)3(a) Albite Anorthite Ca-Montmorillonite Chalcedony Fe(OH)3(a) Gibbsite
Goethite Hematite Illite K-feldspar K-Mica Kaolinite Quartz SiO2(a) Boehmite Diaspore
  -activities          Na+ Al+3 Ca+2 K+ H4SiO4 Al(OH)4- H+
  -molalities          CO2
SOLUTION 1 #       0.00        at atmospheric #Sample taken before addition of CO2
   temp    22
   pH      7
   pe      4
   redox    pe
   units    mol/kgw
   Na      1.36
   Cl      1.36

Mg         9.83E-06 #Measured elemental concentrations, moles/l
Al         9.34E-07
Si         7.05E-06
K          0.00E+00
Ca         9.58E-05
Mn         4.36E-07
Fe         1.44E-07
Sr         5.15E-07
Ba         1.95E-06
Na         1.36E+00

   -water  1.05E-01  # Fluid in vessel, kg

GAS_PHASE 1
   -fixed_pressure
   -pressure          0.00036 #Atmospheric CO2 pressure, bar
   -volume 1
   -temperature       22          #Experimental temperature, celsius
   CO2(g) 0.00036

END
```

```
SOLUTION 1 #       0.00        #Sample taken at time zero: addition of pCO2
   temp    22
   pH      7
   pe      4
   redox   pe
   units   mol/kgw
   Na      1.36
   Cl      1.36

Mg         9.83E-06 #Measured elemental concentrations, moles/l
Al         9.34E-07
Si         7.05E-06
K          0.00E+00
Ca         9.58E-05
Mn         4.36E-07
Fe         1.44E-07
Sr         5.15E-07
Ba         1.95E-06
Na         1.36E+00          #Estimated Na concentration
   -water  1.05E-01

GAS_PHASE 1
   -fixed_pressure
   -pressure          4          #Experimental CO2 pressure, bar
   -volume 1
   -temperature       22
   CO2(g)4

END
```

The above file takes the analysed solution composition of a sample (in this case the sample taken prior to addition of $CO_2$ and the sample taken immediately following pressurisation), applies the experimental $CO_2$ pressure and temperature to it and speciates the elemental concentrations accordingly, also generating saturation indices for phases available in the databases. This procedure also gives an idea of in-situ pH, which in this case will be calculated based on the alkalinity generated by $CO_2$ dissolution, rather than a charge balance.

Additional work was undertaken to model the sandstone experiments , with the inclusion of dissolution kinetics. An example input from one of these runs is on the following pages:

```
DATABASE C:\phreeqc\database\llnl_CO2.dat

selected_output #Removed, but as for previous input files
SOLUTION 1 #Fluid composition measured prior to addition of pCO2
    temp      22
    pressure 4
    pe        4
    redox     pe
    units     mol/kgw
    density   1
Na      1.36
Cl      1.36
Mg          0.000199294
Al          2.3634E-07
Si          1.7937E-05
K           0.000104329
Ca          0.001295212
Mn          8.01292E-07
Fe          0
Sr          2.3387E-06
Ba          6.08872E-07
Alkalinity  0.001295212
Water       0.10439 kg

GAS_PHASE 1
    -fixed_pressure
    -pressure          4
    -volume 1
    -temperature       22
    CO2(g) 4


 Equilibrium_Phases 1-8 #Phases which become oversaturated during the model run
 Beidellite-Ca      0          0
 Beidellite-H       0          0
 Beidellite-K       0          0
 Beidellite-Mg      0          0
 Beidellite-Na      0          0
 Boehmite           0          0
```

```
Corundum        0       0
Dawsonite       0       0
Diaspore 0      0
Gibbsite  0     0
Illite    0     0
Kaolinite 0     0
Mesolite  0     0
Montmor-Ca      0       0
Montmor-K       0       0
Montmor-Mg      0       0
Montmor-Na      0       0
Muscovite       0       0
Paragonite      0       0
Stilbite  0     0

Albite    0     0
Quartz    0     0
Dolomite  0     0
K-feldspar      0       0
#Illite   0     0

Rates 1 #Rates input in BASIC format using formula and values from the USGS Compilation of Rate Parameters
  Quartz
   -start
   10 dif_temp =  (1/TK) - (1/298.15)       #T expression in the rate equation, defined as parameter dif_temp
   20 neutral_rate = ((10^-13.99)*2.718^((-87.6/8.3145)*dif_temp)*(1-(10^SI("Quartz"))))
   30 base_rate = ((10^-16.29)*2.718^((-83/8.3145)*dif_temp)*(ACT("H+"))^-0.5 * (1-(10^SI("Quartz"))))
   40 rate = ( neutral_rate + base_rate )       #using general rate equation from USGS (2004) and values therein:
Knauss and Worley Ea for qtz
   50 moles = parm(1) * rate
   60 save moles * time
   -end

  Dolomite
   -start
   10 dif_temp =  (1/TK) - (1/298.15)       #T expression in the rate equation, defined as parameter dif_temp
   20 acid_rate = ((10^-3.19)*2.718^((-36.1/8.3145)*dif_temp)*(ACT("H+"))^0.5 * (1-(10^SI("Dolomite"))))
   30 neutral_rate = ((10^-7.53)*2.718^((-52.2/8.3145)*dif_temp)*(1-(10^SI("Dolomite"))))
   40 base_rate = ((10^-5.11)*2.718^((-34.8/8.3145)*dif_temp)*(ACT("H+"))^0.5 * (1-(10^SI("Dolomite"))))
   50 rate = ( acid_rate + neutral_rate + base_rate )       #using general rate equation from USGS (2004) and values
therein
   60 moles = parm(1) * rate
   70 save moles * time
   -end

   Albite
    -start
```

```
    10 dif_temp =  (1/TK) - (1/298.15)       #T expression in the rate equation, defined as parameter dif_temp
    20 acid_rate = ((10^-10.16)*2.718^((-65/8.3145)*dif_temp)*(ACT("H+"))^0.457 * (1-(10^SI("Albite"))))
    30 neutral_rate = ((10^-12.56)*2.718^((-69.8/8.3145)*dif_temp)*(1-(10^SI("Albite"))))
    40 base_rate = ((10^-15.6)*2.718^((-71/8.3145)*dif_temp)*(ACT("H+"))^(-0.572) * (1-
(10^(SI(("Albite"))))^0.76)^90)
    50 rate = ( acid_rate + neutral_rate + base_rate )       #using general rate equation from USGS (2004) and
values therein
    60 moles = parm(1) * rate
    70 save moles * time
    -end


  K-Feldspar
   -start
   10 dif_temp =  (1/TK) - (1/298.15)       #T expression in the rate equation, defined as parameter dif_temp
   20 acid_rate = ((10^-10.06)*2.718^((-51.7/8.3145)*dif_temp)*(ACT("H+"))^0.5 * (1-(10^SI("k-feldspar"))))
   30 neutral_rate = ((10^-12.41)*2.718^((-38/8.3145)*dif_temp)*(1-(10^SI("k-feldspar"))))
   40 base_rate = ((10^-21.2)*2.718^((-94.1/8.3145)*dif_temp)*(ACT("H+"))^-0.823 * (1-(10^SI("k-feldspar"))))
   50 rate =( acid_rate + neutral_rate + base_rate )       #using general rate equation from USGS (2004) and values
therein
   60 moles = parm(1) * rate
   70 save moles * time
   -end


    # Illite
    # -start
    # 10 acid_rate = 1.52E-5 * (2.718^(-40 / (8.3145 * TK))) * ((ACT("H+"))^0.592)
    # 20 neutral_rate = 1.29E-11 * (2.718^(-24 / (8.3145 * TK)))
    # 30 base_rate = 6.82E-7 * (2.718^(-33 / (8.3145 * TK))) * (ACT("OH-")^0.747)
    # 40 rate = ( acid_rate + neutral_rate + base_rate)
    # #40 rate = acid_rate
    # 50 moles = parm(1) * rate
    # 60 save moles * time
    # -end


KINETICS 1
 -steps 90 day in 90
 Quartz
     -formula  SiO2  1
     -m        0.530149 #number of moles of mineral in experiment
     -m0       0.530149
     -parms  3.698799068 #parm(1) is the actual mineral surface area in the experiment, m2
 Dolomite
     -formula CaMg(CO3)2 1
     -m       0.017359778
     -m0      0.017359778
     -parms 0.3717386
```

```
K-feldspar
    -formula KAlSi3O8 1
    -m       0.0082
    -m0      0.0082
    -parms 1.338258959

 Albite
     -formula NaAlSi3O8 1
     -m       0.009006333
     -m0      0.009006333
     -parms 0.275086564

  # Illite
 # -formula K0.6Mg0.25Al1.8Al0.5Si3.5O10(OH)2 1
 # -m 0.003535448
 # -m0 0.003535448
 # -parms 0.159847598

-bad_step_max 1000

INCREMENTAL_REACTIONS true #Each new timestep will use the output chemistry from the previous

    USER_PUNCH #Allows output of mineral amounts remaining
 -headings Quartz Dolomite K-Feldspar Albite Illite
 -start
 10 mQuartz = KIN("Quartz")
 20 mDolomite = KIN("Dolomite")
 30 mkfeldspar = KIN("K-Feldspar")
 40 mAlbite = KIN("Albite")
 50 mIllite = KIN("Illite")
 60 punch mQuartz
 70 punch mDolomite
 80 punch mkfeldspar
 90 punch mAlbite
 100 punch mIllite
 -end
```

The above model input takes an initial fluid composition and reacts it, at experimental $pCO_2$ and temperature, with the estimated number of moles of each mineral in the experiment (based on the assumed bulk composition of the sandstone). Primary minerals are allowed to dissolve at the rates specified by the equations and constants given in the USGS Compilation of Rate Parameters (2004). Possible secondary precipitate phases were added to some runs under the equilibrium phases data block (as above), though the main precipitate predicted was Dawsonite and inclusion of this phase made

little difference to the predicted fluid chemistries (see Section 5.1.5 for further details). In this case precipitation rates were not input for secondary minerals, hence any mineral becoming oversaturated was allowed to precipitate instantly at the end of each time-step (in this case every 24 hours of model time).

A similar approach was taken to model the flow-through experiment carried out on a sandstone core (see Section 5.2 for details). The same dissolution rates were used, but a Transport data block was added:

```
TRANSPORT
   -cells               8
   -length              0.005 #Length of each cell in model column, m
   -shifts              1385 #Total number of time steps
   -time_step           1560 # A “shift” of fluid from one cell to the next will occur at the end of every time period of
this length (seconds)
   -boundary_conditions   flux flux #Inlet and outlet b/cs set to flux to allow mass transport
   -punch_cells   1 2 3 4 5 6 7 8 #Specify output for each cell
   -correct_disp true
```

This input will move a parcel of fluid a specified cell length every time step, allow it to react with the minerals present (at the rates specified above) and then move the resulting fluid into the next cell and so on. The input fluid is specified by inputting a “Solution 0”:

```
SOLUTION 0
   temp      70
   pressure 31
   pH       7 charge
   pe       4
   redox     pe
   units     mol/kgw
   density   1
Na 1.36
Cl 1.36
```

And the solution originally inhabiting the column is specified by a data block of the form:

```
SOLUTION 1-8 #Solution in cells 1-8 of the column
   temp      70 #Column temperature
   pressure 31 #Column pressure
   pH       7 Charge #pH is adjusted to achieve charge balance
   pe       4
   redox     pe
   units     mol/kgw
   density   1
Na 1.36
```

```
Cl 1.36
water 0.010387 litres #litres of water in each cell
```

The above kinetic models were designed to provide an immediate comparison between the results of the experimental work detailed in this thesis and the kind of general rate equations (exampled here by those produced by the USGS), often used in predictive modelling of such systems at larger scales.

The other modelling work presented in this thesis was designed largely to provide theoretical fluid chemistries at mineral saturation, with which to compare to experimental results, and to investigate the saturation state and in-situ pH of analysed fluids. Comparisons with modelled results will be made elsewhere in Chapters 4 and 5 of this work, but while doing this it is worth bearing the limitations of this approach in mind, in both the “equilibrium” and the kinetic models detailed above.

Such models are largely limited by the quality of the database used. PHREEQC and other mass-balance type models (as opposed to models which work on the basis of minimising Gibbs Free Energy) rely largely on the equilibrium constants and their associated temperature dependencies present in the database and the method used for calculating the activity of species in solution. The database PHREEQC.dat was largely relied upon in this work as the thermodynamic data present, although limited, is considered to be relatively reliable and consistent. The LLNL.dat database was also used in parts of this work, but due to the large amounts of data present in this database, its quality and consistency may be considered less reliable. Additionally the LLNL.dat database does not contain the data necessary to calculate $CO_2$ partial pressures (Rosenqvist et al. 2012), although where this database has been used, the necessary data has been appended to the database. Despite the above caveats, it is assumed that the thermodynamic data in these databases is of good quality for pure mineral phases, and discrepancies are more likely to arise due to comparison between the pure phases listed in the databases and natural samples, which are unlikely to be completely “pure” chemically.

A greater limitation of the available databases is their inability to accurately model the activity of species in solutions of “high” ionic strength. Using LLNL.dat and PHREEQC.dat will result in activities being calculated using an extended Debye Huckel approach (Parkhurst & Appelo 2013). The terms used in the calculation have been fit using “chloride mean-salt activity coefficient data”, meaning that some non-ideality of the solution is accounted

for and the model may be reasonable at “higher” ionic strengths, particularly where the system is NaCl dominated. What “higher” means in this context is difficult to judge, but it is generally assumed that the model will produce reasonably accurate activites at strengths of up to 0.1M. At strengths of 0.1-1M, the model may produce reasonable results, but is unlikely to be accurate, the discrepancies growing larger as ionic strength increases. Ideally an ion specific interaction approach should be used for calculating activities at higher ionic strengths, the Pitzer activity model for example (Crowe & Longstaffe 1987). However, the major limitation of this approach at present is the lack of available data required to carry out these calculations using aluminosilicate minerals. The Pitzer.dat database which comes with PHREEQC3 for example, lacks data for either Si or Al species. Hence the modelling in this work, for the experiments carried out in 1.36M NaCl brine cannot not be relied upon in detail and while useful as a comparative tool, the limitations of this modelling should be borne in mind.

The kinetic modelling presented here also suffers from the same short-comings described above with the added uncertainties inherent in estimations of mineral quantities and surface areas, which are issues in all calculations related to mineral dissolution and are discussed in more detail in Chapters 5 and 6 of this work.

Despite this such model calculations remain a useful tool in enhancing experimental investigations, such as those presented here, and an essential one in predictions of natural systems and are considered as fit for purpose, as far as their usage in this work goes, as long as their limitations are borne in mind.

A complete listing of the fluid chemistry data used in modelling and dissolution rate calculations is provided in Appendix A.

### 3.4.3 Errors and Uncertainties

Four main types of experimental results are presented in the following work:

1) pH measurements;
2) Dissolved $CO_2$ content of fluids;
3) Elemental concentrations in fluids;
4) Mineral dissolution rates derived from elemental concentrations.

Probes were calibrated before and after pH measurements were made on experimental fluids, so “at the point” pH measurements are assumed to be accurate within 0.1 pH units. Measurements were made external to the experiments, essentially in a flow through cell. In order to flow fluid into the cell, there is necessarily a pressure drop across the system. Likewise there may have been a drop in temperature as fluids from the “hot” (70°C) experiments flowed into the cell. Care was taken to bleed fluids slowly, so as to minimise any pressure gradients arising, however some pressure drop was inevitable. Such a drop will allow $CO_2$ degas, causing the pH in the fluid to rise. Conversely, any drop in temperature would raise the $CO_2$ solubility of the fluid. Unlike in the experiment however, free $CO_2$ was not available within the pH cell, so this was unlikely to have any effect. Degassing of $CO_2$ however was impossible to quantify given the experimental set-up. However, according to PHREEQC calculations, a pressure drop from 31 bar to 15 bar would cause a change in pH from 3.35 to 3.50. Likewise a drop from 4 bar to 2 bar would cause a rise in pH from 3.77 to 3.92. A pressure drop of this magnitude would have been unlikely with the experimental set-up, hence we may reasonably assume that pH measurements reflected the pH of the experimental fluid within 0.5 pH units.

Similar uncertainties arise when considering the values of dissolved $CO_2$ measured. Fluids were samples into NaOH in order to “fix” dissolved $CO_2$, but degassing from some samples was unavoidable. While measurements (made by titration, see Section 3.2.2) on the final samples are assessed to be accurate within 3% (Rosenqvist et al. 2012), when applied to the in-situ experimental fluids, error may be considerably higher (i.e. through sampling error). In order to assess this error multiple samples were taken for solubility where possible (i.e. where there was enough fluid left at the end of the experiment). Standard deviations were calculated for these groups of samples. Deviation was found to be within 10% for the majority of samples.

Standard deviation is presented for individual sets of samples in Sections 4.1 and 5.1.

In order to minimise error in the calculation of dissolved analyte concentrations (and $CO_2$ content) All dilutions and density corrections made to reported elemental concentrations were made using results from a five point balance, rather than relying on volumetric measurements from pipettes etc., greatly reducing experimental error.

The fact that elemental concentrations were measured using different analysts at different times, means that assigning an overall error on dissolved concentrations for the whole dataset is difficult. Analytical precision for each run was monitored by submitting duplicate reference materials for analysis along with the samples. These reference fluids, of known analyte concentration, were prepared as per the samples. Analytical precision has been estimated by calculating the standard deviation between these duplicate samples for each run. This data is presented along with the fluid chemistry data in Appendix A.

The greater error in the chemical data presented comes from random, or sampling errors. This was assessed by taking duplicate samples from the experiments, rough one duplicate for every ten samples taken. These duplicates were prepared and submitted along with the other experimental samples. Based on these duplicates a percentage error (which should in theory include analytical and sampling error) has been calculated on a run by run basis for each analyte used in the calculation of mineral dissolution rates (i.e. error calculated for Ca in the calcite runs, Si in the quartz runs, etc.) and are again presented along with the fluid chemistry data in Appendix A. This error varies greatly depending on the analytical run, but at all times is below 25%, which is considered to be the maximal error on the fluid chemistry data presented here. These errors re illustrated in Figures 4.1.4, 4.1.5, 4.1.7 and 4.1.8 for a selection of the quartz experimental data in Section 4.1.1.

The error in the final calculations of mineral dissolution rates is more difficult to establish. The major errors in this calculation come from analytical uncertainty and the measurement of surface area though the contribution of error from minor variations in the analytical data has been avoided by using the data-smoothing technique described in Section 3.4.1. As discussed in Section 2.1.1.3, an accurate measurement of “reactive” surface area, is difficult to decide upon, but in this work it was decided that surface area as measured by BET would be the standard upon which calculations were

based. In this case, repeat measurements of surface area suggest that the measurements are accurate to within 15% for all samples. Since surface area was not remeasured after the experiments, these measurements necessarily assume that surface area does not change significantly during the experiments, which is not always the case (Stillings & Brantley 1995), though given available SEM evidence, and the relatively short duration of the experiments, this assumption is not without warrant. Assuming very minor contributions to error from measurements of time and fluid volumes (<1%), a reasonable maximum error on calculated mineral dissolution is likely to ±50%, as demonstrated in Figures 4.1.9 – 4.1.12 in Section 4.1.1 for selected quartz dissolution rate data.

# Chapter 4
# Mineral Dissolution Experiments

## 4.1 Silicate Minerals

### 4.1.1 Quartz

#### 4.1.1.1 pH and $CO_2$ Solubility

Six batch experiments were carried out on powdered quartz material (described in Section 3.1.1), the conditions and are summarised in Table 4.1.1.

| Experiment ID | Grain Fraction, µm | Fluid | pCO2, bar (absolute) | Temperature, $^0$C | Run time, volume constant hours | Conditioning period prior to $CO_2$ injection, hours |
|---|---|---|---|---|---|---|
| 121 | 125-180 | 1.36M NaCl | 4 | 22 | 804 | 52 |
| 124 | 125-180 | 1.36M NaCl | 31 | 70 | 1083 | 215 |
| 125 | 125-180 | DI | 4 | 22 | 2685 | 707 |
| 126 | 125-180 | DI | 31 | 70 | 900 | 226 |

**Table 4.1.1**: Summary of experimental conditions for Quartz batch experiments

Figures showing full results of fluid pH calculations and measurements can be found in Appendix B, but selected results, showing measured pH where available, equilibrium pH as calculated by PHREEQC3 and final sample pH as calculated by PHREEQC are shown in Table 4.1.2 which also summarises calculations and measurements of dissolved $CO_2$ content from the batch experiments.

| Run | Fluid/p $CO_2$ (bar)/T(° C) | Equilibrium $CO_2$ PHREEQC3, mol/kg | Final Sample $CO_2$ PHREEQC3, mol/kg | Final Sample $CO_2$ (Measured), mol/kg | Standard Deviation, $CO_2$ (No. of measurements) | Equilibrium pH, PHREEQC3 | Final Sample pH, PHREEEC3 | Final Sample pH, measured |
|---|---|---|---|---|---|---|---|---|
| 121 | NaCl/4/22 | 0.107 | 0.107 | 0.106 | 0.002 (4) | 3.529 | 3.619 | 3.738 |
| 124 | NaCl/31/70 | 0.292 | 0.292 | 0.280 | 0.004 (5) | 3.290 | 3.544 | - |
| 125 | DI/4/22 | 0.146 | 0.146 | - | - | 3.602 | 3.609 | - |
| 126 | DI/31/70 | 0.399 | 0.399 | - | - | 3.352 | 3.608 | - |

**Table 4.1.2**: Summary of pH and $CO_2$ solubility measurements and calculations for Quartz batch experiments

The full results from PHREEQC3 calculations performed on analysed fluid compositions indicate an initial, pre-$CO_2$ injection pH of between 5.59 to 6.12, close to predicted equilibrium range of 5.55 to 5.95. Upon addition of $CO_2$ pH falls rapidly to values close to the respective pure, mineral-free solutions at the same $pCO_2$. Calculated pH ranges from 3.35 to 3.60, while equilibrium pH for the pure fluid ranges from 3.29 to 3.60. This typical response to addition of $CO_2$ is illustrated in Figure 4.1.1, which shows the calculated pH for samples from experiment 121.

Quartz has negligible capacity to buffer $H^+$ and hence the predicted equilibrium pH of quartz-saturated fluids is equal to the equilibrium pH of quartz free fluids. This is reflected in the calculated pH from experiment 125 (Figure 4.1.2) which shows essentially no change over the course of the run. Results from the other three experiments indicate a slight initial rise in pH, such that final calculated and measured pH is above that expected for the equilibrium value of a pure quartz. In all cases this difference in calculated pH was inferred to be due to Fe-metal contaminants causing reduction, consuming $H^+$. Iron was in solution at levels of around $10^{-4}$mol/l in a number of experiments on all minerals and the sandstone material and was likely due to contamination from stainless steel parts used in the gas and sampling systems, which can breakdown rapidly when in contact with $CO_2$ saturated fluids or water saturated $CO_2$.

As for pH, dissolution of quartz should have little effect on $CO_2$ solubility and this is reflected in the calculated and measured $CO_2$ content of the samples (Table 4.1.2). Calculated dissolved $CO_2$ content based on final sample analyses are equal to the predicted equilibrium $CO_2$ content for the systems, which in turn are equal to the predicted equilibrium content of the pure, mineral free fluids. For the two experiments (121 and 124) where $CO_2$ content was measured, measured values agree closely (within 5%) with those predicted by PHREEQC3.

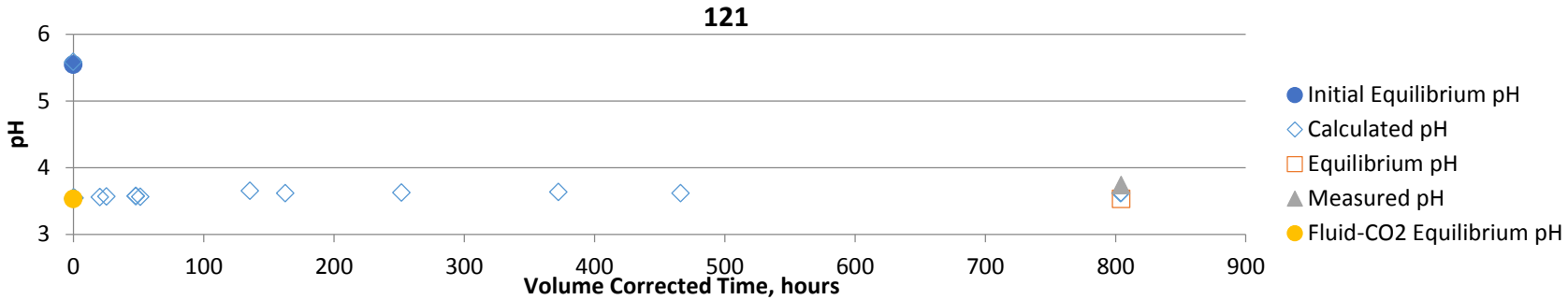


**Figure 4.1.1**: Calculated and measured pH values for experiment 121; calculations were carried out in PHREEQC3 and include pH of fluid samples based on elemental analysis and equilibrium pH

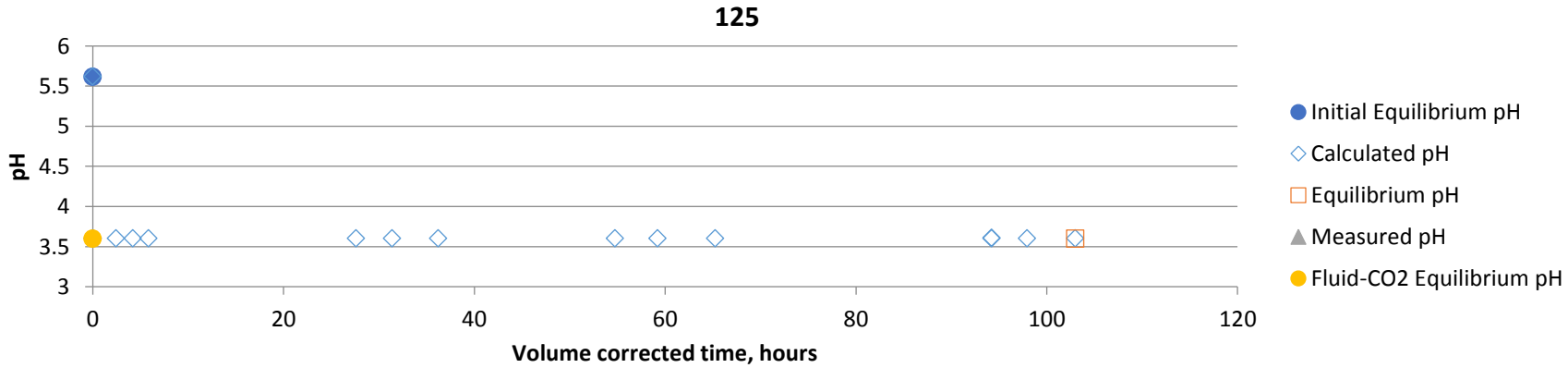


**Figure 4.1.2**: Calculated and measured pH values for experiment 125; calculations were carried out in PHREEQC3 and include pH of fluid samples based on elemental analysis and equilibrium pH

#### 4.1.1.2 Dissolution Behaviour: General Observations

All experiments show an increase in Si concentration (see Figures in Section 4.1.1.3). The two deionised water experiments (125 & 126) show a gradual increase over the whole course of the experiments, while 121 and 124 (conducted in 1.36M NaCl) show sharper increases in concentration initially, before plateauing. These two experiments plateaux at apparent quartz oversaturation, as illustrated in Figure 4.1.3, converging at an SI of around 0.2, while the two deionised experiments remain undersaturated with respect to quartz.

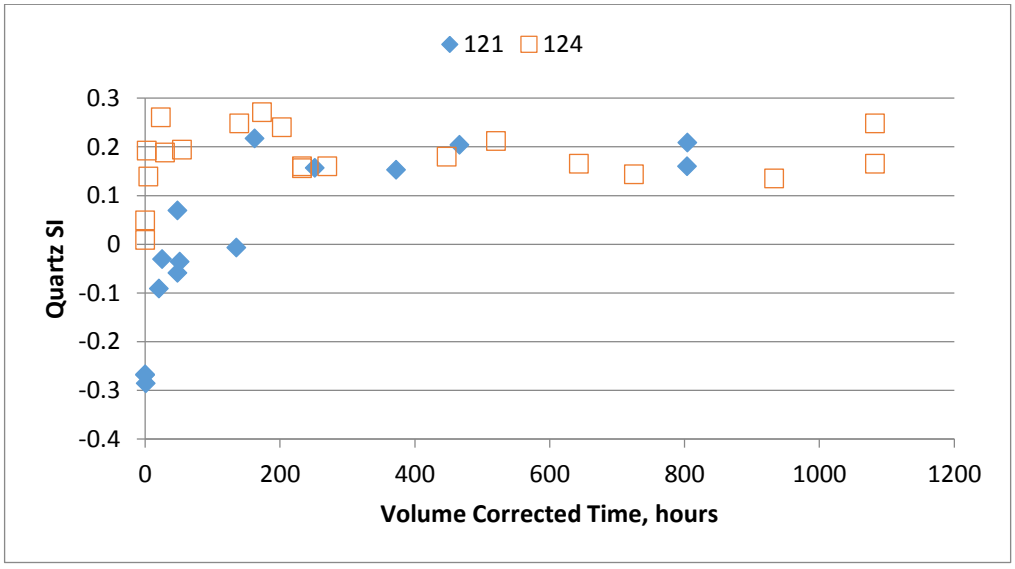


**Figure 4.1.3**: Quartz Saturation Indices for experiments 121 and 124

#### 4.1.1.3 Dissolution Behaviour: Fluid Composition

Figures 4.1.4 and 4.1.5 compare Si release from experiments 121 (1.36M NaCl, 4bar $pCO_2$, 22°C) and 125 (Deionised water, 4bar $pCO_2$, 22°C) and 124 (1.36M NaCl, 31bar $pCO_2$, 70°C) and 126 (Deionised water, 31bar $pCO_2$, 70°C). Figures 4.1.6 also compares calculated quartz dissolution rates for the experiments based on Si release and measured BET surface areas. Note that dissolution rates for experiment 124 could not be calculated since Si concentration plateaux almost immediately in that experiment.

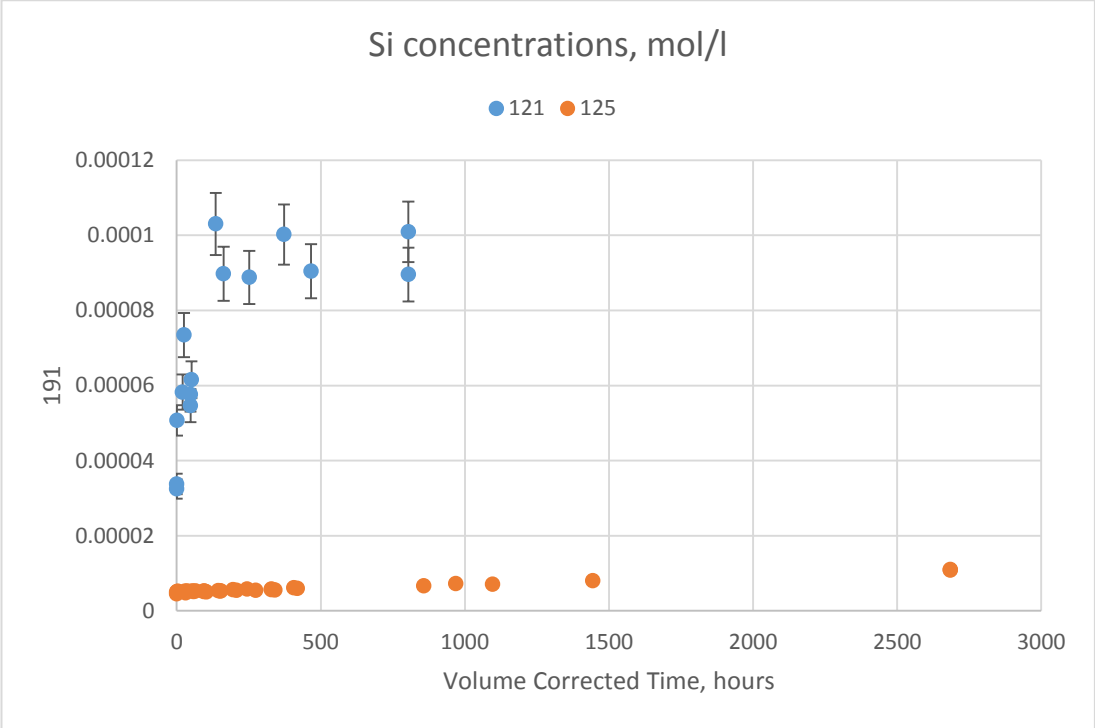


**Figure 4.1.4**: Si release from experiments 121 (NaCl) and 125 (DI)

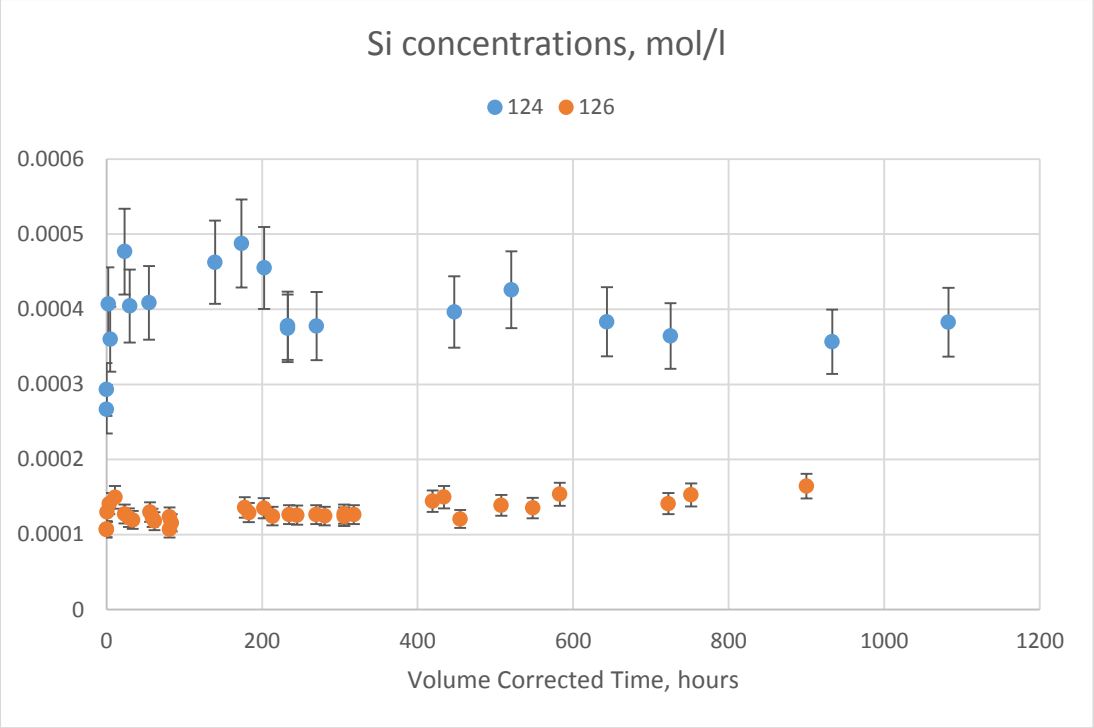


**Figure 4.1.5**: Si release from experiments 124 (NaCl) and 126 (DI)

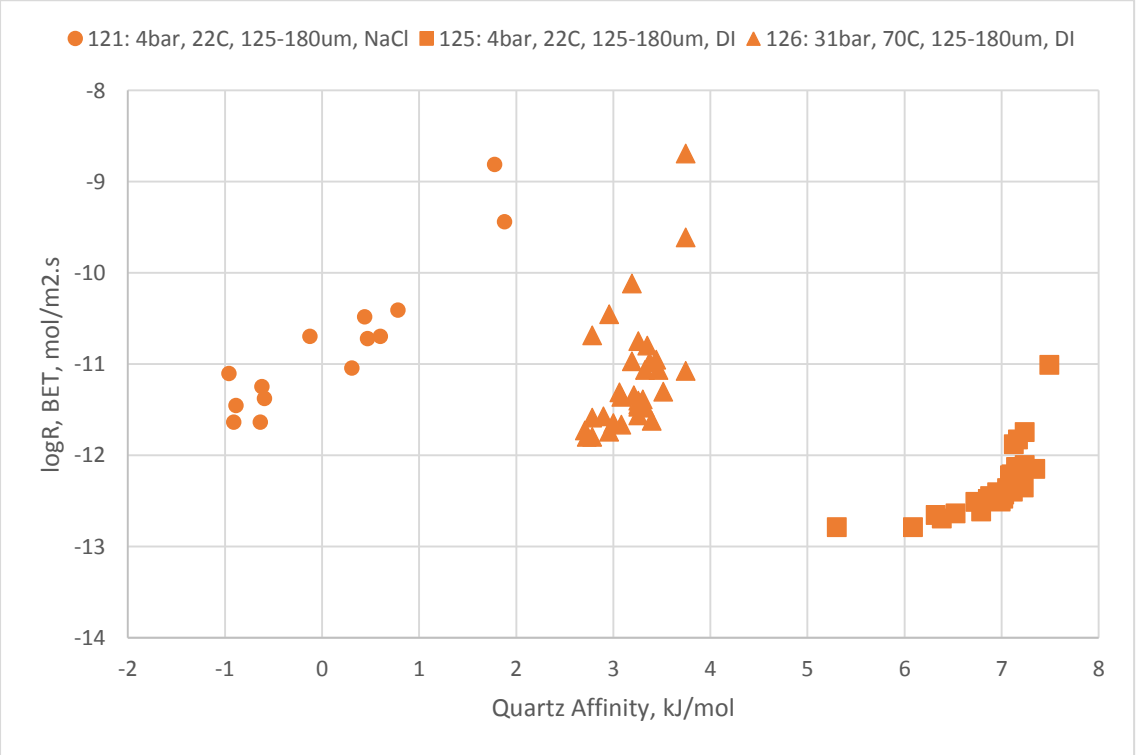


**Figure 4.1.6**: Calculated quartz dissolution rates and quartz affinities for experiments 121, 125 and 126

The effect of using NaCl solution as the fluid is striking. The two experiments carried out in 1.36M NaCl show a relatively sharp initial increase in dissolved Si, both plateauing after around 200 hours. Thereafter concentrations in experiment 121 appear reasonably steady, while those in 124 appear to decrease slightly over the remainder of the experiment. Dissolved Si in the deionised water experiments (125 and 126) increases steadily for the whole duration of the runs. Dissolved Si concentrations in the deionised water experiments remain well below the equilibrium values: final concentration in experiment 125 are around 9x below the predicted equilibrium concentration, while those in 126 are around 4x lower.

In contrast final Si concentrations in the NaCl experiments are higher than those predicted for equilibrium. This is presumably due to the fact that PHREEQC does not take into account any salting effect when calculating dissolved Si concentrations in NaCl bearing fluids (Newton & Manning 2000). Interestingly, the final Si concentrations measured in the NaCl experiments are very close to the predicted equilibrium concentrations for the equivalent deionised water systems.

In terms of dissolution rate , experiment 121, carried out using a NaCl fluid, clearly shows higher dissolution rates than those of its equivalent deionised water experiment (125). Rates in 121 are roughly equal to the deionised water experiment carried out at elevated pressure and temperature (126).

#### 4.1.1.4 Dissolution Behaviour: $pCO_2$ (4bar, 31bar) and temperature (22°C, 70°C)

Figures 4.1.7 and 4.1.8 compare Si release from experiments 121 (4bar $pCO_2$, 22°C, 1.36M NaCl) and 124 (31bar $pCO_2$, 22°C, 1.36M NaCl) and 125 (4bar $pCO_2$, 22°C, deionised water) and 126 (31bar $pCO_2$, 70°C, deionised water). Figure 4.1.6, presented in the previous section, shows calculated quartz dissolution rates and affinities for the experiments.

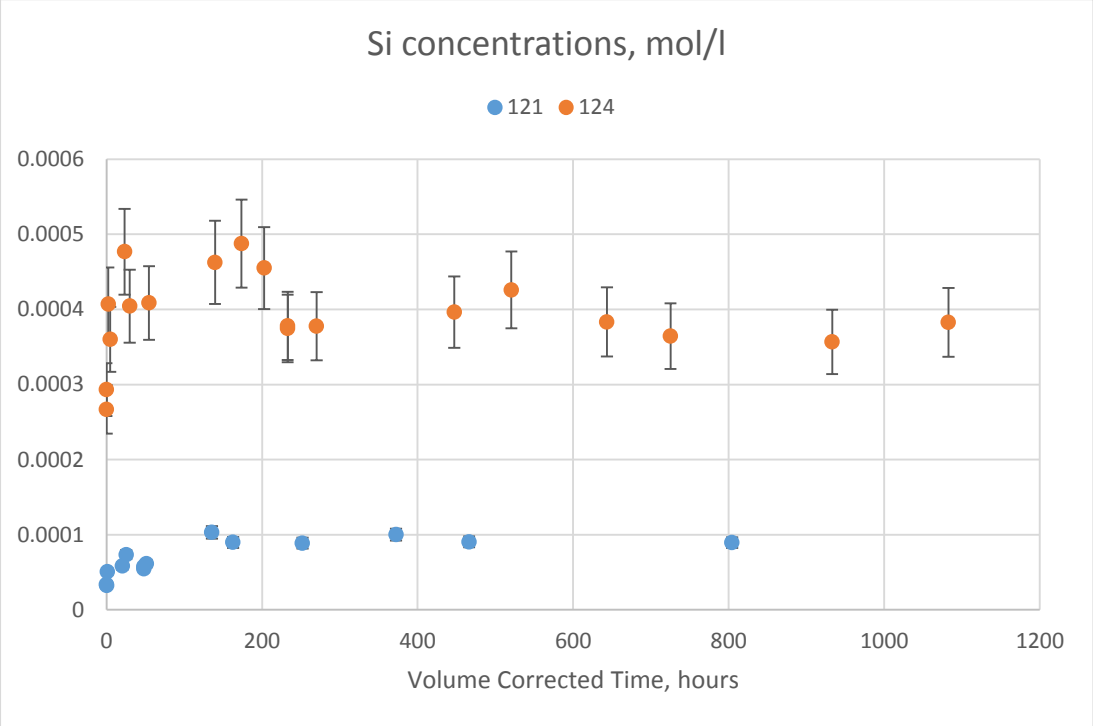


**Figure 4.1.7**: Si release from experiments 121 (4 bar, 22°C) and 124 (31 bar, 70°C)

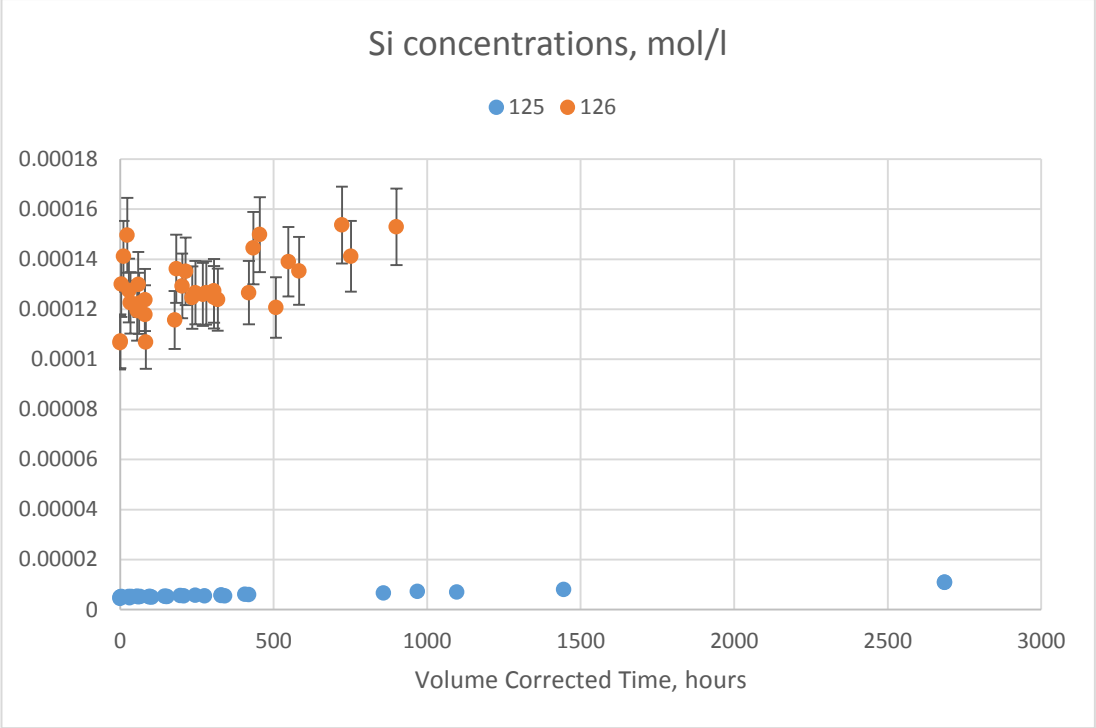


**Figure 4.1.8**: Si release from experiments 125 (4 bar, 22°C) and 126 (31 bar, 70°C)

Again the effect of increased pressure and temperature on quartz dissolution is striking: Si concentrations in the higher temperature/pressure experiments far exceed those measured in the low pressure/temperature experiments, even in experiment 124 where precipitation of silica has a strong effect on Si concentrations. Also of note is the fact that Si concentrations are already very high in the high temperature experiments even prior to $CO_2$ injection and actually change very little over the course of the experiments. This suggests that dissolution has occurred fairly rapidly even prior to addition of $CO_2$ (and hence acidity) and that temperature, rather than $pCO_2$ is the dominant factor in controlling this behaviour.

Direct comparison of dissolution rates from the two deionised water experiments (125 & 126) show that the elevated pressure and temperature enhanced quartz dissolution rates by around 1 – 1.5 orders of magnitude.

#### 4.1.1.5 Quartz Dissolution Rates

Quartz dissolution rates are plotted against quartz affinity in Figures 4.1.9 - 4.1.12. Also plotted are rates calculated using the USGS general rate equation (see Section 2.1.5 for details):

$$\frac{dm}{dt} = -SA\left[\begin{array}{l}\left(k_{acid}^{298.15K} e^{\frac{-E_{acid}}{R}\left(\frac{1}{T}-\frac{1}{298.15K}\right)} a_{H^+}^{n_1}(1-\Omega^{P_1})^{q_1}\right) \\ +\left(k_{neutral}^{298.15K} e^{\frac{-E_{neutral}}{R}\left(\frac{1}{T}-\frac{1}{298.15K}\right)}(1-\Omega^{P_2})^{q_2}\right) \\ +\left(k_{base}^{298.15K} e^{\frac{-E_{base}}{R}\left(\frac{1}{T}-\frac{1}{298.15K}\right)} a_{H^+}^{n_3}(1-\Omega^{P_3})^{q_3}\right)\end{array}\right] \quad (4.1.1)$$

using the published values of E, p, q and n therein. These data came from Tester et al (1994) using BET surface areas and Knauss and Worley (1988). Values for Ω were calculated using the saturation indices produced by PHREEQC3, based on measured analyte concentrations.

Rates are also plotted using the general equation of Tester et al (1995):

$$r_{net} = \frac{dm_{H_4SiO_4}}{dt} = k_f \frac{A_s}{M_w}\left(1 - \frac{m_{H_4SiO_4}}{m_{H_4SiO_4}^{sat}}\right) \quad (4.1.2)$$

Where A is the mineral surface area in $m^2$, M is the mass of water in the system in kg and k is a rate constant. Rate constants have been chosen from a variety of sources to fit experimental temperatures as closely as possible. For 22°C experiments, data from 23°C batch bottle experiments and 25°C packed bed experiments from Tester et al (1994) were used. For 70°C experiments, data from 70°C spinning basked experiments by Tester et al (1994) and shaking bottle experiments by Bennet (1991) were used. Calculated rates from these equations have also been plotted for Experiment 124, although no experimental rate was available due to the precipitation effects discussed above.

Quartz affinity has been calculated using the equation:

$$A = RT \times \ln\left(\frac{K_{Quartz}}{a_{H_4SiO_4}}\right) \quad (4.1.3)$$

Where $K_{Quartz}$ is the equilibrium constant for quartz at the experimental conditions, R is the gas constant, T is the temperature in Kelvin, and $a_{H_4SiO_4}^3$ is the activity of the appropriate ion in solution, as calculated by PHREEQC3 using the measured fluid compositions.

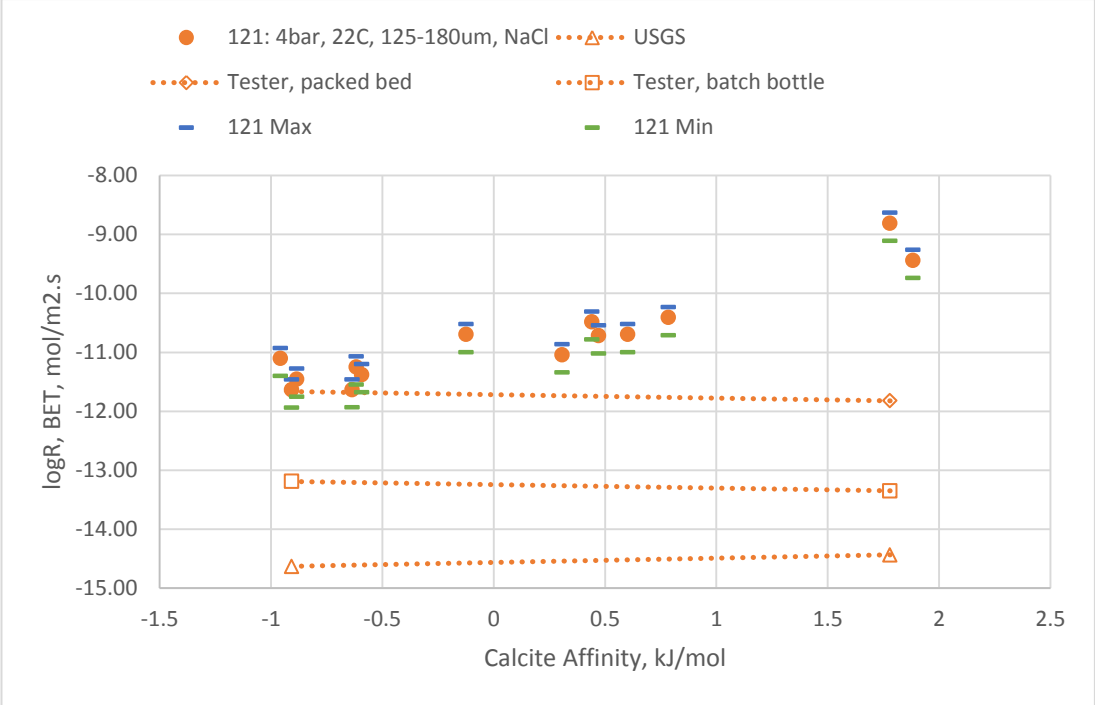


**Figure 4.1.9**: Calculated quartz dissolution rates for experiment 121, based on Si release and BET surface area. Also plotted are calculated rates based on literature equations.

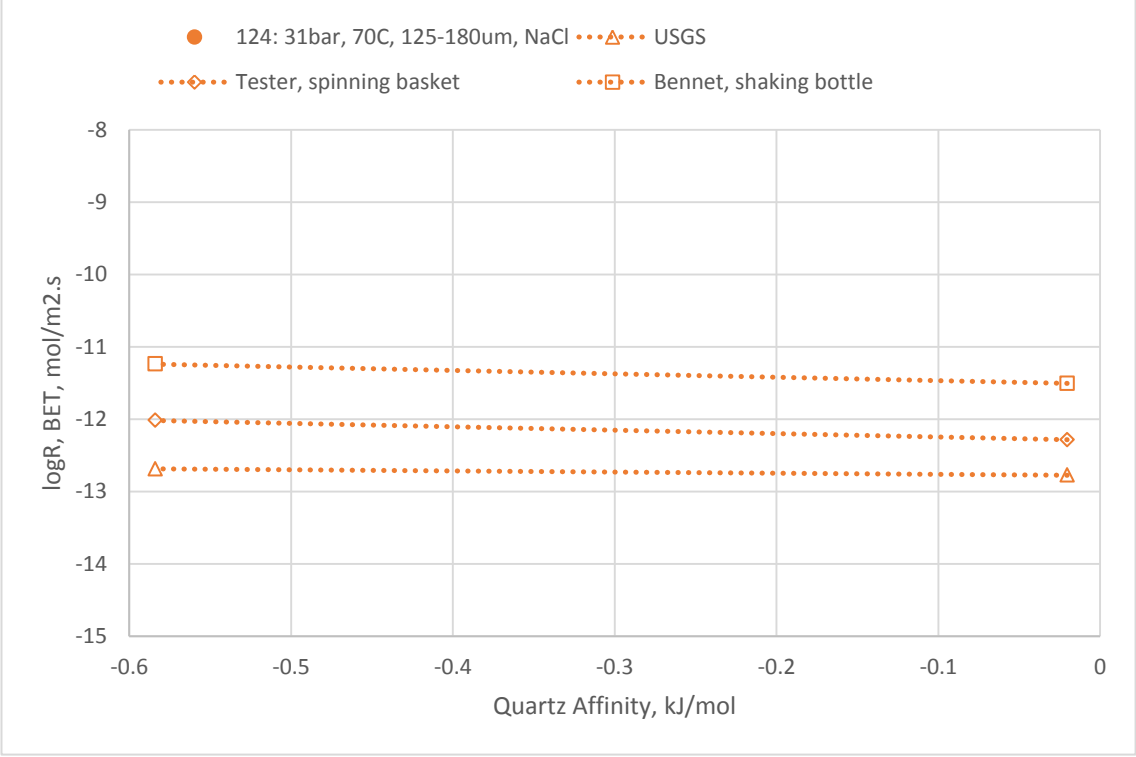


**Figure 4.1.10**: Calculated quartz dissolution rates for experiment 124, based on Si release and BET surface area. Also plotted are calculated rates based on literature equations.

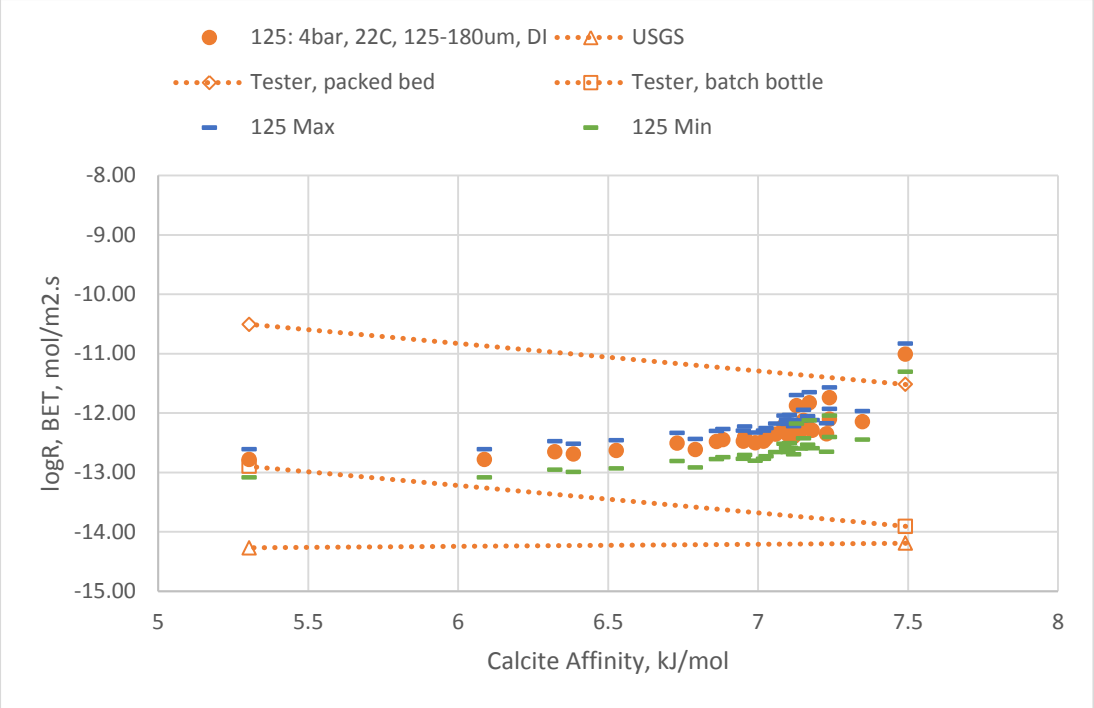


**Figure 4.1.11**: Calculated quartz dissolution rates for experiment 125, based on Si release and BET surface area. Also plotted are calculated rates based on literature equations.

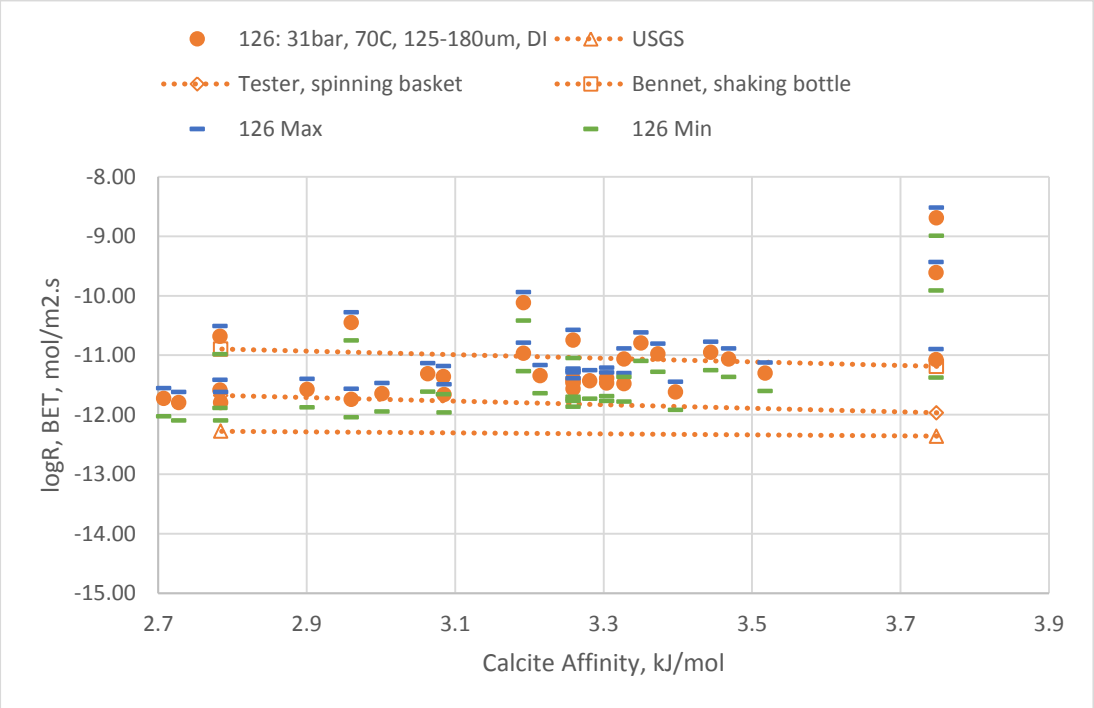


**Figure 4.1.12**: Calculated quartz dissolution rates for experiment 125, based on Si release and BET surface area. Also plotted are calculated rates based on literature equations.

Experimental rates agree reasonably well with the calculated rates. At late times, rates from experiment 121 approach those derived from the Tester packed bed experimental results, though they relatively high at earlier times and are considerably higher than those produced using the Tester batch bottle results or the USGS general rate equation. Late time rates from experiments 125 and 126 (the deionised water experiments) approach those produced using the data from Tester's batch bottle and spinning basket experiments, but again are considerably higher (5–15x) than those produced using the USGS general rate equation.

#### 4.1.1.6 Quartz Experiments Overview and Discussion

Results from measurements of dissolved $CO_2$ and pH in the quartz experiments agree well with model predictions and reflect the very low impact quartz dissolution will have during $CO_2$ injection into a sandstone reservoir. Quartz dissolution, as well as being slow compared to minerals such as carbonates has little effect on pH or on the overall solubility of $CO_2$ on short time scales. While quartz is a major constituent of sandstone reservoirs and is likely to enrich reservoir fluids in silica where it dissolves, other silicate minerals, such as feldspars, are likely to provide more soluble sources of Si and will have a larger impact on the overall chemical changes in the reservoir due to release of various other elements which may act to buffer $CO_2$ solubility and pH.

The addition of NaCl to the experimental matrix had a marked effect on overall Si concentrations in solution. It is well recorded in the literature that alkali cations can increase quartz dissolution rates in NaCl solutions (Blake & Walter 1999), though few results are available for solutions >1M NaCl, the results here follow the same trend: given the very high starting concentrations of Si (immediately prior to $CO_2$ addition) it is clear that even prior to injection, quartz is dissolving relatively rapidly in the NaCl experiments. The two NaCl experiments reach quartz saturation very soon after the experiments start, while those in DI remain very undersaturated w.r.t. quartz for the duration of the experiments. Final Si concentrations are slightly higher than those predicted at equilibrium, suggesting that the addition of NaCl may have a slight effect on quartz solubility. It has been suggested that increased dissolution rates of quartz in NaCl solutions is likely due to disruption of the quartz surface by Na and K cations, which have a high potential for adsorption (relative to other cations, such as Li or Mg) onto the quartz surface (Dove & Crerar 1990).

Calculated quartz dissolution rates are generally quite high compared to those calculated using literature equations, particularly in experiment 121 where quartz affinities are very low. It should also be noted that the quartz dissolution rates obtained from the packed bed and batch bottle experiments of Tester et al, values from which have been used in some of the comparisons above, were noted by the workers as being unusually high themselves. They suggest that, due to the low dissolution rate of quartz at low temperatures, these unusually high rates are due to lack of annealing on the quartz surface, i.e. high energy sites on the quartz surface persist for

longer (Tester et al. 1994). Hence the relatively high quartz dissolution rates observed here may be due to deviation from predictions on close approach to equilibrium, but more likely is that they are due to lack of proper surface preparation, leading to rates which might be considered applicable to fresh quartz surfaces, rather than the lower rates which might be expected in a reservoir setting, where mineral surfaces can be expected to be weathered and lacking in high energy sites.

### 4.1.2 K-Feldspar

Nine experiments were carried out on the alkali feldspar material (described in Section 3.1.2), and are summarised in Table 4.1.3. Three of these experiments were carried out as a test of the effect of different methods of stirring (111, 112, 113). While these three experiments were not designed in the same manner as the other dissolution experiments, the results are relevant in the broader context of K-feldspar dissolution and are used (for example measurements of dissolved $CO_2$ content, etc.) in the following sections. 111 was stirred with a magnetic bead in contact with the mineral powder, 112 was agitated by hand at intervals of c. 12-24 hours and 113 was left completely unstirred. Note that ICP data was not available for experiment 174 due to laboratory issues.

| Experiment ID | Grain Fraction, µm | Fluid | pCO2, bar (absolute) | Temperature, $^0$C | Run time, volume constant hours | Conditioning period prior to $CO_2$ injection, hours |
|---|---|---|---|---|---|---|
| 111 | 500-1000 | DI | 4 | 22 | 900 | 290 |
| 112 | 500-1000 | DI | 4 | 22 | 879 | 302 |
| 113 | 500-1000 | DI | 4 | 22 | 826 | 303 |
| 171 | 125-180 | 1.36M NaCl | 4 | 22 | 1687 | 266 |
| 172 | 500-600 | 1.36M NaCl | 4 | 22 | 1530 | 266 |
| 173 | 125-180 | DI | 4 | 22 | 1480 | 707 |
| 174 | 125-180 | 1.36M NaCl | 31 | 70 | | |
| 175 | 125-180 | 1.36M NaCl | 4 | 70 | 1740 | 219 |
| 176 | 125-180 | DI | 31 | 70 | 1539 | 220 |
| FCO2W10 | 250-500 | DI | 31 | 70 | 2029 | 146 |

**Table 4.1.3**: Summary of K-feldspar experiments

#### 4.1.2.1 pH and $CO_2$ Solubility

Measured and calculated (using PHREEQC3) values for dissolved $CO_2$ content and pH for final experimental samples are presented in Table 4.1.4. Initial (t-1) pH was between 5.6 and 6.5 for all experiments, the highest being for the mechanically stirred experiment, 111, whereas the predicted equilibrium pH for the $CO_2$ free fluids lay between 6.7 and 7.1, depending on experimental conditions. Upon addition of $CO_2$ (t0) calculated pH drops to levels near the predicted pH of the pure, mineral free, fluids under $pCO_2$. Predicted pH for the pure fluids at the applied $pCO_2$ lies between 3.4 and 3.7 depending on conditions, while calculated pH for the experiments at t0 lies between 3.4 and 3.8.

Calculated pH generally changes little during the course of the experiments, varying by only 0.1-0.2 pH units from the initial, t0, pH for the majority of experiments. The mechanically stirred experiment, as described earlier, is the exception to this. This is demonstrated in Figure 4.1.13, where calculated pH values for experiments 111 and 112 are compared. While experiment 112 is typical of the other K-feldspar experiments presented here, in that pH (as calculated using PHREEQC3, based on fluid compositions) varies very little over the course of the run, in experiment 111 there is a pH increase of around 1 pH unit in the first 100 volume constant hours, after which pH remains reasonably constant.

Where pH measurements of final fluid were taken (111, 171, 172, 173) they are in good agreement with the calculated pH based on final fluid composition (Table 4.1.4). The exception is 173, where the measured value is around 0.4 pH units above that of the calculated value. The final calculated pH for all experiments aside from 111 lies between 3.4 and 3.8. All of the measured and calculated final fluid pH values are significantly below the predicted equilibrium pH values for the experiments which lie between 4.4 and 5.7.

Calculated dissolved $CO_2$ concentrations of the final fluids, based on their composition, are generally close to the predicted equilibrium concentrations for the systems: all lie within 0.01 mol/kg of the equilibrium values (Table 4.1.4), with the exception of 171 and 172. For these two experiments, calculated $CO_2$ concentration is around 0.05 mol/kg below the equilibrium value. Dissolved $CO_2$ concentrations were measured for final fluids from 111, 171, 172, 173 and 176 and are generally within 0.03 mol/kg of the calculated concentrations, again with the exception of concentrations

measured in 171 and 172, which are around 0.44 mol/kg below the calculated value. Inspection of PHREEQC output for experiments 171 and 172 indicate that the difference between the computed $CO_2$ concentration of the final sample and the equilibrium concentration is largely due to sodium and calcium bicarbonate ($NaHCO_3$/$CaHCO_3$), which are present in relatively high concentrations in the equilibrium calculations (1E-2 mol/l and 2E-3 mol respectively) but are at relatively low concentrations (1E-4 and 8E-8) in the final sample calculations. Part of the discrepancy probably lies in the use of pure anorthite, pure albite, pure K-feldspar in the equilibrium calculations with no correction for actual activities in the solid phase. The discrepancy between the measured concentration and the calculated final concentration in the brine experiments (171, 172 and 176) may be due to precipitation of sodium bicarbonate  from fluid samples during or after depressurisation.

| Run | Fluid/$pCO_2$ (bar)/T(°C) | Equilibrium $CO_2$ PHREEQC 3, mol/kg | Final Sample $CO_2$ PHREEQC3, mol/kg | Final Sample $CO_2$ (Measured), mol/kg | Standard Deviation, $CO_2$ (No. of measurements) | Equilibrium pH, PHREEQC3 | Final Sample pH, PHREEEC3 | Final Sample pH, measured |
|---|---|---|---|---|---|---|---|---|
| 111 | DI/4/22 | 0.155 | 0.148 | 0.151 | 0.006 (3) | 5.113 | 4.465 | 4.270 |
| 112 | DI/4/22 | 0.155 | 0.146 | - | - | 5.113 | 3.642 | - |
| 113 | DI/4/22 | 0.155 | 0.146 | - | - | 5.113 | 3.632 | - |
| 171 | NaCl/4/22 | 0.159 | 0.107 | 0.063 | 0.007 (5) | 5.652 | 3.642 | 3.450 |
| 172 | NaCl/4/22 | 0.159 | 0.107 | 0.063 | 0.004 (6) | 5.652 | 3.591 | 3.760 |
| 173 | DI/4/22 | 0.155 | 0.146 | 0.171 | 0.020 (2) | 5.113 | 3.797 | 4.220 |
| 175 | NaCl/4/70 | 0.04786 | 0.043 | - | - | 5.011 | 3.80435 | - |
| 176 | DI/31/70 | 0.4038 | 0.400 | 0.376 | n/a (1) | 4.369 | 3.44371 | - |
| FCO2 W10 | DI/31/70 | 0.4038 | 0.400 | 0.400 | 0.020 (2) | 4.369 | 3.35 | 4.37 |

**Table 4.1.4**: Calculated and measured pH and $CO_2$ content of final samples and at equilibrium

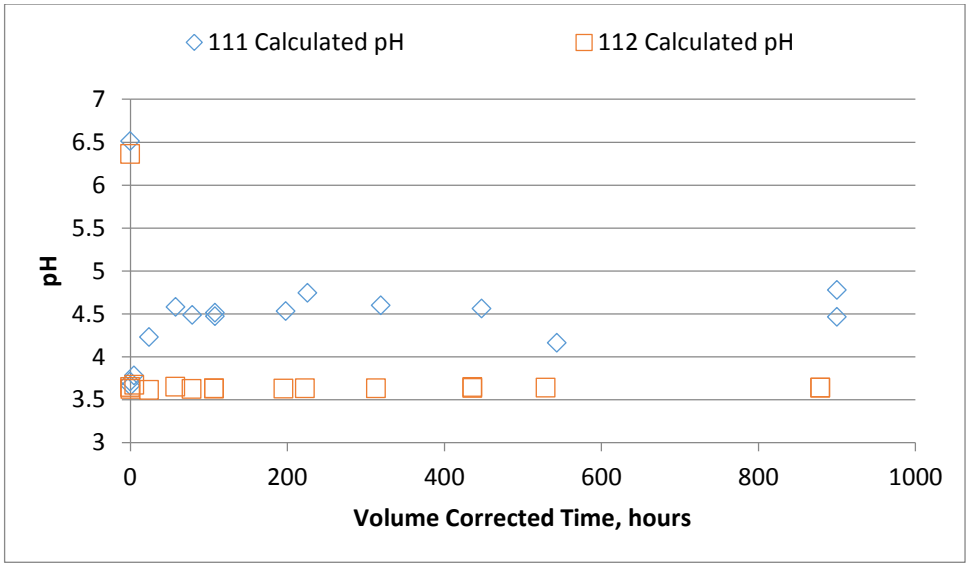


**Figure 4.1.13**: Calculated pH from analysed sample compositions for experiments 111 and 112

#### 4.1.2.2 Dissolution Behaviour: General Observations

Dissolution of alkali feldspar is non-stoichiometric in all of the experiments presented here. Preferential release of potassium and calcium is seen in most cases, while aluminium is generally released with a slight excess relative to silica. These trends are illustrated in Figure 4.1.14, which shows the major elemental concentrations for experiment 172, corrected for mineral proportions.

In terms of saturation indices, as calculated by PHREEQC3 for measured solution compositions, all experiments show relatively rapid rises in saturation with albite, Ca-montmorillonite, gibbsite, kaolinite, K-mica and quartz for the first 200-300 hours of experiment, after which saturations rise more slowly. These trends are illustrated in Figure 4.1.15, which presents the calculated saturation indices for the above minerals for samples from experiment 172.

All experiments, other than 111, remain undersaturated with respect to all of these phases, although experiments 171 and 173 reach quartz saturation at a late (>1400 hours) time. All experiments are close to (SI>-0.5) saturation with quartz by late times and experiment 175 very nearly reaches saturation in kaolinite (SI -0.05) and K-mica (SI -0.79) and experiment 176 nears saturation with gibbsite (SI -0.56). As with the results from other kinetic experiments in this work, all experiments also become oversaturated with respect to goethite and hematite.

The results for saturation indices for experiment 111 differ from those described here due to the mechanical stirring of that experiment. Calculated saturation indices for 111 are illustrated in Figure 4.1.16. Albite reaches saturation and then remains relatively stable, while all of the other phases mentioned above become oversaturated in this experiment.

Experiment 176 shows relatively low Al concentrations compared to Si, while Experiment 175 shows a definite peak in Al concentrations with time, both suggestive of precipitation effects, despite the apparent undersaturation of phases suggested by PHREEQC. Hence further modelling was carried out using the more extensive llnl.dat (as opposed to the standard PHREEQC.dat) database. These calculations indicate that experiments 175 and 176 are oversaturated with respect to diaspore and boehmite, possibly explaining the observed Al behaviour. This modelling also indicated that all experiments became oversaturated with respect to nontronite: a Ca, H, K, Mg, Na bearing smectite. Nontronite is relatively iron rich and it is possible

that iron contamination (see above) allowed this phase to reach oversaturation, although it was not observed as a precipitate by SEM observation of the reacted solids.

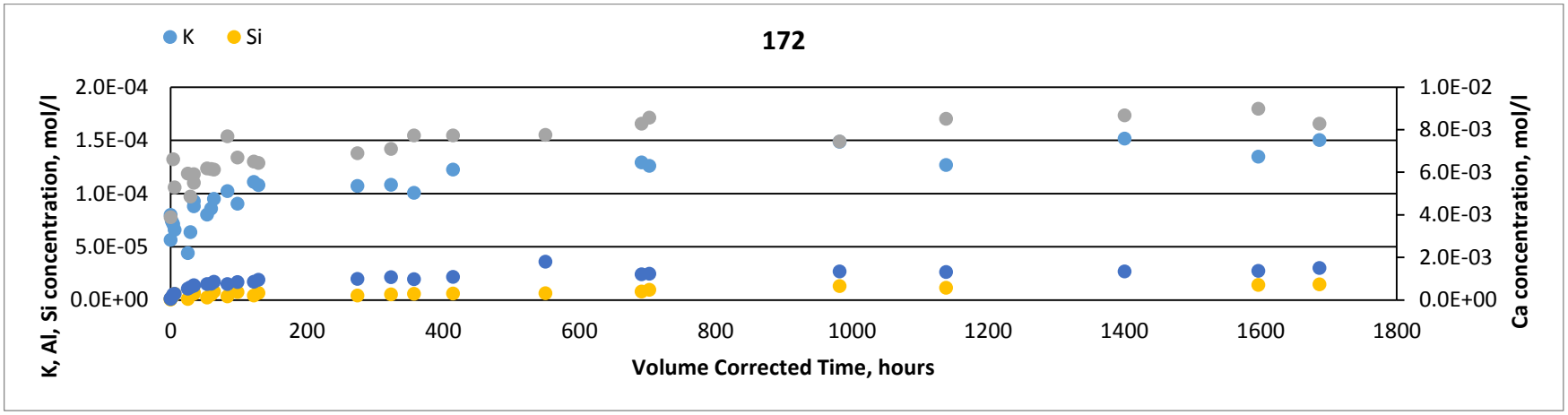


**Figure 4.1.14**: Elemental concentrations for experiment 172

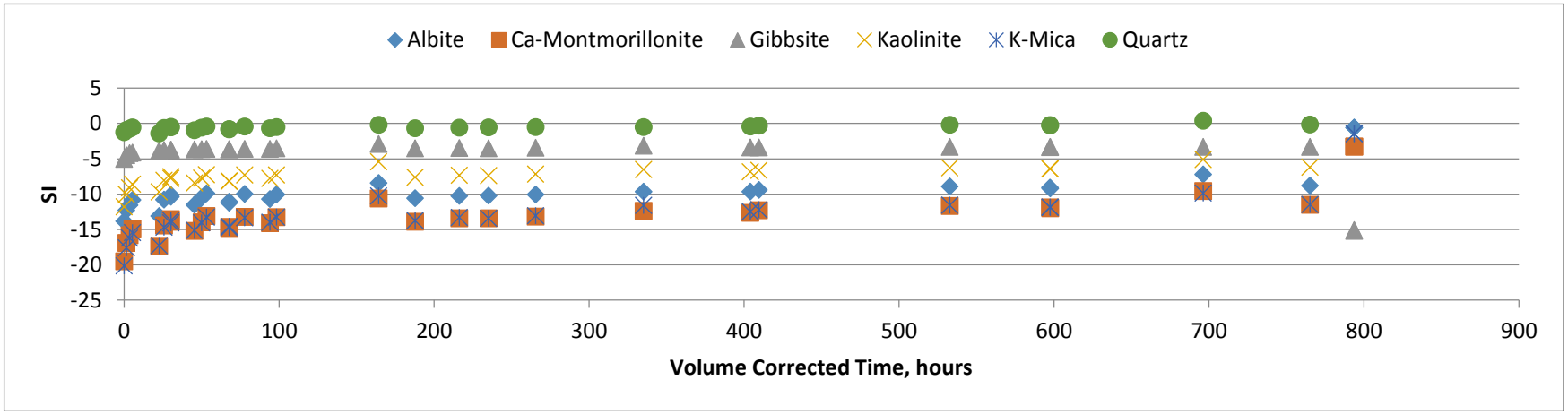


**Figure 4.1.15**: Calculated saturation indices for samples from experiment 172

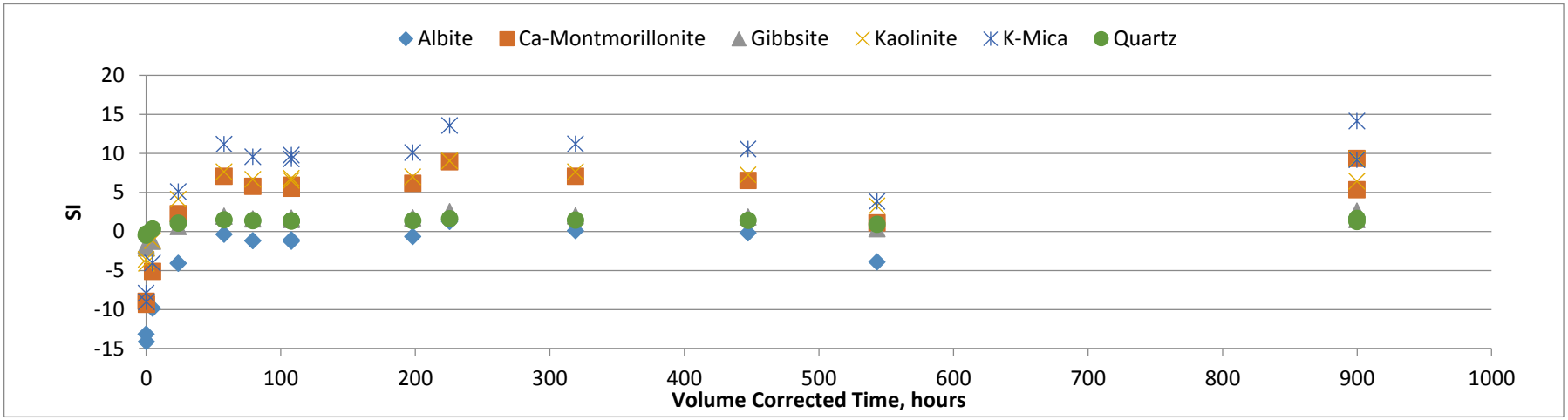


**Figure 4.1.16**: Calculated saturation indices for samples from experiment 111

#### 4.1.2.3 Dissolution Behaviour: Grain Size Effects

Figures 4.1.17 – 4.1.20 compare elemental release from experiments 171 (125-180µm, 4bar $pCO_2$, 22°C, NaCl) and 172 (500-600µm, 4bar $pCO_2$, 22°C, NaCl). Analyte concentrations and trends are broadly similar between the two experiments. Al and Si concentrations in the coarser grained experiment (172) are slightly depressed relative to those from the finer grained experiment, while K concentrations, despite much scatter in the data, are notably higher in 172 than in 171. Despite these differences, actual dissolution rates, as calculated from Si release for the two experiments are very similar (Figure 4.1.21).

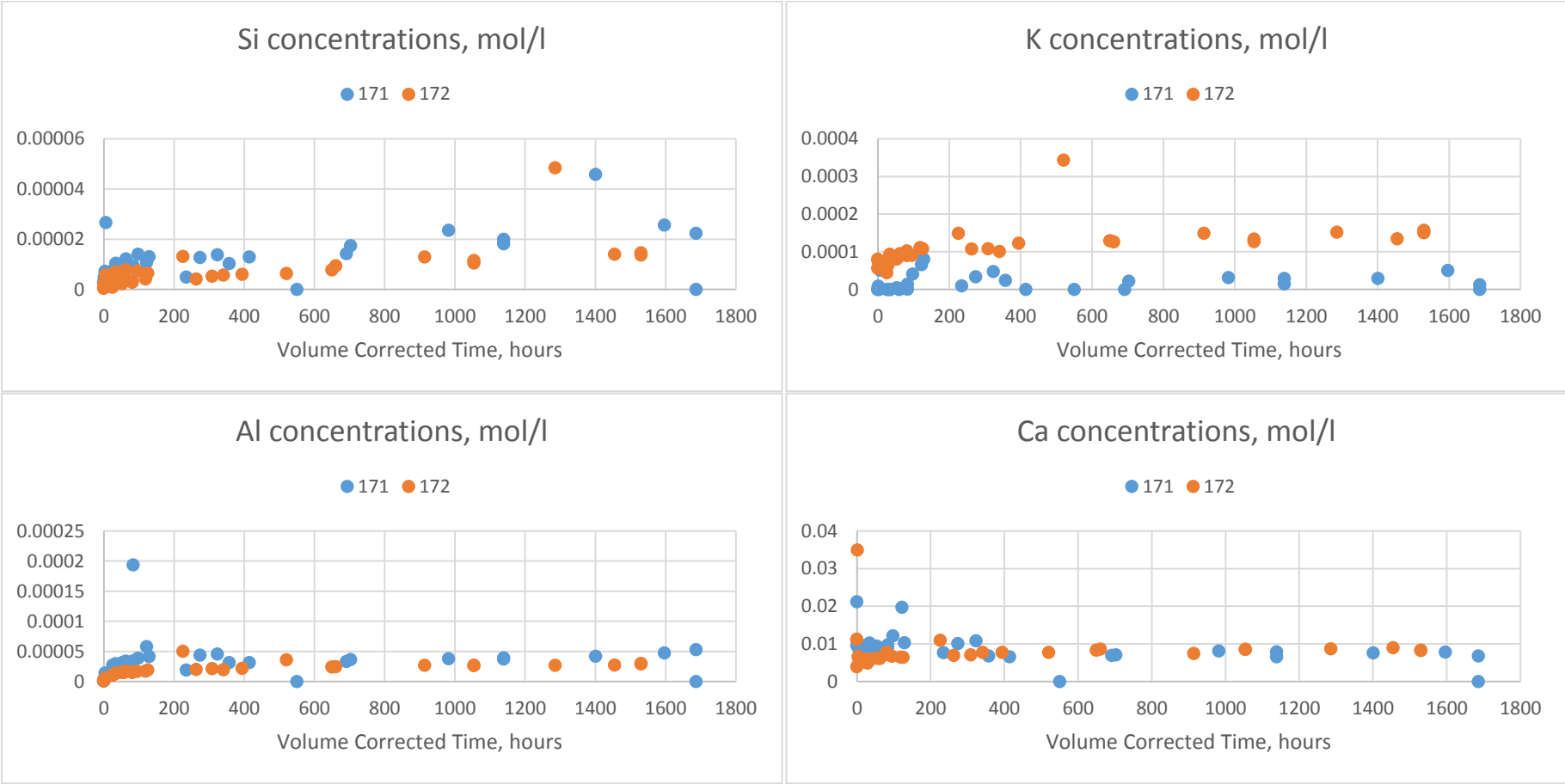


**Figures 4.1.17 – 4.1.20**: Comparative charts of (from top left, moving clockwise) Si, K, Al and Ca concentrations for experiments 171 (125µm - 180µm) and 172 (500µm - 600µm)

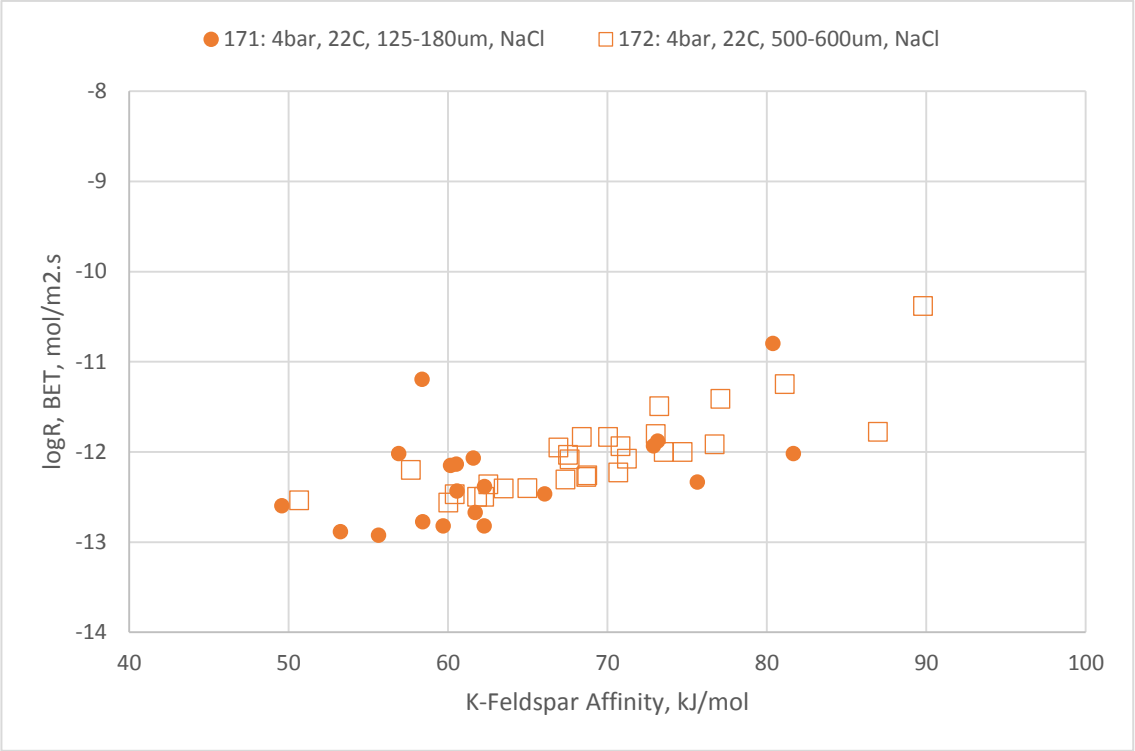


**Figures 4.1.21**: Calculated K-feldspar dissolution rates based on Si release for experiments 171 and 172

#### 4.1.2.4 Dissolution Behaviour: Effect of Fluid Composition

Figures 4.1.22 – 4.1.25 compare elemental release from experiments 171 (1.36M NaCl, 4bar $pCO_2$, 22°C) and 173 (Deionised water, 4bar $pCO_2$, 22°C). Results are broadly comparable for most analytes, with the exception of K, which is notably higher in the deionised water experiment (173). Figure 4.1.26 shows the calculated K-feldspar dissolution rates based on Si release normalized to BET surface area for the two experiments. This also indicates that the NaCl fluid has an inhibitive effect on the dissolution of the feldspar.

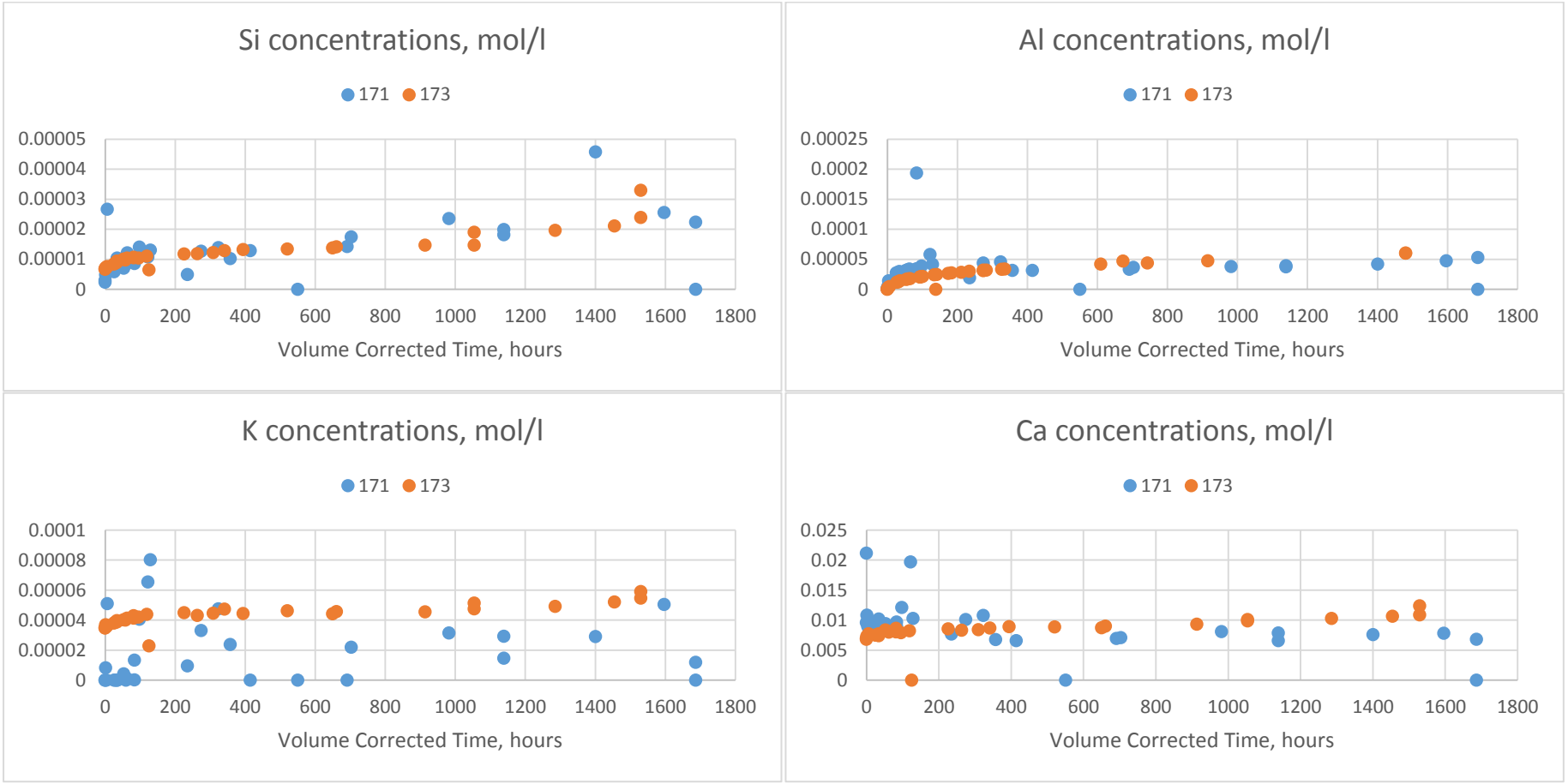


**Figures 4.1.22 – 4.1.25**: Comparative charts of (from top left, moving clockwise) Si, K, Al and Ca concentrations for experiments 171 (1.36M NaCl) and 173 (Deionised Water)

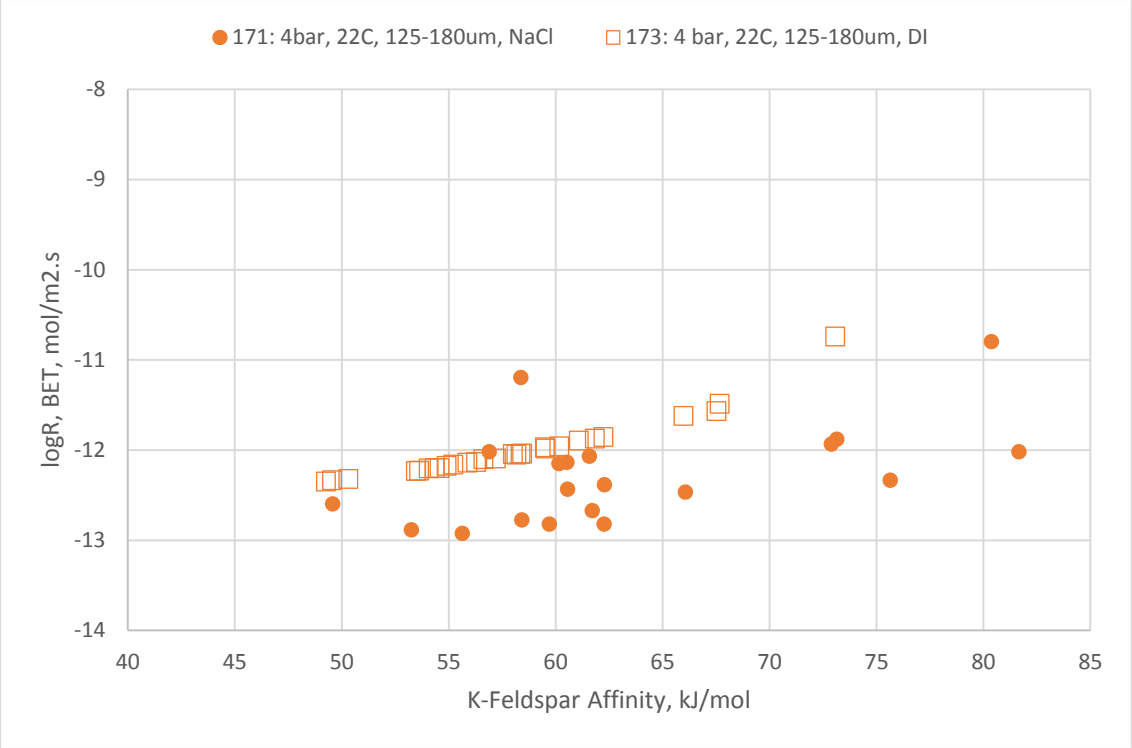


**Figures 4.1.26**: Calculated K-feldspar dissolution rates for experiments 171 and 173. Rates are based on Si release and normalized to BET surface area.

#### 4.1.2.5 Dissolution Behaviour: Effects of $pCO_2$ (4bar, 31bar) and Temperature (22°C, 70°C)

Figures 4.1.27 – 4.1.34 compare elemental release from experiments 171 (4bar $pCO_2$, 22°C, NaCl) and 176 (31bar $pCO_2$, 70°C, NaCl) and experiments 175 (4bar $pCO_2$, 70°C, NaCl) and 171 (4bar $pCO_2$, 22°C, NaCl). Figures 4.1.35 & 4.1.36 compare the calculated K-feldspar dissolution rates, based on Si release, for the two sets of experiments.

Comparing experiments 176 and 171, Si, Ca and K concentrations in experiment 176 are 2-3 times higher than those measured in 171 but Al concentrations on the other hand are consistently higher in the lower temperature experiment 171. Likewise rates of Si and K release are higher for the high P/T experiment, while Al rates are lower, by around 0.5 log units at late times. The higher Si concentrations and dissolution rates in experiment 176 are consistent with higher solubility at higher temperature, the lower Al concentrations, as has already been noted above, are likely due to precipitation of boehmite and/or diaspore. The calculated dissolution rates, based on Si release, are notably (around an order of magnitude) higher for experiment 176.

Likewise, comparing experiments 175 and 171, while Al concentrations are similar, Si concentrations are considerably higher in the higher temperature experiment (175). While Al release may likewise be higher, this is not reflected in the measured concentrations since, as has already been noted, 175 becomes oversaturated with respect to Al bearing phases, which are likely to have precipitated during the experiment. Despite considerable scatter in the Ca and K data, they also show generally higher concentrations in the higher temperature experiment (175). As would be expected based on the measured Si concentrations, K-feldspar dissolution rates are around an order of magnitude higher in the high temperature experiment.

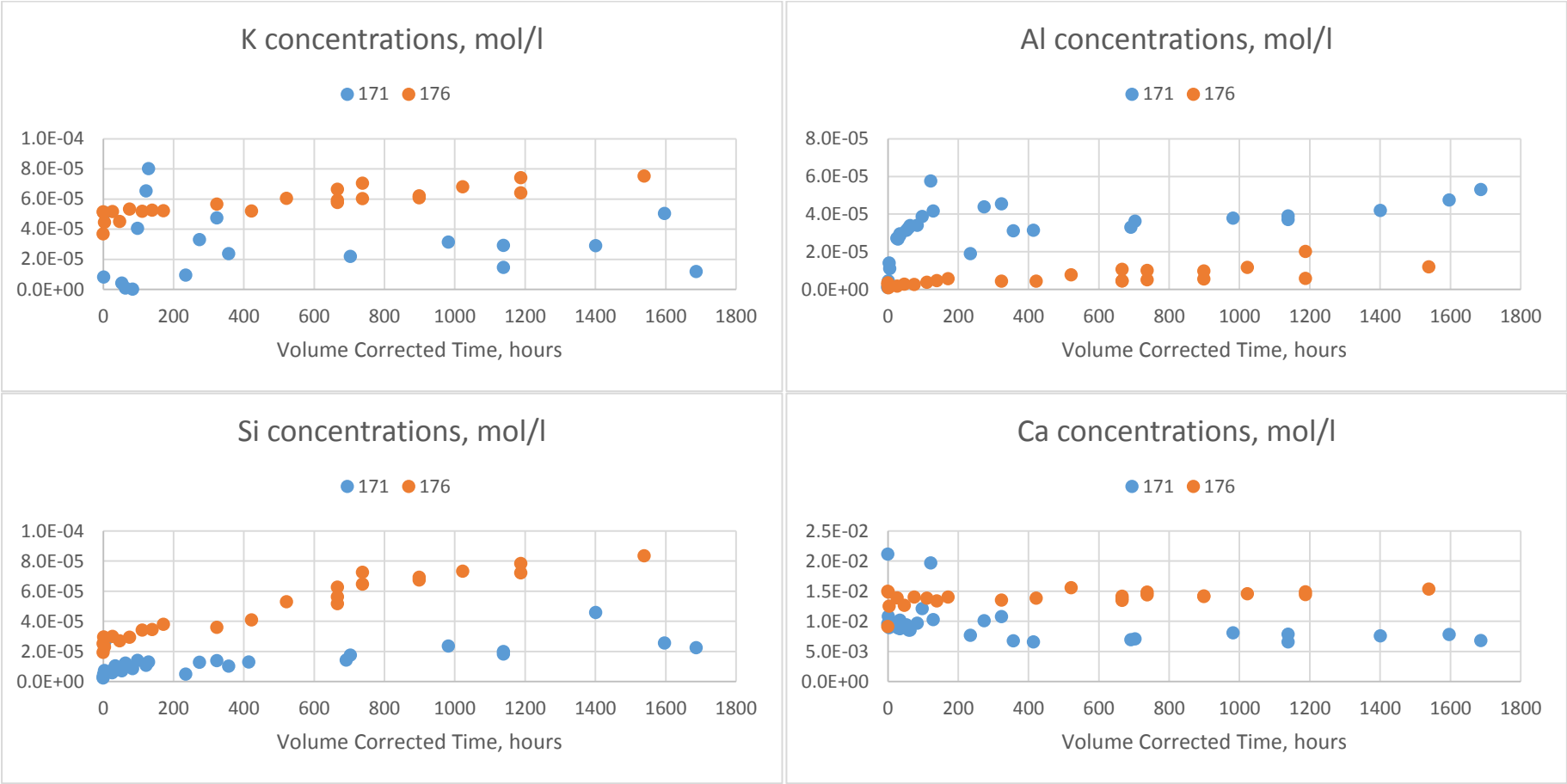


**Figures 4.1.27 – 4.1.30**: Comparative charts of (from top left, moving clockwise) Si, K, Al and Ca concentrations for experiments 171 (4 bar $pCO_2$, 22°C) and 176 (31 bar $pCO_2$, 70°C)

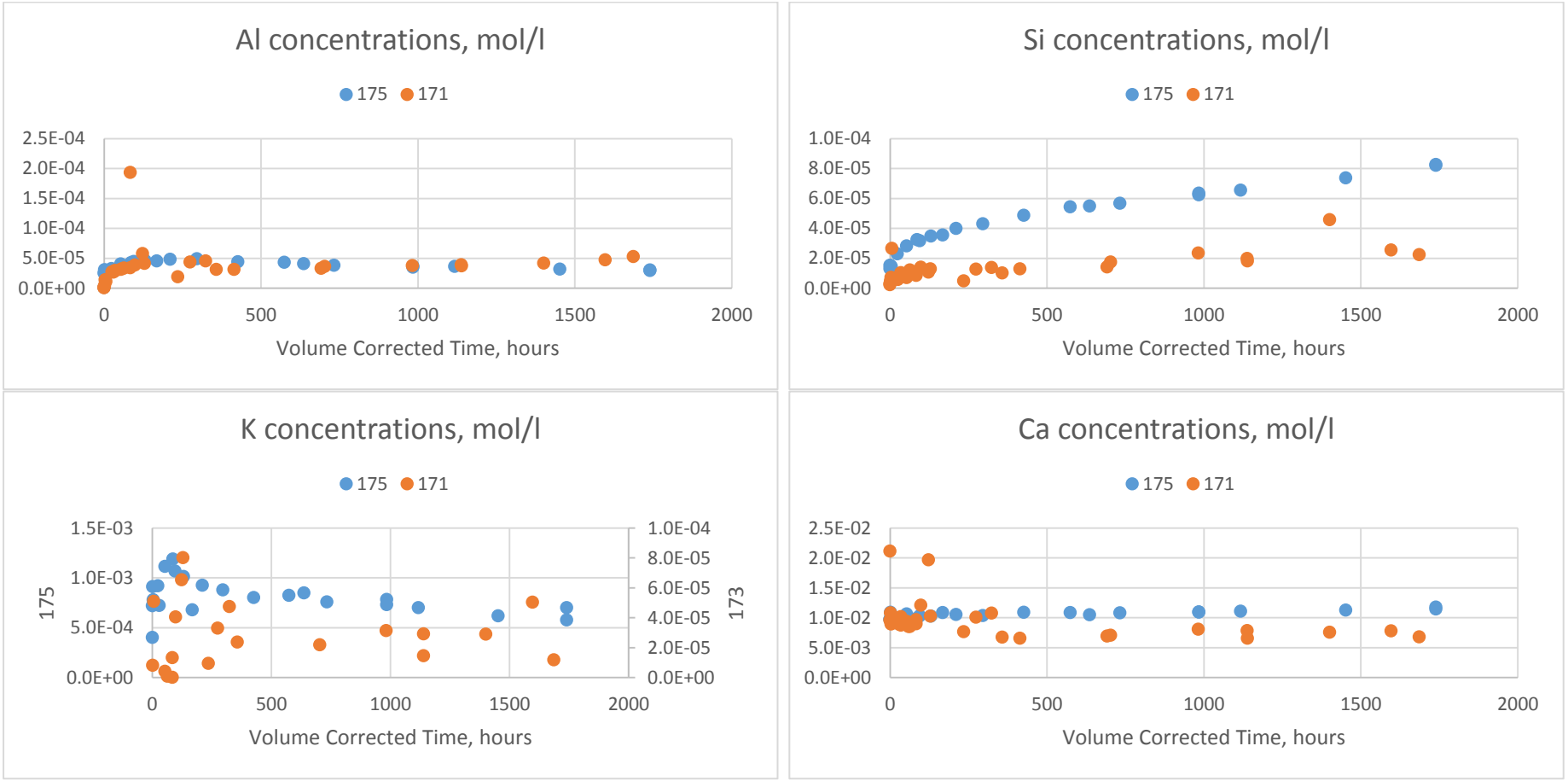


**Figures 4.1.31 – 4.1.34**: Comparative charts of (from top left, moving clockwise) Si, K, Al and Ca concentrations for experiments 175 (4 bar $pCO_2$, 70°C) and 171 (4 bar $pCO_2$, 22°C)

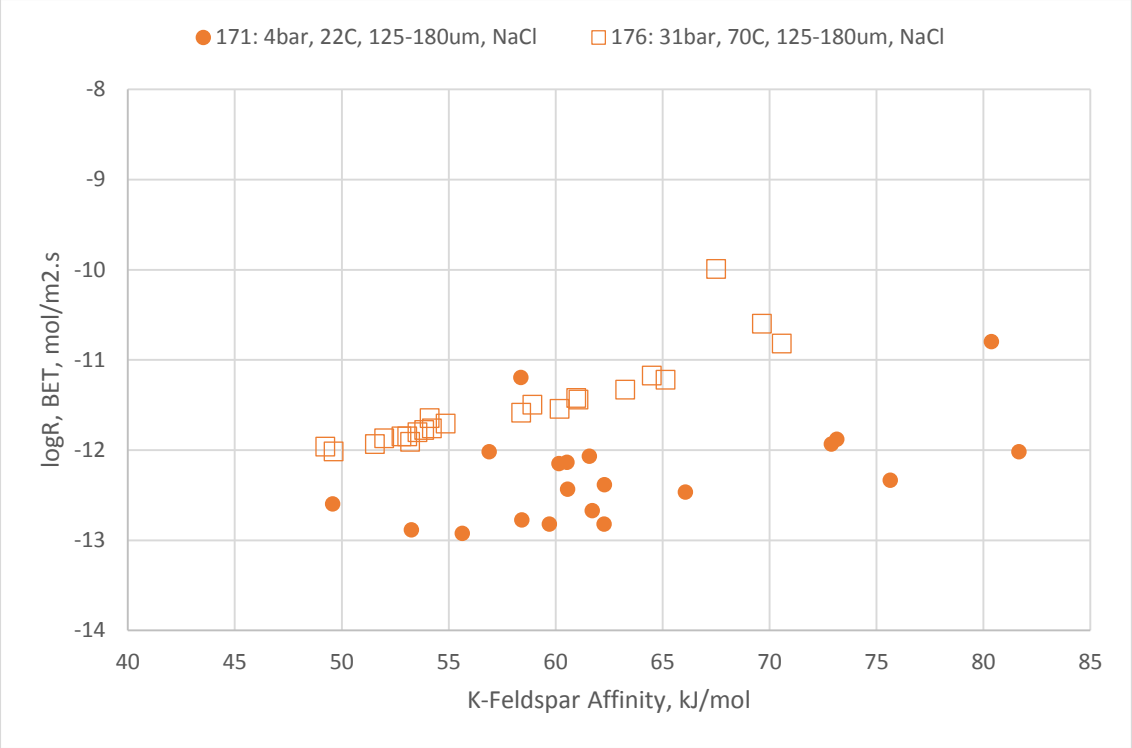


**Figures 4.1.35**: Calculated K-feldspar dissolution rates and affinity for experiments 171 and 176

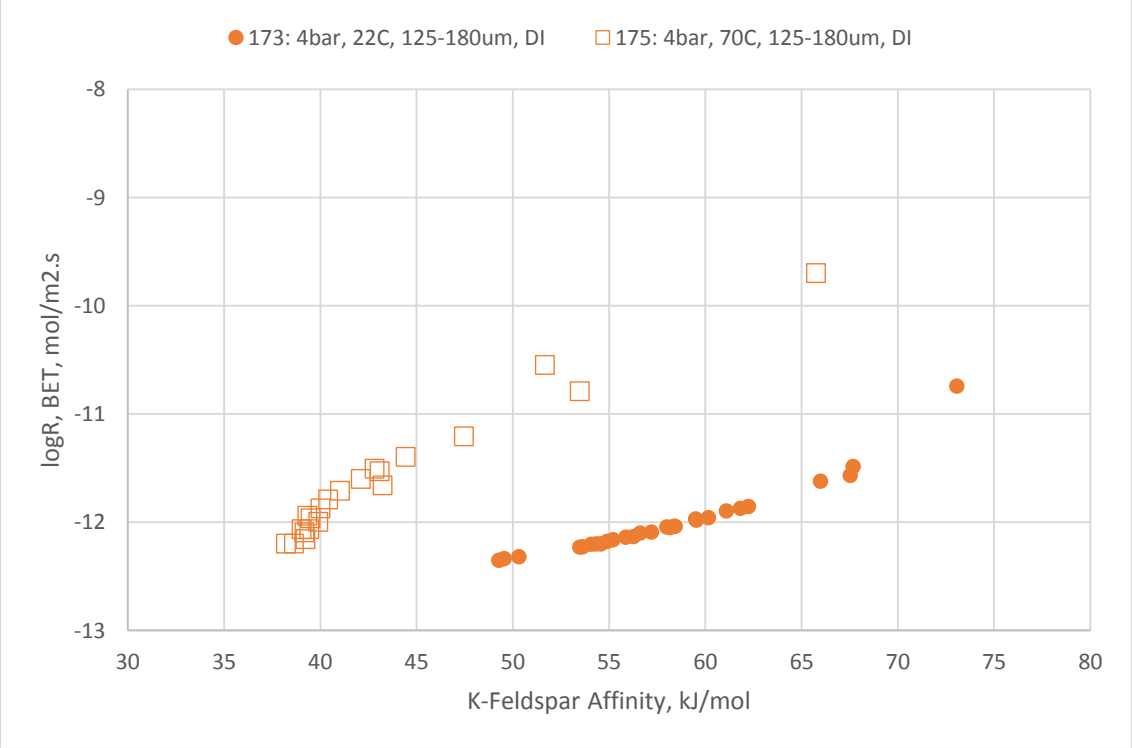


**Figures 4.1.36**: Calculated K-feldspar dissolution rates and affinity for experiments 173 and 175

#### 4.1.2.6 K-Feldspar Dissolution Rates

Experimental dissolution rates, based on bulk Si release and BET surface areas are presented in Figures 4.1.37 – 4.1.44, plotted against K-feldspar affinity. Also plotted are calculated rates using:

1) The USGS general rate equation (see Equation 4.1.1 in Section 4.1.1.6), using values presented in USGS (2004) for K-feldspar.
2) The feldspar dissolution equation, originally presented by Burch et al. (1993):

$$R = k_1[1 - exp(-ng^{m1})] + k_2[1 - exp(-g)]^{m2} \quad (4.1.4)$$

Where $g = \Delta G_r/RT$, $k_1$ and $k_2$ are rate constants and n, m1 and m2 are fitted constants. Values for these constants were taken from Hellmann et al. (2010).

3) The feldspar dissolution equation from Gautier et al. (1994):

$$r = k_+ \left(\frac{1}{a_{AlOH_4^-} a_{H^+}}\right)^{\frac{1}{3}} \left(1 - exp\left(-\frac{A}{3RT}\right)\right) \quad (4.1.5)$$

Where k is a rate constant, taken from the same publication.

K-feldspar affinity has been calculated using the equation:

$$A = RT \times \ln\left(\frac{K_{K-Feldspar}}{(a_{K^+} \times a_{Al(OH)_4^-} \times a^3_{H_4SiO_4})}\right) \quad (4.1.6)$$

Where $K_{K\text{-feldspar}}$ is the equilibrium constant for K-feldspar at the experimental conditions, R is the gas constant, T is the temperature in Kelvin, and $a_{K^+}$, $a_{Al(OH)_4^-}$ and $a^3_{H_4SiO_4}$ are the activities of the appropriate ions in solution, as calculated by PHREEQC3 using the measured fluid compositions.

Experimental rates generally agree very well with those predicted using the USGS general rate equation, particularly at lower chemical affinities. At higher affinities, particularly for experiments 175 and 176, rates are close to those predicted using equation 4.1.4. In all cases, with the exception of the mechanically stirred experiment (111) the equation from Gautier et al (1994) (Equation 4.1.5) considerably over-predicts the dissolution rates, generally by 2-3 log units.

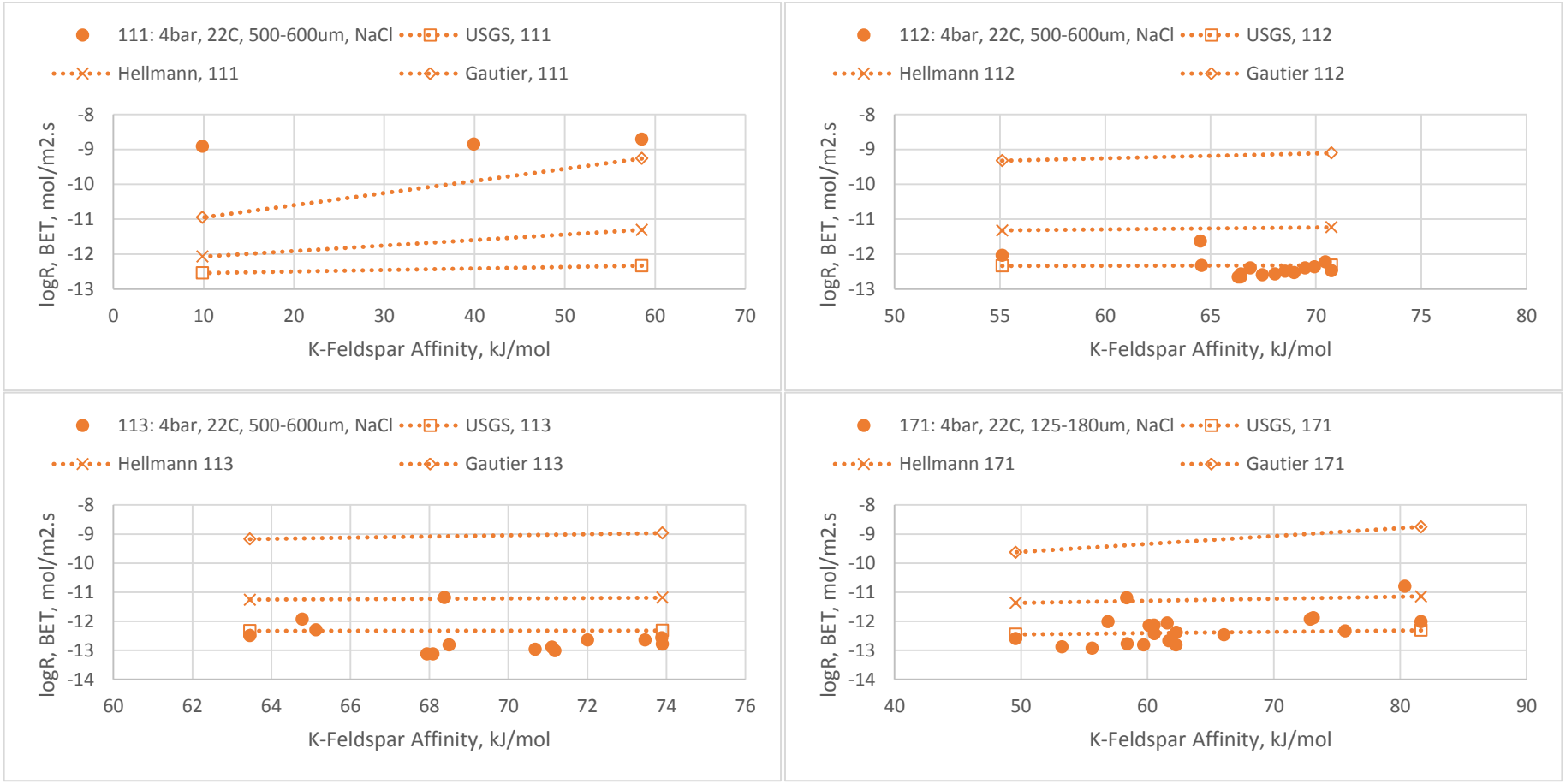


**Figures 4.1.37 – 4.1.40**: Calculated K-feldspar dissolution rates based on Si release and BET surface area, plotted together with various calculated predictions for (from top left moving clockwise) experiments 111, 112, 113 and 171

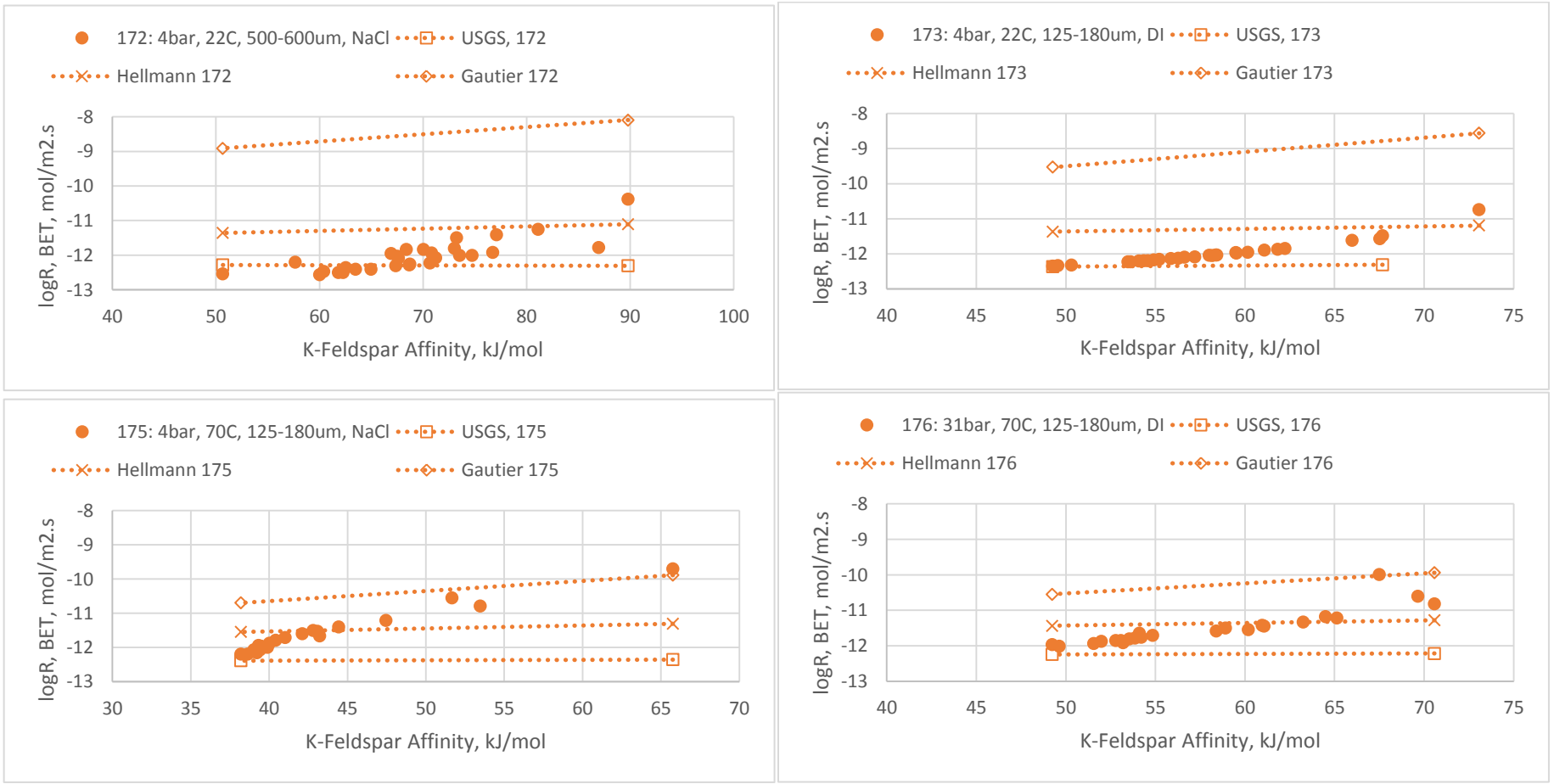


**Figures 4.1.41 – 4.1.44**: Calculated K-feldspar dissolution rates based on Si release and BET surface area, plotted together with various calculated predictions for (from top left moving clockwise) experiments 172, 173, 175 and 176

#### 4.1.2.7 K-feldspar Experiments Overview and Discussion

Of the experiments detailed above, 111, 112 and 113 were carried out as a simple test on the effects of stirring on K-feldspar dissolution. In the case of the test, it was fairly clear that the K-feldspar in experiment 111 would dissolve more rapidly than in the other two experiments, due to the increase in surface area from mechanical grinding by the stirring bead. Experiment 111 is the only experiment presented here in which there is a significant change in pH over the course of the run and despite this the final pH of the experiment remains almost 1 pH unit below the equilibrium pH predicted by PHREEQC3. The differences between experiments 112 (agitated) and 113 (not agitated) are very small, reinforcing the likelihood that the relatively rapid dissolution observed in 111 is due to increased surface area, rather than any transport controls. Additionally, while 111 may work as a useful indicator of the direction in which other, non-mechanically stirred, experiments are reacting, it highlights the dangers of mechanical stirring in increasing surface area. Even when stirrers are not in direct contact with the reacting mineral, it has been noted that grains that are subject to vigorous agitation will undergo spalling and abrasion, with the potential of greatly increasing reactive surface area (Metz & Ganor 2001). These results highlight the benefits of avoiding internal mechanical agitation when undertaking kinetic batch experiments using powders, particularly for silicates, where transport controls on dissolution are likely to be minimal.

As for other single mineral experiments described in this work, $CO_2$ solubilities measured in the experiments are close to the theoretical equilibrium values and likewise modelling of actual solution compositions produces results close to those measured. Minor discrepancies between these values are likely due to the relatively complex nature of the feldspar used, since the actual composition of each solid sample used in the experiments is likely to wander from the average bulk value used in modelling. Major discrepancies, where they appear (i.e. in the NaCl experiments 171 and 172) are likely due to fluid sampling problems, specifically the precipitation of sodium bicarbonate.

While dissolved $CO_2$ concentrations measured in the experiments are generally close to those expected at equilibrium, there is a larger discrepancy between predicted and measured pH. For example, the predicted pH at equilibrium for experiment 171 is 5.65, while the measured value at the end of the experiment is 3.45 and the value predicted based on

modelling of the final solution composition is 3.64. The discrepancy is due to the relatively low concentrations of ions in solution during the experiments compared to what would be expected at equilibrium. For example the predicted equilibrium concentrations of Al and K for experiment 171 are 1.82E-2 mol/l and 4.33E-3 mol/l respectively. Actual concentrations measured towards the end of the experimental run are 4.84E-5 and 3.83E-5. Al speciation in particular has a strong dependence on pH. In the case of experiment 171, raising the Al concentration by three orders of magnitude, brings the calculated pH in line with the predicted equilibrium value.

These results highlight both the sluggish nature of feldspar dissolution and the relative effects of distance from equilibrium on pH and $CO_2$ solubility. $CO_2$ solubility is largely insensitive to changes in fluid composition brought about by silicate dissolution and in these systems, solubility is largely dictated by temperature, pressure and salinity. Hence, in the case of an actual storage system, the solubility achieved shortly after injection is likely to be near the maximum solubility achievable and is unlikely to undergo major changes in the future. pH on the other hand is relatively sensitive to the changes in fluid composition brought about by silicate dissolution and while change, as evidenced by the experiments presented here, is likely to be slow, we would expect that over time pH will climb considerably from its value immediately following $CO_2$ addition.

A notable feature of the dissolution of the feldspar was that it was strongly incongruent. Silica and aluminium release was largely comparable in most experiments, except where Al phases became oversaturated (experiments 175 and 176), however K and Ca release far outstripped these. Incongruent dissolution of feldspars is well documented (Helgeson et al. 1984; Fu et al. 2009; Alekseyev et al. 1997; Stillings & Brantley 1995), with silica release usually lagging behind release of other components. In this case the network modifiers K, Ca and (presumably) Na are preferentially released, likely through exchange for $H^+$ at the mineral surface (Stillings & Brantley 1995). Given the relatively high concentrations of Ca observed in the experiments it is clear that the anorthite component, despite the fact that it makes up a relatively low percentage of the bulk mineral, undergoes preferential dissolution. This is consistent with the thermodynamic instability of anorthite under low-T conditions. The incongruent release of Ca from such a minor component is striking and highlights the impact that such minor components, even within what might be regarded for purposes of modelling as a single phase, can have on fluid chemistry.

The effects of grain size on elemental release or dissolution rates (once normalised to surface area) seem to be minimal in the case of the feldspar material used here. The exception seems to be for K release which was notably higher in the coarser grained experiment. While in theory grain size should make little difference to dissolution rates, once normalised to measured surface area, in practice variation in feldspar dissolution rates with grain size have been noted (Anbeek 1992; Mark E. Hodson 2006). In particular it has been noted that grinding of relatively unweathered mineral (as is the case for the feldspar used here) can have the effect of destroying reactive surface area (Anbeek 1992), which may well be the case here.

As for changes in grain-size, the effect of NaCl on elemental release from the feldspar appears at first glance to be minimal, with the exception of K release, which appears to be slightly higher in the deionised water experiment. It is possible that this reflects the poor K data often collected for the brine experiments; data points often show a lot of scatter and this is presumed to be due to K contamination in the original NaCl solution. However previous studies have noted an inhibitory effect of NaCl on feldspar dissolution (Blake & Walter 1999; Stillings & Brantley 1995) and comparison of calculated dissolution rates from the experiments based on Si release (Figure 4.1.35) do indeed show that rates in the NaCl experiment appear suppressed relative to the deionised water experiment. The effect of the 1.36M NaCl is to lower the dissolution rate of the silicate framework by around 0.5 log units ($mol/m^2.s$). Blake & Walter (1999) observed a decrease of similar magnitude in labradorite dissolution when switching from deionised water to 1M NaCl. The decrease in dissolution rate with increasing NaCl content is generally attributed to increased competition between $Na^+$ and $H^+$ for exchange and adsorption sites on the feldspar surface (Blake & Walter 1999) as is likely the case here for K release.

Comparison of experiments carried out at low vs. high $pCO_2$ and temperature indicate that the increase in temperature from 22°C to 70°C increased the dissolution rate of the feldspar used here by around one order of magnitude. The results indicate that most, if not all of this increase in rate is due to the increased temperature, rather than the increase in $pCO_2$. Other researchers have observed that increased concentrations of dissolved $CO_2$ have little effect on feldspar dissolution (Carroll & Knauss 2005). Enhanced dissolution, rather, occurs as an indirect effect of the decrease in pH of fluids under $pCO_2$. Although feldspar dissolution is dependent upon pH, the additional decrease in pH caused by increasing $pCO_2$ from 4 bar to 31 bar is

only 0.4 pH units (from around 3.5 to 3.1), hence the dissolution rate is relatively insensitive to variations in $pCO_2$ on the magnitude investigated here.

Calculated dissolution rates, based on Si release and BET surface area, agree reasonably well with predictions made with literature sourced equations. At early times and higher K-feldspar affinities, rates generally lie closest to those predicted by the feldspar dissolution equation originally presented by Burch et al. (1993) (Eqn. 4.1.3). The equation presented by Burch et al. was originally derived from a series of dissolution experiments carried out using a flow-through reactor, at “near” equilibrium conditions. The observed dissolution rates showed a sigmoidal shape on approach to equilibrium, with a dissolution “plateau” at affinities greater than around 50kJ/mol and a steep decrease in rates at affinities between around 50 and 25 kJ/mol. The rates presented here are generally for affinities between 50 and 90 kJ/mol, however most of them show a slight decrease in rate with decreasing affinity, suggesting the transition from dissolution plateau to strong dependence on affinity occurs, for the feldspar used here, at slightly higher affinities than predicted by the Burch et al equation. The original equation and the values used by Hellmann et al (2010) are all based on albite dissolution and it is possible that discrepancies are due simply to variations in feldspar composition.

The equation presented by Gautier et al (1994) on the other hand, was produced using results from experiments on K-rich feldspar, but consistently over-predict the dissolution rates in the experiments presented here. K-feldspar affinities in the Gautier et al experiments cover the range 5 – 90kJ/mol, which, as in the Burch et al experiments, were obtained using a flow-through type apparatus. Hence the predictions made by this equation might be expected to be more representative of the experiments presented here. The most likely explanation for the discrepancy is that while the Burch et al equation relies on a series of empirical constants, the Gautier et al equation requires values for $Al(OH)_4$ and $H^+$ activities. In this case these activities were calculated using PHREEQC3 and this introduces additional uncertainties; reliance on the speciation calculations carried out by the modelling programme and their compatibility with the method used to extract data by Gautier et al (1994), the quality of the thermodynamic database and the quality and extent of the analytical data for fluid samples. Hence, while the Gautier equation may well provide accurate predictions of dissolution rate, the additional data required to use it efficiently means that in this case

the more general equations of Burch et al and the USGS general rate equation, provide a better fit to experimental data. It should be noted that the Gautier equation does predict the general trend of rates much more closely than the other two equations: rates calculated using the equation show a decrease with K-feldspar affinity (in the case of the Gautier equation, this decrease is due to the rate dependence on $Al(OH)_4$ activity) similar to that observed in the experiments and not predicted by the other two equations. Hence, while the dependence of rate on K-feldspar affinity is successfully predicted, the overall magnitude of the rates is not.

In conclusion, the results presented here reflect the generally sluggish approach to equilibrium of fluids in contact with K-feldspar, reflected in the persistence of the low pH caused by initial dissolution of $CO_2$. The experiments show some evidence of grain-size effects on K release rates and definite signs of retardation of dissolution rates when NaCl fluids are used. They also highlight the relative insensitivity of feldspar dissolution rate to $pCO_2$. The three literature equations presented here provide useful, if not completely accurate, predictions of the dissolution rates observed in the experiments. The Burch et al and USGS equations predict rates reasonably well, but fail to mirror the trend of decreasing rate with K-feldspar affinity observed in the experiments. The Gautier et al equation, on the other hand, successfully reproduces this dependence, but fails to predict to observed rates as accurately.

### 4.1.3 Albite

Seven experiments were carried out on the albite material (described in Section 3.1.3), under conditions summarised in Table 4.1.5.

| Experiment ID | Grain Fraction, µm | Fluid | pCO2, bar (absolute) | Temperature, $^0$C | Run time, volume constant hours | Conditioning period prior to $CO_2$ injection, hours |
|---|---|---|---|---|---|---|
| 122 | 125-180 | 1.36M NaCl | 4 | 22 | 831 | 52 |
| 123 | 125-180 | 1.36M NaCl | 31 | 70 | 235 | 214 |
| 181 | 500-600 | 1.36M NaCl | 4 | 22 | 1839 | 144 |
| 182 | 500-600 | 1.36M NaCl | 31 | 70 | 1708 | 144 |
| 183 | 125-180 | DI | 4 | 70 | 1644 | 219 |
| 184 | 125-180 | 1.36M NaCl | 31 | 70 | 1621 | 220 |
| 185 | 125-180 | DI | 31 | 70 | 1588 | 220 |

**Table 4.1.5**: Summary of albite dissolution experimental conditions

#### 4.1.3.1 pH and $CO_2$ Solubility

Final sample measured and calculated results for dissolved $CO_2$ and pH are presented in Table 4.1.6. Initial pH (prior to $CO_2$ injection) in each experiment was below the predicted equilibrium pH for the $CO_2$ free system. Initial (t-1) pH was between 5.5 and 6.4, while the predicted equilibrium pH for the $CO_2$ free fluids lay between 6.2 and 7.0, depending on experimental conditions. The exception to this is experiment 182, whose calculated pH is exceptionally high (7.0) due to lack of Al data for early samples. Upon addition of $CO_2$ (t0) calculated pH drops to levels near the predicted pH of the pure, mineral free, fluids under $pCO_2$. Predicted pH for the pure fluids under $pCO_2$ lies between 3.4 and 3.7 depending on conditions, while calculated pH for the experiments at t0 lies between 3.3 to 3.8, again with the exception of experiment 182, whose initial calculated pH (4.7) is abnormally high due to lack of Al data at this time. As an illustration of this pH behaviour Figure 4.1.45 shows calculated pH data for experiment 181.

As for the K-feldspar and quartz dissolution experiments, calculated pH generally changes little during the course of the experiments, varying by only

0.1-0.3 pH units from the initial, t0, pH for the majority of experiments. Measured pH from experiments 122 and 181 are in poor agreement with calculated values: measured pH in experiment 122 is around 0.4 pH units lower than calculated and in experiment 181 is around 0.8 pH units higher. Measured and calculated values in experiment 123 are in good agreement. Discrepancies between measured and calculated pH are likely due to a combination of error introduced while measuring pH under pressure and errors in fluid composition. The final calculated pH for all experiments lies between 3.4 and 4.3. As for the K-feldspar experiments, all of the measured and calculated final fluid pH are significantly below the predicted equilibrium pH for the systems which lie between 3.8 and 4.8, with the exception of experiment 182, whose final calculated pH value lies very close to predicted equilibrium value.

Calculated dissolved $CO_2$ concentrations (Figure 4.1.50) of the final fluids are generally close to the predicted equilibrium concentrations for the systems: all lie within 0.01 mol/kg of the equilibrium values. Dissolved $CO_2$ concentrations were measured for final fluids from 122, 181, 182, 183, 184 and 185 and are generally in good agreement with the calculated concentrations: within 0.03 mol/kg, with the exception of concentrations measured in 184 and 185, which are slightly below (0.03-0.07 mol/kg) below the calculated value.

| Run | Fluid/$pCO_2$ (bar)/T(°C) | Equilibrium $CO_2$ PHREEQC3, mol/kg | Final Sample $CO_2$ PHREEQC3, mol/kg | Final Sample $CO_2$ (Measured), mol/kg | Standard Deviation, $CO_2$ (No. of measurements) | Equilibrium pH, PHREEQC3 | Final Sample pH, PHREEEC3 | Final Sample pH, measured |
|---|---|---|---|---|---|---|---|---|
| 122 | NaCl/4/22 | 0.107 | 0.107 | 0.105 | 0.002 (5) | 4.276 | 3.702 | 3.300 |
| 123 | NaCl/31/70 | 0.292 | 0.299 | - | - | 4.751 | 4.344 | 4.400 |
| 181 | NaCl/4/22 | 0.107 | 0.107 | 0.110 | 0.001 (2) | 4.276 | 3.563 | 4.400 |
| 182 | NaCl/31/70 | 0.292 | 0.295 | 0.295 | 0.024 (3) | 3.847 | 3.881 | - |
| 183 | DI/4/70 | 0.058 | 0.058 | 0.058 | 0.026 (3) | 4.767 | 3.910 | - |
| 184 | NaCl/31/70 | 0.292 | 0.294 | 0.260 | 0.015 (2) | 3.847 | 3.694 | - |
| 185 | DI/31/70 | 0.399 | 0.400 | 0.332 | 0.020 (2) | 4.25 | 3.40862 | - |

**Figure 4.1.6**: Calculated and measured pH and $CO_2$ contents of final samples and at equilibrium

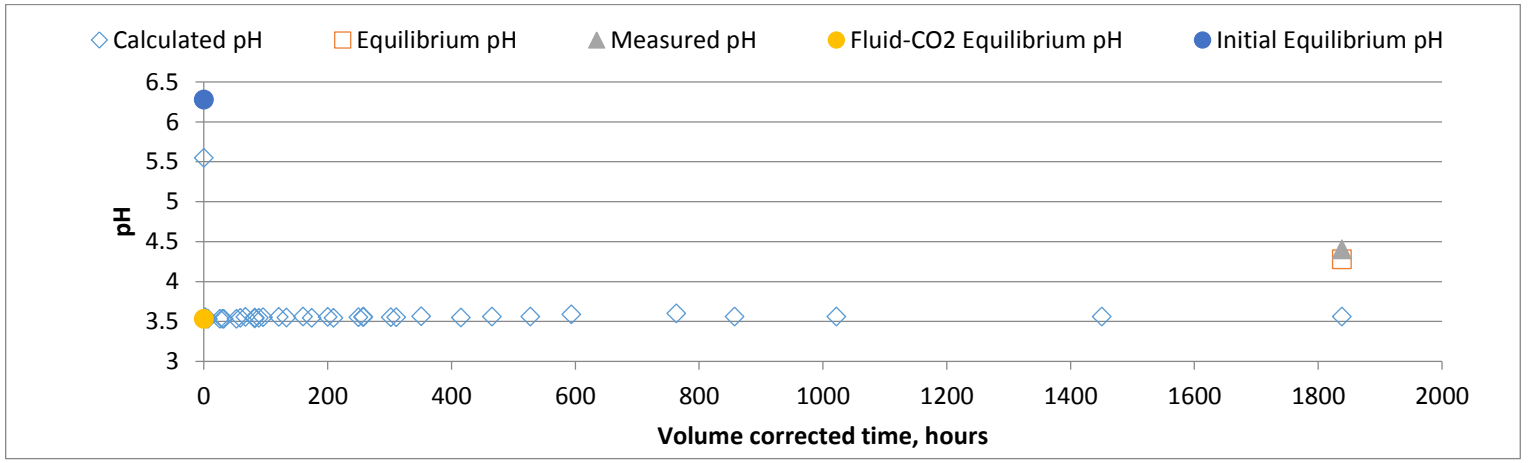


**Figure 4.1.45**: Calculated pH of samples from experiment 181

#### 4.1.3.2 Dissolution Behaviour: General Observations

Elemental releases during the experiments are, for the large part, non-stoichiometric, though Al and Si release are near stoichiometric in experiments 123, 181 and 182. Ca release far outstrips the release of any other element from the bulk mineral. Potassium concentrations tend to start relatively high (at t-1), but remain stable for the duration of the experiments, changing very little, while Al, Si and Ca all show progressive increases as the experiments evolve. These typical behaviours are illustrated in Figure 4.1.46, which shows elemental concentrations for samples taken from experiment 184, corrected for bulk mineral proportions.

Saturation index calculations (carried out in PHREEQC3) indicate that several of the experiments became oversaturated with respect to a variety of phases over the course of the experiments. Experiment 122 reaches saturation with respect to quartz at around 200 hours, 123 with quartz at around 25 hours and gibbsite at around 200 hours, 181 with quartz at around 500 hours, 182 with gibbsite, kaolinite, quartz and K-mica at around 500 hours, and 183 with gibbsite and kaolinite at around 600 hours.

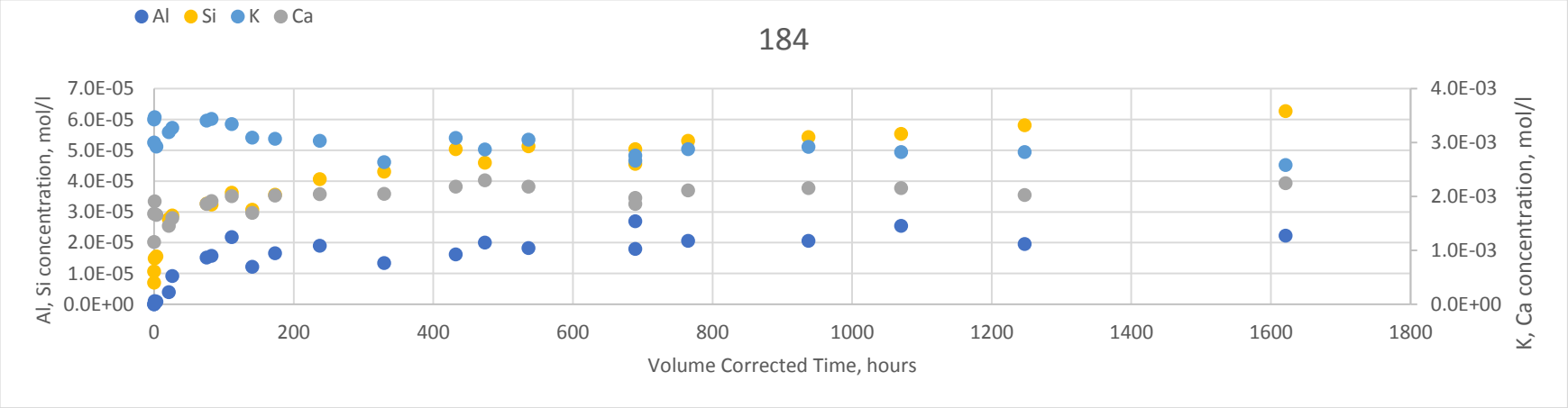


**Figure 4.1.46**: Elemental concentrations for samples from experiment 184, corrected for proportions in bulk mineral

#### 4.1.3.3 Dissolution Behaviour: Grain Size Effects

Experiments 122 (125-180µm, 4bar $pCO_2$, 22°C, NaCl) and 181 (500-600µm, 4bar $pCO_2$, 22°C, NaCl) and experiments 184 (125-180µm, 31bar $pCO_2$, 70°C, NaCl) and 182 (500-600µm, 31bar $pCO_2$, 70°C, NaCl) are compared in Figures 4.1.47 – 4.1.54. In both comparisons, potassium concentrations are elevated in the coarser grained experiments, similar to behaviour observed in the K-feldspar experiments. However, concentrations and release rates of Al, Si and Ca are all lower in the coarser grained experiment (181) at low temperature, while at high temperatures the opposite is true: concentrations of Al, Si and Ca in experiment 182 (coarser grain fraction) are higher than those observed in the fine grained experiment (184) at similar conditions. This behaviour is illustrated in Figures 4.1.55 and 4.1.56, which compare the albite dissolution rates, based on Si release for the two sets of experiments. These results indicate that grain size changes on the order of a few hundred microns can have a dramatic effect on the dissolution behaviour of albite under these conditions.

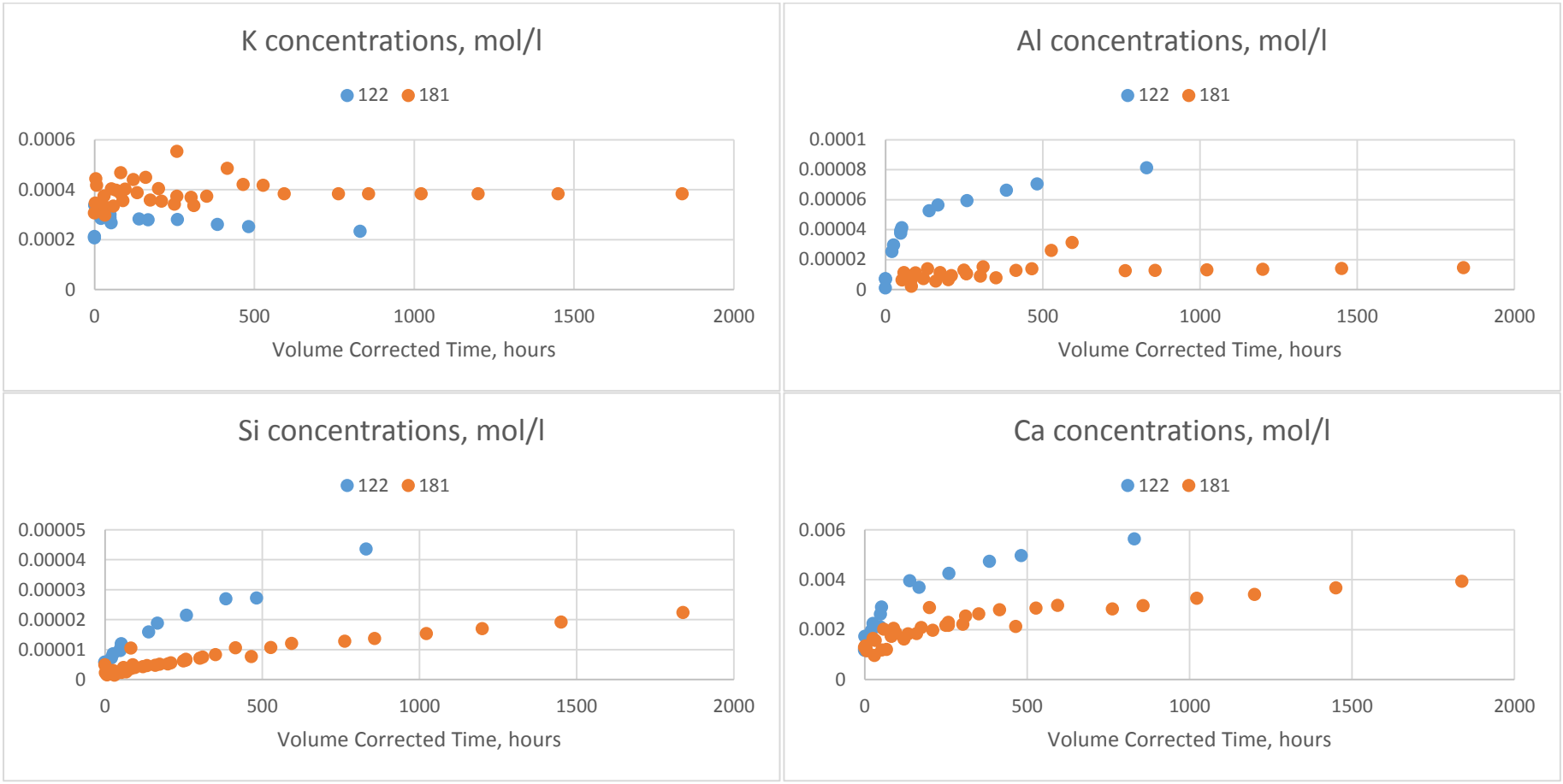


**Figures 4.1.47 – 4.1.50**: Comparative charts of (from top left, moving clockwise) K, Al, Ca and Si concentrations for experiments 122 (125µm - 180µm) and 181 (500µm - 600µm)

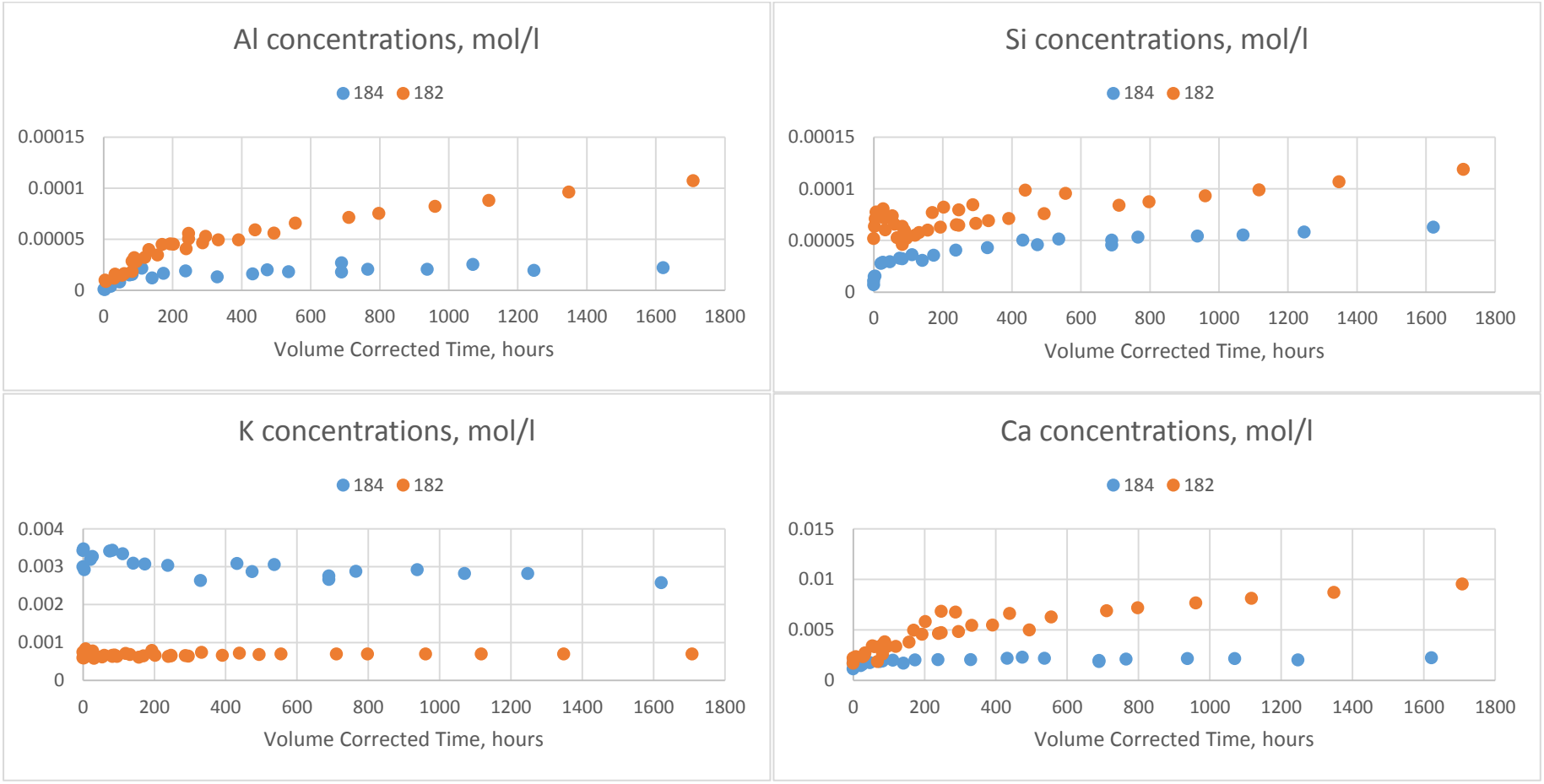


**Figures 4.1.51 – 4.1.54**: Comparative charts of (from top left, moving clockwise) Al, Si, Ca and K concentrations for experiments 184 (125µm - 180µm) and 182 (500µm - 600µm)

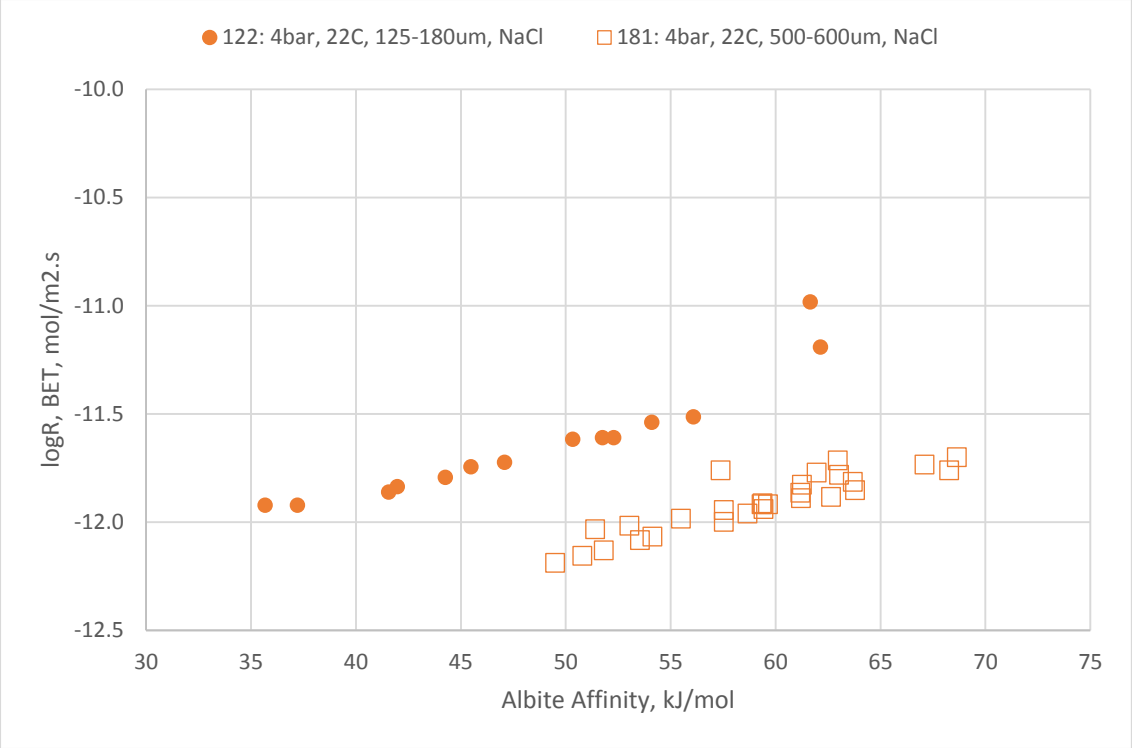


**Figures 4.1.55**: Calculated albite dissolution rates and affinities for experiments 122 and 181

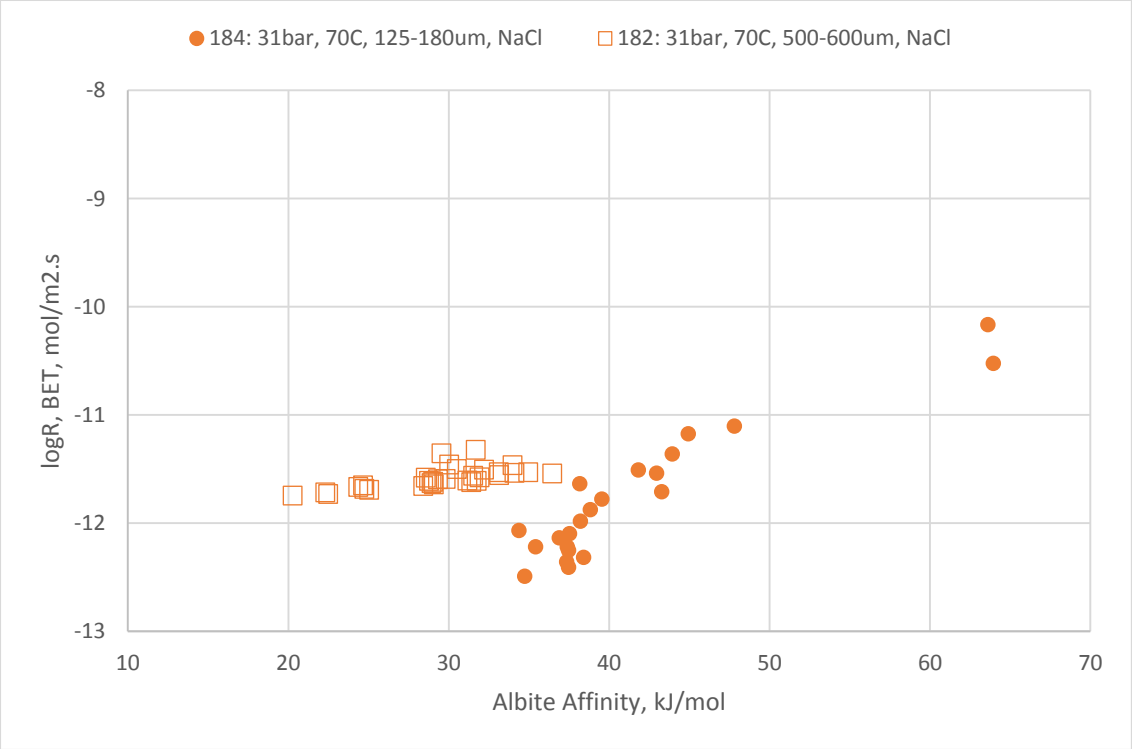


**Figures 4.1.56**: Calculated albite dissolution rates and affinities for experiments 184 and 182

#### 4.1.3.4 Dissolution Behaviour: Effect of Fluid Composition

Experiments 184 (1.36M NaCl, 31bar $pCO_2$, 70°C) and 185 (deionised water, 31bar $pCO_2$, 70°C) are compared in Figures 4.1.57 – 4.1.60. Al and early time Si release are similar between the two experiments, however at later times Si concentrations in the deionised water experiment (185) are notably higher than those observed in the NaCl experiment (184). Ca release rate and overall concentration are likewise higher in experiment 185. Figure 4.1.61 compares the albite dissolution rates, based on Si release for the two experiments. While rates are broadly similar between the two experiments, the calculated dissolution rates in the NaCl experiment (184) appear to show a strong decrease with decreasing albite affinity, as opposed to the results from the deionised water experiment which show little change with affinity. The results suggest that while the introduction of NaCl has little effect on the overall dissolution of the mineral, it does suppress the leaching of Ca from the plagioclaise component.

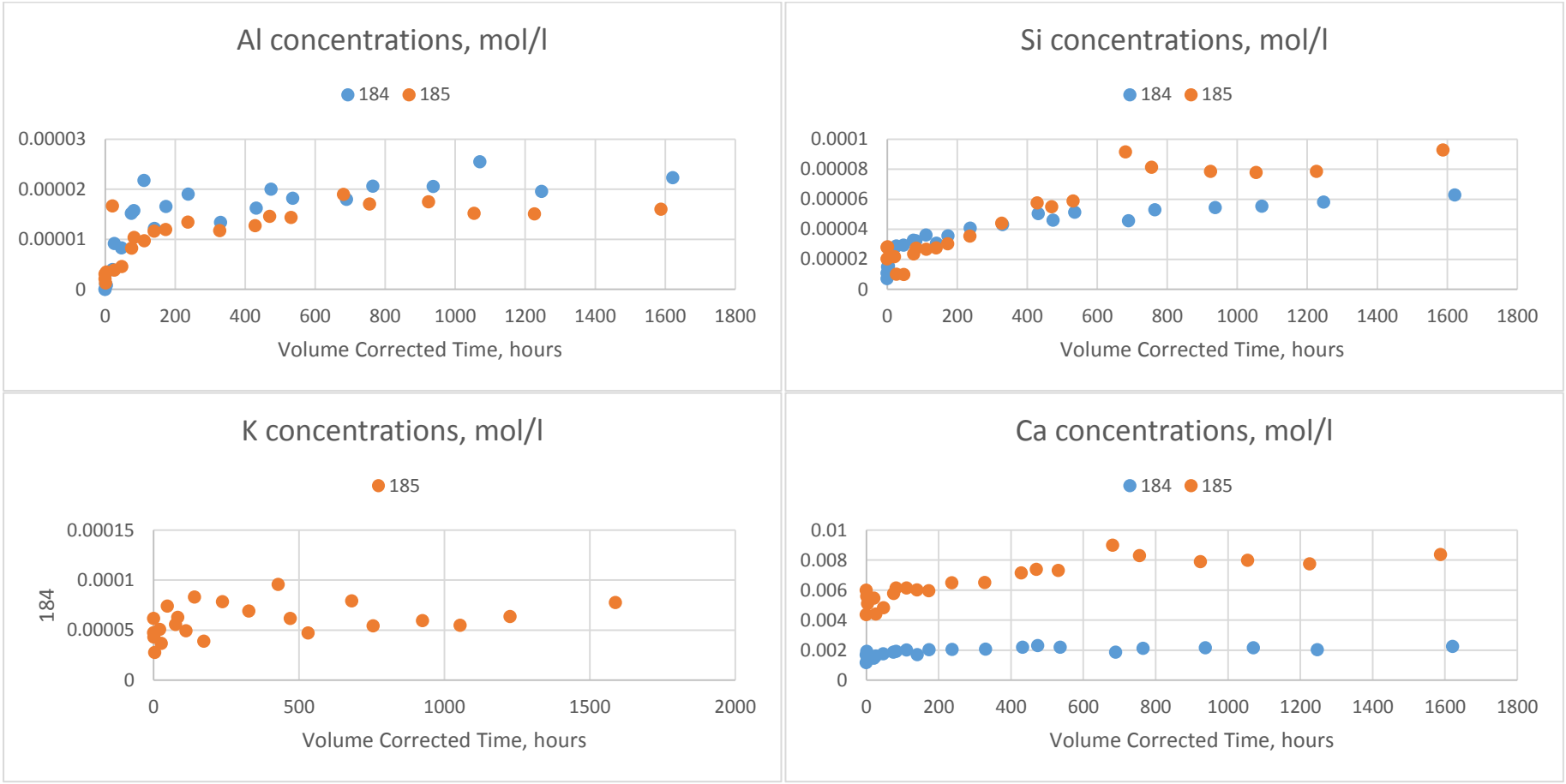


**Figures 4.1.57 – 4.1.60**: Comparative charts of (from top left, moving clockwise) Al, Si, Ca and K concentrations for experiments 184 (NaCl) and 185 (DI)

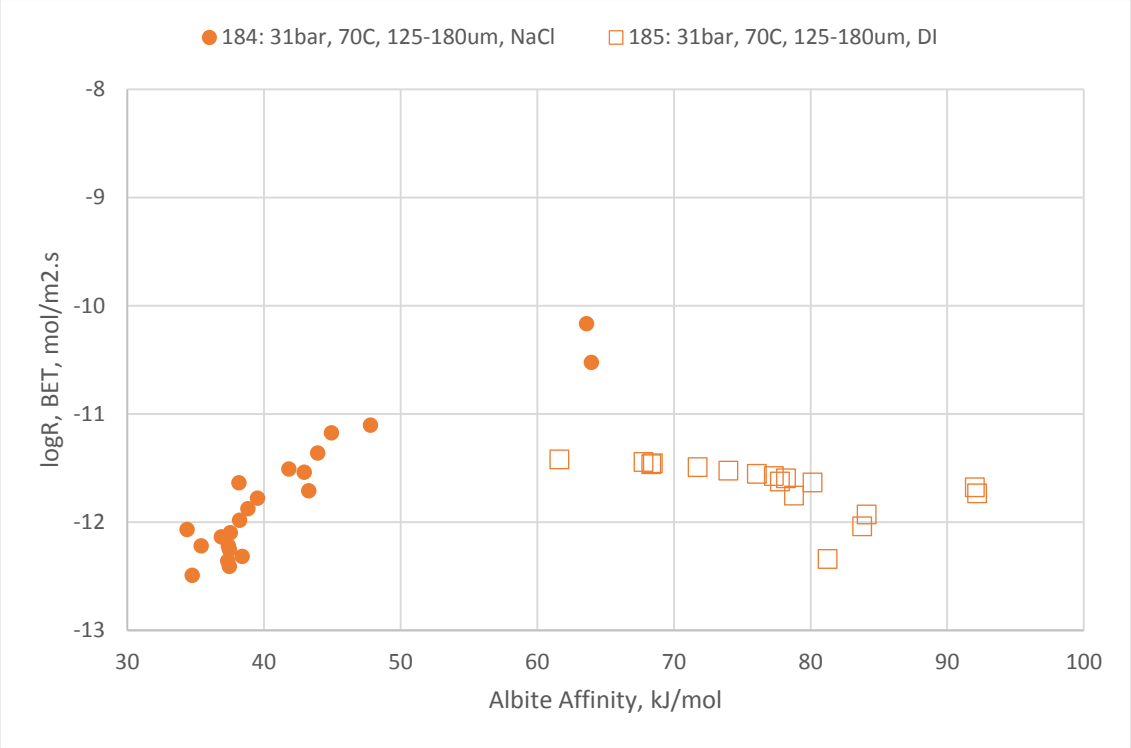


**Figures 4.1.61**: Calculated albite dissolution rates and affinities for experiments 184 and 185

#### 4.1.3.5 Dissolution Behaviour: Effect of Elevated $pCO_2$ (4bar, 31bar) and Temperature (22°C, 70°C)

Elemental release from experiments 122 (4bar $pCO_2$, 22°C, NaCl) and 184 (31bar $pCO_2$, 70°C, NaCl), experiments 181 (4bar $pCO_2$, 22°C, NaCl) and 182 (31bar $pCO_2$, 70°C, NaCl) and experiments 185 (31bar $pCO_2$, 70°C, DI) and 183 (4bar $pCO_2$, 70°C, DI) are compared in Figures 4.1.62 – 4.1.73. Calculated albite dissolution rates based on Si release are compared for the three sets of experiments in Figures 4.1.74 - 4.1.76. Note that K concentrations are not available for experiment 184.

While comparison between experiments 181 (low P/T) and 182 (high P/T) clearly shows higher (around 4-5 times) albite dissolution rates at increased temperature and pressure, the comparison between 122 (low P/T) and 184 (high P/T) is not as clear cut. Si concentrations in the high temperature experiment (184) are clearly higher and Si based dissolution rates are generally higher than in experiment 122, though they converge at late times. However Al and Ca concentrations and release rates are higher in experiment 122 (low P/T). The bulk mineral dissolution rate as calculated from Si release, however, it generally higher for experiment 184 (Figure 4.1.74)

The comparison between experiments 185 and 183, where the only variable is $pCO_2$, indicates that $CO_2$ pressure, and hence acidity has a major effect only on K release, with K concentrations in the lower pressure experiment around 2-3x lower than those in the higher pressure experiment. This increase in K release at higher $pCO_2$ is also reflected in experiment 182 where K concentrations are elevated relative to the low $pCO_2$ comparison experiments.

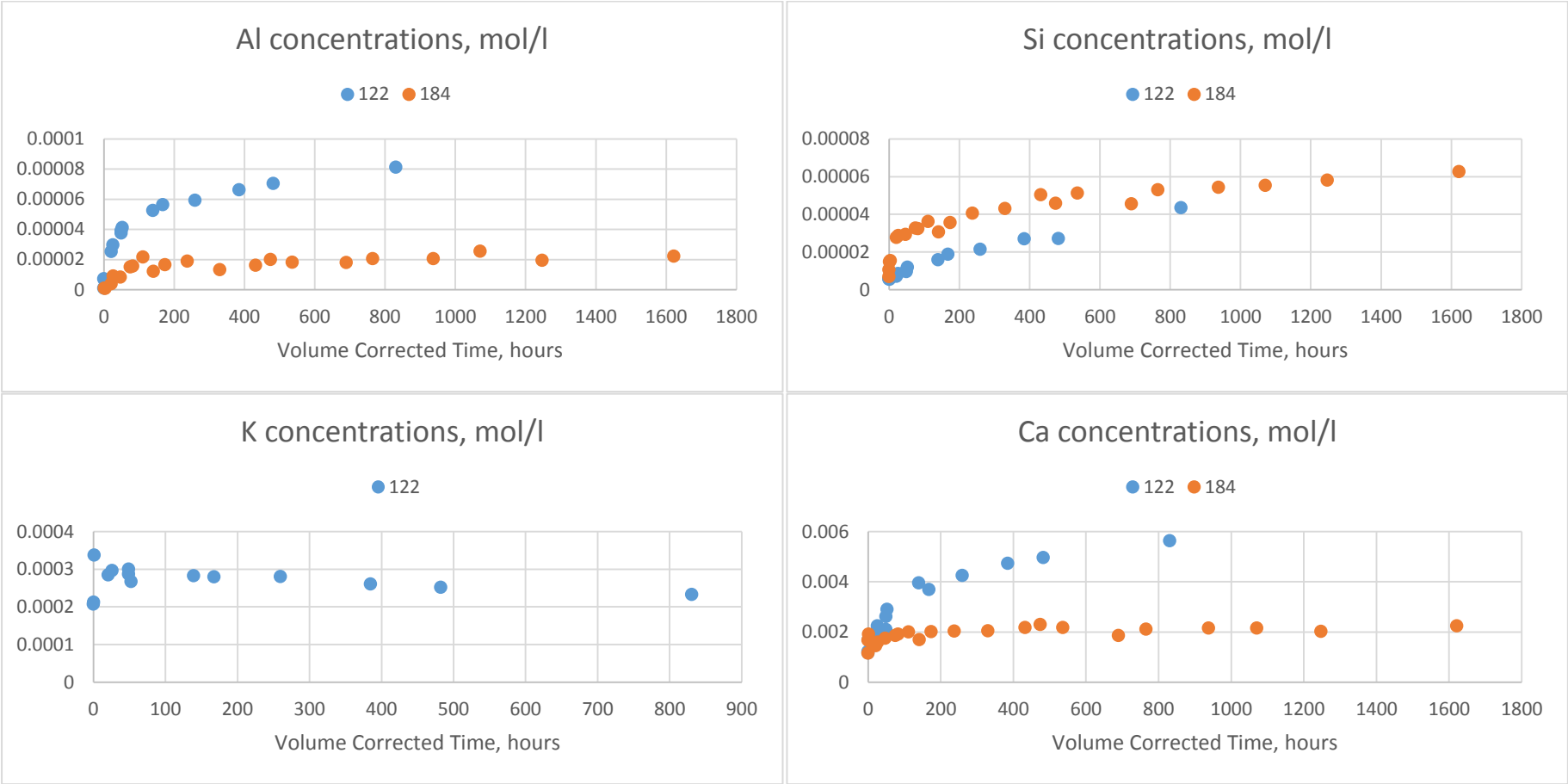


**Figures 4.1.62 – 4.1.65**: Comparative charts of (from top left, moving clockwise) Al, Si, Ca and K concentrations for experiments 122 (4bar, 22°C) and 184 (31bar, 70°C)

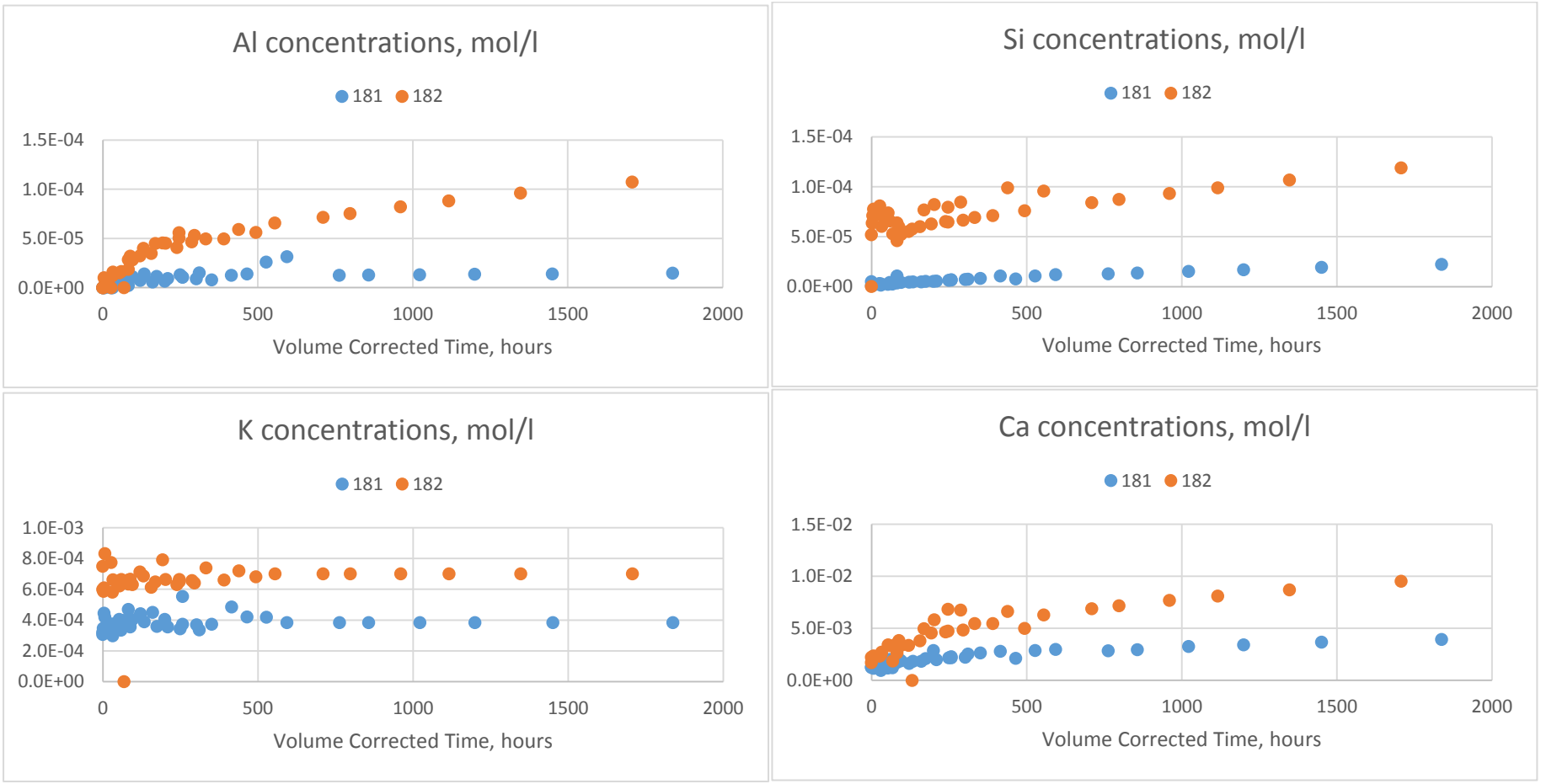


**Figures 4.1.66 – 4.1.69**: Comparative charts of (from top left, moving clockwise) Al, Si, Ca and K concentrations for experiments 181 (4bar, 22°C) and 182 (31bar, 70°C)

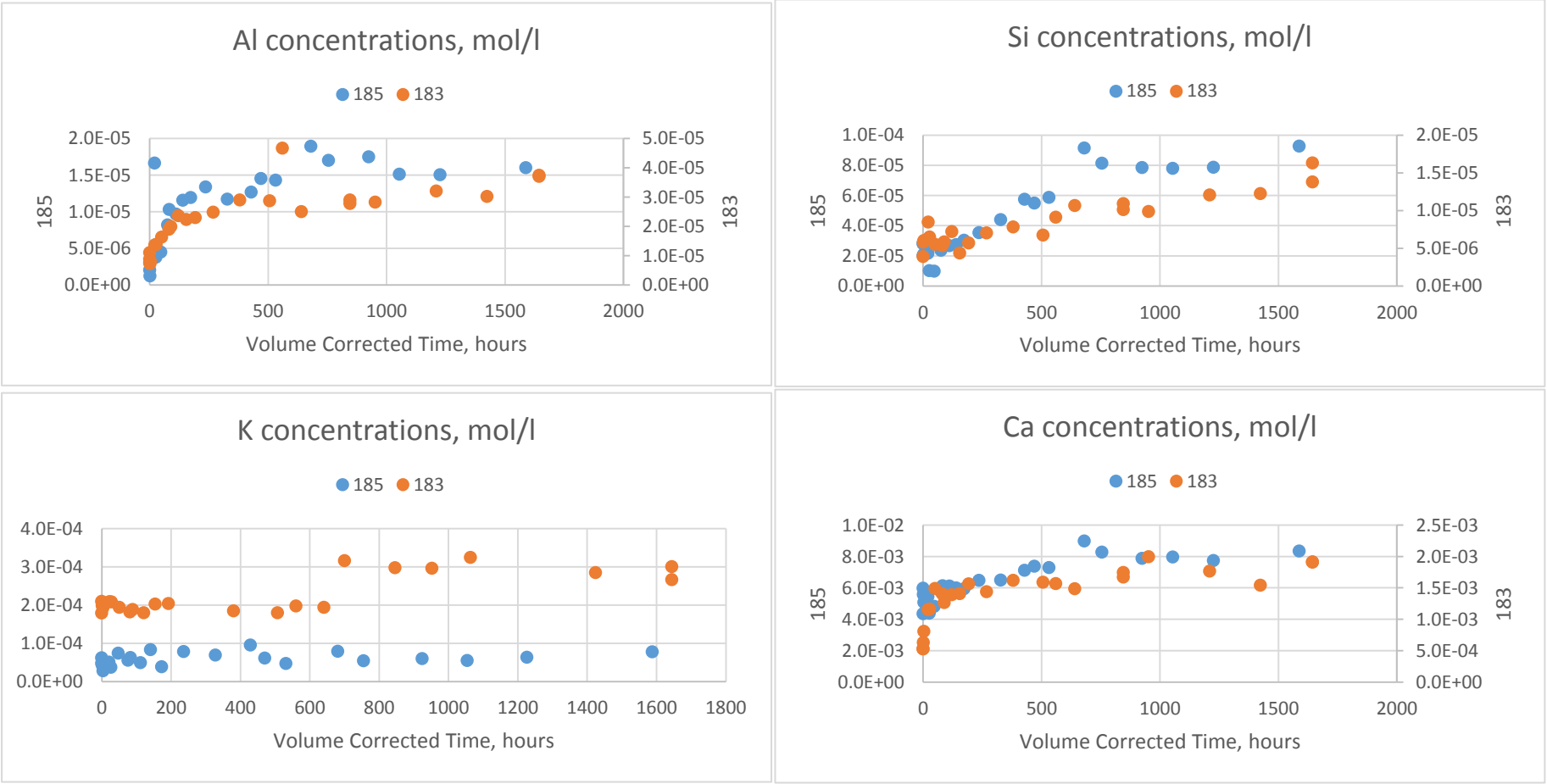


**Figures 4.1.70 – 4.1.73**: Comparative charts of (from top left, moving clockwise) Al, Si, Ca and K concentrations for experiments 185 (31bar, 70°C) and 183 (4bar, 70°C)

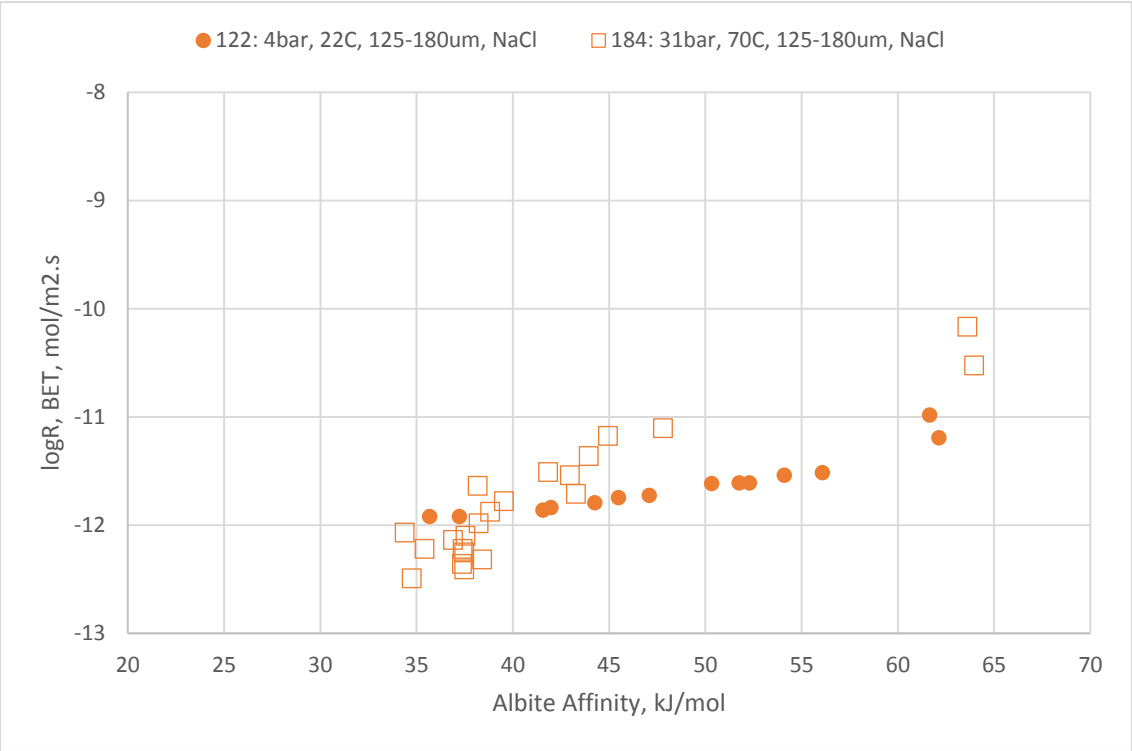


**Figures 4.1.74**: Calculated albite dissolution rates and affinities for experiments 122 and 184

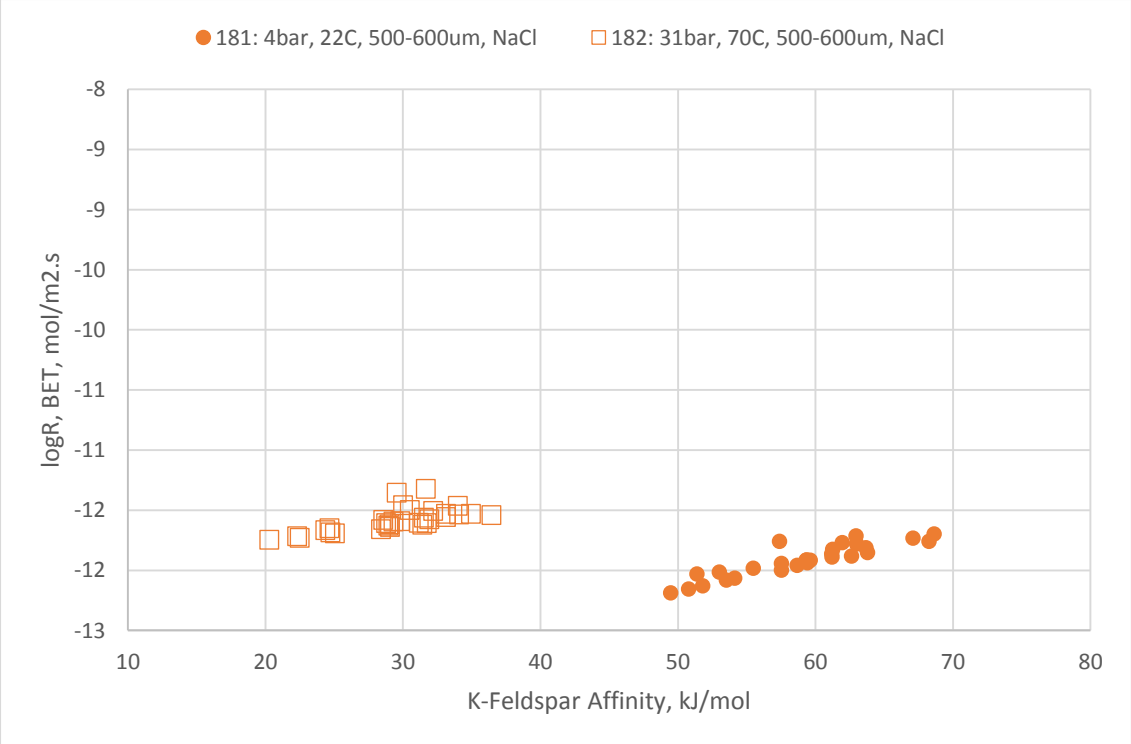


**Figures 4.1.75**: Calculated albite dissolution rates and affinities for experiments 181 and 182

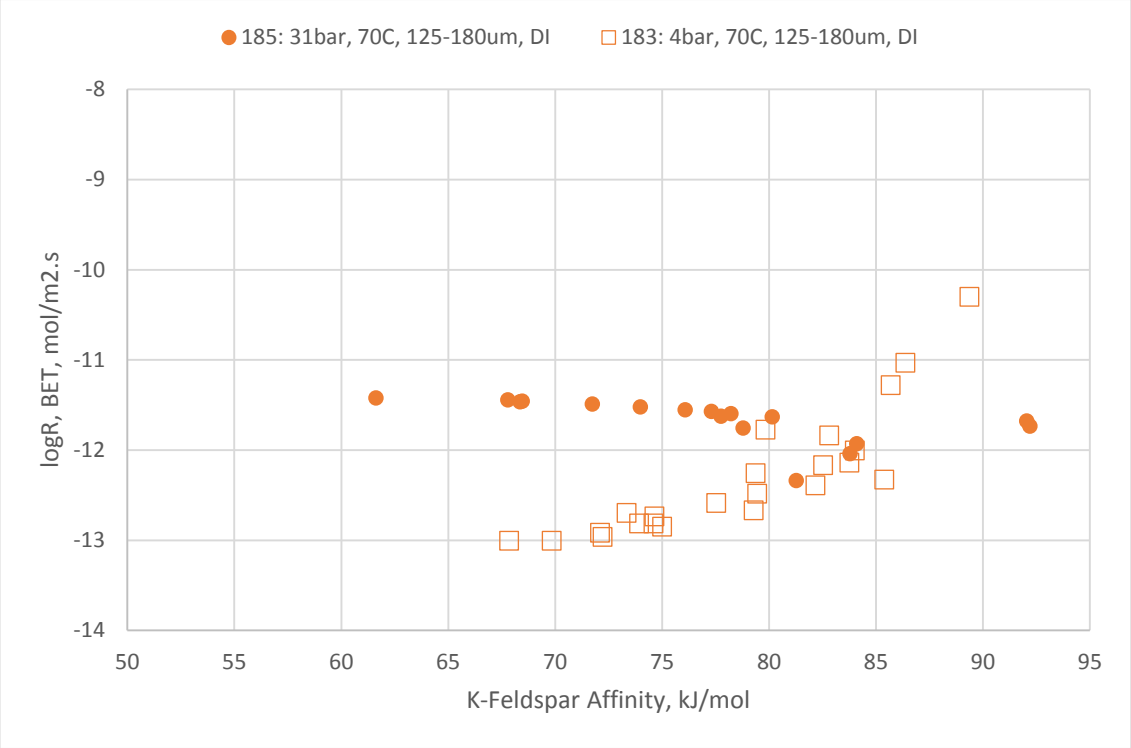


**Figures 4.1.76**: Calculated albite dissolution rates and affinities for experiments 185 and 183

#### 4.1.3.6 Albite Dissolution Rates

Albite dissolution rates have been calculated from the observed Si release and measured BET surface area, and are presented in Figures 4.1.77 – 4.1.83, alongside values predicted by various literature equations. The equations used are those also used in evaluation of the K-feldspar dissolution rates, details of which can be found in Section 4.1.2.6.

Albite affinity has been calculated using the equation:

$$A = RT \times \ln\left(\frac{K_{Albite}}{(a_{Na^+} \times a_{Al(OH)_4^-} \times a^3_{H_4SiO_4})}\right) \quad (4.1.7)$$

Where $K_{Albite}$ is the equilibrium constant for albite at the experimental conditions, R is the gas constant, T is the temperature in Kelvin, and $a_{Na^+}$, $a_{Al(OH)_4^-}$ and $a^3_{H_4SiO_4}$ are the activities of the appropriate ions in solution, as calculated using by PHREEQC3 using the measured fluid compositions. Note that since Na concentrations were not measured they have had to be estimated for the purposes of these calculations. For the brine experiments Na concentrations are assumed to be the starting concentration of the brine (1.36 mol/l) plus the molar equivalent of the measured Si concentration, assuming stoichiometric release. For the deionised water experiments (183 and 185), Na concentrations are assumed to equal to molar equivalent of the measured Si concentration. While these assumptions are probably adequate for the brine experiments, where Na concentrations are dominated by the starting fluid concentrations, the affinities calculated for the deionised water experiments should be treated with more caution. However Si concentrations have a much larger contribution to the product of Equation 4.1.7 and it is assumed that the affinities calculated are reasonable estimates of the actual albite affinities of the experimental fluids.

The results are largely similar to those produced by the analysis of the K-feldspar experiments presented in Section 4.1.2.6: calculated rates generally agree favourably with the rates calculated using the USGS general rate equation and that produced by Burch et al. using values presented in Hellmann et al (2010). The equation presented by Gautier et al generally over-predicts the observed dissolution rates. Observed rates in experiment 123 are higher than all three predictions. Rates generally show less decrease with decreasing affinity than in the K-feldspar experiments, enhancing their fit to the USGS and Burch equation predictions.

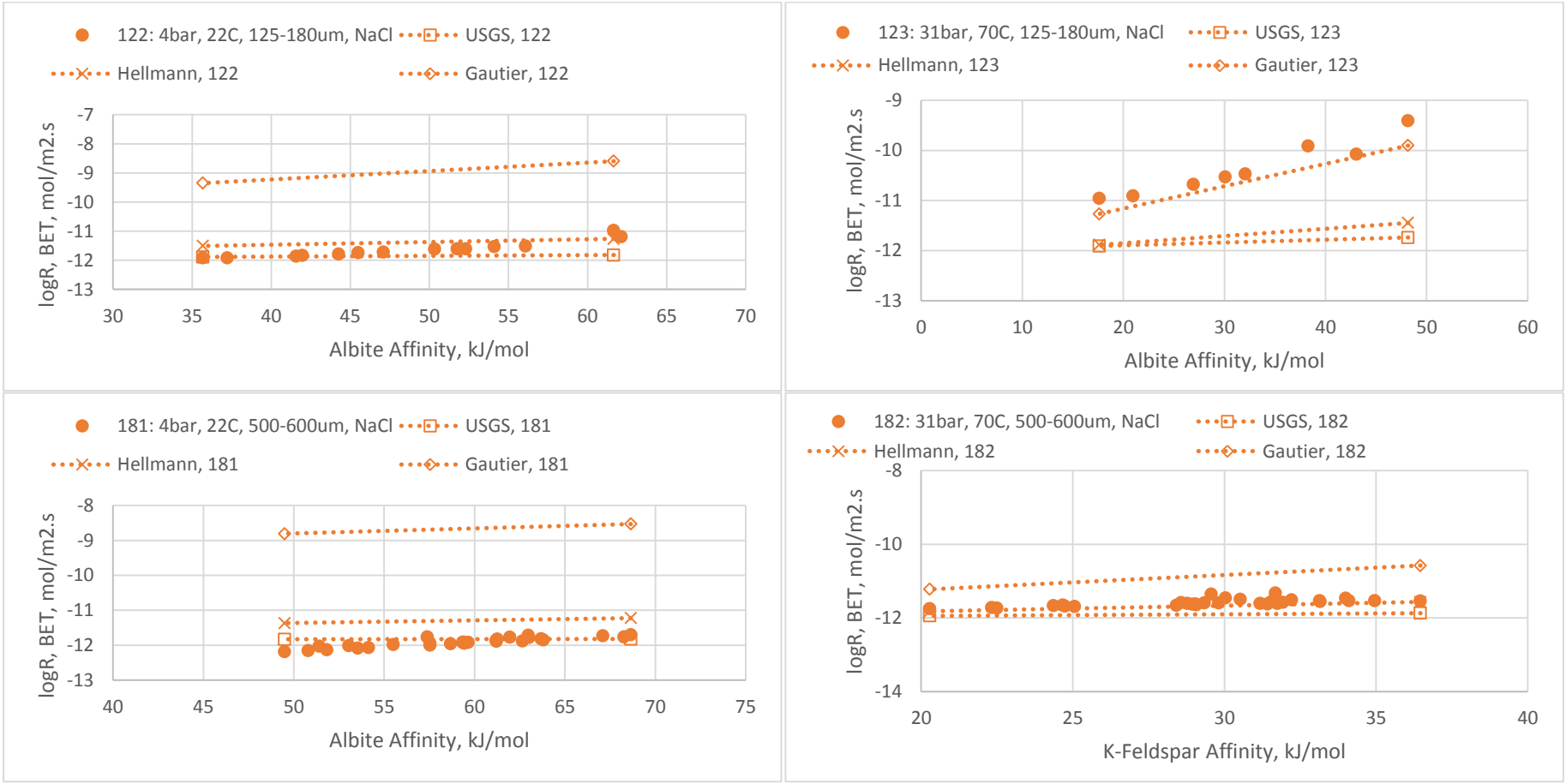


**Figures 4.1.77 – 4.1.80**: Calculated Albite dissolution rates based on Si release and BET surface area, plotted together with various calculated predictions for (from top left moving clockwise) experiments 122, 123, 181 and 182

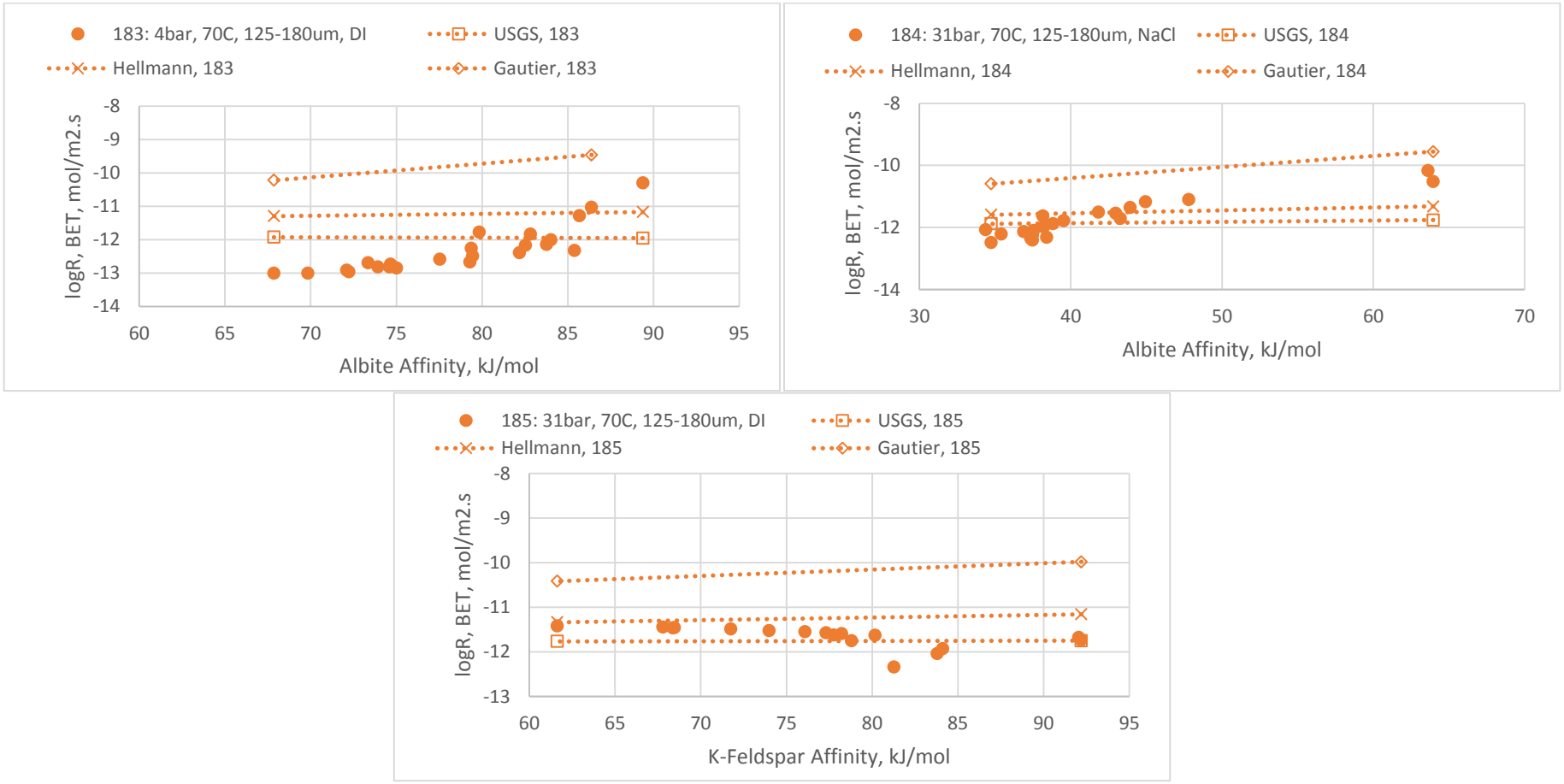


**Figures 4.1.81 – 4.1.83**: Calculated Albite dissolution rates based on Si release and BET surface area, plotted together with various calculated predictions for (from top left moving clockwise) experiments 183, 184 and 185

#### 4.1.3.7 Albite Dissolution Experiments Overview and Discussion

Much of the dissolution behaviour observed in the albite experiments presented above is similar to that discussed for the K-feldspar experiments in Section 4.1.2.7. Hence where appropriate the reader will be referred to that section for details, rather than repeating them here.

As for the K-feldspar experiments and for other single mineral dissolution experiments presented in this work, calculated and measured dissolved $CO_2$ content of samples from the albite experiments are in good agreement and are generally close to the predicted equilibrium values. Also similar to the K-feldspar experiments are the calculated pH values, which change very little over the course of the experiments and are well below the predicted equilibrium values. As for K-feldspar, these results reflect the sluggishness of feldspar dissolution and the relative insensitivity of $CO_2$ solubility to fluid composition.

As for the K-feldspar experiments, elemental release from the albite is non-stoichiometric, with the release of the network modifiers K and Ca outstripping Al and Si release from the silicate framework.

The changes in dissolution behaviour of the albite with grain size appear more complex than those of the K-feldspar. While K release is higher in both coarse grained experiments looked at than in their finer grained counterparts, overall Al and Ca release appears to be higher with the coarser fraction at elevated P/T, but lower at low P/T. The behaviour of K may be explained in the same manner as for the K-feldspar experiments; grinding of minerals may cause destruction of reactive surface area. In this case the K-feldspar component in the experimental feldspar appears to have been most affected i.e. the K-feldspar phase was more susceptible to loss of reactive surface area during grinding. The differing behaviour of the grain sizes at different P/T conditions is more difficult to reconcile with the available data. However, calculated rates for dissolution of the bulk mineral are similar in both cases and it is possible that one of the experiments contained a sample particularly rich in a particular phase or grain type.

The behaviour of the albite material in deionised water vs. NaCl is similar to that of the K-feldspar in that calculated dissolution rates of the bulk mineral a lower in the NaCl fluid. In this case, the rates also show a rapid drop off with affinity, not reproduced in the deionised water experiment. The affinities in experiment 184, in which this decrease is seen, and it may be that the drop in rates represents the switch from dissolution plateau to transitional phase

as equilibrium is approached (see Section 4.1.2.7) (Burch et al. 1993); the affinities for the experiment certainly lie in the 50kJ/mol – 25kJ/mol window suggested by the results of Burch et al (1993).

The comparison between results at low and high P/T conditions indicates that increased temperature enhances bulk mineral dissolution (based on Si release). The increase in $pCO_2$ had little effect except on K release, which was higher at higher pressures. This indicates that the increased acidity at higher pressures had a measurable enhancement on exchange between $K^+$ at the K-feldspar rich parts of the mineral surface and $H^+$ in the fluid, but little overall effect on bulk dissolution of the mineral.

As for the K-feldspar experiments calculated rates are generally in good agreement with those predicted by the Burch et al and USGS rate equations, while the equation produced by Gautier over-predicted dissolution rates. The exception to this general trend is for experiment 123, whose dissolution rates are well predicted by the Gautier equation, though why this is the case is unclear. In general the relative discrepancies between predicted and calculated rates may be explained as for K-feldspar in Section 4.1.2.7.

In conclusion, generally the trends observed in the albite experiments are similar to those observed in the K-feldspar experiments, particularly in terms of fitting dissolution rates to literature equations: again the Burch et al and USGS equations provide the better description of albite dissolution than the Gautier equation under these conditions. As for K-feldspar there is some evidence for grain-size effects and suppression of dissolution rate by the addition of NaCl in these experiments. The addition of $CO_2$ appears to have little effect on bulk mineral dissolution, but does appear to enhance exchange between $K^+$ and $H^+$.

## 4.2 Carbonate Minerals

### 4.2.1 Calcite

#### 4.2.1.1 pH and $CO_2$ Solubility

Six batch experiments were carried out on powdered calcite material, the conditions of which are summarised in Table 4.2.1.

| Experiment ID | Grain Fraction, µm | Fluid | pCO2, bar (absolute) | Temperature, $^0$C | Run time, volume constant hours | Conditioning period prior to $CO_2$ injection, hours |
|---|---|---|---|---|---|---|
| 191 | 125-180 | 1.36M NaCl | 4 | 22 | 1629 | 144 |
| 192 | 125-180 | 1.36M NaCl | 31 | 70 | 1472 | 359 |
| 193 | 125-180 | DI | 4 | 22 | 1206 | 142 |
| 103 | 500-600 | 1.36M NaCl | 4 | 22 | 1405 | 227 |
| 195 | 125-180 | DI | 31 | 70 | 1328 | 144 |
| 196 | 125-180 | 1.36M NaCl | 4 | 70 | 1228 | 219 |

**Table 4.2.1**: Summary of experimental conditions for Calcite batch experiments

Figures showing full results of fluid pH calculations and measurements can be found in Appendix B, but selected results, showing measured pH where available, equilibrium pH as calculated by PHREEQC3 and final sample pH as calculated by PHREEQC are shown in Table 4.2.2 which also summarises calculations and measurements of dissolved $CO_2$ content from the batch experiments.

The full results of pH calculations based on fluid analyses indicate a relatively high initial pH of between 7.5 and 10. Upon injection of $CO_2$, calculations suggest pH falls to values similar to that of a mineral free $CO_2$-fluid-only system: pH 3 - pH 4. Release of $Ca^{2+}$ and associated buffering of pH through formation of bicarbonate initiates immediately and calculated pH suggests rapid buffering for approximately the first 50 hours of experiment. After this initial rapid buffering to a pH of between 4.5 and 5.5, depending on the experiment, pH is generally very stable for the remainder of the

experiments, varying by only 0.1-0.2 pH units. This behaviour is illustrated for experiment 103 in Figure 4.2.1.

| Run | Fluid/ $pCO_2$ (bar)/T (°C) | Equilibrium $CO_2$ PHREEQC3, mol/kg | Final Sample CO2, Duan, mol/kg | Final Sample $CO_2$ PHREEQC3, mol/kg | Final Sample $CO_2$ (Measured), mol/kg | Standard Deviation, $CO_2$ (No. of measurements) | Equilibrium pH, PHREEQC3 | Final Sample pH, PHREEEC3 | Final Sample pH, measured |
|---|---|---|---|---|---|---|---|---|---|
| 196 | NaCl/4/70 | 0.056 | 0.043 | 0.049 | - | - | 5.690 | 5.062 | - |
| 191 | NaCl/4/22 | 0.162 | 0.106 | 0.129 | 0.128 | 0.011 (3) | 5.653 | 5.266 | 5.340 |
| 103 | NaCl/4/22 | 0.162 | 0.106 | 0.129 | 0.139 | 0.001 (3) | 5.653 | 5.283 | 5.370 |
| 193 | DI/4/70 | 0.179 | 0.140 | 0.121 | 0.190 | 0.011 (3) | 5.626 | 5.098 | 5.570 |
| 192 | NaCl/31/70 | 0.342 | 0.308 | 0.311 | 0.328 | 0.038 (3) | 5.138 | 4.761 | - |
| 195 | DI/31/70 | 0.429 | 0.398 | 0.303 | 0.375 | 0.034 (3) | 5.653 | 5.266 | 5.340 |

**Table 4.2.2**: Summary of pH and $CO_2$ solubility measurements and calculations for Calcite batch experiments

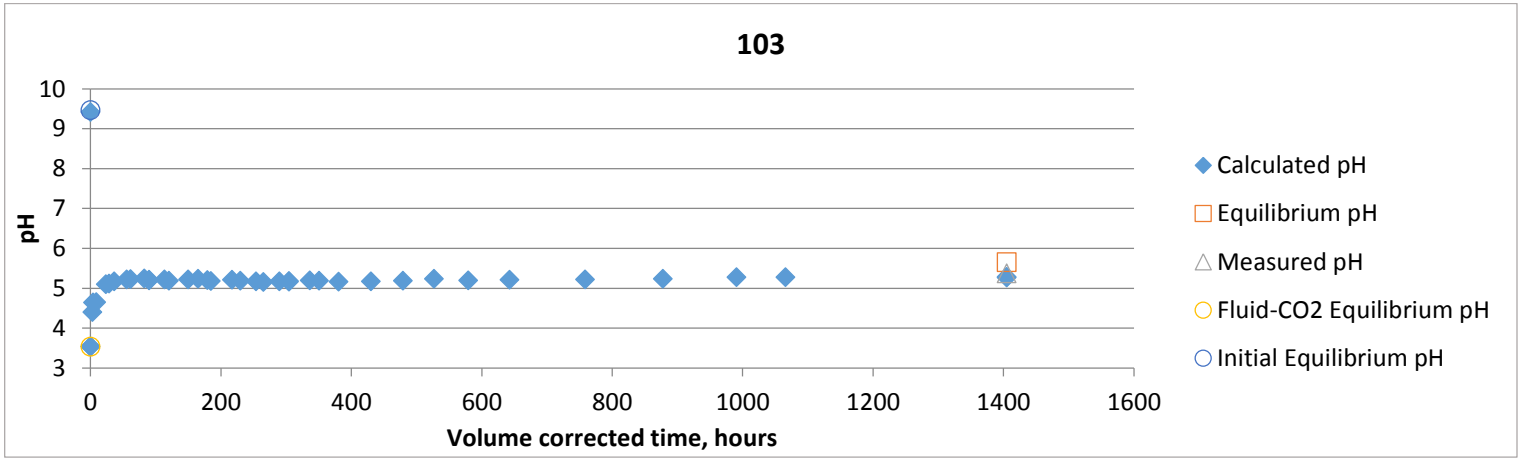


**Figure 4.2.1**: Calculated pH for samples from experiment 103

Despite the apparent stability of pH, in nearly all experiments calculated and measured final sample pH were below the predicted equilibrium pH, though the discrepancy is less than for the feldspar experiments discussed in Sections 4.1.2 and 4.1.3. The one exception to this was for experiment 193, where measured pH and predicted equilibrium pH were very similar. It is likely that this was due to analytical error during the measurement of pH: pH was measured in a flow-through cell and measuring pH in this manner can be problematic if care is not taken to maintain a very low flow, not only because of the effect of fluid movement on the measurement, but also because of potential degassing of carbon dioxide, which would increase pH.

In terms of $CO_2$ solubility, there is generally good agreement between modelled and measured results. $CO_2$ contents of final samples calculated with PHREEQC3 (based on fluid analyses) were all within ±27% of measured values. The simpler model of Duan et al. produced similar results; though it generally underestimated $CO_2$ content of final samples, all calculations were again within ±27% of measured values. Measured values are generally slightly lower than predicted equilibrium values, as calculated by PHREEQC3, but again are reasonably similar, within ±27%.

#### 4.2.1.2 Dissolution Behaviour: General Observations

Ca concentrations generally show increase in all experiments for the first few hundred hours of run time. However Ca concentrations tend to show a small peak and drop at later times for the majority of the calcite experiments, with the exception of experiments 192 and 193. This behaviour is illustrated in Figure 4.2.2 for experiment 103. An explanation for these peaks is not obvious Similar peaks are observed in the low concentrations of Mg and Mn in the experiments. At this point in the experiments pH is well above the level where it should exert a strong influence on dissolution (>pH 4) and is relatively stable. Likewise saturation indices for all Ca containing phases are well below saturation, so precipitation effects do not seem likely. A more likely explanation would be adsorption of cations onto leached sites on the calcite surface. The peaks seem to correspond to a relatively sudden switch between a relatively high release rate beforehand and a considerably lower one afterwards and it is possible that cations in solution begin to reabsorb onto the calcite surface at some threshold value. Such a process may conceivably cause an initial drop in dissolved analyte concentration, followed by a switch a lower release rate regime, where high energy dissolution sites are occupied by adsorbed ions. Dissolution rates following this switch will therefore be a function of adsorbate concentration at the calcite surface as well as dissolved analyte concentration.

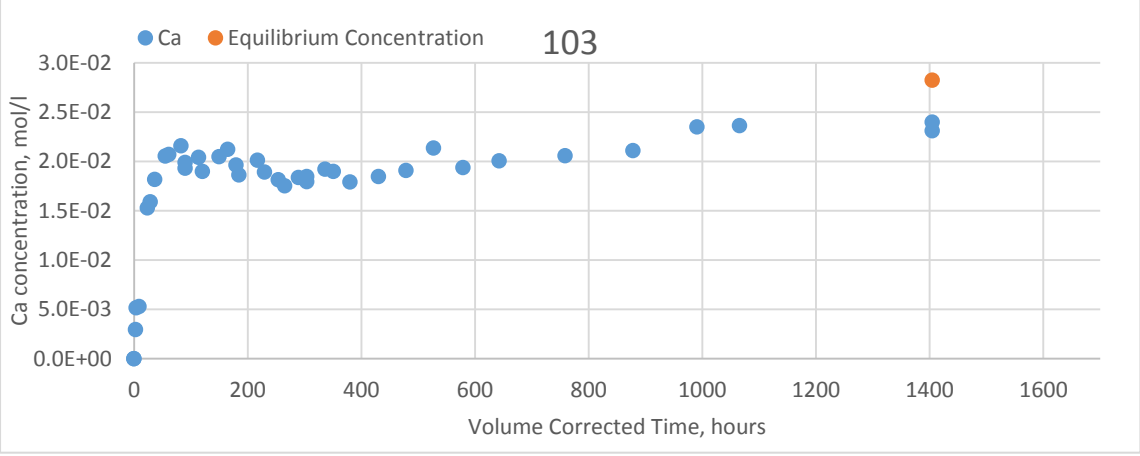


**Figure 4.2.2**: Measured Ca concentrations for experiment 103, showing a small peak in concentrations at around 100 hours

#### 4.2.1.3 Dissolution Behaviour: Grain Size

Figure 4.2.3 compares experiment 191 (125-180µm, 1.36M NaCl, 4bar $pCO_2$, 22°C) with experiment 103 (500-600µm, 1.36M NaCl, 4bar $pCO_2$, 22°C). Figure 4.2.4 compares the calculated calcite dissolution rates for the two experiments, based on Ca release and BET surface area. Calcium release is broadly similar, both in terms of magnitude and rate. A small peak in $Ca^{2+}$ concentration is seen at around 100 hours in both experiments, though It is more apparent in experiment 103, in both cases the peak precedes a more gradual rise in Ca concentration. The results indicate that grain-size (and hence surface area) changes on the scale investigated here have little effect on calcite dissolution.

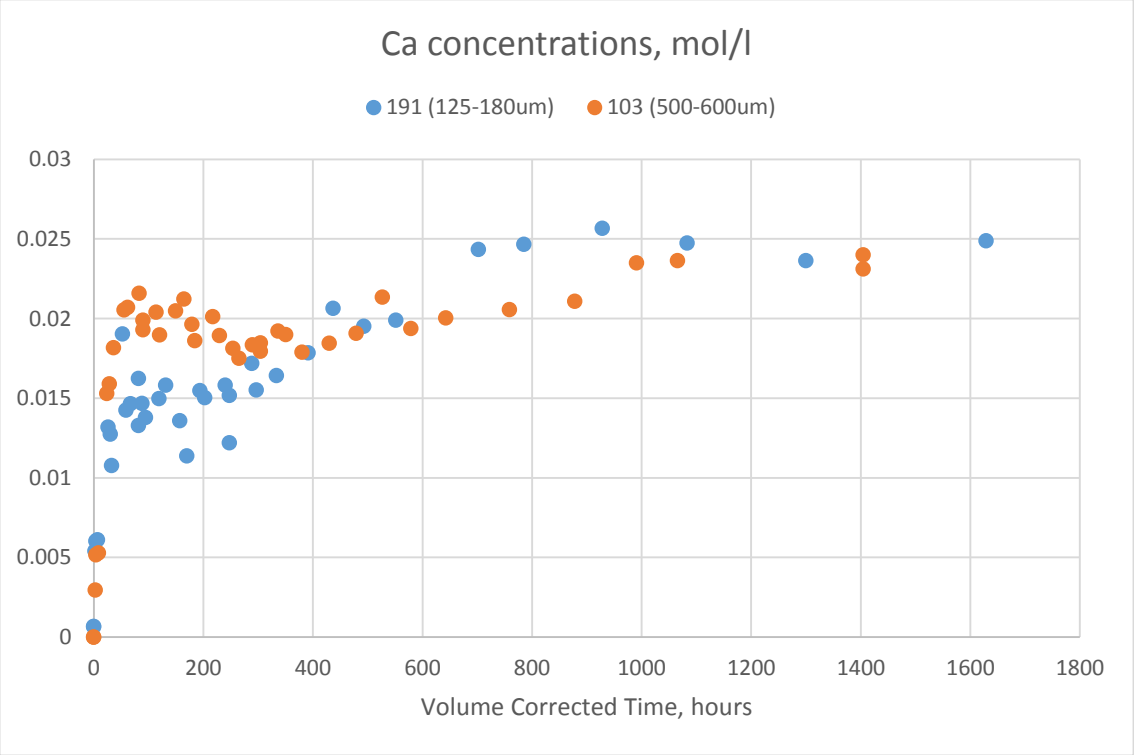


**Figure 4.2.3**: Comparative chart of Ca concentrations for experiments 191 (125µm - 180µm) and 103 (500µm - 600µm)

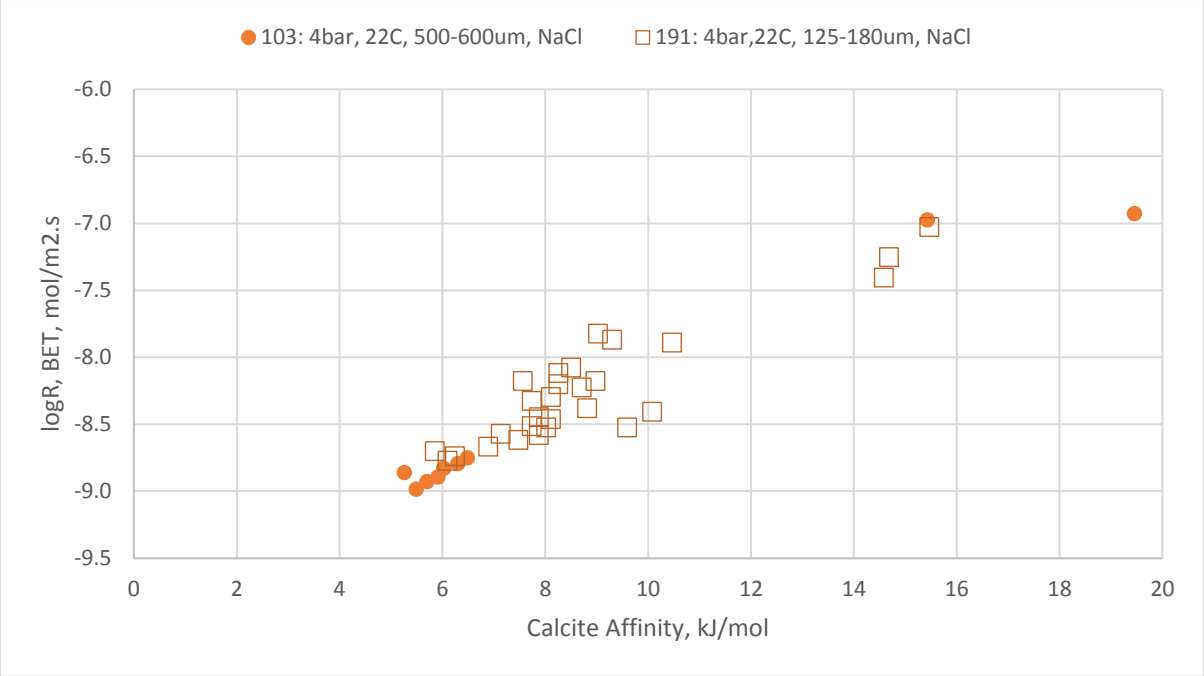


**Figure 4.2.4**: Calculated calcite dissolution rates and affinities for experiments 103 and 191

#### 4.2.1.4 Dissolution Behaviour: Fluid Composition

Figures 4.2.5 and 4.2.6 compare dissolved $Ca^{2+}$ concentrations from experiments 191 (1.36M NaCl, 4bar $pCO_2$, 22°C) and 193 (deionised water, 4bar $pCO_2$, 22°C) and 192 (1.36M NaCl, 31bar $pCO_2$, 70°C) and 195 (deionised water, 31bar $pCO_2$, 70°C). The calculated calcite dissolution rates based on Ca release and BET surface area are compared in Figures 4.2.7 and 4.2.8.

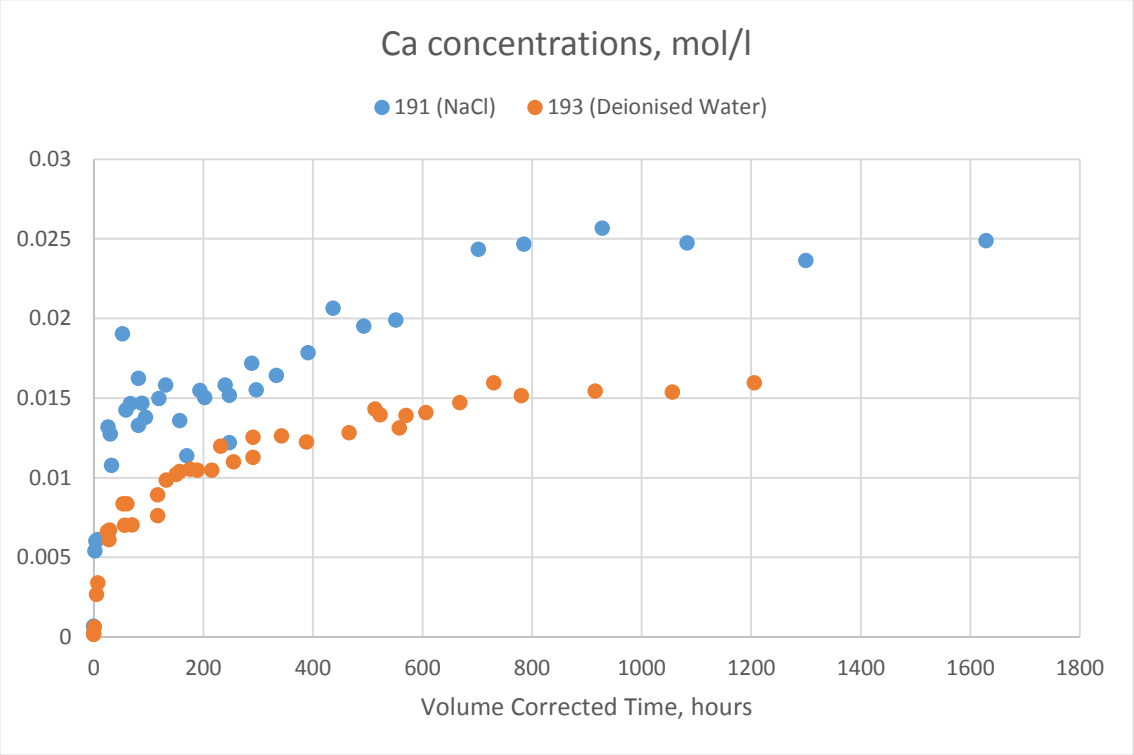


**Figure 4.2.5**: Comparative chart of Ca concentrations for experiments 191 (NaCl) and 193 (DI)

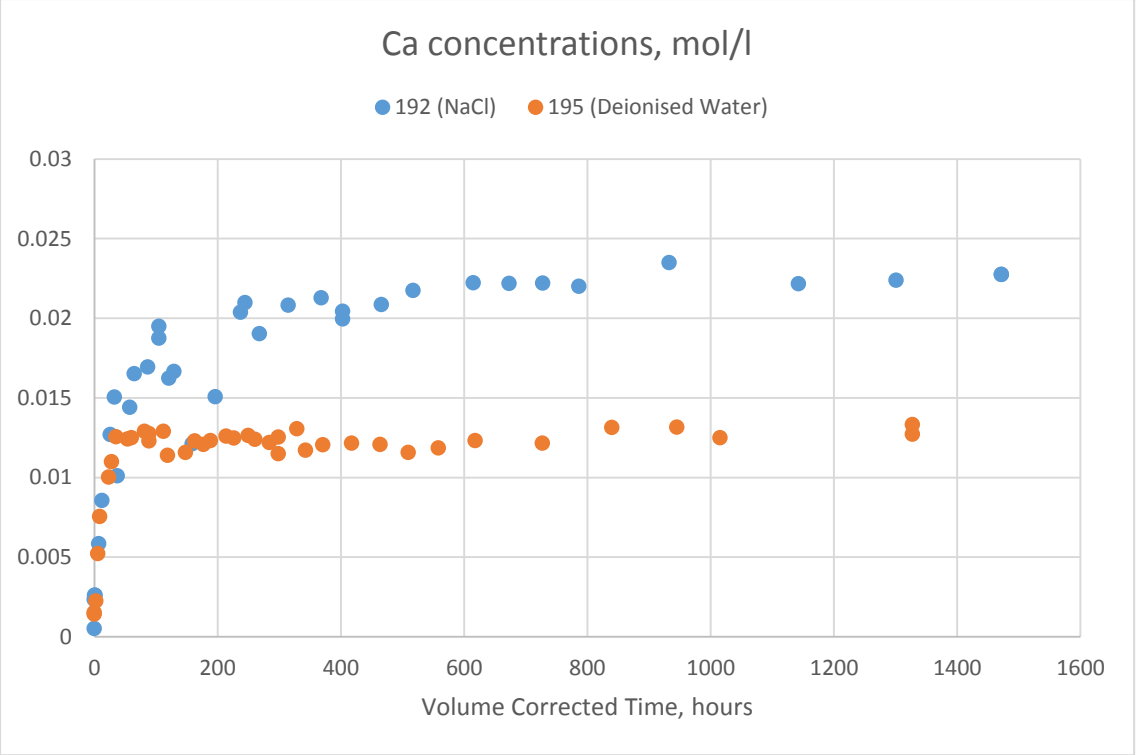


**Figure 4.2.6**: Comparative chart of Ca concentrations for experiments 192 (NaCl) and 195 (DI)

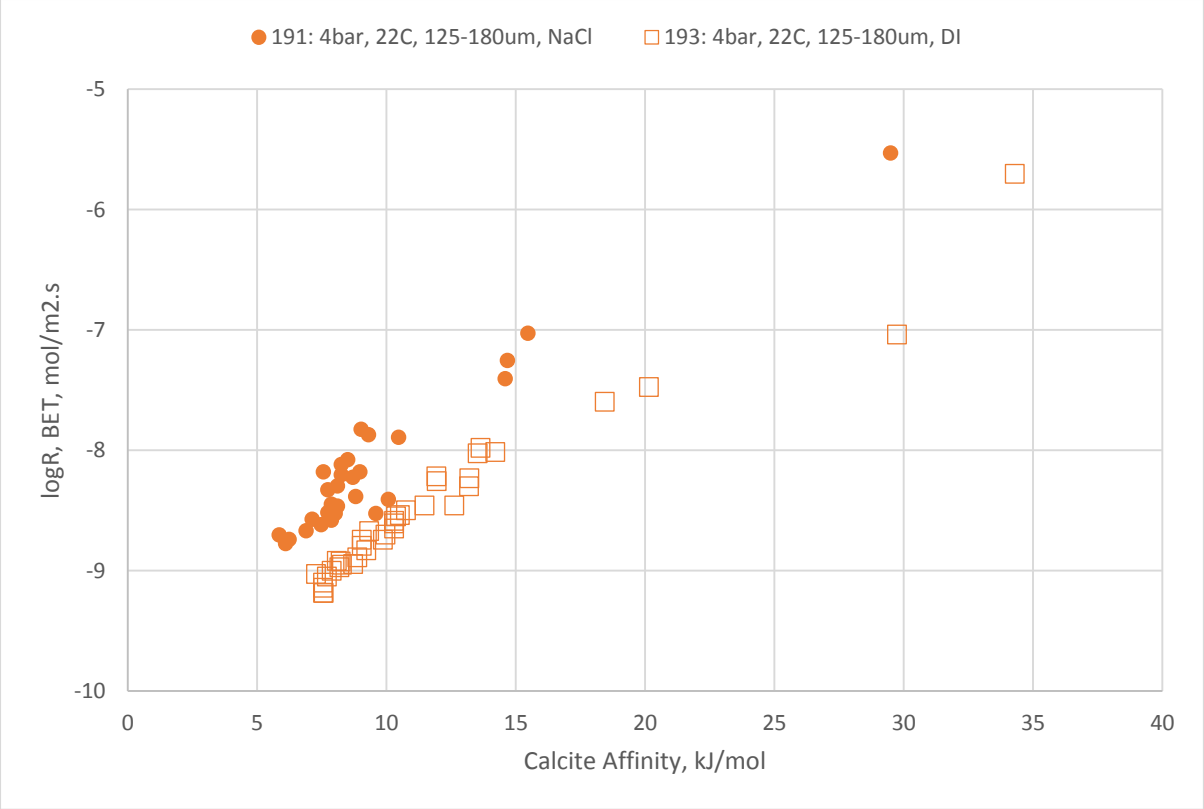


**Figure 4.2.7**: Calculated calcite dissolution rates and affinities for experiments 191 and 193

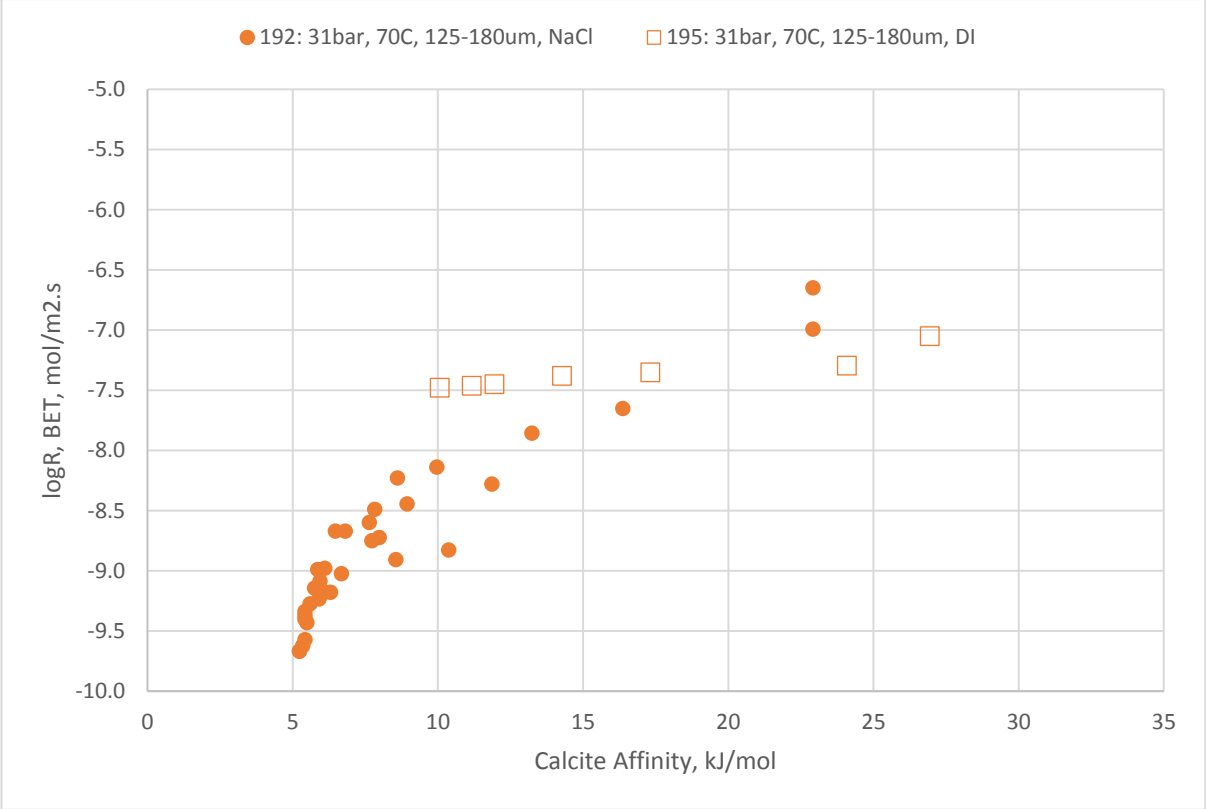


**Figure 4.2.8**: Calculated calcite dissolution rates and affinities for experiments 192 and 195

For both sets of experiments it is clear that overall levels of Ca in solution are increased by the addition of NaCl. Likewise calculated rates of calcite dissolution are consistently higher for experiment 191 than 193 (Figure 4.2.7). Calculation of dissolution rates for experiment 195 are hampered by the sudden cessation of apparent Ca release early in the experiment, but at early times (higher calcite affinities) dissolution rates in 195 (deionised water) are slightly lower than those observed in the NaCl experiment (192) (Figure 4.2.8).

The reason for the sudden cessation of Ca release in experiment 195, not observed in the NaCl experiment at similar conditions in not apparent. Ca bearing phases remain undersaturated according to PHREEQC calculations and so precipitation effects seem unlikely. Again it may be that adsorption of dissolved Ca onto the calcite surface may offer a possible explanation, whereby where available Na is preferentially adsorbed over Ca in systems with NaCl rich solutions, leading to the observed disparity in Ca release behaviour between the two systems.

#### 4.2.1.5 Dissolution Behaviour: $pCO_2$ (4bar, 31bar) and temperature (22°C, 70°C)

Experiments 191 (4bar $pCO_2$, 22°C, 1.36M NaCl) and 192 (31bar $pCO_2$, 70°C, 1.36M NaCl) and experiments 193 (4bar $pCO_2$, 70°C, deionised water) and 195 (31bar $pCO_2$, 70°C, deionised water) are compared in Figures 4.2.9 and 4.2.10. Figures 4.2.11 and 4.2.12 compare calculated calcite dissolution rates, based on Ca release and BET surface area for the two experiments.

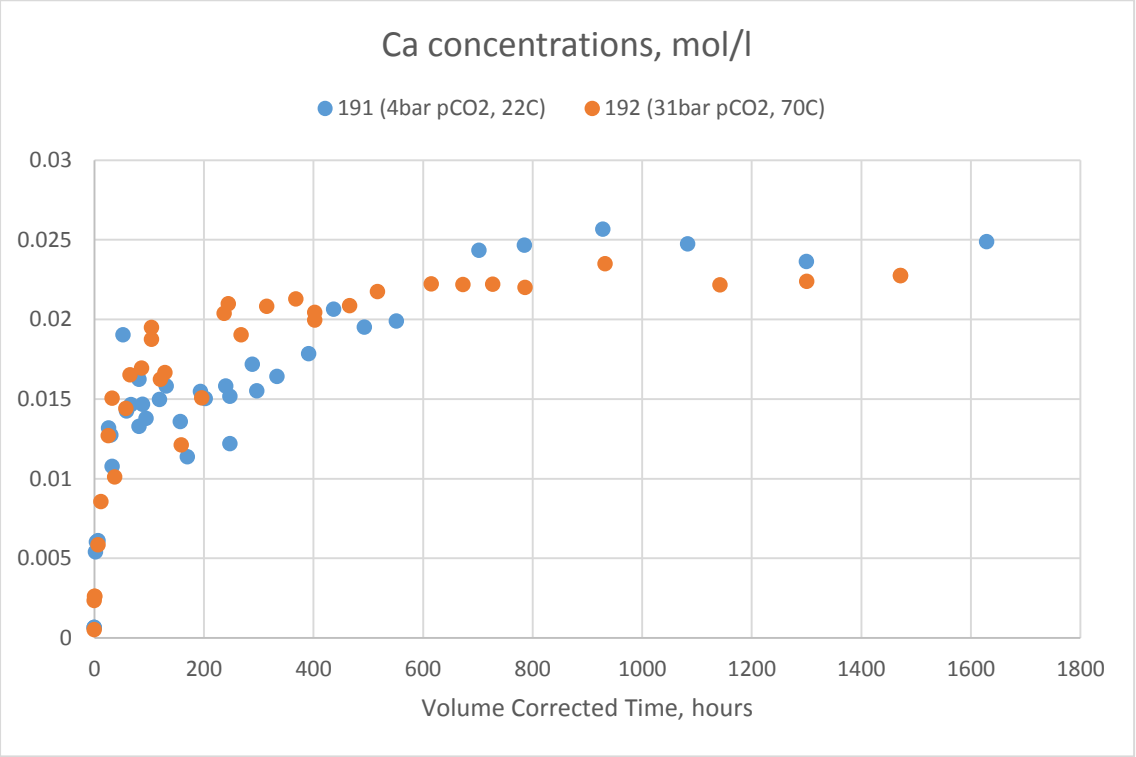


**Figure 4.2.9**: Comparative chart of Ca concentrations for experiments 191 (4 bar, 22°C) and 192 (31 bar, 70°C)

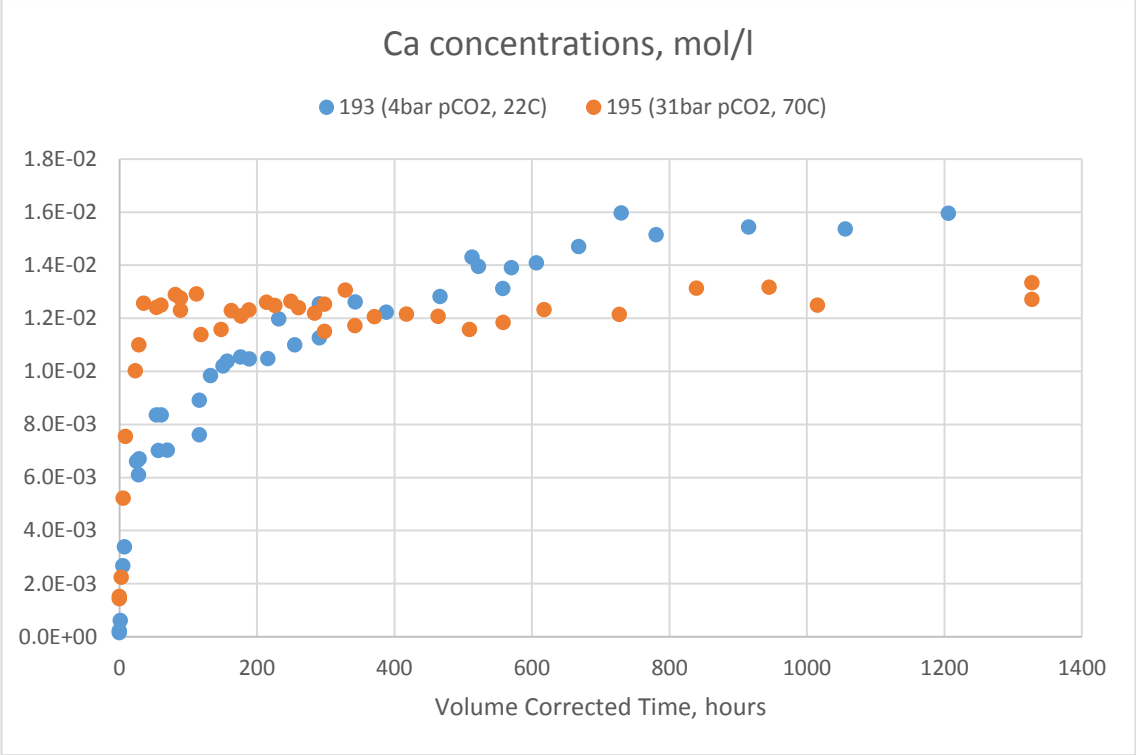


**Figure 4.2.10**: Comparative chart of Ca concentrations for experiments 193 (4 bar, 22°C) and 195 (31 bar, 70°C)

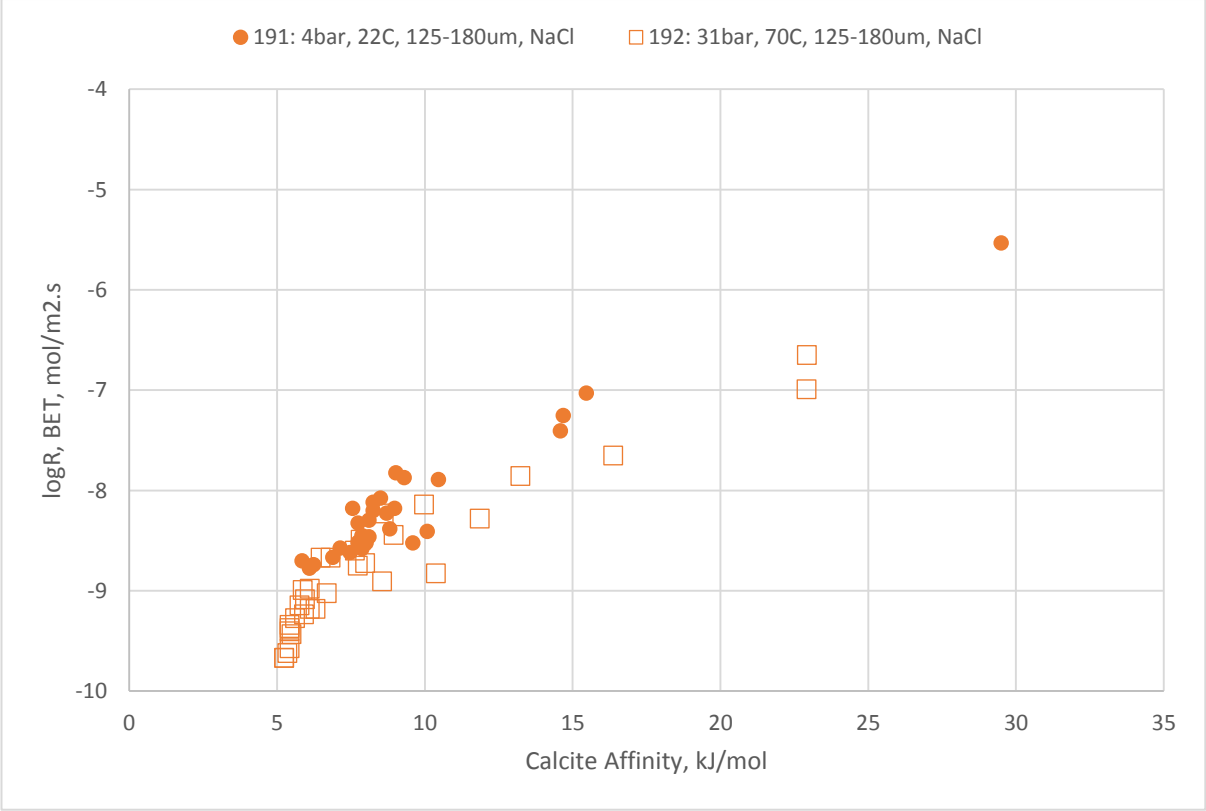


**Figure 4.2.11**: Calculated calcite dissolution rates and affinities for experiments 191 and 192

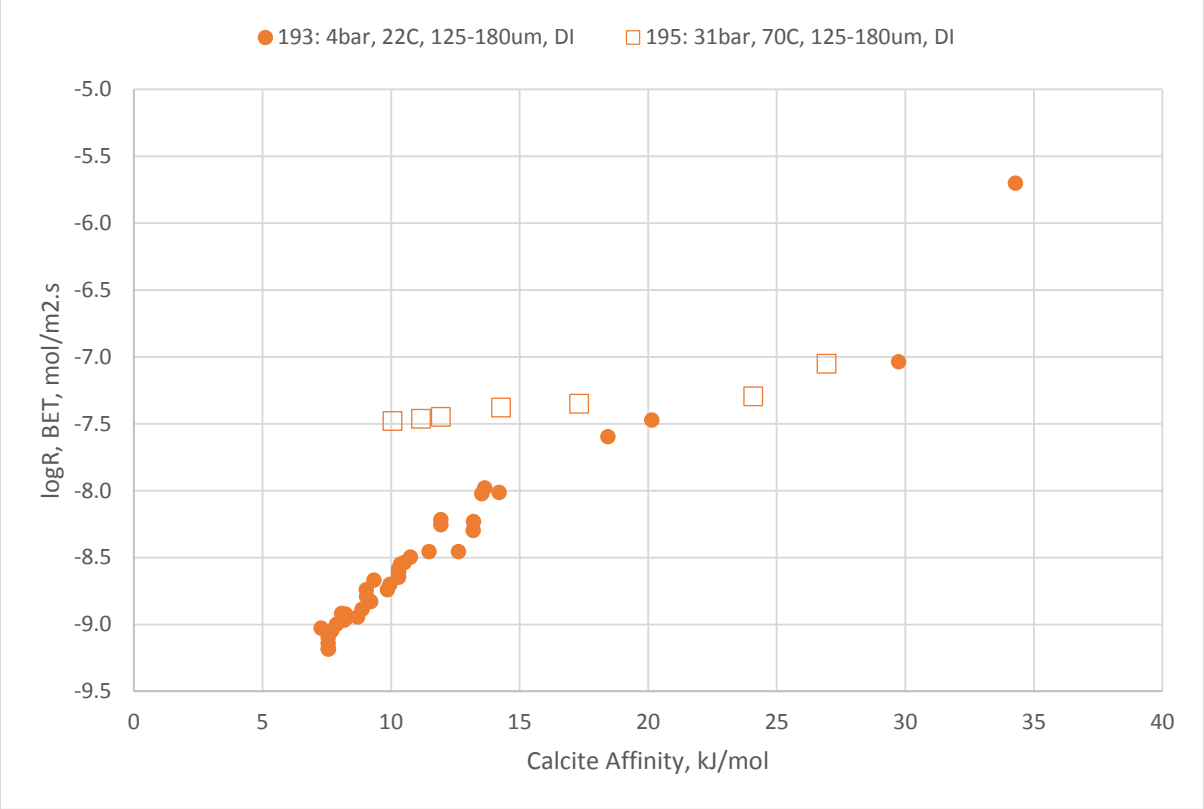


**Figure 4.2.12**: Calculated calcite dissolution rates and affinities for experiments 193 and 195

Dissolved Ca concentrations between the high and low P/T experiments are broadly similar in both sets of comparisons. The dissolution behaviour of experiments 191 and 192 (NaCl experiments) are very similar and dissolution rates, as well as overall Ca concentrations are near identical. There is however a marked difference in Ca concentration behaviour in the deionised water experiment comparison: Ca concentrations in the high P/T experiment (195) climb more rapidly than in the low P/T experiment (193) for the first 100 or so hours of experiment and remain relatively constant thereafter. Concentrations in the low P/T experiment meanwhile follow a much more gradual curve, apparently plateauing, at concentrations above those observed in the high P/T experiment, after around 800 hours.

A control experiment (196) was carried out at 4bar $pCO_2$ and 70°C in an attempt to separate the effects of elevated pressure and temperature on the dissolution behaviours observed in other experiments. However there were considerable problems with leakage from the pressure vessel during this experiment and it is likely that this leakage, with associated depressurisation has influenced the results from this experiment. Measured Ca concentrations

from this experiment were very low compared to all other calcite experiments, despite the elevated temperature and it seems likely that leakage and associated depressurisation of the experiment caused precipitation of a Ca bearing phase during this run, rendering the results unusable as a comparison.

The results compared here indicate that in the context of these experiments, $pCO_2$ and temperature had little effect on the dissolution behaviour of calcite in 1.36M NaCl. The results from the deionised water experiment comparison are somewhat more ambiguous, indicating an increased rate of dissolution at early times under elevated pressure and temperature, but an apparent cessation of dissolution at relatively early times (discussed in Section 4.2.1.3), while the lower P/T experiment shows evidence for continued dissolution.

#### 4.2.1.6 Calcite Dissolution Rates

Calculated rates from each experiment are plotted against calcite affinity in Figures 4.2.13 – 4.2.18. Calculated experimental rates are shown along with early and late time rates as predicted with the following three equations:

1) The rate equation presented in Chout et al. (1989):

$$R = k_1 a_{H^+} k_2 a_{H_2CO_3^*} + k_3 a_{H_2O} - k_b a_{Ca^{2+}} a_{CO_3^{2-}} \quad (4.2.1)$$

Using values of k presented in the original paper upon which the equation is based: Plummer et al. (1978).

2) The empirical rate equation presented by Pokrovsky et al. (2009), based on regression of experimental dissolution rates with respect to $pCO_2$:

$$logR = A + B \times pCO_2 + C \times (pCO_2)^2 \quad (4.2.2)$$

Using values of A, B and C (empirical parameters, dependent on pH and temperature), presented in the same work.

3) The general rate equation presented in the USGS compilation of rate parameters (2004):

$$\frac{dm}{dt} = -SA\left[\begin{array}{l}\left(k_{acid}^{298.15K} e^{\frac{-E_{acid}}{R}\left(\frac{1}{T}-\frac{1}{298.15K}\right)} a_{H^+}^{n_1}(1-\Omega^{P_1})^{q_1}\right) \\ +\left(k_{neutral}^{298.15K} e^{\frac{-E_{neutral}}{R}\left(\frac{1}{T}-\frac{1}{298.15K}\right)}(1-\Omega^{P_2})^{q_2}\right) \\ +\left(k_{base}^{298.15K} e^{\frac{-E_{base}}{R}\left(\frac{1}{T}-\frac{1}{298.15K}\right)} a_{H^+}^{n_3}(1-\Omega^{P_3})^{q_3}\right)\end{array}\right] \quad (4.2.3)$$

Using values of n, p and q presented therein. These values are based on regressed data sourced from Plummer et al. (1978) and Talman et al (1990).

Rates based upon these equations have been calculated using one early time and one late time data point.

Where activities are required, values have been calculated using PHREEQC3. Affinites have been calculated based upon analysed concentrations using the equation:

$$A = RT \times \ln\left(\frac{K_{Calcite}}{(a_{Ca^{2+}} \times a_{CO_3})}\right) \quad (4.2.4)$$

Where $K_{Calcite}$ is the equilibrium constant for calcite at the experimental conditions, R is the gas constant, T is the temperature in Kelvin, and $a_{Ca^{2+}}$ and $a_{CO_3}$ are the activities of the appropriate ions in solution, as calculated using by PHREEQC3 using the measured fluid compositions.

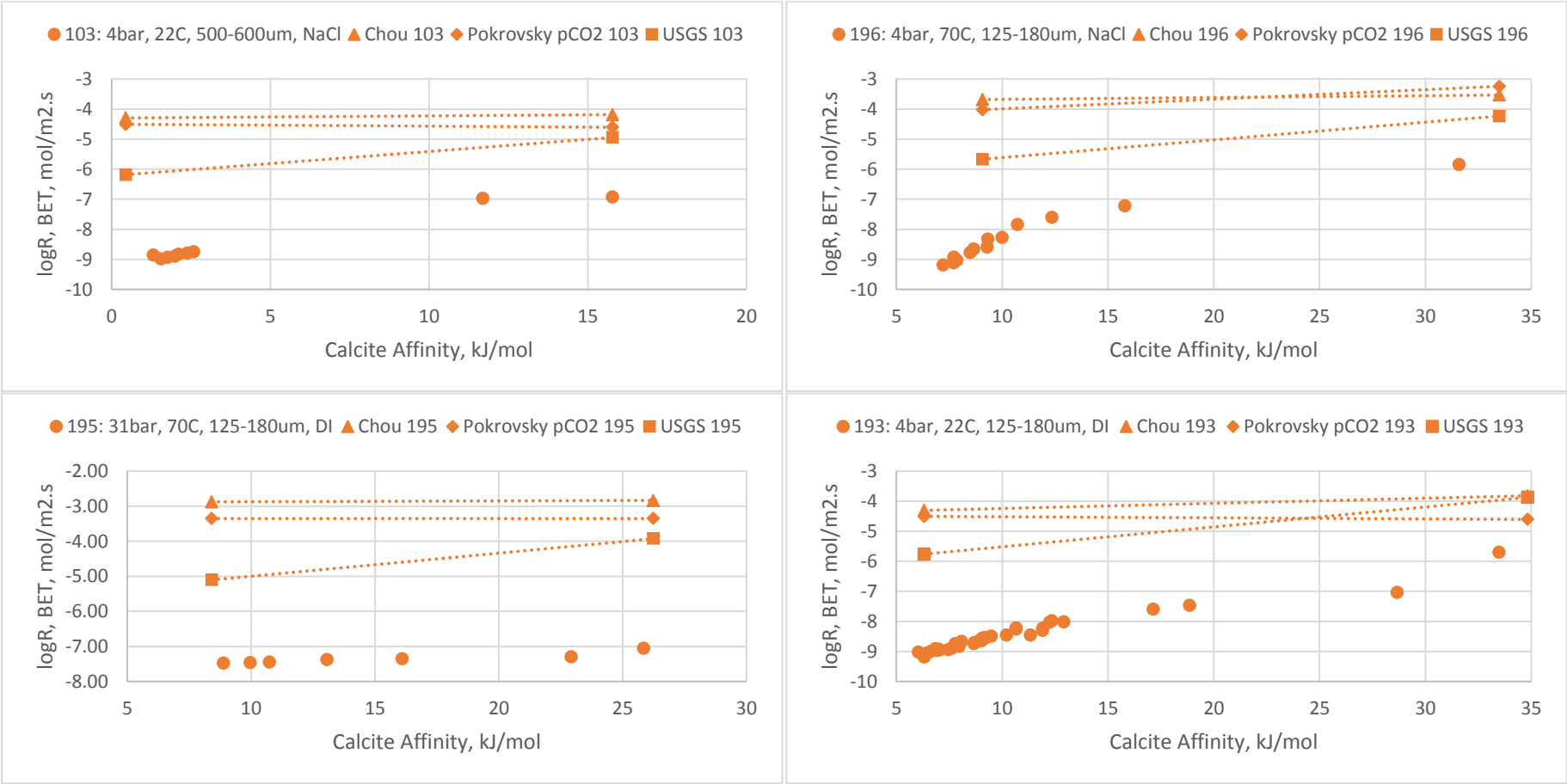


**Figures 4.2.13 – 4.2.16**: Calculated calcite dissolution rates and affinities for experiments (clockwise from top left) 103, 196, 193 and 195, shown together with predicted rates using various literature equations

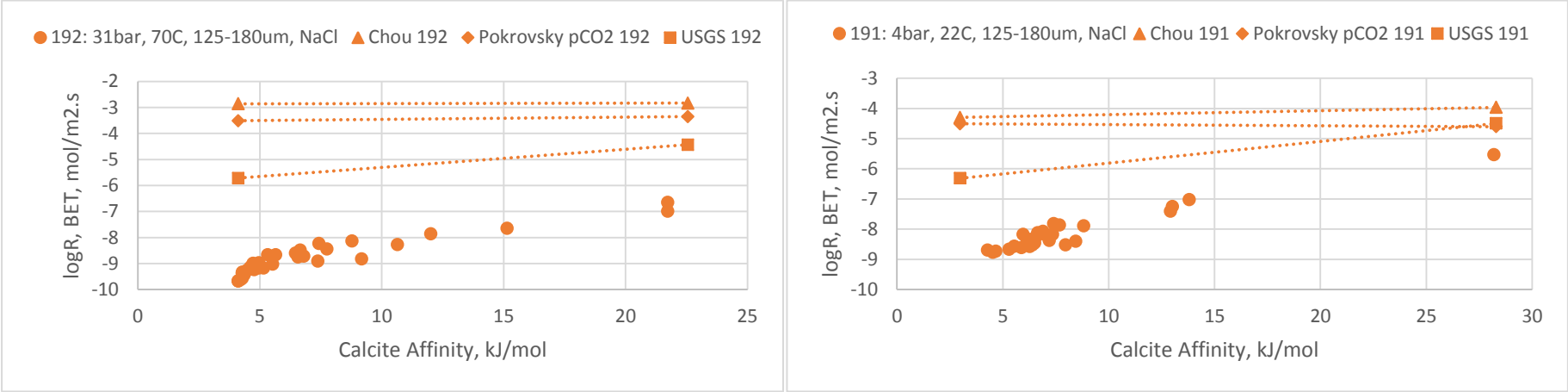


**Figures 4.2.17 – 4.2.18**: Calculated calcite dissolution rates and affinities for experiments 192 (left) and 191 (right), shown together with predicted rates using various literature equations

Experimental rates are consistently lower than those predicted using equations 4.2.1 -4.2.3 and exhibit a strong linear dependence on calcite affinity. Values of $R^2$ for all experimental datasets are higher than 0.85. This strong dependence on chemical affinity is not reflected in the rate equations presented above. In all cases, with the exception of 195, the gradient of the linear fits to experimental data is higher than those predicted. As noted previously, Ca release in experiment 195 apparently ceases very suddenly at around 35 hours into the experiment and hence rates calculated from this experiment (based only on very early time data) should be treated with caution. The USGS general rate equation, perhaps surprising, comes closest to reproducing the dependence of rate on chemical affinity, but the offset between the predicted and experimental rates remains 1-3 orders of magnitude, increasing with decreasing affinity. At high chemical affinities (early times) experimental rates tend toward those predicted by the equations presented above.

It has been shown (Palmer 1991; Svensson & Dreybrodt 1992) that a great number of experimentally derived calcite dissolution rates, including those of Plummer et al. (1978) can be fitted to equations of the form:

$$R = \alpha_1(1 - C/C_s)^{n1} \quad for\ C \leq xC_s \quad (4.2.5)$$

$$R = \alpha_2(1 - C/C_s)^{n2} \quad for\ C > xC_s \quad (4.2.6)$$

Where $\alpha_i$ are dependent on $pCO_2$ and temperature, $n_i$ are reaction orders, C is the Ca concentration and $C_s$ is the predicted equilibrium Ca concentration. x is assumed to be around 0.8, depending on experimental conditions.

Log $(1\text{-}C/C_s)$ vs. log rate is plotted below (Figure 4.2.19) for all experimental calcite dissolution data from this study. Values of $C_s$ were calculated using PHREEQC3.

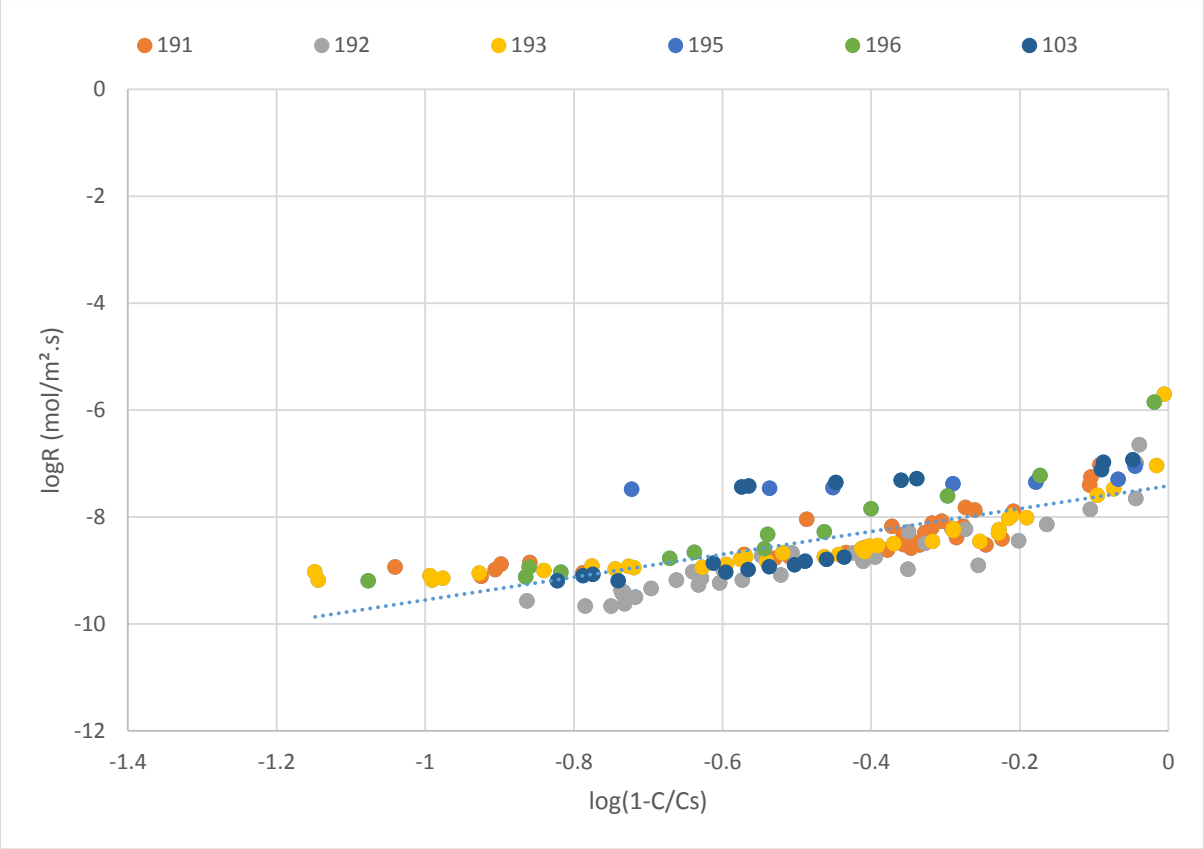


**Figure 4.2.19**: Plot of log Rate vs. log(1-C/Cs) for all experimental data from calcite dissolution experiments

Ignoring very early time data, where pH is relatively low and hence may exert a control on calcite dissolution rate, the majority of experimental data falls on a strong linear trend. Exceptions to this trend are largely from experiment 195 the results of which fall slightly above the general trend. As has already been mentioned, calculated rates from experiment 195 are of low confidence given the sudden cessation of apparent Ca release at early times.

The remaining data were fitted to linear trends to yield values for the reaction constants ($\alpha_i$) and orders ($n_i$) as shown in equations 4.2.5 & 4.2.6 for each experimental run. An inflection point, such that the values of reaction constant or order changed at around $C=xC_s$ was not generally noted, hence only single values of $\alpha$ and n were calculated for each experiment. The results are shown below in Table 4.2.3.

| Experiment | $pCO_2$, bar | T, °C | Solution | Grain size, µm | n | α, $mol/m^2.s$ | $R^2$ | $C/C_s$ min | $C/C_s$ max |
|---|---|---|---|---|---|---|---|---|---|
| 191 | 4 | 22 | NaCl | 125-180 | 1.12 | 1.07E-08 | 0.64 | 0.02 | 0.88 |
| 192 | 31 | 70 | NaCl | 125-180 | 2.26 | 1.66E-08 | 0.87 | 0.02 | 0.84 |
| 193 | 4 | 22 | DI | 125-180 | 1.12 | 8.71E-09 | 0.84 | 0.01 | 0.90 |
| 195 | 31 | 70 | NaCl | 125-180 | 0.29 | 5.01E-08 | 0.94 | 0.10 | 0.86 |
| 196 | 4 | 70 | DI | 125-180 | 2.93 | 2.45E-07 | 0.87 | 0.03 | 0.73 |
| 103 | 4 | 22 | NaCl | 500-600 | 0.55 | 1.55E-09 | 0.85 | 0.10 | 0.85 |

**Table 4.2.3**: Calculated values of n (reaction order) and α (rate constant) with respect to $C/C_s$

#### 4.2.1.7 Calcite Experiments Overview and Discussion

PH during calcite dissolution experiments appears to be well predicted by modelling of fluid compositions using PHREEQC3, as indicated by generally close agreement by measured pH, where available, and predicted pH based on final sample compositions. Discrepancy between the predicted equilibrium pHs and those of the final samples reflect distance from nominal equilibrium: further removal of carbonate from the mineral would continue to drive pH upward through formation of bicarbonate species.

Measured values of dissolved $CO_2$ content agree well with those predicted both by the standalone equation of state based model produced by Duan et al. (which accounts for some major cations in solution) and the more complex PHREEQC3. Both measured and predicted values are relatively close to predicted equilibrium values, highlighting the relative insensitivity of $CO_2$ solubility to fluid-mineral interactions, which remain a long way from equilibrium and the rapidity of $CO_2$ dissolution relative to other processes in the system (i.e. mineral dissolution).

Changes in grain size on the order of 400µm had little to no effect on the dissolution behaviour of calcite. The switch between a deionised water matrix and a 1.36M NaCl matrix on the other hand had a notable effect, with the increase in salinity corresponding to an overall increase in Ca in solution and in calculated dissolution rates, which were up to one order of magnitude greater in the saline matrix. Literature data on calcite dissolution in solutions of salinities =>1M NaCl is relatively scant and often contradictory. Pokrovsky et al. (2005) found that there was little dependence of calcite solubility on salinity at concentrations up to 1M NaCl, though a slight increase in rate is seen in their mixed flow experiments at pH 5.7 at higher salinities. Gledhill & Morse (2006) meanwhile found a relatively strong inhibitory effect of salinity on calcite dissolution rates, in solutions ranging from 0.5M to 4M salinity. Work on very high temperature/pressure fluids (>600°C, 10kbar) has indicated increasing calcite solubility with increasing salinity, eg Newton and Manning (2002), who suggested a relatively simple speciation reaction, possibly of the form:

$$CaCO_3 + 2NaCl_{(aq)} = CaCl_{2(aq)} + Na_2CO_{3(aq)} \quad (4.2.7)$$

to account for the increased solubility. While there is insufficient data here to fully explore this theory, it seems plausible that increased concentrations of sodium carbonate and bicarbonate species formed in NaCl solutions can act to increase calcite dissolution, offering a reasonable explanation for the

increased rates and Ca concentrations observed in the 1.36M NaCl experiments compared to the deionised water experiments presented here. Equilibrium calculation performed in PHREEQC3 partially confirm this, with increased concentrations of $Ca^{2+}$ and $NaHCO_3^-$ in NaCl solutions relative to deionised water, although changes in calcite solubility due to salinity are not accounted for.

The effects of increased $pCO_2$ and temperature on calcite dissolution from the experimental data presented here are somewhat ambiguous. The failure of the control experiment (196) means that separating the effects of $pCO_2$ and temperature is impossible and that results can only be interpreted in terms of a combined effect of the two variables. Results from the deionised water experiments indicate that, at least at very far from equilibrium conditions, dissolution rate is increased by increasing $pCO_2$ and temperature, while the results from the 1.36M NaCl experiments indicate that the two factors have little effect. For a pH of 4, Pokrovsky et al (2005) found that $pCO_2$ had a relatively weak effect on calcite dissolution, increasing dissolution rate by a factor of 3 as $pCO_2$ was raised from 1atm to 50atm. There is relatively little material on the effects of temperature on calcite dissolution, and what work there is indicate a relatively low dependence of dissolution rate on temperature (around 13% increase in rate for every 10°C increase in temperature). Published dependencies of dissolution rate on temperature also vary considerably, generally with distance from equilibrium, from 8-60kJ/mol (Morse & Arvidson 2002). While a detailed analysis of the effects of increased $pCO_2$ and temperature is not possible with the data presented here, the experimental results certainly do not indicate a large effect of increased $pCO_2$ or temperature on calcite dissolution rates.

In terms of calculated dissolution rates, there is a clear discrepancy between the experimentally derived rates produced here and the rates predicted by various empirical models of calcite dissolution (Equations 4.2.1 – 4.2.3). Rates derived from these experiments are substantially (up to five log units) lower than those predicted by the available rate equations. Moreover rates exhibit a strong correlation with chemical affinity, which is not mirrored in the rate equations, with the exception, to a limited degree, of the USGS produced general rate equation. It is possible that transport limitations play a part in this discrepancy: it is well known that transport can be a rate limiting factor in calcite dissolution, particularly at low pH.

As with many general rate equations, equations 4.2.1 – 4.2.3 have been produced through fitting with results from far from equilibrium experiments, often conducted using flow-through reactors of the kind described in Section 2.1.1.1. Here the system is maintained at a set distance from equilibrium, and the effects of processes such as precipitation or adsorption are kept to a minimum. Where closed batch reactors are used, for carbonate minerals at least, a spinning disc set up is often used, such that the surface area to fluid ratio is very low and, again, the system is maintained at relatively far from equilibrium conditions for a long period of time. Svennson and Dreybodt (1992) presented results from a series of dissolution experiments conducted in batch reactors on a mixture of natural calcites and a standard, pure, calcite sample. They found that while the dissolution behaviour of the pure calcite sample obeyed the original rate law proposed by Plummer et al, the natural samples exhibited strong inhibition in dissolution as equilibrium was approached. Other authors have noted this inhibiting behaviour: Herman (1991, original work, unavailable), noted that in her dissolution experiments on calcite discs, in all cases dissolution rates became undetectably small at Ca concentrations around half of the expected equilibrium values. Svennnson and Dreybodt explained such behaviour in terms of adsorption of $Ca^{2+}$ onto the mineral surface at sites where dissolution is active, occupancy of these sites leads to dramatic drops in dissolution rates as equilibrium is approached and hence substantial deviation from the mechanistic model proposed by Plummer et al. and inherent in the equation derived by Chou et al, used in the rate comparison above. The data presented here fits reasonably well within such a model. Results presented in Table 4.2.2 provides values for n and $\alpha$ for use in an equation of the form shown in Equation 4.2.5, which, ignoring some early time data, fits experimentally derived rates reasonably well. With only one experiment per set of experimental conditions, no great confidence can be placed on any particular value of n produced here, but reaction order for the experiments conducted here is generally between 0.5 and 3, dependant on conditions. Figure 4.2.20 shows a plot of calculated rate divided by the rate predicted by the Chou equation (Equation 4.2.1) vs. measured Ca concentration.

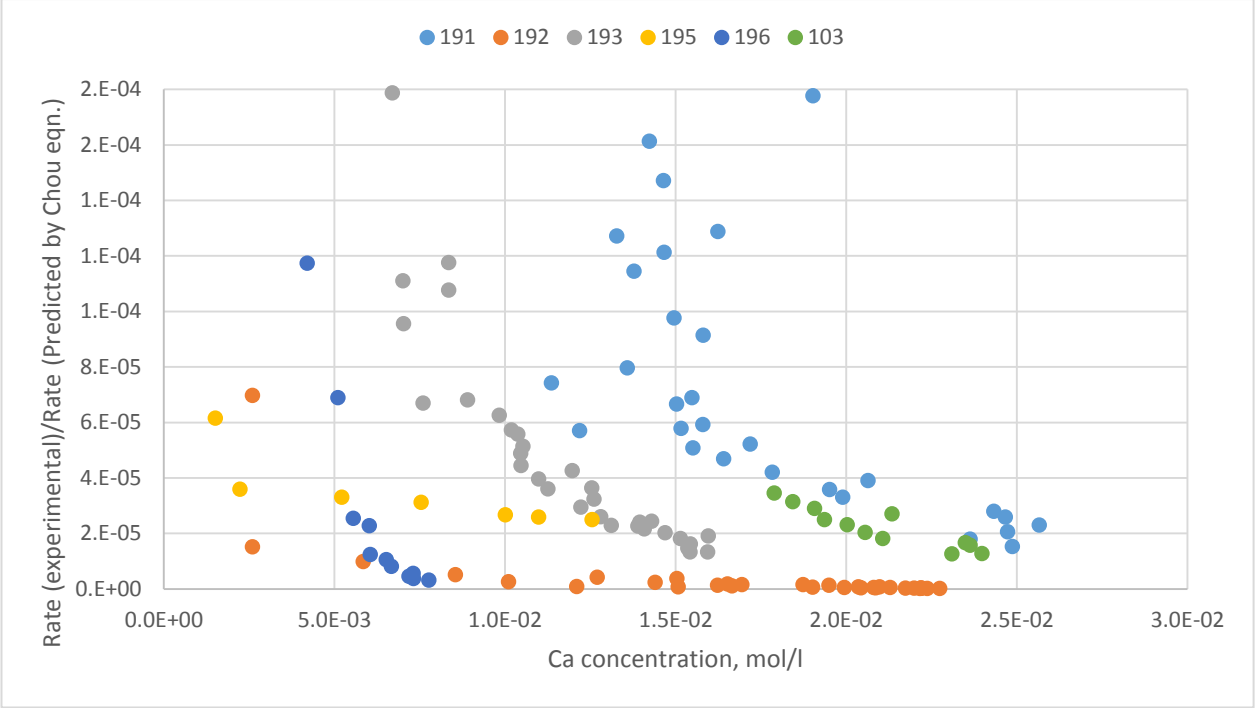


**Figure 4.2.20**: Plot of experimental rate divided by rate calculated from Equation 4.2.1, vs. Ca concentration

Although there is considerable scatter in the data, the results generally show a curve in the data as Ca concentrations tend toward higher values. Svensson and Dreybodt interpreted such data in terms of Fowler-Frumkin isotherms describing increased inhibition of Ca sorption as the surface coverage of inhibitor ions (eg heavy metals from impurities in natural samples) increases. They found that while synthetic calcite exhibited a linear, Langmuir like isotherm, natural samples all exhibited this strong, non-linear behaviour.

The results, in terms of dissolution rates, therefor, fit a conceptual model where calcite dissolution rates become increasingly inhibited on approach to equilibrium, leading to large deviations from the classical models represented by Equations 4.2.1 and 4.2.2. This inhibition is a strong function of calcite affinity and hence Ca concentration and may explained by complex sorption processes at the calcite surface, particularly at high energy sites where dissolution occurs. In terms of CCS the applicability of these results will be highly site dependent. In cases where injection is ongoing, conditions near the well and migrating plume will be relatively dynamic, with short residence times for formation fluid and in this case, the general models represented by equations 4.2.1 and 4.2.2, which have been shown to provide a good fit to experimental data at far from equilibrium and dynamic flow-through conditions, may well be representative of the system. However in

cases where injection has stopped, or in areas trailing the main injection plume, or simply in systems where average residence time is on the order of days-weeks, conditions will be much more static and similar conceptually to the batch experiments presented here. Here dissolved concentrations may build up relatively rapidly. The results presented here suggest that this change chemical affinity is the overriding control on calcite dissolution rates and will lead to large deviations from modelled results.

### 4.2.2 Dolomite

Seven experiments were carried out on powdered dolomite samples to observe dolomite dissolution rates and behaviour in fluids under constant $pCO_2$. The dolomite material used in described in Chapter 3. Experimental conditions are summarised in Table 4.2.4.

| Experiment ID | Grain Fraction, µm | Fluid | pCO2, bar (absolute) | Temperature, $^0C$ | Run time, volume constant hours | Conditioning period prior to $CO_2$ injection, hours |
|---|---|---|---|---|---|---|
| 131 | 125-180 | 1.36M NaCl | 4 | 22 | 721 | 171 |
| 132 | 500-600 | 1.36M NaCl | 4 | 22 | 703 | 171 |
| 133 | 125-180 | DI | 4 | 22 | 1290 | 564 |
| 134 | 125-180 | DI | 31 | 70 | 893 | 226 |
| 135 | 500-600 | DI | 31 | 70 | 729 | 226 |
| 136 | 125-180 | 1.36M NaCl | 4 | 70 | 1119 | 267 |
| 143 | 125-180 | 1.36M NaCl | 31 | 70 | 709 | 1295 |

**Table 4.2.4**: Experimental conditions for dolomite dissolution experiments

#### 4.2.2.1 pH and $CO_2$ Solubility

Figures showing full results of fluid pH calculations and measurements can be found in Appendix B, but selected results, showing measured pH where available, equilibrium pH as calculated by PHREEQC3 and final sample pH as calculated by PHREEQC are shown in Table 4.2.5 which also summarises calculations and measurements of dissolved $CO_2$ content from the batch experiments.

| Run | Fluid/p $CO_2$ (bar)/T(° C) | Equilibrium $CO_2$ PHREEQC3, mol/kg | Final Sample CO2, Duan, mol/kg | Final Sample $CO_2$ PHREEQC3, mol/kg | Final Sample $CO_2$ (Measured), mol/kg | Standard Deviation, $CO_2$ (No. of measurements) | Equilibrium pH, PHREEQC3 | Final Sample pH, PHREEEC3 | Final Sample pH, measured |
|---|---|---|---|---|---|---|---|---|---|
| 131 | NaCl/4/22 | 0.173 | 0.107 | 0.114 | 0.137 | 0.008 (4) | 5.724 | 4.823 | 4.910 |
| 132 | NaCl/4/22 | 0.173 | 0.107 | 0.114 | 0.143 | 0.014 (5) | 5.724 | 4.779 | 5.150 |
| 133 | DI/4/22 | 0.188 | 0.141 | 0.154 | 0.178 | 0.020 (2) | 5.718 | 5.077 | 4.500 |
| 134 | DI/31/70 | 0.434 | 0.399 | 0.406 | - | - | 5.155 | 4.525 | - |
| 135 | DI/31/70 | 0.434 | 0.399 | 0.407 | - | - | 5.155 | 4.565 | - |
| 136 | NaCl/31/70 | 0.072 | 0.043 | 0.064 | - | - | 5.731 | 5.588 | - |
| 143 | NaCl/4/70 | 0.348 | 0.309 | 0.306 | 0.284 | 0.034 (5) | 5.18 | 4.6293 | 4.91 |

**Table 4.2.5**: Summary of pH and CO2 solubility data for dolomite experiments

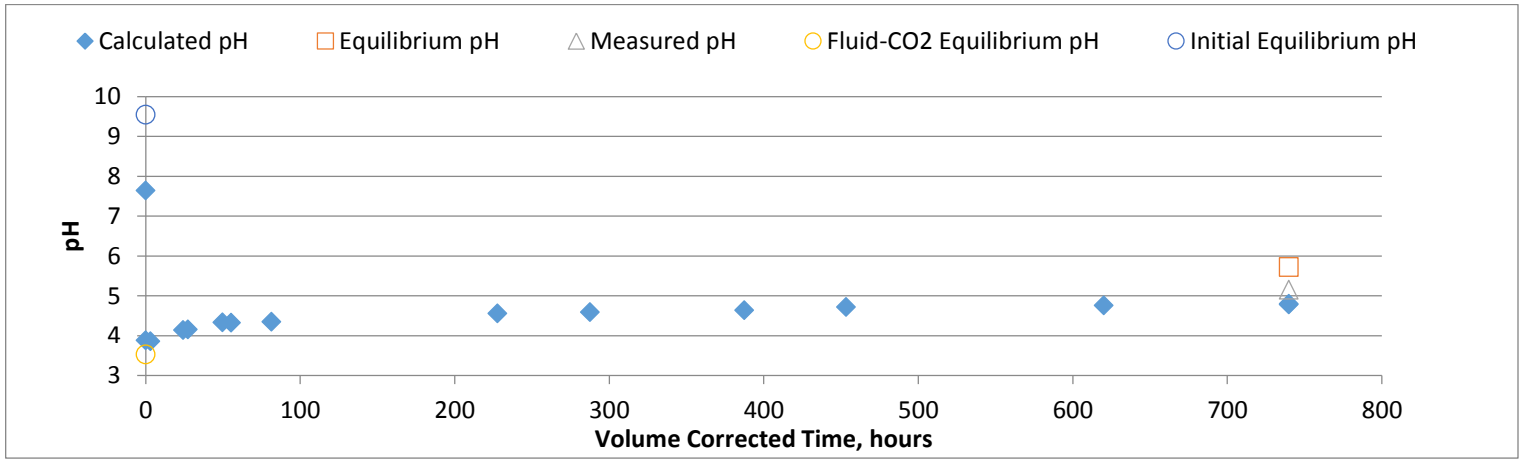


**Figure 4.2.21**: Summary of pH data for experiment 132

PHREEQC3 calculations indicate that the pH of the initial ($CO_2$ free) fluids were relatively high: between 7.6 and 8.7, but substantially below the predicted equilibrium pHs for those systems which range from 8.8 to 9.5. Following injection of $CO_2$, calculated pHs for the experiments fall to values between 3.5 to 4.2, depending on the system. These values are close to those of calculated pH for the equivalent mineral free systems, which lie in the range 3.3-3.7. As dissolution proceeds, pH climbs relatively rapidly, in all experiments, for the first 200-400 hours, before apparently plateauing at values of between 4.5 and 5.6. The exception to this general trend is experiment 136 which shows a continuous rise in calculated pH for the whole experiment. The general behaviour of pH during the experiments is illustrated for experiment 132 in Figure 4.2.21. As illustrated by Table 4.2.5, final pH in all experiments is considerably lower than the predicted equilibrium pH.

Measured $CO_2$ solubility agrees well with values calculated using PHREEQC3 and the Duan standalone model based on final sample analysis. Values calculated using the Duan model are within 25% of measured values and those calculated with PHREEQC3 are within 20%. Calculated values using either method tend to be lower than the measured values. As illustrated in Table 4.2.5, all measured and calculated values for final samples are significantly below the predicted equilibrium values for the system.

The disparity between equilibrium and measured values of dissolved $CO_2$ and pH reflect the distance from equilibrium of the experiments, despite the apparent plateau in calculated values of pH.

#### 4.2.2.2 Dissolution Behaviour: general Observations

The majority of the dolomite experiments showed near stoichiometric release of Ca and Mg, with Ca slightly in excess relative to its proportion in the bulk mineral (illustrated in Figure 4.2.22 for experiment 131). Experiments exhibit rising Ca and Mg concentrations for the duration of the experimental runs, with the exception of experiments 134 and 135. These two experiments experienced a drop in Ca concentrations at around 300-400 hours, which is not reflected in the Mg data. No other dolomite experiment showed a similar pattern and initial modelling using PHREEQC3 and the phreeqc.dat database did not indicate saturation of any Ca bearing phase. However, Fe concentrations showed a similar pattern, with a drop in concentration at around 300-400 hours (Fe in this case is assumed to be associated with contamination from the stainless steel vessels and fittings used in the experiments). Further modelling using the more extensive llnl.dat database indicated saturation with respect to Ca bearing ferrite in these experiments and it is likely that precipitation of this or a similar phase is responsible for the observed drop in Ca concentrations. Similar behaviour was not observed in experiments conducted in brine under the same conditions, so it may be that precipitation of this phase was inhibited by the increased salinity in these cases. Additional evidence for precipitation of a Ca bearing phase comes from SEM observations of occasional precipitate in the reacted solid from experiment 134 (see Figure 4.2.25), although the precipitate was too fine to make as positive identification of the phase.

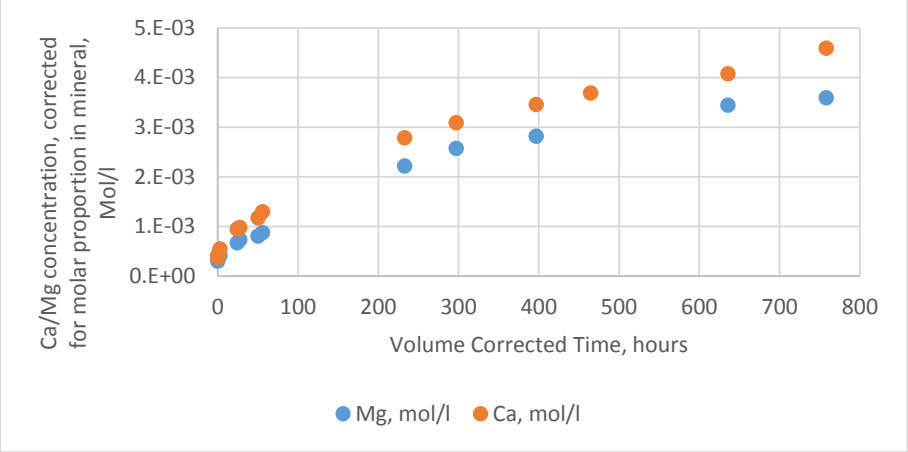


**Figure 4.2.22**: Ca and Mg concentrations, corrected for bulk mineral stoichiometry for experiment 131

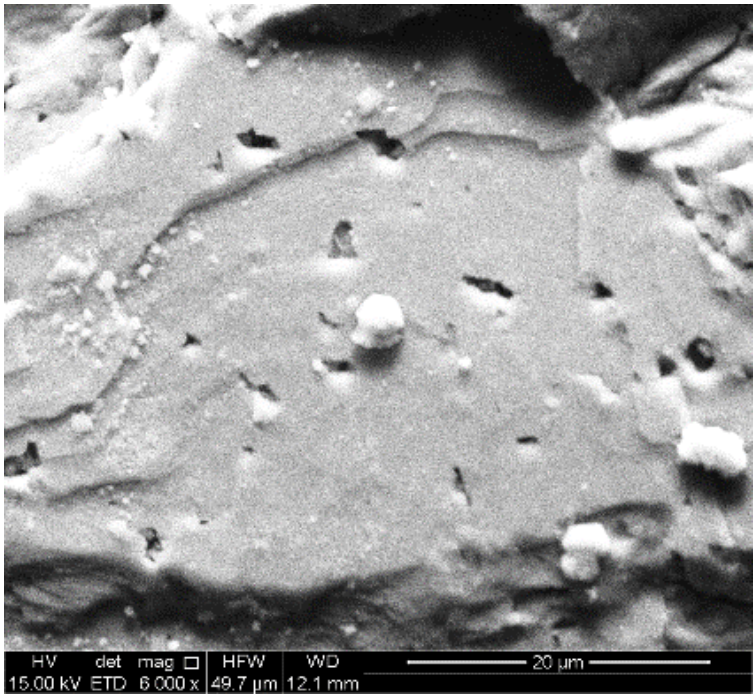


**Figure 4.2.23**: SEM photograph of precipitate on a dolomite grain retrieved from experiment 134

### 4.2.2.3 Dissolution Behaviour: Grain Size

Figures 4.2.24 and 4.2.25 compare Ca release between experiments 131 (125-180µm, 1.36M NaCl, 4bar $pCO_2$, 22°C) and 132 (500-600µm, 1.36M NaCl, 4bar $pCO_2$, 22°C) and between experiments 134 (125-180µm, deionised water, 31bar $pCO_2$, 70°C) and 135 (500-600µm, deionised water, 31bar $pCO_2$, 70°C). Figures 4.2.26 and 4.2.27 compare calculated dolomite dissolution rates for the two sets of experiments. Note that the apparent drop in calculated dissolution rates for experiments 134 and 135 is due to the drop in Ca concentrations discussed in Section 4.2.2.2 and is likely due to precipitation of a Ca bearing phase.

It is clear from the results that grain size changes on this scale have little to no effect on dolomite dissolution. Both comparisons show little difference between fine and coarse fractions, both in terms of overall magnitude of Ca concentrations and release rates.

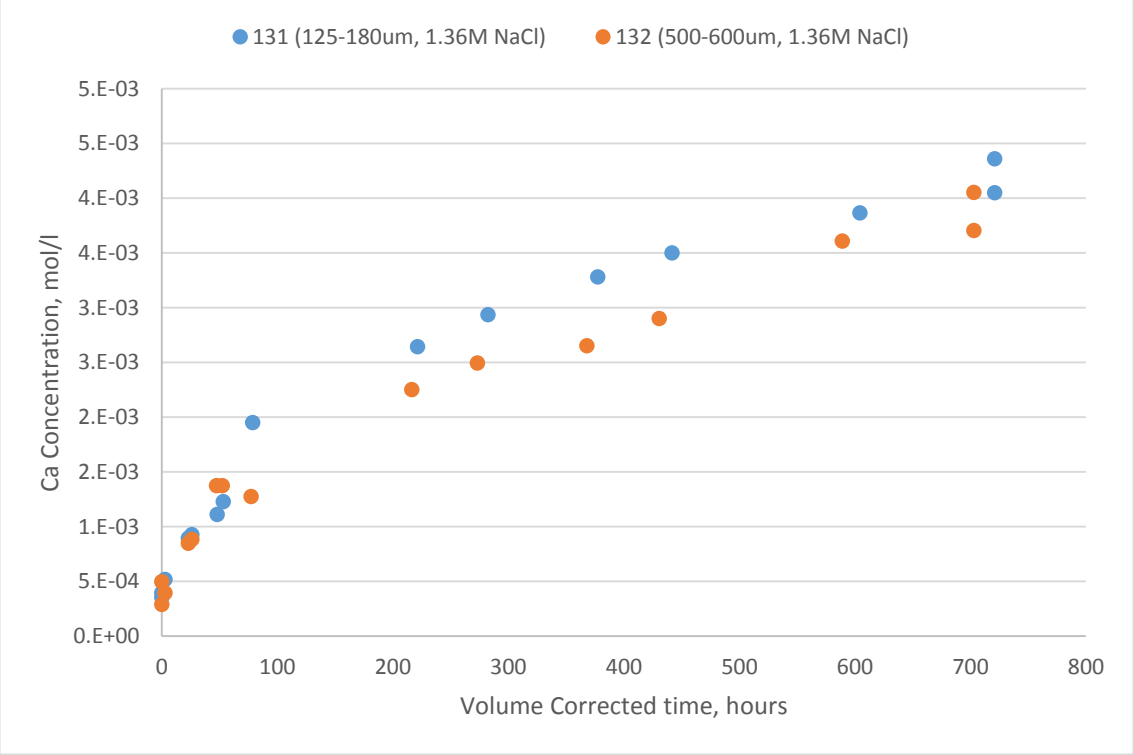


**Figure 4.2.24**: Comparative chart showing Ca release for experiments 131 (125-180µm) and 132 (500-600µm)

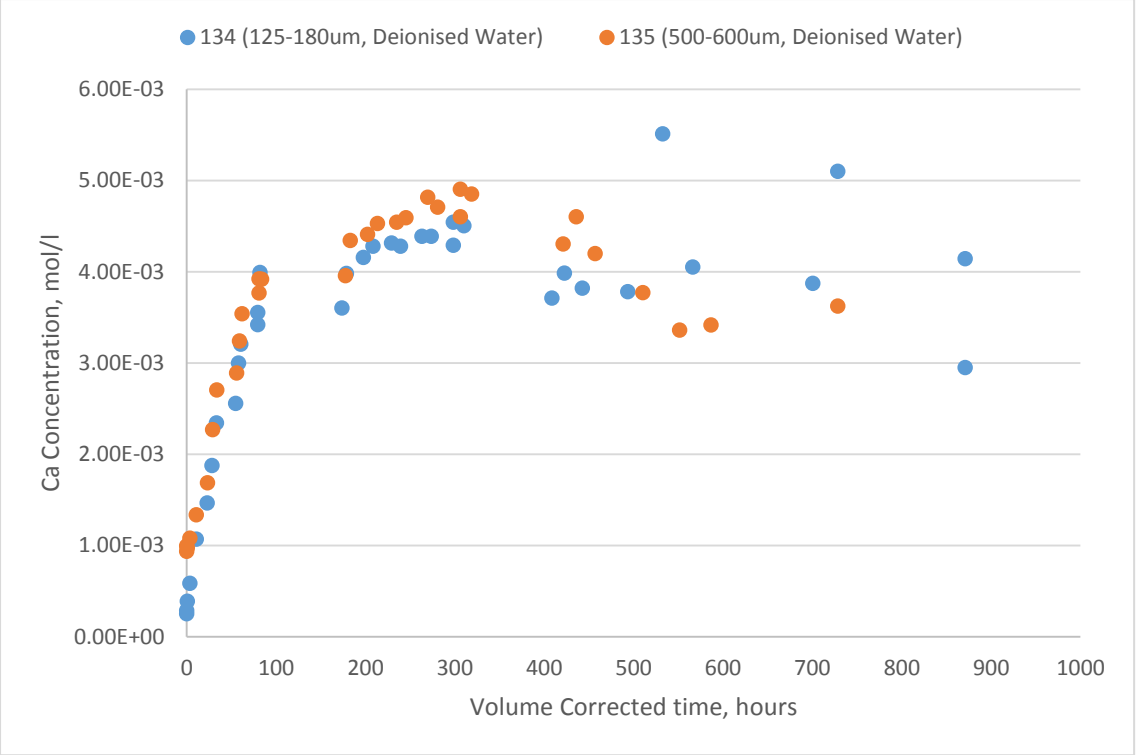


**Figure 4.2.25**: Comparative chart showing Ca release for experiments 134 (125-180µm) and 135 (500-600µm)

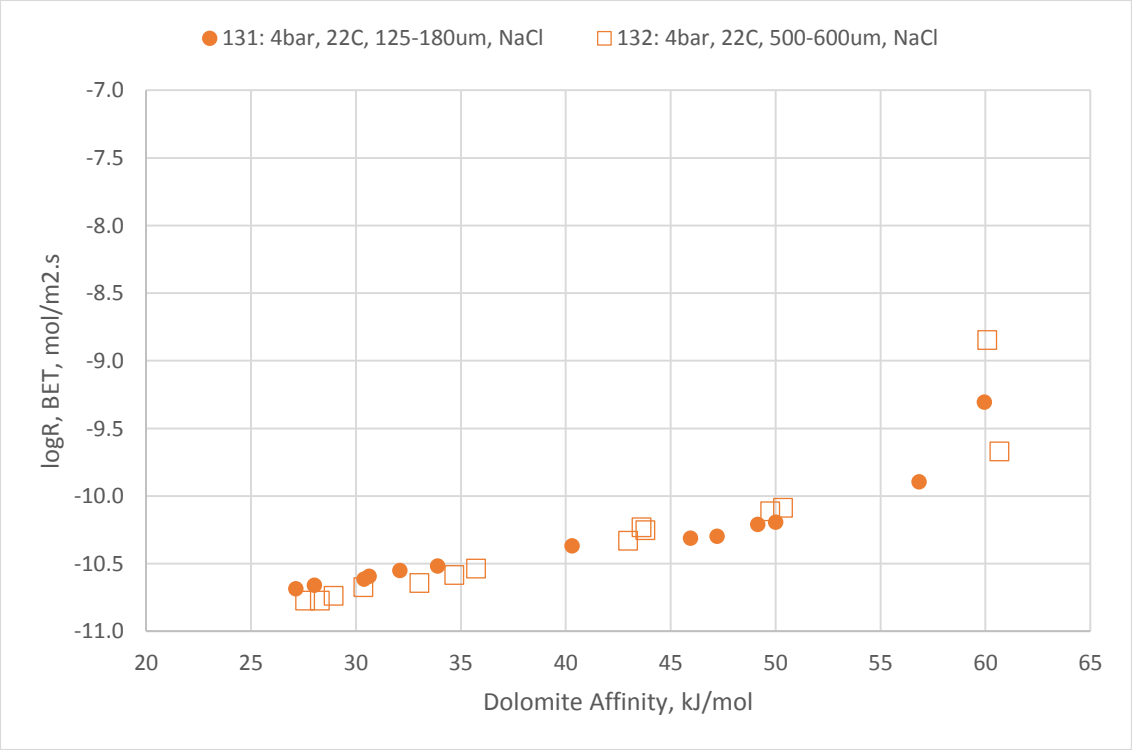


**Figure 4.2.26**: Calculated dolomite dissolution rates and affinities for experiments 131 (125-180µm) and 132 (500-600µm)

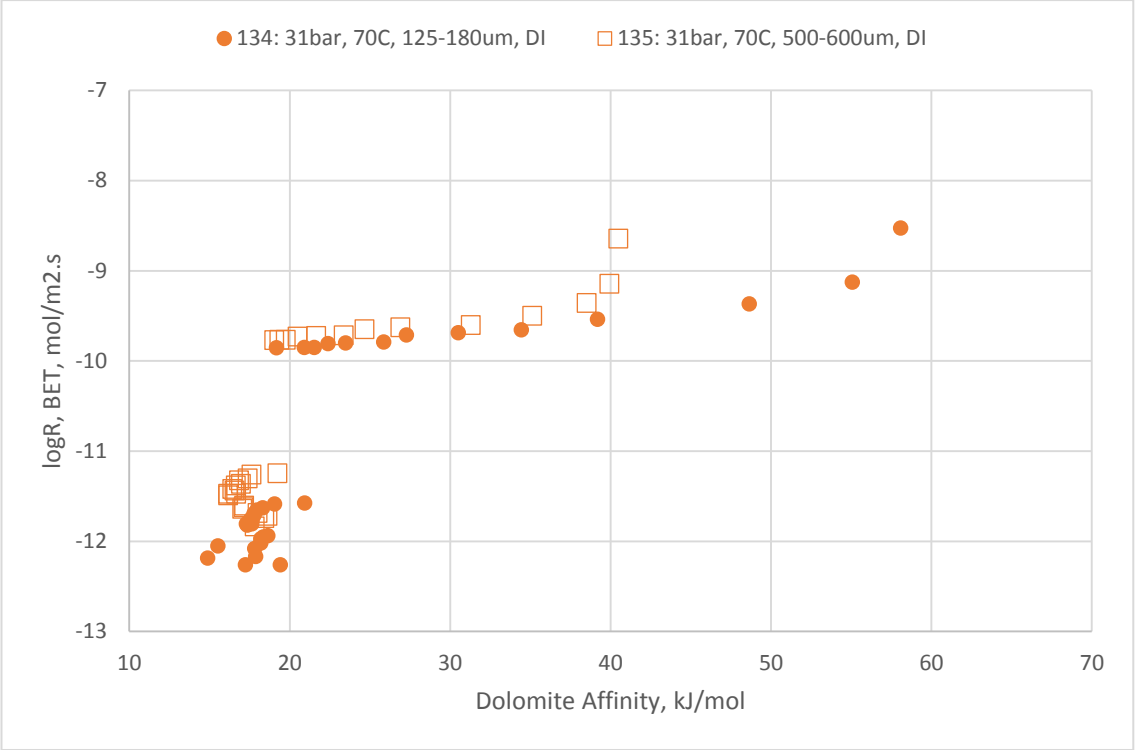


**Figure 4.2.27**: Calculated dolomite dissolution rates and affinities for experiments 134 (125-180µm) and 135 (500-600µm)

#### 4.2.2.4 Dissolution Behaviour: Fluid Composition

Ca release is compared from experiments 131 (1.36M NaCl, 4bar $pCO_2$, 22°C) and 133 (deionised water, 4bar $pCO_2$, 22°C) and experiments 143 (1.36M NaCl, 31bar $pCO_2$, 70°C) and 134 (deionised water, 31bar $pCO_2$, 70°C). Figures 4.2.28 and 4.2.29 compare Ca release from the two sets of experiments. The calculated dolomite dissolution rates for the two sets of experiments are presented in Figures 4.2.30 and 4.2.31.

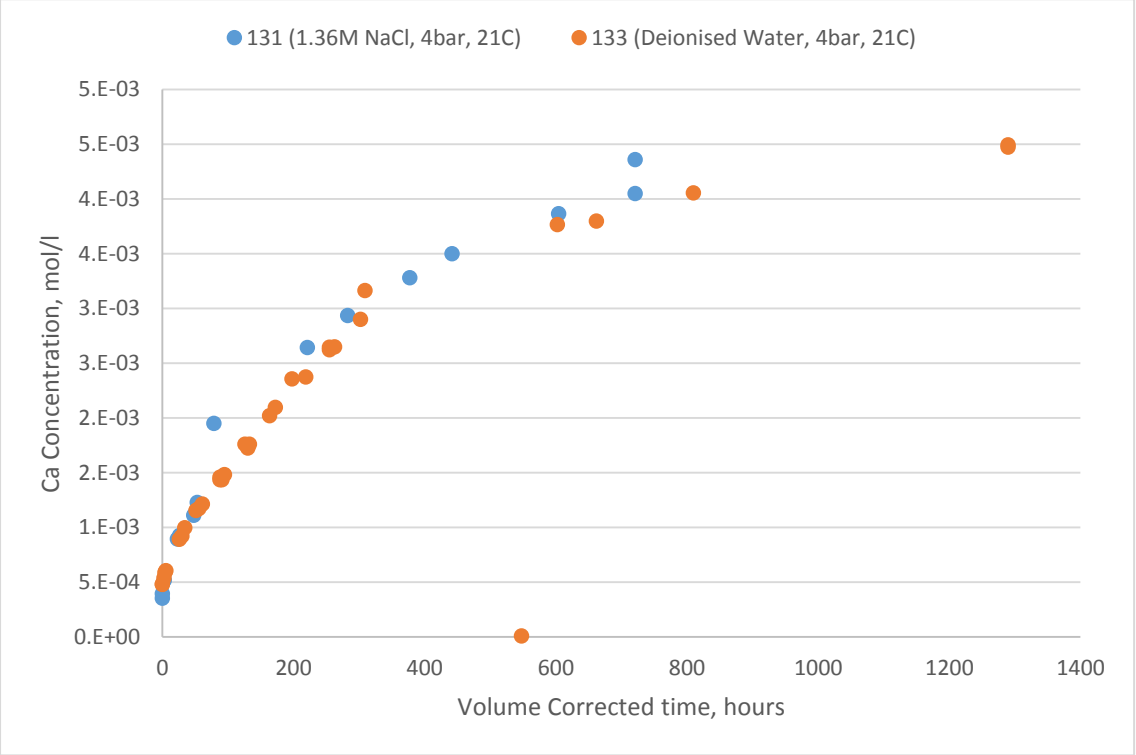


**Figure 4.2.28**: Comparative chart showing Ca release for experiments 131 (NaCl) and 133 (deionised water)

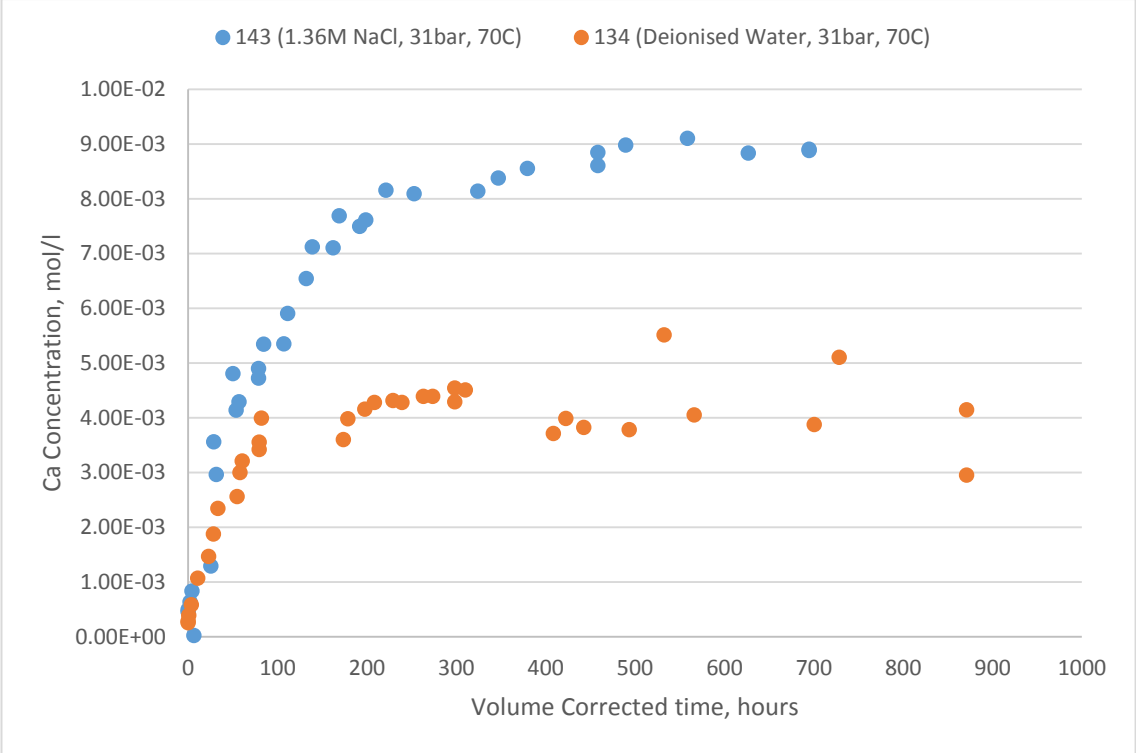


**Figure 4.2.29**: Comparative chart showing Ca release for experiments 143 (NaCl) and 134 (deionised water)

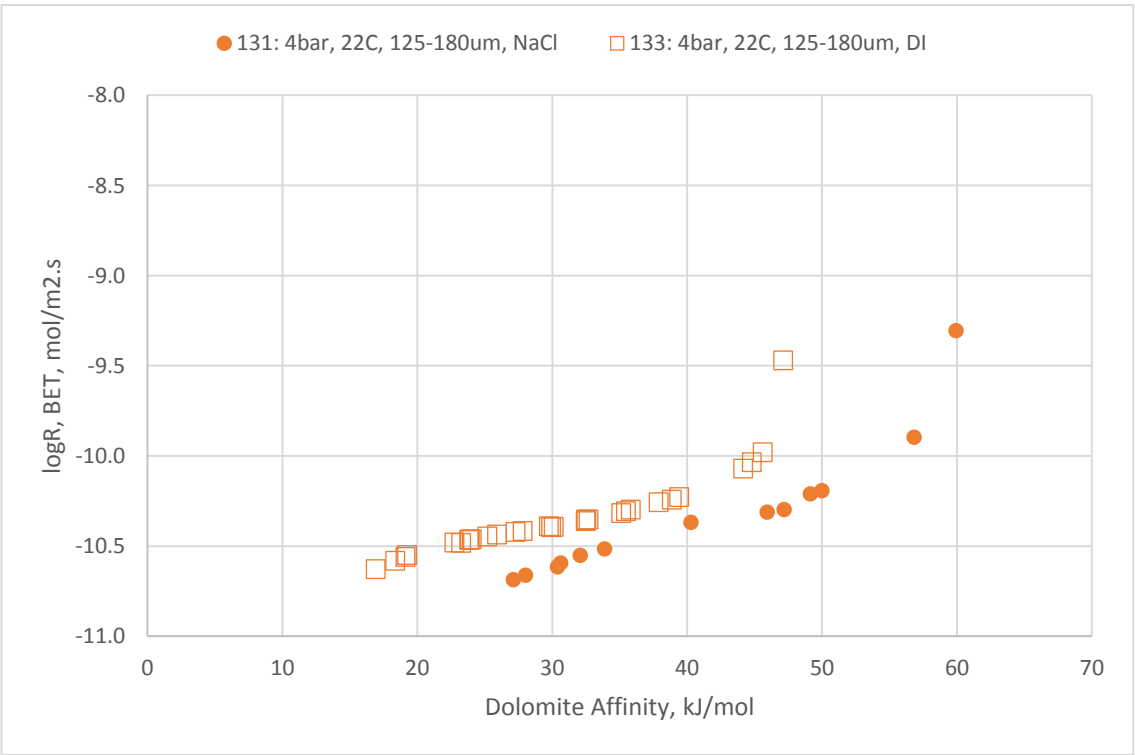


**Figure 4.2.30**: Calculated dolomite dissolution rates and affinities for experiments 131 (NaCl) and 133 (DI)

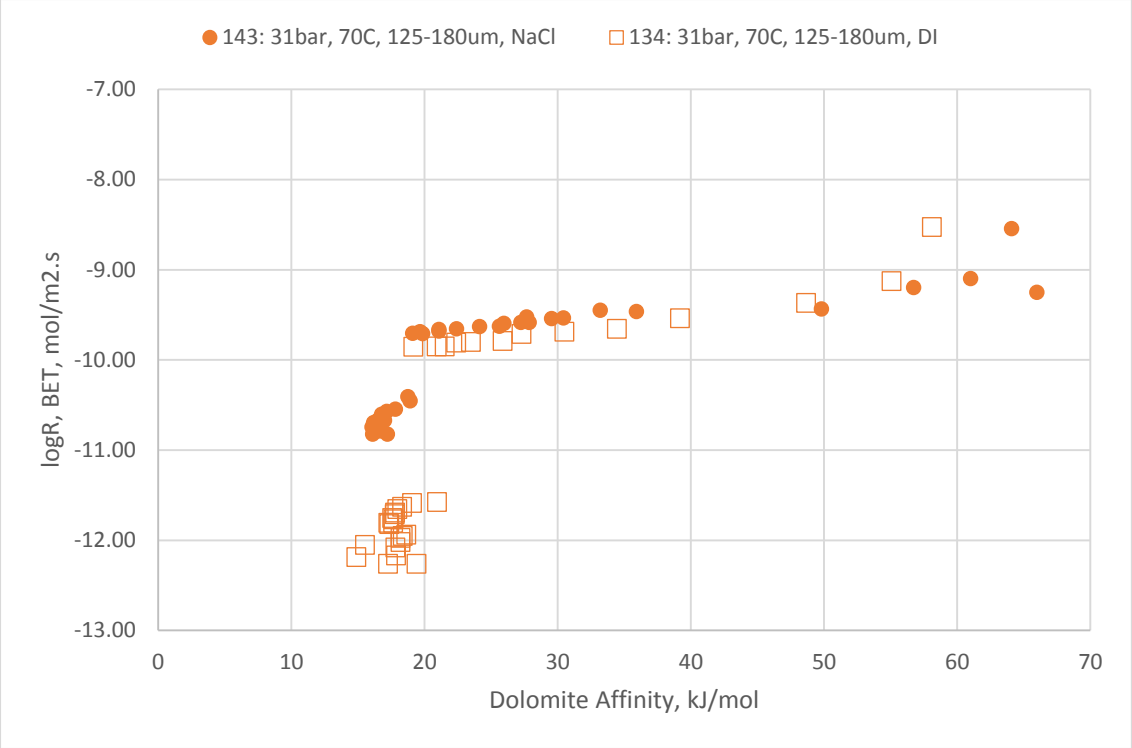


**Figure 4.2.31**: Calculated dolomite dissolution rates and affinities for experiments 143 (NaCl) and 134 (DI)

At low temperatures and pressures (4bar $pCO_2$, 22°C), the change in fluid composition appears to make a small difference to dolomite dissolution rates. While the magnitude of Ca release from experiments 131 and 133 appears similar, the calculated dolomite dissolution rates for the two experiments show that the rate is slightly depressed in the NaCl experiment, relative to that conducted in deionised water. At very early times in the higher pressure and temperature experiments (31bar $pCO_2$, 70°C) the magnitude and rate of Ca release is comparable between the two experiments. However, after around 50 hours, there is a strong deviation in the results, with the NaCl experiment showing a continuing and steep increase in Ca concentrations, while values in the deionised water dropping slightly due, as has been demonstrated in previous sections, to precipitation effects. Calculated rates for the high pressure temperature experiments indicate that dissolution is slightly enhanced in the NaCl experiment, relative to that carried out in deionised water.

### 4.2.2.5 Dissolution Behaviour: $pCO_2$ (4bar, 31bar) and temperature (22°C, 70°C)

Figures 4.2.32 and 4.2.33 compare Ca release from experiments 133 (4bar $pCO_2$, 21°C, DI) and 134 (31bar $pCO_2$, 70°, DI) and experiments 131 (4bar $pCO_2$, 21°C, NaCl) and 143 (31bar $pCO_2$, 70°C, NaCl). The calculated dolomite dissolution rates and affinities for the two sets of experiments are compared in Figures 4.2.34 and 4.2.35.

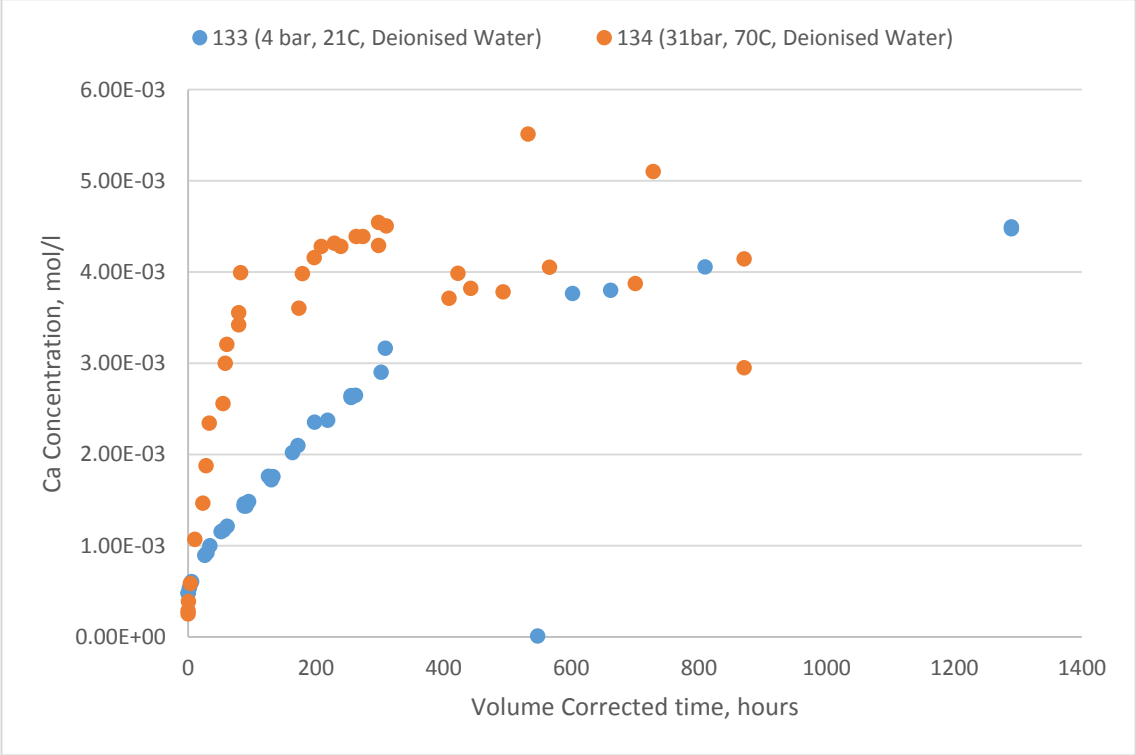


**Figure 4.2.32**: Comparative chart showing Ca release for experiments 133 (low P/T) and 134 (high P/T)

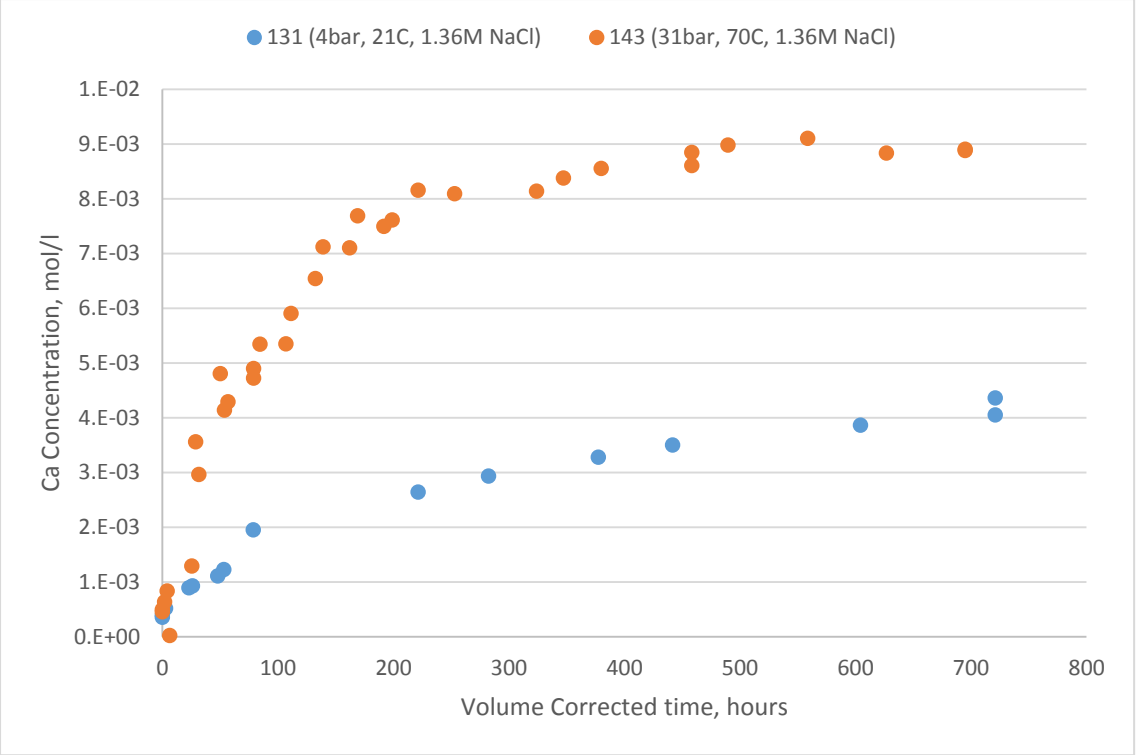


**Figure 4.2.33**: Comparative chart showing Ca release for experiments 131 (low P/T) and 143 (high P/T)

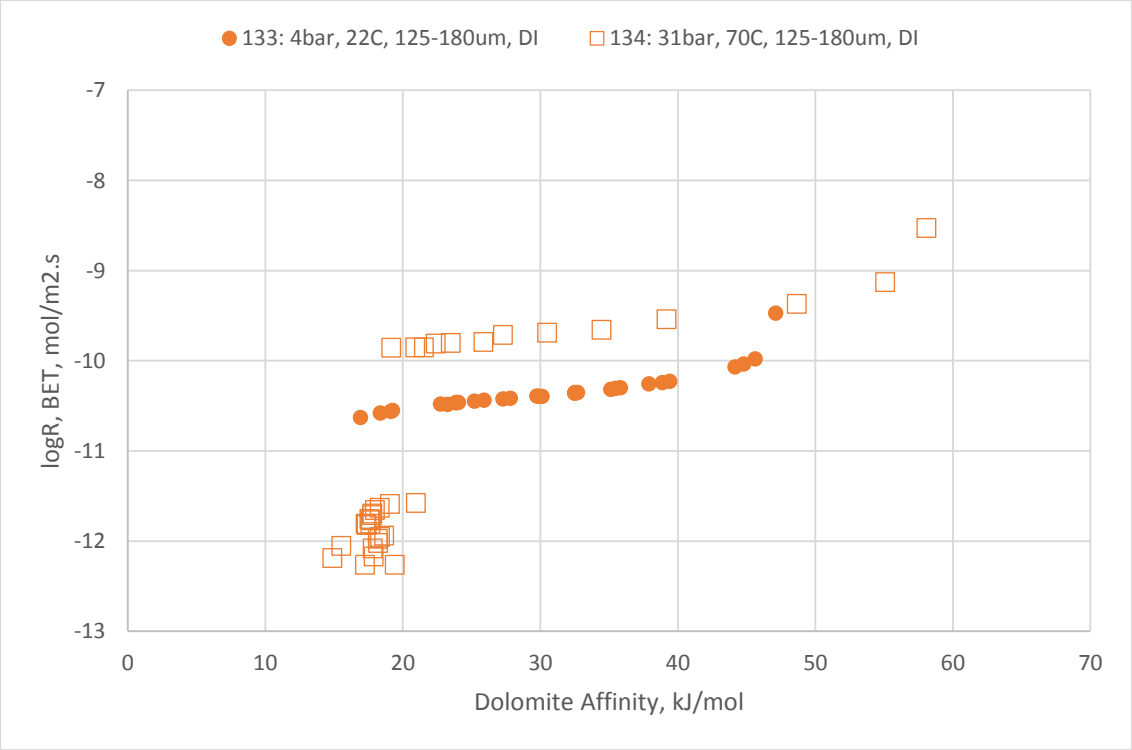


**Figure 4.2.34**: Calculated dolomite dissolution rates and affinities for experiments 133 (low P/T) and 134 (high P/T)

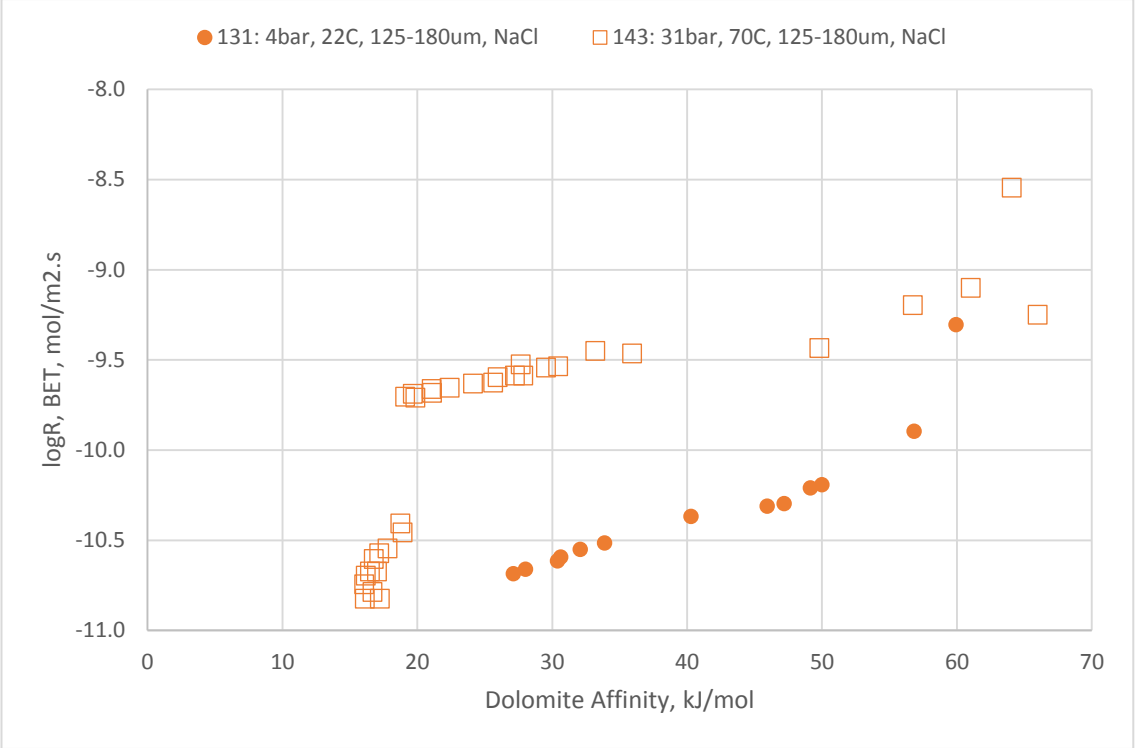


**Figure 4.2.35**: Calculated dolomite dissolution rates and affinities for experiments 131 (low P/T) and 143 (high P/T)

In both sets of experiments (deionised water and 1.36M NaCl), the combined effects of increased $pCO_2$ and temperature are marked. The rate of Ca release from experiment 143 (high P/T) is considerably higher at early time in the experiment (up to 200 hours). After this release rate drops (marked by a clear inflection in Figure 4.2.35), but Ca concentrations remain around 2x higher than those observed in the low P/T experiment (131). The results from the deionised water experiments are not as clear cut, due to the precipitation effects observed in experiment 134, but again it is clear that at early times (up to around 300 hours) Ca release from the high P/T experiment (134) is considerably higher than that observed in 133.

To separate the effects of $pCO_2$ and temperature, a “control” experiment was carried out at 4bar $pCO_2$ and 70°C. Ca release from this experiment (136) is compared to results from experiments 131 (4bar $pCO_2$, 22°C) and 143 (31bar $pCO_2$, 70°C) in Figures 4.2.36 and 4.2.37, while calculated dissolution rates are compared in Figures 4.2.38 and 4.2.39.

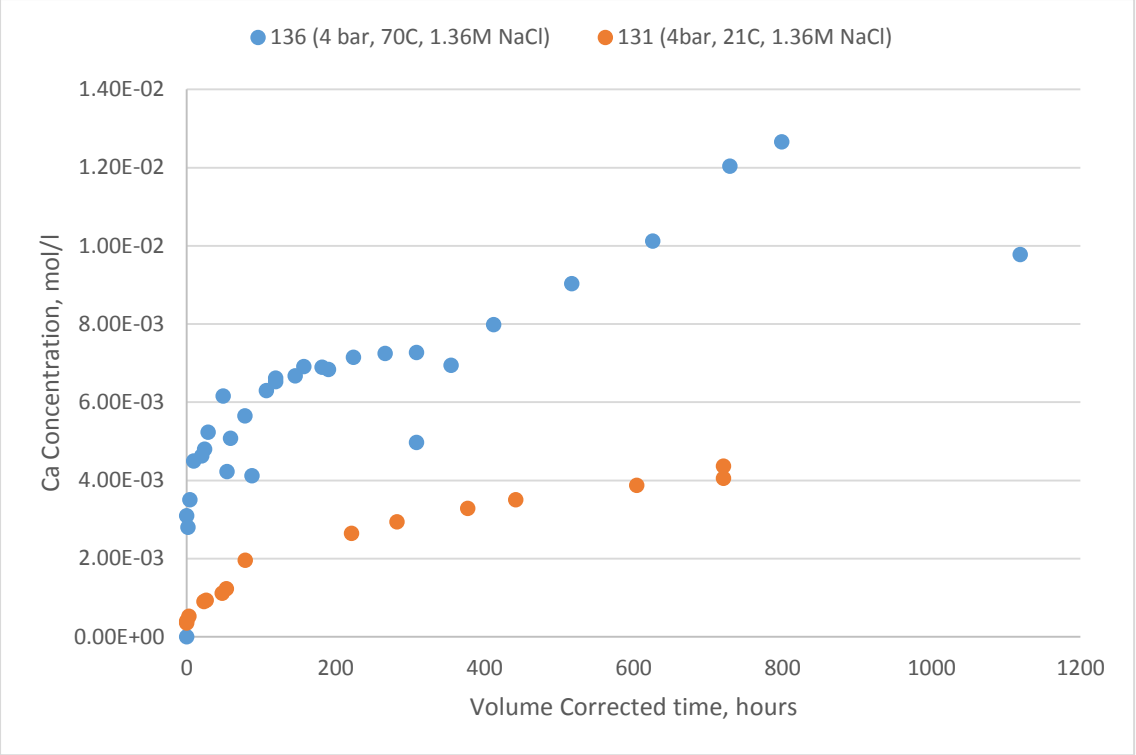


**Figure 4.2.36**: Comparative chart showing Ca release for experiments 136 (control) and 131 (low P/T)

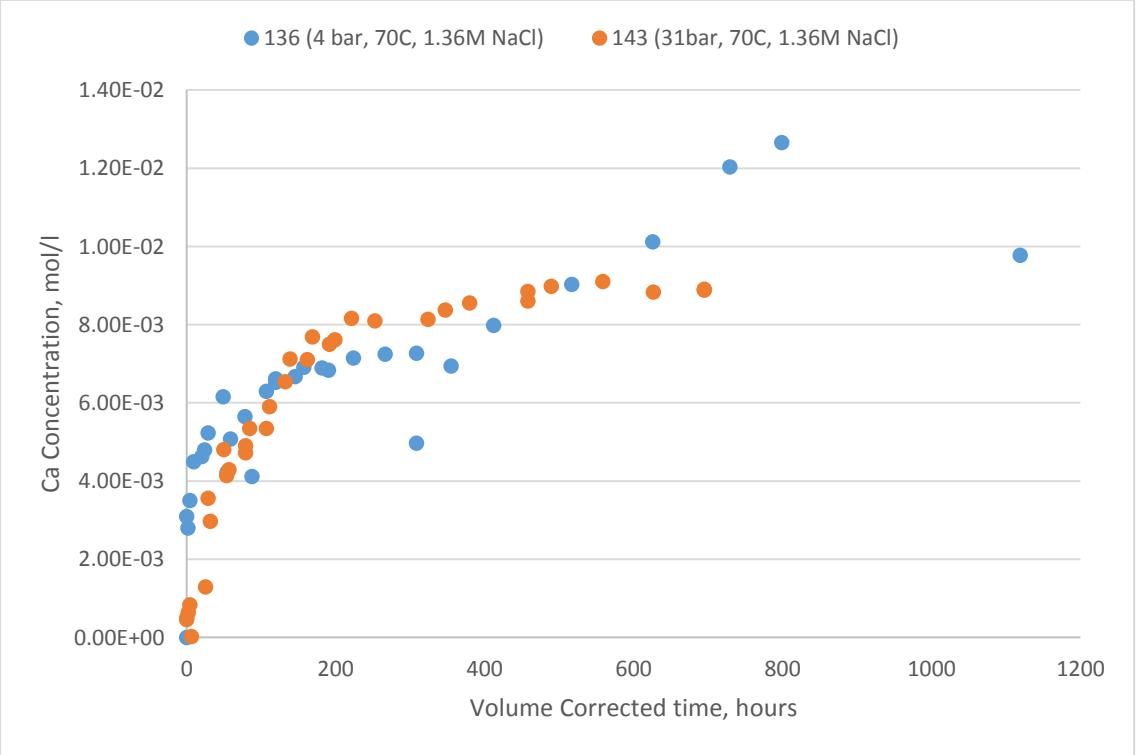


**Figure 4.2.37**: Comparative chart showing Ca release for experiments 136 (control) and 143 (high P/T)

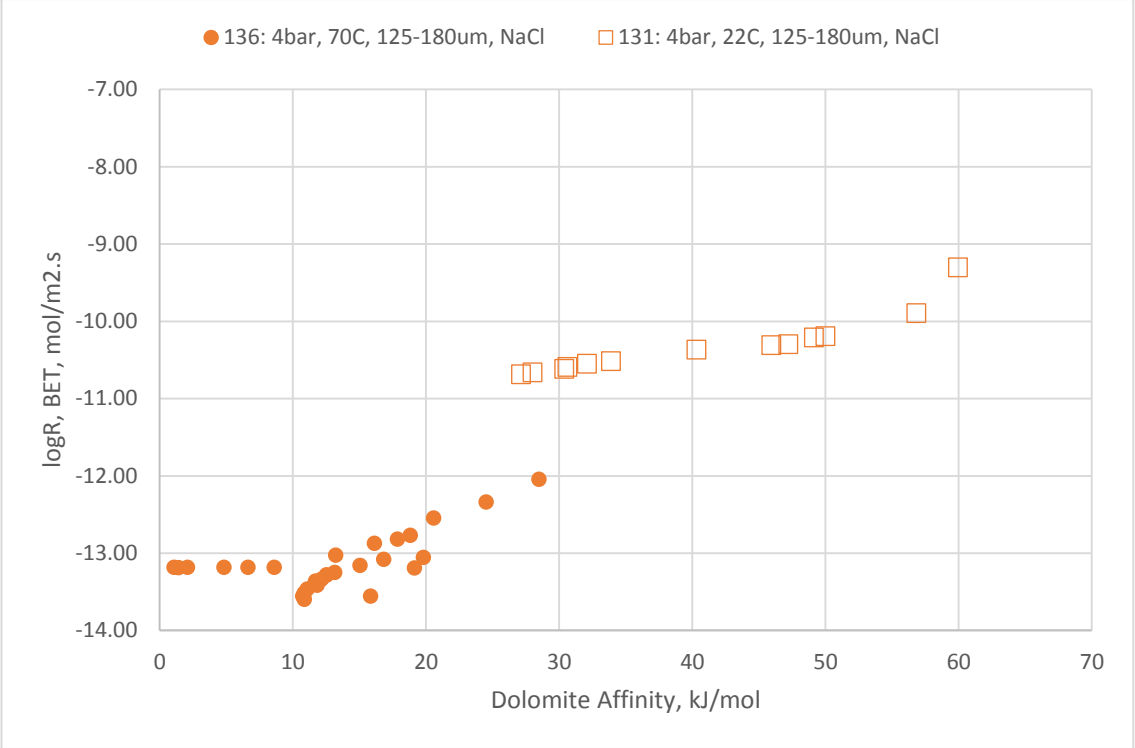


**Figure 4.2.38**: Calculated dolomite dissolution rates and affinities for experiments 136 (control) and 131 (low P/T)

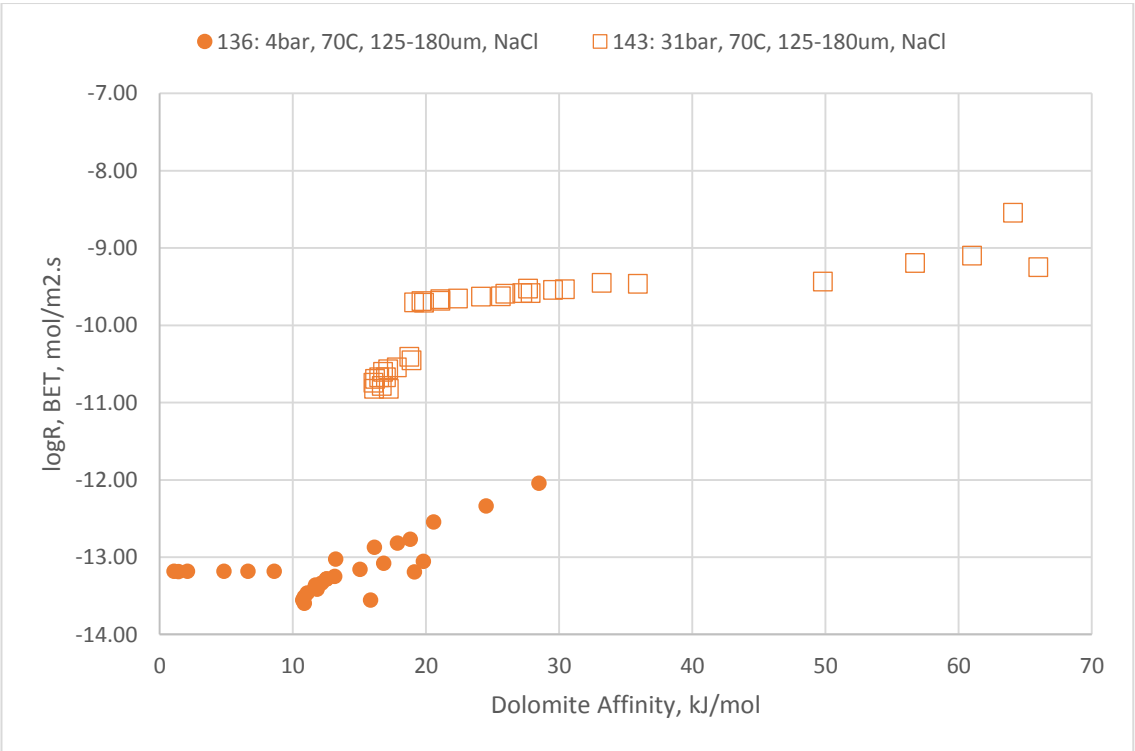


**Figure 4.2.39**: Calculated dolomite dissolution rates and affinities for experiments 136 (control) and 143 (high P/T)

Experiment 136 exhibits some odd behaviour after around 400 hours, where Ca release rates apparently increase, producing a near linear Ca release rate for the remained of the experiment. Despite the relatively high Ca concentrations measured in experiment 136 (comparable to concentrations in 143 and around 2-3x those in experiment 131), the calculated dolomite dissolution rate for the experiment is low relative to both the low pressure/temperature and high pressure/temperature experiments. While it is to be expected the higher $pCO_2$ in experiment 143 would lead to increased dolomite dissolution rates, that the rates observed in 136 are also low relative to the low temperature experiment is more unusual. The relative release rates may be explained by considering that dolomite solubility is proportional to $pCO_2$ and inversely proportional to temperature and that starting concentrations of Ca in the control experiment, 136, are relatively high, around an order of magnitude higher than in the other two experiments considered here. Hence in both cases dolomite affinities are somewhat lower in the control experiment than in the other two experiments compared, particularly 131. It may be that the lower affinity and increased Ca/Mg concentrations retarded the dissolution rate in experiment 136, either through a simple decrease in driving force due to distance from equilibrium or from saturation of surface sites by the relatively high concentrations of ions in solution.

The following section (4.2.2.6) will discuss dissolution rates in more detail, but the results presented here appear to confirm that $pCO_2$ has a strong effect on dolomite dissolution rates. However the effect of temperature is ambiguous from the above results, possibly obscured by affinity effects.

#### 4.2.2.6 Dolomite Dissolution Rates

Dolomite dissolution rates, as calculated from the experimental data are plotted against dolomite affinity (assuming a pure dolomite) in Figures 4.2.40 – 4.2.46. Experimental results are plotted along with calculated results using:

1) The USGS (2004) published general rate equation (Equation 4.2.3), using the values presented therein for ordered dolomite.
2) The dolomite dissolution equation presented by Busenberg and Plummer (1982):
$$R = k_1 a_{H^+}^n + k_2 a_{H_2CO_3^*}^n + k_3 a_{H_2O}^n - k_4 a_{HCO_3^-} \quad (4.2.8)$$
Using values for $k_i$ and n presented therein for dolomite dissolution at 25°C and 65°C (for the 22°C and 70°C experiments respectively).
3) The equation presented by Pokrovsky et al (2001):
$$r = k_{Mg}^{+} \left\{ \frac{K_{CO_3}^* K_{Ca}^*}{K_{CO_3}^* K_{Ca}^* + K_{Ca}^* a_{CO_3^{2-}} + a_{CO_3^{2-}} a_{Ca^{2+}}} \right\}^n \left(1 - exp\left(-\frac{nA}{RT}\right)\right) \quad (4.2.9)$$
Using the values of $k^+_{Mg}$, $K^*_{CO3}$, $K^*_{Ca}$ and n presented by Pokrovsky et al for dolomite dissolution at 25°C, ionic strength of 0.1M, a  and pH>6 (labelled as Pokrovsky 1) and those presented by Gautelier et al (2009) for dolomite dissolution at 80°C.
4) The $CO_2$ dependence of dolomite dissolution rate presented by Pokrovsky et al (2009) (labelled as Pokrovsky 2):
$$logR = A + B \times pCO_2 + C \times (pCO_2)^2 \quad (4.2.10)$$
Using the values of A, B and C presented therein for dolomite dissolution at 25°C or 60°C, in 0.1M NaCl and for 3.1<pH<4.0.

Affinites have been calculated based upon analysed concentrations using the equation:

$$A = RT \times \ln\left(\frac{K_{Dolomite}}{(a_{Ca^{2+}} \times a_{Mg^{2+}} \times a_{CO_3}^2)}\right) \quad (4.2.11)$$

Where $K_{Dolomite}$ is the equilibrium constant for dolomite at the experimental conditions, R is the gas constant, T is the temperature in Kelvin, and $a_{Ca^{2+}}, a_{Mg^{2+}}$ and $a_{CO_3}$ are the activities of the appropriate ions in solution, as calculated using by PHREEQC3 using the measured fluid compositions.

Where activities were required, those calculated from PHREEQC3 using individual fluid analyses have been used. Where literature rate equations

have been used, they have been calculated using one early time point and one late time point.

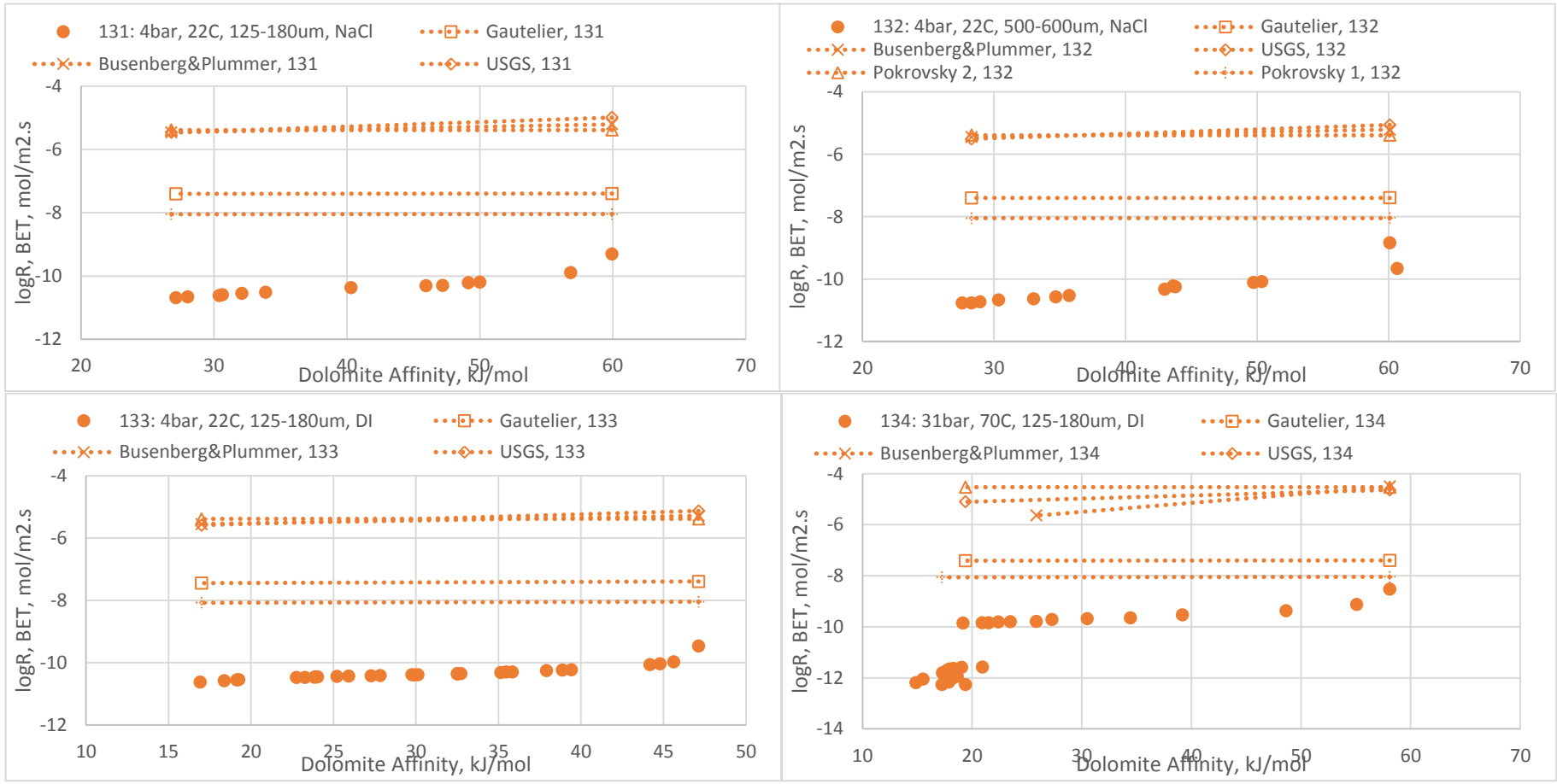


**Figure 4.2.40 – 4.2.43**: Calculated dolomite dissolution rates and affinities for experiments (clockwise from top left) 131, 132, 134 and 133. Experimental rates are plotted together with predicted rates using a variety of literature equations.

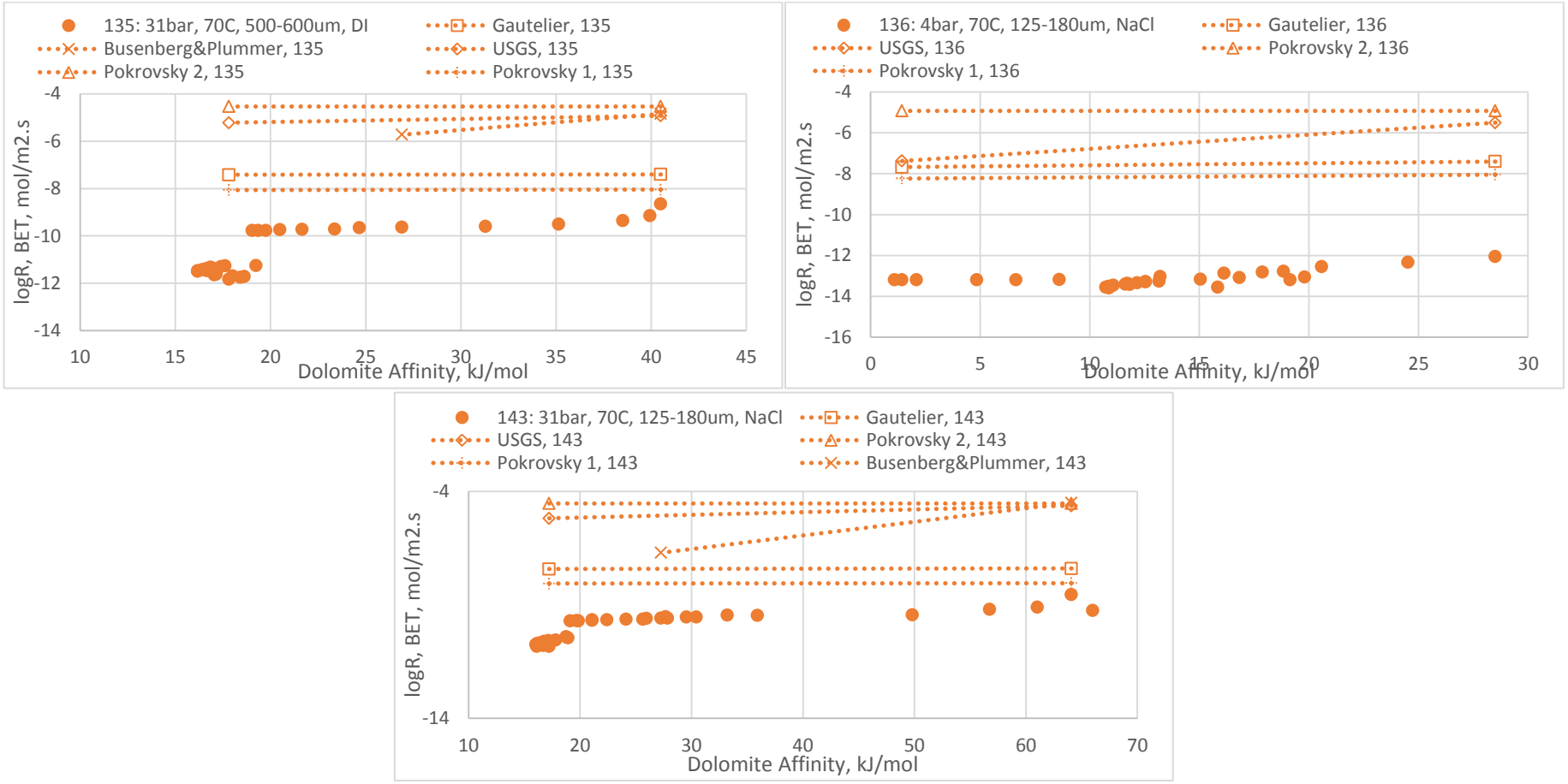


**Figure 4.2.44 - 4.2.46**: Calculated dolomite dissolution rates and affinities for experiments (clockwise from top left) 135, 136 and 143. Experimental rates are plotted together with predicted rates using a variety of literature equations.

As with the calcite experiments presented in Section 4.2.1, rates calculated from the experimental results presented here, consistently fall below those predicted by the literature equations discussed above. The rates predicted using equation 4.2.9 (labelled Pokrovsky 1 and Gautelier) prove the more accurate in terms of agreement with the experimental results and at higher chemical affinities, >40kJ/mol (early times), experimental rates tend toward those predicted by equation 4.2.9, using the values presented in Pokrovsky et al (2001).

The apparent dependence of rate on chemical affinity is weaker than that observed in the calcite experiments. Apparent precipitation or back reaction effects are notable in experiments 134, 135 and 143, where the figures above show a sudden drop in rate and a cluster of points covering a narrow range of affinities. Also notable is the fact that the Busenberg and Plummer equation (Equation 4.2.8) predicts a cessation of dissolution in these experiments. The equation assumes that bicarbonate activity is the main control on the backward reaction and some way into each of these experiments the bicarbonate levels (according to the PHREEQC3 speciation) become high enough to effectively kill the overall dissolution reaction.

Also of note are the results from experiment 136 (Figure 4.2.45). As discussed in Section 4.2.2.5 the rates from this experiment are abnormally low, and suddenly increase to a near constant value towards the end of the experiment. The affinities calculated for this experiment are also very low, which may explain the low rates observed. The affinity in this case is largely dependent on the carbonate ion activities, which are notably elevated in this experiment (again, according to PHREEQC3 speciation calculations).

#### 4.2.2.7 Dolomite Experiments Overview and Discussion

Measured values of dissolved $CO_2$ in the experiments agree well with those predicted by PHREEQC3, using final fluid compositions. Agreement between measured and predicted pH is not as close, but there is no clear systematic deviation between the values and these discrepancies may reflect the difficulty of measuring pH using a flow-through cell and/or sensitivity of predicted pH to errors in fluid analysis. All final sample values of dissolved $CO_2$ and pH (measured and predicted) are below the predicted equilibrium values. Dissolved $CO_2$ was up to 26% below equilibrium values, while pH was up to one pH unit lower. pH has a strong effect on carbonate speciation and on the dissolution of various minerals and hence formation fluid pH will be an important consideration during injection of $CO_2$ into a reservoir. Dolomite will be the main mineral able to buffer pH in many sandstone reservoirs (as is the case in the Sherwood Sandstone) and the results here suggest that in systems where reacted fluids are not rapidly replenished pH will stabilise at values considerably below the equilibrium values predicted by geochemical modelling programmes such as PHREEQC. If pH remains relatively low, $CO_2$ will remain in solution as a dissolved phase, rather than speciating to bicarbonate or carbonate, which in turn will have implications for the capacity of the fluid to dissolve further $CO_2$ and may be of consequence in schemes where the aim is to maximise solubility trapping.

As for calcite variation in grain-size (125-180µm vs. 500-600µm) made little to no difference in the dissolution behaviour of dolomite. Fluid composition (deionised water vs. 1.36M NaCl) on the other hand had a notable impact on dolomite dissolution behaviour. At lower pressures and temperatures, dissolution rates were apparently retarded by the use of NaCl rather than deionised water, while at higher pressures and temperatures the opposite was true. The addition of NaCl should act to slightly increase dolomite solubility through creation of sodium-bicarbonate, driving further dolomite dissolution. This effect is reflected in PHREEQC3 equilibrium calculations, where Ca concentrations are predicted to be 50% higher in the NaCl bearing fluids. It is interesting that this effect is not seen in the low temperature/pressure experiments. It is possible that this is due to the increased temperature enhancing the speed of the reactions and that if the low pressure/temperatures experiments were run for long enough a similar relationship would be observed. Additionally the effect of precipitation in

experiment 134 may have acted to increase the apparent discrepancy between the two experiments: i.e. not all of the difference between the two can be attributed to the fluid composition.

The net effect of increasing temperature and $pCO_2$ was to increase Ca/Mg release rates and the majority of this effect came from the increase in temperature, while there is also some indication that the increase in $CO_2$ pressure increased dissolution rates slightly.

As for the calcite experiments all rates calculated from experimental results are considerably lower than those predicted using the various rate equations presented in section 4.2.2.6. Rates predicted by the USGS general rate equation and those predicted by the Busenberg and Plummer equation are in close agreement, which is unsurprising given that the parameters used in the USGS equation are regressed from the original data produced by Busenberg and Plummer. Rates predicted using Pokrovsky's equation describing rate dependence on $pCO_2$ are also similar to the rates predicted by the Busenberg and Plummer equation. Rates calculated using the more recent equation produced by Pokrovsky et al (2001) are in closer agreement with experimentally derived rates and at high chemical affinities/early times experimental rates tend towards the values predicted by this equation.

The Pokrovsky (2001) equation assumes an early release of Ca relative to Mg from the dolomite surface, with further dissolution being controlled by the hydration of Mg rich surface sites. This forms a precursor complex: $MgOH_2^+$, which is free of Ca or $CO_3$. They proposed that this accounted for the apparent inhibition of rates by calcium and carbonate ions in solution, equivalent to the back-reaction term in the Busenberg and Plummer equation, where dissolution is inhibited by bicarbonate concentrations. Given the discrepancy between the experimentally derived rates and those calculated using the Busenberg and Plummer equation, it is clear that bicarbonate concentrations alone cannot account for the inhibition of dissolution observed in these experiments. Rates calculated using the equation of Pokrovsky and Schotts are much closer to measured rates suggesting that their surface complexation model provides a better description of rate inhibition. It should be noted that the values of $k_{Mg}$, $K_{Ca}$ and $K_{CO3}$ used in their equation are subject to a considerable degree of uncertainty, as they are empirical fitting parameters. The value of $k_{Mg}$ used by Gautelier et al (2007) for example is two orders of magnitude higher than that used in the original Pokrovsky et al paper. Using a $k_{Mg}$ two orders of

magnitude lower than that presented by Pokrovsky and Schott leads to a much better fit with the experimental data presented here but obviously brings into question the utility of such an equation in predictive modelling of carbon dioxide sequestration systems. Additionally, as was the case with calcite, the fits to equations such as those presented by Busenberg and Plummer and Pokrovsky and Schott have been largely calculated using flow-through or rotating disc experiments, where precipitation effects and build-up of surface complexes are minimised. In the experiments presented here all three of the experiments carried out at elevated $pCO_2$ (31bar) show clear evidence of a strong back-reaction, either through precipitation or readsorption. The equation of Busenberg and Plummer partially predicts this (in these experiments the bicarbonate ion concentration becomes so high that the back reaction term in their equation essentially outweighs the forward terms) and it is possible that this effect- the retardation of dissolution through adsorption of ions from solution is present in all of the experiments to some degree.

# Chapter 5
# Sherwood Sandstone Dissolution Experiments Results

Ten dissolution experiments were carried out on the Sherwood Sandstone material described in Chapter 3, the conditions of which are summarised in Table 5.1.1.

| Experiment ID | Grain Fraction, µm | Fluid | pCO2, bar (absolute) | Temperature, $^0$C | Run time, volume constant hours | Conditioning period prior to $CO_2$ injection, hours |
|---|---|---|---|---|---|---|
| 141 | 125-180 | 1.36M NaCl | 4 | 22 | 2177 | 144 |
| 142 | 500-600 | 1.36M NaCl | 4 | 22 | 1933 | 144 |
| 146 | 500-600 | 1.36M NaCl | 31 | 70 | 1064 | 260 |
| 147 | 125-180 | 1.36M NaCl | 31 | 70 | 940 | 139 |
| 144 | 125-180 | Deionised Water | 4 | 22 | 1781 | 266 |
| 148 | 125-180 | Deionised Water | 31 | 70 | 996 | 144 |
| 149 | 125-180 | 1.36M NaCl | 4 | 70 | 1150 | 267 |
| SC2 | Chip | 1.36M NaCl | 31 | 70 | 2744 | 189 |
| SCORE | Core | 1.36M NaCl | 31 | 70 | - | - |
| STATIC | Core | 1.36M NaCl | 13 | 70 | - | - |

**Table 5.1.1**: Summary of experiments carried out on Sherwood Sandstone material

These experiments were designed to assess the behaviour of Sherwood Sandstone type materials under elevated $pCO_2$ and temperature and as a comparison to the results of the single mineral experiments detailed in previous sections.

## 5.1 Powder Batch Experiments

Seven batch experiments were carried out on powdered Sherwood sandstone samples.

### 5.1.1 pH and $CO_2$ Solubility

As in previous sections, modelling has been carried out using PHREEQC3, to estimate equilibrium concentrations and to calculate pH of fluid samples. The full results of the pH and CO2 solubility calculations can be found in Appendix B, but selected results are shown in Table 5.1.2.

Calculated pH of the starting fluids (prior to $CO_2$ injection) is between 7.9 and 8.5. Upon addition of $CO_2$, calculated pH falls rapidly to between 3.6 and 4.5. Calculated pH then tends to rise fairly rapidly for the first few hundred hours of experiment, before levelling off at levels between 4.2 and 4.7. Final pH (calculated and measured) are considerably (1-1.5 pH units) below the predicted equilibrium pH, calculated using the bulk composition outlined above. The results of pH calculations for samples from experiment are presented in Figure 5.1.1 to illustrate this behaviour.

In terms of $CO_2$ solubility, measured and calculated results from the end-time experimental fluids agree reasonably well (within ±15%) and also match relatively closely with the predicted equilibrium values (again, within ±15%).

| Run | Fluid/p $CO_2$ (bar)/T(° C) | Equilibrium $CO_2$ PHREEQC3, mol/kg | Final Sample $CO_2$ PHREEQC3, mol/kg | Final Sample $CO_2$ (Measured), mol/kg | Standard Deviation, $CO_2$ (No. of measurements) | Equilibrium pH, PHREEQC3 | Final Sample pH, PHREEEC3 | Final Sample pH, measured |
|---|---|---|---|---|---|---|---|---|
| 141 | NaCl/4/22 | 0.166 | 0.110 | 0.115 | 0.011 (4) | 5.538 | 4.746 | 4.800 |
| 142 | NaCl/4/22 | 0.166 | 0.1101 | 0.115 | 0.011 (5) | 5.538 | 4.796 | 4.930 |
| 144 | DI/4/22 | 0.177 | 0.146 | 0.145 | 0.033 (5) | 5.615 | 5.021 | 5.430 |
| 146 | NaCl/31/70 | 0.365 | 0.325 | 0.253 | 0.042 (5) | 4.966 | 4.460 | - |
| 147 | NaCl/31/70 | 0.365 | 0.325 | - | - | 4.966 | 4.385 | - |
| 148 | DI/31/70 | 0.436 | 0.415 | 0.375 | 0.033 (3) | 4.903 | 4.591 | - |
| 149 | NaCl/4/70 | 0.077 | 0.045 | 0.051 | n/a (1) | 5.531 | 5.105 | - |

**Figure 5.1.2**: Summary of pH and $CO_2$ solubility data for sandstone powder experiments

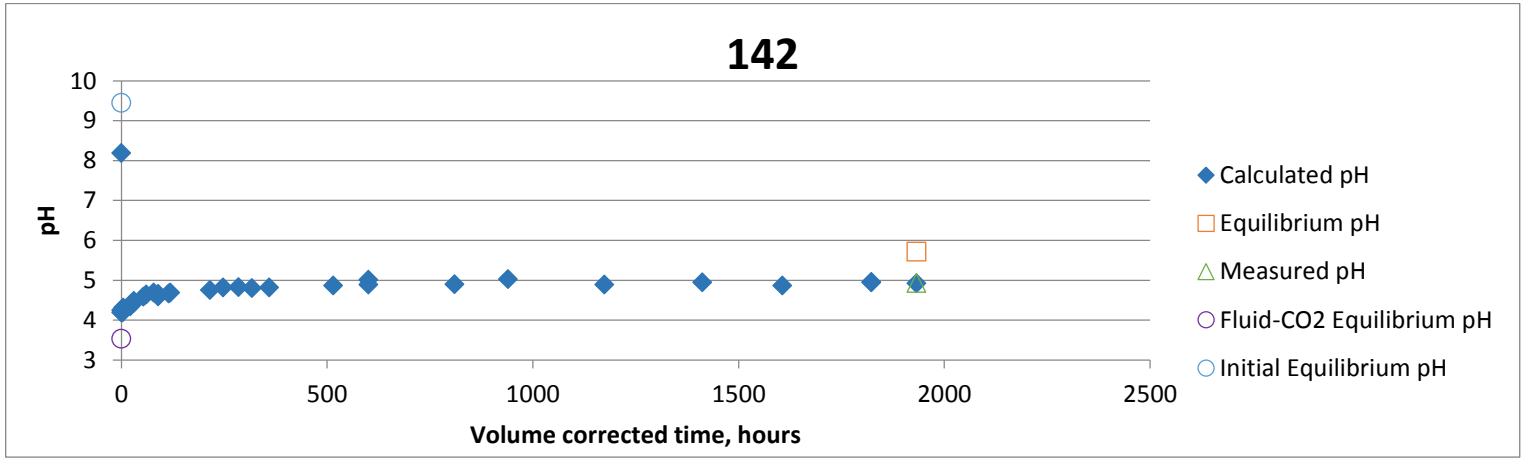


**Figure 5.1.1**: Calculated pH for samples from experiment 142

### 5.1.2 Dissolution Behaviour: Effects of Grain Size

Two pairs of experiments were carried out which differed only in the grain size of the starting materials. Experiments 141 (125-180µm, 4bar $pCO_2$, 22°C, NaCl) and 142 (500-600µm, 4bar $pCO_2$, 22°C, NaCl) and experiments 147 (125-180µm, 31bar $pCO_2$, 70°C, NaCl) and 146 (500-600µm, 31bar $pCO_2$, 70°C, NaCl) are compared in Figures 5.1.2 – 5.1.11. Figures 5.1.12 – 5.1.15 compare calculated K-feldspar and dolomite dissolution rates for the two sets of experiments.

Comparison between experiments 141 and 142 show higher concentrations of K and Al are released in experiment 141 (the finer grained experiment), while other analytes (Mg, Ca, Si) behave in a similar manner in both experiments. Calculated K-feldspar dissolution rates are likewise higher in experiment 141 relative to 142, while dolomite rates are similar.

By comparison, analytes in the high temperature experiments (146 and 147) behave in a similar manner in both the fine and coarse grained experiments and calculated dissolution rates are likewise similar.

These results indicate that while differences in grain size of the magnitude investigated here make little difference at higher pressures and temperatures, where reaction rates are enhanced by other experimental conditions, at lower temperatures and pressures, dissolution of the feldspar component in the sandstone is enhanced if the grain size is finer.

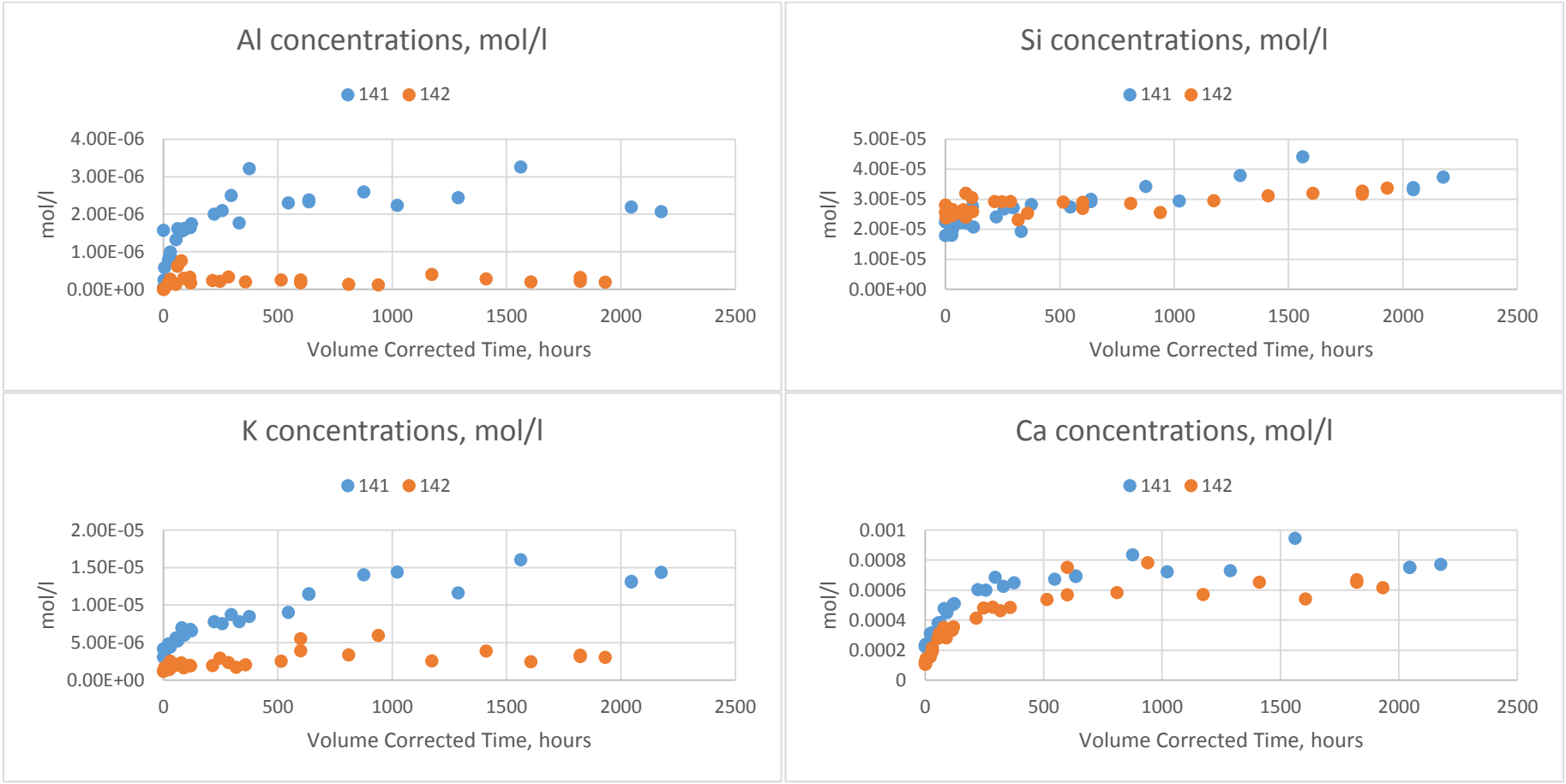


**Figures 5.1.2 – 5.1.5**: Comparative charts showing (clockwise from top left) Al, Si, Ca and K release for experiments 141 (125-180µm) and 142 (500-600µm)

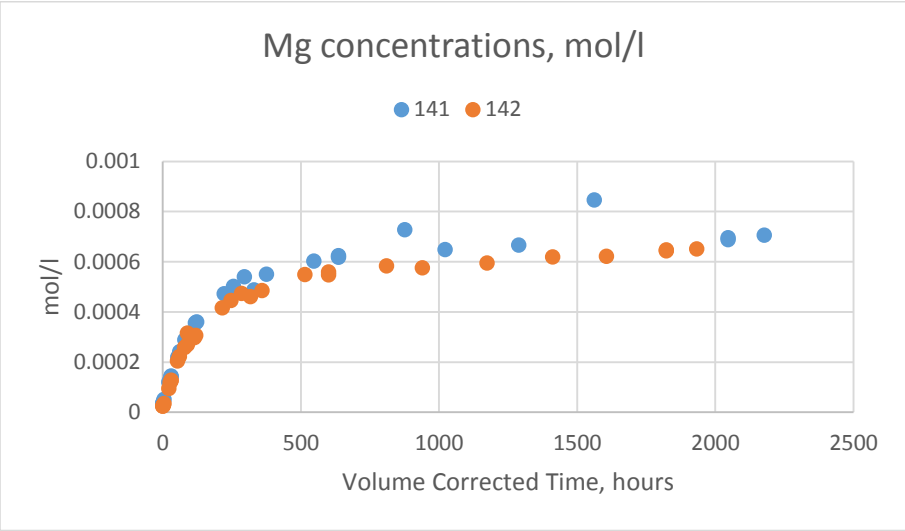


**Figure 5.1.6**: Comparative chart showing Mg release for experiments 141 (125-180µm) and 142 (500-600µm)

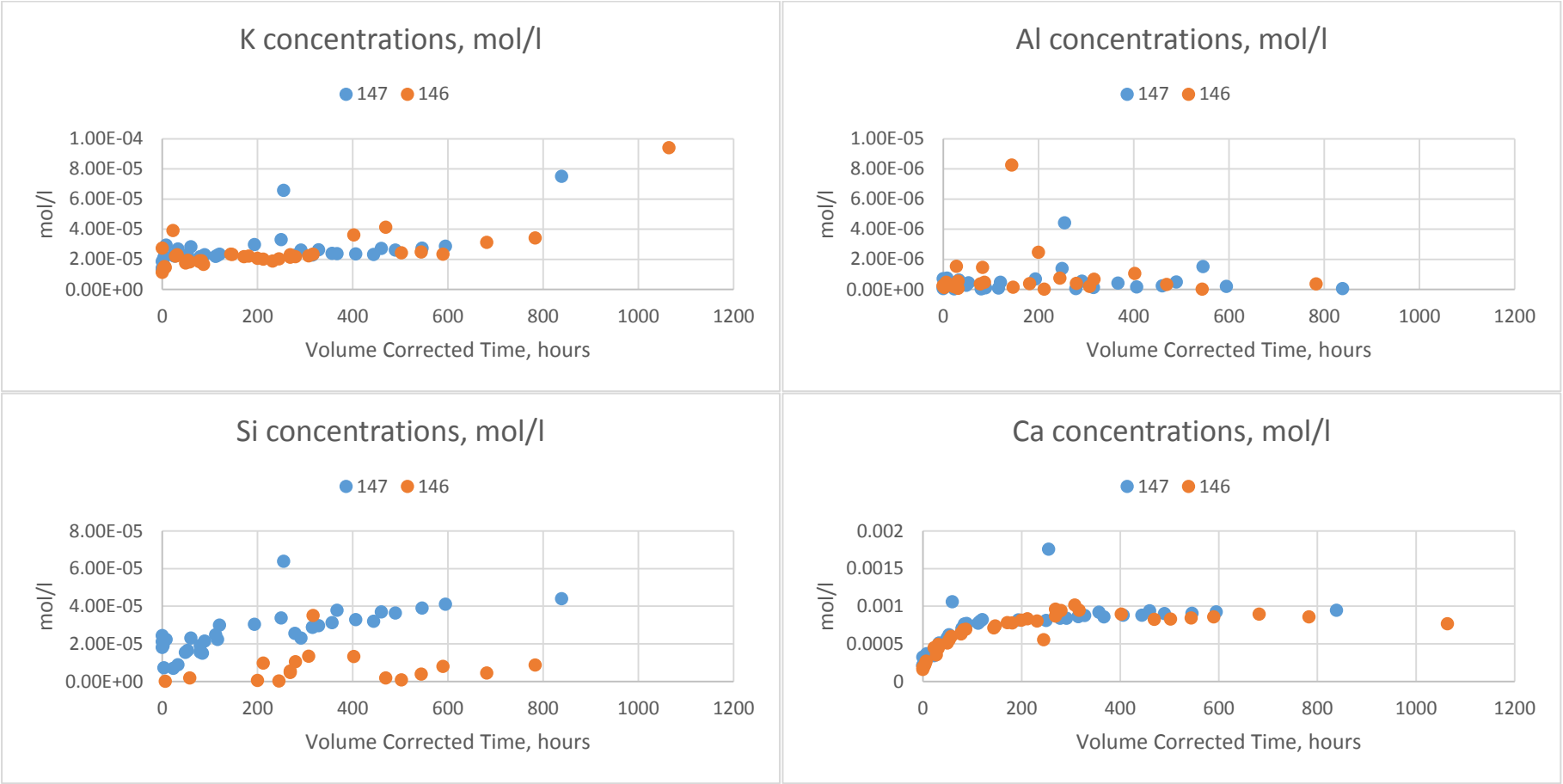


**Figures 5.1.7 – 5.1.10**: Comparative charts showing (clockwise from top left) K, Al, Si, and Ca release for experiments 147 (125-180µm) and 148 (500-600µm)

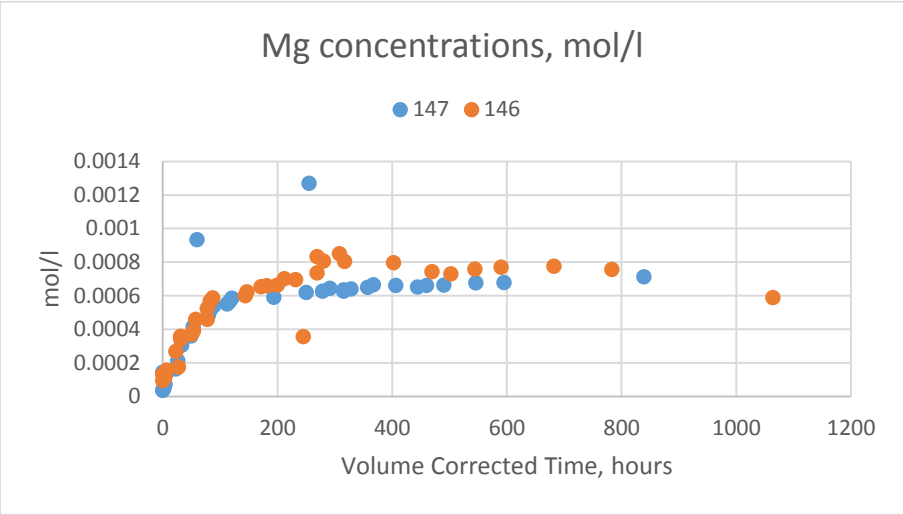


**Figure 5.1.11**: Comparative chart showing Mg release for experiments 147 (125-180µm) and 148 (500-600µm)

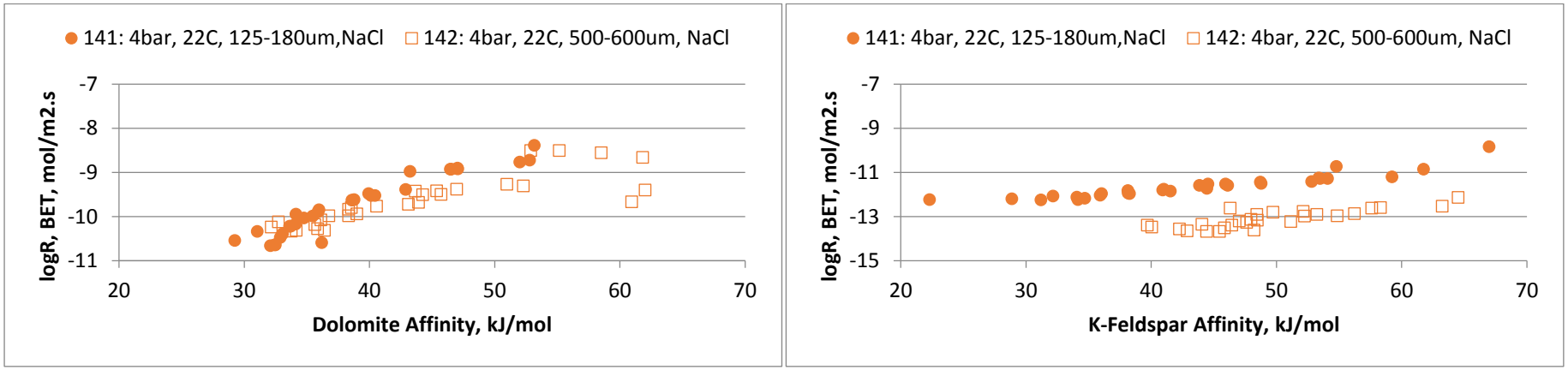


**Figures 5.1.12 – 5.1.13**: Calculated dolomite and K-feldspar dissolution rates for experiments 141 (125-180µm) and 142 (500-600µm).

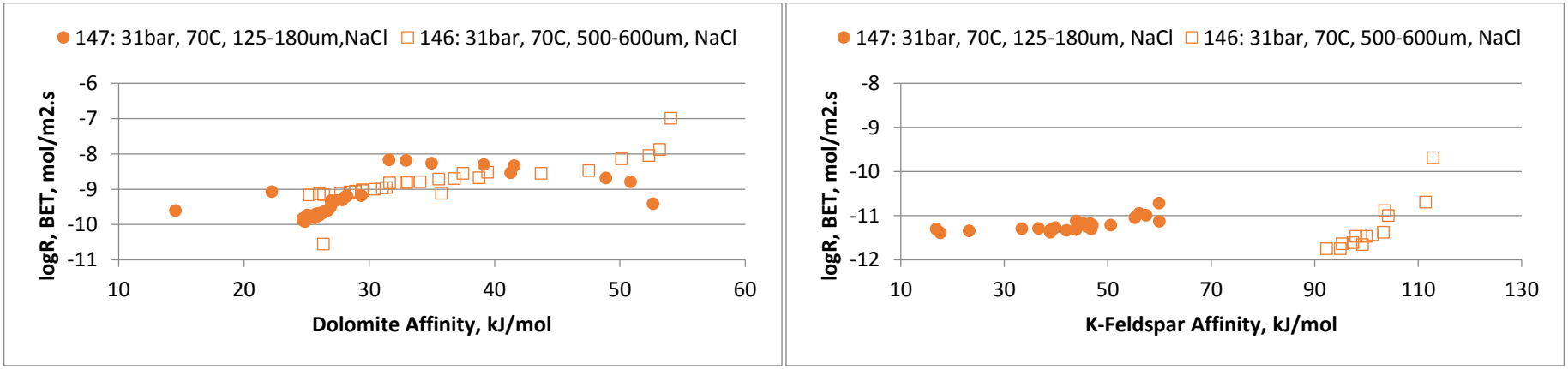


**Figures 5.1.14 – 5.1.15**: Calculated dolomite and K-feldspar dissolution rates for experiments 147 (125-180µm) and 146 (500-600µm).

### 5.1.3 Dissolution Behaviour: Effects of Fluid Salinity

Results from experiments 147 (1.36M NaCl, 31 bar $pCO_2$, 70°C) and 148 (deionised water, 31 bar $pCO_2$, 70°C) and experiments 141 (1.36M NaCl, 4bar $pCO_2$, 22°C) and 144 (deionised water, 4bar $pCO_2$, 22°C) are compared in Figures 5.1.16 – 5.1.25. Calculated dolomite and K-feldspar dissolution rates are shown in Figures 5.1.26 – 5.1.29.

In both the low pressure/temperature and high pressure temperature comparisons, calcium and magnesium concentrations are consistently higher in the NaCl experiments. Aluminium and silica show no consistent differences in the high temperature comparison, but at low temperature concentrations are higher in the NaCl fluid. A comparison of potassium concentrations was not possible for the high temperature/pressure experiments, but for the low temperature experiments, concentrations are very similar. Calculated rates are broadly similar for the compared experiments, with the exception of the calculated dolomite dissolution rates for experiments 141 and 144. Here dolomite dissolution rates appear to be relatively depressed in the NaCl experiment (141), similar to the behaviour observed in the dolomite single mineral experiments discussed in Section 4.2.

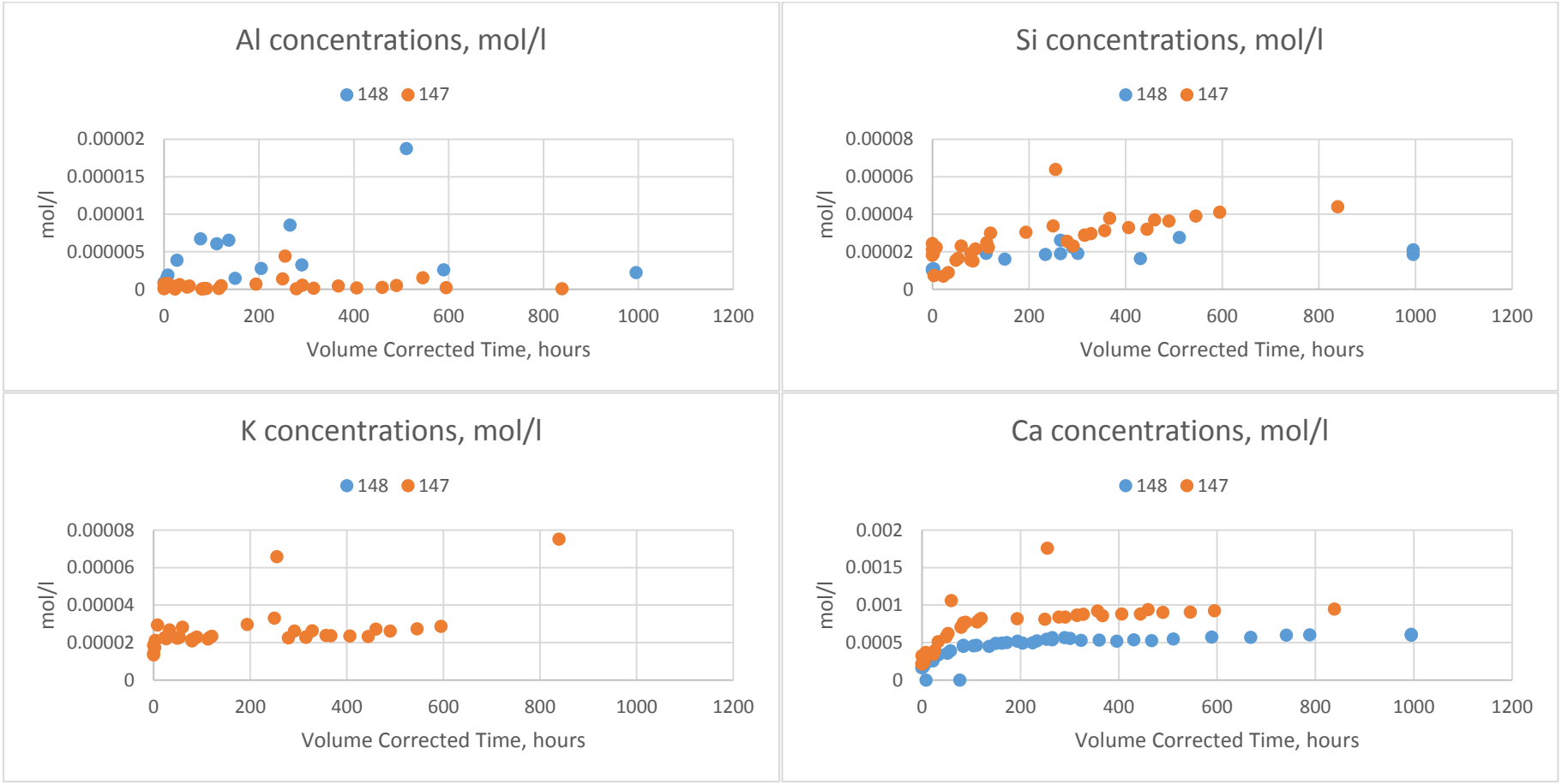


**Figures 5.1.16 – 5.1.19**: Comparative charts showing (clockwise from top left) Al, Si, K and Ca release for experiments 148 (NaCl) and 147 (DI)

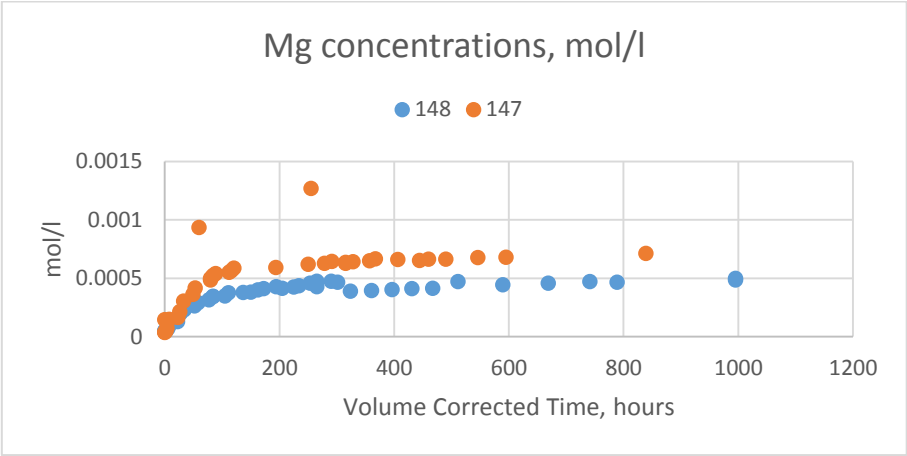


**Figure 5.1.20**: Comparative chart showing Mg release for experiments 148 (NaCl) and 147 (DI)

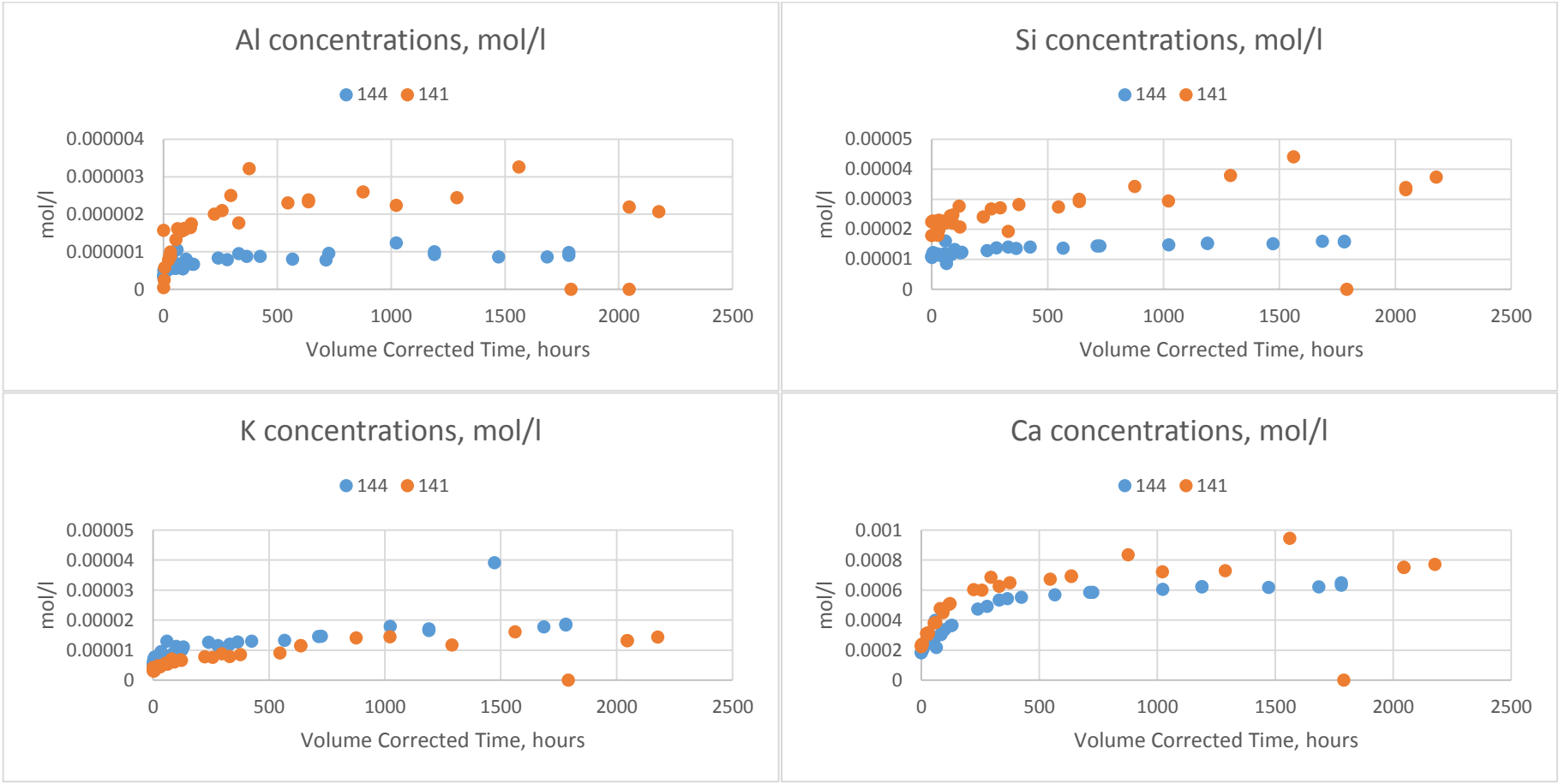


**Figures 5.1.21 – 5.1.24**: Comparative charts showing (clockwise from top left) Al, Si, Ca and K release for experiments 144 (DI) and 141 (NaCl)

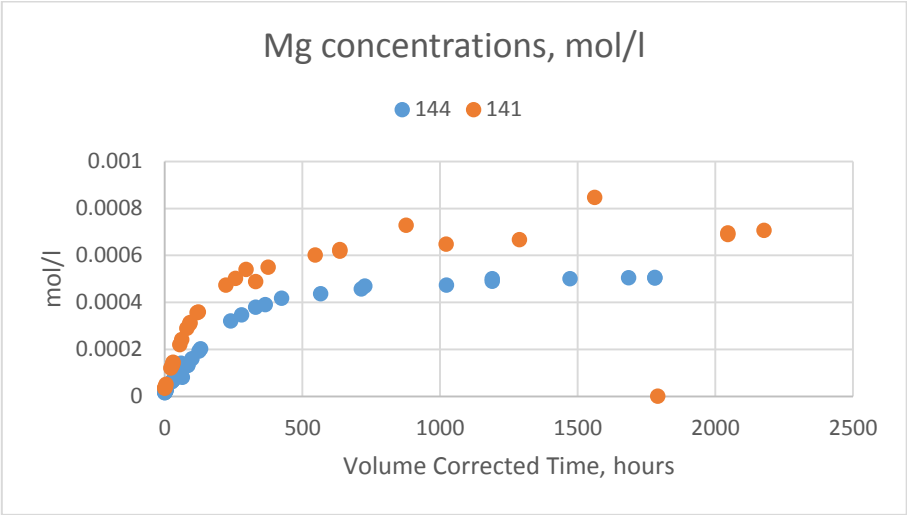


**Figure 5.1.25**: Comparative chart showing Mg release for experiments 144 (DI) and 141 (NaCl)

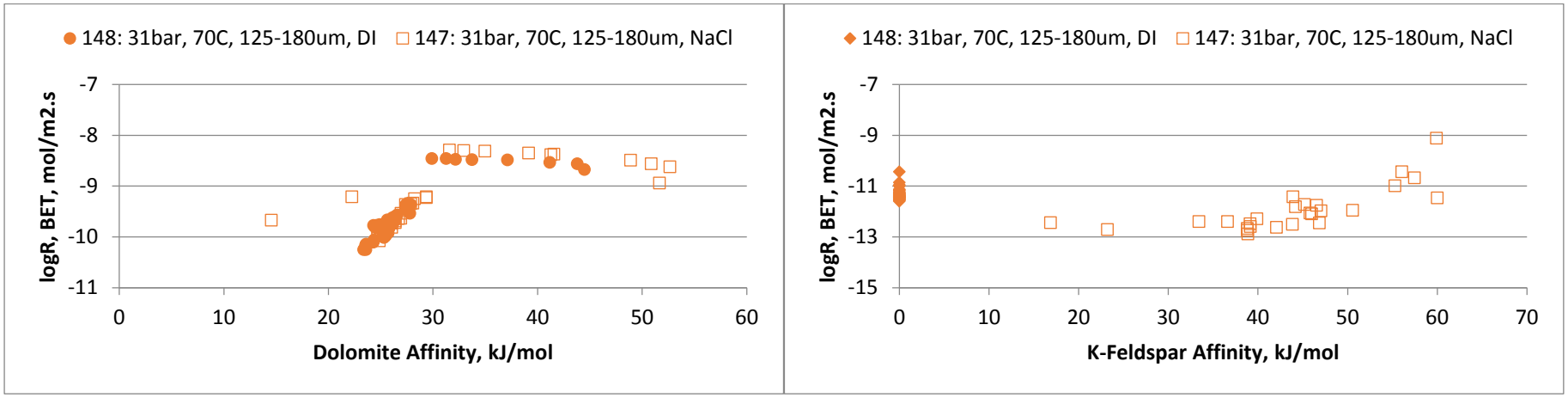


**Figures 5.1.26 – 5.1.27**: Calculated dolomite and K-feldspar dissolution rates for experiments 148 (DI) and 147 (NaCl).

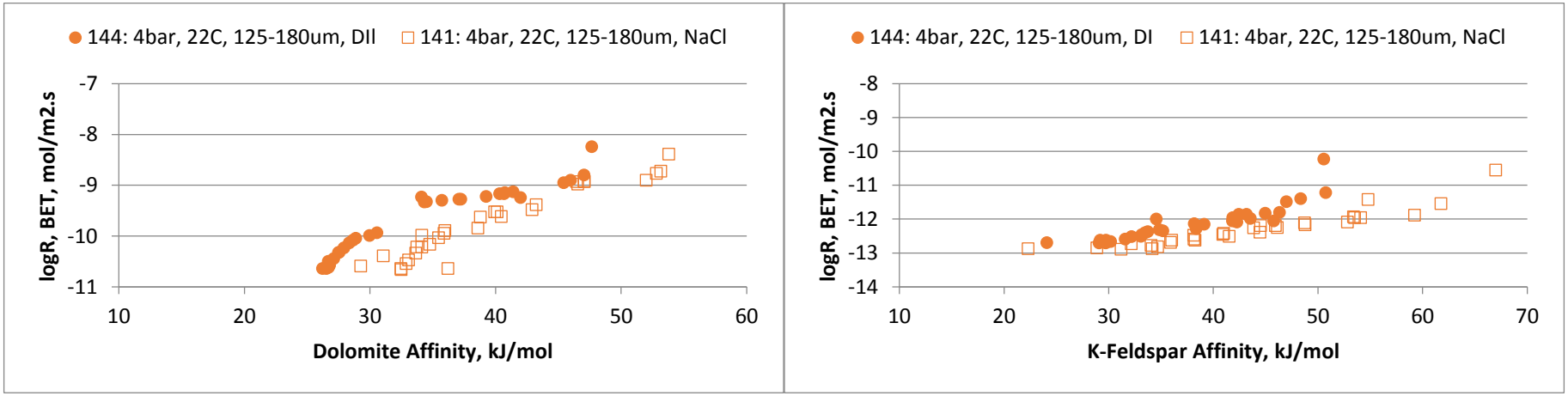


**Figures 5.1.28 – 5.1.29**: Calculated dolomite and K-feldspar dissolution rates for experiments 144 (DI) and 141 (NaCl).

### 5.1.4 Dissolution Behaviour: Effects of $pCO_2$ and Temperature

Figures 5.1.30 – 5.1.49 compare dissolved analyte concentrations from experiment 141 (4bar $pCO_2$, 22°C, 1.36M NaCl) with 147 (31bar $pCO_2$, 70°C, 1.36M NaCl), 144 (4bar $pCO_2$, 22°C, deionised water) with 148 (31bar $pCO_2$, 70°C, deionised water), 141 (4bar $pCO_2$, 22°C, 1.36M NaCl) with 149 (4bar $pCO_2$, 70°C, 1.36M NaCl) and 149 (4bar $pCO_2$, 70°C, 1.36M NaCl) with 147 (31bar $pCO_2$, 70°C, 1.36M NaCl). Figures 5.1.50 – 5.1.57 compare calculated dolomite and K-feldspar dissolution rates for the experiments.

In the comparisons between 141 and 147 and between144 and 148 Ca and Mg release is faster in the high temperature and pressure experiments. Indicative of increased dolomite dissolution at these conditions, although these concentrations tend to similar values at later times, indicating that overall dolomite solubility is relatively similar at the two sets of conditions. Considerable scatter in the Al and Si data from these experiments makes a comparison difficult, but comparison of calculated rates indicate that K-feldspar dissolution is broadly similar at both sets of conditions.

Comparison between experiments 141 and 149 shows little difference in analysed concentrations despite the elevated temperature in experiment 149. Final Ca and Mg concentrations are slightly depressed in experiment 149 relative to 141 possibly due to the retrograde solubility of dolomite with increasing temperature. Calculated dolomite dissolution rates are, at late times (low affinities) notably higher under the elevated pressure/temperature conditions.

Comparison between experiments 149 and 147 show elevated Ca and Mg concentrations and release rates in 147, suggesting that the similar behaviour observed in the comparisons between 141 and 147 and 144 and 148 was largely due to elevated $pCO_2$ rather than temperature. Si concentrations are similarly elevated, suggesting faster dissolution of silicate minerals under increased $pCO_2$, although dissolution rates for K-feldspar could not be calculated for both experiments from the available data.

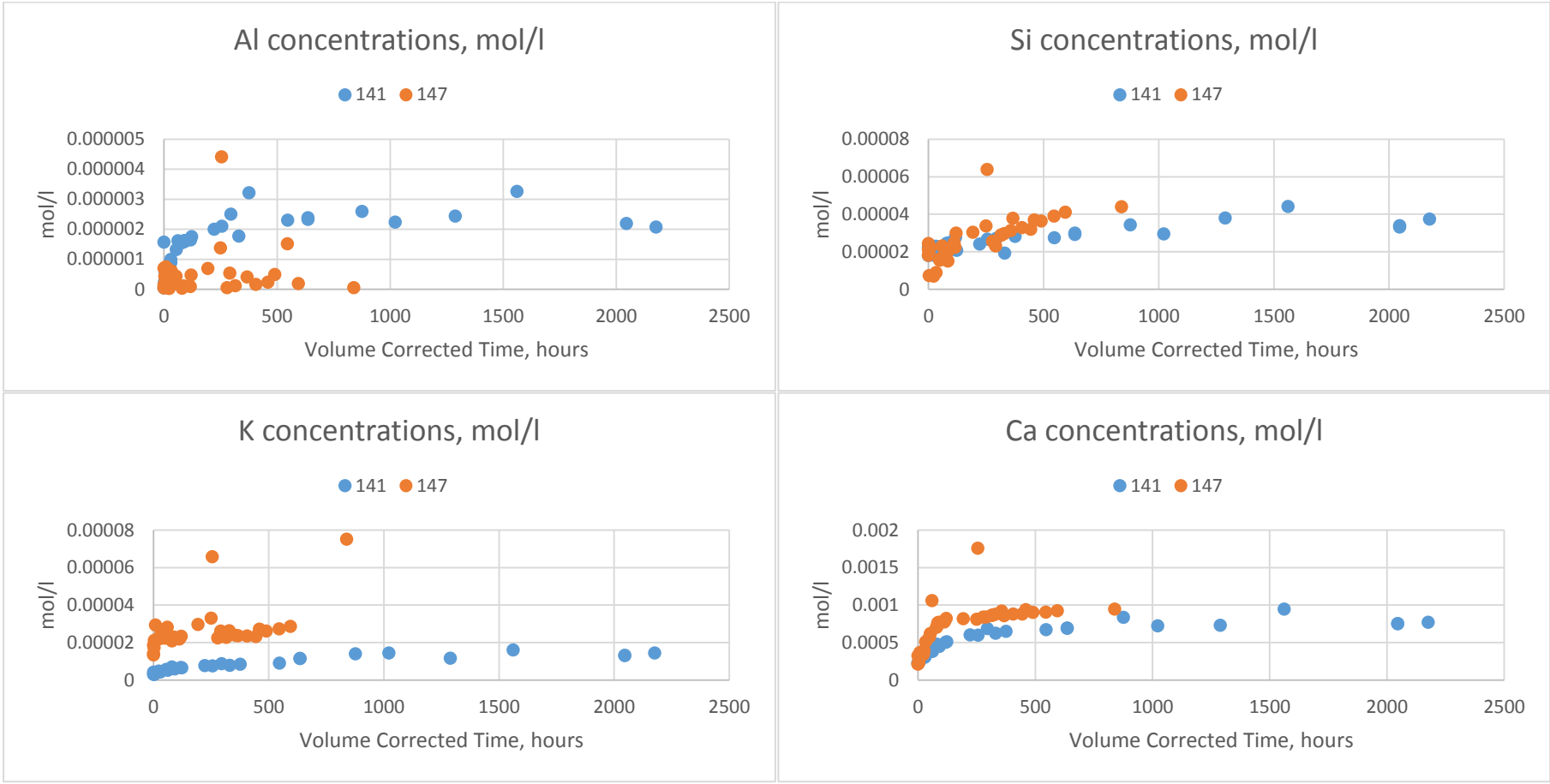


**Figures 5.1.30 – 5.1.33**: Comparative charts showing (clockwise from top left) Al, Si, Ca and K release for experiments 141 (4bar, 22°C) and 147 (31bar, 70°C)

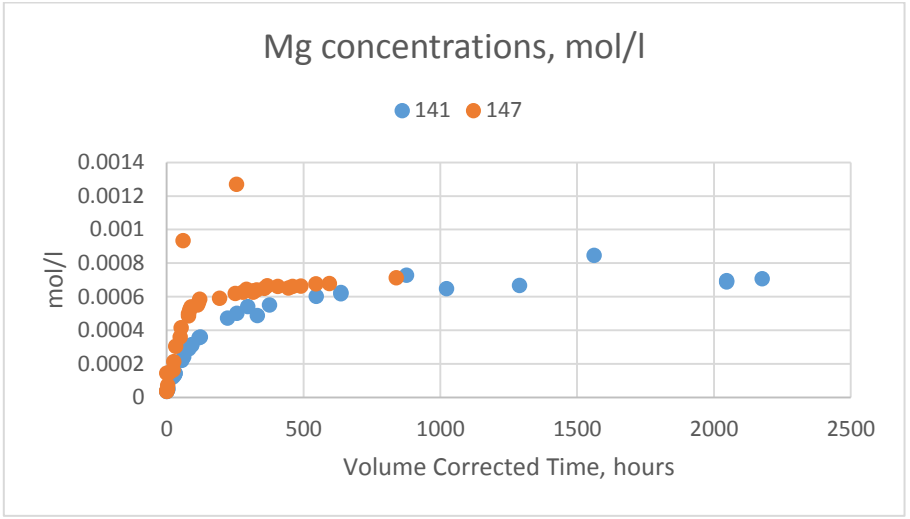


**Figure 5.1.34**: Comparative chart showing Mg release for experiments 141 (4bar, 22°C) and 147 (31bar, 70°C)

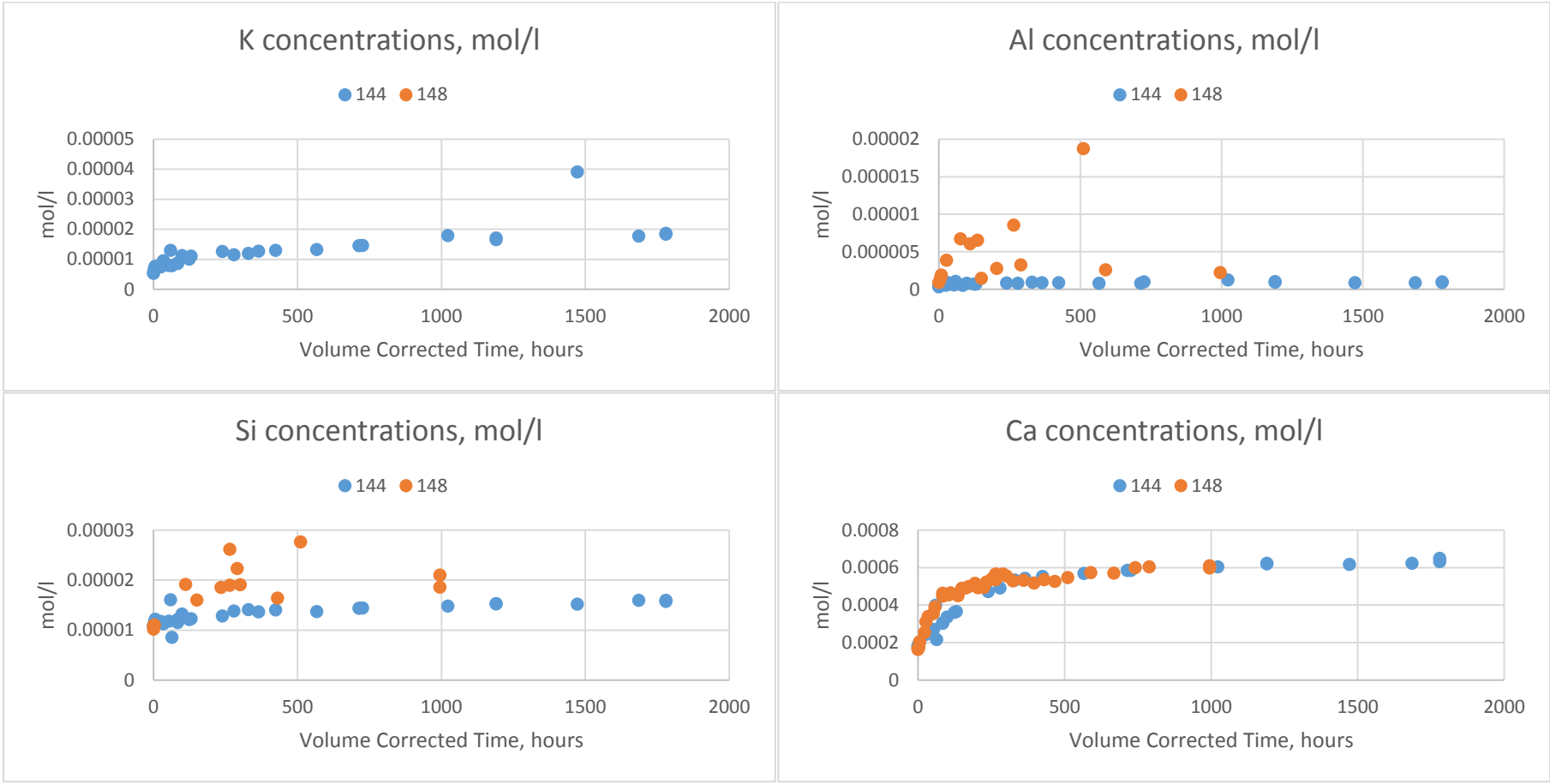


**Figures 5.1.35 – 5.1.438**: Comparative charts showing (clockwise from top left) K, Al, Ca and Si release for experiments 144 (4bar, 22°C) and 148 (31bar, 70°C)

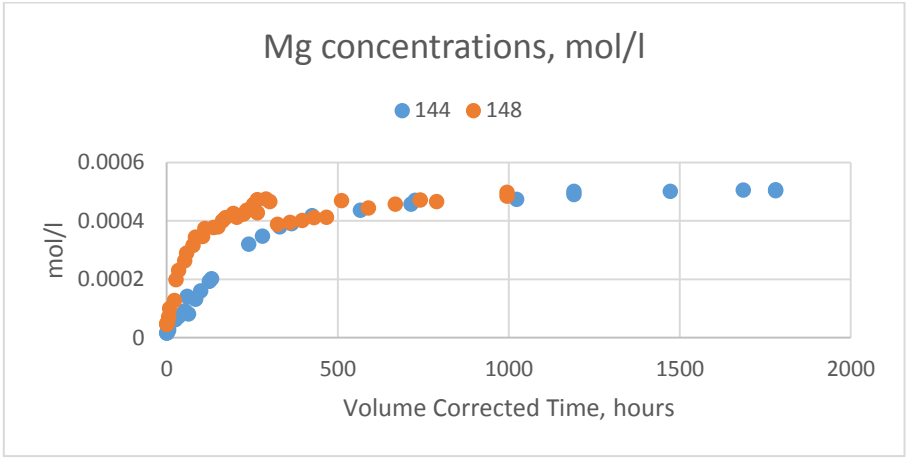


**Figure 5.1.39**: Comparative chart showing Mg release for experiments 144 (4bar, 22°C) and 148 (31bar, 70°C)

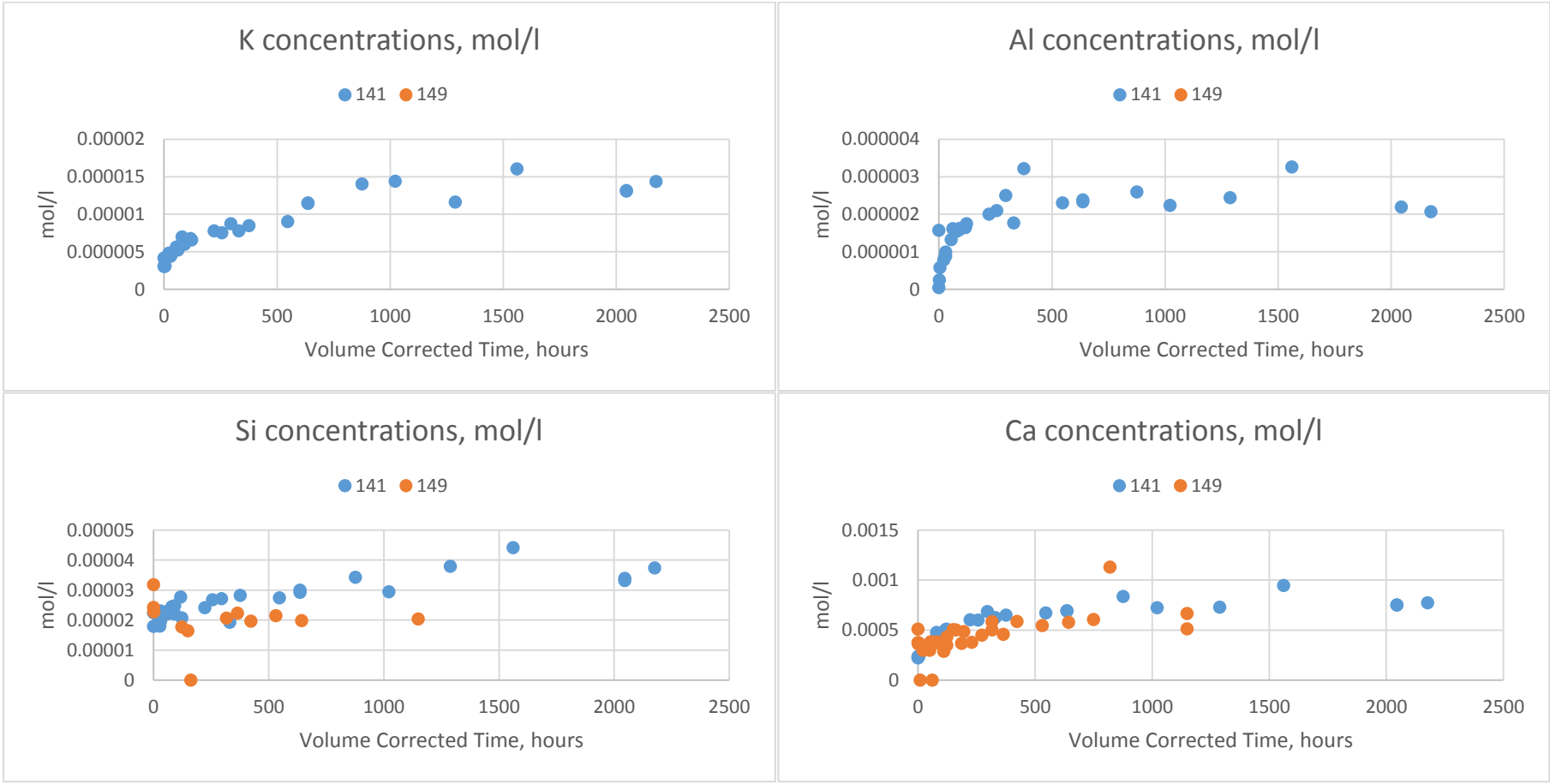


**Figures 5.1.40 – 5.1.43**: Comparative charts showing (clockwise from top left) K, Al, Ca and Si release for experiments 141 (4bar, 22°C) and 149 (4bar, 70°C)

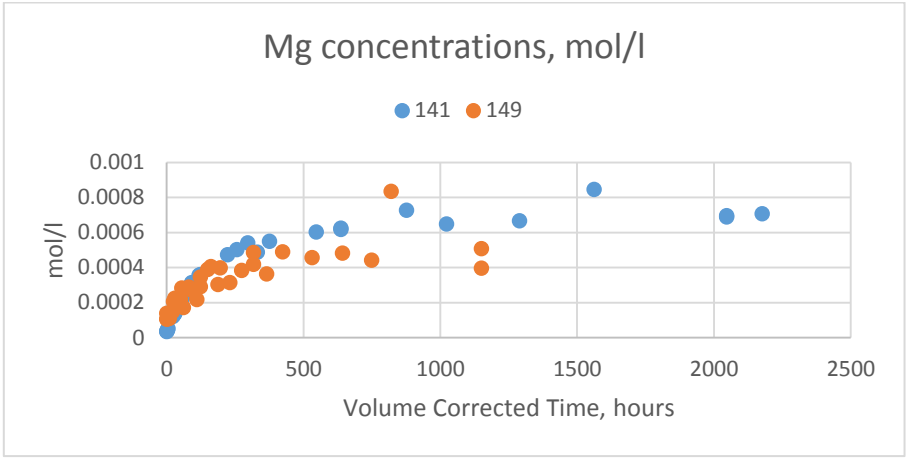


**Figure 5.1.44**: Comparative chart showing Mg release for experiments 141 (4bar, 22°C) and 149 (4bar, 70°C)

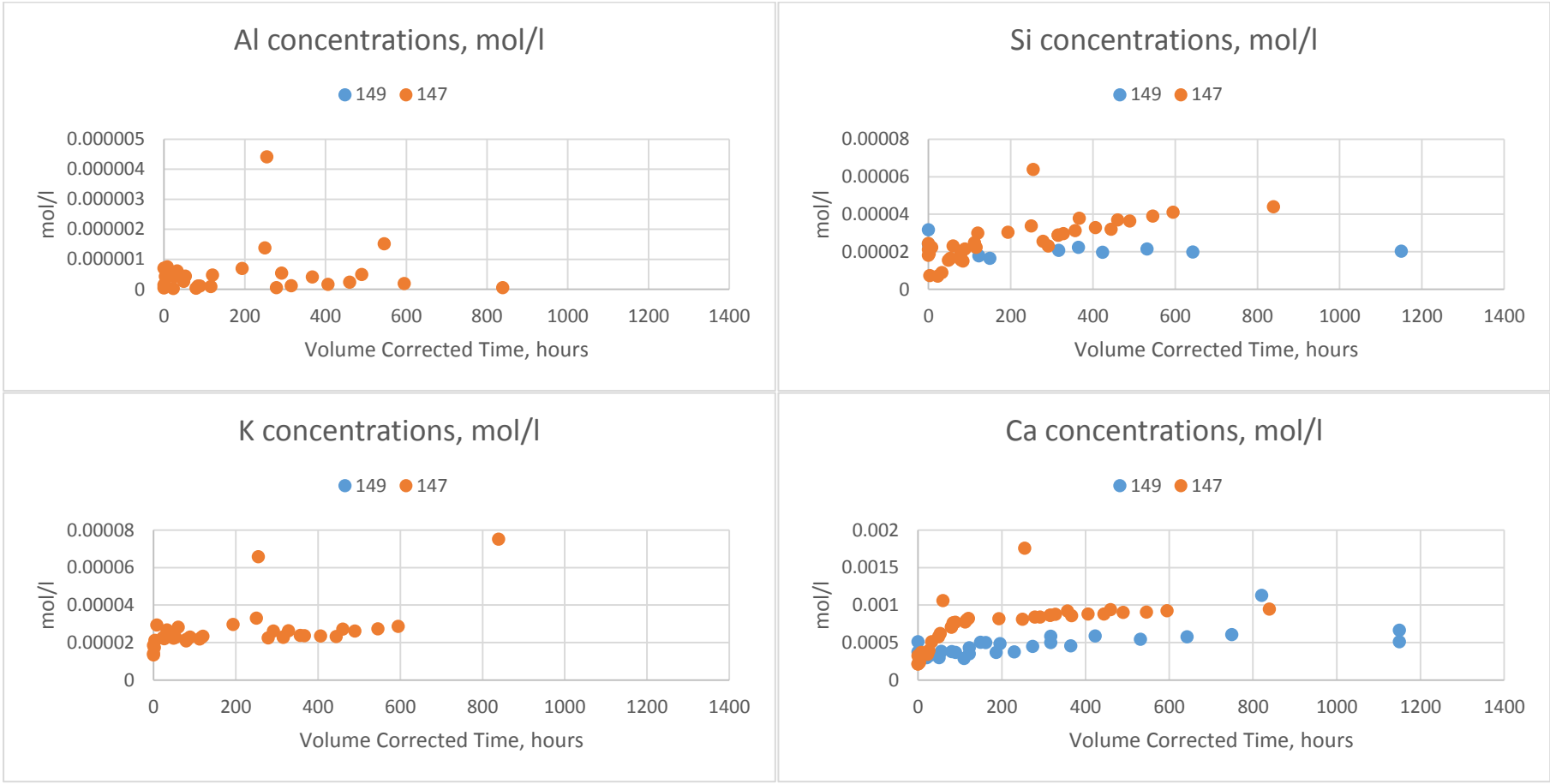


**Figures 5.1.45 – 5.1.48**: Comparative charts showing (clockwise from top left) Al, Si, Ca and K release for experiments 149 (4bar, 70°C) and 147 (31bar, 70°C)

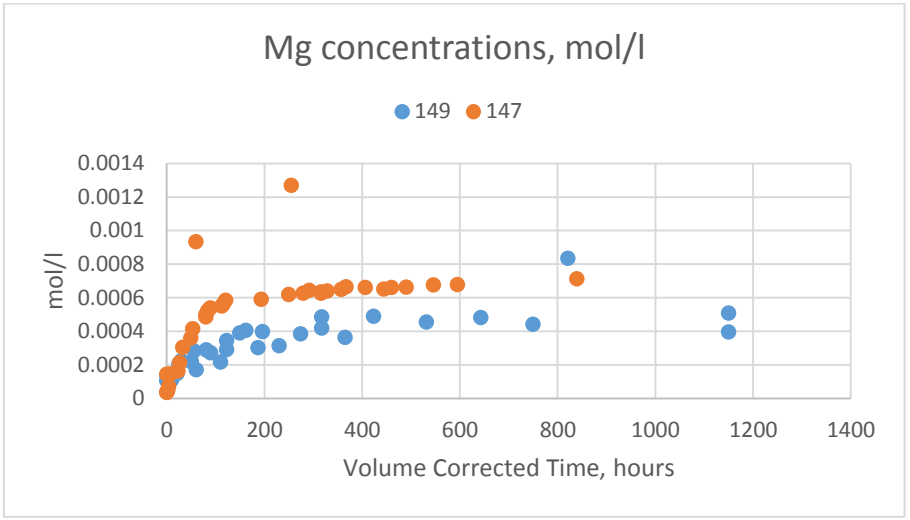


**Figure 5.1.49**: Comparative chart showing Mg release for experiments 149 (4bar, 70°C) and 147 (31bar, 70°C)

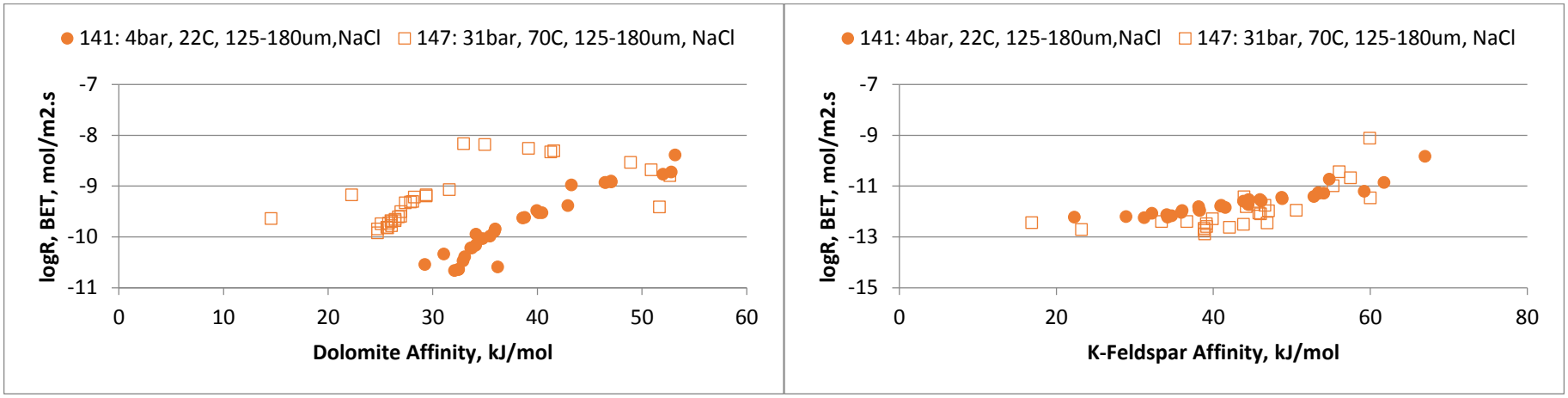


**Figures 5.1.50 – 5.1.51**: Calculated dolomite and K-feldspar dissolution rates for experiments 144 (DI) and 141 (NaCl).

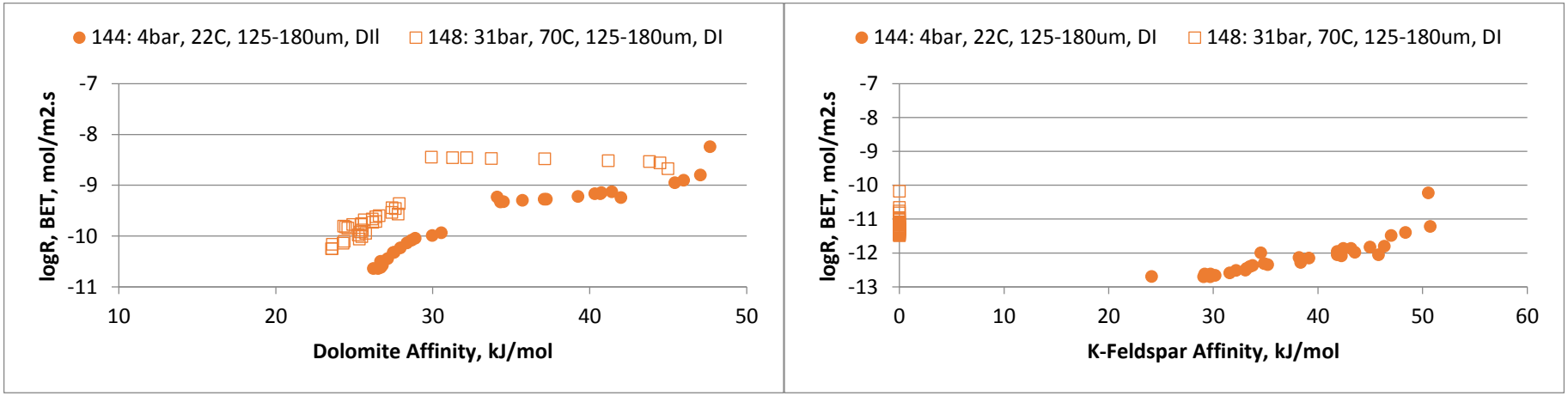


**Figures 5.1.52 – 5.1.53**: Calculated dolomite and K-feldspar dissolution rates for experiments 144 (DI) and 141 (NaCl).

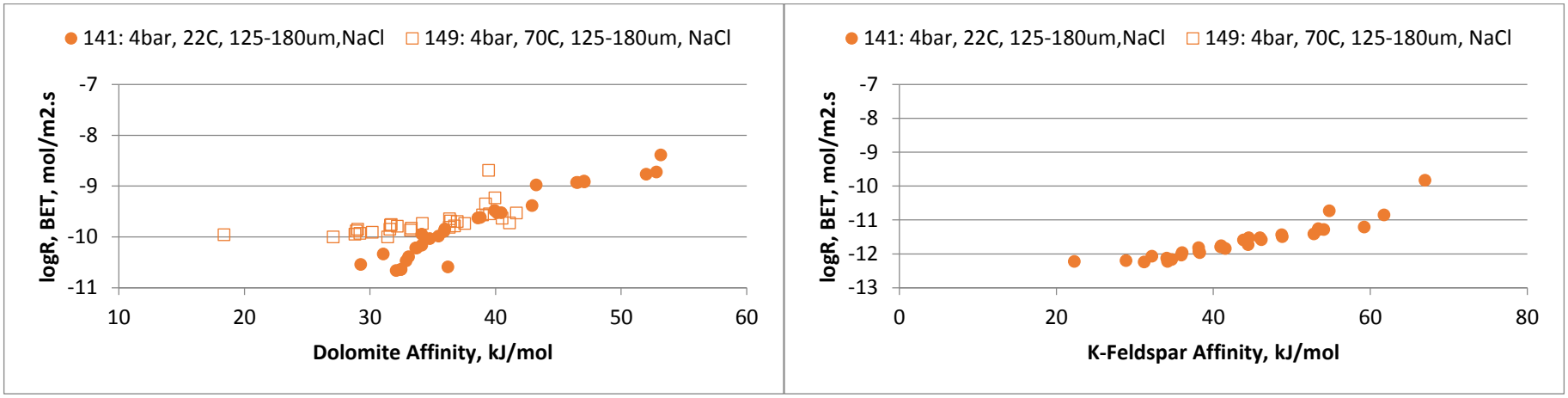


**Figures 5.1.54 – 5.1.55**: Calculated dolomite and K-feldspar dissolution rates for experiments 144 (DI) and 141 (NaCl). Rates have been calculated using Ca and Si release for dolomite and K-feldspar respectively.

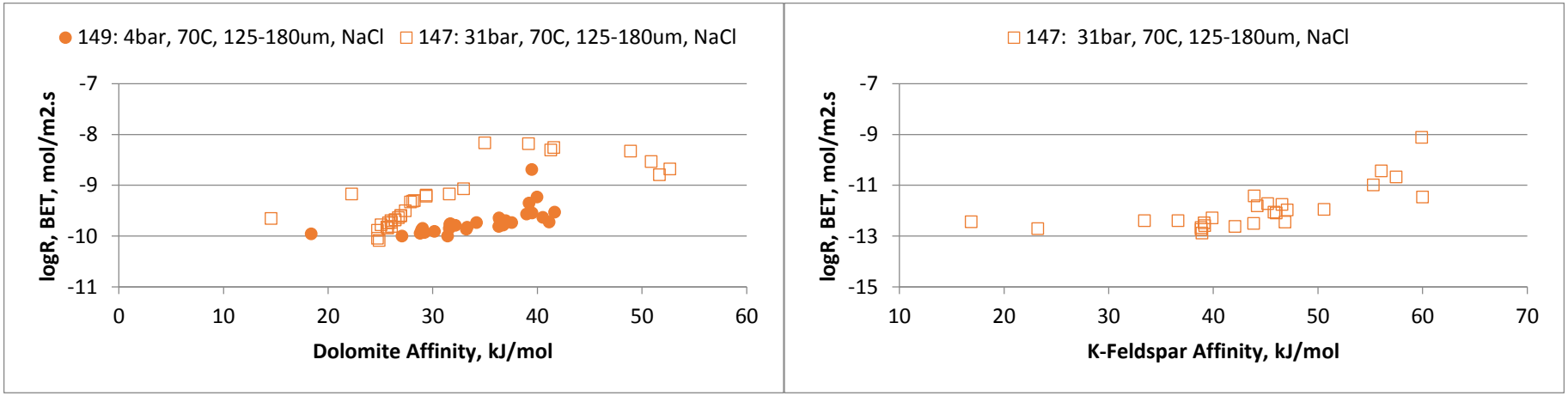


**Figures 5.1.56 – 5.1.57**: Calculated dolomite and K-feldspar dissolution rates for experiments 144 (DI) and 141 (NaCl).

### 5.1.5 Sherwood Sandstone Dissolution Rates

Figures 5.1.60 – 5.1.66 show calculated instantaneous release rates calculate for Ca, Mg, Al, Si and K for each experiment. Where an elemental release rate is not present it is due to poor quality or absence of analytical data. Elemental release rates have been calculated using measured BET surface areas.

Ca and Mg release rates generally plot closely, indicating that the main contribution of these components is from near stoichiometric dissolution of dolomite. The data for Si, K and Al are less consistent, however Si and K plot closely for the majority of experiments where these analytes are available, indicating that the dissolution of K-feldspar is the main contributor of these elements. Al release rates can be seen to be lower than K or Si release in experiments 141 and 144, though this may reflect precipitation of an Al bearing phase rather than slower release of Al from the feldspar structure. PHREEQC calculations showed that a majority of the experiments became supersaturated with respect to $Al(OH)_3$ (predominantly gibbsite) and it therefore possible that some $Al(OH)_3$ phase(s) precipitated during the experiments. However, the precipitated volumes would be very small and no precipitated $Al(OH)_3$ was detected during SEM examination of the reacted solids.

Hence, given the available data and for the purposes of calculating individual mineral dissolution rates, Ca release is assumed to reflect dolomite dissolution, and K release to reflect K-feldspar dissolution. Where K concentrations are not available, Si release has been used as an alternative.

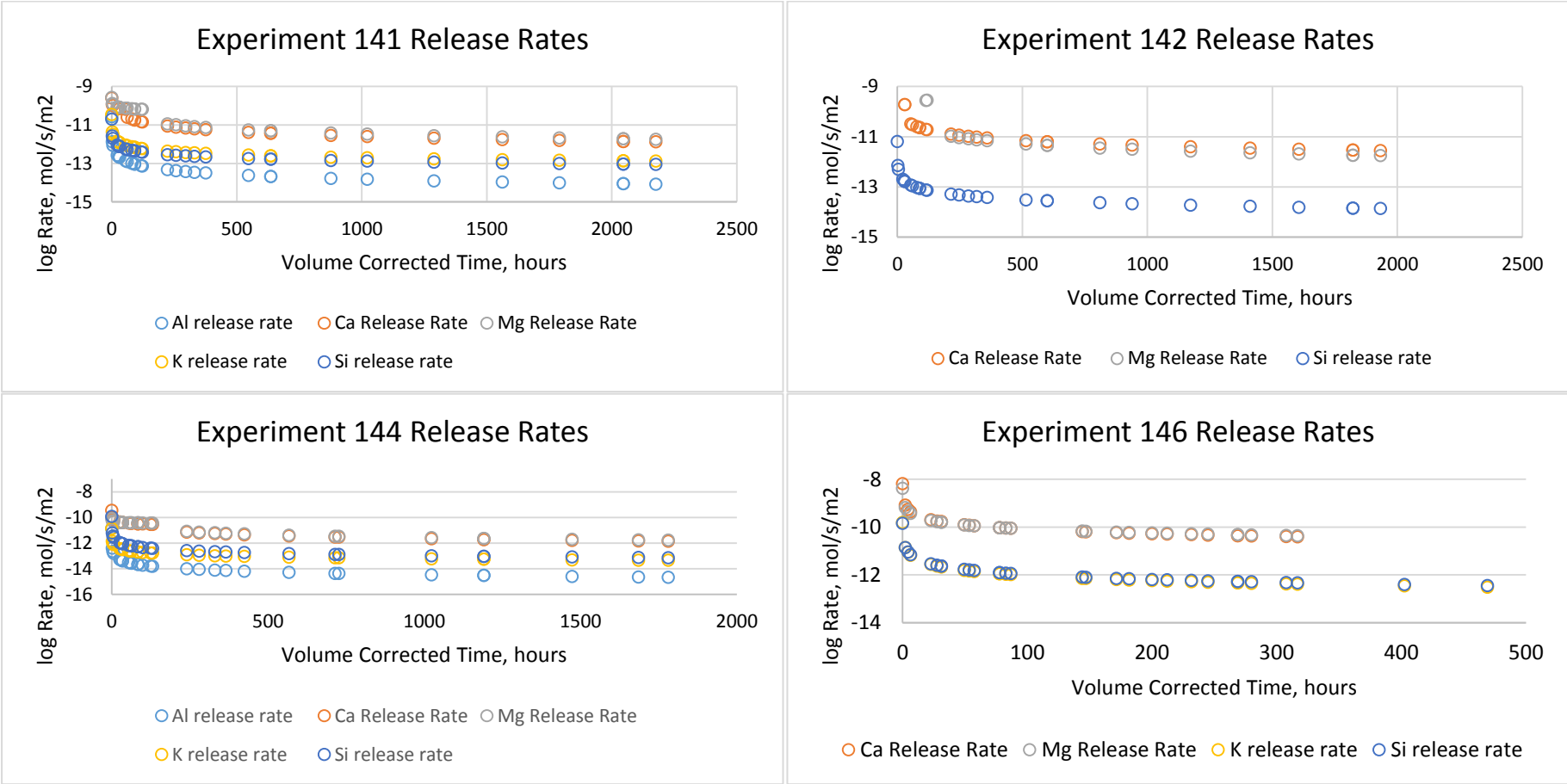


**Figures 5.1.58 – 5.1.61**: Calculated elemental release rates for experiments 141, 142, 144 and 146

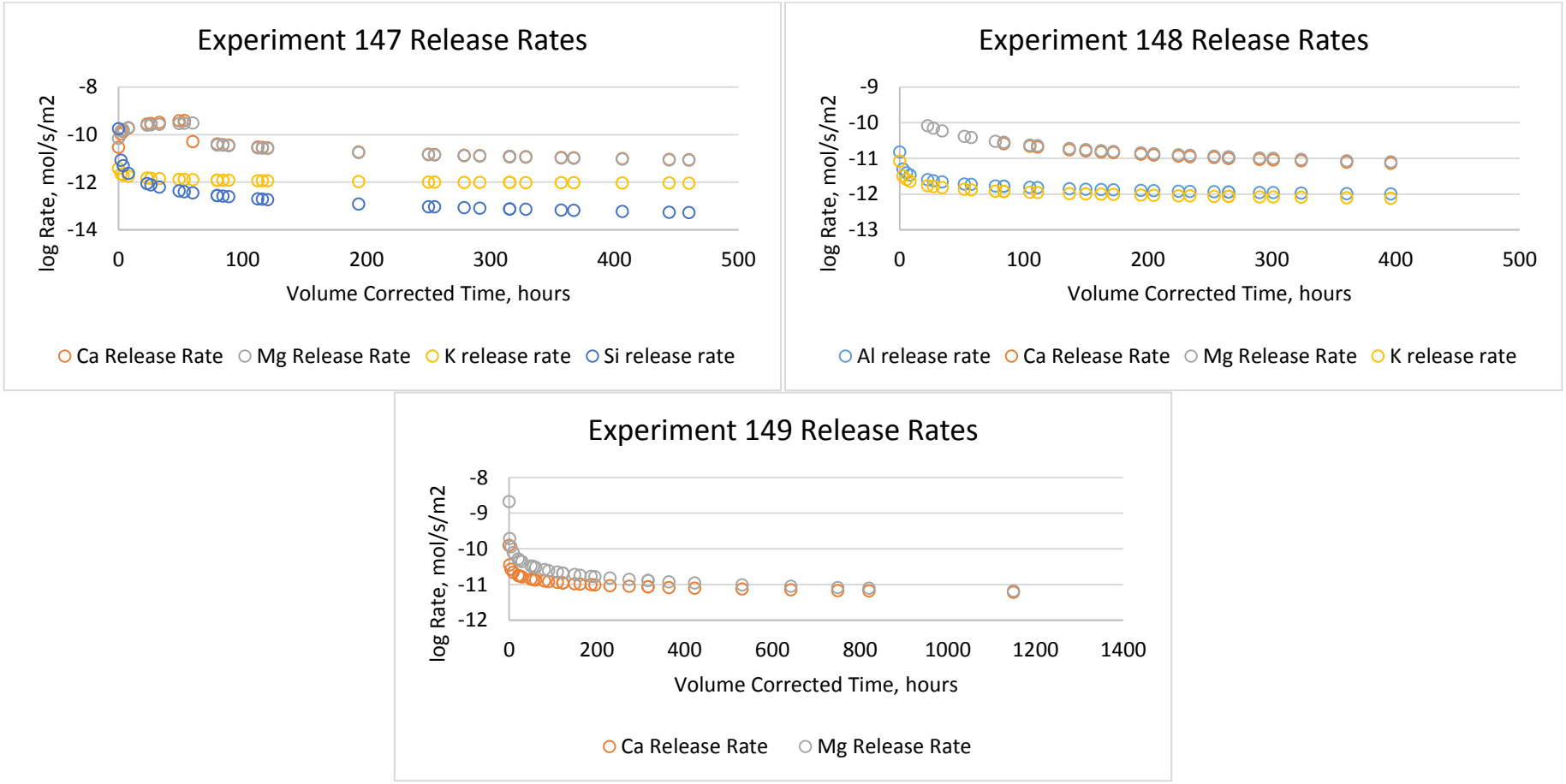


**Figures 5.1.62 – 5.1.64**: Calculated elemental release rates for experiments 147, 148 and 149

Derived rates for dolomite and K-feldspar dissolution have been plotted against chemical affinity for each experiment for which data is available in Figures 5.1.65-5.1.77. Also plotted are dolomite and K-feldspar rates extrapolated from the single mineral experiments most closely matching the experimental conditions in the sandstone experiments. A rate for K-feldspar dissolution could not be calculated from the data available for experiment 149. For experiment 148 a K-feldspar dissolution rate could be calculated, but analytical data was insufficient to calculate K-feldspar affinity. Hence, for this experiment, K-feldspar dissolution rates for the sandstone have been plotted against the Y axis, to provide at least a partial comparison with the single mineral dissolution data.

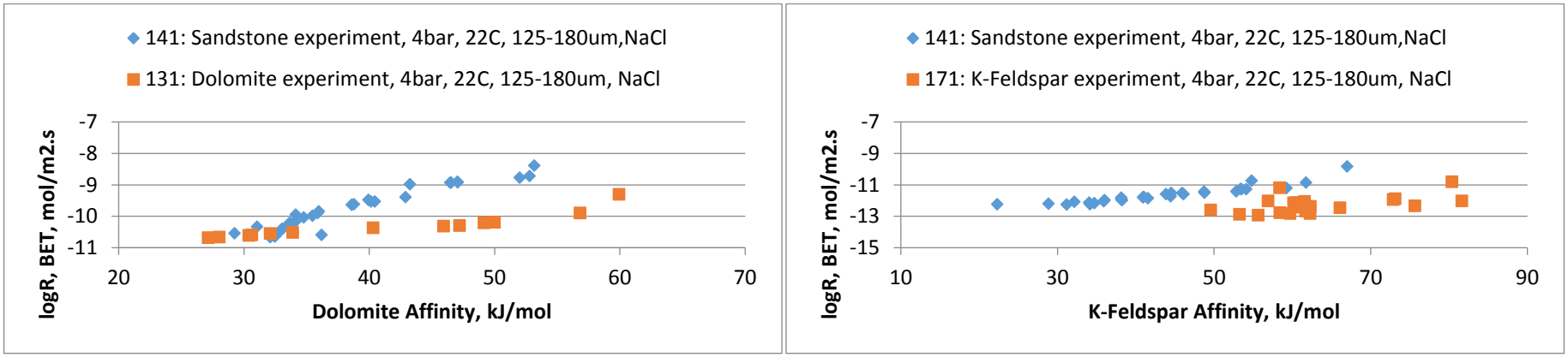


**Figures 5.1.65 – 5.1.66**: Calculated dolomite and K-feldspar dissolution rates for experiment 141. Also plotted are rates calculated for experiments 131 and 171 which were carried out at similar conditions, but using the relevant single minerals.

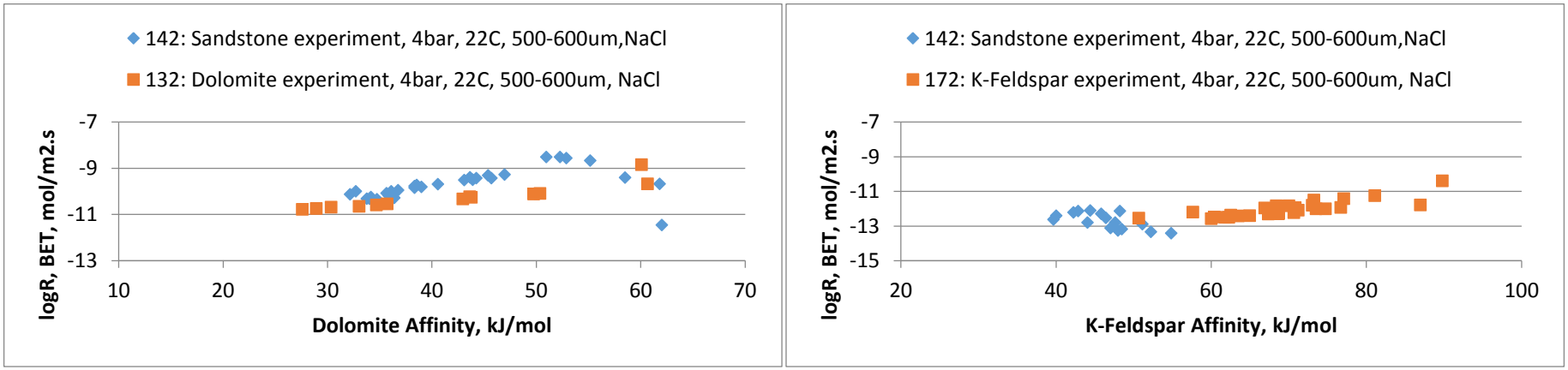


**Figures 5.1.67 – 5.1.68**: Calculated dolomite and K-feldspar dissolution rates for experiment 142. Also plotted are rates calculated for experiments 132 and 172 which were carried out at similar conditions, but using the relevant single minerals.

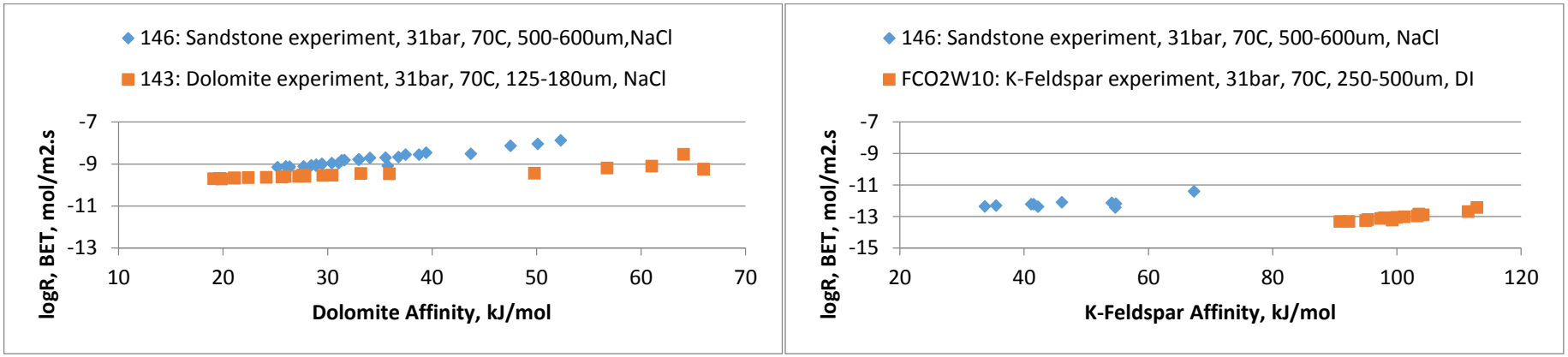


**Figures 5.1.69 – 5.1.70**: Calculated dolomite and K-feldspar dissolution rates for experiment 146. Also plotted are rates calculated for experiments 143 and FCO2W10 which were carried out at similar conditions, but using the relevant single minerals.

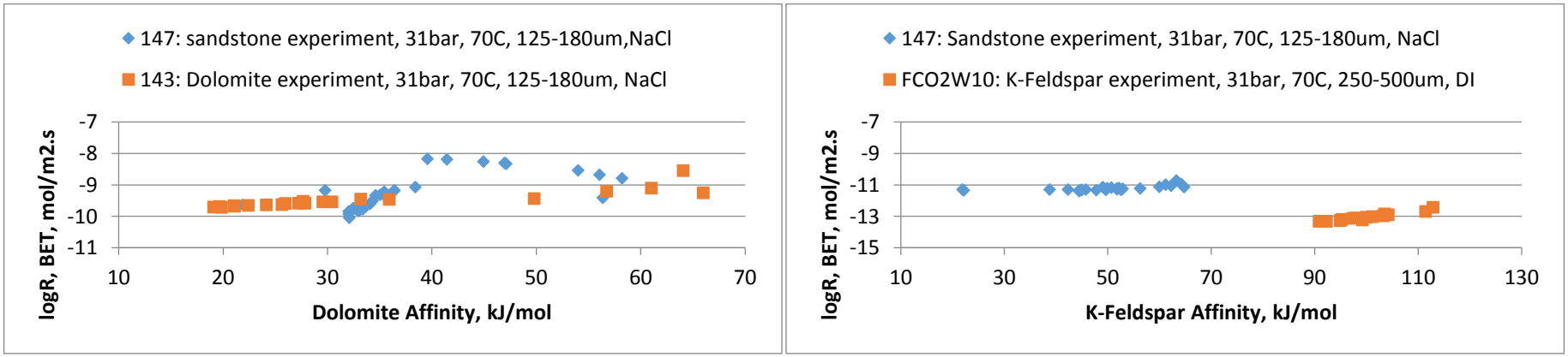


**Figures 5.1.71 – 5.1.72**: Calculated dolomite and K-feldspar dissolution rates for experiment 147. Also plotted are rates calculated for experiments 143 and FCO2W10 which were carried out at similar conditions, but using the relevant single minerals.

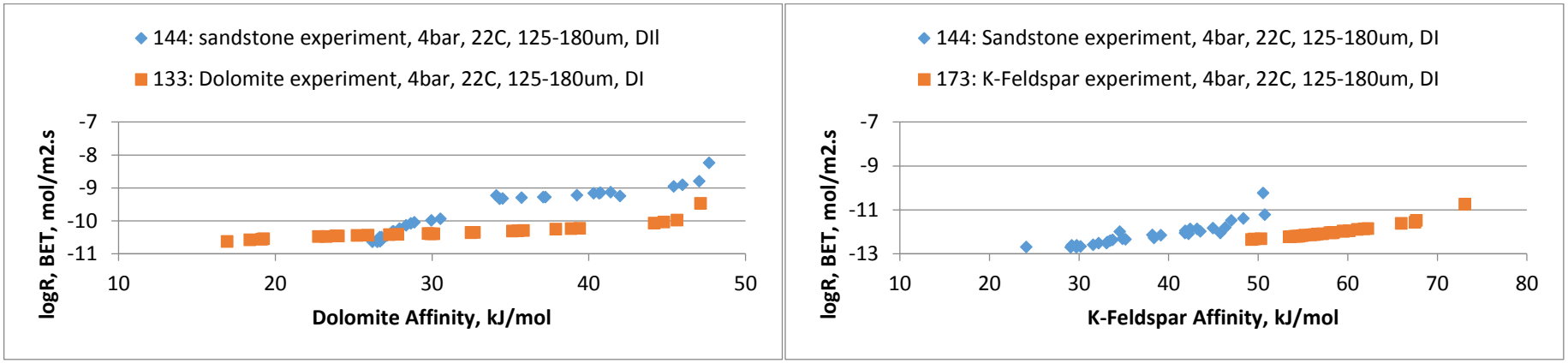


**Figures 5.1.73 – 5.1.74**: Calculated dolomite and K-feldspar dissolution rates for experiment 144. Also plotted are rates calculated for experiments 133 and 173 which were carried out at similar conditions, but using the relevant single minerals.

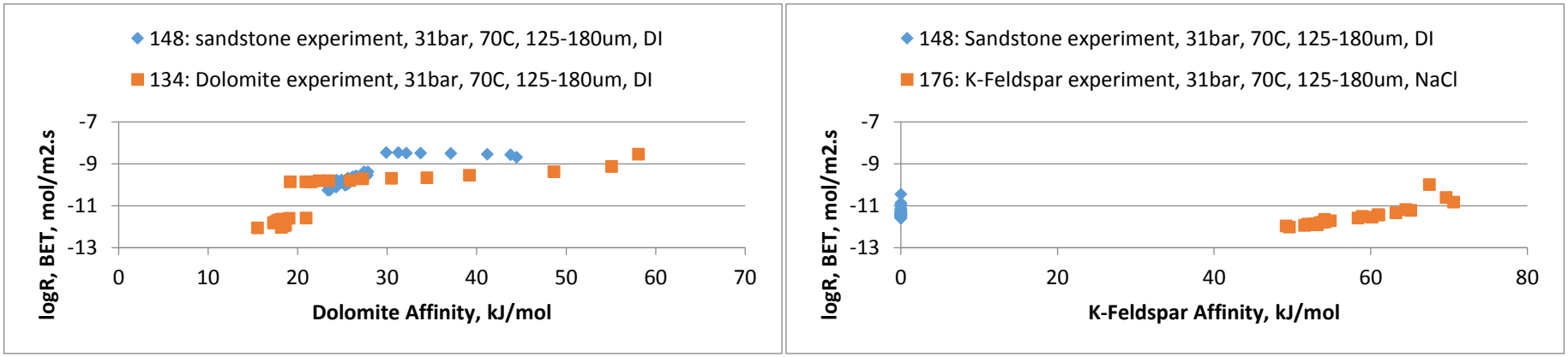


**Figures 5.1.75 – 5.1.76**: Calculated dolomite and K-feldspar dissolution rates for experiment 148. Also plotted are rates calculated for experiments 134 and 176 which were carried out at similar conditions, but using the relevant single minerals.

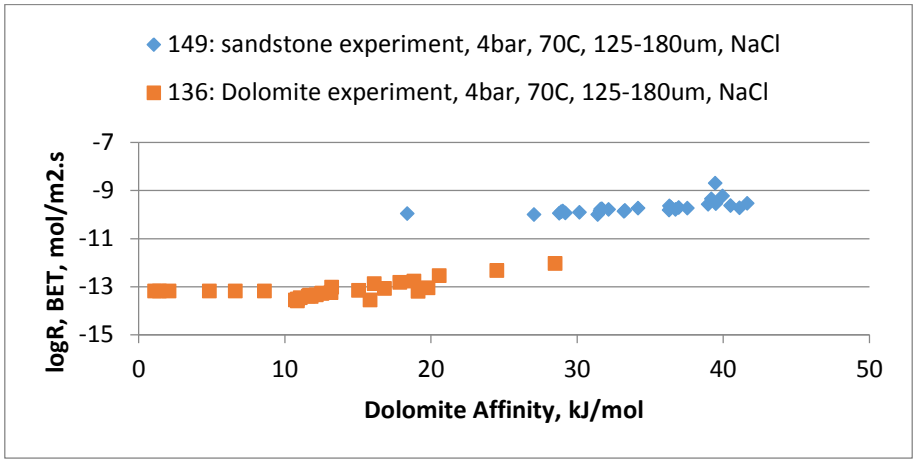


**Figure 5.1.77**: Calculated dolomite dissolution rates for experiment 149. Also plotted are rates calculated for experiment 136 which was carried out at similar conditions, but using the relevant single mineral.

K-feldspar and dolomite dissolution rates calculated from the sandstone experiments tend to agree reasonably well with those calculated from the single mineral experiments. Likewise the trends of dissolution rate variation with mineral affinity are similar in both sets of experiments. The main exception to this is with the feldspar experiment FCO2W10 which shows relatively low rates and chemical affinity relative to those calculated from the sandstone experiment 147. As discussed in section 4.1.2, the experiment FCO2W10 is believed to have been under-stirred, relative to the majority of the other batch kinetic experiments presented here and this is likely to explain this discrepancy.

The dolomite dissolution rates, while similar for the sandstone and single mineral experiments, calculated from the sandstone tend to be slightly higher and tend to have a higher chemical affinity than those calculated for the dolomite only experiments. Likewise, the K-feldspar dissolution rates calculated for the sandstone experiments tend to be slightly higher than those calculated for the single mineral batch experiments, despite the slightly lower K-feldspar affinities calculated for the sandstone experiments. The enhanced dissolution of dolomite and K-feldspar seen at early times in the sandstone experiments are likely due to surface effects: i.e. relatively high concentrations of reactive sites in the more complex sandstone material relative to the single mineral materials.

Given the complexity of bulk rock dissolution, there is no single equation or model which may be employed to predict the dissolution behaviour of the Sherwood Sandstone. However, in order to assess the applicability of the single mineral dissolution rates which are generally employed in the kinetic modelling of such systems, an attempt has been made here to build a kinetic model of Sherwood Sandstone dissolution under experimental conditions using PHREEQC. The kinetic equations used are those presented in the USGS Compilation of rate parameters, details of which and the associated constants used have been discussed in previous sections.

The model uses the bulk sandstone composition given at the start of this chapter. The starting fluids are assumed to be the “t-1” samples, taken prior to $CO_2$ injection. Dolomite, K-feldspar, albite, illite and quartz are allowed to dissolve according to their respective rate equations, with starting amounts of each mineral calculated as per the bulk sandstone composition as presented. Available surface area has been calculated purely as a percentage of the bulk sandstone surface area, i.e. where a mineral

composes 40% of bulk rock composition, it is also assumed to compose 40% of bulk rock surface area.

Initial model runs were carried out ignoring all dissolution or precipitation of phases other than those in the sandstone. Figures 5.1.78 – 5.1.81 illustrate the model output by comparing the modelled elemental release to that measured in experiment 141.

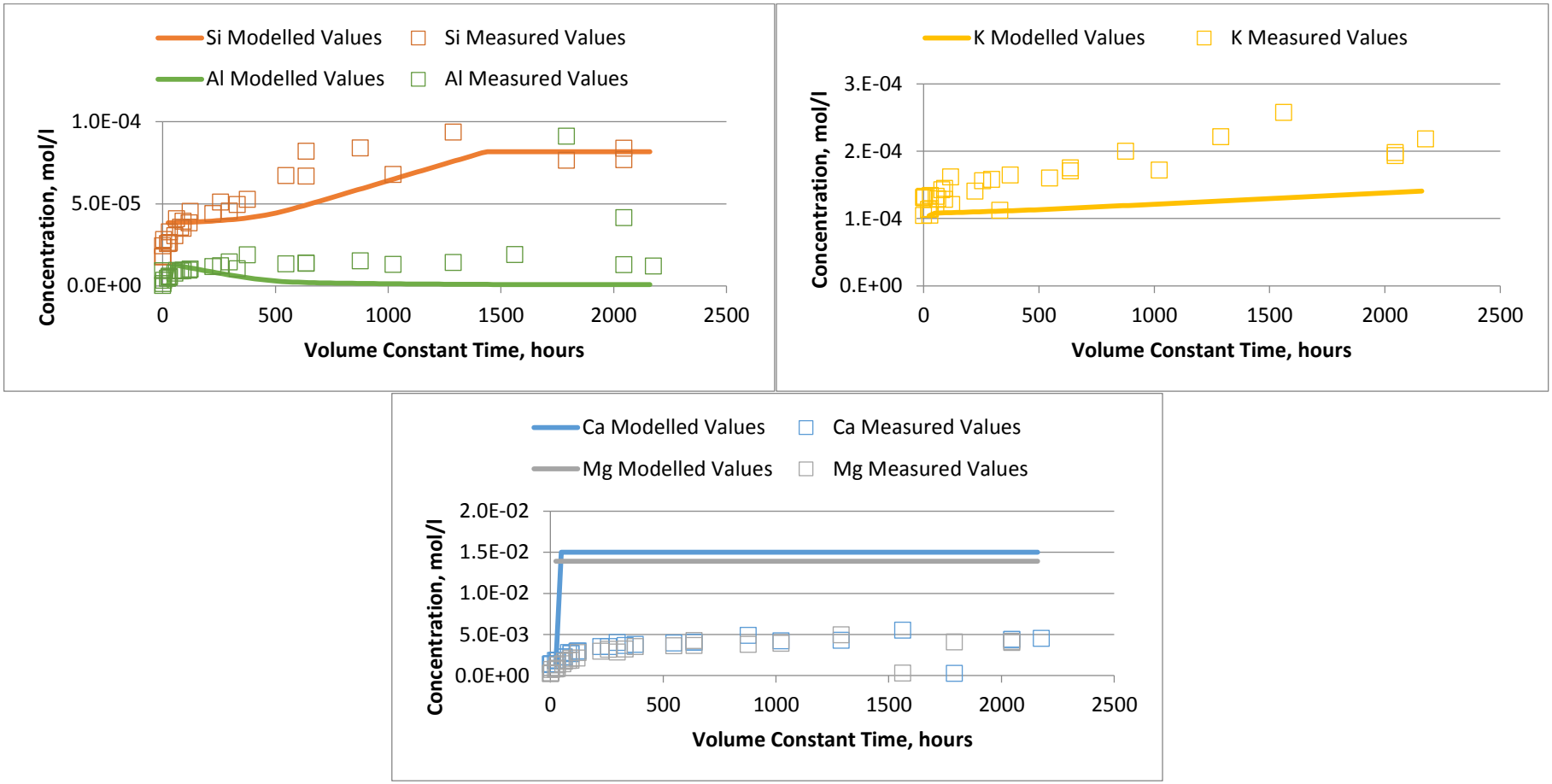


**Figures 5.1.78 – 5.1.80**: Modelled elemental concentrations plotted against measured concentrations for Experiment 141

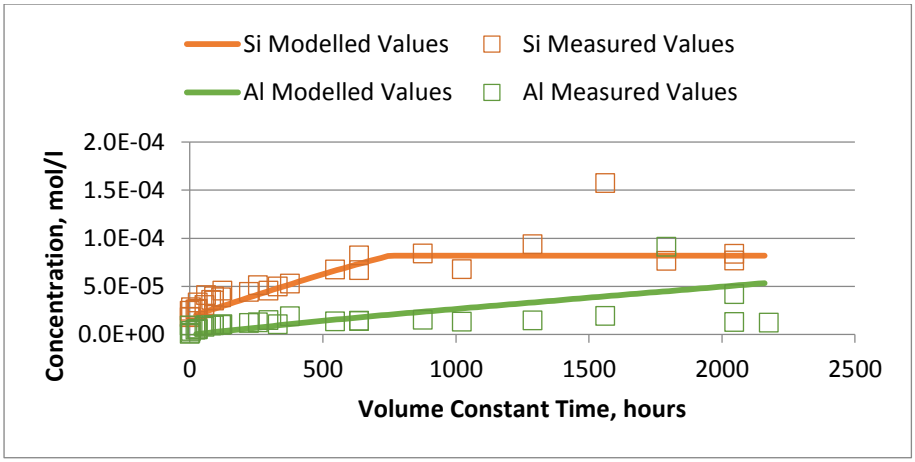


**Figure 5.1.81**: Modelled Si and Al concentrations plotted against measured concentrations for Experiment 141, with Illite removed from model composition.

With no other phases considered, Si release is modelled reasonably well, mirroring the general trend and magnitude observed in the experiment. Modelled concentrations show a general rise until quartz saturation is reached, at around 1500 hours (assuming constant volume). Modelled values of K release are likewise reasonably close to observed values, though tend to be slightly lower than those measured. The modelled aluminium values do not agree so well with those observed in the experiment. Initially the trend appears similar to that observed in the experiment, but after around 250 hours, modelled concentrations drop to very low levels. The cause of this is not clear; given that precipitation of new phases is suppressed, it may be that this is due to reprecipitation of Illite within the model, acting to remove Al from solution faster than it is being added from mineral dissolution. More striking is the disparity between modelled and observed Ca and Mg concentrations. Dolomite and illite dissolve very rapidly in the model, reaching dolomite and illite saturation within the first 24 hours of model time. Ca and Mg hence reach concentrations of around 3x those observed in the experiment in very short order.

The minerals controlling fluid composition within the model are largely K-feldspar and dolomite, removal of albite and quartz have very little effect on model output. Removal of illite from the model leads to a much better fit for observed Si concentrations (Figure 5.1.81) and increases Al concentrations such that they are overestimated by the model. Addition of the various equilibrium phases mentioned above make little to no difference to any

predicted concentrations except for Al, concentrations of which become suppressed to very low levels due to precipitation of various Al phases, primarily dawsonite.

Plots of models for each sandstone experiment can be found in Appendix B, however the broad conclusions are the same for all batch experiments: the model based on the USGS rate equations generally provide a good fit for Si and K concentrations, provided Illite is not included as a dissolving phase. Ca and Mg concentrations and rates of release are consistently overestimated by the model however, whereas Al concentrations are underestimated due to precipitation of various Al-bearing phases in the model.

### 5.1.6 Sherwood Sandstone Batch Experiments: Overview and Discussion

The sandstone batch experiments, from which selected results have been presented in the preceding sections, were carried out in order to:

- Observe the dissolution behaviour of the Sherwood Sandstone under $pCO_2$;
- To assess whether modelling using a bulk composition would adequately predict the fluid chemistry produced;
- To assess whether dissolution rates and behaviours derived from single mineral experiments are sufficient to predict the dissolution of the bulk rock.

As with the single mineral experiments detailed in preceding chapters, calculated values of $CO_2$ solubility in the sandstone experiments agree reasonably well (within 15%) with both predicted equilibrium and final measured values of dissolved $CO_2$. The discrepancies are interpreted as due to the distance from equilibrium of the actual experimental fluids and also, likely, the simplification of the bulk sandstone composition for modelling. Modelled values of equilibrium pH on the other hand are considerably (up to 1.5 pH units) higher than those observed during the experiments. Equilibrium pH, calculated for sandstone models, is largely controlled by dolomite dissolution and as inspection of Figures 5.1.75 – 5.1.79 shows, all of the sandstone experiments remain some distance from equilibrium with respect to dolomite. In general the sandstone experiments are further from dolomite equilibrium (i.e. they have higher dolomite affinities) than the single mineral experiments, also shown in the plots. As in the single mineral experiments, it seems likely that dolomite dissolution, under these experimental conditions, is transport limited and since the experiments are subject only to relatively gentle mixing, dolomite dissolution is suppressed while still far from equilibrium (Pokrovsky et al. 2009). Were further dolomite dissolution to occur, pH would be driven upward, towards the equilibrium value for the model bulk sandstone.

As for the majority of the single mineral experiments, changes in grain size on the order of a few hundred micron appear to make little difference to the dissolution of the sandstone, particularly at higher $CO_2$ pressures and

temperatures, though at lower pressures and temperatures there is some evidence for enhanced dissolution of the feldspar components from the finer grained fraction. This is consistent with evidence from the albite and K-feldspar single mineral experiments described in previous chapters.

As for the dolomite experiments, at lower pressures and temperatures Ca and Mg release are depressed in NaCl solutions relative to deionised water and as for the quartz experiments Si concentrations are similarly enhanced. These effects, as for the single mineral experiments, are likely due to the enhanced solubility of dolomite in NaCl fluids and to similar “salting-in” effects on quartz dissolving in brines (Shmulovich et al. 2006; Newton & Manning 2000).

As would be expected, elemental release is increased under higher $pCO_2$ and temperature, with release of Ca and Mg from dolomite and Si, Al and K from the silicates all being enhanced. The increase in $pCO_2$ appears to be the more important factor in increasing dissolution in the case of the sandstone, particularly for the dolomite component, similar to the behaviour observed in the single mineral experiments and in other work (e.g. O. S. Pokrovsky et al., 2009).

The analytical evidence suggests that K-feldspar and dolomite dissolution are the main processes controlling evolution of the fluids during the experiments. It is not surprising that these minerals exert more control on composition than albite or quartz, given that the former appears only in small amounts in the sandstone and the latter should be unreactive relative to feldspar, however it is surprising that dissolution of illite, given its relatively high surface area and reactivity, does not exert more of a control. Possibly the estimate of illite within the bulk sandstone is too high for the experiment due to loss of Illite during preparation of the sandstone for the experiments. Previous work comparing single mineral dissolution to whole rock behaviour also noted the relative reactivity of feldspars compared to other silicates and their importance in describing whole rock dissolution (Allan et al. 2011) This will be discussed in more detail below, but it appears that dissolution of the sandstone can be adequately described through dissolution of K-feldspar and dolomite alone.

Comparison of dissolution rates calculated for these two phases from sandstone experiments with those calculated from the single mineral experiments shows largely good agreement. Perhaps surprisingly K-feldspar affinity appears more evolved (closer to equilibrium), and dissolution rates

slightly higher, in the sandstone experiments than in the single mineral experiments. This may be due to dissolution of other silicates in the sandstone: enhancing elemental concentrations or could reflect greater distance between K-feldspar grains. Additionally, the sandstone material is generally more weathered than the single mineral materials, perhaps enhancing feldspar surface area available for reaction.

As for the single mineral experiments, an attempt has been made to model the dissolution of the bulk sandstone in terms of the rate equations and constants presented in the USGS compilation of rate parameters, details of which can be found in the appropriate single mineral sections. The model fit to observed Si and K values is, perhaps surprisingly, relatively close, particularly when illite is removed from the model, providing further evidence that illite is not present in the expected quantities in the processed sandstone material, or at least is effectively unreactive. As in the single mineral experiments, the largest discrepancy between observed and predicted dissolution is for the dolomite-hosted components. Ca and Mg concentrations are consistently over-estimated by the model by up to an order of magnitude. As for the single mineral experiments, it seems likely that this discrepancy is due to transport limitations within the experiment, retarding dissolution relative to what may be expected in a “well-mixed” system. The other discrepancy is in Al concentrations. Where equilibration with other Al bearing phases is considered, Al concentrations are sometimes several orders of magnitude below, those observed. On the other hand, where precipitation of other phases is suppressed Al concentrations tend to be higher than those observed. The model will precipitate phases to maintain a saturation index of 1. It seems likely that the observed results arise when one or more Al bearing phases has become oversaturated in the sandstone experiments and as a result that phase, or a precursor, has precipitated in small amounts, lowering Al concentrations to levels below those predicted for a precipitate-free system, but not reaching the concentrations expected at equilibrium.

The results for the dissolution of Sherwood Sandstone material presented here agree well with those reported earlier for single mineral dissolution. The composition of fluids in contact with the sandstone is largely controlled by K-feldspar and dolomite dissolution, with some minor contribution from other silicate phases. Illite dissolution appears to have little effect on fluid evolution, perhaps because the majority of illite was removed from the sandstone during the cleaning of the material.. The results suggest that for

systems where transport of dissolved elements is rapid, existing surface reaction rate laws will describe, reasonably accurately, the dissolution of bulk material. However, where dissolution of an important mineral may become transport limited, as is the case for dolomite, both in the single mineral and bulk sandstone experiments, general rate laws are not sufficient to describe fluid evolution. This is especially important in the case of dolomite, given its important role in controlling pH and hence its effect on the dissolution rate of other minerals (Rochelle et al. 2004). These results are discussed in a broader (GCS) context in Section 7.2.

## 5.2 Consolidated Sandstone Experiments

In addition to the powdered batch experiments described above, two experiments on Sherwood Sandstone cores, taken from the same borehole interval, were carried out. Details on experimental set-up for these experiments have been presented in Section 3.4.

A summary of experimental conditions is presented in Table 5.2.1. One core was used in a flow-through experiment, with NaCl solution passing through it at a steady rate, while the other was flushed and saturated with brine initially, before being sealed at pressure and temperature and left to react.

| Experiment Name | Type | Fluid | Temperature, °C | $pCO_2$, bar | Experiment Duration, hours |
|---|---|---|---|---|---|
| SCORE | Flow-through | 1.36M NaCl | 70 | 31 | 580 |
| STATIC | Batch experiment (core) | 1.36M NaCl | 70 | 31 | 1100 |
| SC2 | Batch experiment (chip) | 1.36M NaCl | 70 | 31 | 2740 |

**Table 5.2.1**: Summary of consolidated sandstone experiments

Samples were taken from the outlet of the flow-through experiment at regular intervals, while only a single sample was retrieved from the “static” experiment, immediately prior to disassembly.

A further batch experiment (SC2) was carried out on a single chip of the Sandstone material. This experiment was carried out as for the powder batch experiments, replacing the powdered sandstone with an irregular 1.5g chip of the same material (Figure 5.2.1). This experiment was originally designed as a means of observing specific points on the rock surface before and after dissolution using SEM imaging. Following reaction, finding specific areas on the surface proved problematic, however the chemical analyses from the experiment still provide a useful comparison for the other two whole rock experiments presented in this section.

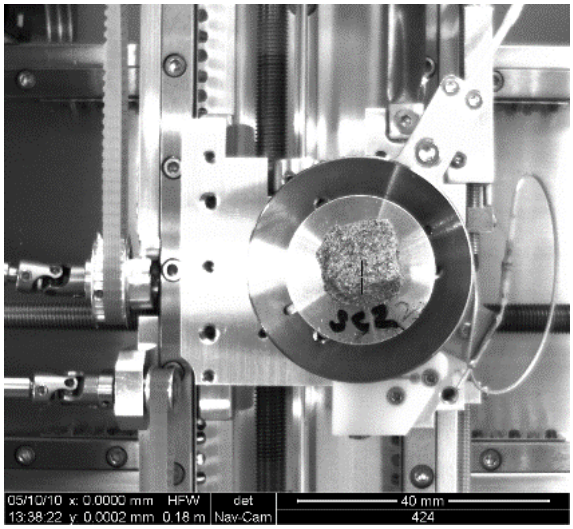


**Figure 5.2.1**: Sherwood Sandstone chip used in experiment SC2

Experiment 147, a batch experiment on powdered sandstone material, was carried out under the same conditions (1.36M NaCl, 70°C, 31bar $pCO_2$) as the other experiments presented in this section and hence results from this experiment will be used as a comparison to those obtained from the whole experiments presented here.

The flow rate used for the flow-through experiment was 0.05$cm^3$/min, with a pore volume of around 10.4$cm^3$ and assuming plug flow, a conservative estimate of the residence time of an aliquot of fluid passing through the core is 208 minutes. Both cores were flushed with several pore volumes of 1.36M NaCl, at experimental pressure, prior to heating and addition of $pCO_2$ to the inlet fluid reservoir.

Mineral surface area available for reaction within the cores is very difficult to estimate with any precision. In this case, average pore width within the consolidated sandstone material has been estimated from SEM observations. Average pore width was found to be 0.01cm. For the purposes of calculations, pores are assumed to be perfectly spherical. Based on porosity measurements made on the core these assumptions yield available surface areas of 0.55$m^2$ for the core used in the SCORE experiment, 0.55$m^2$ for the core used in the STATIC experiment and 0.01$m^2$ for the sandstone chip. Mineral surface areas where used, have been calculated based on their percentage contribution to bulk composition, as described for the sandstone batch experiments in preceding sections.

### 5.2.1 Chemical Results

Figures 5.2.2 – 5.2.5 compare analyte concentrations from the consolidated rock experiments described above and to those from the appropriate powder batch experiments. Experimental results included are from the core flow-through experiment (SCORE), the score static experiment (STATIC), a batch powder sandstone experiment carried out under the same conditions (Experiment 147), the batch experiment on a sandstone chip (SC2), a batch powder K-feldspar experiment carried out under similar conditions (Experiment 176, which used deionised water, rather than the 1.36M NaCl brine) and batch powder experiments carried out on quartz and dolomite at the same conditions as the core experiments (Experiments 124 and 143 respectively). Also included are the predicted equilibrium concentrations for the batch sandstone experiment (147) as calculated using PHREEQC3.

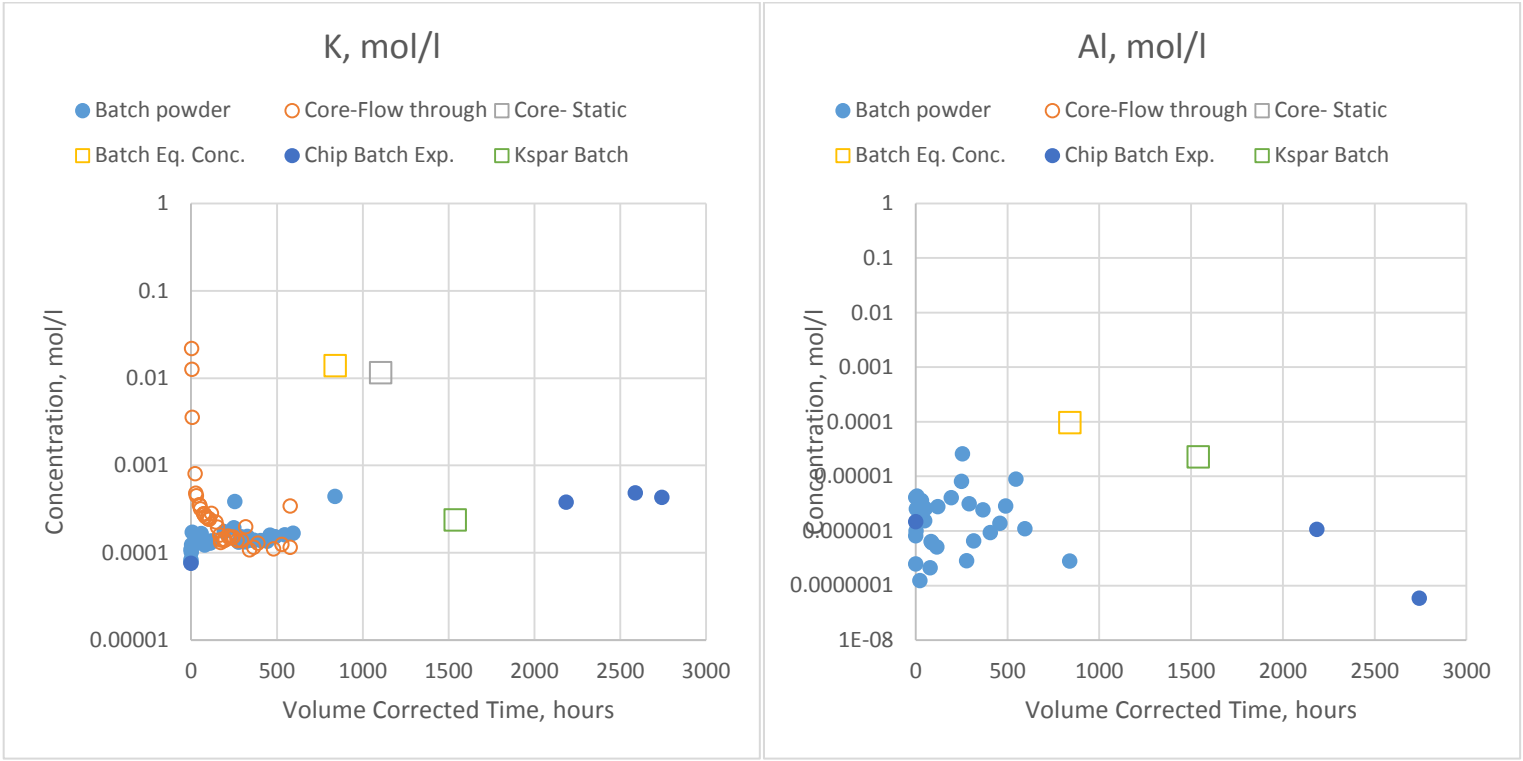


**Figures 5.2.2 – 5.2.3**: K (left) and Al (right) concentrations for samples from consolidated sandstone experiments. Also plotted are values from the powder experiment 147 and from single mineral experiments conducted at similar conditions

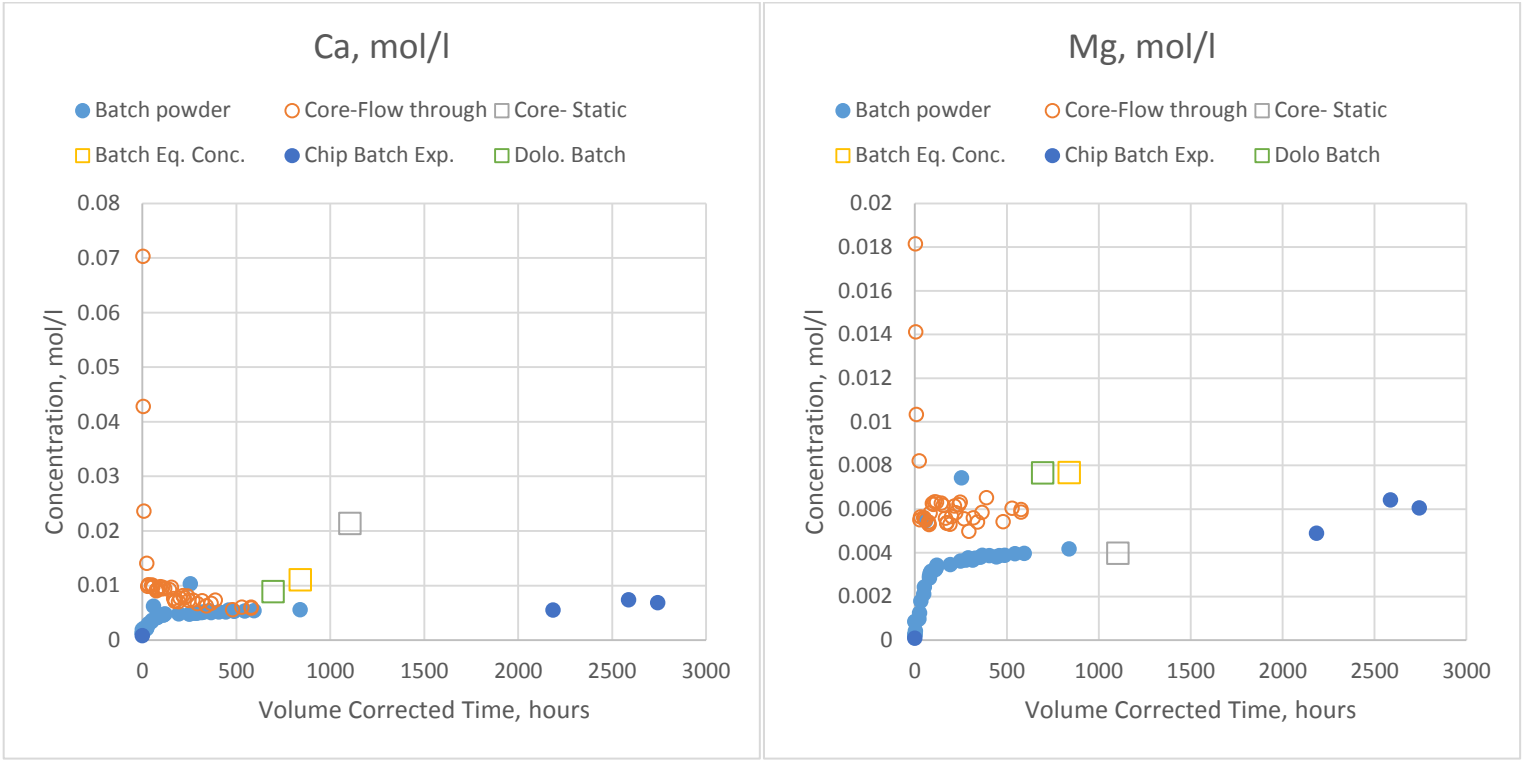


**Figures 5.2.4 – 5.2.5**: Ca (left) and Mg (right) concentrations for samples from consolidated sandstone experiments. Also plotted are values from the powder experiment 147 and from single mineral experiments conducted at similar conditions

Results from the chip batch experiment are consistent with those from the powder batch experiment. Although few samples were taken, measured concentrations from the batch chip experiment are similar to those at late times of the powder experiment, where concentrations have levelled off after the relatively rapid initial reaction phase. The STATIC experiment produced results which are often inconsistent with the other data and this may reflect sampling issues noted above.

Similarly, analyte concentrations in the effluent from the SCORE experiment tend toward those of the batch experiments at late times.

In terms of silica release, while concentrations and trend from the sandstone chip (SC2) and powder batch experiments are comparable, peaking at around quartz saturation, they are both higher than those measured from either the quartz or K-feldspar experiments at similar conditions. While the relatively low concentration observed in the quartz experiment may simply be explained by the relatively low dissolution rate of quartz compared to K-feldspar, the low Si concentration observed in the K-feldspar powder experiment suggests that the K-feldspar in the sandstone is dissolved more easily than the single mineral material. Partly this is due to fluid composition: the single mineral experiment used in the comparison is a deionised water experiment, rather than one using an NaCl brine. However the result is also consistent with the generally higher apparent K-feldspar dissolution rates calculated from the sandstone batch experiments in Section 5.1 compared to those calculated from the single mineral experiments (Section 4.1). Hence it seems likely that dissolution of other trace phases in the sandstone is enhancing the apparent dissolution rate for K-feldspar, through increased Si release, or there is a structural difference between the K-feldspar in the sandstone and that used in the single mineral experiments.

Final K concentrations on the other hand are all broadly comparable between the SCORE, sandstone powder and chip batch and K-feldspar powder batch experiments. K concentrations in all of these experiments are well below the predicted equilibrium concentration for the sandstone batch experiment. It is likely that in all experiments K concentrations were suppressed by precipitation of a K-bearing phase, such as a phyllosilicate. Relatively low Al concentrations in the powder and chip experiments are likely due to the same cause. The very high initial K concentration in the outflow from the SCORE experiment suggests an initially low pH in the pore fluid in the core, possibly an artefact of the experimental design.

Ca and Mg concentrations behave similarly for all experiments: for the batch powder and sandstone chip experiments concentrations tend toward, but remain below dolomite saturation. Concentrations from the flow-through experiment are initially well above dolomite saturation, but rapidly drop to levels similar to those observed in the batch experiments.

Results from the static core experiment are inconsistent. Si concentrations are apparently far above quartz saturation. K and Ca concentrations are considerably higher than those measured in any of the other experiments compared, while the measured Mg concentrations is very similar to those measured in the other experiments. It should be emphasised that the results from the static core experiment are based on a single sample, which was relatively difficult to obtain from the core at the end of the experiment, hence these results cannot be relied upon for accuracy.

### 5.2.2 Core Observations

Following reaction, the cores used for the SCORE and STATIC experiments were sliced and prepared for SEM analysis. Sections from both the inlet and outlet ends were taken as well as transects along the cores lengths.

Helium porosimetry and NMR pore size distribution analyses were carried out on both cores, both before and after reaction.

Sample images from the inlet and outlet ends of each core are shown in Figures 5.2.6 – 5.2.9.

The SCORE core generally shows more weathering/dissolution of mineral grains than does the core from the STATIC experiment. Also, as would be expected, the inlet end of the flow-through core, shows more evidence of dissolution than does the outlet end. Of particular note is the extensive dissolution of dolomite observed in the flow-through core, along its whole length. Very few dolomite grains have been left intact and most show the extensive dissolution illustrated in Figures 5.2.10 & 5.2.11.

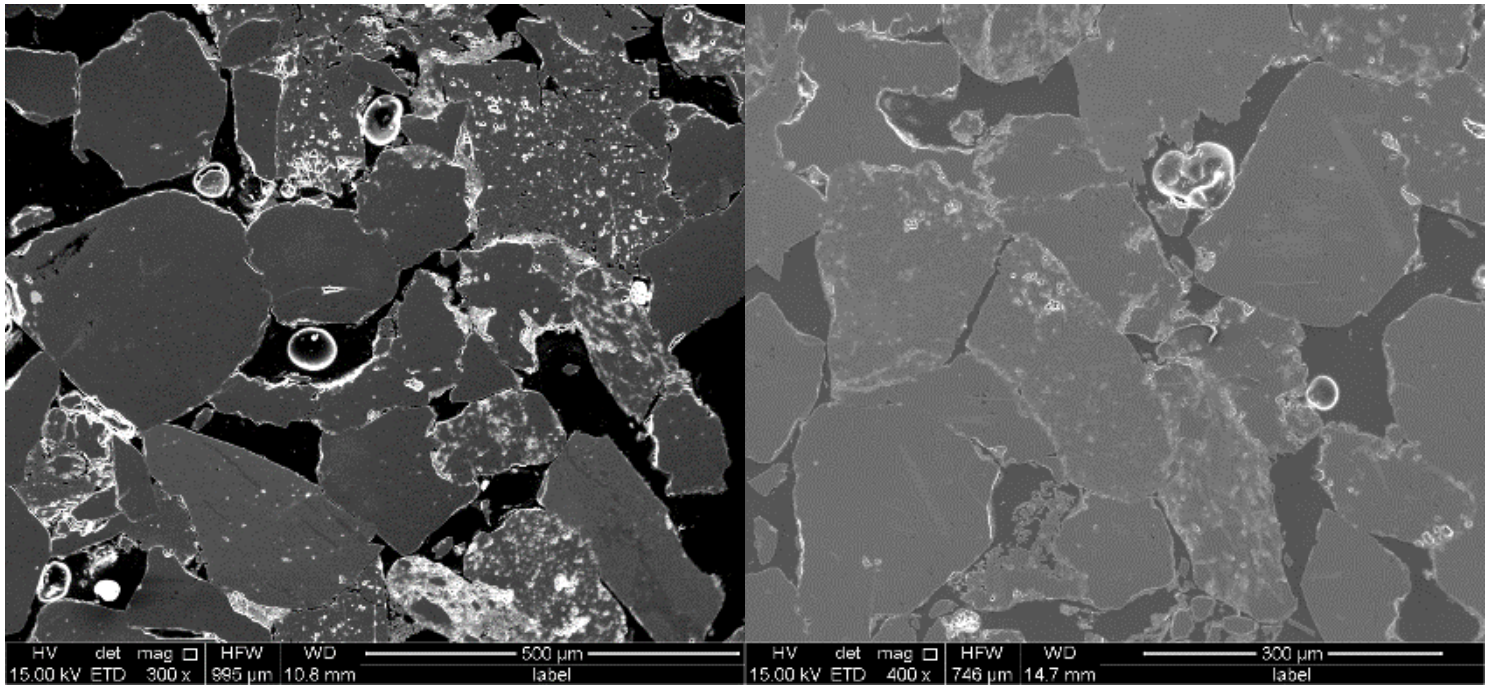


**Figure 5.2.6 & 5.2.7**: SEM images of SCORE Inlet (Left) and STATIC Inlet (Right). Observations from SCORE generally show more dissolution features (increased porosity and pitting) than those from STATIC

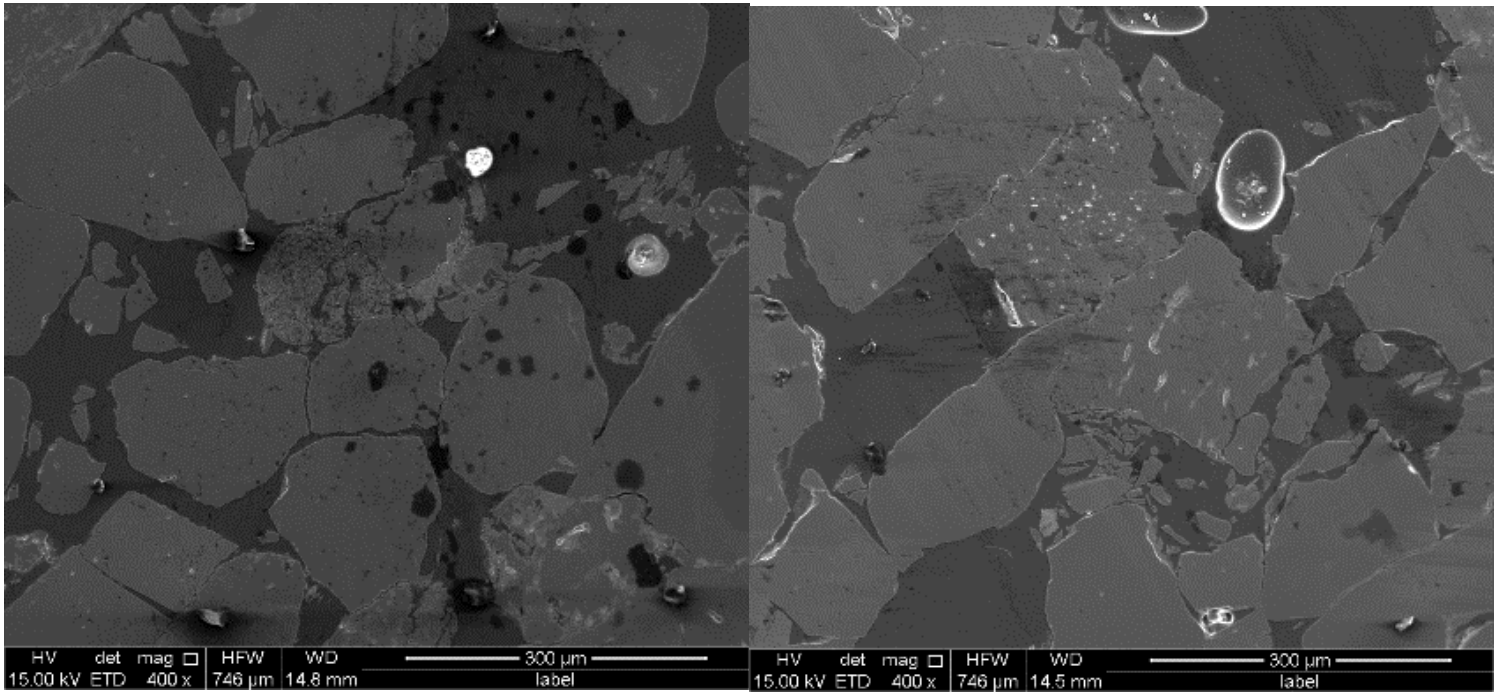


**Figures 5.2.8 & 5.2.9**: SEM images of SCORE outlet (Left) and STATIC outlet (Right). Observations from SCORE generally show more dissolution features (increased porosity and pitting) than those from STATIC

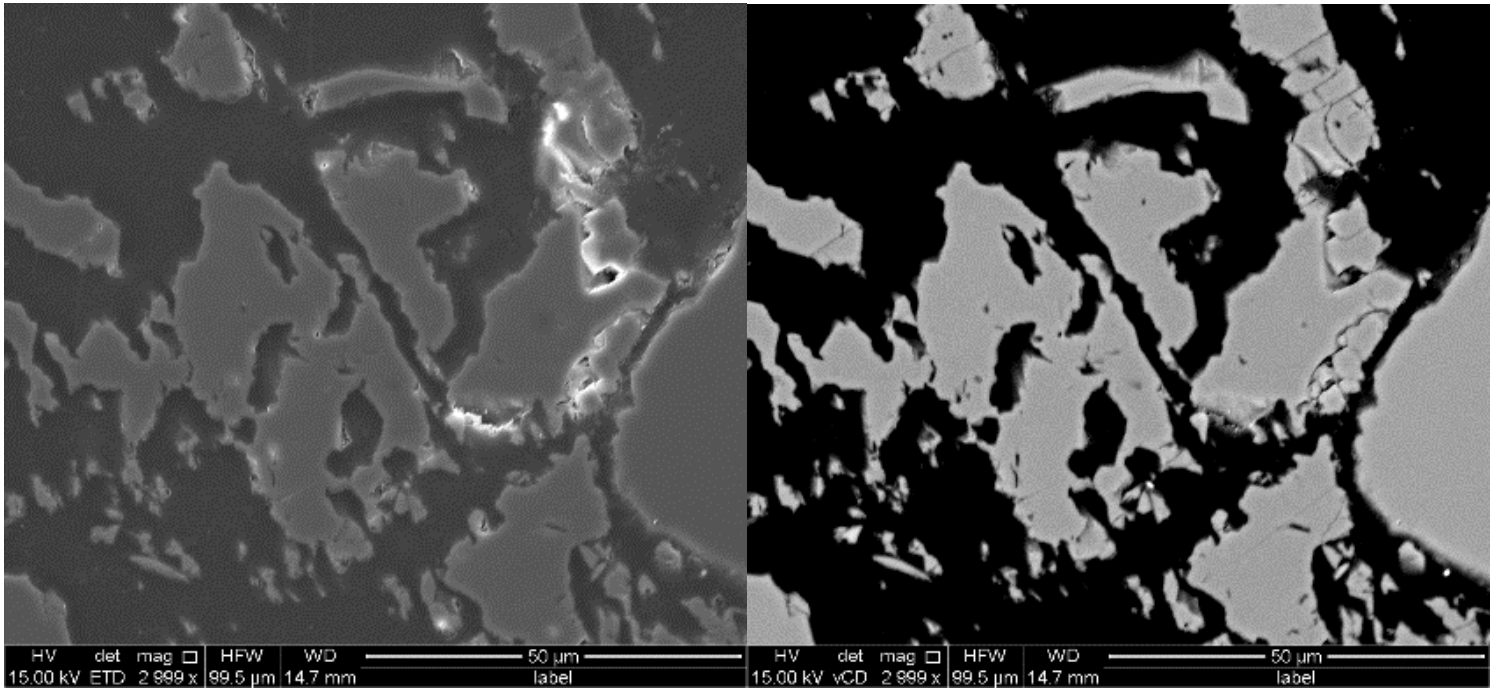


**Figures 5.2.10 & 5.2.11**: SEM images of Heavily dissolved dolomite grain from SCORE in secondary electron (left) and backscatter (right) modes

In keeping with this extreme dissolution of dolomite grains, porosity in both of the cores increased over the course of the experiments, from values of around 24% before reaction, to values of around 26% following reaction. Likewise the pore size distribution shifted considerably, shown in Figures 5.2.12 – 5.2.15. Although absolute values of pore size etc. cannot be obtained directly from this data, the x-axes on these charts may be considered to represent pore size, while the y-axes represent the number of pores. Hence pore sizes in both cases shift from the smooth distribution observed before the experiment to a more complex distribution following reaction. In this case there is a general shift in distribution towards smaller pore sizes, which is likely related to the disintegration of dolomite grains noted above. Also of note is that the shift in distribution is better developed in the SCORE experiment, which is consistent with the SEM observations, in Figures 5.2.6 – 5.2.11.

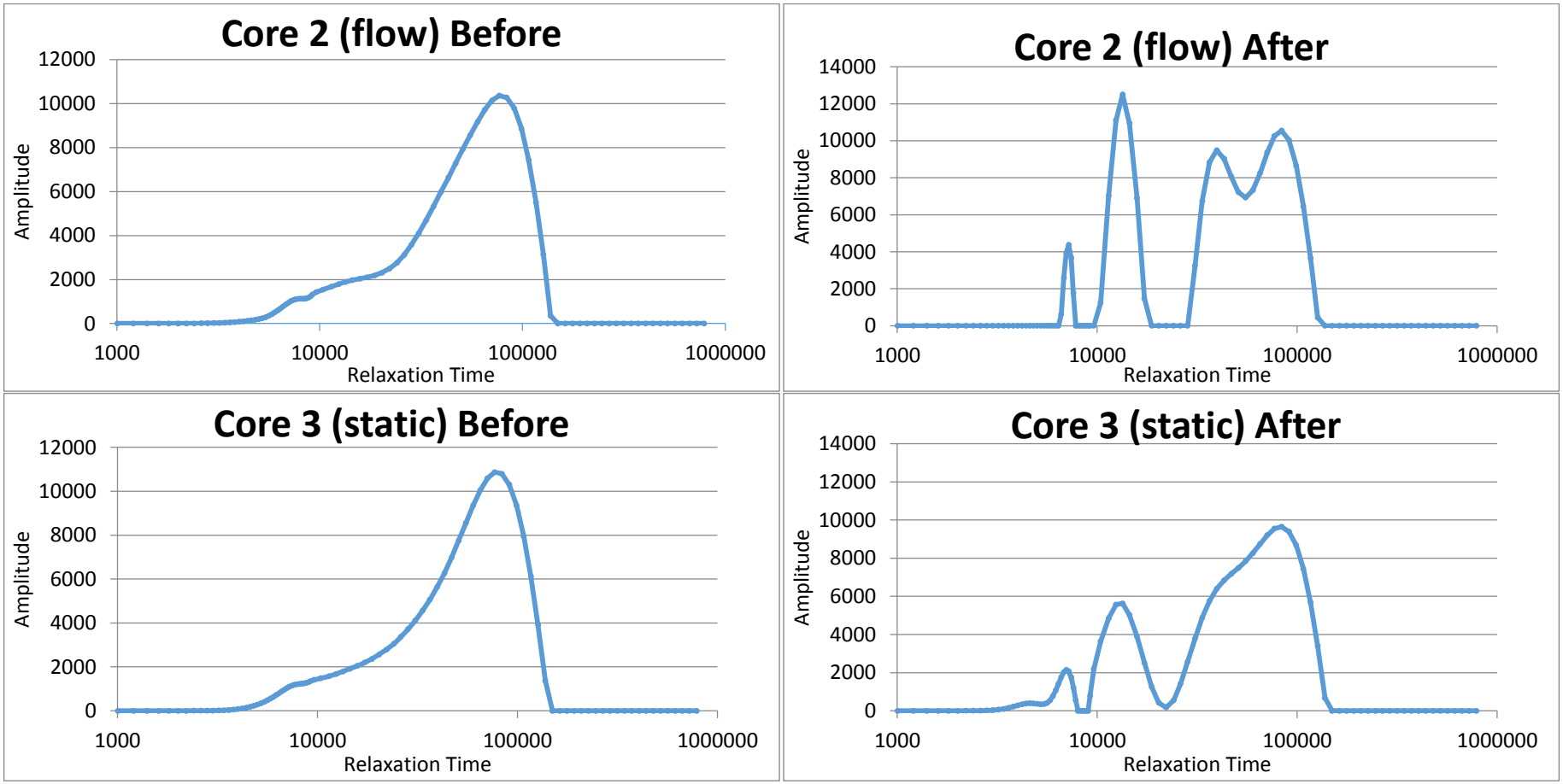


**Figures 5.2.12 - 5.2.15**: NMR measurements for both SCORE and STATIC cores, before and after reaction

### 5.2.3 Flow-through Modelling

The SCORE experiment, was modelled using PHREEQC3. Mineral dissolution kinetics were implemented as for the sandstone batch experiment modelling, discussed in Chapter 6, using equations and values presented in the USGS Compilation of Rate Parameters (USGS 2004).

Eights cells, each of length 0.05m were used to model the core and the model shifts and times steps were adjusted so as to give each parcel of fluid passing through the core a residence time of 208 minutes. Results are presented in Figures 5.2.16 – 5.2.22, along with analysed results from the flow-through experiment.

Modelled results are, at best, ambiguous, especially given the lack of good analytical data for Si or Al concentrations from the experiment. K concentrations are dramatically under-predicted. Likewise both Ca and Mg concentrations are under predicted. Partly this is due to the relatively rapid dissolution of dolomite predicted by the model; all dolomite in the core is predicted to have dissolved after only a few days of reaction time, after which Ca and Mg concentrations fall to zero. While SEM evidence shows that dolomite is heavily attacked by the flow-through fluid, it is clear both from SEM observations and the continued detection of Ca and Mg in the effluent, that dolomite persists within the core for the duration of the experiment. Additionally even when dolomite is added to the model, in such quantities that it persists for the whole of the model run, predicted concentrations at the outflow remain well below those analysed during the experiment. It seems likely that model concentrations are suppressed by precipitation of a secondary phase/phases. However these could not be identified from the model output. Certainly the model fluids remain well below dolomite, calcite and illite saturation.

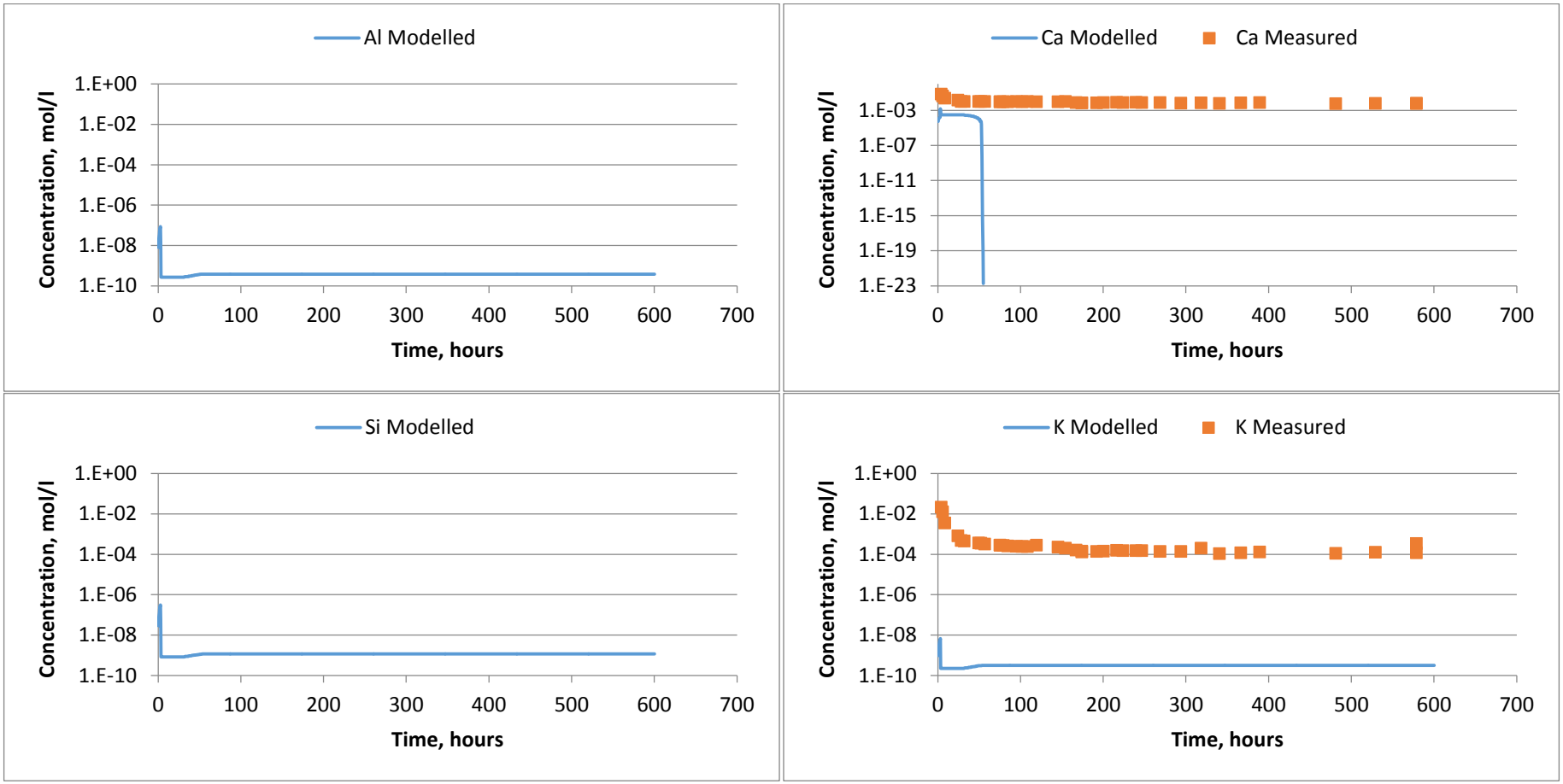


**Figures 5.2.16 - 5.2.19**: Modelled and measured elemental concentrations for SCORE

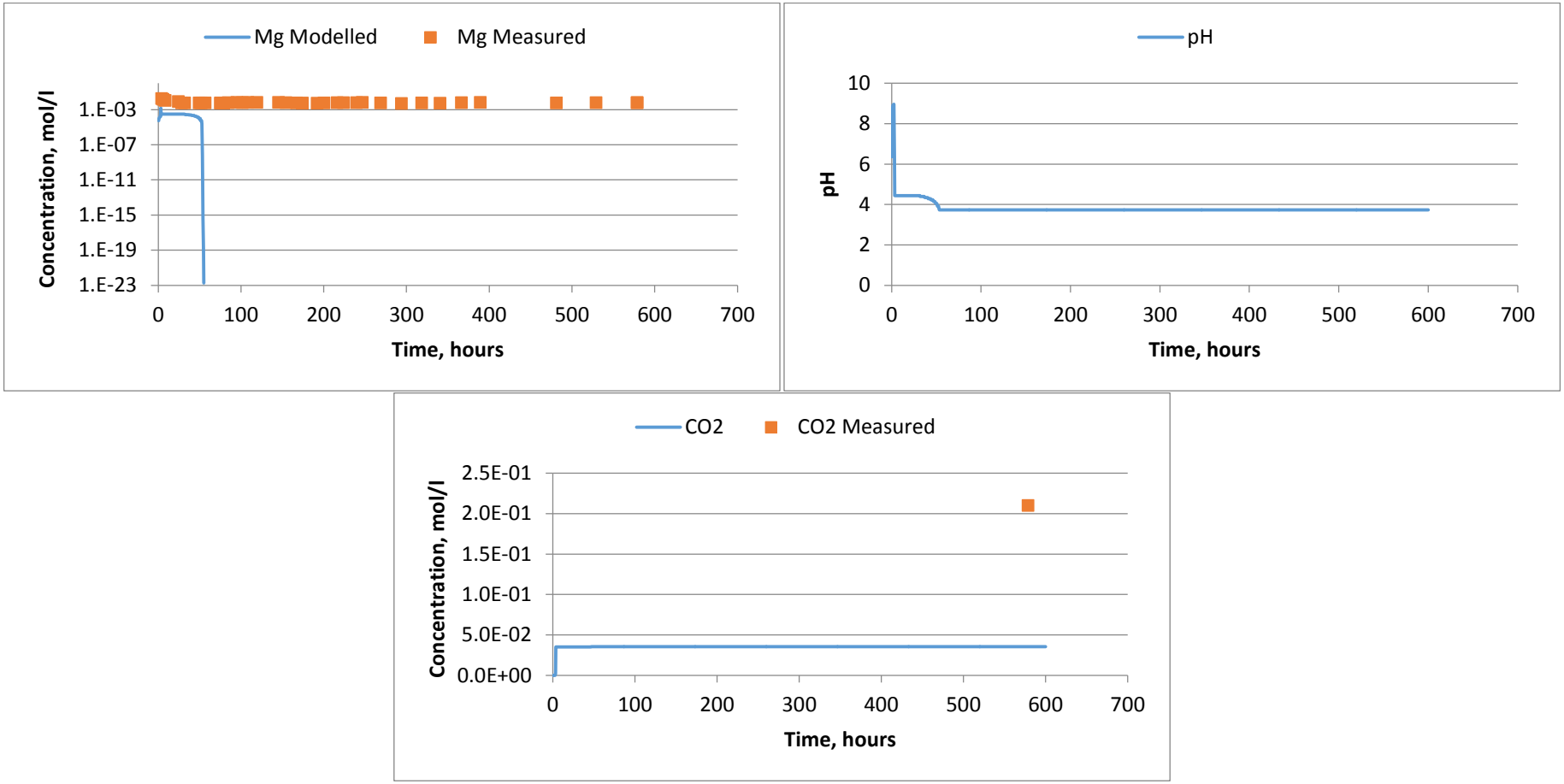


**Figures 5.2.20 - 5.2.22**: Modelled and measured Mg concentrations, pH and dissolved $CO_2$ content for SCORE

### 5.2.4 Dissolution Rates

Dissolution rates have been calculated for dolomite and K-feldspar for the SCORE experiment and are compared to those calculated from Experiment 147 in Figures 5.2.23 & 5.2.24. Dissolution rates have likewise been calculated for the other two experiments conducted on consolidated sandstone; STATIC and SC2, although these data are very sparse, being based on a single point in the case of STATIC and only four points for SC2. Dolomite dissolution rates have been calculated based on Ca release, while K-feldspar rates have been calculated based on K release.

Calculated rates for the flow-through experiment are generally higher than those calculated for the powdered batch experiment (147). Both the dolomite and K-feldspar rates follow a characteristic trend when plotted against mineral affinity: a sharp decline in dissolution rate a small decrease in affinity, followed by a period of reasonably steady dissolution rate. The steep declines in rate are from the earliest samples in the experiment, where dissolution rates are relatively high before the output transitions to steadier conditions later in the experiment. As well as calculated rates, mineral affinities are also lower than would be expected from the general trends indicated by the batch powder experiment. The dissolution rate calculated for SCORE agrees closely with the predicted rate for the single mineral experiment 134 (carried out under the same conditions), using the original dissolution equation presented by Busenberg and Plummer.

Interestingly, the rates from the chip batch experiment are also relatively high, with affinities somewhere between those observed in the flow-through and powdered batch experiments. The dolomite rate calculated from the static core experiment, on the other hand, is much closer to those seen towards the end of the powder batch experiment than the relatively high values calculated for the flow-through core experiment.

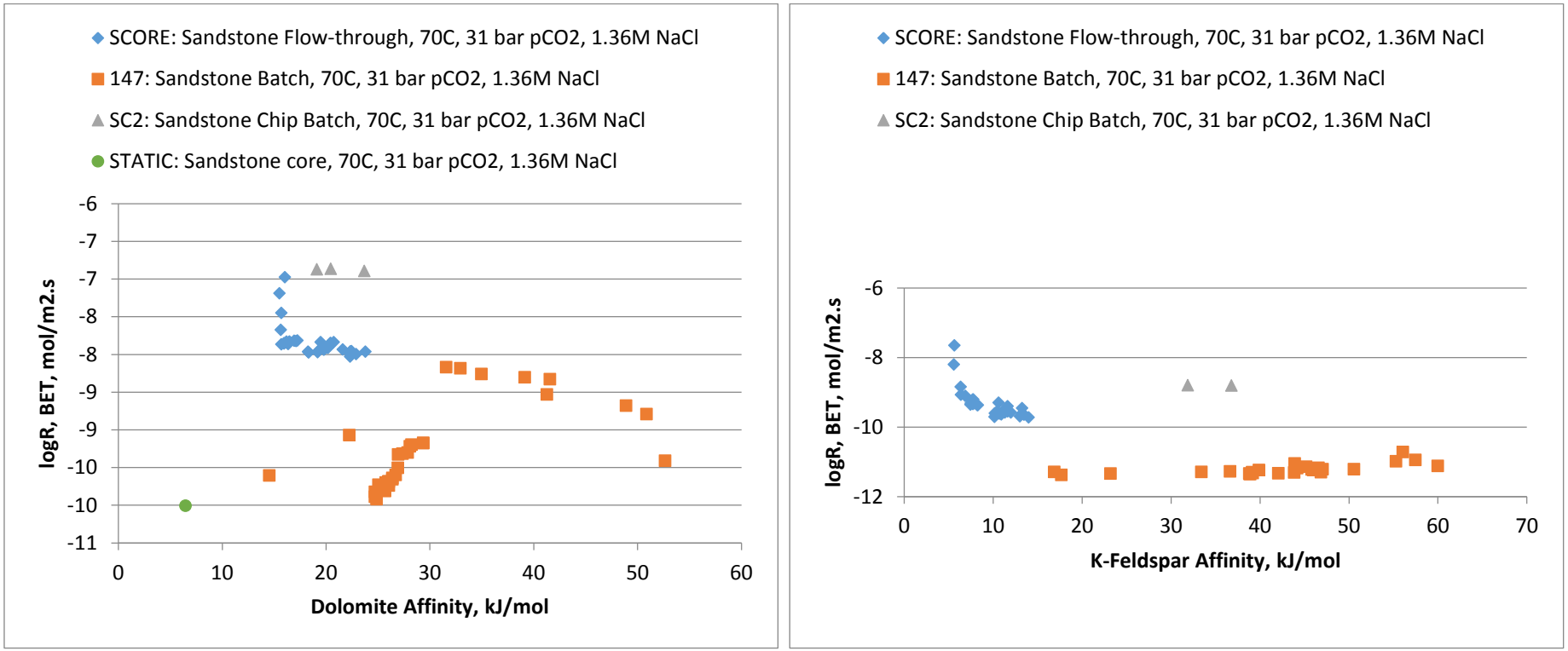


**Figures 5.2.23 - 5.2.24**: Calculated dolomite and K-feldspar dissolution rates for consolidated sandstone experiments and powder experiment 147

### 5.2.5 Intact Experiments: Overview and Discussion

The three “intact-rock” experiments described in this section were designed as a comparison to the powdered rock experiments detailed in previous sections. While powder batch experiments are relatively simple to carry out and maximise available surface areas so as to increase reaction, experiments on the original rock are evidently closer to natural systems. The flow-through experiment is of particular importance, more closely mimicking the dynamic, flowing, nature of an actual reservoir system.

The static core experiment is also of interest as it represents the type of stagnant conditions one may expect to find after active reservoir management has ceased, or in various pockets of trapped $CO_2$ left behind the main body of a migrating plume.

While analytical data is relatively poor for the two core experiments (particularly for Al and Si), the results from the experiments remain useful.

In terms of measured concentrations and mineral affinities, results from the powder batch and chip batch experiments are broadly comparable. The large difference comes in the apparent dissolution rates, which are considerably higher, for both dolomite and K-feldspar, in the chip batch experiment. It is possible that this apparent discrepancy is due to the surface areas used in the rate calculations. The surface area for the powdered sandstone is a measured one, and while the surface area contributions of individual mineral phases remain unknown, we might consider this a reasonable estimate of available surface area. The surface areas available for reaction for the chip (and both of the cores) have, by necessity, been estimated geometrically, based on porosity and average pore size. Surface roughness, or the relative accessibility of minerals, have not been taken into account and hence we might consider this to be a lower estimate of available surface area. This highlights the difficulty in both estimating surface areas for whole rock samples (and by extension, natural reservoirs) and in direct comparisons between rates obtained from experiments of these two types.

That being said, the heavy dissolution of dolomite grains observed in the flow-through experiment, not generally observed in the batch powder experiments, suggests that dissolution rates in the system were relatively high, such that not all the discrepancy between rates may be attributed to errors in surface area calculations. Indeed one would expect that in a system where fresh fluid is being constantly injected, dissolution rates would remain relatively high for longer. Late time dolomite dissolution rates in the flow-

through experiment, where dissolution has reached apparent steady state, tend toward the early time rates obtained from the powder batch experiment and agree well with predictions made for dolomite dissolution using the equation of Busenberg and Plummer (Equation 4.2.8 in Section 4.2). This suggests that in the case of the flow-through experiments, dolomite dissolution rates are not limited by transport as observed in the batch experiments. Apparent K-feldspar dissolution rates in the flow-through experiment do not reach steady state and continue to drop for the duration of the experiment, however we might assume that had the experiment ran for longer, they too would reach a steady state. This makes sense if we consider each input of fresh fluid to be equivalent to starting a new batch experiment, allowing the system to maintain the relatively high reaction rates seen early on in the batch experiments for a longer duration. Additionally, effects of increased Al concentrations, which have been cited as having a major impact on feldspar dissolution (Oelkers et al. 1994).

The static core experiment on the other hand, provides the opposite end member, where no fresh fluid is introduced. In this case the calculated dolomite dissolution rate is comparable to those from the late times of the powder batch experiment. Here concentrations build up in the fluid and on the surface of the mineral, essentially killing any further reaction. As in the powder batch experiments, observations from the static core did not reveal the significant dolomite dissolution seen in the flow-through core.

Modelling of the flow-through experiment proved problematic. K, Ca and Mg concentrations are significantly under-estimated, while the actual extent of dolomite dissolution is overestimated. Hence the model is both over-predicting the dissolution rate of dolomite, and apparently predicting the precipitation of Ca and Mg bearing phases, which do not actually occur in the experiment. Whether or not this interpretation is correct, it is clear that the relatively simplistic kinetic model was insufficient to predict the behaviour observed. Underestimation of dissolved solid concentrations will necessarily have a knock on effect on calculated pH and $CO_2$ solubilities, which, while insignificant at the lab scale, may be of greater import at the field scale.

Observed physical changes in the cores are also significant: both saw a relatively large increase in porosity. Interestingly this increase was similar in both cores, despite the fact that dolomite dissolution was observed to be far more advanced in the flow-through core. Likewise significant changes in the distribution of pore sizes occurred; in this case the effect was clearly more

developed in the flow-through experiment, though the general direction of changes (increases in the number of smaller pores) was the same in both cases. This is significant both in terms of potentially enhanced flow within reservoirs and also because of the fact the effect is strong in both stagnant and flowing systems, suggesting that physical changes to the rock may occur relatively rapidly even in areas where flow is stagnant or retarded. The main impact of this rapid carbonate dissolution, is likely to be an increase in permeability and reactive surface area (Kieffer et al. 1999), thereby leading to increased reaction and, if occurring near the injection well, as would likely be the case, improved injectivity (Lamy-Chappuis & Angus 2014).

Further discussion of these results, in the broader context of GCS, is presented in Section 7.2.

# Chapter 6
# Hele-Shaw Cell Experiments

## 6.1 Introduction and Methodology

Some background to the importance of density driven flow in GCS and the utility of Hele-Shaw cells has been given in Section 2.2. As highlighted there, some limited experimental work has been done in utilising Hele-Shaw cells to investigate processes during GCS specifically (Kneafsey & Pruess 2011; Neufeld et al. 2010; Faisal et al. 2013). The work of Neufeld et al (2010) utilised a mixture of methanol and ethylene glycol (MEG) and water to simulate the density difference between $CO_2$ saturated and $CO_2$ unsaturated fluids, while the work of Kneafsey & Pruess (2011) and Faisal et al (2013) used actual $CO_2$ dissolving into a solution of bromocresol green pH indicator, highlighting the acidified and hence $CO_2$ rich areas in the cell. Images from these works, reproduced as published, are shown below.

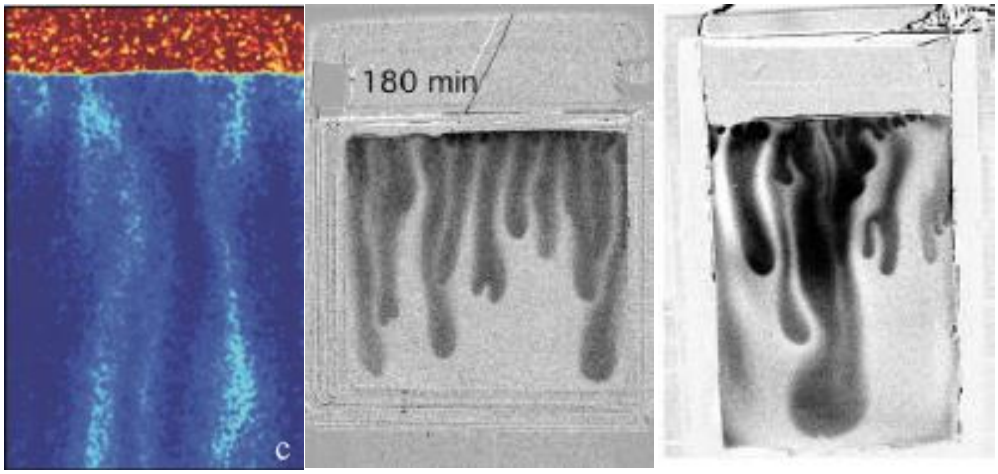


**Figure 6.1.1**: Processed images of Hele-Shaw cell experiments from the published work of: LEFT- Neufeld et al (2010); MIDDLE- Kneafsey & Pruess (2011); RIGHT- Faisal et al (2013)

Consistent among these works is the generally low quality of the images, which require considerable post-processing in order to enhance the contrast between the two fluids of interest, particularly for the experiments of Neufeld et al where an analog fluid is used. The experiments using pH indicator produce more striking results, but still require post processing to enhance the images in order for comparison with models. Both sets of experiments also

experienced several problems relating to experimental design, including contamination and non-heterogeneity of cells (Kneafsey & Pruess 2011) , uneven apertures and shearing along the gas-fluid boundary (Faisal et al. 2013).

Moreover, despite the utilisation of pH indicator in these two experiments, very little thought seems to have been given to the movement of pH gradients within the cell, the focus largely being on the physical process of convection. This essentially amounts to a simplification of the experimental system, where the focus is on defining a sharp boundary between $CO_2$ rich and $CO_2$ poor fluid. In reality of course the $CO_2$ content (and hence pH) of the fluid will vary from that produced by atmospheric $CO_2$ pressure to that produced by the $pCO_2$ at the fluid-gas interface. Movement of pH fronts within GCS systems will be of first order importance since, even over relatively short time periods, acidified porewaters can greatly impact formation fluid composition through ion exchange and mineral dissolution processes.

The Hele-Shaw cell, particularly when used in conjunction with pH indicator solutions can be an excellent tool for investigating these issues: both in terms of providing actual observations of systems in action to compare with models and as a visually striking demonstrative tool for communicating such science, particularly to the general public. The new work presented here therefor, was undertaken to reproduce and refine the experiments originally carried out by Kneafsey & Pruess, with a focus on improving experimental design, improving the quality and visual impact of the images produced and with a particular focus on how these cells may be used to more effectively investigate the pH gradients produced in such systems, rather than merely producing a direct comparison between physical convection in them.

Two sets of experiments were carried out, using an experimental setup based on the work presented by Kneafsey & Pruess (2010). These two sets of experiments used differing cell designs. Both designs, as it turned out, were slightly flawed, but the results using the second cell design are considered of higher quality. Nevertheless, some results from the first set of tests are of interest and so the background to both sets of experiments will be presented here.

The original set of experiments utilised two cells, each made from two cut glass panels measuring 0.3m x 0.3m. The apertures between the panels were measured as 2.4mm and 1.24mm respectively. The glass panels were

spaced using a metal strip, around which the panels were sealed, leaving the top edge open.

The newer cell was created using thick sheets of Perspex, spaced using a rubber strip. The two panels could be fully removed from one another to allow cleaning and were sealed together around the rubber strip using screwing tighteners.

The two cell designs are shown below in Figures 6.1.1 & 6.1.2.

Solution used with the cells varied. All runs using the initial cell design were carried out using 0.1g/l bromocresol purple, diluted in either deionised water, 1M NaCl or 4M NaCl depending on the experiment. Bromocresol purple changes colour from purple to yellow at between pH 6.8 and pH 5.2 and at the concentrations used in these experiments proved to be a good indicator of $CO_2$ dissolution. However the colour change is rather sharp, making any gradients in concentration (pH) hard to distinguish.

The second set of experiments were designed to monitor pH gradients within the cell and hence a broader range pH indicator than the bromocresol purple used in the original experiments was required. Various solutions were tested, but the solution giving the best results was a mixture of three parts 0.5g/l phenol red to six parts 0.5g/l bromocresol green to one part deionised water.

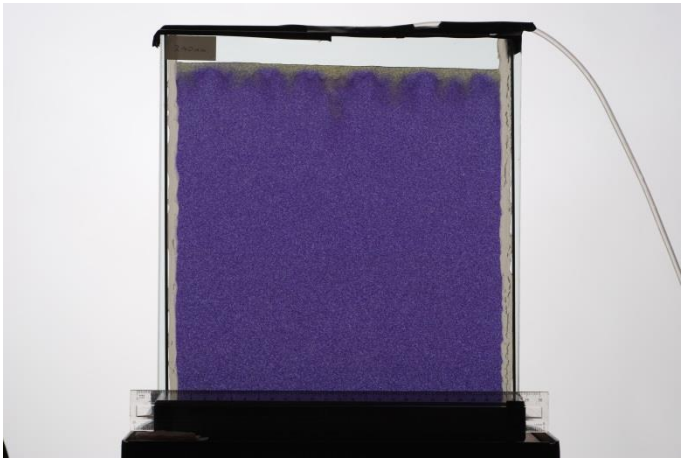

**Figure 6.1.2**: Original Hele-Shaw cell design

**Figure 6.1.3**: Revised, openable Hele-Shaw cell design

In both sets of experiments cells were loaded with solution and the top sealed with a rubber tube connected to a pump loaded with $CO_2$. $CO_2$ was introduced to the top surface of the fluid through apertures in the tubing and excess gas was allowed to escape through a hole at the top corner of the cell.

Cell runs were set-up in a photography studio at the British Geological Survey building in Keyworth and were photographed once per minute for the duration of the run. Room temperature during the runs was monitored and maintained at 25.5 ± 0.5°C.

## 6.2 Initial Experiments

The initial experiments, using the original cell design are summarised in Table 6.2.1 and Figures 6.2.1 – 6.2.7. In both runs 1 and 2 (Figures 6.2.1 & 6.2.2) a pre-existing instability, caused in this case by a streak of contamination from previous tests down the centre of the cell, “forces” plume development. Any minor instabilities forming at the top surface were rapidly dragged into the central plumes, essentially focussing all plume development in one point.

Runs 3, 4 & 7 (Figures 6.2.3, 6.2.4 & 6.2.7) demonstrate another problem with the original cell design; that of shearing of the top fluid surface by the gas passing across it. In this case the shear forced all of the developing plumes to migrate to the right

Runs 4 and 6 use NaCl solutions rather than the deionised water used in other experiments. Although problems with the runs, mentioned above, makes assessment of the results difficult, comparison of the early time pictures, where numerous small plumes have formed at the top layer of fluid, the retarding effect of NaCl on plume formation is noticeable. The effect is particularly strong in run 6, where a strong, 4M NaCl solution was used. In this case the initial instabilities along the top surface are barely noticeable when compared to the 1M NaCl (run 4) or deionised water runs. The introduction of NaCl not only lowers $CO_2$ solubility but also decreases the density difference between the native fluid and the $CO_2$ saturated fluid forming along the top boundary. Hence instabilities take longer to form and migrate as NaCl concentration is increased.

For Run 5 the cell was filled with 0.4-0.6mm diameter glass beads, in order to lower the test permeability to a value more closely approaching that of an actual rock. While the pure fluid cells have theoretical permeabilities on the order of $10^{-7}m^2$ permeability using the glass beads is likely to be several orders of magnitude lower. After one week, plume migration is considerably less than that observed in other cell runs in an hour, demonstrating how slow the process is likely to be in an actual aquifer. The beaded cell run had its own problems, notably short-circuiting of some fluid around the outside of glass beads, creating the ghosting visible in the one week photo. Additionally fluid evaporation form the top of the cell was an issue, causing unintended drying out and concentration gradients at the top of the cell.

Despite some of the problems with the setup used here, the results from these initial tests demonstrated the retarding effect of NaCl and lowering permeability has on the formation of these density plumes, as well as the utility of such experiments in demonstrating plume migration in a laboratory setting.

| Experiment No. | Cell dimensions | Fluid | Duration | Comments |
|---|---|---|---|---|
| **1** | 0.3x0.3x0.0024 | 0.1g/l Bromocresol Purple in DI | 3hrs 49mins | Plume simply followed streak of contamination down centre |
| **2** | 0.3x0.3x0.0024 | 0.1g/l Bromocresol Purple in DI | 2hrs 4mins | Same problem as Exp. 1, One major plume |
| **3** | 0.3x0.3x0.00124 | 0.1g/l Bromocresol Purple in DI | 2hrs 2mins | Better, but plumes all down one side of cell |
| **4** | 0.3x0.3x0.00124 | 0.1g/l Bromocresol Purple in 1M NaCl | 3hrs 36mins | Plume starts in centre and "flows" to right side of cell |
| **5** | 0.3x0.3x0.0024 | 0.1g/l Bromocresol Purple in DI in homogenous glass beads | Weeks | Plumes very slow, problems with drying out of solution and shortcutting |
| **6** | 0.3x0.3x0.00124 | 0.1g/l Bromocresol Purple in 4M NaCl | 1hr 11mins | One thin plume in centre, metal lining reacting with solution |
| **7** | 0.3x0.3x0.00124 | 0.1g/l Bromocresol Purple in DI | 1hr 51mins | Better, again pulling of plumes to right |

**Table 6.2.1**: Summary of original Hele-Shaw Cell experiments

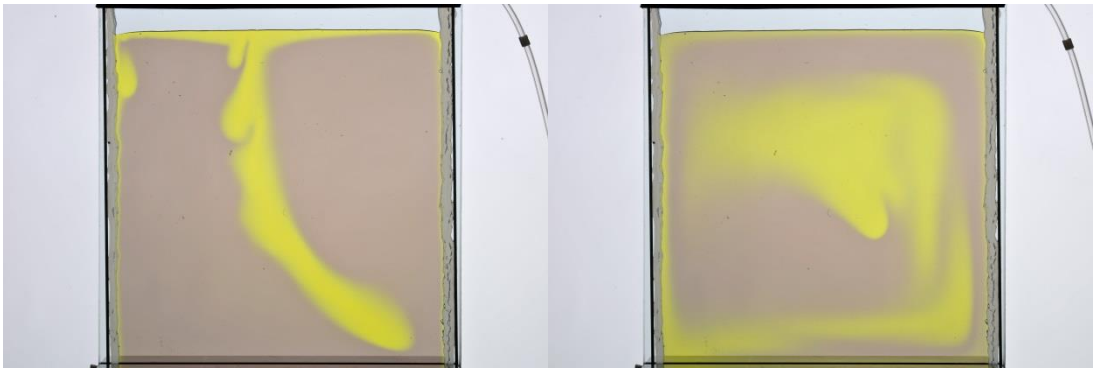

**Figure 6.2.1**: Run 1 at 0.5 hours (left) and 2 hours (right)

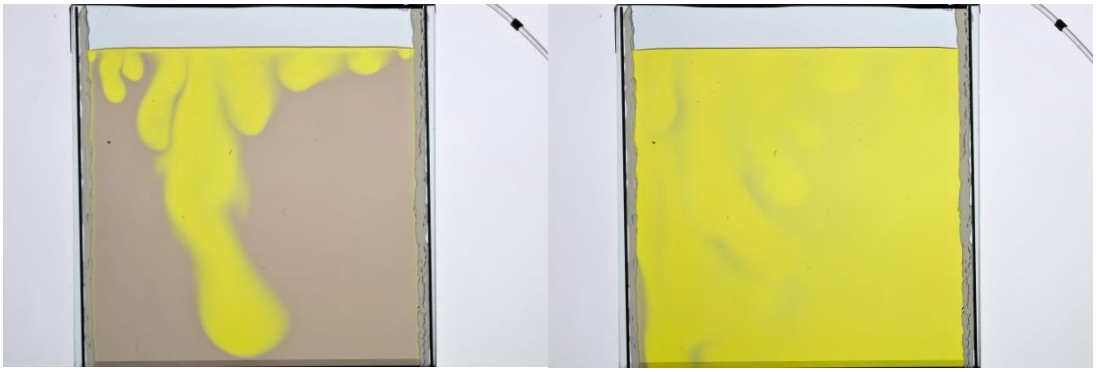

**Figure 6.2.2**: Run 2 at 0.5 hours (left) and 2 hours (right)

**Figure 6.2.3**: Run 3 at 0.5 hours (left) and 2 hours (right)

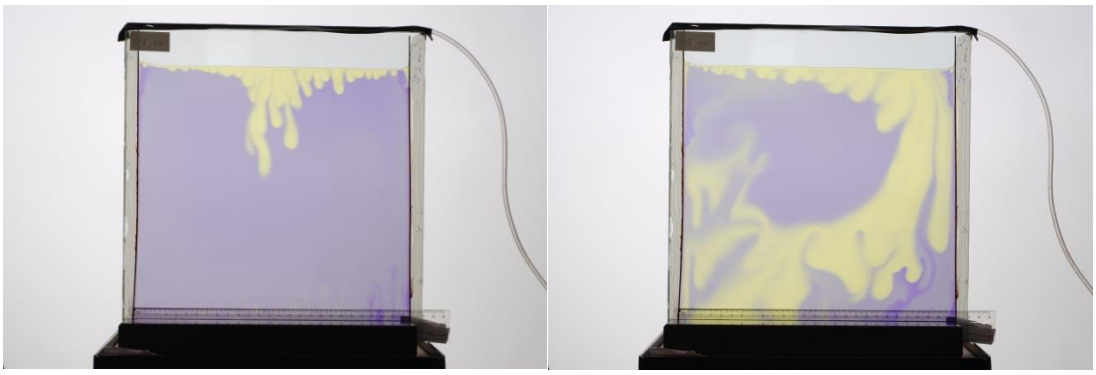

**Figure 6.2.4**: Run 4 at 0.5 hours (left) and 2 hours (right)

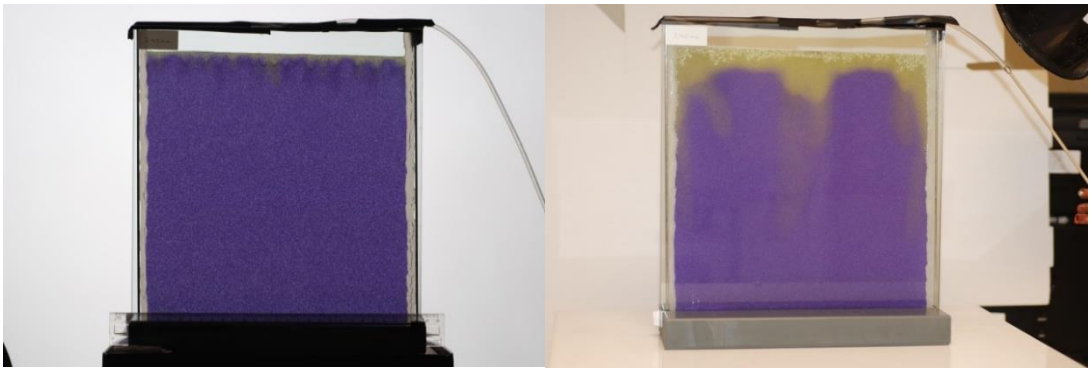

**Figure 6.2.5**: Run 5 at 24 hours (left) and one week (right)

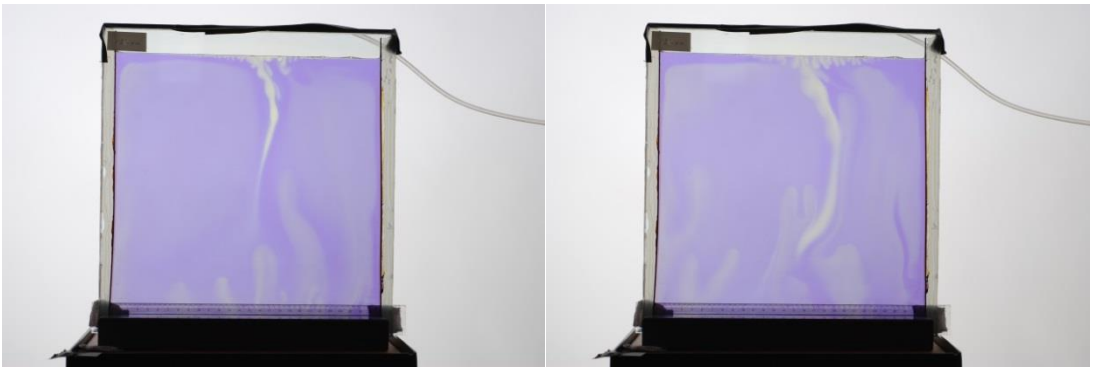

**Figure 6.2.6**: Run 6 at 0.5 hours (left) and 1 hour (right)

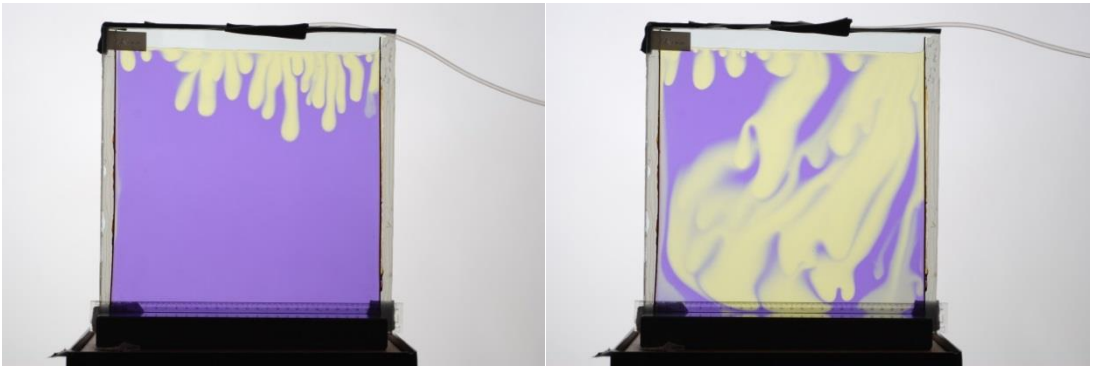

**Figure 6.2.7**: Run 7 at 0.5 hours (left) and 1 hour (right)

## 6.3 pH Gradient Experiment

A single experiment was carried out using the improved cell design described in Section 6.1. The openable cell allowed cleaning following tests, to prevent plumes forming along pre-existing instabilities. Metal parts were removed to prevent reaction with fluid seen in previous runs along the edges of the cell. Additionally $CO_2$ was introduced through a series of holes in the tubing running along the top of the cell, rather than having one inlet, to reduce the problems associated with shearing observed in earlier experiments. The improved cell dimensions are 0.5m x 0.5m with a 0.0005m aperture, corresponding to a theoretical water permeability of 2.5E-8 $m^2$.

The experiment was designed in order to observe the formation of pH gradients within the cell during the formation of $CO_2$ rich plumes and to compare the results with modelled predictions. Earlier runs, apart from experimental problems, were carried out using a fairly narrow range pH indicator, the result being that, in theory, not all of the $CO_2$ enriched water would undergo a colour change. The broader range used in this experiment was sufficient to cover all possible $CO_2$ saturations and the resultant pH range.

A selection of raw photographs, taken from various time periods over the 16 hour run are presented in Figures 6.3.1 – 6.3.6. As is evident, despite some “ghosting” from previous tests, the run was successful in avoiding most of the problems associated with the earlier experiments detailed above.

By 10 minutes into the run numerous small (<1cm) instabilities have formed along the top surface of the fluid, where $CO_2$ is dissolving. These instabilities rapidly develop and grow into individual plumes, around 50-60 in number by 30 minutes. These plumes continue to move downward and amalgamate, such that by 5 hours the 50-60 individual plumes have coalesced into around 20 or so distinct bodies. In the gaps between these plumes at the top surface small instabilities continue to form as fluid free of $CO_2$ upwells, though at a much reduced rate. Eventually the plumes almost completely coalesce, though some plume centres, where $CO_2$ concentrations are particularly high, can still be distinguished. By 16 hours almost all of the fluid within the cell has “seen” $CO_2$ such that only some fluid around the bottom edges of the cell is $CO_2$ free. This effect is thought to be due to bowing of the plastic cell when filled with fluid, such that the aperture in the very centre is slightly larger than elsewhere. This would have increased the permeability in this area, leading

to a slight preference of the plumes to move toward the centre, hence avoiding the edges of the cell.

A definite gradient is visible even in the unedited photos shown in Figures 6.3.1 – 6.3.6, from blue to green to yellow as pH decreases (and, correspondingly, dissolved $CO_2$ increases). In order to differentiate areas of varying pH, images were processed using the image editing software ImageJ and using calibration images. These calibration images were created by filling the cell with the same fluid mixture used during the run, but with the pH adjusted to measured values using HCl acid. These images therefor provide a measure of the colour intensity expected for a given pH. The measured pH values of calibration images were 3.4, 3.9, 4.5, 5.0, 5.5, 5.9, 6.4 and 7.2.

Image processing involved initially cropping an image. Each calibration image was then subtracted from the shot, producing 8 images for each timeslice, one for each calibration value. Each of these images should in theory have a pixel value of zero (black) where the colour (i.e. pH) of the appropriate calibration image matches that of the original image. Each of these images was then converted to greyscale. This data was then exported to Excel where all non-zero values were converted to 255 (white), such that the images, when recompiled, consisted only of black and white pixels, black pixels corresponding to areas matching the target pH. These 8 images of specific pH were then reduced to 7 images illustrating pH ranges. These were created simply by using ImageJ to produce a “difference” image from the two original end member images. In these images, due to the “difference” operation, white areas correspond to areas within the cell which match the target pH range, while black areas fall out-with the given range. Final edits of the run photos are shown in Figures 6.3.7 – 6.3.48.

The processed images appear to pick out areas of a given pH range well. The topmost surface of the fluid appears to have a pH of between 3-4 – 4.9. The theoretical pH of water saturated with $CO_2$ at 1bar, should be around 3.9 (according to PHREEQC3 calculations), hence this top layer appears to correspond to a layer of $CO_2$ saturated fluid. The plumes themselves however tend to have a higher pH, ranging from around 4.5 in the centre of the plumes up 6.5-7.0 at the plume edges where mixing and diffusion with the $CO_2$ free fluid will occur.

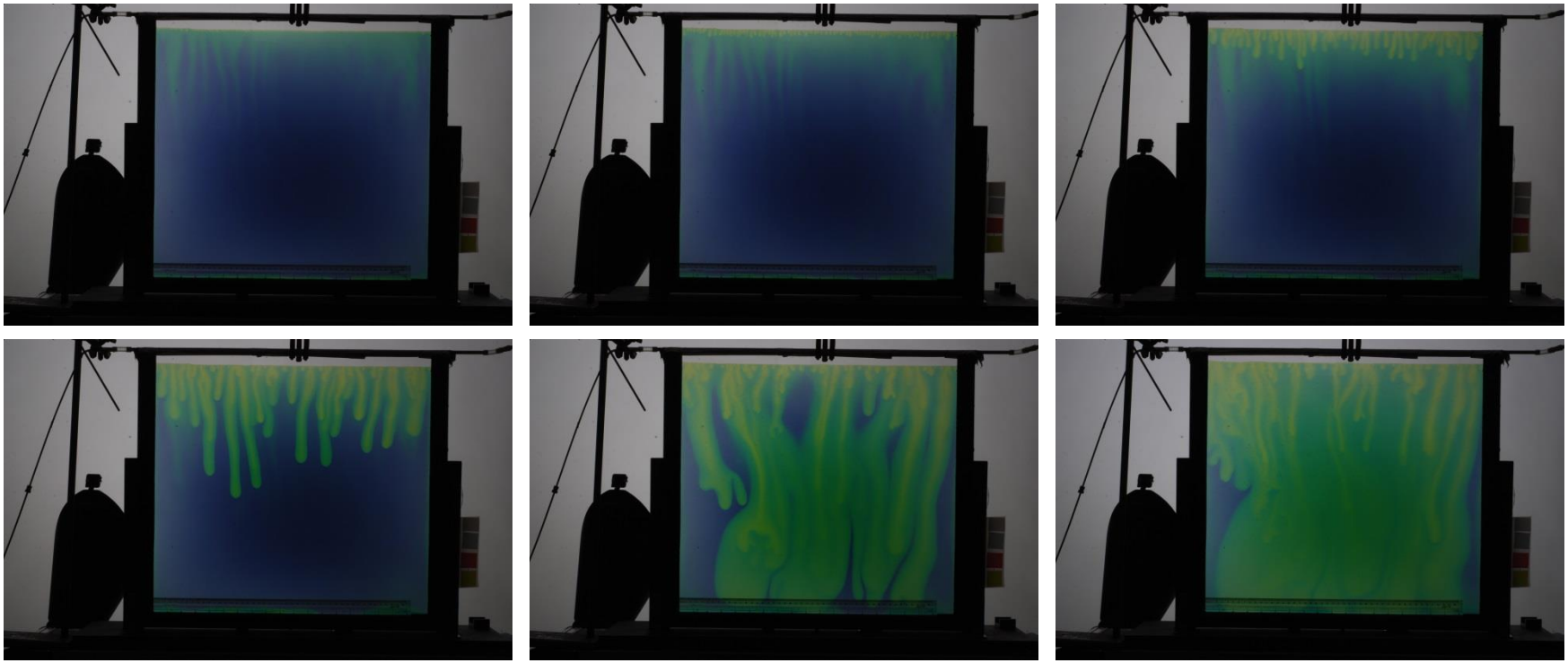

**Figures 6.3.1 – 6.3.6**: Photographs from pH gradient experiment taken at 10 minutes (top left), 30 minutes (top centre), 2 hours (top right), 5 hours (bottom left), 12 hours (bottom centre) and 16 hours (bottom right). The cell interior forms a square of 0.5m x 0.5m.

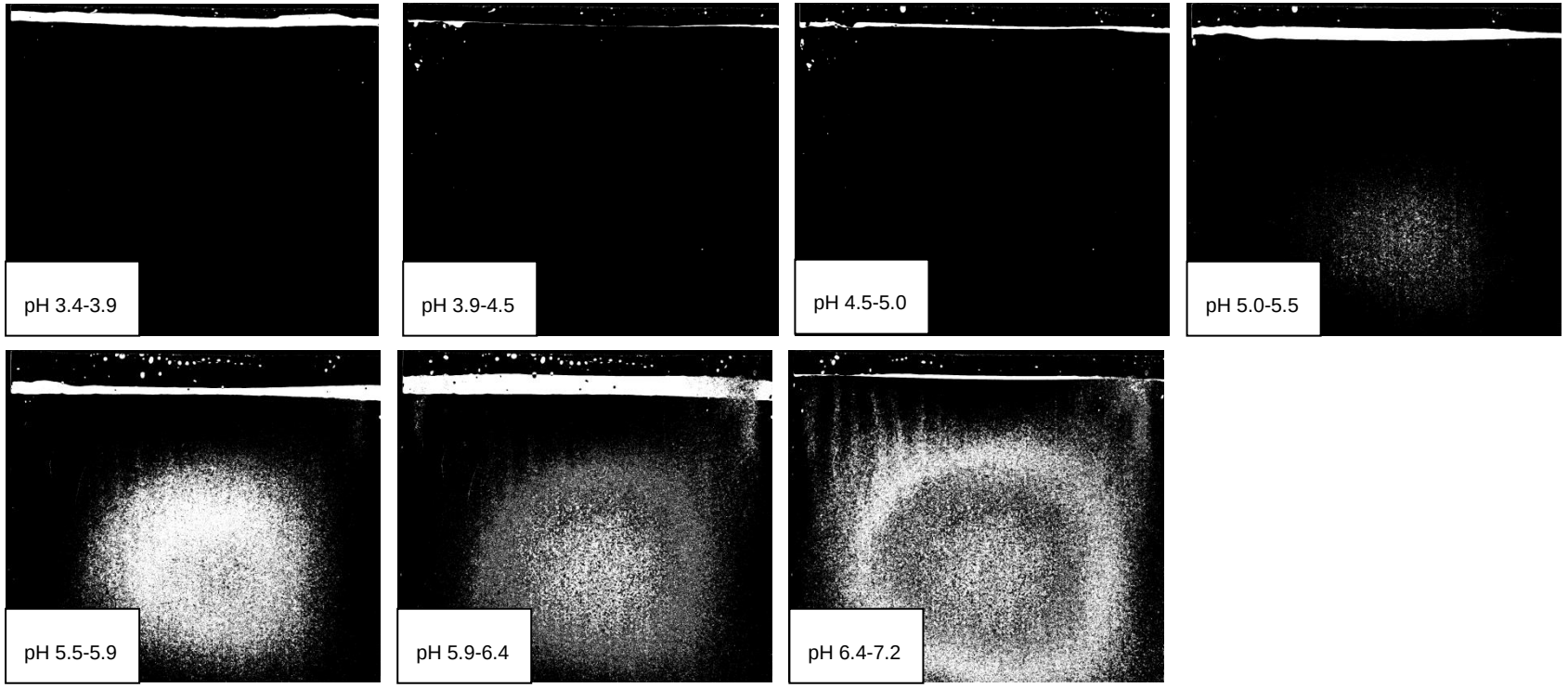


**Figure 6.3.7 – 6.3.13**: Processed 10 minute image showing various pH ranges. White areas correspond to the appropriate pH.

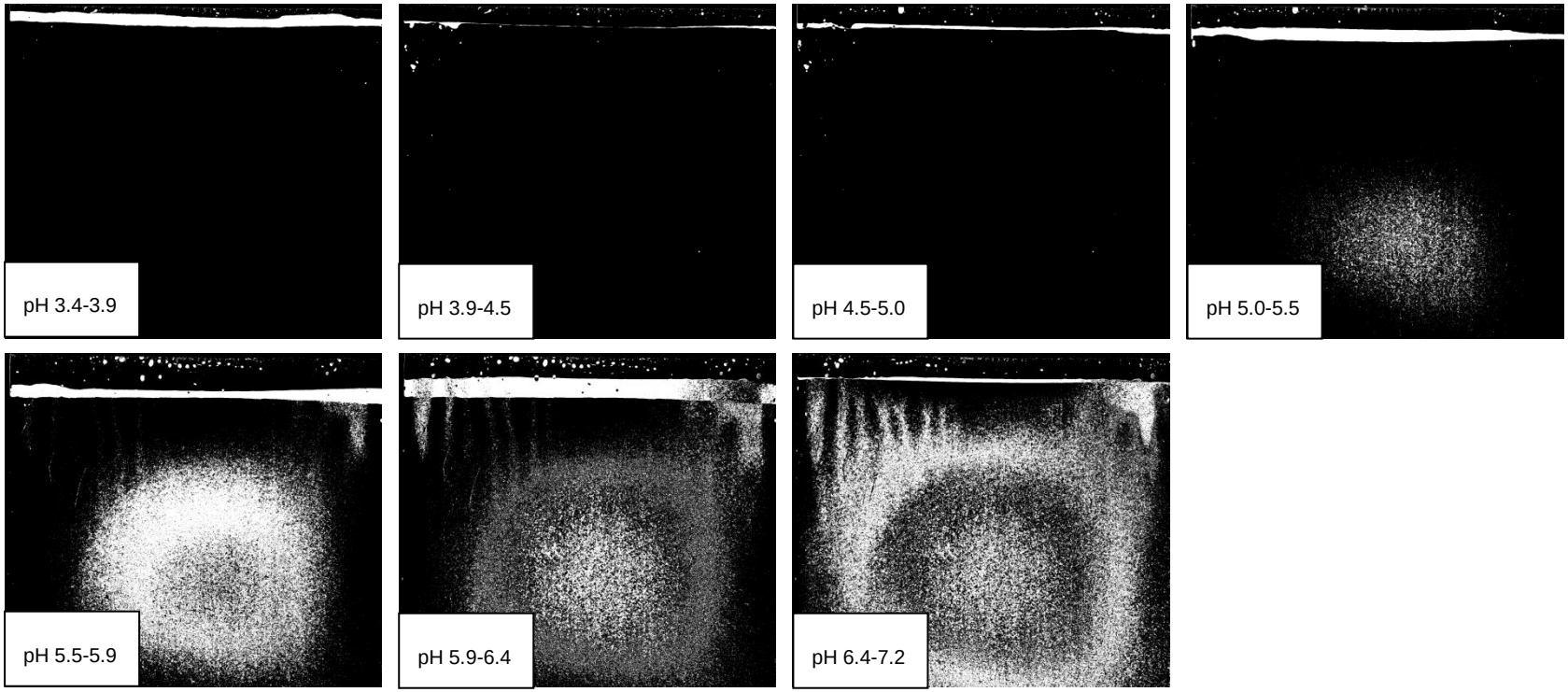


**Figure 6.3.14 – 6.3.20**: Processed 30 minute image showing various pH ranges. White areas correspond to the appropriate pH.

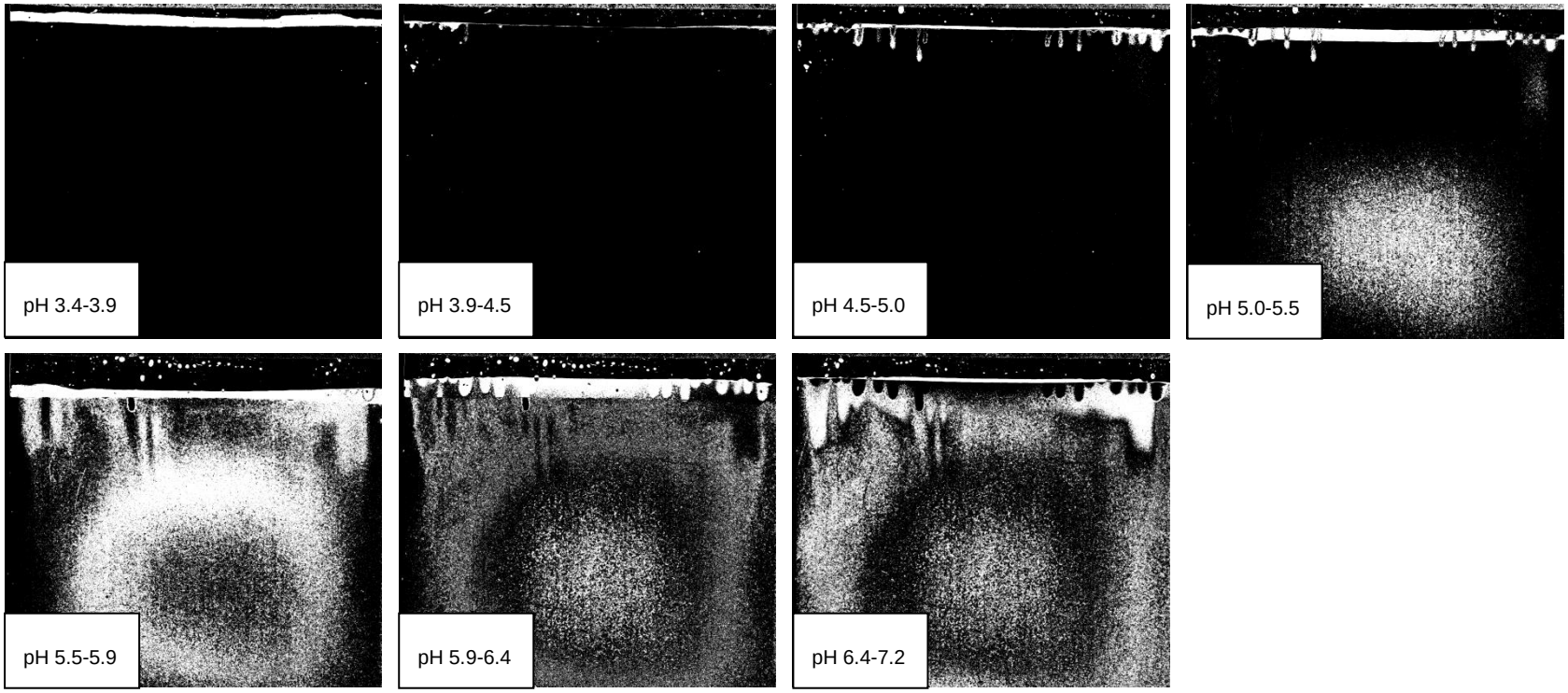


**Figure 6.3.21 – 6.3.27**: Processed 2 hour image showing various pH ranges. White areas correspond to the appropriate pH.

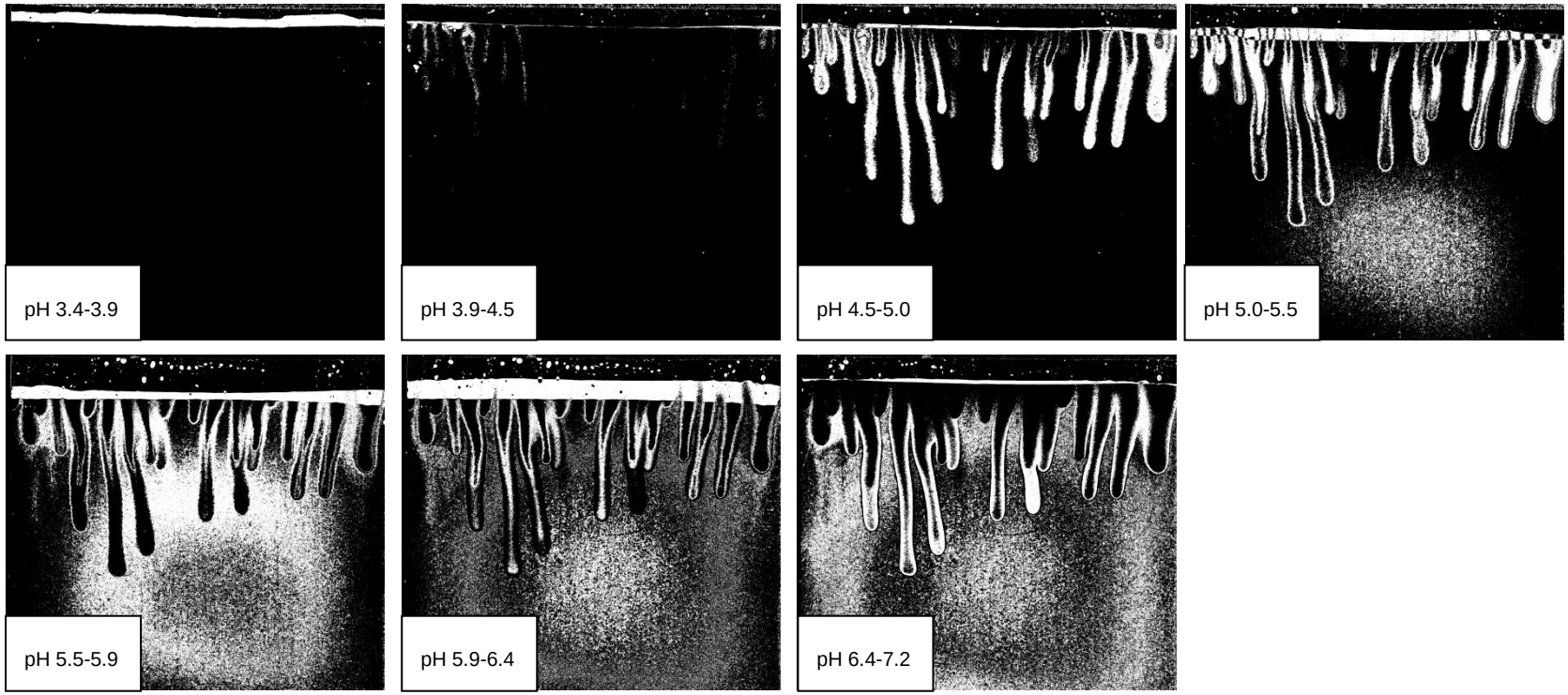


**Figures 6.3.28 – 6.3.34**: Processed 5 hour image showing various pH ranges. White areas correspond to the appropriate pH.

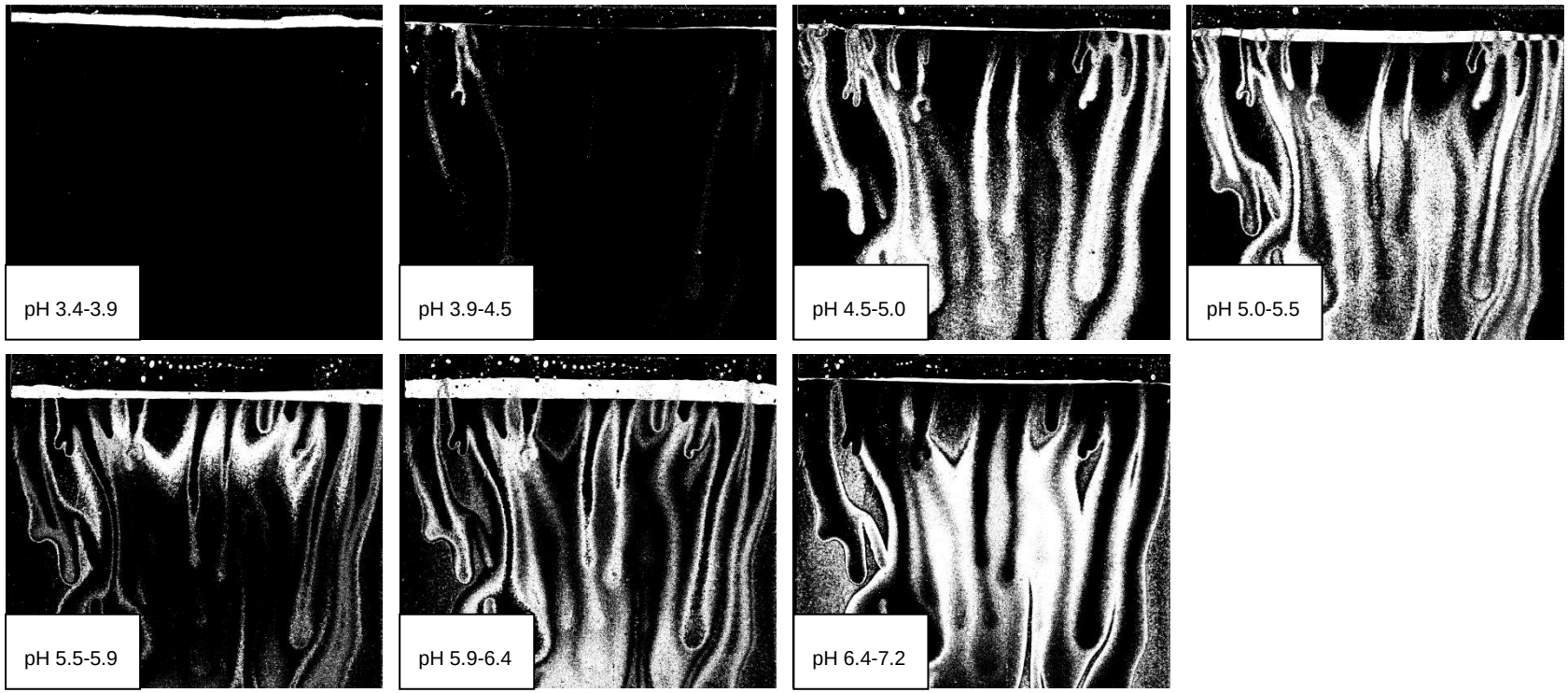


**Figures 6.3.35 – 6.3.41**: Processed 12 hour image showing various pH ranges. White areas correspond to the appropriate pH.

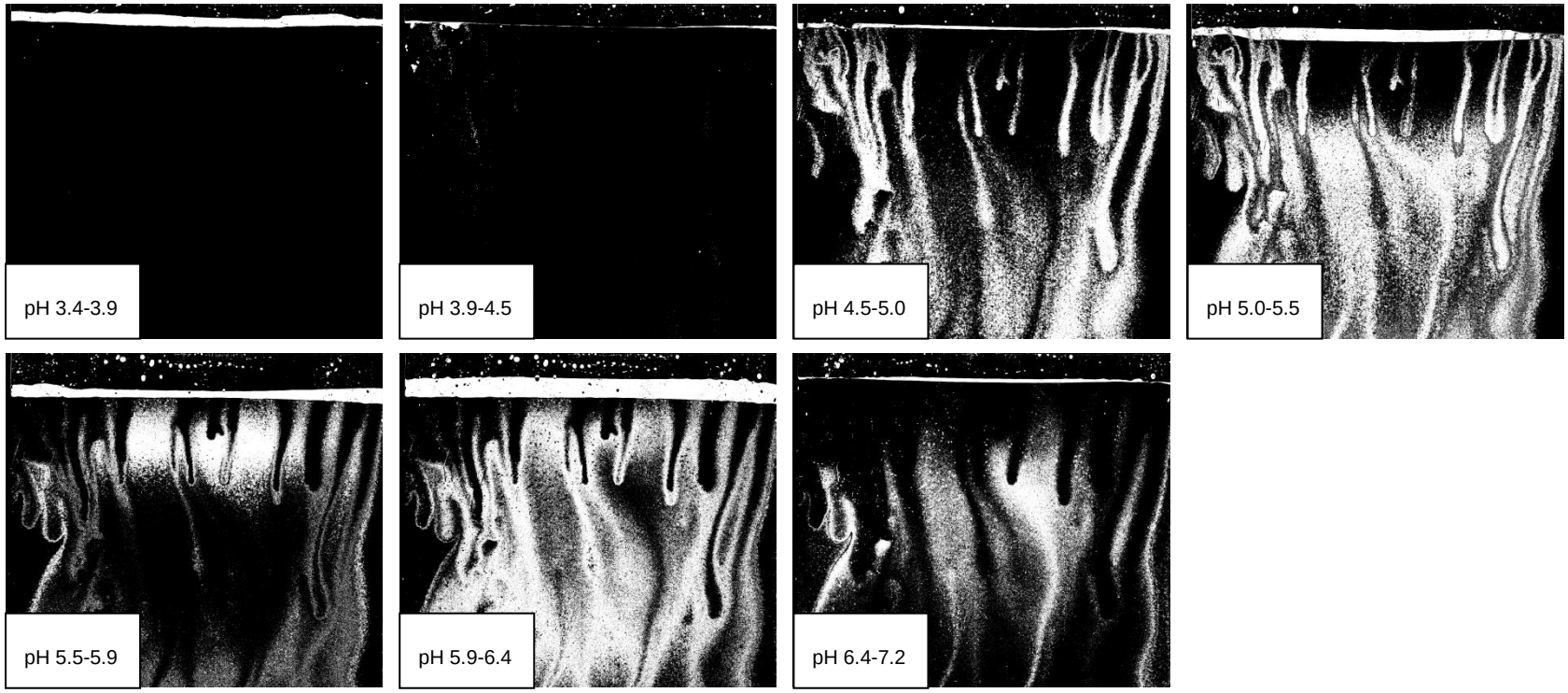


**Figure 6.3.42 – 6.3.48**: Processed 16 hour image showing various pH ranges. White areas correspond to the appropriate pH.

The pH gradient experiment was modelled, using TOUGH2, operated from the GUI software Petrasim. The dimensions of the cell were recreated exactly and the fluid filled section assigned a permeability equivalent to the theoretical permeability of the cell. A 7000 cell mesh was created to model the cell (Figure 6.3.49); 200 cells wide by 35 cells tall. The mesh was refined as the top of the cell was approached, so as to better capture the very small instabilities seen in this area during the early times of the experiment. The top 5 layers of the model are “air”, with a $CO_2$ injection well along the top-most boundary. All boundaries are under no-flow conditions, such that no mass may enter or leave the model.

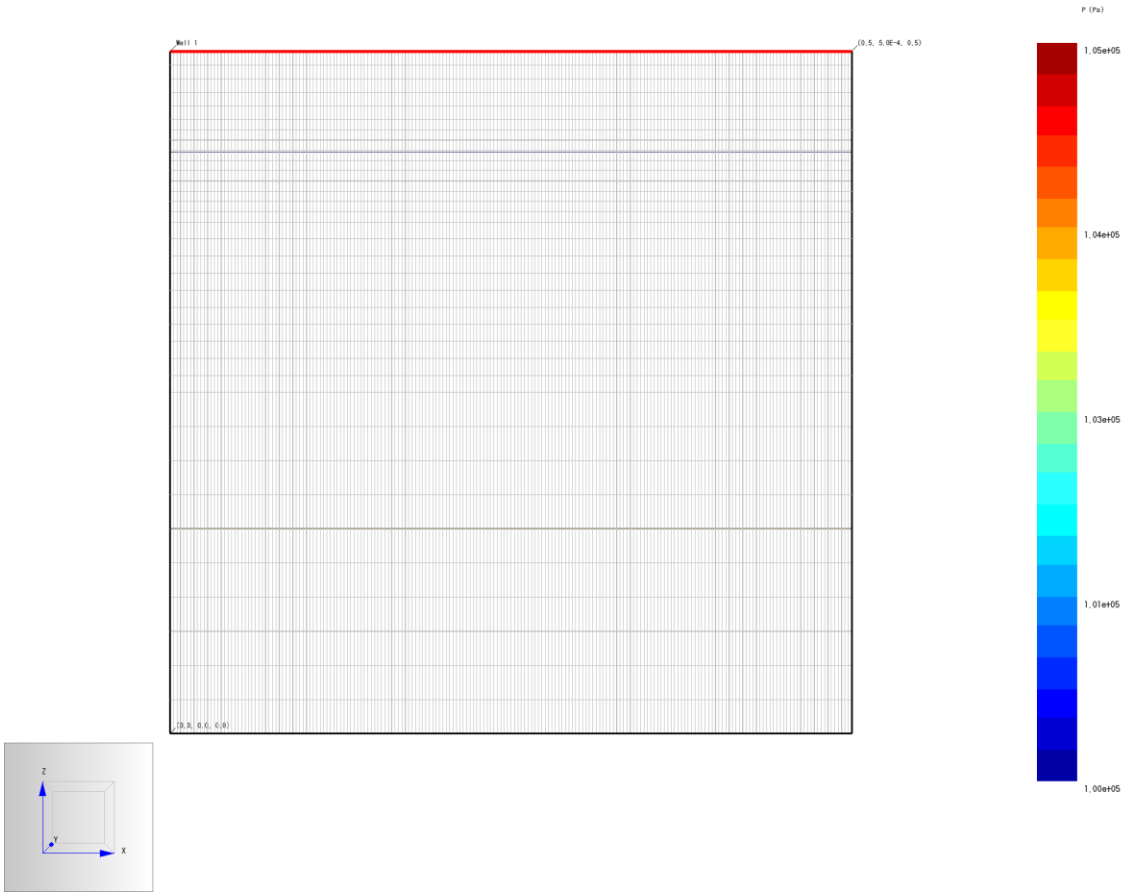


**Figure 6.3.49**: Image of the model grid used to simulate the pH gradient experiment

The model results after 12 hours are shown in Figures 6.3.50 – 6.3.59. The model output is not capable of producing pH values, but does give values of dissolved $CO_2$. Hence the appropriate values of dissolved $CO_2$ for a given pH range have been calculated and the final model output produced accordingly.

The model reproduces the number and width of the plumes reasonably well. However, most striking in the output is that it under predicts the vertical extent of the plumes, such that while in the experiment by 12 hours the plumes have reached the cell base, the model plumes reach only around the half-way mark. In terms of pH the model produces reasonable results, with most plume centres having a model $CO_2$ content correspondent to a pH of 4.5 – 5.5, with the plume rims reaching increasingly high ranges moving outward. Apparent discrepancies between the experimental and modelled images at higher pH ranges (6-7) occur because the model is not reproducing pH, but dissolved $CO_2$ content, hence the “background” pH of the $CO_2$ free fluid is not represented in the model figures, but is captured in the experimental images.

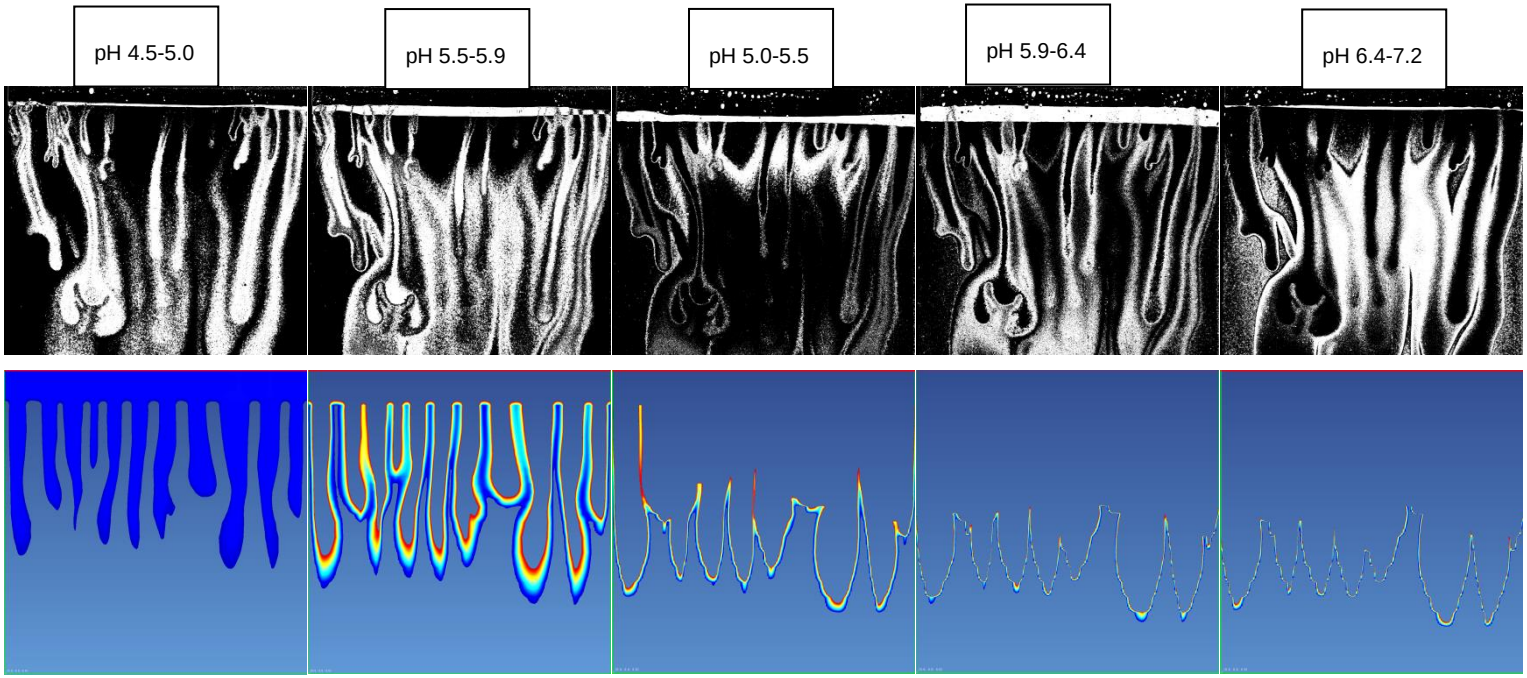


**Figure 6.3.50 – 6.3.59**: Processed 12 hour image showing various pH ranges (top) and corresponding model images (bottom). White areas correspond to the appropriate pH range in the top figures, while coloured areas (dark blue to red corresponding to high pH to low pH) correspond to the appropriate range in the modelled images.

## 6.4 Conclusions

The Hele-Shaw cell work presented here, despite various experimental problems, demonstrates the utility of such experiments in studying density driven flow, relevant to GCS, in a laboratory setting. The results of the initial experiments demonstrate the retarding effect of NaCl on the formation of plumes, both through reduced $CO_2$ solubility and reduced density contrasts between the fluids involved. The cell run carried out using glass-beads also demonstrates the relative speed of these processes in something approaching real reservoir materials: plume migration is limited to only a few centimetres, over the course of a week, even in what, in terms of sandstones, would be considered a relatively permeable medium. Despite this, plumes do begin to form relatively rapidly, generally within a few minutes for the pure fluid cells and results from several of the initial experiments illustrate that heterogeneities (in this case contamination within the cell, but the same processes are likely to occur where physical heterogeneities are present in a reservoir) can have a huge effect in focusing and accelerating these density plumes. Heterogeneities such as permeable faults on the reservoir scale may well dominate the behaviour of such systems and if correctly characterised may be useful in enhancing the movement of $CO_2$ saturated fluids away from the main plume body a relatively rapid rates, allowing fresh, unsaturated fluid to up-well, thereby increasing solubility trapping.

Further work demonstrates a novel method for observing pH gradients created during such cell experiments. While previous work has focused on using limited range pH indicator only to study the physical movement of $CO_2$ rich water, the work presented here demonstrates that if appropriate methodology is applied, similar experiments can be of great utility in observing relatively small pH gradients. Perhaps the most striking outcome of this work is the underestimation of plume migration by the modelling software used. It is possible that part of this discrepancy is due to the enhanced permeability present in the centre of the cell, where it was bowed during the experiments. However other work has noted similar disparities while modelling laboratory experiments (Kneafsey & Pruess 2011), suggesting that there may be fundamental discrepancy between the modelled and experimental system. This has obvious implications for field-scale deployment of GCS, where predictive modelling of these plumes may

be involved and where density driven flow may be relied upon to increase the long-term security of storage.

Further discussion of these results, in the broader context of GCS, can be found in Section 7.3.

# Chapter 7
# Synthesis: Applying Laboratory Derived Results to GCS

The results presented in Chapters 4, 5 & 6 of this work cover a number of processes which may occur at a variety of spatial and temporal scales during GCS, from early dissolution of $CO_2$ into, and acidification of, pore-waters, to mineral dissolution, which will begin relatively rapidly, but may continue for very long periods of time, to processes such as density driven convection which may act to increase storage security over relatively short time-scales. The following sections will discuss how the results and processes discussed in previous sections fit into the broader picture of GCS as a whole and their significance at the reservoir scale.

## 7.1 Kicking Off: $CO_2$ solubility and pH

Among the first reactions that take place following injection of $CO_2$ into a geological reservoir will be dissolution of free-phase $CO_2$ into the reservoir brine. Dissolution of $CO_2$ will be accompanied by a drop in formation-fluid pH as dissolved $CO_2$ dissociates (Rochelle et al. 2004; Gilfillan et. al. 2009; Gunter et al. 2004).

The dissolution and overall solubility of $CO_2$ in a given reservoir are of significance for a number of reasons. The solubility of $CO_2$ and its dissolution rate will place restrictions on both injection rates and the ultimate storage capacity of a given reservoir: the faster free-phase $CO_2$ dissolves, the faster "fresh" $CO_2$ can be injected without driving up formation pressure and more $CO_2$ can be trapped as a dissolved phase, ultimately increasing storage security. Additionally, if increases in formation pressure can be kept to a minimum, the need for production of formation waters to relieve pressure can be avoided. The rate of $CO_2$ dissolution will not be governed by the inherent rate of dissolution, but rather on the contact area between free-phase $CO_2$ and unsaturated formation fluid.

Secondly, the pH drop associated with dissolving $CO_2$ will "kick-start" the dissolution of minerals (particularly carbonates) within the reservoir and the rate of these reactions will be dependant in the case of many minerals on the exact value of pH (Gaus 2010). Mineral dissolution will act to buffer pH and secure dissolved $CO_2$ as various ionic species, which in turn will allow more $CO_2$ to dissolve (Gunter et al. 2004). This feedback mechanism will be relatively slow and long-lasting for many silicate minerals, which exhibit

relatively slow reaction rates. For carbonates, dissolution of which will rapidly buffer pH, the feedback will have more impact on the short-term, but may be relatively short-lived as fluids rapidly become saturated with respect to, for example, calcite or dolomite. This behaviour is observable in the experiments presented here: results from calcite and dolomite batch experiments (Section 4.2) indicate that pH is rapidly buffered at early experimental times, where dissolution is relatively fast, but slows relatively soon (e.g. Figure 4.2.3 for calcite). The final pH values in these experiments, despite being apparently stable, remain up to 0.5 pH units below the expected values at mineral saturation. This is in contrast to other experimental studies on carbonate dissolution under $pCO_2$, where higher pH is attained in less time (e.g. Crockford & Telmer (2011)). This issue is related to the relatively low dissolution rates obtained for calcite and dolomite in this study, which is discussed in more detail below. In other systems, for example where mixing is more efficient or surface area greater, we would expect pH to continue climbing for longer, reaching higher levels and plateauing as calcite or dolomite become saturated.

The experiments carried out on silicate minerals meanwhile, show very little variation in pH. The results of the stirring test on K-feldspar (Section 4.1.2, Figure 4.1.13) show that silicate dissolution can have a marked effect on pH. In this case grinding caused by the use of magnetic stirrer beads increased the surface area available for reaction. No measurement was made of the final surface area, but the powder removed from the experiment was very fine, as opposed to the relatively coarse, granular starting material. This increase in surface area “sped-up” the dissolution of the K-feldspar very effectively, revealing effects, such as the increase in pH, which would otherwise not be observed on these time-scales. It should be noted that the apparent increase in dissolution rate (of around three log units) in this experiment relative to unstirred experiments, is likely largely an artefact of the changing surface area not being taken into account in the final calculations of rate, though other processes such as transport effects and changes in mineral structure due to grinding may also have had a “real” effect on the dissolution rate. Therefor in a natural system, where surface area of silicates will change only very gradually, the effect of silicate dissolution on pH will only become significant over very long (years) periods of time. Even if silicate dissolution were reasonably fast, such effects would in any case be masked by the much stronger and more rapid effect of carbonate dissolution in the short term. It is however worth bearing in mind

that In the longer term, if carbonates were eventually removed from the system through complete dissolution, silicates dissolution would have a more marked effect on pH and this should be borne in mind for long-term storage schemes..

While $CO_2$ solubility is thought to be fairly well constrained, high quality experimental data on $CO_2$ dissolution using mineral and rock suspensions are generally lacking, especially for conditions relevant to GCS. The results for dissolved $CO_2$ content and pH of experimental fluids presented here therefor are vital in understanding the processes likely to occur during GCS (Rosenqvist et al. 2012).

$CO_2$ dissolution, along with the associated drop in pH should occur rapidly as was the case in the experiments presented here and in Rosenqvist et al (2013) which presents results from $CO_2$ dissolution experiments carried out using the same experimental set-up. In all experiments presented here, calculated pH for the fluid samples drops from relatively high (pH>7) to relatively low (pH 3-4) values (e.g. Figure 4.1.45 for albite, Section 4.1.3). In the case of the silicate minerals studied here, pH shows relatively little change thereafter, while for the carbonate minerals looked at, pH is buffered relatively rapidly to higher values. In all cases final experimental pH was below that predicted at equilibrium for the experiments. In the case of the feldspar experiments, pH buffering is largely limited by the relatively sluggish nature of feldspar dissolution. Likewise slow carbonate dissolution in the batch experiments here lead to the discrepancy in pH, though in this case the slow dissolution was likely due to transport limitations. Hence the pH and $CO_2$ solubility results for the mineral experiments presented here are representative of the period of movement from far from equilibrium conditions to “nearer” to equilibrium conditions that will take place following initial $CO_2$ injection. In terms of where in space these results are applicable, they will apply to various parts of the system at different stages in its evolution.

There was generally less discrepancy between dissolved $CO_2$ content in the experiments and that predicted by, for example, PHREEQC or the Duan solubility equations than for pH. This is because $CO_2$ solubility is largely dictated, in the short term, by pressure, temperature and salinity conditions, rather than fluid-mineral interactions.  Worth noting is the fact that earlier versions of PHREEQC did not take into account the variation in activity of dissolved $CO_2$ with partial-pressure, necessitating the use of fugacity coefficients to calculate an “effective” partial pressure (see work presented in

Rosenqvist et al, 2013, for details). While PHREEQC3 now automatically corrects for this effect if using the default database (PHREEQC.dat), use of alternative databases will lead to similar problems unless they are updated with the appropriate thermodynamic data.

Applying these results to an actual storage setting, we would expect a rapid drop in pH and a concurrent increase in the dissolved $CO_2$ content of the formation fluid and these effects have been observed at numerous $CO_2$ injection sites as well as in laboratory experiments (Wilkinson et al. 2009; Hovorka et al. 2006; Rochelle et al. 2004). Fluid in contact with injected $CO_2$ will rapidly become saturated in $CO_2$. While ongoing reactions may well act to remove or speciate dissolved $CO_2$ (in the form of carbonate minerals, for example), these reactions are relatively sluggish compared to the dissolution rate of free-phase $CO_2$. These reactions will continue to shift the equilibrium of the $CO_2$-fluid system, allowing continued $CO_2$ dissolution into what was once saturated fluid, but in the short term $CO_2$ solubility will be controlled by reservoir conditions and dissolution will be limited by the contact area between fresh formation fluid and the main body of $CO_2$.

Therefore, the results presented in this work (and in Rosenqvist et al, 2013) for $CO_2$ solubility in mineral suspensions, provide a conservative estimate for $CO_2$ solubilities in an actual storage setting. Long term dissolution of minerals will act to increase the volume of $CO_2$ that may be dissolved into a given reservoir. The actual volume of $CO_2$ that can be dissolved will also depend on the flow dynamics of the reservoir (Bradshaw et al. 2007). Groundwater flow is often very sluggish in deep aquifers and hence, without additional engineering (e.g. through pumping and extracting from various wells to manipulate fluid flow in the reservoir), $CO_2$ dissolution may be quite limited. On the other hand, as will be discussed in Section 7.3, the dissolution of $CO_2$ into, and the associated density increase of, formation fluids may kick-start further processes, such as large scale convection, which will in time act to increase the volume of $CO_2$ stored as a dissolved phase (Faisal et al. 2013).

In terms of pH, the work presented here is of significance as it indicates that even where carbonate minerals exist to buffer acidity caused by $CO_2$ dissolution, if transport becomes a limiting factor, pH will remain a good deal below that expected for equilibrium, as experienced in the dolomite and calcite experiments detailed in Section 4.2. Hence in areas where flow is low, e.g. far from the injection point, or where $CO_2$ is trapped in stagnant pockets

trailing the main plume, areas of low pH will persist and any assumptions on the rapid buffering of pH to high levels by carbonate minerals are likely to be misplaced.

## 7.2 The Long Haul: Mineral Interactions

### 7.2.1 Mineral Dissolution and Precipitation

Following the initial dissolution of $CO_2$ and rapid changes in pH discussed above, minerals in the host rock will begin to dissolve during and after injection of $CO_2$. This is likely to be a long-term, on-going process, particularly in silicate reservoirs, where movement toward equilibrium will be sluggish. The preceding chapters have presented the results from dissolution experiments on a number of important rock-forming minerals which are common in sandstone and carbonate reservoirs. When designing and monitoring GCS systems at an industrial scale, rates and equations derived from such experiments are necessary in predicting the behaviour of the target reservoir. As has been discussed in the preceding section, mineral dissolution will ultimately affect the solubility of $CO_2$ in the reservoir, the potential for long-term mineral trapping and, just as importantly, can have a major impact on aquifer properties such as permeability and porosity (Lamy-Chappuis & Angus 2014). Hence it is important to carefully consider the results from such experiments in the context of the problem to which they're being applied.

As has been discussed in Section 2.1, mineral dissolution rates are often derived from a variety of experimental types, though they can be broadly divided into two categories: the constant distance from equilibrium flow-through type experiment or the evolving batch type experiments (Allan et al. 2011; DePaolo et al. 2013). All of the results for single minerals presented here are from batch-type reactors, with a changing volume and an evolving fluid composition. This can allow study of any precipitation reactions and the changes in rate as a fluid moves towards equilibrium with the dissolving mineral, but can also mean that "true" rates are masked by precipitation effects or transport limitations, which are generally avoided in flow-through type experiments.

Which type of rate is applicable is entirely dependent on where in the GCS system attention is focused. Conditions will vary hugely from near the injection well to far-field. The area around the injection and immediately surrounding the main body of $CO_2$ is likely to be relatively dynamic, with a good deal of groundwater movement, especially if the system has been engineered to maximise contact between groundwater and $CO_2$. Here, the results from flow-through type experiments, which can maintain far from

equilibrium conditions and dissolution rates will be applicable. However, the system will also contain relatively stagnant areas, far from the injection well, where $CO_2$ saturated fluid is relatively static or where slow acting, density driven fluid movement is in effect. In these areas the chemistry of the pore-waters will move toward equilibrium and it is here that results from the type of experiments conducted in this work become more relevant. The temporal dimension should also be considered. While the experiments detailed here may be “approaching” equilibrium, dissolution rates are likely to vary dramatically on very close approach to equilibrium (Kampman et al. 2009; Arvidson & Luttge 2010). This reinforces the point that no single set of experimentally derived rates are sufficient to describe the entirety of a GCS system on a spatial and temporal scale and careful consideration is required when applying experimental rates to such systems.

From the results from single mineral experiments presented here, it appears that rates derived from batch experiments on quartz and feldspar are comparable to those predicted by equations derived from flow-through experiments, albeit with some discrepancies. A careful comparison between the experiments detailed here serves to highlight and explain some of these differences.

At low temperature and in deionised water the rates calculated for quartz dissolution from experiment 125 (22C, 4bar $pCO_2$), tend very closely to those calculated from the Tester et al. batch bottle experiment, which was carried out under very similar conditions. The addition of NaCl (experiment 121: 22C, 4bar $pCO_2$) acted to increase the quartz dissolution rate significantly, such that the calculated rates tend towards those produced by Tester et al. using a packed bed reactor, a set-up which, other conditions being equal, would be expected to produce relatively high dissolution rates, being maintained at a distance from equilibrium. The addition of NaCl has been noted to enhance quartz dissolution rates in past work (Blake & Walter 1999), though few experiments could be found carried out in solutions of ionic strength comparable to what may be expected in a GCS setting, making the striking increase in rate observed here (an increase of 1-2 log units) particularly worthy of note. These dissolution rates however are considerably (up to 2-3 log units) higher than the rates calculated using the general rate equation used as a comparison in this work (USGS 2004). The close agreement between the results produced here and those of Tester et al. suggest that as in those experiments sample preparation and lack of conditioning of the sample surface has caused this discrepancy (see Section

4.1.1.5). Further evidence for this lies in the fact that calculated dissolution rates for the higher temperature experiment (126: 31bar $pCO_2$, 70C) are much closer (within 0.5 log units), of the prediction of the general rate equation. At higher temperatures it would be assumed that annealing of the quartz surface will occur more rapidly, perhaps during the preconditioning stage, prior to $CO_2$ addition, thus removing higher energy sites, leading to dissolution rates more comparable to those predicted using general equations. Hence the results presented here for quartz dissolution are useful in terms of comparison of conditional effects, such as pressure, temperature etc. but the results from the lower temperature experiments are not expected to reflect dissolution rates in systems where the quartz surface is not fresh.

Comparison of the experimental results for the feldspars is more complex: feldspars have a more complex structure than quartz, with more elements available for relatively rapid surface exchange processes, which may mask “true” dissolution of the feldspar structure. Hence, where possible, dissolution rates produced here have been calculated based on Si release on the assumption that this reflects actual breakdown of the feldspar structure. This does however mean that dissolution of minor phases in the complex feldspars used (some albite in the K-feldspar material and vice-versa) could not be quantified accurately and that calculated dissolution rates must be assumed to apply to the bulk mineral, rather than individual, pure phases. For the majority of the K-feldspar experiments, calculated rates towards the end of the experiments fit the predictions made by the general rate equation (USGS 2004) very closely (generally within 0.1-0.2 log units). At earlier times calculated rates agree closely with those predicted using the equation of Burch et al. (1993) with the values produced by Hellmann & Tisserand (2006) for albite dissolution under elevated $pCO_2$ (90 bar). The experiments of Hellmann and Tisserand were carried out at a higher $pCO_2$ and temperature (150$^{o}$C) than those produced here and so it is not surprising that rates produced in these experiments are generally lower than those predicted using their rate constants. Where early time rates agree with those predicted using their values, it may be that the minor albitic component of the bulk mineral is dissolving relatively quickly, producing elevated dissolution rates.

Comparison of experimental K-feldspar dissolution rates with those predicted by the equation of Gautier et al. (1994) are less favourable: experimental rates are generally 2-3 orders of magnitude lower than those predicted using this equation. A clear explanation for this discrepancy could not be found, but

it is notable that this equation relies on having accurate information on ion activities and speciation (specifically for $AlOH^{-}_{4}$ and $H^{+}$). In this case of this work, these were calculated using PHREEQC. This introduces additional uncertainties into the calculation, relying as it does on the thermodynamic data used by PHREEQC rather than on direct empirical measurements. Perhaps more importantly (certainly for the experiments carried out using NaCl) accurate thermodynamic data (particularly for Al and Si species) to accurately carry out these calculations at elevated ionic strengths is not generally available (see Section 3.4.2), meaning that for the experiments carried out in brine a direct comparison to rates calculated using this data is not justified.

The results obtained for albite dissolution follow similar trends, with dissolution rates lying very close to those predicted using the general rate equation (USGS 2004) and that produced by Burch et al. (1993) and generally much lower than those suggested by the equation of Gautier et al. (1994). One feature of these experiments, not noted in the K-feldspar experiments, was that several of them became oversaturated with respect to quartz, kaolinite and gibbsite. No precipitate was noted in the final samples, but this is unsurprising given that any precipitation is likely to only have occurred in very small amounts. It is worth noting however, since feldspar dissolution in the experiments presented here appeared largely non-stoichiometric. Whether this was an effect of surface exchange processes or precipitation is not clear, but if precipitation were occurring, it may be that actual break-down of the feldspar was more rapid than the rates calculated here allow for and that the apparent dissolution is under-predicted due to this effect. If this were the case, the rates predicted by the equation of Gautier et al. (1994) may not be as erroneous as the presented data suggests.

Despite these complications, the behaviour of the silicate minerals in the experimental systems used here, appears to be relatively well predicted using available literature data and models. In these experiments, transport does not appear to be a limiting factor on dissolution. However, where transport is a limiting factor, as appears to be the case for the dolomite and calcite results presented here, mineral dissolution rates can be several orders of magnitude less than those predicted (see Figures 4.2.15 – 4.2.20 in Section 4.2.1). This discrepancy is true for all literature based rates and equations used. Predicted calcite dissolution rates are generally 2-3 log units lower than the nearest literature based rates (those predicted using the USGS general rate equation). Likewise dolomite rates are generally 2-2.5 log

units below the nearest literature based rates, though at very early times (high dolomite affinities) rates tend towards those predicted by the work presented in Pokrovsky & Schott (2001). The calcite and, to a lesser extent, the dolomite dissolution rates calculated from the experiments presented here exhibit a strong decrease with decreasing affinity, not generally predicted by the literature data. This is consistent with inhibition of dissolution at the carbonate surface, by rapid build-up of concentrations in solution at the mineral-fluid interface. Such inhibitive behaviour has been noted in natural carbonates previously (Svensson & Dreybrodt 1992) and it has been attributed to various mechanisms, including $Ca^{2+}$ adsorption (Svensson & Dreybrodt 1992) and bicarbonate concentrations (Busenberg & Plummer 1982). Given that the back reaction involving bicarbonate is already accounted for in the rates calculated using the equation of Busenberg & Plummer (1982) (see section 2.1.4), the model proposed by Svensson and Dreybodt, whereby surface occupancy if monopolised by $Ca^{2+}$, greatly lowering dissolution rates seems the more likely model in this case. In the experiments carried out by Svensson & Dreybrodt (1992) calcite dissolution rates were seen to drop dramatically for natural calcite samples relative to those predicted by, for example, the equation produced by L. N. L. Plummer et al. (1978) as $Ca^{2+}$ rose. While a surface transport affect along these lines seems likely in the case of the experiments presented here, its exact nature cannot easily be deduced from the available data. What the results do demonstrate however, is that carbonate dissolution, in some systems where transport is limited, can be extremely sluggish, much more so than might be predicted using rates and equations generally found in the literature.

Carbonate minerals can be of particular importance in GCS, since their dissolution will act to rapidly buffer the pH of $CO_2$ saturated fluids. Since carbonate dissolution is generally considered to be relatively rapid, their dissolution rates are also of great importance when assessing the likely impacts of $CO_2$ injection on formation properties such as porosity and permeability (Lamy-Chappuis & Angus 2014) and if in certain parts of the system, where transport is low, carbonate dissolution is likely to be considerably slower than might generally be assumed, this may have considerable implications for the design of such a system. For example, pH may remain relatively low, preventing further dissolution of $CO_2$ and more persistent acidity will have a knock on effect on the dissolution of other (i.e. silicate) minerals.

The results presented here on single mineral dissolution rates stress the fact that not all parts of an injection site may be considered equal and that the experimental sources of data used for prediction should be carefully considered when modelling different parts of a large scale GCS system.

Other factors to consider when assessing the applicability of these and experimental results to field systems include surface area calculations (White & Brantley 2003) and variations in mineral composition (Lu et al. 2013). All of the final mineral dissolution rates presented here have been carried out using BET surface areas, since this is considered the most realistic estimation of surface area available for reaction. Geometric estimates of surface area are often used in rate calculations and this can have a large impact on the final values calculated. For example, using a simple geometric estimate for surface area for the calculations used here, would increase calculated dissolution rates of dolomite in the batch experiments by 1-2 orders of magnitude. While more complex geometric estimates might include factors to compensate for surface roughness etc., thereby lowering calculated rates, it is important to bear in mind how surface areas are calculated when applying results to large scale systems. While the question of estimating reactive surface area is a complex subject and one that is unlikely to be satisfactorily resolved in the near future (Brantley 2008), it is important to at least be consistent in the manner of surface area estimation when applying laboratory derived rates to large-scale systems. Additional complications arise when considering how surface area may change as reactions progress; dissolution can act to greatly increase surface areas, even for relatively slow-reacting minerals such as feldspars, the surface area of which has been observed to increase up to 5x during dissolution experiments (Stillings & Brantley 1995). Such an increase would lead to a spuriously high dissolution rate. Hence, ideally, rates calculated from laboratory experiments should account for this change, through measurement of surface area both before and after reaction. This is rarely done however and was not done in this study.

In terms of mineral composition, laboratory derived dissolution rates tend to be measured for pure or near pure phases. This assists in elucidating fundamental dissolution processes and behaviours, but again it is worth bearing in mind that a real system is unlikely to behave in such an ideal manner. The feldspars used in the mineral dissolution experiments presented here are “complex”, in that they each contain significant amounts of another feldspar phase, as is often the case for feldspars in natural

systems (Lu et al. 2013). While bulk mineral dissolution rates, as predicted using literature derived equations have proved sufficient to predict the bulk mineral dissolution, what may be overlooked is the contribution the relatively minor phases might make to fluid composition. For example, calcium release from the minority phases in the K-feldspar material used here, far outstripped any other elemental release rate. While effects of such non-stoichiometric behaviour might be negligible in systems including carbonate minerals (such as the Sherwood Sandstone) it will have knock on effects on the dissolution rates of other minerals, overall fluid composition and hence $CO_2$ solubility. Hence, such complexities are worth considering, where predictions of fluid composition are required .

Precipitation of carbonate minerals is often cited as a long-term goal for GCS schemes, since it increases storage security (Matter & Kelemen 2009; Bachu et al. 1994). However, precipitation of such minerals is a long-term effect of GCS and is difficult to assess at the scales investigated in laboratory experiments. While some experimental studies have shown evidence for carbonate precipitation under elevated $pCO_2$ (e.g. Bateman, Rochelle, Lacinska, & Wagner, 2011; Fu et al., 2009), none of the experiments presented here show evidence for such. Partly, as discussed above, it is likely that any precipitation occurring would be in very small amounts over the timescales and in the systems investigated here, making them difficult to detect. However, over longer timescales and in natural systems where dissolved concentrations may build up relatively quickly due to the lower fluid:rock ratio, precipitation can have significant impact on aquifer properties, in much the same way that mineral dissolution will effect porosity and permeability, however once again it is important to apply such consideration appropriately. While such processes are of greater importance around the injection well, where clogging by precipitates may have a detrimental effect on injectivity,  the likelihood of them occurring is reduced in areas where flow is relatively high and dissolved solid concentrations do not have a chance to build up to levels sufficient for precipitation to occur. As the reaction front moves outward from the injection well and in more stagnant areas, where fluid-rock interaction can progress toward equilibrium the chances of precipitation may be higher, but again, as indicated by the experiments presented here, it seems unlikely that they will be of significance in conventional sandstone reservoirs in the short-term: none of the experiments detailed in this work showed evidence for significant mineral precipitation during reaction.

### 7.2.2 From Single Minerals to Whole Rock Reservoirs

As discussed above, the majority of mineral dissolution rates are calculated from experiments on single minerals. This is obviously necessary in order to understand the fundamental processes governing mineral dissolution, however comparison of these rates to “whole-rock” systems using the same experimental set-ups and within the same study are rare (e.g. Allan et al., 2011). Such comparisons are of fundamental importance to the prediction of behaviour in GCS systems since if such systems cannot be accurately modelled using the single mineral data available, a great deal of effort would need to be expended in specific characterisation and experimental work on each site.

Specific problems include mineral complexity and estimation of reactive surface area (as discussed in Section 7.2.1) and the surface area problem becomes even more acute as we move from powdered materials, where BET measurements are relatively straight-forward, to consolidated rocks, such as those used in experiments described in Section 5.2 (Scislewski & Zuddas 2010). While BET measurements in this work appear to be reasonably accurate (see section 3.4.2), the assumptions used in calculations of individual mineral surface areas in the sandstone material are more suspect, as they assume that surface area is distributed evenly based on molar weight. Such uncertainties were not quantified as part of this work, but certainly the division of surface area is one of the largest problems in predicting the behaviour of minerals as part of a bulk system. Such problems may be alleviated by careful characterisation of mineral surfaces under the microscope, or perhaps by preparing mineral separates from the bulk material and performing individual surface area measurements. Despite this, the relatively close agreement between the single mineral and bulk sandstone dissolution results in this work suggests that the assumptions used in calculation of surface area here were not drastically damaging to the comparison.

Additionally, while experimental work on single minerals is often carried out on treated samples, with relatively clean, unweathered surfaces, natural reservoirs will often be comprised of minerals which have been weathered, by passage of meteoric fluids through the reservoir for example. A good example of this is given in this work, where the quartz dissolution rates from the batch experiments are discussed (Sections 4.1.1 and 7.2.1). Here, quartz dissolution rates are relatively high, likely because the quartz surfaces are

fresh (having been powdered) and are slow to anneal at low temperatures. Where quartz surfaces are annealed, as would be the case in a sandstone aquifer, dissolution rates are expected to be a good deal slower (Tester et al. 1994). Further, dissolution experiments are often carried out in relatively pure fluids, deionised water or NaCl brines for example, while natural formation fluids will be, at least partially, in equilibrium with the whole rock assemblage, with relatively high concentrations of dissolved solids. This means that in many injection scenarios formation fluid, following saturation with $CO_2$, will be considerably closer to equilibrium than would be the case in a laboratory experiment where $CO_2$ saturated fluid is introduced directly to a dry mineral, which would initially produce relatively high, “far from equilibrium” reaction rates. While effects of lack of fluid:mineral prequilibration are not quantified here, the experiments presented in this work have attempted to, at least partially, negate such effects by subjecting the mineral and rock suspensions to a preconditioning period. Fluid samples taken prior to $CO_2$ injection show that this procedure was successful in shifting the systems towards fluid equilibrium (though few achieved full equilibrium in the time periods available).

The results of experiments carried out on powdered and consolidated sandstone material presented in this work go some way to addressing some of the uncertainties in applying single mineral rates to whole rocks. Results suggest that fluid chemistry, in the case of the Sherwood Sandstone-fluid-$CO_2$ is largely controlled by dolomite and K-feldspar dissolution. The comparison between results obtained from K-feldspar experiments and those carried out on the sandstone suggest that the majority of Si released from the sandstone is contributed by the K-feldspar, due to its higher dissolution rate and the fact that the quartz present in the sandstone is more likely to be annealed (i.e. have a lower surface energy) than the material used in the quartz dissolution experiments presented here.

While preferential release of Ca and Na from minor components in the K-feldspar present may well be occurring, such effects are negligible when considered in the context of a relatively high molar brine (1.36M NaCl in this case) and a carbonate bearing assemblage, where Ca concentrations are dominated by dolomite dissolution. Such results are important, as they allow simplifying assumptions to be made when modelling the system. If a target reservoir can be reasonably characterised by two or three, relatively reactive, minerals this will save great amounts of processor time when making “first-pass” estimates of how the reservoir is likely to behave during GCS. Despite

the increased uncertainty in surface area estimation inherent in using sandstone material which is texturally relatively complex, calculated dissolution rates for K-feldspar and dolomite from the sandstone experiments are comparable to those produced from single mineral experiments.

Modelled behaviour using the USGS general rate equation (USGS 2004), as would be inferred from the results of the single mineral experiments, predicts silicate dissolution in the sandstone closely (see Section 5.1.5), but over-predicts dolomite dissolution relative to that observed in the experiment. As discussed in Section 7.2.1, discrepancies between model and literature rates, and those produced from the experiments presented here for calcite and dolomite are almost certainly due to transport limitations.

Hence, we may say that the results from the single mineral presented here are applicable to whole rock dissolution under similar conditions, i.e. using powdered material and in a relatively low transport environment. Similar observations have been made elsewhere (Allan et al. 2011), but generally, comparative work on application of single mineral rates to whole rocks is lacking, at least partly because comparisons generally should be internal to a study, to avoid differences in experimental set-up and analysis which will affect the comparison of such results. Work such as this is important as it provides greater confidence in the modelling of natural systems and also highlights issues such as those of estimating surface area and the possible impact of transport effects, which should be carefully considered when using experimental results.

What, however, of application of such results to consolidated materials and in situations where fluid movement is relatively high, as opposed to the static nature of the batch experiments? The results presented here from the flow-through experiment on a sandstone core, show relatively high dolomite and K-feldspar dissolution rates when compared to the batch experiments. This is to be expected for the dolomite, dissolution of  which appeared transport limited in the batch experiments, and indeed the dolomite dissolution rates calculated for the flow-through experiment compare much more favourably (generally within 0.5 log units) with the rates predicted using the work of Pokrovsky & Schott (2001) and Gautelier et al. (2007) than the rates calculated in the batch experiments which would seem to confirm a heavy transport limitation.

The discrepancy in K-feldspar dissolution rates (of around 0.5 log units) is more difficult to reconcile. While the effects of grinding to produced powdered materials for the batch experiments may have played a part, also of concern is, once again, estimation of surface area. In the case of the consolidated rock experiments presented, surface area was necessarily estimated using various geometric assumptions, likely to produce a relatively high dissolution rate. Similar problems are encountered when assessing the surface area available for reaction in a potential $CO_2$ reservoir. Again, the key is consistency: the results presented here highlight the fact no matter how good the measurement of surface area on single minerals during dissolution experiments is, poor estimation of surface area in the system to which they are being applied will lead to discrepancies. Such results may be used as an argument for greater prevalence of the use of geometric surface areas when interpreting the results from dissolution experiments, since more realistic BET surface areas are unlikely to be available for actual reservoir materials. Also of note is that silica data was unavailable for this experiment and K-feldspar dissolution was instead estimated based on potassium release. Hence these rates may not represent true dissolution of the mineral matrix, but rather preferential release of $K^+$ from the mineral structure, producing spuriously high dissolution rates.

Another possibility is that due to the relatively dynamic nature of the flow-through experiment (in terms of fluid and hence dissolved solid movement) and hence the relatively low analyte concentrations, prevented inhibition of feldspar dissolution by elevated Al concentrations, which may occur during batch experiments where fluids are more evolved (Oelkers et al. 1994). This, once again highlights the need for careful consideration of where in a particular system, particular rates are applied. Additionally, careful consideration of the distance from equilibrium of the system is required. It is well documented that natural systems tend to exhibit very low dissolution rates relative to laboratory experiments and it has been suggested that this is due, at least in part, to the close to equilibrium nature of the reactions occurring in natural reservoirs (Kampman et al. 2009).

The preceding pages have highlighted some of the difficulties in using single mineral data to predict whole rock dissolution. From the results presented in this thesis however, it is evident that such predictions can be made with reasonable accuracy, despite simplifying assumptions of surface area, as long as these assumptions and the experimental set-up used to generate the

single mineral rates are considered carefully when applying them to other systems.

## 7.3 Meanwhile…: The Effect of Density Plumes on GCS

While solubility trapping, as discussed in Section 7.1 will act to make stored $CO_2$ relatively secure in the short term and mineral dissolution and precipitation may increase security in the long term, the migration of $CO_2$ saturated fluid away from the main $CO_2$ body may have great impact on GCS shortly after $CO_2$ dissolution. Fluid movement, driven by density changes where $CO_2$ has saturated formation brines will act to remove $CO_2$ saturated fluid from the immediate injection vicinity and allow upwelling of fresh brine, which in turn can become saturated, a cycle which will act to greatly enhance the overall storage potential of any reservoir. Moreover, movement of plumes, driven as they are by gravity, will be largely downward, away from the cap-rock, greatly reducing the likelihood of compromising cap-rock integrity through dissolution or degassing of $CO_2$ from solution due to pressure drops (Faisal et al. 2013; Kneafsey & Pruess 2011).

The experiments presented in Chapter 6 of this work serve to illustrate how such processes may be studied successfully in a laboratory setting. Such work has been fairly scant so far and the results presented here, together with those presented by Kneafesy and Pruess, indicate that while migration of density plumes is a will be relatively slow at the permeabilities common to most sandstone reservoirs, current models underestimate the speed of migration of such plumes, though modelling work carried out by others has had more success in recreating the results produced using Hele-Shaw cells (e.g. Faisal et al., 2013).

The laboratory experiments presented here suggest that density instabilities form relatively rapidly following $CO_2$ dissolution. For example Figure 6.3.2 in Section 6.3, shows that numerous instabilities have formed within 30 minutes of $CO_2$ being introduced to a cell. Complete “turnover”, i.e. cell scale convection of fluid, is achieved within 16 hours (Figure 6.3.6). These processes will act to move saturated fluid away from the main plume body at rates much higher than would be achieved through diffusion, or natural groundwater movement alone.

The experiments also indicate that heterogeneities, whether physical or chemical, can act to focus and greatly increase the rapidity of movement of $CO_2$ saturated fluids. Figure 6.2.6 in Section 6.2 illustrates such an effect; where a small streak of contamination in the centre of the cell acted as a

conduit for rapid movement of plumes to the base of the cell. Such effects will be of particular importance in natural reservoirs where heterogeneities, such as zones of increased permeability, are likely to be commonplace. Conversely, horizontal layers of low permeability material will act in the opposite direction, cutting off density driven convection. Hence, a proper understanding of aquifer heterogeneity, one which can be built into numerical models, is essential for modelling such systems, if the maximum storage potential of a reservoir is to be reasonably predicted.

The experiments presented here using Hele-Shaw cells, demonstrate not only how information regarding plume movement can be generated from such experiments (information that is vital to the ground-truthing of predictive models), but also how, with careful experimental design, these cells can also provide relatively high resolution data on the generation and movement of pH gradients within such systems. Previous work has generally ignored this potentially useful aspect of the experiments and it is hoped that future work will make use of the experimental designs described here in more closely investigating these processes.

# Chapter 8
# Conclusions and Future Work

Quartz dissolution experiments carried out at elevated $pCO_2$ indicate that quartz dissolution has little ability to buffer pH or affect $CO_2$ solubility following injection of $CO_2$. Dissolution of quartz is enhanced in NaCl fluids relative to pure water, by around one order of magnitude at the conditions used here. A similar increase in dissolution rate is seen as temperature and $pCO_2$ are increased from 22°C to 70°C and 4 bar to 31 bar. Calculated dissolution rates for the quartz material agree well with values predicted using the equation from Tester et al (1995), but are relatively high for quartz dissolution in general and the USGS general rate equation used for comparison consistently under-predicts observed dissolution rates. It is believed that this is due to lack of annealing of the quartz surface, leading to abnormally high dissolution rates.

Stirring tests carried out on K-feldspar show the effect of mechanical stirring on observed dissolution rates: increasing surface area during the stirred experiment caused an increase in observed dissolution rate of over three orders of magnitude. While grain size changes on the order of 100µm have no effect on K-feldspar dissolution under elevated $pCO_2$, rates are depressed in NaCl bearing fluids relative to deionised water by around 5x. Increasing experimental temperature and $pCO_2$ from 22°C - 70°C and 4 bar to 31 bar, increase observed dissolution rates by 1 – 2 orders of magnitude. The USGS general rate equation and the feldspar specific equation of Burch et al (1993) both provide predictions in good agreement with observed dissolution rates, while the equation of Gautier et al (1994) over-predicts the observed rate, likely due to its reliance on calculated activities, which must be estimated using a speciation model such as PHREEQC.

Variations in grain size have more effect on the dissolution of the albite material used here than on the K-feldspar: at low pressures and temperatures finer fractions show higher dissolution rates (around 5x higher), while at increased pressure and temperature the coarser fraction has higher (around 5x) dissolution rates at late times. The reason for this behaviour is unclear. As for K-feldspar, albite dissolution rates are depressed in NaCl bearing fluids relative to deionised water by up to one order of magnitude. Bulk mineral dissolution rates are generally higher at increased temperature and $pCO_2$. Increased $pCO_2$ has a direct effect only on K release from the K-feldspar component within the albite, increases in bulk dissolution rate are

largely due to the temperature increase. As for K-feldspar, rate predicted by the USGS general rate equation and the equation from Burch et al (1993) agree well with observed rates, while that of Gautier et al (1994) over-predicts observed rates.

While calcite and dolomite dissolution under elevated $pCO_2$ has the ability to buffer pH to higher values, dissolution levels off well before pH is increased to the predicted equilibrium values. While variations in grain size on the order of 100µm have no effect on calcite or dolomite dissolution, calcite dissolution rates are apparently enhanced in NaCl bearing fluids relative to deionised water. Calcite and dolomite dissolution is inhibited by transport effects, meaning that observed effects of increased $pCO_2$ and temperature are minimal and that observed rates are all significantly below those predicted using various literature equations. These results highlight the sluggish nature of carbonate dissolution in areas of GCS reservoirs where flow is low.

Sherwood Sandstone dissolution under elevated $pCO_2$ is largely dominated by dissolution of dolomite and K-feldspar. Similar to the results of the single mineral experiments dissolution of the feldspar component is enhanced using finer grain fractions and dissolution of dolomite is depressed in NaCl bearing fluids relative to deionised water. K-feldspar and dolomite dissolution rates are in good agreement with calculated rates from single mineral experiments at late times, showing that results from single mineral experiments can be used to predict the behaviour of more complex rock compositions successfully. Kinetic modelling of sandstone dissolution using the USGS general rate equation predicts K-feldspar dissolution reasonably well, but under-predicts dolomite dissolution, again due to transport effects, reinforcing the importance of considering the system in question when applying literature derived dissolution rates.

Dolomite dissolution in the flow-through experiments was similar to predictions made using literature based equations, indicating that under flowing conditions transport effects are minimised. K-feldspar dissolution rates were also apparently higher under flowing conditions, though this may have been an artefact of the method used to estimate geometric surface area. This highlights the importance of consistency in methods used to calculate reactive surface area in reservoirs where direct BET measurements are impossible. Dolomite dissolution under flowing conditions is considerable, and it is thought that the 2% increase in porosity and the shift

in pore-size distribution of the reacted core was due largely to loss of dolomite.

Use of Hele-Shaw cells can be used successfully to visualise density driven flow caused by relatively dense $CO_2$ saturated fluids. $CO_2$ saturation is observed indirectly, via pH, using pH indicator solution. Results from these experiments highlight the sluggish nature of this process and the retarding effect of NaCl bearing fluids on plume formation and movement relative to deionised water. Physio-chemical heterogeneities in such systems greatly enhance the focus and transport of $CO_2$ saturated fluids. Results also indicate that predictive modelling of such plumes may under-estimate the rapidity of their formation in and movement through porous media. The methodological work presented here also demonstrates how Hele-Shaw cells can be used to observe relatively small gradients in pH, which will occur within such systems as acidified pore-waters migrate. These cells have not been used in this manner in previous work, despite the importance of pH in GCS in terms of mineral dissolution and ion exchange and it is hoped that future work with Hele-Shaw cells can expand upon the experimental methods presented here to investigate these processes further and compare the results with more detailed geochemical modelling.

Many of the uncertainties, and hence focus for future work, in predicting geochemical behaviour during GCS are the same uncertainties inherent in the understanding of many natural geochemical systems. Perhaps most fundamental of these are the questions of estimation of reactive surface area and the relative distance from equilibrium of natural systems compared to those studied in the lab (White & Brantley 2003; Wigley et al. 2013; Kampman et al. 2009). While a great deal of work comparing the various merits of different measurements of surface area is ongoing (e.g. M.E. Hodson, 2006) and the debate over how best to estimate surface area is likely to continue for many years to come, as has already been mentioned, key to any approach of this problem is consistency in the measurement and application of surface areas. The effect of close approach to equilibrium on dissolution rates is likewise an area of continued research and debate, but such effects are fundamental to our understanding of the behaviour of natural systems. Recent work has taken advantage of advanced interferometry techniques in order to measure dissolution rates at very near to equilibrium conditions: rates which would be very difficult to measure using traditional batch experiments due to the very small mass transfers involved (e.g. Arvidson & Luttge, 2010).

More directly related to GCS is the question of the effect of density plumes on overall storage of $CO_2$. As has been discussed in Chapters 6 & 7, relatively minor heterogeneities can have a huge impact on the formation and migration of dense plumes of $CO_2$ saturated fluid. A better understanding of how heterogeneities will effect plumes will allow improved targeting of reservoirs likely to be conducive to enhanced movement of plumes, which in turn has the potential to greatly increase the volume and security of storage. Further laboratory based experiments coupled with more complex modelling work would greatly enhance our understanding of these processes.

# Bibliography

Akinfiev, N.N. & Diamond, L.W., 2010. Thermodynamic model of aqueous CO2-H2O-NaCl solutions from-22 to 100 °C and from 0.1 to 100 MPa. *Fluid Phase Equilibria*, In Press, (1), pp.104–124.

Alekseyev, V. a. et al., 1997. Change in the dissolution rates of alkali feldspars as a result of secondary mineral precipitation and approach to equilibrium. *Geochimica et Cosmochimica Acta*, 61(6), pp.1125–1142.

Allan, M.M., Turner, A. & Yardley, B.W.D., 2011. Relation between the dissolution rates of single minerals and reservoir rocks in acidified pore waters. *Applied Geochemistry*, 26(8), pp.1289–1301.

Anbeek, C., 1992. The dependence of dissolution rates on grain size for some fresh and weathered feldspars. *Geochimica et Cosmochimica Acta*, 56(11), pp.3957–3970.

Arvidson, R.S. & Luttge, A., 2010. Mineral dissolution kinetics as a function of distance from equilibrium – New experimental results. *Chemical Geology*, 269(1-2), pp.79–88.

Bachu, S., 2002. From Regional Characterization to Site Selection. *Energy Conversion and Management*, 41(9), pp.87–102.

Bachu, S. & Adams, J.J., 2003. Sequestration of CO2 in geological media in response to climate change: capacity of deep saline aquifers to sequester CO2 in solution. *Energy Conversion and Management*, 44(20), pp.3151–3175.

Bachu, S. & Bennion, B., 2008. Effects of in-situ conditions on relative permeability characteristics of CO2-brine systems. *Environmental Geology*, 54(8), pp.1707–1722.

Bachu, S., Gunter, W.D. & Perkins, E.H., 1994. Aquifer disposal of CO2: Hydrodynamic and mineral trapping. *Energy Conversion and Management*, 35(4), pp.269–279.

Baines, S.J. & Worden, R.H., 2004. The long-term fate of CO2 in the subsurface: natural analogues for CO2 storage. *Geological Society, London, Special Publications*, 233(1), pp.59–85.

Bateman, K. et al., 2011. CO2-porewater-rock reactions-Large-scale column experiment (Big Rig II). *Energy Procedia*, pp.0–7.

Berg, A. & Banwart, S. a., 2000. Carbon dioxide mediated dissolution of Ca-feldspar: implications for silicate weathering. *Chemical Geology*, 163(1-4), pp.25–42.

Blake, R. & Walter, L., 1999. Kinetics of feldspar and quartz dissolution at 70–80 C and near-neutral pH: effects of organic acids and NaCl. *Geochimica et Cosmochimica Acta*, 63(13), pp.2043–2059.

Bradshaw, J. et al., 2007. CO2 storage capacity estimation: Issues and development of standards. *International Journal of Greenhouse Gas Control*, 1(1), pp.62–68.

Brady, P. V. & Walther, J. V., 1990. Kinetics of quartz dissolution at low temperatures. *Chemical Geology*, 82, pp.253–264.

Brantley, S., 2008. Kinetics of mineral dissolution. In *Kinetics of water-rock interaction*.

Brantley, S.L. & Stillings, L., 1996. Feldspar dissolution at 25 degrees C and low pH. *Am J Sci*, 296(2), pp.101–127.

British Geological Survey, 1985. *Cleethorpes No. 1 Geothermal Well - a preliminary assessment of the resource*,

British Geological Survey, 2006. *Industrial Carbon Dioxide Emissions and carbon Dioxide Storage Potential in the UK*,

Burch, T.E., Nagy, K.L. & Lasaga, A.C., 1993. Free energy dependence of albite dissolution kinetics at 80 ° C. *Chemical Geology*, 105(1-3), pp.137–162.

Burley, S., 1984. Patterns of diagenesis in the Sherwood Sandstone Group (Triassic), United Kingdom. *Clay Minerals*, pp.403–440.

Busenberg, E. & Clemency, C. V, 1976. The dissolution kinetics of feldspars at 25°C and 1 atm CO2 partial pressure. *Geochimica et Cosmochimica Acta*, 40(1), pp.41–49.

Busenberg, E. & Plummer, L.N., 1982. The kinetics of dissolution of dolomite in CO 2 -H 2 O systems at 1.5 to 65 degrees C and O to 1 atm PCO 2. *American Journal of Science*, 282, pp.45–78.

Carroll, S.A. & Knauss, K.G., 2005. Dependence of labradorite dissolution kinetics on CO2(aq), Al(aq), and temperature. *Chemical Geology*, 217(3-4), pp.213–225.

Celia, M.A. & Nordbotten, J.M., 2009. Practical modeling approaches for geological storage of carbon dioxide. *Ground Water*, 47(5), pp.627–638.

Choo, W.L., Jeffrey, M.I. & Robertson, S.G., 2006. Analysis of leaching and cementation reaction kinetics: Correcting for volume changes in laboratory studies. *Hydrometallurgy*, 82(1-2), pp.110–116.

Chou, L., Garrels, R. & Wollast, R., 1989. Comparative study of the kinetics and mechanisms of dissolution of carbonate minerals. *Chemical Geology*, 78, pp.269–282.

Crockford, P. & Telmer, K., 2011. Dissolution Kinetics of Keg River dolomites and implications for spectra energy's Fort Nelson CCS project. *Energy Procedia*.

Crowe, A. & Longstaffe, F., 1987. Extension of geochemical modelling techniques to brines: coupling of the Pitzer equations to PHREEQE. *Proc. of the National Water Well Conf. on ….*

Deer, Howie & Zussman, 1992. *The Rock Forming Minerals*,

DePaolo, D.J. et al., 2013. *Geochemistry of Geologic CO2 Sequestration*,

Dove, P.M. & Crerar, D. a., 1990. Kinetics of quartz dissolution in electrolyte solutions using a hydrothermal mixed flow reactor. *Geochimica et Cosmochimica Acta*, 54(4), pp.955–969.

Dreybrodt, W., Lauckner, J. & Zaihua, L., 1996. The kinetics of the reaction CO2+ H2O--> H++ HCO3-as one of the rate limiting steps for the dissolution of calcite in the system H2O---CO2---CaCO3. *Geochimica et Cosmochimica Acta*, 60(18), pp.3375–3381.

Duan R., Z. and S., 2003. An improved model calculating CO2 solubility in pure water and aqueous NaCl solutions from 273 to 533 K and from 0 to 2000 bar. *Chemical Geology*, 193, pp.257–271.

Duan, Z. et al., 2006. An improved model for the calculation of CO2 solubility in aqueous solutions containing Na+, K+, Ca2+, Mg2+, Cl-, and SO42. *Marine Chemistry*, 98(2-4), pp.131–139.

Van Eldik, R. & Palmer, D., 1982. Effects of pressure on the kinetics of the dehydration of carbonic acid and the hydrolysis of CO 2 in aqueous solution. *Journal of Solution Chemistry*, 11(5), pp.339–346.

Ennis-King, J.P. & Paterson, L., 2005. Role of Convective Mixing in the Long-Term Storage of Carbon Dioxide in Deep Saline Formations. *SPE Journal*, 10(3), pp.pp. 349–356.

Faisal, T.F., Chevalier, S. & Sassi, M., 2013. Experimental and Numerical Studies of Density Driven Natural Convection in Saturated Porous Media with Application to CO2 geological storage. *Energy Procedia*, 37, pp.5323–5330.

Fu, Q. et al., 2009. Coupled alkali-feldspar dissolution and secondary mineral precipitation in batch systems: 1. New experiments at 200 °C and 300 bars. *Chemical Geology*, 258(3–4), pp.125–135.

Gale, J., 2004. Why do we need to consider geological storage of CO2. *Geological Society, London, Special Publications*, 233(1), pp.7–15.

Gaus, I. et al., 2007. Geochemical and solute transport modelling for CO2 storage, what to expect from it? In *4th Trondheim Conference on CO2 Capture, Transport and Storage*. Trondheim, NORWAY: Elsevier Sci Ltd, pp. 605–625.

Gaus, I., 2010. Role and impact of CO2–rock interactions during CO2 storage in sedimentary rocks. *International Journal of Greenhouse Gas Control*, 4(1), pp.73–89.

Gautelier, M., Oelkers, E.H. & Schott, J., 1999. An experimental study of dolomite dissolution rates as a function of pH from -0.5 to 5 and temperature from 25 to 80C.

Gautelier, M., Schott, J. & Oelkers, E., 2007. An experimental study of dolomite dissolution rates at 80 °C as a function of chemical affinity and solution composition. *Chemical Geology*, 242(3-4), pp.509–517.

Gautier, J., Oelkers, E. & Schott, J., 2001. Are quartz dissolution rates proportional to BET surface areas? *Geochimica et Cosmochimica Acta*, 65(7), pp.1059–1070.

Gautier, J.-M., Oelkers, E.H. & Schott, J., 1994. Experimental study of K-feldspar dissolution rates as a function of chemical affinity at 150°C and pH 9. *Geochimica et Cosmochimica Acta*, 58(21), pp.4549–4560.

Gilfillan et. al., S.M. V, 2009. Solubility Trapping in formation water as dominant CO2 sink in natural gas fields. *nature*, 458(April 2009), pp.614–618.

Gunter, W.D., Bachu, S. & Benson, S., 2004. The role of hydrogeological and geochemical trapping in sedimentary basins for secure geological storage of carbon dioxide. *Geological Society, London, Special Publications*, 233(1), pp.129–145.

Helgeson, H.C., Murphy, W.M. & Aagaard, P., 1984. Thermodynamic and kinetic constraints on reaction rates among minerals and aqueous solutions. II. Rate constants, effective surface area, and the hydrolysis of feldspar. *Geochimica et Cosmochimica Acta*, 48(12), pp.2405–2432.

Hellmann, R., Daval, D. & Tisserand, D., 2010. The dependence of albite feldspar dissolution kinetics on fluid saturation state at acid and basic pH: Progress towards a universal relation. *Comptes Rendus Geoscience*, 342(7-8), pp.676–684.

Hellmann, R. & Tisserand, D., 2006. Dissolution kinetics as a function of the Gibbs free energy of reaction: An experimental study based on albite feldspar. *Geochimica et Cosmochimica Acta*, 70(2), pp.364–383.

Hemingway, B.S. & Robie, R.A., 1994. Enthalpy and Gibbs energy of formation of dolomite, CaMg(C03 ) 2 , at 298.15 K from HC1 solution calorimetry. *USGS publication*.

Herman, J.S. & White, W.B., 1985. Dissolution kinetics of dolomite: Effects of lithology and fluid flow velocity. *Geochimica et Cosmochimica Acta*, 49(10), pp.2017–2026.

Hodson, M.E., 2006. Does reactive surface area depend on grain size? Results from pH 3, 25°C far-from-equilibrium flow-through dissolution experiments on anorthite and biotite. *Geochimica et Cosmochimica Acta*, 70(7), pp.1655–1667.

Hodson, M.E., 2006. Searching for the perfect surface area normalizing term—a comparison of BET surface area-, geometric surface area- and mass-normalized dissolution rates of anorthite and biotite. *Journal of Geochemical Exploration*, 88(1-3), pp.288–291.

Hodson, M.E., Langan, S.J. & Meriau, S., 1998. Determination of mineral surface area in relation to the calculation of weathering rates. *Geoderma*, 83(1-2), pp.35–54.

Hovorka, S.D. et al., 2006. Measuring permanence of CO2 storage in saline formations: the Frio experiment. *Environmental Geosciences*, 13(2), pp.105–121.

IPCC, 2005. *Carbon Dioxide Capture and Storage*, Cambridge University Press.

Juanes, R. et al., 2006. Impact of relative permeability hysteresis on geological CO2 storage. *Water Resour. Res.*, 42.

Kampman, N. et al., 2009. Feldspar dissolution kinetics and Gibbs free energy dependence in a CO2-enriched groundwater system, Green River, Utah. *Earth and Planetary Science Letters*, 284(3-4), pp.473–488.

Kaszuba, J.P., Yardley, B.W.D. & Andreani, M., 2013. Experimental perspectives of mineral dissolution and precipitation due to carbon dioxide-water-rock interactions. *Reviews in Mineralogy and Geochemistry*, 77, pp.153–188.

Kieffer, B. et al., 1999. An experimental study of the reactive surface area of the Fontainebleau sandstone as a function of porosity, permeability, and fluid flow rate. *Geochimica et Cosmochimica Acta*, 63(21), pp.3525–3534.

Kneafsey, T.J. & Pruess, K., 2011. Laboratory experiments and numerical simulation studies of convectively enhanced carbon dioxide dissolution. *Energy Procedia*, 4(0), pp.5114–5121.

Kumar, A. et al., 2004. Reservoir Simulation of CO2 Storage in Deep Saline Aquifers. *SPE/DOE Symposium on Improved Oil Recovery*.

Lagache, M., 1976. New data on the kinetics of the dissolution of alkali feldspars at 200°C in CO2 charged water. *Geochimica et Cosmochimica Acta*, 40(2), pp.157–161.

Lamy-Chappuis, B. & Angus, D., 2014. Rapid porosity and permeability changes of calcareous sandstone due to CO2-enriched brine injection. *Geophysical …*, (Figure 1), pp.399–406.

Lu, P. et al., 2013. Coupled alkali feldspar dissolution and secondary mineral precipitation in batch systems – 2: New experiments with supercritical CO2 and implications for carbon sequestration. *Applied Geochemistry*, 30, pp.75–90.

Al Mansoori, S.K. et al., 2009. Measurements of non-wetting phase trapping applied to carbon dioxide storage. *International Journal of Greenhouse Gas Control*, 4(2), pp.283–288.

Martinez, M. & White, W., 1999. A laboratory investigation of the relative dissolution rates of the Lirio Limestone and the Isla de Mona Dolomite and implications for cave and karst development. *… of Cave and …*, 61(April), pp.7–12.

Matter, J.M. & Kelemen, P.B., 2009. Permanent storage of carbon dioxide in geological reservoirs by mineral carbonation. *Nature Geosci*, 2(12), pp.837–841.

Metz, V. & Ganor, J., 2001. Stirring effect on kaolinite dissolution rate. *Geochimica et Cosmochimica Acta*, 65(20), pp.3475–3490.

Michael, K. et al., 2009. CO2 storage in saline aquifers I--Current state of scientific knowledge. *Energy Procedia*, 1(1), pp.3197–3204.

Morse, J.W. & Arvidson, R.S., 2002. The dissolution kinetics of major sedimentary carbonate minerals. *Earth-Science Reviews*, 58(1-2), pp.51–84.

Neufeld, J. a. et al., 2010. Convective dissolution of carbon dioxide in saline aquifers. *Geophysical Research Letters*, 37(22), pp.2–6.

Neufeld, J. a. & Huppert, H.E., 2009. Modelling carbon dioxide sequestration in layered strata. *Journal of Fluid Mechanics*, 625, p.353.

Newton, R.C. & Manning, C.E., 2000. Quartz solubility in H2O-NaCl and H2O-CO2 solutions at deep crust-upper mantle pressures and temperatures: 2–15 kbar and 500–900°C. *Geochimica et Cosmochimica Acta*, 64(17), pp.2993–3005.

Oelkers, E. & Schott, J., 1995. Experimental study of anorthite dissolution and the relative mechanism of feldspar hydrolysis. *Geochimica et Cosmochimica Acta*, 59(24), pp.5039–5053.

Oelkers, E., Schott, J. & Devidal, J., 2001. interpretation of closed system mineral dissolution experiments: comment on “Mechanism of kaolinite dissolution at room temperature and pressure part II: *Geochimica et cosmochimica acta*, 65(23), pp.4429–4432.

Oelkers, E.H., Schott, J. & Devidal, J.-L., 1994. The effect of aluminum, pH, and chemical affinity on the rates of aluminosilicate dissolution reactions. *Geochimica et Cosmochimica Acta*, 58(9), pp.2011–2024.

Oloruntobi, O.S. & LaForce, T.C., 2009. Effect of Aquifer Heterogeneity on CO2 Sequestration. *EUROPEC/EAGE Conference and Exhibition*.

Palmer, A., 1991. Origin and morphology of limestone caves. *Geological Society of America Bulletin*.

Parkhurst, D. & Appelo, C., 2013. Input and Examples for PHREEQC Version 3--a Computer Program for Speciation, Batch-reaction, One-dimensional Transport, and Inverse Geochemical. *Groundwater Book*.

Plummer, L., Wigley, T.M.L. & Parkhurst, D., 1978. The kinetics of calcite dissolution in CO2-water systems at 5C to 60C and 0.0 to 1.0 atm CO2. *American Journal of Science*, 278, pp.179–216.

Plummer, L.N., Busenberg, E. & Survey, U.S.G., 1982. The solubilities of calcite, aragonite and vaterite in CO2-H2O solutions between 0 and 90°C, and an evaluation of the aqueous model for the system CaCO3-CO2-H2O. *Geochimica et Cosmochimica Acta*, 46(6), pp.1011–1040.

Plummer, L.N.L. et al., 1978. The kinetics of calcite dissolution in CO2 -water systems at 5 degrees to 60 degrees C and 0.0 to 1.0 atm CO2. *American Journal of Science*, 278(2), pp.179–216.

Plunder, a. et al., 2012. How continuous and precise is the record of P-T paths? Insights from combined thermobarometry and thermodynamic modelling into subduction dynamics (Schistes Lustrés, W. Alps). *Journal of Metamorphic Geology*, 30(3), pp.323–346.

Pokrovsky, O. & Schott, J., 2001. Kinetics and mechanism of dolomite dissolution in neutral to alkaline solutions revisited. *American Journal of Science*, 301(September), pp.597–626.

Pokrovsky, O., Schott, J. & Thomas, F., 1999. Dolomite surface speciation and reactivity in aquatic systems. *Geochimica et cosmochimica acta*, 63(19), pp.3133–3143.

Pokrovsky, O.S. et al., 2009. Calcite, dolomite and magnesite dissolution kinetics in aqueous solutions at acid to circumneutral pH, 25 to 150 °C and 1 to 55 atm pCO2: New constraints on CO2 sequestration in sedimentary basins. *Chemical Geology*, 265(1-2), pp.20–32.

Pokrovsky, O.S., Golubev, S. V. & Schott, J., 2005. Experimental determination of the effect of dissolved CO2 on the dissolution kinetics of Mg and Ca silicates at 25 8C. *Chemical Geology*, 217(3-4), pp.239–255.

Portier, S. & Rochelle, C., 2005. Modelling CO2 solubility in pure water and NaCl-type waters from 0 to 300 °C and from 1 to 300 bar: Application to the Utsira Formation at Sleipner. *Chemical Geology*, 217(3-4), pp.187–199.

Rochelle, C.A., Czernichowski-Lauriol, I. & Milodowski, A.E., 2004. The impact of chemical reactions on CO2 storage in geological formations: a brief review. *Geological Society, London, Special Publications*, 233(1), pp.87–106.

Rosenqvist, J., Kilpatrick, A.D. & Yardley, B.W.D., 2012. Solubility of carbon dioxide in aqueous fluids and mineral suspensions at 294K and subcritical pressures. *Applied Geochemistry*, 27(8), pp.1610–1614.

Saylor, B.Z. & Zerai, B., 2004. Injection and trapping of carbon dioxide in deep saline aquifers. *Geological Society, London, Special Publications*, 236(1), pp.285–296.

Sciences, A., 1999. The dissolution kinetics of quartz in aqueous mixed cation solutions. , 63(22), pp.3715–3727. Available at: http://www.geochem.geos.vt.edu/bgep/pubs/99 dove_geochimica cosmochimica acta.pdf [Accessed April 11, 2014].

Scislewski, A. & Zuddas, P., 2010. Estimation of reactive mineral surface area during water–rock interaction using fluid chemical data. *Geochimica et Cosmochimica Acta*, 74(24), pp.6996–7007.

Sherman, L.A. & Barak, P., 2000. Solubility and dissolution kinetics of dolomite in Ca-Mg-HCO3/CO3 Solutions at 25C and 0.1MPa Carbon Dioxide. *Soil Science Society of America Journal*, 64(1978), pp.1959–1968.

Shmulovich, K.I., Yardley, B.W.D. & Graham, C.M., 2006. Solubility of quartz in crustal fluids: experiments and general equations for salt solutions and H2O-CO2 mixtures at 400-800oC and 0.1-0.9 GPa. *Geofluids*, 6(2), pp.154–167.

Spycher, N. & Pruess, K., 2005. CO2-H2O mixtures in the geological sequestration of CO2. II. Partitioning in chloride brines at 12-100°C and

up to 600 bar. *Geochimica et Cosmochimica Acta*, 69(13), pp.3309–3320.

Stillings, L. & Brantley, S., 1995. Feldspar dissolution at 25 C and pH 3: Reaction stoichiometry and the effect of cations. *Geochimica et Cosmochimica Acta*, 59(X).

Svensson, U. & Dreybrodt, W., 1992. Dissolution kinetics of natural calcite minerals in CO2-water systems approaching calcite equilibrium. *Chemical Geology*, 100(1-2), pp.129–145.

Tester, J.W. et al., 1994. Correlating quartz dissolution kinetics in pure water from 25 to 625°C. *Geochimica et Cosmochimica Acta*, 58(11), pp.2407–2420.

USGS, 2004. *A compilation of rate parameters of water-mineral interaction kinetics for application to geochemical modelling*,

Velbel, M. a. & Losiak, a. I., 2008. Influence of surface-area estimation on rates of plagioclase weathering determined from naturally weathered 3400 y old Hawaiian basalt. *Mineralogical Magazine*, 72(1), pp.91–94.

White, A.F. & Brantley, S.L., 2003. The effect of time on the weathering of silicate minerals: why do weathering rates differ in the laboratory and field? *Chemical Geology*, 202(3-4), pp.479–506.

Wigley, M. et al., 2013. Controls of sluggish, CO2-promoted, hematite and K-feldspar dissolution kinetics in sandstones. *Earth and Planetary Science Letters*, 362, pp.76–87.

Wilkinson, M. et al., 2009. CO2-Mineral Reaction in a Natural Analogue for CO2 Storage--Implications for Modeling. *Journal of Sedimentary Research*, 79(7), pp.486–494.

Worley, W.G., 1994. *Dissolution kinetics and mechanisms in quartz and granite systems*.

Xu, T. et al., 2010. Reactive transport modeling to study changes in water chemistry induced by CO2 injection at the Frio-I Brine Pilot. *Chemical Geology*, In Press, .

Xu, T., Apps, J.A. & Pruess, K., 2003. Reactive geochemical transport simulation to study mineral trapping for CO2 disposal in deep arenaceous formations. *J. Geophys. Res.*, 108.

Zaihua, L. & Dreybodt, W., 2001. Kinetics and rate-limiting mechanisms of dolomite dissolution at various CO2 partial pressures. *Science in China Series B: Chemistry*, 44(5), pp.500–509.

# Appendix A: Fluid Chemistry Data

The following appendix presents the fluid chemistry data used in the PHREEQC modelling and dissolution rate calculations presented in this work. Corrections for dilutions and background values have been made, as detailed in Section 3.4.1. The precision for each analyte has been estimated using the analytical results of repeat measurements on reference material duplicates and is included as a “std. dev.” column. Sample times and the “volume corrected times” used in dissolution rate calculations have both been included. Where an analyte has been used to calculate a mineral dissolution rate, it has been highlighted in red and supplied with a % error, based on analysed concentrations from duplicate samples. Where columns have been left blank, solutions have not been analysed for reasons of economy. Where concentrations are recorded as zero, the respective analyte was below the detection limit and omitted from any modelling.

# A.1 Quartz Fluid Chemistry Data

| 121: 1.36M NaCl, 4bar pCO2, 22C | | | | | | | | | | | | | | | | |
|---|---|---|---|---|---|---|---|---|---|---|---|---|---|---|---|---|
| Time, hours | Std. Dev. Mol/l | -0.12 | 0.17 | 1.08 | 19.43 | 24.13 | 44.88 | 44.90 | 47.88 | 119.88 | 142.55 | 214.38 | 307.95 | 378.53 | 622.67 | 622.88 |
| VCT, hours | - | 0.00 | 0.17 | 1.11 | 20.31 | 25.35 | 48.03 | 48.05 | 51.43 | 135.46 | 162.66 | 251.97 | 372.27 | 466.24 | 803.99 | 804.30 |
| Mg, mol/l | 6.47E-06 | 2.91E-06 | 1.18E-05 | 9.47E-06 | 8.71E-06 | 8.87E-06 | 8.71E-06 | 8.15E-06 | 8.04E-06 | 1.00E-05 | 1.14E-05 | 1.09E-05 | 1.07E-05 | 1.09E-05 | 1.10E-05 | 1.13E-05 |
| Al, mol/l | 5.09E-08 | 2.06E-07 | 8.87E-06 | 1.42E-06 | 2.82E-06 | 1.95E-06 | 2.18E-06 | 2.59E-06 | 6.00E-06 | 5.93E-06 | 3.72E-06 | 3.55E-06 | 2.84E-06 | 2.85E-06 | 2.72E-06 | 2.96E-06 |
| Si, mol/l (±8%) | 2.64E-07 | 3.38E-05 | 3.24E-05 | 5.07E-05 | 5.83E-05 | 7.34E-05 | 5.46E-05 | 5.76E-05 | 6.16E-05 | 1.03E-04 | 8.97E-05 | 8.88E-05 | 1.00E-04 | 9.04E-05 | 1.01E-04 | 8.96E-05 |
| K, mol/l | 2.33E-06 | 1.05E-05 | 4.44E-03 | 2.54E-03 | 1.57E-03 | 1.17E-03 | 6.64E-04 | 5.03E-04 | 3.63E-04 | 4.72E-04 | 3.41E-04 | 2.27E-04 | 1.87E-04 | 1.49E-04 | 1.57E-04 | 1.43E-04 |
| Ca, mol/l | 7.19E-06 | 1.99E-05 | 4.10E-05 | 2.60E-05 | 2.42E-05 | 2.89E-05 | 1.34E-05 | 1.35E-05 | 1.99E-05 | 2.38E-05 | 1.95E-05 | 2.38E-05 | 2.16E-05 | 2.47E-05 | 2.78E-05 | 2.60E-05 |
| Mn, mol/l | 1.65E-09 | 5.31E-07 | 2.77E-05 | 3.80E-05 | 6.03E-05 | 5.64E-05 | 8.70E-05 | 7.72E-05 | 5.34E-05 | 2.70E-04 | 1.63E-04 | 1.39E-04 | 1.41E-04 | 1.12E-04 | 1.21E-04 | 9.68E-05 |
| Fe, mol/l | 9.78E-09 | 1.61E-07 | 1.26E-04 | 3.17E-04 | 5.61E-04 | 7.85E-04 | 9.76E-04 | 8.87E-04 | 5.29E-04 | 2.90E-03 | 1.96E-03 | 2.21E-03 | 2.49E-03 | 2.00E-03 | 2.08E-03 | 2.12E-03 |
| Sr, mol/l | 8.95E-09 | 1.38E-07 | 1.56E-07 | 1.99E-07 | 1.87E-07 | 2.03E-07 | 1.85E-07 | 1.75E-07 | 1.90E-07 | 1.96E-07 | 2.02E-07 | 2.14E-07 | 1.97E-07 | 1.98E-07 | 2.03E-07 | 2.03E-07 |
| Ba, mol/l | 1.96E-09 | 4.45E-08 | 1.83E-07 | 1.01E-07 | 1.24E-07 | 9.38E-08 | 1.21E-07 | 1.30E-07 | 1.02E-07 | 1.08E-07 | 1.45E-07 | 1.51E-07 | 1.36E-07 | 2.14E-07 | 8.96E-08 | 1.07E-07 |
| Na (est), mol/l | - | 1.36E+00 | 1.36E+00 | 1.36E+00 | 1.36E+00 | 1.36E+00 | 1.36E+00 | 1.36E+00 | 1.36E+00 | 1.36E+00 | 1.36E+00 | 1.36E+00 | 1.36E+00 | 1.36E+00 | 1.36E+00 | 1.36E+00 |
| Fluid in exp. (kg) | - | 0.100 | 0.099 | 0.096 | 0.094 | 0.092 | 0.090 | 0.088 | 0.087 | 0.085 | 0.082 | 0.079 | 0.077 | 0.074 | 0.071 | 0.069 |

| 124: 1.36M NaCl, 31bar pCO2, 70C | | | | | | | | | | | | | | | | |
|---|---|---|---|---|---|---|---|---|---|---|---|---|---|---|---|---|
| Time, hours | Std. Dev. Mol/l | -1.33 | 0.08 | 2.22 | 4.42 | 20.82 | 26.52 | 47.42 | 117.17 | 144.23 | 166.65 | 189.18 | 189.20 | 215.57 | 333.23 | 380.02 |
| VCT, hours | - | 0.00 | 0.08 | 2.32 | 4.74 | 23.19 | 29.79 | 54.60 | 139.50 | 173.56 | 202.72 | 232.95 | 232.97 | 270.05 | 447.22 | 520.54 |
| Mg, mol/l | 6.47E-06 | 1.50E-05 | 1.44E-05 | 1.52E-05 | 1.38E-05 | 1.53E-05 | 1.32E-05 | 1.35E-05 | 1.55E-05 | 1.54E-05 | 1.52E-05 | 1.43E-05 | 1.52E-05 | 1.52E-05 | 1.73E-05 | 1.71E-05 |
| Al, mol/l | 5.09E-08 | 1.24E-08 | 0.00E+00 | 7.05E-07 | 1.29E-06 | 3.89E-07 | 5.91E-07 | 6.82E-07 | 2.08E-06 | 2.18E-06 | 2.77E-06 | 5.03E-06 | 2.37E-06 | 2.50E-06 | 3.67E-06 | 6.78E-06 |
| Si, mol/l (±12%) | 2.64E-07 | 2.93E-04 | 2.67E-04 | 4.07E-04 | 3.60E-04 | 4.77E-04 | 4.04E-04 | 4.09E-04 | 4.63E-04 | 4.88E-04 | 4.55E-04 | 3.75E-04 | 3.78E-04 | 3.78E-04 | 3.96E-04 | 4.26E-04 |
| K, mol/l | 2.33E-06 | 2.01E-05 | 4.84E-06 | 1.48E-05 | 9.15E-06 | 1.11E-05 | 3.55E-08 | 0.00E+00 | 1.26E-05 | 1.64E-05 | 1.47E-05 | 1.07E-05 | 1.01E-05 | 5.68E-06 | 1.45E-05 | 1.14E-05 |
| Ca, mol/l | 7.19E-06 | 4.95E-04 | 7.59E-04 | 2.06E-03 | 1.38E-03 | 7.02E-04 | 4.24E-04 | 4.27E-04 | 4.58E-04 | 4.56E-04 | 4.29E-04 | 3.84E-04 | 4.11E-04 | 4.62E-04 | 4.78E-04 | 5.53E-04 |
| Mn, mol/l | 1.65E-09 | 3.58E-05 | 2.28E-05 | 4.80E-05 | 2.23E-05 | 3.50E-05 | 2.26E-05 | 2.27E-05 | 3.59E-05 | 3.43E-05 | 2.69E-05 | 2.25E-05 | 2.07E-05 | 1.75E-05 | 3.23E-05 | 2.73E-05 |
| Fe, mol/l | 9.78E-09 | 2.92E-04 | 4.16E-05 | 3.56E-04 | 3.23E-04 | 8.21E-04 | 5.20E-04 | 5.69E-04 | 1.05E-03 | 1.07E-03 | 8.17E-04 | 6.49E-04 | 5.58E-04 | 4.30E-04 | 8.92E-04 | 7.39E-04 |
| Sr, mol/l | 8.95E-09 | 4.93E-07 | 3.94E-07 | 6.11E-07 | 4.55E-07 | 4.78E-07 | 3.33E-07 | 3.51E-07 | 4.42E-07 | 4.16E-07 | 3.79E-07 | 3.43E-07 | 3.50E-07 | 3.52E-07 | 3.99E-07 | 5.48E-07 |
| Ba, mol/l | 1.96E-09 | 5.96E-08 | 6.10E-08 | 8.14E-08 | 1.53E-07 | 6.27E-08 | 3.98E-08 | 8.73E-08 | 6.15E-08 | 5.76E-08 | 1.26E-07 | 9.66E-08 | 3.75E-08 | 2.73E-08 | 1.39E-07 | 6.14E-08 |
| Na (est), mol/l | - | 1.36E+00 | 1.36E+00 | 1.36E+00 | 1.36E+00 | 1.36E+00 | 1.36E+00 | 1.36E+00 | 1.36E+00 | 1.36E+00 | 1.36E+00 | 1.36E+00 | 1.36E+00 | 1.36E+00 | 1.36E+00 | 1.36E+00 |
| Fluid in exp. (kg) | - | 0.101 | 0.096 | 0.091 | 0.087 | 0.085 | 0.083 | 0.081 | 0.079 | 0.076 | 0.074 | 0.071 | 0.069 | 0.068 | 0.064 | 0.061 |

| 124 cont.: 1.36M NaCl, 31bar pCO2, 70C | | | | | | |
|---|---|---|---|---|---|---|
| Time, hours | Std. Dev. Mol/l | 455.50 | 503.65 | 620.65 | 701.42 | 701.45 |
| VCT, hours | - | 643.44 | 725.19 | 933.02 | 1082.47 | 1082.54 |
| Mg, mol/l | 6.47E-06 | 1.63E-05 | 1.55E-05 | 1.61E-05 | 1.72E-05 | 1.71E-05 |
| Al, mol/l | 5.09E-08 | 4.04E-06 | 2.66E-06 | 2.47E-06 | 2.40E-06 | 2.47E-06 |
| Si, mol/l (±12%) | 2.64E-07 | 3.83E-04 | 3.64E-04 | 3.57E-04 | 4.63E-04 | 3.83E-04 |
| K, mol/l | 2.33E-06 | 8.67E-06 | 6.60E-06 | 1.15E-06 | 9.23E-06 | 7.45E-06 |
| Ca, mol/l | 7.19E-06 | 5.02E-04 | 5.13E-04 | 5.05E-04 | 6.71E-04 | 5.81E-04 |
| Mn, mol/l | 1.65E-09 | 2.41E-05 | 1.85E-05 | 1.89E-05 | 1.92E-05 | 1.55E-05 |
| Fe, mol/l | 9.78E-09 | 6.67E-04 | 5.47E-04 | 5.84E-04 | 6.23E-04 | 5.53E-04 |
| Sr, mol/l | 8.95E-09 | 3.76E-07 | 3.90E-07 | 3.71E-07 | 4.52E-07 | 4.52E-07 |
| Ba, mol/l | 1.96E-09 | 4.57E-08 | 4.34E-08 | 5.76E-08 | 3.10E-08 | 1.23E-07 |
| Na (est), mol/l | - | 1.36E+00 | 1.36E+00 | 1.36E+00 | 1.36E+00 | 1.36E+00 |
| Fluid in exp. (kg) | - | 0.059 | 0.056 | 0.054 | 0.052 | 0.049 |

| 125: DI, 4bar pCO2, 22C | | | | | | | | | | | | | | | | |
|---|---|---|---|---|---|---|---|---|---|---|---|---|---|---|---|---|
| Time, hours | Std. Dev. Mol/l | -0.35 | 0.00 | 2.32 | 3.95 | 5.43 | 24.18 | 27.32 | 31.18 | 45.57 | 48.90 | 53.28 | 73.48 | 73.48 | 75.57 | 78.23 |
| VCT, hours | - | 0.00 | 0.02 | 2.42 | 4.19 | 5.85 | 27.61 | 31.39 | 36.21 | 54.76 | 59.20 | 65.26 | 94.23 | 94.23 | 97.95 | 102.99 |
| Mg, mol/l | 4.46E-06 | 7.31E-06 | 1.22E-05 | 7.62E-06 | 8.97E-06 | 7.61E-06 | 7.59E-06 | 7.57E-06 | 7.56E-06 | 7.79E-06 | 7.97E-06 | 7.62E-06 | 7.60E-06 | 7.67E-06 | 7.77E-06 | 7.59E-06 |
| Al, mol/l | 3.05E-06 | 0.00E+00 | 0.00E+00 | 0.00E+00 | 0.00E+00 | 0.00E+00 | 0.00E+00 | 0.00E+00 | 1.47E-08 | 0.00E+00 | 0.00E+00 | 3.15E-07 | 2.32E-06 | 0.00E+00 | 0.00E+00 | 0.00E+00 |
| Si, mol/l (±3%) | 7.67E-06 | 4.51E-06 | 5.00E-06 | 5.14E-06 | 5.23E-06 | 5.00E-06 | 5.18E-06 | 4.78E-06 | 5.28E-06 | 5.32E-06 | 5.15E-06 | 5.27E-06 | 5.30E-06 | 5.12E-06 | 5.20E-06 | 5.02E-06 |
| K, mol/l | 3.15E-06 | 0.00E+00 | 1.09E-06 | 0.00E+00 | 1.54E-05 | 0.00E+00 | 0.00E+00 | 0.00E+00 | 0.00E+00 | 0.00E+00 | 0.00E+00 | 0.00E+00 | 0.00E+00 | 0.00E+00 | 0.00E+00 | 0.00E+00 |
| Ca, mol/l | 6.88E-05 | 1.31E-05 | 2.61E-05 | 1.46E-05 | 2.84E-05 | 1.28E-05 | 1.26E-05 | 1.25E-05 | 1.29E-05 | 1.53E-05 | 2.74E-05 | 1.33E-05 | 1.25E-05 | 1.35E-05 | 1.45E-05 | 1.36E-05 |
| Mn, mol/l | 3.59E-08 | 2.49E-06 | 4.08E-06 | 2.76E-06 | 2.59E-06 | 2.74E-06 | 2.62E-06 | 2.57E-06 | 2.61E-06 | 2.71E-06 | 2.61E-06 | 2.65E-06 | 2.60E-06 | 2.59E-06 | 2.68E-06 | 2.62E-06 |
| Fe, mol/l | 2.62E-07 | 4.62E-07 | 5.92E-07 | 6.26E-07 | 7.23E-07 | 7.16E-07 | 8.92E-07 | 1.09E-06 | 1.06E-06 | 8.75E-07 | 9.50E-07 | 9.73E-07 | 1.03E-06 | 9.44E-07 | 1.04E-06 | 1.05E-06 |
| Sr, mol/l | 3.17E-08 | 8.02E-08 | 1.02E-07 | 8.26E-08 | 9.15E-08 | 7.87E-08 | 9.15E-08 | 8.93E-08 | 9.49E-08 | 9.51E-08 | 9.52E-08 | 9.20E-08 | 9.73E-08 | 8.95E-08 | 8.63E-08 | 9.54E-08 |
| Ba, mol/l | 2.02E-08 | 1.38E-07 | 3.35E-07 | 1.46E-07 | 1.99E-07 | 6.92E-08 | 1.04E-07 | 1.17E-07 | 8.03E-08 | 1.15E-07 | 8.49E-08 | 6.40E-08 | 5.09E-08 | 7.91E-08 | 5.57E-08 | 1.00E-07 |
| Na (est), mol/l | - | 0.00E+00 | 0.00E+00 | 0.00E+00 | 0.00E+00 | 0.00E+00 | 0.00E+00 | 0.00E+00 | 0.00E+00 | 0.00E+00 | 0.00E+00 | 0.00E+00 | 0.00E+00 | 0.00E+00 | 0.00E+00 | 0.00E+00 |
| Fluid in exp. (kg) | - | 0.098 | 0.097 | 0.092 | 0.089 | 0.086 | 0.083 | 0.080 | 0.077 | 0.075 | 0.072 | 0.070 | 0.067 | 0.065 | 0.054 | 0.051 |

| 125 cont.: DI, 4bar pCO2, 22C | | | | | | | | | | | | | | | | | | | |
|---|---|---|---|---|---|---|---|---|---|---|---|---|---|---|---|---|---|---|---|
| Time, hours | Std. Dev. Mol/l | 98.90 | 101.48 | 103.07 | 121.15 | 126.07 | 139.95 | 150.68 | 169.02 | 169.02 | 172.52 | 190.42 | 193.40 | 290.03 | 311.12 | 332.53 | 382.15 | 531.08 | 531.08 |
| VCT, hours | - | 144.31 | 149.75 | 153.27 | 195.60 | 207.79 | 244.43 | 274.56 | 329.44 | 329.44 | 341.18 | 406.86 | 418.98 | 857.36 | 968.20 | 1096.46 | 1444.52 | 2685.30 | 2685.30 |
| Mg, mol/l | 4.46E-06 | 7.80E-06 | 7.89E-06 | 7.85E-06 | 7.96E-06 | 8.03E-06 | 7.93E-06 | 8.17E-06 | 8.53E-06 | 8.52E-06 | 8.44E-06 | 8.30E-06 | 8.63E-06 | 8.81E-06 | 8.88E-06 | 1.06E-05 | 8.87E-06 | 9.97E-06 | 9.49E-06 |
| Al, mol/l | 3.05E-06 | 0.00E+00 | 6.05E-08 | 8.27E-08 | 7.79E-08 | 3.13E-07 | 2.32E-07 | 7.15E-08 | 2.27E-07 | 5.38E-07 | 2.81E-07 | 4.16E-07 | 3.11E-07 | 1.34E-06 | 7.51E-07 | 6.43E-07 | 1.05E-06 | 1.69E-06 | 2.02E-06 |
| Si, mol/l | 7.67E-06 | 5.38E-06 | 5.29E-06 | 5.25E-06 | 5.61E-06 | 5.45E-06 | 5.78E-06 | 5.47E-06 | 5.62E-06 | 5.83E-06 | 5.53E-06 | 6.15E-06 | 6.00E-06 | 6.68E-06 | 7.26E-06 | 7.08E-06 | 7.99E-06 | 1.10E-05 | 1.09E-05 |
| K, mol/l | 3.15E-06 | 0.00E+00 | 0.00E+00 | 0.00E+00 | 0.00E+00 | 0.00E+00 | 0.00E+00 | 0.00E+00 | 0.00E+00 | 0.00E+00 | 0.00E+00 | 0.00E+00 | 1.49E-07 | 0.00E+00 | 0.00E+00 | 0.00E+00 | 0.00E+00 | 0.00E+00 | 0.00E+00 |
| Ca, mol/l | 6.88E-05 | 1.39E-05 | 1.41E-05 | 1.43E-05 | 1.47E-05 | 1.53E-05 | 1.37E-05 | 1.49E-05 | 1.70E-05 | 1.82E-05 | 1.79E-05 | 2.02E-05 | 1.86E-05 | 2.02E-05 | 2.20E-05 | 2.35E-05 | 2.46E-05 | 3.32E-05 | 2.90E-05 |
| Mn, mol/l | 3.59E-08 | 2.67E-06 | 2.66E-06 | 2.67E-06 | 2.66E-06 | 2.69E-06 | 2.73E-06 | 2.80E-06 | 2.83E-06 | 2.77E-06 | 2.77E-06 | 2.79E-06 | 2.74E-06 | 2.89E-06 | 2.89E-06 | 2.96E-06 | 3.04E-06 | 4.09E-06 | 3.55E-06 |
| Fe, mol/l | 2.62E-07 | 1.14E-06 | 1.28E-06 | 1.20E-06 | 1.44E-06 | 1.26E-06 | 1.27E-06 | 1.23E-06 | 1.71E-06 | 1.26E-06 | 1.37E-06 | 1.34E-06 | 1.38E-06 | 1.65E-06 | 1.74E-06 | 1.43E-06 | 1.92E-06 | 2.51E-06 | 2.29E-06 |
| Sr, mol/l | 3.17E-08 | 9.86E-08 | 9.84E-08 | 9.92E-08 | 9.77E-08 | 9.74E-08 | 1.03E-07 | 1.07E-07 | 1.24E-07 | 1.22E-07 | 1.21E-07 | 1.16E-07 | 1.29E-07 | 1.44E-07 | 1.47E-07 | 1.46E-07 | 1.55E-07 | 1.83E-07 | 1.70E-07 |
| Ba, mol/l | 2.02E-08 | 3.32E-08 | 3.85E-08 | 5.87E-08 | 7.61E-08 | 2.94E-08 | 3.69E-08 | 5.46E-08 | 9.45E-08 | 9.40E-08 | 6.13E-08 | 7.11E-08 | 7.54E-08 | 1.01E-07 | 1.06E-07 | 3.58E-08 | 1.93E-07 | 1.12E-07 | 1.16E-07 |
| Na (est), mol/l | - | 0.00E+00 | 0.00E+00 | 0.00E+00 | 0.00E+00 | 0.00E+00 | 0.00E+00 | 0.00E+00 | 0.00E+00 | 0.00E+00 | 0.00E+00 | 0.00E+00 | 0.00E+00 | 0.00E+00 | 0.00E+00 | 0.00E+00 | 0.00E+00 | 0.00E+00 | 0.00E+00 |
| Fluid in exp. (kg) | - | 0.048 | 0.046 | 0.043 | 0.041 | 0.039 | 0.037 | 0.034 | 0.032 | 0.030 | 0.029 | 0.026 | 0.024 | 0.021 | 0.018 | 0.016 | 0.014 | 0.012 | 0.009 |

| 126: 1.36M NaCl, 31bar pCO2, 70C | | | | | | | | | | | | | | | | | | |
|---|---|---|---|---|---|---|---|---|---|---|---|---|---|---|---|---|---|---|
| Time, hours | Std. Dev. Mol/l | -1.03 | 0.03 | 0.67 | 3.47 | 10.30 | 21.80 | 26.77 | 31.13 | 50.50 | 53.35 | 55.55 | 71.47 | 71.47 | 73.63 | 147.98 | 152.12 | 166.82 |
| VCT, hours | - | 0.00 | 0.03 | 0.68 | 3.60 | 10.86 | 23.25 | 28.75 | 33.64 | 55.82 | 59.13 | 61.75 | 80.97 | 80.97 | 83.66 | 177.65 | 182.97 | 202.29 |
| Mg, mol/l | 4.81E-06 | 2.10E-05 | 2.83E-05 | 2.80E-05 | 2.58E-05 | 2.48E-05 | 2.37E-05 | 2.64E-05 | 2.49E-05 | 2.68E-05 | 2.58E-05 | 2.53E-05 | 2.61E-05 | 2.27E-05 | 2.53E-05 | 2.75E-05 | 2.61E-05 | 2.72E-05 |
| Al, mol/l | 1.72E-06 | 0.00E+00 | 1.77E-07 | 1.60E-06 | 3.44E-06 | 4.67E-06 | 3.61E-06 | 2.83E-06 | 3.44E-06 | 4.14E-06 | 7.08E-06 | 3.13E-06 | 3.86E-06 | 3.25E-06 | 3.37E-06 | 4.18E-06 | 4.12E-06 | 4.54E-06 |
| Si, mol/l (±10%) | 1.76E-06 | 1.07E-04 | 1.07E-04 | 1.30E-04 | 1.41E-04 | 1.50E-04 | 1.27E-04 | 1.23E-04 | 1.19E-04 | 1.30E-04 | 1.22E-04 | 1.18E-04 | 1.24E-04 | 1.07E-04 | 1.16E-04 | 1.36E-04 | 1.29E-04 | 1.35E-04 |
| K, mol/l | 7.99E-06 | 2.29E-06 | 1.06E-03 | 5.08E-04 | 3.46E-04 | 2.94E-04 | 1.18E-04 | 6.83E-05 | 5.81E-05 | 7.00E-05 | 5.56E-05 | 4.21E-05 | 6.43E-05 | 6.31E-05 | 4.02E-05 | 8.33E-05 | 6.01E-05 | 4.38E-05 |
| Ca, mol/l | 1.75E-05 | 3.91E-05 | 5.68E-05 | 7.66E-05 | 6.74E-05 | 5.50E-05 | 4.58E-05 | 4.68E-05 | 4.75E-05 | 5.27E-05 | 4.99E-05 | 4.90E-05 | 4.97E-05 | 4.08E-05 | 4.75E-05 | 5.29E-05 | 5.33E-05 | 5.81E-05 |
| Mn, mol/l | 3.76E-08 | 1.16E-05 | 7.68E-05 | 1.99E-04 | 2.19E-04 | 1.97E-04 | 7.91E-05 | 6.06E-05 | 4.74E-05 | 5.41E-05 | 4.08E-05 | 3.42E-05 | 4.40E-05 | 3.38E-05 | 3.05E-05 | 6.18E-05 | 4.57E-05 | 3.84E-05 |
| Fe, mol/l | 4.79E-07 | 1.29E-07 | 5.18E-05 | 1.52E-04 | 2.72E-04 | 6.27E-04 | 6.13E-04 | 4.69E-04 | 3.76E-04 | 5.16E-04 | 3.85E-04 | 2.69E-04 | 3.87E-04 | 2.84E-04 | 1.91E-04 | 8.05E-04 | 6.02E-04 | 4.91E-04 |
| Sr, mol/l | 3.15E-08 | 1.93E-07 | 2.02E-07 | 2.23E-07 | 2.31E-07 | 2.33E-07 | 1.96E-07 | 2.53E-07 | 2.01E-07 | 2.17E-07 | 2.16E-07 | 2.20E-07 | 2.17E-07 | 1.98E-07 | 2.17E-07 | 2.26E-07 | 2.27E-07 | 2.48E-07 |
| Ba, mol/l | 2.72E-08 | 5.85E-07 | 2.80E-07 | 2.81E-07 | 2.67E-07 | 2.48E-07 | 1.32E-07 | 2.63E-07 | 5.02E-08 | 1.73E-07 | 2.24E-07 | 3.07E-07 | 1.40E-07 | 2.60E-07 | 9.24E-08 | 7.92E-08 | 1.29E-07 | 1.23E-07 |
| Na (est), mol/l | - | 0.00E+00 | 0.00E+00 | 0.00E+00 | 0.00E+00 | 0.00E+00 | 0.00E+00 | 0.00E+00 | 0.00E+00 | 0.00E+00 | 0.00E+00 | 0.00E+00 | 0.00E+00 | 0.00E+00 | 0.00E+00 | 0.00E+00 | 0.00E+00 | 0.00E+00 |
| Fluid in exp. (kg) | - | 0.147 | 0.146 | 0.143 | 0.140 | 0.138 | 0.136 | 0.132 | 0.130 | 0.128 | 0.126 | 0.123 | 0.121 | 0.119 | 0.118 | 0.116 | 0.114 | 0.111 |

| 126 cont.: 1.36M NaCl, 31bar pCO2, 70C | | | | | | | | | | | | | | | | | | |
|---|---|---|---|---|---|---|---|---|---|---|---|---|---|---|---|---|---|---|
| Time, hours | Std. Dev. Mol/l | 175.08 | 190.77 | 198.08 | 215.38 | 222.97 | 239.88 | 239.88 | 247.97 | 312.97 | 322.13 | 334.90 | 366.32 | 389.88 | 409.63 | 487.05 | 502.83 | 581.03 | 581.03 |
| VCT, hours | - | 213.35 | 234.75 | 244.95 | 269.53 | 280.53 | 305.58 | 305.58 | 317.92 | 419.33 | 433.94 | 454.77 | 507.54 | 548.05 | 582.85 | 722.46 | 751.64 | 900.07 | 900.07 |
| Mg, mol/l | 4.81E-06 | 2.65E-05 | 2.68E-05 | 2.74E-05 | 2.70E-05 | 2.72E-05 | 2.79E-05 | 2.79E-05 | 2.78E-05 | 3.12E-05 | 2.96E-05 | 3.10E-05 | 3.12E-05 | 2.96E-05 | 3.24E-05 | 3.03E-05 | 3.00E-05 | 3.01E-05 | 3.11E-05 |
| Al, mol/l | 1.72E-06 | 6.82E-06 | 4.15E-06 | 4.19E-06 | 4.21E-06 | 5.41E-06 | 4.56E-06 | 7.18E-06 | 5.80E-06 | 2.91E-06 | 1.42E-06 | 1.20E-06 | 4.98E-07 | 1.75E-06 | 9.74E-04 | 2.55E-07 | 3.79E-07 | 7.25E-08 | 2.49E-06 |
| Si, mol/l (±10%) | 1.76E-06 | 1.25E-04 | 1.27E-04 | 1.26E-04 | 1.27E-04 | 1.25E-04 | 1.27E-04 | 1.24E-04 | 1.27E-04 | 1.44E-04 | 1.50E-04 | 1.21E-04 | 1.39E-04 | 1.35E-04 | 1.54E-04 | 1.41E-04 | 1.53E-04 | 1.50E-04 | 1.64E-04 |
| K, mol/l | 7.99E-06 | 3.95E-05 | 3.22E-05 | 2.76E-05 | 3.49E-05 | 3.71E-05 | 3.51E-05 | 3.80E-05 | 3.24E-05 | 3.59E-05 | 3.81E-05 | 2.99E-05 | 3.36E-05 | 3.23E-05 | 2.90E-05 | 2.85E-05 | 2.50E-05 | 2.55E-05 | 2.63E-05 |
| Ca, mol/l | 1.75E-05 | 5.53E-05 | 5.49E-05 | 6.30E-05 | 5.70E-05 | 5.60E-05 | 6.04E-05 | 5.99E-05 | 6.50E-05 | 5.90E-05 | 5.38E-04 | 5.42E-05 | 6.30E-05 | 6.19E-05 | 7.26E-05 | 6.06E-05 | 6.83E-05 | 6.45E-05 | 7.18E-05 |
| Mn, mol/l | 3.76E-08 | 3.27E-05 | 3.26E-05 | 3.04E-05 | 3.17E-05 | 3.09E-05 | 3.16E-05 | 3.00E-05 | 2.79E-05 | 4.84E-05 | 4.19E-05 | 3.99E-05 | 4.11E-05 | 3.84E-05 | 3.87E-05 | 5.03E-05 | 4.25E-05 | 4.76E-05 | 4.37E-05 |
| Fe, mol/l | 4.79E-07 | 3.97E-04 | 4.15E-04 | 3.30E-04 | 3.77E-04 | 3.21E-04 | 3.34E-04 | 2.97E-04 | 2.43E-04 | 6.23E-04 | 5.24E-04 | 3.96E-04 | 4.27E-04 | 3.95E-04 | 3.94E-04 | 6.08E-04 | 4.94E-04 | 5.99E-04 | 5.35E-04 |
| Sr, mol/l | 3.15E-08 | 2.40E-07 | 2.42E-07 | 2.60E-07 | 2.49E-07 | 2.62E-07 | 2.60E-07 | 2.66E-07 | 2.65E-07 | 3.05E-07 | 4.27E-07 | 3.09E-07 | 3.13E-07 | 2.98E-07 | 3.30E-07 | 3.02E-07 | 3.07E-07 | 3.07E-07 | 3.18E-07 |
| Ba, mol/l | 2.72E-08 | 7.79E-08 | 1.51E-07 | 1.13E-07 | 1.64E-07 | 1.78E-07 | 1.70E-08 | 2.63E-08 | 2.58E-08 | 2.97E-08 | 0.00E+00 | 0.00E+00 | 0.00E+00 | 0.00E+00 | 1.72E-07 | 0.00E+00 | 0.00E+00 | 0.00E+00 | 0.00E+00 |
| Na (est), mol/l | - | 0.00E+00 | 0.00E+00 | 0.00E+00 | 0.00E+00 | 0.00E+00 | 0.00E+00 | 0.00E+00 | 0.00E+00 | 0.00E+00 | 0.00E+00 | 0.00E+00 | 0.00E+00 | 0.00E+00 | 0.00E+00 | 0.00E+00 | 0.00E+00 | 0.00E+00 | 0.00E+00 |
| Fluid in exp. (kg) | - | 0.109 | 0.107 | 0.105 | 0.103 | 0.101 | 0.099 | 0.097 | 0.096 | 0.094 | 0.092 | 0.090 | 0.087 | 0.085 | 0.083 | 0.081 | 0.079 | 0.077 | 0.075 |

# A.2 K-Feldspar Fluid Chemistry Data

| 111: DI, 4bar pCO2, 22C | | | | | | | | | | | | | | | | |
|---|---|---|---|---|---|---|---|---|---|---|---|---|---|---|---|---|
| Time, hours | Std. Dev. Mol/l | -116.53 | 0.17 | 4.77 | 22.93 | 54.07 | 73.12 | 98.00 | 98.02 | 173.02 | 195.35 | 267.52 | 362.60 | 431.60 | 675.85 | 675.88 |
| VCT, hours | | 0.00 | 0.17 | 4.88 | 23.85 | 57.84 | 79.19 | 107.97 | 107.99 | 198.12 | 225.63 | 319.18 | 447.46 | 543.32 | 900.03 | 900.07 |
| Mg, mol/l | 2.23E-06 | 5.48E-06 | 1.01E-07 | 0.00E+00 | 1.19E-06 | 2.75E-06 | 1.42E-06 | 1.44E-06 | 1.87E-06 | 2.00E-06 | 3.30E-06 | 1.95E-06 | 1.74E-06 | 9.87E-07 | 4.30E-06 | 1.25E-06 |
| Al, mol/l | 3.78E-08 | 3.39E-05 | 1.82E-05 | 5.74E-05 | 2.80E-04 | 7.02E-04 | 5.49E-04 | 5.31E-04 | 5.87E-04 | 6.19E-04 | 1.08E-03 | 7.40E-04 | 6.73E-04 | 2.37E-04 | 1.19E-03 | 5.17E-04 |
| Si, mol/l (±2%) | 1.40E-07 | 3.06E-05 | 4.37E-05 | 1.78E-04 | 1.00E-03 | 2.77E-03 | 2.10E-03 | 1.96E-03 | 2.01E-03 | 2.15E-03 | 3.72E-03 | 2.62E-03 | 2.35E-03 | 7.45E-04 | 4.14E-03 | 1.76E-03 |
| K, mol/l | 9.46E-07 | 2.50E-05 | 1.27E-05 | 4.11E-05 | 2.13E-04 | 6.22E-04 | 4.87E-04 | 4.65E-04 | 4.50E-04 | 5.36E-04 | 8.70E-04 | 6.41E-04 | 6.13E-04 | 2.74E-04 | 1.22E-03 | 5.41E-04 |
| Ca, mol/l | 9.70E-07 | 1.56E-05 | 1.07E-05 | 1.15E-05 | 1.78E-05 | 2.12E-05 | 2.11E-05 | 2.15E-05 | 2.34E-05 | 2.58E-05 | 2.54E-05 | 2.53E-05 | 2.53E-05 | 2.33E-05 | 4.67E-05 | 2.01E-05 |
| Mn, mol/l | 2.59E-09 | 1.19E-07 | 3.79E-07 | 4.23E-07 | 8.21E-07 | 8.65E-07 | 7.87E-07 | 8.18E-07 | 8.99E-07 | 9.38E-07 | 1.00E-06 | 1.01E-06 | 1.07E-06 | 1.17E-06 | 2.44E-06 | 1.03E-06 |
| Fe, mol/l | 5.26E-08 | 1.39E-06 | 9.37E-06 | 4.70E-06 | 5.56E-06 | 9.24E-06 | 5.56E-06 | 9.18E-06 | 8.69E-06 | 7.25E-06 | 1.27E-05 | 6.22E-06 | 6.54E-06 | 3.81E-06 | 1.46E-05 | 4.56E-06 |
| Sr, mol/l | 2.51E-07 | 1.24E-07 | 1.35E-07 | 1.71E-07 | 3.53E-07 | 6.18E-07 | 5.40E-07 | 5.51E-07 | 6.04E-07 | 6.06E-07 | 7.87E-07 | 7.03E-07 | 6.88E-07 | 4.57E-07 | 1.35E-06 | 5.82E-07 |
| Ba, mol/l | 4.28E-08 | 1.35E-06 | 9.80E-07 | 1.72E-07 | 5.78E-07 | 1.32E-06 | 1.18E-06 | 1.15E-06 | 1.30E-06 | 1.20E-06 | 1.88E-06 | 1.57E-06 | 1.43E-06 | 7.40E-07 | 2.75E-06 | 1.23E-06 |
| Na (est), mol/l | | 7.57E-06 | 8.10E-07 | 2.55E-05 | 3.83E-04 | 2.03E-03 | 1.96E-03 | 2.31E-03 | 2.23E-03 | 4.01E-03 | 7.09E-03 | 6.60E-03 | 7.14E-03 | 3.18E-03 | 1.42E-02 | 6.30E-03 |
| Fluid in exp. (kg) | | 0.099 | 0.098 | 0.096 | 0.094 | 0.090 | 0.088 | 0.085 | 0.083 | 0.082 | 0.080 | 0.076 | 0.073 | 0.071 | 0.067 | 0.066 |

| 112: DI, 4bar pCO2, 22C | | | | | | | | | | | | | | | | |
|---|---|---|---|---|---|---|---|---|---|---|---|---|---|---|---|---|
| Time, hours | Std. Dev. Mol/l | -116.42 | 0.17 | 4.90 | 22.90 | 54.00 | 73.05 | 98.13 | 98.17 | 173.00 | 195.30 | 267.47 | 362.55 | 362.58 | 431.68 | 676.00 | 676.05 |
| VCT, hours | | 0.00 | 0.17 | 5.02 | 23.86 | 57.23 | 78.16 | 106.66 | 106.70 | 195.24 | 222.39 | 312.88 | 435.86 | 435.91 | 529.03 | 879.01 | 879.09 |
| Mg, mol/l | 2.23E-06 | 8.22E-07 | 8.11E-07 | 1.15E-06 | 0.00E+00 | 0.00E+00 | 0.00E+00 | 0.00E+00 | 3.13E-07 | 0.00E+00 | 0.00E+00 | 0.00E+00 | 0.00E+00 | 0.00E+00 | 0.00E+00 | 0.00E+00 | 0.00E+00 |
| Al, mol/l | 3.78E-08 | 1.46E-05 | 6.57E-06 | 2.21E-05 | 3.31E-06 | 1.50E-05 | 6.88E-06 | 7.74E-06 | 9.15E-06 | 8.70E-06 | 9.54E-06 | 9.16E-06 | 1.04E-05 | 1.37E-05 | 1.12E-05 | 1.20E-05 | 1.20E-05 |
| Si, mol/l (±8%) | 1.40E-07 | 2.43E-05 | 2.21E-05 | 4.17E-05 | 1.79E-05 | 2.49E-05 | 1.32E-05 | 1.45E-05 | 1.62E-05 | 1.26E-05 | 1.81E-05 | 1.69E-05 | 1.72E-05 | 1.89E-05 | 1.87E-05 | 2.08E-05 | 2.13E-05 |
| K, mol/l | 9.46E-07 | 5.60E-06 | 3.32E-05 | 4.41E-05 | 1.21E-05 | 7.82E-06 | 1.64E-05 | 1.28E-05 | 2.17E-05 | 1.02E-05 | 7.49E-06 | 8.15E-06 | 9.56E-06 | 9.60E-06 | 8.57E-06 | 8.66E-06 | 8.47E-06 |
| Ca, mol/l | 9.70E-07 | 6.74E-06 | 8.84E-06 | 1.39E-05 | 9.02E-06 | 1.02E-05 | 1.52E-05 | 1.42E-05 | 1.51E-05 | 1.70E-05 | 1.60E-05 | 1.52E-05 | 1.69E-05 | 1.78E-05 | 1.82E-05 | 1.82E-05 | 1.76E-05 |
| Mn, mol/l | 2.59E-09 | 8.97E-08 | 5.79E-07 | 4.14E-07 | 6.11E-07 | 4.24E-07 | 5.03E-07 | 5.64E-07 | 6.11E-07 | 7.18E-07 | 7.00E-07 | 7.02E-07 | 7.83E-07 | 8.10E-07 | 8.89E-07 | 8.95E-07 | 8.53E-07 |
| Fe, mol/l | 5.26E-08 | 1.47E-06 | 2.36E-06 | 4.78E-06 | 4.15E-06 | 3.59E-06 | 2.29E-06 | 2.36E-06 | 2.70E-06 | 4.98E-06 | 3.50E-06 | 3.52E-06 | 4.28E-06 | 4.59E-06 | 5.48E-06 | 5.27E-06 | 4.55E-06 |
| Sr, mol/l | 2.51E-07 | 7.90E-08 | 1.08E-07 | 1.65E-07 | 1.32E-07 | 1.19E-07 | 1.61E-07 | 1.70E-07 | 1.90E-07 | 1.80E-07 | 1.82E-07 | 1.78E-07 | 1.87E-07 | 1.94E-07 | 2.02E-07 | 1.99E-07 | 1.93E-07 |
| Ba, mol/l | 4.28E-08 | 4.46E-07 | 5.42E-07 | 5.31E-08 | 1.63E-07 | 1.02E-07 | 2.20E-07 | 2.70E-07 | 2.72E-07 | 1.18E-07 | 2.44E-07 | 1.72E-07 | 1.77E-07 | 1.33E-07 | 1.93E-07 | 2.17E-07 | 1.96E-07 |
| Na (est), mol/l | | 1.69E-06 | 2.12E-06 | 2.78E-05 | 2.18E-05 | 2.54E-05 | 6.57E-05 | 6.32E-05 | 1.07E-04 | 7.53E-05 | 6.05E-05 | 8.28E-05 | 1.11E-04 | 1.12E-04 | 9.97E-05 | 1.01E-04 | 9.86E-05 |
| Fluid in exp. (kg) | | 0.099 | 0.098 | 0.096 | 0.094 | 0.092 | 0.090 | 0.087 | 0.084 | 0.083 | 0.081 | 0.079 | 0.076 | 0.074 | 0.073 | 0.069 | 0.066 |

| 113: DI, 4bar pCO2, 22C | | | | | | | | | | | | | | | | |
|---|---|---|---|---|---|---|---|---|---|---|---|---|---|---|---|---|
| Time, hours | Std. Dev. Mol/l | -116.35 | 0.22 | 4.95 | 23.03 | 53.87 | 72.70 | 98.20 | 98.22 | 172.92 | 195.17 | 267.48 | 362.48 | 431.72 | 676.05 | 676.08 |
| VCT, hours | | 0.00 | 0.22 | 5.07 | 23.90 | 56.61 | 76.98 | 105.33 | 105.35 | 191.21 | 217.35 | 304.32 | 421.33 | 508.72 | 826.17 | 826.22 |
| Mg, mol/l | 2.23E-06 | 0.00E+00 | 0.00E+00 | 0.00E+00 | 0.00E+00 | 0.00E+00 | 0.00E+00 | 0.00E+00 | 0.00E+00 | 0.00E+00 | 0.00E+00 | 0.00E+00 | 0.00E+00 | 0.00E+00 | 0.00E+00 | 3.87E-06 |
| Al, mol/l | 3.78E-08 | 1.31E-05 | 8.14E-06 | 1.30E-05 | 1.24E-05 | 1.41E-05 | 4.13E-06 | 5.74E-06 | 5.45E-06 | 6.17E-06 | 7.10E-06 | 6.71E-06 | 7.65E-06 | 7.97E-06 | 9.94E-06 | 9.22E-06 |
| Si, mol/l (±7%) | 1.40E-07 | 2.30E-05 | 2.50E-05 | 3.22E-05 | 2.69E-05 | 3.00E-05 | 1.27E-05 | 1.41E-05 | 1.28E-05 | 1.01E-05 | 1.70E-05 | 1.43E-05 | 1.65E-05 | 1.46E-05 | 1.80E-05 | 1.72E-05 |
| K, mol/l | 9.46E-07 | 2.80E-06 | 3.65E-06 | 4.04E-06 | 6.40E-06 | 7.67E-06 | 6.62E-06 | 7.16E-06 | 5.60E-06 | 8.28E-06 | 1.34E-05 | 8.29E-06 | 5.47E-06 | 6.14E-06 | 8.80E-06 | 1.19E-05 |
| Ca, mol/l | 9.70E-07 | 6.20E-06 | 8.77E-06 | 1.02E-05 | 1.41E-05 | 1.94E-05 | 2.23E-05 | 2.50E-05 | 2.32E-05 | 2.56E-05 | 2.59E-05 | 2.52E-05 | 2.49E-05 | 2.63E-05 | 2.94E-05 | 2.81E-05 |
| Mn, mol/l | 2.59E-09 | 1.06E-07 | 3.05E-07 | 2.13E-07 | 3.71E-07 | 4.35E-07 | 4.24E-07 | 4.90E-07 | 4.44E-07 | 5.62E-07 | 6.05E-07 | 5.97E-07 | 6.55E-07 | 7.14E-07 | 8.22E-07 | 7.72E-07 |
| Fe, mol/l | 5.26E-08 | 2.38E-07 | 2.73E-06 | 3.23E-06 | 9.57E-06 | 1.08E-05 | 1.18E-06 | 1.20E-06 | 9.60E-07 | 4.52E-06 | 2.19E-06 | 2.78E-06 | 1.21E-06 | 1.47E-06 | 1.47E-06 | 1.74E-06 |
| Sr, mol/l | 2.51E-07 | 7.27E-08 | 9.69E-08 | 1.07E-07 | 1.33E-07 | 1.50E-07 | 1.57E-07 | 1.80E-07 | 1.64E-07 | 1.72E-07 | 1.90E-07 | 1.84E-07 | 2.11E-07 | 1.97E-07 | 2.13E-07 | 2.03E-07 |
| Ba, mol/l | 4.28E-08 | 1.81E-07 | 7.26E-07 | 8.24E-09 | 5.67E-08 | 6.97E-08 | 1.28E-07 | 2.08E-07 | 1.29E-07 | 9.07E-08 | 3.65E-07 | 1.96E-07 | 1.12E-06 | 1.59E-07 | 1.68E-07 | 1.99E-07 |
| Na (est), mol/l | | 8.47E-07 | 2.78E-07 | 2.56E-06 | 1.15E-05 | 2.47E-05 | 2.62E-05 | 3.50E-05 | 2.74E-05 | 6.05E-05 | 1.07E-04 | 8.27E-05 | 6.37E-05 | 7.15E-05 | 1.02E-04 | 1.39E-04 |
| Fluid in exp. (kg) | | 0.100 | 0.099 | 0.096 | 0.095 | 0.093 | 0.091 | 0.089 | 0.087 | 0.086 | 0.084 | 0.082 | 0.080 | 0.078 | 0.076 | 0.073 |

| 173: DI, 4bar pCO2, 22C | | | | | | | | | | | | | | | | | |
|---|---|---|---|---|---|---|---|---|---|---|---|---|---|---|---|---|---|
| Time, hours | Std. Dev. Mol/l | -0.33 | 0.00 | 2.25 | 3.88 | 5.37 | 24.10 | 27.25 | 31.12 | 45.50 | 48.83 | 53.22 | 73.42 | 73.42 | 75.50 | 78.17 | 98.83 | 101.42 |
| VCT, hours | | 0.00 | 0.02 | 2.35 | 4.10 | 5.75 | 27.31 | 31.08 | 35.85 | 54.22 | 58.63 | 64.64 | 93.34 | 93.34 | 96.45 | 100.61 | 133.94 | 138.30 |
| Mg, mol/l | 4.81E-06 | 3.03E-06 | 3.36E-06 | 3.37E-06 | 2.91E-06 | 6.35E-06 | 3.23E-06 | 3.28E-06 | 3.20E-06 | 3.41E-06 | 3.44E-06 | 3.71E-06 | 3.72E-06 | 3.93E-06 | 3.67E-06 | 3.53E-06 | 3.85E-06 | 1.60E-03 |
| Al, mol/l | 1.72E-06 | 0.00E+00 | 4.25E-07 | 2.71E-06 | 2.94E-06 | 4.53E-06 | 1.17E-05 | 1.24E-05 | 1.43E-05 | 1.65E-05 | 1.73E-05 | 1.80E-05 | 2.07E-05 | 2.08E-05 | 2.15E-05 | 2.19E-05 | 2.45E-05 | 0.00E+00 |
| Si, mol/l (±2%) | 1.76E-06 | 2.04E-05 | 1.99E-05 | 2.14E-05 | 2.15E-05 | 2.26E-05 | 2.51E-05 | 2.57E-05 | 2.66E-05 | 2.79E-05 | 2.98E-05 | 2.91E-05 | 3.11E-05 | 3.13E-05 | 3.19E-05 | 3.11E-05 | 3.29E-05 | 1.92E-05 |
| K, mol/l | 7.99E-06 | 2.65E-05 | 2.63E-05 | 2.81E-05 | 2.71E-05 | 2.73E-05 | 2.88E-05 | 2.93E-05 | 2.94E-05 | 3.01E-05 | 3.05E-05 | 3.04E-05 | 3.13E-05 | 3.13E-05 | 3.26E-05 | 3.18E-05 | 3.32E-05 | 1.72E-05 |
| Ca, mol/l | 1.75E-05 | 6.97E-05 | 6.77E-05 | 7.31E-05 | 7.33E-05 | 7.68E-05 | 7.48E-05 | 7.52E-05 | 7.40E-05 | 7.69E-05 | 8.32E-05 | 8.16E-05 | 7.96E-05 | 8.00E-05 | 8.63E-05 | 7.86E-05 | 8.20E-05 | 1.76E-03 |
| Mn, mol/l | 3.76E-08 | 9.45E-07 | 2.24E-06 | 2.54E-06 | 1.92E-06 | 1.57E-06 | 1.28E-06 | 1.41E-06 | 1.31E-06 | 1.60E-06 | 1.42E-06 | 1.35E-06 | 1.43E-06 | 1.43E-06 | 1.43E-06 | 1.48E-06 | 1.51E-06 | 4.05E-05 |
| Fe, mol/l | 4.79E-07 | 2.28E-07 | 1.06E-05 | 1.28E-05 | 8.27E-06 | 4.97E-06 | 1.36E-05 | 1.44E-05 | 1.47E-05 | 2.11E-05 | 2.01E-05 | 2.00E-05 | 2.55E-05 | 2.56E-05 | 2.57E-05 | 2.66E-05 | 2.90E-05 | 6.40E-06 |
| Sr, mol/l | 3.15E-08 | 1.85E-06 | 1.89E-06 | 2.00E-06 | 2.00E-06 | 2.07E-06 | 2.10E-06 | 2.12E-06 | 2.13E-06 | 2.13E-06 | 2.18E-06 | 2.13E-06 | 2.19E-06 | 2.16E-06 | 2.18E-06 | 2.19E-06 | 2.20E-06 | 6.21E-07 |
| Ba, mol/l | 2.72E-08 | 4.56E-07 | 3.72E-07 | 3.16E-07 | 2.89E-07 | 3.94E-07 | 6.12E-07 | 6.14E-07 | 6.48E-07 | 6.53E-07 | 6.55E-07 | 6.47E-07 | 7.17E-07 | 7.51E-07 | 6.75E-07 | 6.73E-07 | 7.16E-07 | 0.00E+00 |
| Na (est), mol/l | | 8.02E-06 | 3.57E-07 | 1.06E-05 | 1.49E-05 | 1.89E-05 | 5.67E-05 | 6.29E-05 | 6.96E-05 | 9.40E-05 | 1.01E-04 | 1.07E-04 | 1.41E-04 | 1.41E-04 | 1.50E-04 | 1.51E-04 | 1.91E-04 | 1.01E-04 |
| Fluid in exp. (kg) | | 0.099 | 0.097 | 0.093 | 0.090 | 0.087 | 0.084 | 0.081 | 0.079 | 0.076 | 0.073 | 0.071 | 0.068 | 0.066 | 0.065 | 0.062 | 0.060 | 0.058 |

| 173 cont.: DI, 4bar pCO2, 22C | | | | | | | | | | | | | | | | | |
|---|---|---|---|---|---|---|---|---|---|---|---|---|---|---|---|---|---|
| Time, hours | Std. Dev. Mol/l | 103.00 | 121.08 | 126.00 | 139.88 | 150.62 | 168.95 | 168.95 | 172.45 | 190.35 | 193.33 | 289.97 | 311.05 | 332.47 | 382.08 | 531.02 | 531.02 |
| VCT, hours | | 141.09 | 174.15 | 183.55 | 211.40 | 233.90 | 274.23 | 274.23 | 282.51 | 327.14 | 335.06 | 609.44 | 673.24 | 742.64 | 915.31 | 1480.26 | 1480.26 |
| Mg, mol/l | 4.81E-06 | 4.10E-06 | 4.04E-06 | 4.25E-06 | 4.78E-06 | 5.38E-06 | 5.01E-06 | 4.64E-06 | 4.81E-06 | 5.22E-06 | 5.37E-06 | 7.05E-06 | 7.11E-06 | 7.76E-06 | 8.71E-06 | 1.16E-05 | 1.17E-05 |
| Al, mol/l | 1.72E-06 | 2.50E-05 | 2.70E-05 | 2.78E-05 | 2.89E-05 | 3.06E-05 | 3.16E-05 | 3.26E-05 | 3.25E-05 | 3.38E-05 | 3.43E-05 | 4.25E-05 | 4.77E-05 | 4.46E-05 | 4.82E-05 | 6.14E-05 | 6.15E-05 |
| Si, mol/l (±2%) | 1.76E-06 | 3.50E-05 | 3.55E-05 | 3.65E-05 | 3.83E-05 | 3.94E-05 | 4.00E-05 | 4.10E-05 | 4.22E-05 | 4.39E-05 | 4.38E-05 | 5.68E-05 | 5.86E-05 | 6.30E-05 | 7.13E-05 | 9.85E-05 | 9.71E-05 |
| K, mol/l | 7.99E-06 | 3.40E-05 | 3.28E-05 | 3.38E-05 | 3.59E-05 | 3.37E-05 | 3.50E-05 | 3.35E-05 | 3.46E-05 | 3.45E-05 | 3.60E-05 | 3.89E-05 | 3.74E-05 | 3.95E-05 | 4.14E-05 | 4.48E-05 | 4.59E-05 |
| Ca, mol/l | 1.75E-05 | 8.52E-05 | 8.28E-05 | 8.41E-05 | 8.65E-05 | 8.89E-05 | 8.83E-05 | 8.71E-05 | 8.97E-05 | 9.29E-05 | 9.84E-05 | 1.01E-04 | 1.02E-04 | 1.06E-04 | 1.08E-04 | 1.24E-04 | 1.26E-04 |
| Mn, mol/l | 3.76E-08 | 1.50E-06 | 1.59E-06 | 1.60E-06 | 1.61E-06 | 1.66E-06 | 1.69E-06 | 1.63E-06 | 1.69E-06 | 1.73E-06 | 1.74E-06 | 2.12E-06 | 2.15E-06 | 2.16E-06 | 2.42E-06 | 2.93E-06 | 2.75E-06 |
| Fe, mol/l | 4.79E-07 | 2.87E-05 | 2.99E-05 | 3.14E-05 | 3.07E-05 | 3.12E-05 | 3.12E-05 | 3.02E-05 | 3.12E-05 | 3.09E-05 | 3.12E-05 | 3.60E-05 | 3.53E-05 | 3.51E-05 | 5.79E-05 | 4.67E-05 | 4.58E-05 |
| Sr, mol/l | 3.15E-08 | 2.19E-06 | 2.23E-06 | 2.21E-06 | 2.23E-06 | 2.27E-06 | 2.30E-06 | 2.23E-06 | 2.26E-06 | 2.27E-06 | 2.30E-06 | 2.37E-06 | 2.35E-06 | 2.37E-06 | 2.37E-06 | 2.56E-06 | 2.48E-06 |
| Ba, mol/l | 2.72E-08 | 7.20E-07 | 7.42E-07 | 8.33E-07 | 7.91E-07 | 7.96E-07 | 8.45E-07 | 8.01E-07 | 7.81E-07 | 8.26E-07 | 8.32E-07 | 9.66E-07 | 1.05E-06 | 9.64E-07 | 1.10E-06 | 1.36E-06 | 1.35E-06 |
| Na (est), mol/l | | 2.02E-04 | 2.25E-04 | 2.40E-04 | 2.80E-04 | 2.82E-04 | 3.26E-04 | 3.12E-04 | 3.28E-04 | 3.61E-04 | 3.83E-04 | 4.53E-04 | 4.35E-04 | 4.60E-04 | 4.82E-04 | 5.21E-04 | 5.34E-04 |
| Fluid in exp. (kg) | | 0.055 | 0.053 | 0.051 | 0.048 | 0.046 | 0.044 | 0.042 | 0.041 | 0.039 | 0.037 | 0.034 | 0.032 | 0.030 | 0.028 | 0.026 | 0.023 |

| 171: 1.36M NaCl, 4bar pCO2, 22C | | | | | | | | | | | | | | | | | |
|---|---|---|---|---|---|---|---|---|---|---|---|---|---|---|---|---|---|
| Time, hours | Std. Dev. Mol/l | -23.13 | 0.02 | 1.53 | 3.57 | 5.40 | 22.70 | 25.87 | 30.20 | 30.20 | 45.45 | 50.07 | 53.28 | 67.78 | 67.78 | 77.87 | 94.22 | 98.45 |
| VCT, hours | | 0.00 | 0.02 | 1.59 | 3.76 | 5.78 | 25.45 | 29.15 | 34.33 | 34.33 | 53.35 | 59.32 | 63.59 | 83.53 | 83.53 | 98.06 | 122.41 | 128.93 |
| Mg, mol/l | 7.13E-08 | 9.83E-06 | 1.11E-04 | 1.61E-05 | 7.10E-06 | 4.75E-06 | 6.17E-06 | 4.96E-06 | 6.22E-06 | 5.56E-06 | 5.67E-06 | 5.56E-06 | 5.65E-06 | 7.03E-06 | 6.16E-06 | 8.05E-06 | 1.31E-04 | 3.30E-05 |
| Al, mol/l | 1.63E-08 | 9.34E-07 | 1.21E-06 | 4.54E-06 | 1.43E-05 | 1.13E-05 | 2.77E-05 | 2.72E-05 | 2.91E-05 | 3.01E-05 | 3.20E-05 | 3.33E-05 | 3.45E-05 | 3.46E-05 | 1.98E-04 | 3.95E-05 | 5.87E-05 | 4.24E-05 |
| Si, mol/l (±16%) | 2.15E-07 | 7.05E-06 | 8.85E-06 | 1.43E-05 | 2.16E-05 | 7.96E-05 | 1.75E-05 | 2.34E-05 | 3.10E-05 | 2.89E-05 | 2.08E-05 | 2.75E-05 | 3.63E-05 | 2.57E-05 | 2.80E-05 | 4.18E-05 | 3.20E-05 | 3.88E-05 |
| K, mol/l | 2.90E-07 | 0.00E+00 | 0.00E+00 | 6.15E-06 | 0.00E+00 | 3.87E-05 | 0.00E+00 | 0.00E+00 | 0.00E+00 | 0.00E+00 | 3.20E-06 | 0.00E+00 | 5.91E-07 | 4.64E-08 | 1.01E-05 | 3.08E-05 | 4.97E-05 | 6.09E-05 |
| Ca, mol/l | 1.18E-06 | 9.58E-05 | 2.11E-04 | 1.08E-04 | 8.94E-05 | 9.80E-05 | 9.48E-05 | 8.87E-05 | 8.73E-05 | 1.02E-04 | 9.38E-05 | 8.51E-05 | 8.53E-05 | 9.67E-05 | 8.98E-05 | 1.21E-04 | 1.97E-04 | 1.03E-04 |
| Mn, mol/l | 4.58E-10 | 4.36E-07 | 7.12E-06 | 4.30E-06 | 1.87E-06 | 4.54E-05 | 1.62E-06 | 9.69E-07 | 1.31E-06 | 9.20E-07 | 1.11E-06 | 1.01E-06 | 1.01E-06 | 1.26E-06 | 1.27E-06 | 1.25E-06 | 1.37E-06 | 1.32E-06 |
| Fe, mol/l | 1.43E-08 | 1.44E-07 | 3.16E-05 | 1.07E-05 | 1.09E-05 | 2.67E-03 | 8.73E-06 | 5.94E-06 | 5.78E-06 | 4.07E-06 | 6.26E-06 | 4.94E-06 | 3.28E-06 | 9.34E-06 | 3.80E-06 | 5.53E-06 | 8.37E-06 | 4.12E-06 |
| Sr, mol/l | 1.34E-09 | 5.15E-07 | 5.65E-07 | 5.45E-07 | 5.93E-07 | 5.91E-07 | 6.47E-07 | 7.01E-07 | 9.41E-07 | 9.89E-07 | 5.72E-07 | 7.61E-07 | 7.20E-07 | 7.13E-07 | 7.24E-07 | 1.27E-06 | 6.49E-07 | 6.50E-07 |
| Ba, mol/l | 1.58E-09 | 1.95E-06 | 1.85E-06 | 2.43E-06 | 2.57E-06 | 4.68E-06 | 7.96E-06 | 1.05E-05 | 2.72E-05 | 3.05E-05 | 3.85E-06 | 1.53E-05 | 1.23E-05 | 1.03E-05 | 1.25E-05 | 4.61E-05 | 2.33E-06 | 2.85E-06 |
| Na (est), mol/l | | 1.36E+00 | 1.36E+00 | 1.36E+00 | 1.36E+00 | 1.36E+00 | 1.36E+00 | 1.36E+00 | 1.36E+00 | 1.36E+00 | 1.36E+00 | 1.36E+00 | 1.36E+00 | 1.36E+00 | 1.36E+00 | 1.36E+00 | 1.36E+00 | 1.36E+00 |
| Fluid in exp. (kg) | | 0.105 | 0.103 | 0.100 | 0.097 | 0.094 | 0.091 | 0.089 | 0.086 | 0.084 | 0.083 | 0.080 | 0.078 | 0.075 | 0.073 | 0.072 | 0.069 | 0.067 |

| 171 cont.: 1.36M NaCl, 4bar pCO2, 22C | | | | | | | | | | | | | | | | |
|---|---|---|---|---|---|---|---|---|---|---|---|---|---|---|---|---|
| Time, hours | Std. Dev. Mol/l | 164.45 | 187.92 | 216.32 | 235.25 | 265.75 | 335.35 | 404.25 | 409.70 | 532.83 | 597.62 | 597.63 | 696.37 | 765.28 | 793.78 | 793.78 |
| VCT, hours | | 234.90 | 274.27 | 323.44 | 357.35 | 414.49 | 550.46 | 691.33 | 703.00 | 982.06 | 1138.53 | 1138.57 | 1400.71 | 1596.71 | 1686.53 | 1686.53 |
| Mg, mol/l | 7.13E-08 | 1.40E-05 | 1.81E-05 | 1.73E-05 | 1.29E-05 | 1.69E-05 | 2.57E-05 | 2.15E-05 | 2.72E-05 | 3.00E-05 | 3.38E-05 | 2.95E-05 | 3.84E-05 | 4.37E-05 | | 3.73E-05 |
| Al, mol/l | 1.63E-08 | 1.93E-05 | 4.46E-05 | 4.63E-05 | 3.17E-05 | 3.19E-05 | 2.54E-04 | 3.36E-05 | 3.69E-05 | 3.86E-05 | 3.98E-05 | 3.78E-05 | 4.27E-05 | 4.84E-05 | | 5.40E-05 |
| Si, mol/l (±16%) | 2.15E-07 | 1.45E-05 | 3.78E-05 | 4.13E-05 | 3.05E-05 | 3.85E-05 | 4.46E-05 | 4.25E-05 | 5.20E-05 | 7.03E-05 | 5.94E-05 | 5.43E-05 | 1.37E-04 | 7.65E-05 | | 6.69E-05 |
| K, mol/l | 2.90E-07 | 7.20E-06 | 2.51E-05 | 3.60E-05 | 1.79E-05 | 0.00E+00 | 1.85E-05 | 0.00E+00 | 1.66E-05 | 2.38E-05 | 2.21E-05 | 1.11E-05 | 2.20E-05 | 3.83E-05 | | 9.01E-06 |
| Ca, mol/l | 1.18E-06 | 7.64E-05 | 1.01E-04 | 1.08E-04 | 6.75E-05 | 6.55E-05 | 4.03E-04 | 6.94E-05 | 7.07E-05 | 8.05E-05 | 7.84E-05 | 6.55E-05 | 7.57E-05 | 7.80E-05 | | 6.79E-05 |
| Mn, mol/l | 4.58E-10 | 8.05E-07 | 1.77E-06 | 2.11E-06 | 1.58E-06 | 1.63E-06 | 2.01E-06 | 2.03E-06 | 2.20E-06 | 2.16E-06 | 2.12E-06 | 1.64E-06 | 2.35E-06 | 2.06E-06 | | 1.08E-06 |
| Fe, mol/l | 1.43E-08 | 8.47E-06 | 1.17E-05 | 2.72E-05 | 7.51E-05 | 9.17E-05 | 9.11E-05 | 9.95E-05 | 8.82E-05 | 8.23E-05 | 8.77E-05 | 8.93E-05 | 9.39E-05 | 7.08E-05 | | 1.89E-05 |
| Sr, mol/l | 1.34E-09 | 3.51E-07 | 6.49E-07 | 6.94E-07 | 4.48E-07 | 4.53E-07 | 6.29E-07 | 4.69E-07 | 5.40E-07 | 6.67E-07 | 6.07E-07 | 5.86E-07 | 5.32E-07 | 5.87E-07 | | 5.68E-07 |
| Ba, mol/l | 1.58E-09 | 6.52E-07 | 2.50E-06 | 4.05E-06 | 2.54E-06 | 3.28E-06 | 8.46E-06 | 2.36E-06 | 8.36E-06 | 1.52E-05 | 1.09E-05 | 1.27E-05 | 4.82E-06 | 7.26E-06 | | 9.41E-06 |
| Na (est), mol/l | | 1.36E+00 | 1.36E+00 | 1.36E+00 | 1.36E+00 | 1.36E+00 | 1.36E+00 | 1.36E+00 | 1.36E+00 | 1.36E+00 | 1.36E+00 | 1.36E+00 | 1.36E+00 | 1.36E+00 | | 1.36E+00 |
| Fluid in exp. (kg) | | 0.064 | 0.062 | 0.060 | 0.058 | 0.055 | 0.053 | 0.051 | 0.048 | 0.046 | 0.043 | 0.040 | 0.039 | 0.036 | 0.033 | 0.032 |

| 172: 1.36M NaCl, 4bar pCO2, 22C | | | | | | | | | | | | | | | | | |
|---|---|---|---|---|---|---|---|---|---|---|---|---|---|---|---|---|---|
| Time, hours | Std. Dev. Mol/l | -23.17 | 0.02 | 1.50 | 3.53 | 5.37 | 22.67 | 25.83 | 30.17 | 30.17 | 45.42 | 50.03 | 53.25 | 67.75 | 67.75 | 77.83 | 94.18 | 98.42 |
| VCT, hours | | 0.00 | 0.02 | 1.56 | 3.73 | 5.73 | 25.12 | 28.73 | 33.78 | 33.78 | 52.34 | 58.12 | 62.26 | 81.47 | 81.47 | 95.50 | 118.93 | 125.19 |
| Mg, mol/l | 7.13E-08 | 8.44E-07 | 1.10E-05 | 1.03E-05 | 2.44E-06 | 2.06E-06 | 7.19E-07 | 1.11E-06 | 3.17E-06 | 2.35E-06 | 3.23E-06 | 3.37E-06 | 3.21E-06 | 4.52E-06 | 3.86E-06 | 3.85E-06 | 1.76E-05 | 3.53E-05 |
| Al, mol/l | 1.63E-08 | 1.54E-06 | 7.91E-07 | 2.60E-06 | 5.19E-06 | 5.82E-06 | 1.07E-05 | 1.23E-05 | 1.34E-05 | 1.40E-05 | 1.52E-05 | 1.54E-05 | 1.73E-05 | 1.52E-05 | 1.61E-05 | 1.72E-05 | 1.74E-05 | 1.94E-05 |
| Si, mol/l (±15%) | 2.15E-07 | 1.19E-06 | 3.40E-06 | 7.53E-06 | 1.03E-05 | 1.71E-05 | 2.40E-06 | 1.33E-05 | 1.73E-05 | 2.09E-05 | 6.83E-06 | 1.48E-05 | 2.31E-05 | 9.73E-06 | 8.42E-06 | 2.17E-05 | 1.22E-05 | 1.91E-05 |
| K, mol/l | 2.90E-07 | 4.28E-05 | 6.07E-05 | 5.63E-05 | 5.41E-05 | 5.00E-05 | 3.35E-05 | 4.84E-05 | 6.69E-05 | 7.06E-05 | 6.08E-05 | 6.51E-05 | 7.21E-05 | 7.76E-05 | 6.82E-05 | 6.86E-05 | 8.43E-05 | 8.21E-05 |
| Ca, mol/l | 1.18E-06 | 3.88E-05 | 1.12E-04 | 3.49E-04 | 6.61E-05 | 5.28E-05 | 5.94E-05 | 4.85E-05 | 5.49E-05 | 5.90E-05 | 6.17E-05 | 6.15E-05 | 6.12E-05 | 7.69E-05 | 7.16E-05 | 6.68E-05 | 6.50E-05 | 6.43E-05 |
| Mn, mol/l | 4.58E-10 | 0.00E+00 | 2.90E-06 | 6.43E-06 | 9.14E-07 | 6.57E-07 | 8.69E-07 | 4.14E-07 | 4.22E-07 | 3.66E-07 | 6.44E-07 | 4.33E-07 | 4.58E-07 | 5.33E-07 | 3.82E-07 | 3.60E-07 | 4.80E-07 | 4.59E-07 |
| Fe, mol/l | 1.43E-08 | 3.41E-07 | 8.70E-06 | 1.69E-05 | 8.19E-06 | 6.16E-06 | 5.83E-06 | 4.38E-06 | 3.31E-06 | 3.75E-06 | 5.63E-06 | 3.17E-06 | 2.82E-06 | 3.81E-06 | 1.67E-06 | 3.21E-06 | 5.99E-06 | 3.45E-06 |
| Sr, mol/l | 1.34E-09 | 2.92E-07 | 2.86E-07 | 3.88E-07 | 3.80E-07 | 3.02E-07 | 3.80E-07 | 4.54E-07 | 5.75E-07 | 4.70E-07 | 4.31E-07 | 7.35E-07 | 8.28E-07 | 3.37E-07 | 4.22E-07 | 5.07E-07 | 3.55E-07 | 3.59E-07 |
| Ba, mol/l | 1.58E-09 | 9.94E-07 | 6.18E-07 | 1.33E-06 | 2.75E-06 | 2.53E-06 | 4.63E-06 | 1.24E-05 | 2.17E-05 | 1.26E-05 | 7.72E-06 | 3.12E-05 | 4.09E-05 | 1.47E-06 | 6.70E-06 | 1.50E-05 | 1.04E-06 | 2.77E-06 |
| Na (est), mol/l | | 1.36E+00 | 1.36E+00 | 1.36E+00 | 1.36E+00 | 1.36E+00 | 1.36E+00 | 1.36E+00 | 1.36E+00 | 1.36E+00 | 1.36E+00 | 1.36E+00 | 1.36E+00 | 1.36E+00 | 1.36E+00 | 1.36E+00 | 1.36E+00 | 1.36E+00 |
| Fluid in exp. (kg) | | 0.105 | 0.104 | 0.100 | 0.097 | 0.095 | 0.093 | 0.091 | 0.089 | 0.086 | 0.085 | 0.083 | 0.081 | 0.078 | 0.076 | 0.075 | 0.073 | 0.070 |

| 172 cont.: 1.36M NaCl, 4bar pCO2, 22C | | | | | | | | | | | | | | | | |
|---|---|---|---|---|---|---|---|---|---|---|---|---|---|---|---|---|
| Time, hours | Std. Dev. Mol/l | 164.42 | 187.88 | 216.28 | 235.22 | 265.72 | 335.32 | 404.22 | 409.67 | 532.80 | 597.58 | 597.60 | 696.33 | 765.25 | 793.75 | 793.75 |
| VCT, hours | | 226.02 | 262.95 | 309.08 | 341.02 | 394.39 | 520.60 | 649.79 | 660.49 | 913.75 | 1054.00 | 1054.04 | 1285.74 | 1454.79 | 1529.76 | 1529.76 |
| Mg, mol/l | 7.13E-08 | 1.10E-04 | 1.30E-05 | 8.27E-06 | 8.91E-06 | 9.81E-06 | 1.33E-05 | 1.63E-05 | 1.70E-05 | 2.10E-05 | 2.32E-05 | 2.24E-05 | 2.63E-05 | 3.18E-05 | 3.15E-05 | 3.18E-05 |
| Al, mol/l | 1.63E-08 | 5.12E-05 | 2.02E-05 | 2.17E-05 | 1.98E-05 | 2.22E-05 | 3.66E-05 | 2.45E-05 | 2.52E-05 | 2.74E-05 | 2.67E-05 | 2.75E-05 | 2.73E-05 | 2.78E-05 | 3.04E-05 | 2.95E-05 |
| Si, mol/l (±15%) | 2.15E-07 | 3.93E-05 | 1.24E-05 | 1.56E-05 | 1.68E-05 | 1.78E-05 | 1.88E-05 | 2.31E-05 | 2.81E-05 | 3.87E-05 | 3.42E-05 | 3.12E-05 | 1.45E-04 | 4.19E-05 | 4.34E-05 | 4.09E-05 |
| K, mol/l | 2.90E-07 | 1.13E-04 | 8.14E-05 | 8.21E-05 | 7.64E-05 | 9.30E-05 | 2.61E-04 | 9.82E-05 | 9.58E-05 | 1.13E-04 | 9.62E-05 | 1.01E-04 | 1.15E-04 | 1.02E-04 | 1.14E-04 | 1.19E-04 |
| Ca, mol/l | 1.18E-06 | 1.09E-04 | 6.89E-05 | 7.09E-05 | 7.72E-05 | 7.72E-05 | 7.75E-05 | 8.28E-05 | 8.56E-05 | 7.44E-05 | 8.51E-05 | 8.54E-05 | 8.66E-05 | 8.98E-05 | 8.27E-05 | 8.25E-05 |
| Mn, mol/l | 4.58E-10 | 1.88E-06 | 7.58E-07 | 8.55E-07 | 7.47E-07 | 9.69E-07 | 9.57E-07 | 1.10E-06 | 1.02E-06 | 1.06E-06 | 1.22E-06 | 1.02E-06 | 1.14E-06 | 1.28E-06 | 1.21E-06 | 1.20E-06 |
| Fe, mol/l | 1.43E-08 | 1.34E-05 | 1.53E-05 | 6.71E-06 | 4.30E-06 | 6.90E-06 | 8.98E-06 | 8.04E-06 | 5.84E-06 | 7.18E-06 | 6.20E-06 | 5.06E-06 | 6.94E-06 | 7.02E-06 | 5.42E-06 | 5.85E-06 |
| Sr, mol/l | 1.34E-09 | 6.70E-07 | 3.51E-07 | 3.72E-07 | 4.27E-07 | 4.13E-07 | 3.98E-07 | 4.29E-07 | 3.97E-07 | 9.18E-07 | 4.41E-07 | 4.91E-07 | 3.74E-07 | 4.36E-07 | 4.97E-07 | 6.21E-07 |
| Ba, mol/l | 1.58E-09 | 2.58E-06 | 9.15E-07 | 1.59E-06 | 4.91E-06 | 3.57E-06 | 1.69E-06 | 6.58E-06 | 4.96E-06 | 4.44E-05 | 7.20E-06 | 8.46E-06 | 3.49E-06 | 3.45E-06 | 8.40E-06 | 1.88E-05 |
| Na (est), mol/l | | 1.36E+00 | 1.36E+00 | 1.36E+00 | 1.36E+00 | 1.36E+00 | 1.36E+00 | 1.36E+00 | 1.36E+00 | 1.36E+00 | 1.36E+00 | 1.36E+00 | 1.36E+00 | 1.36E+00 | 1.36E+00 | 1.36E+00 |
| Fluid in exp. (kg) | | 0.068 | 0.066 | 0.064 | 0.062 | 0.059 | 0.057 | 0.055 | 0.053 | 0.051 | 0.048 | 0.045 | 0.044 | 0.042 | 0.040 | 0.037 |

| 175: 1.36M NaCl, 4bar pCO2, 70C | | | | | | | | | | | | | | | | |
|---|---|---|---|---|---|---|---|---|---|---|---|---|---|---|---|---|
| Time, hours | Std. Dev. Mol/l | -0.10 | 0.03 | 1.22 | 3.42 | 6.35 | 19.85 | 24.67 | 43.47 | 51.57 | 67.70 | 73.82 | 97.48 | 97.48 | 120.68 | 146.32 |
| VCT, hours | | 0.00 | 0.03 | 1.34 | 3.84 | 7.26 | 23.44 | 29.37 | 53.33 | 64.05 | 86.25 | 95.08 | 130.68 | 130.68 | 167.73 | 210.23 |
| Mg, mol/l | 3.32E-06 | 0.00E+00 | 0.00E+00 | 0.00E+00 | 0.00E+00 | | 0.00E+00 | 4.59E-05 | 0.00E+00 | | 0.00E+00 | 0.00E+00 | 0.00E+00 | | 0.00E+00 | 0.00E+00 |
| Al, mol/l | 2.94E-06 | 2.60E-05 | 1.00E-06 | 3.13E-05 | 2.63E-05 | | 3.33E-05 | 0.00E+00 | 4.11E-05 | | 4.35E-05 | 4.52E-05 | 4.74E-05 | | 4.63E-05 | 4.94E-05 |
| Si, mol/l (±1%) | 7.55E-06 | 4.56E-05 | 3.91E-05 | 4.53E-05 | 4.34E-05 | | 6.86E-05 | 0.00E+00 | 8.44E-05 | | 9.69E-05 | 9.49E-05 | 1.04E-04 | | 1.06E-04 | 1.19E-04 |
| K, mol/l | 3.89E-05 | 3.05E-04 | 5.46E-04 | 6.92E-04 | 5.92E-04 | | 6.99E-04 | 5.49E-04 | 8.46E-04 | | 9.02E-04 | 8.12E-04 | 7.69E-04 | | 5.16E-04 | 7.03E-04 |
| Ca, mol/l | 1.36E-05 | 9.75E-05 | 9.72E-05 | 1.09E-04 | 9.66E-05 | | 9.89E-05 | 7.52E-03 | 1.06E-04 | | 9.90E-05 | 1.03E-04 | 1.03E-04 | | 1.08E-04 | 1.05E-04 |
| Mn, mol/l | 0.00E+00 | 0.00E+00 | 0.00E+00 | 0.00E+00 | 0.00E+00 | | 0.00E+00 | 0.00E+00 | 0.00E+00 | | 0.00E+00 | 0.00E+00 | 0.00E+00 | | 0.00E+00 | 0.00E+00 |
| Fe, mol/l | 0.00E+00 | 0.00E+00 | 0.00E+00 | 7.81E-06 | 1.10E-06 | | 2.13E-05 | 0.00E+00 | 3.39E-06 | | 6.24E-07 | 0.00E+00 | 3.16E-06 | | 2.91E-06 | 8.52E-07 |
| Sr, mol/l | 6.42E-08 | 2.20E-07 | 1.65E-07 | 1.69E-07 | 8.60E-08 | | 1.72E-07 | 1.88E-06 | 2.43E-07 | | 2.67E-07 | 2.34E-07 | 2.48E-07 | | 2.26E-07 | 2.75E-07 |
| Ba, mol/l | 2.98E-08 | 5.40E-06 | 4.07E-06 | 3.20E-06 | 3.39E-06 | | 3.18E-06 | 0.00E+00 | 3.38E-06 | | 3.18E-06 | 4.04E-06 | 3.43E-06 | | 4.53E-06 | 4.36E-06 |
| Na (est), mol/l | | 1.36E+00 | 1.36E+00 | 1.36E+00 | 1.36E+00 | | 1.36E+00 | 1.36E+00 | 1.36E+00 | | 1.36E+00 | 1.36E+00 | 1.36E+00 | | 1.36E+00 | 1.37E+00 |
| Fluid in exp. (kg) | | 0.098 | 0.097 | 0.088 | 0.085 | 0.083 | 0.081 | 0.079 | 0.076 | 0.073 | 0.070 | 0.067 | 0.064 | 0.062 | 0.061 | 0.058 |

| 175 cont.: 1.36M NaCl, 4bar pCO2, 70C | | | | | | | | | | | | | | | |
|---|---|---|---|---|---|---|---|---|---|---|---|---|---|---|---|
| Time, hours | Std. Dev. Mol/l | 170.90 | 194.48 | 261.32 | 333.82 | 362.73 | 404.45 | 434.10 | 502.48 | 502.48 | 548.62 | 593.98 | 648.40 | 721.90 | 721.90 |
| VCT, hours | | 253.05 | 296.20 | 426.04 | 573.86 | 636.42 | 732.77 | 805.56 | 984.19 | 984.19 | 1117.64 | 1261.10 | 1452.15 | 1739.86 | 1739.86 |
| Mg, mol/l | 3.32E-06 | | 0.00E+00 | 0.00E+00 | 0.00E+00 | 0.00E+00 | 0.00E+00 | | 0.00E+00 | 0.00E+00 | 0.00E+00 | | 0.00E+00 | 0.00E+00 | 0.00E+00 |
| Al, mol/l | 2.94E-06 | | 4.99E-05 | 4.49E-05 | 4.41E-05 | 4.17E-05 | 3.89E-05 | | 3.57E-05 | 3.75E-05 | 3.70E-05 | | 3.24E-05 | 3.03E-05 | 3.11E-05 |
| Si, mol/l (±1%) | 7.55E-06 | | 1.29E-04 | 1.46E-04 | 1.63E-04 | 1.64E-04 | 1.70E-04 | | 1.90E-04 | 1.86E-04 | 1.96E-04 | | 2.20E-04 | 2.45E-04 | 2.47E-04 |
| K, mol/l | 3.89E-05 | | 6.68E-04 | 6.10E-04 | 6.27E-04 | 6.45E-04 | 5.77E-04 | | 5.95E-04 | 5.56E-04 | 5.32E-04 | | 4.69E-04 | 5.31E-04 | 4.38E-04 |
| Ca, mol/l | 1.36E-05 | | 1.04E-04 | 1.09E-04 | 1.08E-04 | 1.05E-04 | 1.08E-04 | | 1.10E-04 | 1.10E-04 | 1.11E-04 | | 1.12E-04 | 1.14E-04 | 1.18E-04 |
| Mn, mol/l | 0.00E+00 | | 0.00E+00 | 0.00E+00 | 0.00E+00 | 0.00E+00 | 0.00E+00 | | 0.00E+00 | 0.00E+00 | 0.00E+00 | | 0.00E+00 | 0.00E+00 | 0.00E+00 |
| Fe, mol/l | 0.00E+00 | | 6.09E-07 | 1.05E-05 | 0.00E+00 | 4.29E-07 | 3.55E-07 | | 1.24E-05 | 0.00E+00 | 0.00E+00 | | 0.00E+00 | 3.23E-06 | 0.00E+00 |
| Sr, mol/l | 6.42E-08 | | 2.38E-07 | 2.40E-07 | 2.51E-07 | 2.63E-07 | 2.40E-07 | | 3.10E-07 | 2.67E-07 | 2.55E-07 | | 2.92E-07 | 2.86E-07 | 2.44E-07 |
| Ba, mol/l | 2.98E-08 | | 3.22E-06 | 3.80E-06 | 3.21E-06 | 3.15E-06 | 3.28E-06 | | 4.48E-06 | 3.72E-06 | 3.20E-06 | | 4.02E-06 | 3.60E-06 | 3.98E-06 |
| Na (est), mol/l | | | 1.37E+00 | 1.37E+00 | 1.37E+00 | 1.37E+00 | 1.37E+00 | | 1.37E+00 | 1.37E+00 | 1.37E+00 | | 1.37E+00 | 1.37E+00 | 1.37E+00 |
| Fluid in exp. (kg) | | 0.056 | 0.053 | 0.050 | 0.047 | 0.045 | 0.042 | 0.039 | 0.037 | 0.035 | 0.033 | 0.031 | 0.028 | 0.025 | 0.022 |

| 176: DI, 31bar pCO2, 70C | | | | | | | | | | | | | | | | | |
|---|---|---|---|---|---|---|---|---|---|---|---|---|---|---|---|---|---|
| Time, hours | Std. Dev. Mol/l | -0.15 | 0.05 | 1.10 | 3.33 | 6.02 | 19.73 | 24.58 | 43.18 | 51.28 | 67.42 | 73.53 | 97.20 | 97.20 | 120.40 | 146.03 | 170.62 |
| VCT, hours | | 0.00 | 0.05 | 1.12 | 3.46 | 21.14 | 26.48 | 47.29 | 75.17 | 82.39 | 110.76 | 139.36 | 171.56 | 233.89 | 323.03 | 421.87 | 462.17 |
| Mg, mol/l | 1.16E-06 | 0.00E+00 | 0.00E+00 | 0.00E+00 | 0.00E+00 | | 0.00E+00 | 0.00E+00 | 0.00E+00 | | 0.00E+00 | 0.00E+00 | 0.00E+00 | | 0.00E+00 | 0.00E+00 | |
| Al, mol/l | 1.51E-07 | 3.57E-06 | 2.60E-06 | 7.91E-07 | 1.24E-06 | | 1.73E-06 | 2.74E-06 | 2.55E-06 | | 3.79E-06 | 4.68E-06 | 5.73E-06 | | 4.38E-06 | 4.42E-06 | |
| Si, mol/l (±9%) | 1.21E-05 | 5.79E-05 | 7.51E-05 | 8.80E-05 | 6.87E-05 | | 8.94E-05 | 8.05E-05 | 8.75E-05 | | 1.02E-04 | 1.03E-04 | 1.13E-04 | | 1.07E-04 | 1.22E-04 | |
| K, mol/l | 7.46E-07 | 2.80E-05 | 3.91E-05 | 3.87E-05 | 3.38E-05 | | 3.93E-05 | 3.42E-05 | 4.05E-05 | | 3.94E-05 | 4.00E-05 | 3.97E-05 | | 4.29E-05 | 3.95E-05 | |
| Ca, mol/l | 5.67E-06 | 9.12E-05 | 1.50E-04 | 1.48E-04 | 1.25E-04 | | 1.39E-04 | 1.26E-04 | 1.40E-04 | | 1.38E-04 | 1.34E-04 | 1.40E-04 | | 1.35E-04 | 1.38E-04 | |
| Mn, mol/l | 0.00E+00 | 0.00E+00 | 4.53E-06 | 1.14E-05 | 9.98E-06 | | 8.28E-06 | 1.30E-06 | 1.36E-06 | | 0.00E+00 | 0.00E+00 | 0.00E+00 | | 0.00E+00 | 0.00E+00 | |
| Fe, mol/l | 0.00E+00 | 0.00E+00 | 0.00E+00 | 0.00E+00 | 2.01E-05 | | 2.27E-04 | 1.64E-04 | 2.47E-04 | | 2.37E-04 | 1.59E-04 | 2.29E-04 | | 2.13E-04 | 2.95E-04 | |
| Sr, mol/l | 1.59E-08 | 1.91E-07 | 2.83E-07 | 3.32E-07 | 2.84E-07 | | 2.79E-07 | 2.14E-07 | 2.38E-07 | | 2.56E-07 | 2.43E-07 | 2.65E-07 | | 2.12E-07 | 2.59E-07 | |
| Ba, mol/l | 3.24E-08 | 1.92E-06 | 1.13E-06 | 2.07E-07 | 3.30E-07 | | 6.22E-07 | 4.97E-07 | 6.01E-07 | | 6.78E-07 | 5.66E-07 | 6.15E-07 | | 8.53E-07 | 6.95E-07 | |
| Na (est), mol/l | | 8.48E-06 | 1.11E-06 | 8.92E-06 | 1.66E-05 | | 7.59E-05 | 9.75E-05 | 1.58E-04 | | 1.99E-04 | 2.36E-04 | 2.69E-04 | | 4.46E-04 | 4.59E-04 | |
| Fluid in exp. (kg) | | 0.157 | 0.156 | 0.153 | 0.149 | 0.147 | 0.144 | 0.142 | 0.139 | 0.137 | 0.135 | 0.132 | 0.130 | 0.128 | 0.126 | 0.124 | 0.122 |

| 176 cont.: DI, 31bar pCO2, 70C | | | | | | | | | | | | | | | | |
|---|---|---|---|---|---|---|---|---|---|---|---|---|---|---|---|---|
| Time, hours | Std. Dev. Mol/l | 194.20 | 261.03 | 333.53 | 362.45 | 404.17 | 433.82 | 502.20 | 502.20 | 548.33 | 593.70 | 648.12 | 721.62 | 815.98 | 1007.62 | 1007.62 |
| VCT, hours | | 521.55 | 666.42 | 666.42 | 737.44 | 898.62 | 1022.84 | 1187.76 | 666.42 | 737.44 | 809.46 | 898.62 | 1022.84 | 1187.76 | 1538.53 | 1538.53 |
| Mg, mol/l | 1.16E-06 | 0.00E+00 | 0.00E+00 | 0.00E+00 | 0.00E+00 | 0.00E+00 | | 0.00E+00 | 0.00E+00 | 0.00E+00 | | 0.00E+00 | 0.00E+00 | 0.00E+00 | 0.00E+00 | 0.00E+00 |
| Al, mol/l | 1.51E-07 | 7.82E-06 | 4.53E-06 | 4.48E-06 | 5.19E-06 | 5.61E-06 | | 5.85E-06 | 1.08E-05 | 1.01E-05 | | 9.98E-06 | 1.18E-05 | 2.06E-05 | 1.21E-05 | 2.28E-05 |
| Si, mol/l (±9%) | 1.21E-05 | 1.58E-04 | 1.55E-04 | 1.68E-04 | 1.93E-04 | 2.07E-04 | | 2.16E-04 | 1.87E-04 | 2.16E-04 | | 2.01E-04 | 2.19E-04 | 2.34E-04 | 2.50E-04 | 2.37E-04 |
| K, mol/l | 7.46E-07 | 4.59E-05 | 4.38E-05 | 4.50E-05 | 4.58E-05 | 4.62E-05 | | 4.87E-05 | 5.05E-05 | 5.35E-05 | | 4.72E-05 | 5.17E-05 | 5.64E-05 | 5.72E-05 | 5.60E-05 |
| Ca, mol/l | 5.67E-06 | 1.55E-04 | 1.38E-04 | 1.41E-04 | 1.44E-04 | 1.42E-04 | | 1.44E-04 | 1.35E-04 | 1.48E-04 | | 1.41E-04 | 1.45E-04 | 1.49E-04 | 1.53E-04 | 1.50E-04 |
| Mn, mol/l | 0.00E+00 | 4.59E-07 | 5.72E-07 | 1.13E-06 | 0.00E+00 | 0.00E+00 | | 0.00E+00 | 0.00E+00 | 0.00E+00 | | 0.00E+00 | 0.00E+00 | 0.00E+00 | 0.00E+00 | 0.00E+00 |
| Fe, mol/l | 0.00E+00 | 2.88E-04 | 4.09E-04 | 4.00E-04 | 2.68E-04 | 2.18E-04 | | 2.03E-04 | 1.57E-04 | 1.27E-04 | | 1.08E-04 | 1.17E-04 | 8.43E-05 | 1.56E-04 | 1.03E-04 |
| Sr, mol/l | 1.59E-08 | 3.35E-07 | 2.71E-07 | 2.90E-07 | 2.89E-07 | 3.05E-07 | | 3.24E-07 | 2.75E-07 | 3.46E-07 | | 3.01E-07 | 3.52E-07 | 3.55E-07 | 3.80E-07 | 3.59E-07 |
| Ba, mol/l | 3.24E-08 | 8.35E-07 | 8.89E-07 | 1.07E-06 | 9.74E-07 | 1.04E-06 | | 1.13E-06 | 1.09E-06 | 1.52E-06 | | 1.45E-06 | 1.56E-06 | 1.74E-06 | 1.90E-06 | 1.77E-06 |
| Na (est), mol/l | | 5.35E-04 | 5.10E-04 | 5.24E-04 | 5.33E-04 | 5.38E-04 | | 5.67E-04 | 5.88E-04 | 6.23E-04 | | 5.49E-04 | 6.01E-04 | 6.56E-04 | 6.65E-04 | 6.52E-04 |
| Fluid in exp. (kg) | | 0.119 | 0.117 | 0.114 | 0.112 | 0.110 | 0.107 | 0.105 | 0.102 | 0.101 | 0.098 | 0.095 | 0.092 | 0.089 | 0.085 | 0.082 |

| FCO2W10: DI, 31bar pCO2, 70C | | | | | | | | | | | | | | | | |
|---|---|---|---|---|---|---|---|---|---|---|---|---|---|---|---|---|
| Time, hours | Std. Dev. Mol/l | -0.90 | 25.80 | 93.43 | 188.90 | 238.48 | 335.05 | 431.73 | 529.90 | 623.32 | 676.65 | 935.40 | 1103.73 | 1274.07 | 1558.90 | 1558.98 |
| VCT, hours | | 0.00 | 25.80 | 95.27 | 195.90 | 249.43 | 356.41 | 466.40 | 583.04 | 698.12 | 766.28 | 1120.15 | 1358.81 | 1605.43 | 2029.32 | 2029.45 |
| Mg, mol/l | 6.47E-06 | 0.00E+00 | 0.00E+00 | 0.00E+00 | 0.00E+00 | 0.00E+00 | 0.00E+00 | 0.00E+00 | 0.00E+00 | 0.00E+00 | 0.00E+00 | 0.00E+00 | 0.00E+00 | 0.00E+00 | 0.00E+00 | 0.00E+00 |
| Al, mol/l | 5.09E-08 | 1.42E-06 | 1.58E-06 | 1.29E-06 | 1.47E-06 | 1.37E-06 | 1.34E-06 | 1.19E-06 | 1.24E-06 | 1.20E-06 | 1.15E-06 | 1.35E-06 | 1.42E-06 | 1.14E-06 | 1.23E-06 | 1.13E-06 |
| Si, mol/l (±11%) | 2.64E-07 | 6.43E-07 | 9.75E-07 | 1.34E-06 | 2.50E-06 | 2.28E-06 | 2.54E-06 | 3.18E-06 | 3.46E-06 | 4.14E-06 | 4.35E-06 | 5.26E-06 | 2.81E-06 | 4.98E-06 | 6.39E-06 | 7.37E-06 |
| K, mol/l | 2.33E-06 | 1.98E-06 | 3.46E-06 | 2.67E-06 | 5.87E-06 | 6.50E-06 | 6.72E-06 | 8.07E-06 | 9.16E-06 | 1.11E-05 | 1.23E-05 | 1.22E-05 | 1.98E-05 | 1.97E-05 | 2.20E-05 | 2.62E-05 |
| Ca, mol/l | 7.19E-06 | 5.47E-06 | 4.23E-06 | 3.34E-06 | 9.73E-06 | 4.63E-06 | 5.86E-06 | 4.15E-06 | 4.23E-06 | 4.49E-06 | 4.94E-06 | 5.36E-06 | 6.22E-06 | 5.18E-06 | 5.66E-06 | 6.62E-06 |
| Mn, mol/l | 1.65E-09 | 1.74E-06 | 2.10E-06 | 1.15E-06 | 2.40E-06 | 1.81E-06 | 2.46E-06 | 1.30E-06 | 1.31E-06 | 1.29E-06 | 1.26E-06 | 1.88E-06 | 1.55E-06 | 1.38E-06 | 1.43E-06 | 1.32E-06 |
| Fe, mol/l | 9.78E-09 | 6.81E-07 | 2.64E-06 | 1.18E-06 | 1.25E-06 | 1.21E-06 | 1.24E-06 | 9.69E-07 | 9.84E-07 | 9.79E-07 | 8.66E-07 | 1.17E-06 | 2.94E-06 | 1.50E-06 | 1.66E-06 | 9.88E-07 |
| Sr, mol/l | 8.95E-09 | 3.26E-06 | 2.60E-05 | 8.24E-06 | 1.07E-05 | 5.42E-06 | 5.42E-06 | 2.37E-06 | 2.36E-06 | 1.52E-06 | 1.39E-06 | 2.10E-06 | 5.98E-05 | 1.91E-05 | 6.00E-06 | 3.36E-06 |
| Ba, mol/l | 1.96E-09 | 5.00E-08 | 4.17E-08 | 9.72E-09 | 1.00E-07 | 3.58E-08 | 1.29E-07 | 2.50E-08 | 1.19E-08 | 1.18E-08 | 1.13E-08 | 1.61E-08 | 1.49E-08 | 1.35E-08 | 1.52E-08 | 1.42E-08 |
| Na (est), mol/l | - | 5.99E-07 | 6.57E-06 | 1.22E-05 | 4.35E-05 | 5.67E-05 | 7.45E-05 | 9.40E-05 | 1.07E-04 | 1.29E-04 | 1.44E-04 | 1.42E-04 | 2.30E-04 | 2.29E-04 | 2.57E-04 | 3.05E-04 |
| Fluid in exp. (kg) | - | 0.150 | 0.146 | 0.143 | 0.139 | 0.136 | 0.132 | 0.129 | 0.123 | 0.119 | 0.115 | 0.107 | 0.103 | 0.101 | 0.098 | 0.097 |

# A.3 Plagioclase Fluid Chemistry Data

| 122: 1.36M NaCl, 4bar pCO2, 22C | | | | | | | | | | | | | | | | |
|---|---|---|---|---|---|---|---|---|---|---|---|---|---|---|---|---|
| Time, hours | Std. Dev. Mol/l | -0.08 | 0.17 | 1.08 | 19.52 | 24.23 | 44.97 | 45.00 | 47.92 | 119.83 | 142.57 | 214.42 | 307.92 | 378.58 | 622.70 | 622.75 |
| VCT, hours | | 0.00 | 0.17 | 1.11 | 20.68 | 25.83 | 49.00 | 49.04 | 52.46 | 139.23 | 167.52 | 259.46 | 384.58 | 482.36 | 830.50 | 830.58 |
| Mg, mol/l | 6.47E-06 | 3.93E-06 | 3.39E-06 | 4.29E-06 | 4.48E-06 | 4.91E-06 | 5.95E-06 | 6.1E-06 | 5.86E-06 | 7.05E-06 | 7.27E-06 | 6.6E-06 | 6.94E-06 | 6.82E-06 | 6.85E-06 | 6.82E-06 |
| Al, mol/l | 5.09E-08 | 1.09E-06 | 7.41E-06 | 7.11E-06 | 2.60E-05 | 3.06E-05 | 3.88E-05 | 4.04E-05 | 4.25E-05 | 5.42E-05 | 5.81E-05 | 6.11E-05 | 6.83E-05 | 7.25E-05 | 8.34E-05 | 8.36E-05 |
| Si, mol/l (±11%) | 2.64E-07 | 1.72E-05 | 1.69E-05 | 1.61E-05 | 2.11E-05 | 2.54E-05 | 2.85E-05 | 2.99E-05 | 3.52E-05 | 4.69E-05 | 5.56E-05 | 6.34E-05 | 7.97E-05 | 8.05E-05 | 1.54E-04 | 1.29E-04 |
| K, mol/l | 2.33E-06 | 1.86E-05 | 1.91E-05 | 3.03E-05 | 2.56E-05 | 2.67E-05 | 2.58E-05 | 2.70E-05 | 2.41E-05 | 2.54E-05 | 2.51E-05 | 2.52E-05 | 2.34E-05 | 2.26E-05 | 2.24E-05 | 2.10E-05 |
| Ca, mol/l | 7.19E-06 | 3.68E-05 | 3.51E-05 | 5.17E-05 | 5.88E-05 | 6.71E-05 | 6.30E-05 | 7.84E-05 | 8.69E-05 | 1.18E-04 | 1.11E-04 | 1.28E-04 | 1.42E-04 | 1.49E-04 | 1.93E-04 | 1.69E-04 |
| Mn, mol/l | 1.65E-09 | 2.93E-07 | 9.51E-07 | 5.73E-07 | 7.39E-07 | 6.77E-07 | 7.48E-07 | 7.13E-07 | 7.04E-07 | 8.87E-07 | 8.25E-07 | 8.05E-07 | 1.12E-06 | 1.33E-06 | 2.26E-05 | 3.85E-06 |
| Fe, mol/l | 9.78E-09 | 8.97E-06 | 1.75E-05 | 5.51E-06 | 4.75E-06 | 3.96E-06 | 4.70E-06 | 1.22E-05 | 6.97E-06 | 1.12E-05 | 8.13E-06 | 6.29E-06 | 1.15E-05 | 1.21E-05 | 3.92E-04 | 6.08E-05 |
| Sr, mol/l | 8.95E-09 | 2.49E-07 | 2.00E-07 | 2.52E-07 | 2.84E-07 | 2.86E-07 | 3.03E-07 | 2.97E-07 | 3.02E-07 | 3.08E-07 | 3.07E-07 | 3.17E-07 | 3.26E-07 | 3.30E-07 | 3.24E-07 | 3.29E-07 |
| Ba, mol/l | 1.96E-09 | 1.60E-07 | 1.44E-07 | 2.06E-07 | 1.84E-07 | 1.89E-07 | 2.65E-07 | 3.20E-07 | 3.59E-07 | 2.17E-07 | 3.71E-07 | 4.50E-07 | 2.37E-07 | 4.10E-07 | 3.73E-07 | 3.03E-07 |
| Na (est), mol/l | - | 1.36E+00 | 1.36E+00 | 1.36E+00 | 1.36E+00 | 1.36E+00 | 1.36E+00 | 1.36E+00 | 1.36E+00 | 1.36E+00 | 1.36E+00 | 1.36E+00 | 1.36E+00 | 1.36E+00 | 1.36E+00 | 1.36E+00 |
| Fluid in exp. (kg) | - | 0.100 | 0.099 | 0.096 | 0.093 | 0.090 | 0.088 | 0.085 | 0.084 | 0.082 | 0.079 | 0.077 | 0.074 | 0.071 | 0.069 | 0.067 |

| 123: 1.36M NaCl, 31bar pCO2, 70C | | | | | | | | | | | |
|---|---|---|---|---|---|---|---|---|---|---|---|
| Time, hours | Std. Dev. Mol/l | -1.10 | 0.30 | 2.42 | 4.67 | 21.10 | 26.75 | 47.67 | 117.42 | 144.58 | 166.90 |
| VCT, hours | | 0.00 | 0.30 | 2.48 | 4.89 | 26.12 | 33.63 | 62.38 | 161.20 | 200.90 | 235.08 |
| Mg, mol/l | 6.47E-06 | 1.04E-05 | 1.12E-05 | 2.53E-05 | 4.99E-06 | 1.01E-05 | 9.02E-06 | 8.58E-06 | 8.71E-06 | 9.14E-06 | 5.57E-05 |
| Al, mol/l | 5.09E-08 | 3.92E-06 | 5.78E-06 | 1.94E-05 | 4.39E-05 | 6.08E-05 | 8.72E-05 | 1.05E-04 | 1.44E-04 | 1.99E-04 | 1.42E-03 |
| Si, mol/l (±25%) | 2.64E-07 | 1.14E-04 | 1.83E-04 | 2.76E-04 | 1.49E-04 | 2.83E-04 | 2.99E-04 | 3.42E-04 | 4.81E-04 | 5.41E-04 | 3.21E-03 |
| K, mol/l | 2.33E-06 | 2.54E-05 | 2.74E-05 | 2.60E-05 | 2.26E-05 | 2.68E-05 | 2.28E-05 | 1.90E-05 | 2.22E-05 | 2.54E-05 | 2.48E-04 |
| Ca, mol/l | 7.19E-06 | 1.46E-04 | 1.58E-04 | 1.19E-04 | 1.35E-04 | 1.12E-04 | 1.55E-04 | 1.88E-04 | 2.46E-04 | 3.49E-04 | 2.42E-03 |
| Mn, mol/l | 1.65E-09 | 4.40E-06 | 3.62E-06 | 8.61E-06 | 1.49E-06 | 1.17E-05 | 1.05E-05 | 1.24E-05 | 2.04E-05 | 2.63E-05 | 1.24E-04 |
| Fe, mol/l | 9.78E-09 | 2.67E-05 | 4.68E-05 | 2.44E-04 | 4.51E-05 | 4.19E-04 | 4.08E-04 | 5.49E-04 | 7.76E-04 | 8.90E-04 | 3.94E-03 |
| Sr, mol/l | 8.95E-09 | 6.01E-07 | 6.59E-07 | 4.45E-07 | 3.32E-07 | 3.40E-07 | 3.44E-07 | 3.40E-07 | 3.96E-07 | 4.81E-07 | 3.22E-06 |
| Ba, mol/l | 1.96E-09 | 4.90E-07 | 4.26E-07 | 4.11E-07 | 2.77E-07 | 4.02E-07 | 6.36E-07 | 2.77E-07 | 3.39E-07 | 3.27E-07 | 2.02E-06 |
| Na (est), mol/l | - | 1.36E+00 | 1.36E+00 | 1.36E+00 | 1.36E+00 | 1.36E+00 | 1.36E+00 | 1.36E+00 | 1.36E+00 | 1.36E+00 | 1.36E+00 |
| Fluid in exp. (kg) | - | 0.102 | 0.098 | 0.095 | 0.092 | 0.076 | 0.074 | 0.071 | 0.069 | 0.067 | 0.064 |

| 181: 1.36M NaCl, 4bar pCO2, 22C | | | | | | | | | | | | | | | | | | | | | |
|---|---|---|---|---|---|---|---|---|---|---|---|---|---|---|---|---|---|---|---|---|---|
| Time, hours | Std. Dev. Mol/l | -0.07 | 0.02 | 1.97 | 3.98 | 6.40 | 23.68 | 27.28 | 29.12 | 45.83 | 50.85 | 57.30 | 68.12 | 68.12 | 72.75 | 77.52 | 94.20 | 102.22 | 118.75 | 127.00 | 141.62 | 146.83 |
| VCT, hours | | 0.00 | 0.02 | 2.04 | 4.19 | 6.83 | 26.11 | 30.26 | 32.42 | 52.81 | 59.13 | 67.57 | 82.26 | 82.26 | 88.84 | 95.83 | 121.23 | 133.78 | 160.46 | 174.33 | 200.02 | 209.54 |
| Mg, mol/l | 5.36E-06 | 4.67E-06 | 4.65E-06 | 9.46E-06 | 5.11E-06 | 4.51E-06 | 4.78E-06 | 5.20E-06 | 4.08E-06 | 6.64E-06 | 5.43E-06 | 5.76E-06 | 5.70E-06 | 5.33E-06 | 5.21E-06 | 5.74E-06 | 5.13E-06 | 5.72E-06 | 5.20E-06 | 5.51E-06 | 5.29E-06 | 6.22E-06 |
| Al, mol/l | 4.18E-08 | 0.00E+00 | 0.00E+00 | 0.00E+00 | 0.00E+00 | 0.00E+00 | 0.00E+00 | 0.00E+00 | 0.00E+00 | 6.57E-06 | 1.15E-05 | 8.73E-06 | 2.15E-06 | 6.84E-06 | 9.88E-06 | 1.13E-05 | 7.52E-06 | 1.43E-05 | 5.74E-06 | 1.16E-05 | 6.73E-06 | 9.46E-06 |
| Si, mol/l (±3%) | 8.61E-06 | 3.04E-06 | 1.44E-05 | 6.57E-06 | 5.45E-06 | 4.50E-06 | 8.91E-06 | 4.29E-06 | 7.70E-06 | 6.85E-06 | 1.19E-05 | 7.58E-06 | 1.07E-05 | 3.11E-05 | 1.45E-05 | 1.19E-05 | 1.27E-05 | 1.37E-05 | 1.39E-05 | 1.51E-05 | 1.53E-05 | 1.63E-05 |
| K, mol/l | 2.69E-06 | 2.88E-05 | 2.76E-05 | 3.11E-05 | 3.99E-05 | 3.75E-05 | 3.04E-05 | 3.37E-05 | 2.68E-05 | 3.63E-05 | 3.00E-05 | 3.58E-05 | 4.21E-05 | 3.46E-05 | 3.20E-05 | 3.62E-05 | 3.97E-05 | 3.49E-05 | 4.04E-05 | 3.22E-05 | 3.64E-05 | 3.18E-05 |
| Ca, mol/l | 1.73E-06 | 3.73E-05 | 3.88E-05 | 4.01E-05 | 3.80E-05 | 3.43E-05 | 4.93E-05 | 2.87E-05 | 4.70E-05 | 3.53E-05 | 6.03E-05 | 3.61E-05 | 5.20E-05 | 5.23E-05 | 6.14E-05 | 5.61E-05 | 4.86E-05 | 5.47E-05 | 5.52E-05 | 6.23E-05 | 8.63E-05 | 5.92E-05 |
| Mn, mol/l | 2.55E-06 | 3.30E-07 | 1.21E-05 | 2.90E-06 | 1.05E-06 | 9.80E-07 | 5.99E-07 | 5.77E-07 | 4.74E-07 | 7.22E-07 | 6.55E-07 | 6.13E-07 | 1.40E-06 | 7.76E-07 | 8.86E-07 | 7.51E-07 | 1.58E-06 | 8.99E-07 | 1.17E-06 | 8.42E-07 | 8.93E-07 | 1.11E-06 |
| Fe, mol/l | 1.15E-06 | 0.00E+00 | 5.41E-04 | 1.27E-04 | 3.60E-05 | 3.20E-05 | 9.98E-06 | 8.77E-06 | 4.62E-06 | 1.13E-05 | 1.03E-05 | 7.21E-06 | 5.00E-05 | 1.36E-05 | 2.03E-05 | 1.42E-05 | 6.04E-05 | 2.18E-05 | 1.97E-05 | 1.54E-05 | 2.24E-05 | 2.90E-05 |
| Sr, mol/l | 8.33E-09 | 1.92E-07 | 2.00E-07 | 2.06E-07 | 2.00E-07 | 2.04E-07 | 2.13E-07 | 2.23E-07 | 1.85E-07 | 2.47E-07 | 2.21E-07 | 2.35E-07 | 2.36E-07 | 2.24E-07 | 2.28E-07 | 2.29E-07 | 2.17E-07 | 2.30E-07 | 2.19E-07 | 2.23E-07 | 2.39E-07 | 2.89E-07 |
| Ba, mol/l | 1.35E-06 | 5.49E-07 | 1.17E-06 | 7.69E-07 | 5.48E-07 | 3.87E-07 | 4.03E-07 | 8.92E-07 | 2.72E-07 | 1.17E-06 | 1.11E-06 | 9.11E-07 | 7.65E-07 | 1.09E-06 | 1.05E-06 | 1.11E-06 | 4.72E-07 | 9.12E-07 | 2.98E-07 | 4.48E-07 | 1.00E-06 | 1.51E-06 |
| Na (est), mol/l | | 1.36E+00 | 1.36E+00 | 1.36E+00 | 1.36E+00 | 1.36E+00 | 1.36E+00 | 1.36E+00 | 1.36E+00 | 1.36E+00 | 1.36E+00 | 1.36E+00 | 1.36E+00 | 1.36E+00 | 1.36E+00 | 1.36E+00 | 1.36E+00 | 1.36E+00 | 1.36E+00 | 1.36E+00 | 1.36E+00 | 1.36E+00 |
| Fluid in exp. (kg) | | 0.100 | 0.098 | 0.095 | 0.092 | 0.090 | 0.088 | 0.085 | 0.083 | 0.081 | 0.078 | 0.075 | 0.072 | 0.070 | 0.069 | 0.067 | 0.065 | 0.063 | 0.061 | 0.058 | 0.056 | 0.054 |

| 181 cont.: 1.36M NaCl, 4bar pCO2, 22C | | | | | | | | | | | | | | | | | |
|---|---|---|---|---|---|---|---|---|---|---|---|---|---|---|---|---|---|
| Time, hours | Std. Dev. Mol/l | 168.08 | 172.02 | 172.02 | 193.57 | 197.68 | 215.70 | 243.02 | 263.67 | 288.15 | 312.93 | 372.78 | 404.35 | 455.97 | 508.62 | 576.93 | 675.03 |
| VCT, hours | | 249.87 | 257.59 | 257.59 | 302.16 | 311.01 | 351.46 | 415.24 | 465.46 | 527.40 | 593.94 | 763.26 | 857.67 | 1022.21 | 1200.19 | 1450.83 | 1838.55 |
| Mg, mol/l | 5.36E-06 | 6.08E-06 | 5.99E-06 | 6.85E-06 | 5.86E-06 | 6.29E-06 | 5.56E-06 | 6.63E-06 | 6.63E-06 | 7.69E-06 | 6.69E-06 | 0.00E+00 | 0.00E+00 | 3.41E-05 | 1.46E-06 | 0.00E+00 | 0.00E+00 |
| Al, mol/l | 4.18E-08 | 1.33E-05 | 1.09E-05 | 1.09E-05 | 9.19E-06 | 1.55E-05 | 8.06E-06 | 1.30E-05 | 1.43E-05 | 2.68E-05 | 3.24E-05 | 1.29E-05 | 1.31E-05 | 1.35E-05 | 1.39E-05 | 1.44E-05 | 1.50E-05 |
| Si, mol/l (±3%) | 8.61E-06 | 1.82E-05 | 1.91E-05 | 1.99E-05 | 2.10E-05 | 2.20E-05 | 2.45E-05 | 3.12E-05 | 2.27E-05 | 3.14E-05 | 3.55E-05 | 3.76E-05 | 4.05E-05 | 4.52E-05 | 5.01E-05 | 5.67E-05 | 6.61E-05 |
| K, mol/l | 2.69E-06 | 3.08E-05 | 3.36E-05 | 4.98E-05 | 3.32E-05 | 3.02E-05 | 3.36E-05 | 4.36E-05 | 3.78E-05 | 3.75E-05 | 3.45E-05 | 3.45E-05 | 3.45E-05 | 3.45E-05 | 3.45E-05 | 3.45E-05 | 3.45E-05 |
| Ca, mol/l | 1.73E-06 | 6.49E-05 | 6.84E-05 | 6.50E-05 | 6.64E-05 | 7.61E-05 | 7.88E-05 | 8.37E-05 | 6.36E-05 | 8.58E-05 | 8.91E-05 | 8.48E-05 | 8.86E-05 | 9.75E-05 | 1.02E-04 | 1.10E-04 | 1.18E-04 |
| Mn, mol/l | 2.55E-06 | 1.09E-06 | 8.26E-07 | 9.69E-07 | 1.18E-06 | 7.95E-07 | 9.52E-07 | 9.64E-07 | 1.04E-06 | 8.36E-07 | 9.77E-07 | 7.97E-07 | 8.05E-07 | 9.50E-07 | 7.52E-07 | 9.50E-07 | 1.28E-06 |
| Fe, mol/l | 1.15E-06 | 3.63E-05 | 1.36E-05 | 1.73E-05 | 3.68E-05 | 1.05E-05 | 3.01E-05 | 2.09E-05 | 3.04E-05 | 1.20E-05 | 2.24E-05 | 2.75E-05 | 2.57E-05 | 3.43E-05 | 0.00E+00 | 0.00E+00 | 4.99E-05 |
| Sr, mol/l | 8.33E-09 | 2.60E-07 | 2.71E-07 | 2.66E-07 | 2.71E-07 | 2.52E-07 | 2.59E-07 | 3.14E-07 | 3.17E-07 | 2.83E-07 | 2.69E-07 | 0.00E+00 | 0.00E+00 | 0.00E+00 | 0.00E+00 | 0.00E+00 | 0.00E+00 |
| Ba, mol/l | 1.35E-06 | 7.76E-07 | 7.65E-07 | 2.25E-07 | 5.35E-07 | 7.13E-07 | 9.44E-07 | 1.82E-06 | 2.61E-06 | 1.44E-06 | 4.71E-07 | 3.09E-07 | 1.34E-07 | 5.21E-07 | 1.40E-06 | 2.11E-07 | 1.70E-07 |
| Na (est), mol/l | | 1.36E+00 | 1.36E+00 | 1.36E+00 | 1.36E+00 | 1.36E+00 | 1.36E+00 | 1.36E+00 | 1.36E+00 | 1.36E+00 | 1.36E+00 | 1.36E+00 | 1.36E+00 | 1.36E+00 | 1.36E+00 | 1.36E+00 | 1.36E+00 |
| Fluid in exp. (kg) | | 0.052 | 0.050 | 0.048 | 0.047 | 0.046 | 0.044 | 0.042 | 0.040 | 0.039 | 0.037 | 0.035 | 0.033 | 0.031 | 0.029 | 0.027 | 0.025 |

| 182: 1.36M NaCl, 31bar pCO2, 70C | | | | | | | | | | | | | | | | | | | | | | |
|---|---|---|---|---|---|---|---|---|---|---|---|---|---|---|---|---|---|---|---|---|---|---|
| Time, hours | Std. Dev. Mol/l | -0.23 | 0.08 | 2.35 | 4.32 | 6.73 | 24.02 | 27.60 | 29.43 | 46.15 | 51.17 | 57.60 | 68.45 | 68.45 | 73.07 | 77.85 | 94.52 | 102.53 | 119.00 | 127.33 | 141.85 | 147.17 |
| VCT, hours | | 0.00 | 0.08 | 2.45 | 4.57 | 7.24 | 26.92 | 31.08 | 33.27 | 53.72 | 60.03 | 68.33 | 82.57 | 82.57 | 88.87 | 95.57 | 119.56 | 131.44 | 156.54 | 169.68 | 193.36 | 202.34 |
| Mg, mol/l | 5.36E-06 | 5.87E-06 | 4.34E-06 | 5.41E-06 | 6.54E-06 | 8.07E-06 | 7.68E-06 | 7.23E-06 | 7.00E-06 | 7.73E-06 | 7.65E-06 | 2.55E-06 | 7.50E-06 | 8.24E-06 | 8.42E-06 | 7.52E-06 | 7.68E-06 | 8.19E-06 | 8.16E-06 | 8.29E-06 | 1.02E-05 | 8.29E-06 |
| Al, mol/l | 4.18E-08 | 0.00E+00 | 0.00E+00 | 0.00E+00 | 1.04E-05 | 8.93E-06 | 0.00E+00 | 1.23E-05 | 1.63E-05 | 1.53E-05 | 1.69E-05 | 0.00E+00 | 1.91E-05 | 2.94E-05 | 3.29E-05 | 2.90E-05 | 3.32E-05 | 4.10E-05 | 3.57E-05 | 4.62E-05 | 4.68E-05 | 4.65E-05 |
| Si, mol/l (±20%) | 8.61E-06 | 3.53E-04 | 1.53E-04 | 1.88E-04 | 2.10E-04 | 2.29E-04 | 2.39E-04 | 2.12E-04 | 1.78E-04 | 2.19E-04 | 1.94E-04 | 1.56E-04 | 1.88E-04 | 1.36E-04 | 1.77E-04 | 1.54E-04 | 1.63E-04 | 1.70E-04 | 1.77E-04 | 2.27E-04 | 1.86E-04 | 2.43E-04 |
| K, mol/l | 2.69E-06 | 6.74E-05 | 5.37E-05 | 5.28E-05 | 5.48E-05 | 7.48E-05 | 6.96E-05 | 5.23E-05 | 5.94E-05 | 5.59E-05 | 5.96E-05 | 1.29E-04 | 5.93E-05 | 5.70E-05 | 5.99E-05 | 5.66E-05 | 6.41E-05 | 6.16E-05 | 5.50E-05 | 5.82E-05 | 7.12E-05 | 5.97E-05 |
| Ca, mol/l | 1.73E-06 | 5.07E-05 | 6.66E-05 | 6.56E-05 | 6.80E-05 | 7.07E-05 | 7.00E-05 | 7.43E-05 | 8.14E-05 | 1.03E-04 | 9.99E-05 | 5.58E-05 | 1.06E-04 | 7.87E-05 | 1.14E-04 | 1.01E-04 | 1.01E-04 | 1.06E-04 | 1.14E-04 | 1.49E-04 | 1.36E-04 | 1.74E-04 |
| Mn, mol/l | 2.55E-06 | 1.30E-03 | 2.69E-04 | 1.93E-04 | 1.69E-04 | 1.48E-04 | 1.41E-04 | 1.03E-04 | 6.32E-05 | 9.54E-05 | 7.76E-05 | 6.32E-05 | 6.82E-05 | 5.97E-05 | 4.68E-05 | 4.23E-05 | 6.48E-05 | 6.52E-05 | 6.33E-05 | 6.17E-05 | 6.71E-05 | 5.04E-05 |
| Fe, mol/l | 1.15E-06 | 2.37E-02 | 3.31E-03 | 2.14E-03 | 2.03E-03 | 2.62E-03 | 2.43E-03 | 2.36E-03 | 1.46E-03 | 1.93E-03 | 1.68E-03 | 1.38E-03 | 1.44E-03 | 1.35E-03 | 1.01E-03 | 8.89E-04 | 1.32E-03 | 1.44E-03 | 1.38E-03 | 1.46E-03 | 1.56E-03 | 1.17E-03 |
| Sr, mol/l | 8.33E-09 | 2.09E-07 | 2.37E-07 | 2.56E-07 | 2.77E-07 | 3.10E-07 | 2.69E-07 | 2.38E-07 | 2.73E-07 | 2.58E-07 | 2.83E-07 | 1.78E-07 | 2.83E-07 | 2.88E-07 | 2.73E-07 | 2.77E-07 | 2.97E-07 | 2.74E-07 | 3.04E-07 | 2.89E-07 | 3.75E-07 | 3.20E-07 |
| Ba, mol/l | 1.35E-06 | 2.67E-07 | 7.49E-07 | 1.39E-06 | 1.31E-06 | 8.91E-07 | 1.27E-06 | 9.45E-07 | 1.37E-06 | 4.15E-07 | 1.80E-06 | 0.00E+00 | 1.40E-06 | 1.56E-06 | 4.74E-07 | 1.65E-06 | 1.73E-06 | 5.32E-07 | 1.66E-06 | 8.17E-07 | 1.46E-06 | 1.62E-06 |
| Na (est), mol/l | | 1.36E+00 | 1.36E+00 | 1.36E+00 | 1.36E+00 | 1.36E+00 | 1.36E+00 | 1.36E+00 | 1.36E+00 | 1.36E+00 | 1.36E+00 | 1.36E+00 | 1.36E+00 | 1.36E+00 | 1.36E+00 | 1.36E+00 | 1.36E+00 | 1.36E+00 | 1.36E+00 | 1.36E+00 | 1.36E+00 | 1.36E+00 |
| Fluid in exp. (kg) | | 0.100 | 0.099 | 0.094 | 0.091 | 0.089 | 0.087 | 0.085 | 0.083 | 0.081 | 0.078 | 0.076 | 0.075 | 0.073 | 0.072 | 0.070 | 0.068 | 0.067 | 0.065 | 0.063 | 0.060 | 0.058 |

| 182 cont.: 1.36M NaCl, 31bar pCO2, 70C | | | | | | | | | | | | | | | | | |
|---|---|---|---|---|---|---|---|---|---|---|---|---|---|---|---|---|---|
| Time, hours | Std. Dev. Mol/l | 168.40 | 172.37 | 172.37 | 193.88 | 198.00 | 216.03 | 243.35 | 264.73 | 288.40 | 313.27 | 373.10 | 404.70 | 460.20 | 509.40 | 577.45 | 675.47 |
| VCT, hours | | 239.41 | 246.57 | 246.57 | 287.40 | 295.51 | 332.51 | 390.98 | 438.72 | 494.23 | 555.37 | 710.71 | 797.80 | 960.77 | 1116.58 | 1347.73 | 1708.00 |
| Mg, mol/l | 5.36E-06 | 9.07E-06 | 9.33E-06 | 8.79E-06 | 9.55E-06 | 8.94E-06 | 1.52E-05 | 9.53E-06 | 9.95E-06 | 9.26E-06 | 9.45E-06 | 0.00E+00 | 7.95E-06 | 0.00E+00 | 1.08E-04 | 0.00E+00 | 2.02E-06 |
| Al, mol/l | 4.18E-08 | 4.18E-05 | 5.20E-05 | 5.75E-05 | 4.79E-05 | 5.45E-05 | 5.08E-05 | 5.10E-05 | 6.09E-05 | 5.76E-05 | 6.77E-05 | 7.34E-05 | 7.75E-05 | 8.45E-05 | 9.07E-05 | 9.90E-05 | 1.11E-04 |
| Si, mol/l (±20%) | 8.61E-06 | 1.92E-04 | 2.35E-04 | 1.91E-04 | 2.50E-04 | 1.97E-04 | 2.05E-04 | 2.10E-04 | 2.92E-04 | 2.25E-04 | 2.82E-04 | 2.49E-04 | 2.58E-04 | 2.76E-04 | 2.92E-04 | 3.16E-04 | 3.52E-04 |
| K, mol/l | 2.69E-06 | 5.67E-05 | 5.84E-05 | 5.96E-05 | 5.89E-05 | 5.76E-05 | 6.65E-05 | 5.93E-05 | 6.47E-05 | 6.11E-05 | 6.29E-05 | 6.29E-05 | 6.29E-05 | 6.29E-05 | 6.29E-05 | 6.29E-05 | 6.29E-05 |
| Ca, mol/l | 1.73E-06 | 1.39E-04 | 2.05E-04 | 1.42E-04 | 2.03E-04 | 1.45E-04 | 1.63E-04 | 1.64E-04 | 1.99E-04 | 1.49E-04 | 1.88E-04 | 2.06E-04 | 2.15E-04 | 2.30E-04 | 2.43E-04 | 2.61E-04 | 2.86E-04 |
| Mn, mol/l | 2.55E-06 | 5.81E-05 | 5.22E-05 | 4.07E-05 | 5.20E-05 | 4.32E-05 | 6.04E-05 | 6.11E-05 | 6.75E-05 | 5.64E-05 | 6.80E-05 | 6.78E-05 | 5.99E-05 | 5.79E-05 | 7.36E-05 | 6.29E-05 | 7.17E-05 |
| Fe, mol/l | 1.15E-06 | 1.28E-03 | 1.26E-03 | 9.65E-04 | 1.16E-03 | 1.01E-03 | 1.50E-03 | 1.42E-03 | 1.65E-03 | 1.34E-03 | 1.71E-03 | 1.82E-03 | 1.60E-03 | 1.54E-03 | 1.90E-03 | 1.57E-03 | 1.80E-03 |
| Sr, mol/l | 8.33E-09 | 3.31E-07 | 3.62E-07 | 3.46E-07 | 3.51E-07 | 3.59E-07 | 5.58E-07 | 3.79E-07 | 3.75E-07 | 3.74E-07 | 3.54E-07 | 0.00E+00 | 0.00E+00 | 0.00E+00 | 4.69E-06 | 0.00E+00 | 0.00E+00 |
| Ba, mol/l | 1.35E-06 | 8.77E-07 | 8.74E-07 | 1.18E-06 | 4.09E-07 | 1.21E-06 | 1.15E-06 | 2.25E-06 | 6.21E-07 | 2.14E-06 | 5.51E-07 | 3.76E-07 | 6.36E-07 | 5.28E-07 | 3.11E-07 | 2.43E-07 | 3.03E-07 |
| Na (est), mol/l | | 1.36E+00 | 1.36E+00 | 1.36E+00 | 1.36E+00 | 1.36E+00 | 1.36E+00 | 1.36E+00 | 1.36E+00 | 1.36E+00 | 1.36E+00 | 1.36E+00 | 1.36E+00 | 1.36E+00 | 1.36E+00 | 1.36E+00 | 1.36E+00 |
| Fluid in exp. (kg) | | 0.056 | 0.055 | 0.053 | 0.052 | 0.050 | 0.048 | 0.046 | 0.044 | 0.042 | 0.040 | 0.038 | 0.036 | 0.034 | 0.031 | 0.029 | 0.027 |

| 183: DI, 4bar pCO2, 70C | | | | | | | | | | | | | | | | | |
|---|---|---|---|---|---|---|---|---|---|---|---|---|---|---|---|---|---|
| Time, hours | Std. Dev. Mol/l | -0.12 | 0.13 | 1.65 | 3.85 | 6.73 | 20.28 | 25.10 | 43.90 | 52.00 | 68.13 | 74.25 | 97.92 | 97.92 | 121.12 | 146.75 | 171.33 |
| VCT, hours | | 0.00 | 0.13 | 1.70 | 4.04 | 7.19 | 22.43 | 28.03 | 50.50 | 60.48 | 81.02 | 89.05 | 121.24 | 121.24 | 154.41 | 192.63 | 230.63 |
| Mg, mol/l | 1.16E-06 | 0.00E+00 | 0.00E+00 | 0.00E+00 | 0.00E+00 | | 0.00E+00 | 0.00E+00 | 0.00E+00 | | 0.00E+00 | 0.00E+00 | 0.00E+00 | | 0.00E+00 | 0.00E+00 | |
| Al, mol/l | 1.51E-07 | 9.14E-06 | 1.14E-05 | 7.45E-06 | 8.18E-06 | | 1.41E-05 | 1.42E-05 | 1.69E-05 | | 1.96E-05 | 2.05E-05 | 2.43E-05 | | 2.30E-05 | 2.37E-05 | |
| Si, mol/l (±16%) | 1.21E-05 | 0.00E+00 | 1.16E-05 | 1.72E-05 | 1.78E-05 | | 2.50E-05 | 1.92E-05 | 1.63E-05 | | 1.58E-05 | 1.73E-05 | 2.14E-05 | | 1.29E-05 | 1.69E-05 | |
| K, mol/l | 7.46E-07 | 1.88E-05 | 1.61E-05 | 1.79E-05 | 1.74E-05 | | 1.88E-05 | 1.87E-05 | 1.74E-05 | | 1.64E-05 | 1.69E-05 | 1.62E-05 | | 1.82E-05 | 1.83E-05 | |
| Ca, mol/l | 5.67E-06 | 1.59E-05 | 1.60E-05 | 1.89E-05 | 2.43E-05 | | 3.47E-05 | 3.49E-05 | 4.48E-05 | | 4.21E-05 | 3.80E-05 | 4.17E-05 | | 4.22E-05 | 4.69E-05 | |
| Mn, mol/l | 0.00E+00 | 0.00E+00 | 0.00E+00 | 0.00E+00 | 0.00E+00 | | 0.00E+00 | 0.00E+00 | 0.00E+00 | | 0.00E+00 | 0.00E+00 | 0.00E+00 | | 0.00E+00 | 0.00E+00 | |
| Fe, mol/l | 0.00E+00 | 0.00E+00 | 0.00E+00 | 0.00E+00 | 0.00E+00 | | 0.00E+00 | 0.00E+00 | 0.00E+00 | | 0.00E+00 | 0.00E+00 | 0.00E+00 | | 0.00E+00 | 0.00E+00 | |
| Sr, mol/l | 1.59E-08 | 0.00E+00 | 0.00E+00 | 0.00E+00 | 0.00E+00 | | 0.00E+00 | 0.00E+00 | 0.00E+00 | | 0.00E+00 | 0.00E+00 | 0.00E+00 | | 0.00E+00 | 0.00E+00 | |
| Ba, mol/l | 3.24E-08 | 1.47E-06 | 1.08E-06 | 1.37E-06 | 1.37E-06 | | 2.59E-06 | 2.22E-06 | 1.16E-06 | | 1.96E-06 | 1.96E-06 | 1.69E-06 | | 1.98E-06 | 1.39E-06 | |
| Na (est), mol/l | | 0.00E+00 | 3.52E-06 | 5.23E-06 | 5.41E-06 | | 7.60E-06 | 5.84E-06 | 4.95E-06 | | 4.80E-06 | 5.25E-06 | 6.49E-06 | | 3.91E-06 | 5.13E-06 | |
| Fluid in exp. (kg) | | 0.098 | 0.096 | 0.093 | 0.091 | 0.088 | 0.086 | 0.083 | 0.080 | 0.078 | 0.076 | 0.073 | 0.071 | 0.068 | 0.067 | 0.065 | 0.062 |

| 183 cont.: DI, 4bar pCO2, 70C | | | | | | | | | | | | | | | |
|---|---|---|---|---|---|---|---|---|---|---|---|---|---|---|---|
| Time, hours | Std. Dev. Mol/l | 194.92 | 261.75 | 334.25 | 363.17 | 404.88 | 434.53 | 502.92 | 502.92 | 549.05 | 594.42 | 648.83 | 722.33 | 792.17 | 792.17 |
| VCT, hours | | 268.54 | 380.17 | 506.98 | 560.05 | 640.57 | 700.50 | 845.74 | 845.74 | 952.42 | 1063.21 | 1209.57 | 1424.14 | 1644.38 | 1644.38 |
| Mg, mol/l | 1.16E-06 | 0.00E+00 | 0.00E+00 | 0.00E+00 | 0.00E+00 | 0.00E+00 | 0.00E+00 | 0.00E+00 | 0.00E+00 | 0.00E+00 | 0.00E+00 | 0.00E+00 | 0.00E+00 | 0.00E+00 | 0.00E+00 |
| Al, mol/l | 1.51E-07 | 2.56E-05 | 2.99E-05 | 2.96E-05 | 4.81E-05 | 2.58E-05 | 0.00E+00 | 2.86E-05 | 2.99E-05 | 2.91E-05 | 0.00E+00 | 3.30E-05 | 3.11E-05 | 3.86E-05 | 3.82E-05 |
| Si, mol/l (±16%) | 1.21E-05 | 2.08E-05 | 2.31E-05 | 1.99E-05 | 2.69E-05 | 3.16E-05 | 0.00E+00 | 3.23E-05 | 2.99E-05 | 2.92E-05 | 0.00E+00 | 3.57E-05 | 3.62E-05 | 4.83E-05 | 4.08E-05 |
| K, mol/l | 7.46E-07 | 0.00E+00 | 1.66E-05 | 1.62E-05 | 1.77E-05 | 1.74E-05 | 2.84E-05 | 0.00E+00 | 2.68E-05 | 2.66E-05 | 2.92E-05 | 0.00E+00 | 2.56E-05 | 2.39E-05 | 2.70E-05 |
| Ca, mol/l | 5.67E-06 | 4.31E-05 | 4.87E-05 | 4.77E-05 | 4.70E-05 | 4.46E-05 | 0.00E+00 | 5.01E-05 | 5.24E-05 | 5.99E-05 | 0.00E+00 | 5.30E-05 | 4.62E-05 | 5.75E-05 | 5.72E-05 |
| Mn, mol/l | 0.00E+00 | 0.00E+00 | 0.00E+00 | 0.00E+00 | 0.00E+00 | 0.00E+00 | 0.00E+00 | 0.00E+00 | 0.00E+00 | 0.00E+00 | 0.00E+00 | 0.00E+00 | 0.00E+00 | 0.00E+00 | 0.00E+00 |
| Fe, mol/l | 0.00E+00 | 0.00E+00 | 1.65E-07 | 0.00E+00 | 0.00E+00 | 0.00E+00 | 0.00E+00 | 0.00E+00 | 0.00E+00 | 0.00E+00 | 0.00E+00 | 0.00E+00 | 0.00E+00 | 1.35E-07 | 0.00E+00 |
| Sr, mol/l | 1.59E-08 | 0.00E+00 | 0.00E+00 | 0.00E+00 | 0.00E+00 | 1.34E-08 | 0.00E+00 | 2.72E-08 | 6.63E-08 | 1.52E-09 | 0.00E+00 | 4.99E-08 | 3.09E-08 | 7.31E-08 | 5.25E-08 |
| Ba, mol/l | 3.24E-08 | 1.84E-06 | 1.40E-06 | 1.90E-06 | 1.27E-06 | 1.70E-06 | 0.00E+00 | 1.68E-06 | 1.61E-06 | 1.67E-06 | 0.00E+00 | 3.90E-07 | 1.73E-07 | 3.98E-07 | 1.56E-07 |
| Na (est), mol/l | | 6.32E-06 | 7.03E-06 | 6.06E-06 | 8.19E-06 | 9.59E-06 | 0.00E+00 | 9.82E-06 | 9.10E-06 | 8.87E-06 | 0.00E+00 | 1.08E-05 | 1.10E-05 | 1.47E-05 | 1.24E-05 |
| Fluid in exp. (kg) | | 0.060 | 0.058 | 0.055 | 0.052 | 0.050 | 0.048 | 0.045 | 0.043 | 0.042 | 0.039 | 0.036 | 0.033 | 0.030 | 0.028 |

| 184: 1.36M NaCl, 31bar pCO2, 70C | | | | | | | | | | | | | | | | | |
|---|---|---|---|---|---|---|---|---|---|---|---|---|---|---|---|---|---|
| Time, hours | Std. Dev. Mol/l | -0.20 | 0.05 | 1.10 | 3.33 | 6.07 | 19.73 | 24.58 | 43.18 | 51.28 | 67.42 | 73.53 | 97.20 | 97.20 | 120.40 | 146.03 | 170.62 |
| VCT, hours | | 0.00 | 0.05 | 1.12 | 3.44 | 6.32 | 21.03 | 26.35 | 47.18 | 56.43 | 75.24 | 82.54 | 111.42 | 111.42 | 140.64 | 173.62 | 205.93 |
| Mg, mol/l | 3.32E-06 | 0.00E+00 | 0.00E+00 | 0.00E+00 | 0.00E+00 | | 0.00E+00 | 0.00E+00 | 0.00E+00 | | 0.00E+00 | 0.00E+00 | | 0.00E+00 | 0.00E+00 | 0.00E+00 | |
| Al, mol/l | 2.94E-06 | 0.00E+00 | 0.00E+00 | 1.03E-06 | 8.21E-07 | | 4.02E-06 | 9.39E-06 | 8.51E-06 | | 1.56E-05 | 1.62E-05 | | 2.24E-05 | 1.25E-05 | 1.70E-05 | |
| Si, mol/l (±7%) | 7.55E-06 | 2.08E-05 | 3.16E-05 | 4.40E-05 | 4.58E-05 | | 8.18E-05 | 8.52E-05 | 8.66E-05 | | 9.65E-05 | 9.57E-05 | | 1.07E-04 | 9.08E-05 | 1.05E-04 | |
| K, mol/l | 3.89E-05 | 2.70E-04 | 3.08E-04 | 3.12E-04 | 2.63E-04 | | 2.87E-04 | 2.94E-04 | 3.85E-04 | | 3.07E-04 | 3.09E-04 | | 3.00E-04 | 2.78E-04 | 2.76E-04 | |
| Ca, mol/l | 1.36E-05 | 3.46E-05 | 5.02E-05 | 5.73E-05 | 4.97E-05 | | 4.35E-05 | 4.79E-05 | 5.26E-05 | | 5.57E-05 | 5.73E-05 | | 6.01E-05 | 5.08E-05 | 6.04E-05 | |
| Mn, mol/l | 0.00E+00 | 3.48E-06 | 2.76E-05 | 4.90E-05 | 5.03E-05 | | 4.16E-05 | 3.31E-05 | 3.57E-05 | | 3.29E-05 | 2.82E-05 | | 4.13E-05 | 3.04E-05 | 3.80E-05 | |
| Fe, mol/l | 0.00E+00 | 4.85E-07 | 2.48E-04 | 1.81E-04 | 1.79E-04 | | 9.07E-04 | 9.09E-04 | 1.10E-03 | | 9.87E-04 | 8.04E-04 | | 1.29E-03 | 9.47E-04 | 1.22E-03 | |
| Sr, mol/l | 6.42E-08 | 8.88E-08 | 5.21E-08 | 6.12E-08 | 7.51E-08 | | 6.20E-08 | 7.28E-08 | 6.89E-08 | | 1.05E-07 | 1.18E-07 | | 9.35E-08 | 4.28E-08 | 1.13E-08 | |
| Ba, mol/l | 2.98E-08 | 3.21E-06 | 1.65E-07 | 1.55E-07 | 1.51E-07 | | 2.16E-07 | 2.57E-07 | 2.68E-07 | | 4.09E-07 | 5.95E-07 | | 4.21E-07 | 5.95E-07 | 1.75E-07 | |
| Na (est), mol/l | | 1.36E+00 | 1.36E+00 | 1.36E+00 | 1.36E+00 | | 1.36E+00 | 1.36E+00 | 1.36E+00 | | 1.36E+00 | 1.36E+00 | | 1.36E+00 | 1.36E+00 | 1.36E+00 | |
| Fluid in exp. (kg) | | 0.157 | 0.156 | 0.153 | 0.150 | 0.148 | 0.145 | 0.142 | 0.139 | 0.136 | 0.134 | 0.131 | 0.128 | 0.125 | 0.124 | 0.121 | 0.119 |

| 184 cont.: 1.36M NaCl, 31bar pCO2, 70C | | | | | | | | | | | | | | | |
|---|---|---|---|---|---|---|---|---|---|---|---|---|---|---|---|
| Time, hours | Std. Dev. Mol/l | 194.20 | 261.03 | 333.53 | 362.45 | 404.17 | 433.82 | 502.20 | 502.20 | 548.33 | 593.70 | 648.12 | 721.62 | 815.98 | 1007.62 |
| VCT, hours | | 237.63 | 329.75 | 432.13 | 474.13 | 536.33 | 581.83 | 689.63 | 689.63 | 765.32 | 842.25 | 937.57 | 1070.30 | 1247.31 | 1621.47 |
| Mg, mol/l | 3.32E-06 | 0.00E+00 | 0.00E+00 | 0.00E+00 | 0.00E+00 | 0.00E+00 | | 0.00E+00 | 0.00E+00 | 0.00E+00 | | 0.00E+00 | 0.00E+00 | 0.00E+00 | 0.00E+00 |
| Al, mol/l | 2.94E-06 | 1.96E-05 | 1.37E-05 | 1.67E-05 | 2.06E-05 | 1.87E-05 | | 1.85E-05 | 2.78E-05 | 2.12E-05 | | 2.12E-05 | 2.62E-05 | 2.01E-05 | 2.29E-05 |
| Si, mol/l (±7%) | 7.55E-06 | 1.20E-04 | 1.27E-04 | 1.49E-04 | 1.36E-04 | 1.52E-04 | | 1.35E-04 | 1.49E-04 | 1.57E-04 | | 1.61E-04 | 1.64E-04 | 1.72E-04 | 1.86E-04 |
| K, mol/l | 3.89E-05 | 2.73E-04 | 2.37E-04 | 2.78E-04 | 2.58E-04 | 2.75E-04 | | 2.39E-04 | 2.48E-04 | 2.59E-04 | | 2.63E-04 | 2.54E-04 | 2.54E-04 | 2.32E-04 |
| Ca, mol/l | 1.36E-05 | 6.12E-05 | 6.14E-05 | 6.54E-05 | 6.89E-05 | 6.54E-05 | | 5.58E-05 | 5.92E-05 | 6.34E-05 | | 6.45E-05 | 6.46E-05 | 6.08E-05 | 6.73E-05 |
| Mn, mol/l | 0.00E+00 | 3.50E-05 | 3.99E-05 | 5.33E-05 | 3.41E-05 | 3.47E-05 | | 3.59E-05 | 3.71E-05 | 2.97E-05 | | 2.54E-05 | 2.58E-05 | 2.81E-05 | 3.74E-05 |
| Fe, mol/l | 0.00E+00 | 1.06E-03 | 1.29E-03 | 1.71E-03 | 1.07E-03 | 1.07E-03 | | 1.17E-03 | 1.14E-03 | 8.64E-04 | | 6.98E-04 | 7.26E-04 | 7.73E-04 | 1.03E-03 |
| Sr, mol/l | 6.42E-08 | 9.87E-08 | 6.19E-08 | 1.13E-07 | 5.85E-08 | 1.01E-07 | | 0.00E+00 | 4.83E-08 | 6.81E-08 | | 6.01E-08 | 3.75E-08 | 8.72E-08 | 4.61E-08 |
| Ba, mol/l | 2.98E-08 | 4.61E-07 | 6.43E-07 | 4.48E-07 | 6.69E-07 | 7.46E-07 | | 1.59E-07 | 1.67E-07 | 7.98E-08 | | 3.78E-07 | 1.33E-07 | 4.73E-07 | 3.43E-07 |
| Na (est), mol/l | | 1.36E+00 | 1.36E+00 | 1.36E+00 | 1.36E+00 | 1.36E+00 | | 1.36E+00 | 1.36E+00 | 1.36E+00 | | 1.36E+00 | 1.36E+00 | 1.36E+00 | 1.36E+00 |
| Fluid in exp. (kg) | | 0.116 | 0.113 | 0.110 | 0.107 | 0.105 | 0.102 | 0.099 | 0.096 | 0.095 | 0.092 | 0.089 | 0.086 | 0.083 | 0.080 |

| 185: DI, 31bar pCO2, 70C | | | | | | | | | | | | | | | |
|---|---|---|---|---|---|---|---|---|---|---|---|---|---|---|---|
| Time, hours | Std. Dev. Mol/l | -0.18 | 0.05 | 1.10 | 3.33 | 6.07 | 19.73 | 24.58 | 43.18 | 51.28 | 67.42 | 73.53 | 97.20 | 97.20 | 120.40 |
| VCT, hours | | 0.00 | 0.05 | 1.13 | 3.47 | 6.39 | 21.25 | 26.62 | 47.56 | 56.83 | 75.64 | 82.91 | 111.60 | 111.60 | 140.54 |
| Mg, mol/l | 1.16E-06 | 0.00E+00 | 0.00E+00 | 0.00E+00 | 0.00E+00 | | 0.00E+00 | 0.00E+00 | 0.00E+00 | | 0.00E+00 | 0.00E+00 | 0.00E+00 | | 0.00E+00 |
| Al, mol/l | 1.51E-07 | 2.10E-06 | 3.16E-06 | 1.26E-06 | 3.51E-06 | | 1.71E-05 | 3.92E-06 | 4.64E-06 | | 8.45E-06 | 1.06E-05 | 9.95E-06 | | 1.19E-05 |
| Si, mol/l (±19%) | 1.21E-05 | 6.00E-05 | 8.25E-05 | 8.37E-05 | 6.24E-05 | | 6.39E-05 | 2.98E-05 | 2.89E-05 | | 6.98E-05 | 8.08E-05 | 7.90E-05 | | 8.12E-05 |
| K, mol/l | 7.46E-07 | 4.27E-06 | 5.54E-06 | 3.86E-06 | 2.48E-06 | | 4.55E-06 | 3.30E-06 | 6.64E-06 | | 4.98E-06 | 5.63E-06 | 4.42E-06 | | 7.47E-06 |
| Ca, mol/l | 5.67E-06 | 1.31E-04 | 1.79E-04 | 1.68E-04 | 1.52E-04 | | 1.64E-04 | 1.32E-04 | 1.45E-04 | | 1.73E-04 | 1.84E-04 | 1.84E-04 | | 1.80E-04 |
| Mn, mol/l | 0.00E+00 | 0.00E+00 | 0.00E+00 | 0.00E+00 | 0.00E+00 | | 0.00E+00 | 0.00E+00 | 0.00E+00 | | 0.00E+00 | 0.00E+00 | 0.00E+00 | | 0.00E+00 |
| Fe, mol/l | 0.00E+00 | 0.00E+00 | 0.00E+00 | 0.00E+00 | 0.00E+00 | | 9.42E-07 | 0.00E+00 | 0.00E+00 | | 0.00E+00 | 0.00E+00 | 1.46E-06 | | 9.48E-07 |
| Sr, mol/l | 1.59E-08 | 1.13E-08 | 6.97E-08 | 4.55E-08 | 1.07E-08 | | 3.02E-08 | 0.00E+00 | 0.00E+00 | | 0.00E+00 | 2.55E-09 | 0.00E+00 | | 0.00E+00 |
| Ba, mol/l | 3.24E-08 | 9.81E-07 | 6.32E-07 | 0.00E+00 | 4.59E-08 | | 2.25E-08 | 4.08E-07 | 1.12E-07 | | 3.10E-07 | 1.81E-07 | 1.49E-07 | | 1.30E-07 |
| Na (est), mol/l | | 1.83E-05 | 2.51E-05 | 2.54E-05 | 1.90E-05 | | 1.94E-05 | 9.05E-06 | 8.79E-06 | | 2.12E-05 | 2.46E-05 | 2.40E-05 | | 2.47E-05 |
| Fluid in exp. (kg) | | 0.147 | 0.145 | 0.142 | 0.138 | 0.136 | 0.133 | 0.131 | 0.129 | 0.127 | 0.124 | 0.122 | 0.120 | 0.117 | 0.116 |

| 185 cont.: DI, 31bar pCO2, 70C | | | | | | | | | | | | | | | | | | |
|---|---|---|---|---|---|---|---|---|---|---|---|---|---|---|---|---|---|---|
| Time, hours | Std. Dev. Mol/l | 146.03 | 170.62 | 194.20 | 261.03 | 333.53 | 362.45 | 404.17 | 433.82 | 502.20 | 502.20 | 548.33 | 593.70 | 648.12 | 721.62 | 815.98 | 1007.62 | 1007.62 |
| VCT, hours | | 173.21 | 205.20 | 236.61 | 327.68 | 428.88 | 470.22 | 531.36 | 575.91 | 681.14 | 681.14 | 755.46 | 831.06 | 924.38 | 1054.30 | 1226.30 | 1588.08 | |
| Mg, mol/l | 1.16E-06 | 0.00E+00 | | 0.00E+00 | 0.00E+00 | 0.00E+00 | 0.00E+00 | 0.00E+00 | | 0.00E+00 | 0.00E+00 | 0.00E+00 | | 0.00E+00 | 0.00E+00 | 0.00E+00 | 0.00E+00 | |
| Al, mol/l | 1.51E-07 | 1.23E-05 | | 1.38E-05 | 1.21E-05 | 1.30E-05 | 1.50E-05 | 1.47E-05 | | 1.95E-05 | 2.27E-05 | 1.75E-05 | | 1.80E-05 | 1.56E-05 | 1.55E-05 | 1.65E-05 | |
| Si, mol/l (±19%) | 1.21E-05 | 8.93E-05 | | 1.04E-04 | 1.30E-04 | 1.70E-04 | 1.63E-04 | 1.74E-04 | | 2.71E-04 | 1.99E-04 | 2.41E-04 | | 2.32E-04 | 2.30E-04 | 2.33E-04 | 2.74E-04 | |
| K, mol/l | 7.46E-07 | 3.49E-06 | | 7.04E-06 | 6.22E-06 | 8.60E-06 | 5.53E-06 | 4.24E-06 | | 7.12E-06 | 6.56E-06 | 4.88E-06 | | 5.35E-06 | 4.91E-06 | 5.72E-06 | 6.97E-06 | |
| Ca, mol/l | 5.67E-06 | 1.79E-04 | | 1.94E-04 | 1.95E-04 | 2.14E-04 | 2.21E-04 | 2.19E-04 | | 2.70E-04 | 2.30E-04 | 2.48E-04 | | 2.37E-04 | 2.39E-04 | 2.32E-04 | 2.51E-04 | |
| Mn, mol/l | 0.00E+00 | 0.00E+00 | | 0.00E+00 | 0.00E+00 | 0.00E+00 | 0.00E+00 | 0.00E+00 | | 0.00E+00 | 0.00E+00 | 0.00E+00 | | 0.00E+00 | 0.00E+00 | 0.00E+00 | 0.00E+00 | |
| Fe, mol/l | 0.00E+00 | 2.69E-06 | | 1.88E-06 | 1.29E-05 | 2.16E-05 | 1.43E-05 | 1.34E-05 | | 2.63E-05 | 8.93E-06 | 1.46E-05 | | 1.84E-05 | 2.61E-05 | 3.31E-05 | 5.46E-05 | |
| Sr, mol/l | 1.59E-08 | 1.84E-09 | | 0.00E+00 | 0.00E+00 | 2.24E-08 | 1.91E-08 | 2.02E-08 | | 1.22E-07 | 1.92E-08 | 6.21E-08 | | 3.51E-08 | 1.77E-08 | 3.99E-09 | 3.40E-08 | |
| Ba, mol/l | 3.24E-08 | 1.37E-09 | | 1.01E-07 | 3.88E-08 | 9.08E-08 | 1.10E-07 | 1.06E-07 | | 2.86E-07 | 1.18E-08 | 7.05E-08 | | 0.00E+00 | 5.26E-08 | 0.00E+00 | 1.38E-07 | |
| Na (est), mol/l | | 2.72E-05 | | 3.17E-05 | 3.96E-05 | 5.17E-05 | 4.94E-05 | 5.28E-05 | | 8.23E-05 | 6.06E-05 | 7.31E-05 | | 7.06E-05 | 7.01E-05 | 7.07E-05 | 8.34E-05 | |
| Fluid in exp. (kg) | | 0.114 | 0.112 | 0.109 | 0.107 | 0.104 | 0.102 | 0.099 | 0.097 | 0.094 | 0.091 | 0.090 | 0.087 | 0.085 | 0.082 | 0.080 | 0.077 | 0.074 |

# A.4 Calcite Fluid Chemistry Data

| 191: 1.36M NaCl, 4bar pCO2, 22C | | | | | | | | | | | | | | | | | | | | |
|---|---|---|---|---|---|---|---|---|---|---|---|---|---|---|---|---|---|---|---|---|
| Time, hours | Std. Dev. Mol/l | -0.07 | 0.02 | 1.97 | 3.98 | 6.40 | 23.68 | 27.28 | 29.12 | 45.83 | 50.85 | 57.30 | 68.12 | 68.12 | 72.75 | 77.52 | 94.20 | 102.22 | 118.75 | 127.00 |
| VCT, hours | | 0.00 | 0.02 | 2.03 | 4.19 | 6.83 | 26.19 | 30.33 | 32.49 | 52.65 | 58.87 | 67.13 | 81.51 | 81.51 | 87.93 | 94.71 | 119.11 | 131.16 | 156.80 | 169.96 |
| Mg, mol/l | 5.36E-06 | 2.39E-05 | 2.67E-05 | 4.91E-05 | 5.88E-05 | 6.40E-05 | 1.13E-04 | 1.11E-04 | 1.13E-04 | 1.28E-04 | 1.20E-04 | 1.16E-04 | 1.20E-04 | 1.10E-04 | 1.11E-04 | 1.13E-04 | 1.24E-04 | 1.25E-04 | 1.28E-04 | 1.26E-04 |
| Al, mol/l | 4.18E-08 | 0.00E+00 | 0.00E+00 | 0.00E+00 | 0.00E+00 | 0.00E+00 | 0.00E+00 | 0.00E+00 | 0.00E+00 | 0.00E+00 | 0.00E+00 | 0.00E+00 | 0.00E+00 | 0.00E+00 | 0.00E+00 | 0.00E+00 | 0.00E+00 | 0.00E+00 | 0.00E+00 | 0.00E+00 |
| Si, mol/l | 8.61E-06 | 4.51E-06 | 6.50E-06 | 5.26E-06 | 2.22E-06 | 9.22E-06 | 3.16E-06 | 1.92E-06 | 1.43E-06 | 6.83E-06 | 4.27E-06 | 4.16E-06 | 6.11E-06 | 3.72E-06 | 3.89E-06 | 2.67E-06 | 2.17E-06 | 2.97E-06 | 1.22E-06 | 3.51E-07 |
| K, mol/l | 2.69E-06 | 0.00E+00 | 0.00E+00 | 0.00E+00 | 0.00E+00 | 0.00E+00 | 0.00E+00 | 0.00E+00 | 0.00E+00 | 0.00E+00 | 0.00E+00 | 0.00E+00 | 0.00E+00 | 0.00E+00 | 0.00E+00 | 0.00E+00 | 0.00E+00 | 0.00E+00 | 0.00E+00 | 0.00E+00 |
| Ca, mol/l (±14%) | 1.73E-06 | 6.46E-04 | 6.53E-04 | 5.40E-03 | 6.02E-03 | 6.10E-03 | 1.32E-02 | 1.27E-02 | 1.08E-02 | 1.90E-02 | 1.42E-02 | 1.47E-02 | 1.62E-02 | 1.33E-02 | 1.47E-02 | 1.38E-02 | 1.50E-02 | 1.58E-02 | 1.36E-02 | 1.14E-02 |
| Mn, mol/l | 2.55E-06 | 1.23E-08 | 4.44E-06 | 3.15E-06 | 1.98E-06 | 1.77E-06 | 2.81E-06 | 2.60E-06 | 2.59E-06 | 4.36E-06 | 4.67E-06 | 3.70E-06 | 4.57E-06 | 4.58E-06 | 2.79E-06 | 2.73E-06 | 3.14E-06 | 3.17E-06 | 3.21E-06 | 3.67E-06 |
| Fe, mol/l | 1.15E-06 | 2.74E-07 | 2.40E-04 | 1.41E-04 | 5.48E-05 | 2.99E-05 | 6.02E-06 | 3.69E-06 | 7.79E-06 | 8.05E-05 | 1.14E-04 | 6.48E-05 | 1.06E-04 | 1.15E-04 | 9.24E-06 | 9.01E-06 | 8.66E-06 | 8.82E-06 | 4.10E-06 | 2.61E-05 |
| Sr, mol/l | 8.33E-09 | 1.06E-06 | 1.20E-06 | 2.72E-06 | 3.32E-06 | 3.67E-06 | 6.72E-06 | 6.61E-06 | 6.72E-06 | 7.61E-06 | 7.09E-06 | 6.77E-06 | 7.16E-06 | 6.58E-06 | 6.73E-06 | 6.81E-06 | 7.48E-06 | 7.65E-06 | 7.90E-06 | 7.72E-06 |
| Ba, mol/l | 1.35E-06 | 8.93E-08 | 4.03E-07 | 2.19E-07 | 1.74E-07 | 6.33E-08 | 1.33E-09 | 0.00E+00 | 0.00E+00 | 1.32E-08 | 0.00E+00 | 0.00E+00 | 2.09E-08 | 1.01E-07 | 0.00E+00 | 2.17E-08 | 0.00E+00 | 1.86E-08 | 0.00E+00 | 1.69E-08 |
| Na (est), mol/l | | 1.36E+00 | 1.36E+00 | 1.36E+00 | 1.36E+00 | 1.36E+00 | 1.36E+00 | 1.36E+00 | 1.36E+00 | 1.36E+00 | 1.36E+00 | 1.36E+00 | 1.36E+00 | 1.36E+00 | 1.36E+00 | 1.36E+00 | 1.36E+00 | 1.36E+00 | 1.36E+00 | 1.36E+00 |
| Alkalinity(est), mol/l | | 6.46E-04 | 6.53E-04 | 5.40E-03 | 6.02E-03 | 6.10E-03 | 1.32E-02 | 1.27E-02 | 1.08E-02 | 1.90E-02 | 1.42E-02 | 1.47E-02 | 1.62E-02 | 1.33E-02 | 1.47E-02 | 1.38E-02 | 1.50E-02 | 1.58E-02 | 1.36E-02 | 1.14E-02 |
| Fluid in exp. (kg) | | 0.100 | 0.098 | 0.095 | 0.092 | 0.090 | 0.088 | 0.085 | 0.084 | 0.081 | 0.079 | 0.077 | 0.074 | 0.072 | 0.071 | 0.069 | 0.067 | 0.065 | 0.063 | 0.061 |

| 191 cont.: 1.36M NaCl, 4bar pCO2, 22C | | | | | | | | | | | | | | | | | | | |
|---|---|---|---|---|---|---|---|---|---|---|---|---|---|---|---|---|---|---|---|
| Time, hours | Std. Dev. Mol/l | 141.62 | 146.83 | 168.08 | 172.02 | 172.02 | 193.57 | 197.68 | 215.70 | 243.02 | 263.67 | 288.15 | 312.93 | 372.78 | 404.35 | 455.97 | 508.55 | 576.93 | 675.03 |
| VCT, hours | | 193.99 | 202.90 | 240.35 | 247.49 | 247.49 | 288.61 | 296.74 | 333.61 | 391.53 | 436.89 | 492.77 | 551.77 | 702.18 | 785.39 | 928.59 | 1083.14 | 1299.81 | 1628.84 |
| Mg, mol/l | 5.36E-06 | 1.31E-04 | 1.22E-04 | 1.21E-04 | 1.19E-04 | 1.24E-04 | 1.24E-04 | 1.22E-04 | 1.28E-04 | 1.40E-04 | 1.50E-04 | 1.50E-04 | 1.55E-04 | 1.41E-04 | 1.32E-04 | 1.51E-04 | 1.26E-04 | 1.25E-04 | 1.51E-04 |
| Al, mol/l | 4.18E-08 | 0.00E+00 | 0.00E+00 | 0.00E+00 | 0.00E+00 | 0.00E+00 | 0.00E+00 | 0.00E+00 | 0.00E+00 | 0.00E+00 | 0.00E+00 | 0.00E+00 | 0.00E+00 | 0.00E+00 | 0.00E+00 | 0.00E+00 | 0.00E+00 | 0.00E+00 | 0.00E+00 |
| Si, mol/l | 8.61E-06 | 2.63E-06 | 2.08E-06 | 1.71E-06 | 2.19E-06 | 7.41E-07 | 2.60E-06 | 9.36E-06 | 2.25E-06 | 1.03E-06 | 2.45E-06 | 3.34E-06 | 2.61E-06 | 0.00E+00 | 0.00E+00 | 0.00E+00 | 0.00E+00 | 0.00E+00 | 0.00E+00 |
| K, mol/l | 2.69E-06 | 0.00E+00 | 0.00E+00 | 0.00E+00 | 0.00E+00 | 0.00E+00 | 0.00E+00 | 0.00E+00 | 0.00E+00 | 0.00E+00 | 0.00E+00 | 0.00E+00 | 0.00E+00 | 0.00E+00 | 0.00E+00 | 0.00E+00 | 0.00E+00 | 0.00E+00 | 0.00E+00 |
| Ca, mol/l (±14%) | 1.73E-06 | 1.55E-02 | 1.50E-02 | 1.58E-02 | 1.52E-02 | 1.22E-02 | 1.72E-02 | 1.55E-02 | 1.64E-02 | 1.78E-02 | 2.06E-02 | 1.95E-02 | 1.99E-02 | 2.43E-02 | 2.47E-02 | 2.57E-02 | 2.47E-02 | 2.36E-02 | 2.49E-02 |
| Mn, mol/l | 2.55E-06 | 3.38E-06 | 3.08E-06 | 3.10E-06 | 2.98E-06 | 3.05E-06 | 3.01E-06 | 3.05E-06 | 4.74E-06 | 3.61E-06 | 3.90E-06 | 3.98E-06 | 5.76E-06 | 3.51E-06 | 3.27E-06 | 3.75E-06 | 3.44E-06 | 3.41E-06 | 4.16E-06 |
| Fe, mol/l | 1.15E-06 | 5.02E-06 | 6.90E-06 | 4.11E-06 | 5.51E-06 | 4.82E-06 | 9.34E-06 | 6.19E-06 | 8.05E-05 | 7.11E-06 | 1.26E-05 | 1.40E-05 | 1.29E-04 | 4.51E-05 | 4.00E-05 | 5.76E-05 | 3.97E-05 | 4.30E-05 | 6.55E-05 |
| Sr, mol/l | 8.33E-09 | 8.19E-06 | 7.61E-06 | 7.68E-06 | 7.49E-06 | 7.83E-06 | 7.79E-06 | 7.83E-06 | 8.31E-06 | 9.06E-06 | 9.61E-06 | 9.74E-06 | 9.96E-06 | 6.24E-06 | 6.23E-06 | 6.90E-06 | 6.84E-06 | 6.20E-06 | 6.76E-06 |
| Ba, mol/l | 1.35E-06 | 0.00E+00 | 5.67E-08 | 4.16E-08 | 1.75E-07 | 1.02E-08 | 0.00E+00 | 5.47E-08 | 2.32E-08 | 4.78E-08 | 2.56E-07 | 2.03E-08 | 0.00E+00 | 0.00E+00 | 0.00E+00 | 0.00E+00 | 9.62E-08 | 0.00E+00 | 0.00E+00 |
| Na (est), mol/l | | 1.36E+00 | 1.36E+00 | 1.36E+00 | 1.36E+00 | 1.36E+00 | 1.36E+00 | 1.36E+00 | 1.36E+00 | 1.36E+00 | 1.36E+00 | 1.36E+00 | 1.36E+00 | 1.36E+00 | 1.36E+00 | 1.36E+00 | 1.36E+00 | 1.36E+00 | 1.36E+00 |
| Alkalinity(est), mol/l | | 1.55E-02 | 1.50E-02 | 1.58E-02 | 1.52E-02 | 1.22E-02 | 1.72E-02 | 1.55E-02 | 1.64E-02 | 1.78E-02 | 2.06E-02 | 1.95E-02 | 1.99E-02 | 2.43E-02 | 2.47E-02 | 2.57E-02 | 2.47E-02 | 2.36E-02 | 2.49E-02 |
| Fluid in exp. (kg) | | 0.060 | 0.057 | 0.056 | 0.054 | 0.052 | 0.051 | 0.050 | 0.048 | 0.046 | 0.045 | 0.043 | 0.041 | 0.039 | 0.037 | 0.035 | 0.033 | 0.031 | 0.029 |

| 192: 1.36M NaCl, 31bar pCO2, 70C | | | | | | | | | | | | | | | | | | | | |
|---|---|---|---|---|---|---|---|---|---|---|---|---|---|---|---|---|---|---|---|---|
| Time, hours | Std. Dev. Mol/l | -0.42 | -0.42 | 0.07 | 0.75 | 6.08 | 10.57 | 22.32 | 28.07 | 31.92 | 48.35 | 54.22 | 70.62 | 84.02 | 84.02 | 95.53 | 101.37 | 121.10 | 145.50 | 171.32 |
| VCT, hours | | 0.00 | 0.00 | 0.50 | 1.23 | 7.09 | 12.15 | 25.72 | 32.52 | 37.19 | 57.60 | 65.07 | 86.55 | 104.65 | 104.65 | 120.80 | 129.22 | 158.66 | 196.22 | 237.38 |
| Mg, mol/l | 5.36E-06 | 7.87E-05 | 7.87E-05 | 7.21E-05 | 7.95E-05 | 9.44E-05 | 1.09E-04 | 1.33E-04 | 1.49E-04 | 1.49E-04 | 1.46E-04 | 1.52E-04 | 1.97E-04 | 1.41E-04 | 1.78E-04 | 1.57E-04 | 1.61E-04 | 1.67E-04 | 1.68E-04 | 1.37E-04 |
| Al, mol/l | 4.18E-08 | 0.00E+00 | 0.00E+00 | 0.00E+00 | 0.00E+00 | 0.00E+00 | 0.00E+00 | 0.00E+00 | 0.00E+00 | 0.00E+00 | 0.00E+00 | 0.00E+00 | 0.00E+00 | 0.00E+00 | 0.00E+00 | 0.00E+00 | 0.00E+00 | 0.00E+00 | 0.00E+00 | 0.00E+00 |
| Si, mol/l | 8.61E-06 | 4.68E-05 | 4.68E-05 | 3.31E-05 | 3.68E-05 | 1.04E-04 | 8.56E-05 | 9.83E-05 | 7.24E-05 | 2.94E-05 | 4.83E-05 | 4.41E-05 | 4.51E-05 | 4.60E-05 | 4.18E-05 | 3.32E-05 | 2.67E-05 | 2.24E-05 | 3.25E-05 | 0.00E+00 |
| K, mol/l | 2.69E-06 | 5.83E-05 | 5.83E-05 | 2.71E-05 | 3.03E-05 | 2.12E-05 | 9.48E-06 | 1.05E-05 | 2.26E-05 | 2.08E-05 | 0.00E+00 | 1.13E-05 | 4.41E-05 | 6.35E-06 | 3.12E-05 | 1.23E-05 | 1.47E-05 | 1.77E-05 | 1.76E-05 | 0.00E+00 |
| Ca, mol/l (±3%) | 1.73E-06 | 2.34E-03 | 2.34E-03 | 2.60E-03 | 2.60E-03 | 5.85E-03 | 8.55E-03 | 1.27E-02 | 1.50E-02 | 1.01E-02 | 1.44E-02 | 1.65E-02 | 1.69E-02 | 1.87E-02 | 1.95E-02 | 1.62E-02 | 1.67E-02 | 1.21E-02 | 1.51E-02 | 2.04E-02 |
| Mn, mol/l | 2.55E-06 | 1.02E-04 | 1.02E-04 | 5.82E-05 | 3.57E-05 | 6.71E-05 | 5.01E-05 | 5.23E-05 | 4.10E-05 | 3.31E-05 | 4.40E-05 | 3.78E-05 | 5.39E-05 | 3.73E-05 | 4.16E-05 | 4.33E-05 | 3.29E-05 | 4.14E-05 | 4.71E-05 | 3.51E-05 |
| Fe, mol/l | 1.15E-06 | | | | | | | | | | | | | | | | | | | |
| Sr, mol/l | 8.33E-09 | 2.58E-06 | 2.58E-06 | 2.67E-06 | 3.07E-06 | 4.08E-06 | 5.06E-06 | 6.48E-06 | 7.09E-06 | 7.61E-06 | 7.60E-06 | 8.00E-06 | 1.02E-05 | 7.37E-06 | 9.47E-06 | 8.34E-06 | 8.56E-06 | 8.85E-06 | 8.65E-06 | 5.18E-06 |
| Ba, mol/l | 1.35E-06 | 4.12E-07 | 4.12E-07 | 4.99E-07 | 1.58E-06 | 2.30E-07 | 3.67E-08 | 0.00E+00 | 1.03E-07 | 0.00E+00 | 0.00E+00 | 2.19E-08 | 0.00E+00 | 0.00E+00 | 4.12E-08 | 0.00E+00 | 0.00E+00 | 0.00E+00 | 2.77E-08 | 0.00E+00 |
| Na (est), mol/l | | 1.36E+00 | 1.36E+00 | 1.36E+00 | 1.36E+00 | 1.36E+00 | 1.36E+00 | 1.36E+00 | 1.36E+00 | 1.36E+00 | 1.36E+00 | 1.36E+00 | 1.36E+00 | 1.36E+00 | 1.36E+00 | 1.36E+00 | 1.36E+00 | 1.36E+00 | 1.36E+00 | 1.36E+00 |
| Alkalinity(est), mol/l | | 2.34E-03 | 2.34E-03 | 2.60E-03 | 2.60E-03 | 5.85E-03 | 8.55E-03 | 1.27E-02 | 1.50E-02 | 1.01E-02 | 1.44E-02 | 1.65E-02 | 1.69E-02 | 1.87E-02 | 1.95E-02 | 1.62E-02 | 1.67E-02 | 1.21E-02 | 1.51E-02 | 2.04E-02 |
| Fluid in exp. (kg) | | 0.091 | 0.091 | 0.088 | 0.085 | 0.083 | 0.081 | 0.079 | 0.078 | 0.076 | 0.074 | 0.072 | 0.070 | 0.068 | 0.067 | 0.065 | 0.063 | 0.061 | 0.059 | 0.057 |

| 192 cont.: 1.36M NaCl, 31bar pCO2, 70C | | | | | | | | | | | | | | | | | | |
|---|---|---|---|---|---|---|---|---|---|---|---|---|---|---|---|---|---|---|
| Time, hours | Std. Dev. Mol/l | 175.68 | 189.42 | 215.90 | 244.92 | 263.08 | 263.08 | 294.15 | 318.15 | 362.17 | 386.92 | 409.03 | 431.32 | 483.67 | 553.92 | 603.95 | 654.55 | 654.55 |
| VCT, hours | | 244.60 | 268.05 | 314.77 | 367.95 | 402.71 | 402.71 | 465.92 | 517.06 | 614.90 | 672.87 | 727.63 | 786.24 | 932.61 | 1142.30 | 1300.72 | 1471.80 | 1471.80 |
| Mg, mol/l | 5.36E-06 | 1.33E-04 | 1.36E-04 | 1.39E-04 | 1.61E-04 | 1.33E-04 | 1.40E-04 | 1.41E-04 | 1.41E-04 | 1.57E-04 | 1.55E-04 | 1.52E-04 | 1.46E-04 | 1.58E-04 | 1.39E-04 | 1.44E-04 | 1.48E-04 | 1.54E-04 |
| Al, mol/l | 4.18E-08 | 0.00E+00 | 0.00E+00 | 0.00E+00 | 0.00E+00 | 0.00E+00 | 0.00E+00 | 0.00E+00 | 0.00E+00 | 0.00E+00 | 0.00E+00 | 0.00E+00 | 0.00E+00 | 0.00E+00 | 0.00E+00 | 0.00E+00 | 0.00E+00 | 0.00E+00 |
| Si, mol/l | 8.61E-06 | 0.00E+00 | 0.00E+00 | 0.00E+00 | 0.00E+00 | 0.00E+00 | 0.00E+00 | 0.00E+00 | 0.00E+00 | 0.00E+00 | 0.00E+00 | 0.00E+00 | 0.00E+00 | 0.00E+00 | 0.00E+00 | 0.00E+00 | 0.00E+00 | 0.00E+00 |
| K, mol/l | 2.69E-06 | 0.00E+00 | 0.00E+00 | 0.00E+00 | 0.00E+00 | 0.00E+00 | 0.00E+00 | 0.00E+00 | 0.00E+00 | 0.00E+00 | 0.00E+00 | 0.00E+00 | 0.00E+00 | 0.00E+00 | 0.00E+00 | 0.00E+00 | 0.00E+00 | 0.00E+00 |
| Ca, mol/l (±3%) | 1.73E-06 | 2.10E-02 | 1.90E-02 | 2.08E-02 | 2.13E-02 | 1.99E-02 | 2.04E-02 | 2.09E-02 | 2.17E-02 | 2.22E-02 | 2.22E-02 | 2.22E-02 | 2.20E-02 | 2.35E-02 | 2.22E-02 | 2.24E-02 | 2.27E-02 | 2.27E-02 |
| Mn, mol/l | 2.55E-06 | 3.59E-05 | 2.58E-05 | 2.89E-05 | 3.09E-05 | 2.78E-05 | 2.30E-05 | 2.55E-05 | 2.78E-05 | 2.92E-05 | 2.52E-05 | 2.36E-05 | 2.33E-05 | 2.72E-05 | 2.65E-05 | 2.77E-05 | 2.56E-05 | 2.35E-05 |
| Fe, mol/l | 1.15E-06 | | | | | | | | | | | | | | | | | |
| Sr, mol/l | 8.33E-09 | 5.21E-06 | 4.45E-06 | 5.06E-06 | 5.39E-06 | 5.06E-06 | 5.31E-06 | 5.55E-06 | 5.41E-06 | 5.80E-06 | 5.67E-06 | 5.78E-06 | 5.84E-06 | 6.00E-06 | 5.35E-06 | 5.77E-06 | 5.55E-06 | 5.49E-06 |
| Ba, mol/l | 1.35E-06 | 0.00E+00 | 0.00E+00 | 0.00E+00 | 0.00E+00 | 0.00E+00 | 0.00E+00 | 0.00E+00 | 0.00E+00 | 0.00E+00 | 0.00E+00 | 0.00E+00 | 2.72E-08 | 0.00E+00 | 0.00E+00 | 0.00E+00 | 0.00E+00 | 0.00E+00 |
| Na (est), mol/l | | 1.36E+00 | 1.36E+00 | 1.36E+00 | 1.36E+00 | 1.36E+00 | 1.36E+00 | 1.36E+00 | 1.36E+00 | 1.36E+00 | 1.36E+00 | 1.36E+00 | 1.36E+00 | 1.36E+00 | 1.36E+00 | 1.36E+00 | 1.36E+00 | 1.36E+00 |
| Alkalinity(est), mol/l | | 2.10E-02 | 1.90E-02 | 2.08E-02 | 2.13E-02 | 1.99E-02 | 2.04E-02 | 2.09E-02 | 2.17E-02 | 2.22E-02 | 2.22E-02 | 2.22E-02 | 2.20E-02 | 2.35E-02 | 2.22E-02 | 2.24E-02 | 2.27E-02 | 2.27E-02 |
| Fluid in exp. (kg) | | 0.055 | 0.053 | 0.051 | 0.049 | 0.047 | 0.046 | 0.044 | 0.042 | 0.040 | 0.038 | 0.036 | 0.034 | 0.031 | 0.030 | 0.028 | 0.026 | 0.027 |

| 193: DI, 4bar pCO2, 22C | | | | | | | | | | | | | | | | | | | | |
|---|---|---|---|---|---|---|---|---|---|---|---|---|---|---|---|---|---|---|---|---|
| Time, hours | Std. Dev. Mol/l | -0.08 | 0.02 | 1.20 | 4.78 | 7.05 | 23.45 | 26.05 | 26.87 | 48.38 | 50.82 | 54.22 | 61.68 | 98.33 | 98.33 | 110.65 | 124.17 | 128.53 | 142.18 | 150.88 |
| VCT, hours | | 0.00 | 0.02 | 1.21 | 4.93 | 7.34 | 25.15 | 28.03 | 28.96 | 53.86 | 56.73 | 60.83 | 70.01 | 116.51 | 116.51 | 132.67 | 150.88 | 156.94 | 176.34 | 189.04 |
| Mg, mol/l | 4.75E-06 | 1.44E-05 | 1.19E-05 | 1.56E-05 | 3.78E-05 | 3.74E-05 | 9.17E-05 | 6.91E-05 | 7.04E-05 | 7.61E-05 | 7.22E-05 | 7.18E-05 | 7.15E-05 | 7.68E-05 | 7.58E-05 | 6.81E-05 | 2.85E-04 | 7.26E-05 | 7.25E-05 | 7.04E-05 |
| Al, mol/l | 1.29E-05 | 2.98E-05 | 0.00E+00 | 0.00E+00 | 0.00E+00 | 0.00E+00 | 0.00E+00 | 0.00E+00 | 0.00E+00 | 0.00E+00 | 0.00E+00 | 0.00E+00 | 0.00E+00 | 0.00E+00 | 0.00E+00 | 0.00E+00 | 7.81E-05 | 5.17E-05 | 0.00E+00 | 0.00E+00 |
| Si, mol/l | 0.00E+00 | 4.70E-06 | 6.05E-06 | 3.76E-06 | 3.96E-06 | 4.14E-06 | 5.59E-06 | 5.13E-06 | 5.09E-06 | 6.09E-06 | 5.54E-06 | 7.34E-06 | 1.12E-05 | 4.90E-06 | 7.79E-06 | 0.00E+00 | 0.00E+00 | 0.00E+00 | 0.00E+00 | 0.00E+00 |
| K, mol/l | 2.48E-06 | 1.88E-06 | 3.15E-06 | 3.50E-06 | 5.75E-06 | 7.42E-06 | 9.57E-06 | 4.31E-06 | 2.64E-06 | 2.95E-06 | 2.83E-06 | 7.30E-06 | 4.86E-06 | 3.88E-06 | 3.23E-06 | 0.00E+00 | 1.39E-04 | 0.00E+00 | 0.00E+00 | 0.00E+00 |
| Ca, mol/l (±12%) | 2.30E-06 | 1.54E-04 | 2.21E-04 | 6.06E-04 | 2.67E-03 | 3.39E-03 | 6.60E-03 | 6.10E-03 | 6.70E-03 | 8.36E-03 | 7.01E-03 | 8.35E-03 | 7.02E-03 | 7.60E-03 | 8.91E-03 | 9.84E-03 | 1.02E-02 | 1.04E-02 | 1.05E-02 | 1.05E-02 |
| Mn, mol/l | 3.09E-06 | 4.08E-08 | 3.96E-06 | 3.56E-07 | 7.84E-07 | 7.22E-07 | 1.77E-06 | 1.55E-06 | 1.37E-06 | 1.48E-06 | 1.71E-06 | 1.43E-06 | 1.66E-06 | 1.93E-06 | 2.09E-06 | 1.58E-06 | 1.80E-06 | 1.58E-06 | 1.89E-06 | 1.56E-06 |
| Fe, mol/l | 0.00E+00 | 2.69E-07 | 4.07E-06 | 1.41E-06 | 1.79E-06 | 6.38E-06 | 3.94E-06 | 2.55E-06 | 2.57E-06 | 3.18E-06 | 3.11E-06 | 2.84E-06 | 3.12E-06 | 3.28E-06 | 4.09E-06 | 0.00E+00 | 3.49E-05 | 0.00E+00 | 0.00E+00 | 0.00E+00 |
| Sr, mol/l | 0.00E+00 | 4.32E-07 | 4.29E-07 | 6.86E-07 | 2.05E-06 | 2.08E-06 | 5.13E-06 | 3.84E-06 | 3.92E-06 | 4.25E-06 | 4.06E-06 | 4.04E-06 | 4.10E-06 | 4.40E-06 | 4.31E-06 | 3.38E-06 | 3.52E-06 | 3.46E-06 | 3.56E-06 | 3.49E-06 |
| Ba, mol/l | 1.06E-05 | 0.00E+00 | 0.00E+00 | 0.00E+00 | 0.00E+00 | 0.00E+00 | 0.00E+00 | 0.00E+00 | 0.00E+00 | 0.00E+00 | 0.00E+00 | 3.54E-07 | 0.00E+00 | 0.00E+00 | 0.00E+00 | 0.00E+00 | 5.33E-08 | 0.00E+00 | 0.00E+00 | 0.00E+00 |
| Na (est), mol/l | | 0.00E+00 | 0.00E+00 | 0.00E+00 | 0.00E+00 | 0.00E+00 | 0.00E+00 | 0.00E+00 | 0.00E+00 | 0.00E+00 | 0.00E+00 | 0.00E+00 | 0.00E+00 | 0.00E+00 | 0.00E+00 | 0.00E+00 | 0.00E+00 | 0.00E+00 | 0.00E+00 | 0.00E+00 |
| Alkalinity(est), mol/l | | 1.54E-04 | 2.21E-04 | 6.06E-04 | 2.67E-03 | 3.39E-03 | 6.60E-03 | 6.10E-03 | 6.70E-03 | 8.36E-03 | 7.01E-03 | 8.35E-03 | 7.02E-03 | 7.60E-03 | 8.91E-03 | 9.84E-03 | 1.02E-02 | 1.04E-02 | 1.05E-02 | 1.05E-02 |
| Fluid in exp. (kg) | | 0.100 | 0.099 | 0.097 | 0.095 | 0.093 | 0.091 | 0.089 | 0.087 | 0.085 | 0.083 | 0.082 | 0.080 | 0.078 | 0.076 | 0.075 | 0.073 | 0.071 | 0.069 | 0.068 |

| 193 cont.: DI, 4bar pCO2, 22C | | | | | | | | | | | | | | | | | | | | | |
|---|---|---|---|---|---|---|---|---|---|---|---|---|---|---|---|---|---|---|---|---|---|
| Time, hours | Std. Dev. Mol/l | 168.77 | 179.27 | 193.85 | 215.92 | 215.92 | 246.43 | 272.15 | 314.92 | 339.78 | 344.58 | 361.90 | 367.77 | 384.18 | 411.03 | 436.45 | 456.22 | 506.78 | 556.82 | 607.42 | 607.42 |
| VCT, hours | | 215.78 | 231.90 | 255.00 | 290.93 | 290.93 | 342.92 | 388.38 | 466.37 | 513.25 | 522.62 | 557.86 | 570.29 | 606.58 | 668.12 | 730.19 | 780.66 | 915.53 | 1056.21 | 1205.84 | 1205.84 |
| Mg, mol/l | 4.75E-06 | 7.86E-05 | 7.52E-05 | 7.50E-05 | 8.12E-05 | | 6.86E-04 | 8.03E-05 | 1.03E-04 | 8.99E-05 | 8.82E-05 | 7.56E-05 | 7.72E-05 | 8.02E-05 | 8.19E-05 | 8.88E-05 | 8.35E-05 | 9.03E-05 | 8.50E-05 | 1.49E-04 | 8.75E-05 |
| Al, mol/l | 1.29E-05 | 0.00E+00 | 0.00E+00 | 0.00E+00 | 0.00E+00 | | 4.22E-04 | 0.00E+00 | 9.88E-06 | 0.00E+00 | 0.00E+00 | 0.00E+00 | 0.00E+00 | 0.00E+00 | 0.00E+00 | 0.00E+00 | 0.00E+00 | 0.00E+00 | 0.00E+00 | 2.41E-05 | 0.00E+00 |
| Si, mol/l | 0.00E+00 | 0.00E+00 | 0.00E+00 | 0.00E+00 | 0.00E+00 | 0.00E+00 | 0.00E+00 | 0.00E+00 | 0.00E+00 | 0.00E+00 | 0.00E+00 | 0.00E+00 | 0.00E+00 | 0.00E+00 | 0.00E+00 | 0.00E+00 | 0.00E+00 | 0.00E+00 | 0.00E+00 | 0.00E+00 | 0.00E+00 |
| K, mol/l | 2.48E-06 | 0.00E+00 | 0.00E+00 | 0.00E+00 | 0.00E+00 | 0.00E+00 | 0.00E+00 | 0.00E+00 | 0.00E+00 | 0.00E+00 | 0.00E+00 | 0.00E+00 | 0.00E+00 | 0.00E+00 | 0.00E+00 | 0.00E+00 | 0.00E+00 | 0.00E+00 | 0.00E+00 | 0.00E+00 | 0.00E+00 |
| Ca, mol/l (±12%) | 2.30E-06 | 1.05E-02 | 1.20E-02 | 1.10E-02 | 1.25E-02 | 1.13E-02 | 1.26E-02 | 1.22E-02 | 1.28E-02 | 1.43E-02 | 1.40E-02 | 1.31E-02 | 1.39E-02 | 1.41E-02 | 1.47E-02 | 1.60E-02 | 1.51E-02 | 1.54E-02 | 1.54E-02 | 1.59E-02 | 1.54E-02 |
| Mn, mol/l | 3.09E-06 | 1.65E-06 | 1.67E-06 | 1.71E-06 | 1.72E-06 | | 4.15E-05 | 1.81E-06 | 1.92E-06 | 1.99E-06 | 1.94E-06 | 1.94E-06 | 2.01E-06 | 2.05E-06 | 2.10E-06 | 2.28E-06 | 2.21E-06 | 2.32E-06 | 2.32E-06 | 2.44E-06 | 2.25E-06 |
| Fe, mol/l | 0.00E+00 | 0.00E+00 | 0.00E+00 | 0.00E+00 | 0.00E+00 | 3.02E-03 | 1.76E-04 | 0.00E+00 | 0.00E+00 | 0.00E+00 | 0.00E+00 | 0.00E+00 | 0.00E+00 | 0.00E+00 | 0.00E+00 | 0.00E+00 | 0.00E+00 | 0.00E+00 | 0.00E+00 | 0.00E+00 | 0.00E+00 |
| Sr, mol/l | 0.00E+00 | 3.52E-06 | 3.75E-06 | 3.72E-06 | 3.91E-06 | 3.93E-06 | 4.11E-06 | 4.11E-06 | 4.15E-06 | 4.74E-06 | 4.48E-06 | 4.47E-06 | 4.63E-06 | 4.75E-06 | 4.86E-06 | 5.20E-06 | 4.97E-06 | 5.14E-06 | 4.98E-06 | 5.20E-06 | 4.77E-06 |
| Ba, mol/l | 1.06E-05 | 0.00E+00 | 0.00E+00 | 0.00E+00 | 0.00E+00 | 0.00E+00 | 0.00E+00 | 0.00E+00 | 0.00E+00 | 0.00E+00 | 0.00E+00 | 0.00E+00 | 0.00E+00 | 0.00E+00 | 0.00E+00 | 0.00E+00 | 0.00E+00 | 0.00E+00 | 0.00E+00 | 0.00E+00 | 0.00E+00 |
| Na (est), mol/l | | 0.00E+00 | 0.00E+00 | 0.00E+00 | 0.00E+00 | 0.00E+00 | 0.00E+00 | 0.00E+00 | 0.00E+00 | 0.00E+00 | 0.00E+00 | 0.00E+00 | 0.00E+00 | 0.00E+00 | 0.00E+00 | 0.00E+00 | 0.00E+00 | 0.00E+00 | 0.00E+00 | 0.00E+00 | 0.00E+00 |
| Alkalinity(est), mol/l | | 1.05E-02 | 1.20E-02 | 1.10E-02 | 1.25E-02 | 1.13E-02 | 1.26E-02 | 1.22E-02 | 1.28E-02 | 1.43E-02 | 1.40E-02 | 1.31E-02 | 1.39E-02 | 1.41E-02 | 1.47E-02 | 1.60E-02 | 1.51E-02 | 1.54E-02 | 1.54E-02 | 1.59E-02 | 1.54E-02 |
| Fluid in exp. (kg) | | 0.066 | 0.064 | 0.062 | 0.061 | 0.059 | 0.058 | 0.056 | 0.054 | 0.052 | 0.051 | 0.048 | 0.047 | 0.045 | 0.043 | 0.040 | 0.039 | 0.037 | 0.035 | 0.033 | 0.031 |

| 103: 1.36M NaCl, 4bar pCO2, 22C | | | | | | | | | | | | | | | | | | | | |
|---|---|---|---|---|---|---|---|---|---|---|---|---|---|---|---|---|---|---|---|---|
| Time, hours | Std. Dev. Mol/l | -0.12 | 0.03 | 2.93 | 3.85 | 8.45 | 21.80 | 26.13 | 32.68 | 48.67 | 53.80 | 70.83 | 76.75 | 76.75 | 94.80 | 99.88 | 121.37 | 132.32 | 142.47 | 146.15 |
| VCT, hours | | 0.00 | 0.03 | 3.02 | 3.98 | 8.95 | 23.84 | 28.78 | 36.40 | 55.35 | 61.58 | 82.65 | 90.12 | 90.12 | 113.59 | 120.35 | 149.66 | 164.91 | 179.39 | 184.77 |
| Mg, mol/l | 4.75E-06 | 2.76E-06 | 6.71E-06 | 2.05E-05 | 3.20E-05 | 3.39E-05 | 8.69E-05 | 8.80E-05 | 9.81E-05 | 1.37E-04 | 1.13E-04 | 1.28E-04 | 1.14E-04 | 1.22E-04 | 1.31E-04 | 1.70E-04 | 1.13E-04 | 1.23E-04 | 1.21E-04 | 9.68E-05 |
| Al, mol/l | 1.29E-05 | 0.00E+00 | 3.58E-06 | 0.00E+00 | 0.00E+00 | 0.00E+00 | 0.00E+00 | 8.11E-06 | 4.02E-06 | 1.52E-05 | 8.35E-06 | 6.41E-06 | 0.00E+00 | 1.32E-05 | 4.48E-06 | 2.80E-05 | 0.00E+00 | 0.00E+00 | 0.00E+00 | 0.00E+00 |
| Si, mol/l | 0.00E+00 | 0.00E+00 | 0.00E+00 | 0.00E+00 | 0.00E+00 | 0.00E+00 | 0.00E+00 | 0.00E+00 | 0.00E+00 | 0.00E+00 | 0.00E+00 | 0.00E+00 | 0.00E+00 | 0.00E+00 | 0.00E+00 | 0.00E+00 | 0.00E+00 | 0.00E+00 | 0.00E+00 | 0.00E+00 |
| K, mol/l | 2.48E-06 | 0.00E+00 | 0.00E+00 | 0.00E+00 | 0.00E+00 | 0.00E+00 | 0.00E+00 | 0.00E+00 | 0.00E+00 | 0.00E+00 | 0.00E+00 | 0.00E+00 | 0.00E+00 | 0.00E+00 | 0.00E+00 | 0.00E+00 | 0.00E+00 | 0.00E+00 | 0.00E+00 | 0.00E+00 |
| Ca, mol/l (±3%) | 2.30E-06 | 0.00E+00 | 0.00E+00 | 2.94E-03 | 5.15E-03 | 5.27E-03 | 1.53E-02 | 1.59E-02 | 1.82E-02 | 2.05E-02 | 2.07E-02 | 2.16E-02 | 1.93E-02 | 1.99E-02 | 2.04E-02 | 1.90E-02 | 2.05E-02 | 2.12E-02 | 1.96E-02 | 1.86E-02 |
| Mn, mol/l | 3.09E-06 | 0.00E+00 | 9.81E-07 | 4.25E-07 | 6.06E-07 | 5.80E-07 | 1.76E-06 | 1.79E-06 | 2.05E-06 | 2.49E-06 | 2.50E-06 | 2.71E-06 | 2.58E-06 | 2.48E-06 | 2.54E-06 | 2.49E-06 | 2.88E-06 | 2.60E-06 | 2.38E-06 | 2.24E-06 |
| Fe, mol/l | 0.00E+00 | 0.00E+00 | 0.00E+00 | 0.00E+00 | 0.00E+00 | 0.00E+00 | 0.00E+00 | 0.00E+00 | 2.61E-05 | 3.89E-05 | 3.05E-05 | 3.30E-05 | 0.00E+00 | 3.01E-05 | 0.00E+00 | 4.21E-05 | 3.16E-05 | 3.38E-05 | 2.76E-05 | 0.00E+00 |
| Sr, mol/l | 0.00E+00 | 0.00E+00 | 0.00E+00 | 6.72E-07 | 1.39E-06 | 1.34E-06 | 3.98E-06 | 4.22E-06 | 4.72E-06 | 5.23E-06 | 5.26E-06 | 5.61E-06 | 5.17E-06 | 5.18E-06 | 5.08E-06 | 5.05E-06 | 5.26E-06 | 5.63E-06 | 5.28E-06 | 4.81E-06 |
| Ba, mol/l | 1.06E-05 | 0.00E+00 | 0.00E+00 | 0.00E+00 | 0.00E+00 | 0.00E+00 | 0.00E+00 | 0.00E+00 | 0.00E+00 | 0.00E+00 | 0.00E+00 | 0.00E+00 | 0.00E+00 | 0.00E+00 | 0.00E+00 | 0.00E+00 | 0.00E+00 | 0.00E+00 | 0.00E+00 | 0.00E+00 |
| Na (est), mol/l | | 1.36E+00 | 1.36E+00 | 1.36E+00 | 1.36E+00 | 1.36E+00 | 1.36E+00 | 1.36E+00 | 1.36E+00 | 1.36E+00 | 1.36E+00 | 1.36E+00 | 1.36E+00 | 1.36E+00 | 1.36E+00 | 1.36E+00 | 1.36E+00 | 1.36E+00 | 1.36E+00 | 1.36E+00 |
| Alkalinity(est), mol/l | | 0.00E+00 | 0.00E+00 | 2.94E-03 | 5.15E-03 | 5.27E-03 | 1.53E-02 | 1.59E-02 | 1.82E-02 | 2.05E-02 | 2.07E-02 | 2.16E-02 | 1.93E-02 | 1.99E-02 | 2.04E-02 | 1.90E-02 | 2.05E-02 | 2.12E-02 | 1.96E-02 | 1.86E-02 |
| Fluid in exp. (kg) | | 0.110 | 0.109 | 0.106 | 0.103 | 0.101 | 0.097 | 0.095 | 0.093 | 0.092 | 0.090 | 0.088 | 0.086 | 0.084 | 0.084 | 0.082 | 0.080 | 0.078 | 0.076 | 0.074 |

| 103 cont.: 1.36M NaCl, 4bar pCO2, 22C | | | | | | | | | | | | | | | | | | | | | |
|---|---|---|---|---|---|---|---|---|---|---|---|---|---|---|---|---|---|---|---|---|---|
| Time, hours | Std. Dev. Mol/l | 167.88 | 176.08 | 191.43 | 198.55 | 213.17 | 221.80 | 221.80 | 239.93 | 247.78 | 263.48 | 288.88 | 312.93 | 335.88 | 359.95 | 388.10 | 437.60 | 486.43 | 530.83 | 558.97 | 680.00 | 680.00 |
| VCT, hours | | 217.29 | 229.82 | 253.91 | 265.38 | 289.59 | 304.25 | 304.25 | 336.30 | 350.65 | 380.39 | 430.15 | 478.96 | 527.00 | 579.15 | 642.81 | 758.75 | 877.95 | 990.64 | 1065.74 | 1404.84 | 1404.84 |
| Mg, mol/l | 4.75E-06 | 1.53E-04 | 1.17E-04 | 1.13E-04 | 8.78E-05 | 9.32E-05 | 8.74E-05 | 9.32E-05 | 9.90E-05 | 9.18E-05 | 9.16E-05 | 2.06E-04 | 8.96E-05 | 9.99E-05 | 9.51E-05 | 1.13E-04 | 1.04E-04 | 1.16E-04 | 1.17E-04 | 1.23E-04 | 1.21E-04 | 1.29E-04 |
| Al, mol/l | 1.29E-05 | 1.61E-05 | 7.18E-06 | 0.00E+00 | 6.47E-05 | 7.19E-05 | 0.00E+00 | 0.00E+00 | 0.00E+00 | 2.35E-06 | 1.10E-05 | 6.18E-05 | 0.00E+00 | 1.52E-05 | 3.44E-06 | 1.19E-05 | 6.25E-06 | 0.00E+00 | 6.56E-06 | 9.33E-06 | 5.70E-06 | 6.45E-06 |
| Si, mol/l | 0.00E+00 | 0.00E+00 | 0.00E+00 | 0.00E+00 | 0.00E+00 | 0.00E+00 | 0.00E+00 | 0.00E+00 | 0.00E+00 | 0.00E+00 | 0.00E+00 | 0.00E+00 | 0.00E+00 | 0.00E+00 | 0.00E+00 | 0.00E+00 | 0.00E+00 | 0.00E+00 | 0.00E+00 | 0.00E+00 | 0.00E+00 | 0.00E+00 |
| K, mol/l | 2.48E-06 | 0.00E+00 | 0.00E+00 | 0.00E+00 | 0.00E+00 | 0.00E+00 | 0.00E+00 | 0.00E+00 | 0.00E+00 | 0.00E+00 | 0.00E+00 | 0.00E+00 | 0.00E+00 | 0.00E+00 | 0.00E+00 | 0.00E+00 | 0.00E+00 | 0.00E+00 | 0.00E+00 | 0.00E+00 | 0.00E+00 | 0.00E+00 |
| Ca, mol/l (±3%) | 2.30E-06 | 2.01E-02 | 1.89E-02 | 1.81E-02 | 1.75E-02 | 1.84E-02 | 1.79E-02 | 1.85E-02 | 1.92E-02 | 1.90E-02 | 1.79E-02 | 1.84E-02 | 1.91E-02 | 2.13E-02 | 1.94E-02 | 2.00E-02 | 2.06E-02 | 2.11E-02 | 2.35E-02 | 2.36E-02 | 2.31E-02 | 2.40E-02 |
| Mn, mol/l | 3.09E-06 | 2.54E-06 | 2.69E-06 | 2.28E-06 | 2.26E-06 | 2.34E-06 | 2.23E-06 | 2.34E-06 | 2.38E-06 | 2.31E-06 | 2.24E-06 | 2.39E-06 | 2.22E-06 | 2.59E-06 | 2.27E-06 | 2.52E-06 | 2.36E-06 | 2.92E-06 | 2.78E-06 | 2.87E-06 | 2.83E-06 | 2.99E-06 |
| Fe, mol/l | 0.00E+00 | 3.86E-05 | 3.09E-05 | 0.00E+00 | 0.00E+00 | 0.00E+00 | 2.44E-05 | 0.00E+00 | 2.69E-05 | 2.84E-05 | 4.65E-05 | 5.01E-05 | 0.00E+00 | 4.08E-05 | 0.00E+00 | 0.00E+00 | 0.00E+00 | 0.00E+00 | 0.00E+00 | 0.00E+00 | 0.00E+00 | -5.66E-06 |
| Sr, mol/l | 0.00E+00 | 5.38E-06 | 5.10E-06 | 5.08E-06 | 4.88E-06 | 5.05E-06 | 4.97E-06 | 4.92E-06 | 5.39E-06 | 5.36E-06 | 4.84E-06 | 5.09E-06 | 5.31E-06 | 6.77E-06 | 6.29E-06 | 6.55E-06 | 6.65E-06 | 6.88E-06 | 7.31E-06 | 7.49E-06 | 7.46E-06 | 7.84E-06 |
| Ba, mol/l | 1.06E-05 | 0.00E+00 | 0.00E+00 | 0.00E+00 | 0.00E+00 | 0.00E+00 | 0.00E+00 | 0.00E+00 | 0.00E+00 | 0.00E+00 | 0.00E+00 | 0.00E+00 | 0.00E+00 | 0.00E+00 | 0.00E+00 | 0.00E+00 | 0.00E+00 | 0.00E+00 | 0.00E+00 | 0.00E+00 | 0.00E+00 | 0.00E+00 |
| Na (est), mol/l | | 1.36E+00 | 1.36E+00 | 1.36E+00 | 1.36E+00 | 1.36E+00 | 1.36E+00 | 1.36E+00 | 1.36E+00 | 1.36E+00 | 1.36E+00 | 1.36E+00 | 1.36E+00 | 1.36E+00 | 1.36E+00 | 1.36E+00 | 1.36E+00 | 1.36E+00 | 1.36E+00 | 1.36E+00 | 1.36E+00 | 1.36E+00 |
| Alkalinity(est), mol/l | | 2.01E-02 | 1.89E-02 | 1.81E-02 | 1.75E-02 | 1.84E-02 | 1.79E-02 | 1.85E-02 | 1.92E-02 | 1.90E-02 | 1.79E-02 | 1.84E-02 | 1.91E-02 | 2.13E-02 | 1.94E-02 | 2.00E-02 | 2.06E-02 | 2.11E-02 | 2.35E-02 | 2.36E-02 | 2.31E-02 | 2.40E-02 |
| Fluid in exp. (kg) | | 0.073 | 0.071 | 0.069 | 0.067 | 0.066 | 0.064 | 0.062 | 0.061 | 0.059 | 0.057 | 0.055 | 0.054 | 0.052 | 0.050 | 0.048 | 0.046 | 0.044 | 0.043 | 0.041 | 0.039 | 0.037 |

| 195: DI, 31bar pCO2, 70C | | | | | | | | | | | | | | | | | | | | | |
|---|---|---|---|---|---|---|---|---|---|---|---|---|---|---|---|---|---|---|---|---|---|
| Time, hours | Std. Dev. Mol/l | -0.18 | 0.08 | 2.58 | 5.45 | 8.12 | 21.42 | 25.77 | 32.17 | 48.22 | 53.28 | 70.32 | 76.28 | 76.28 | 94.30 | 99.38 | 120.88 | 131.87 | 141.98 | 149.98 | 167.37 | 175.58 |
| VCT, hours | | 0.00 | 0.08 | 2.67 | 5.72 | 8.61 | 23.28 | 28.16 | 35.48 | 54.16 | 60.30 | 81.34 | 88.85 | 88.85 | 112.17 | 118.88 | 147.83 | 162.89 | 177.04 | 188.48 | 213.93 | 226.18 |
| Mg, mol/l | 4.75E-06 | 4.14E-05 | 3.53E-05 | 5.78E-05 | 4.89E-05 | 7.40E-05 | 8.39E-05 | 1.02E-04 | 1.07E-04 | 1.36E-04 | 1.01E-04 | 1.88E-04 | 1.11E-04 | 1.19E-04 | 9.65E-05 | 9.72E-05 | 9.46E-05 | 1.20E-04 | 9.10E-05 | 1.01E-04 | 1.12E-04 | 9.70E-05 |
| Al, mol/l | 1.29E-05 | 1.11E-05 | 5.28E-06 | 2.70E-05 | 1.57E-05 | 1.31E-05 | 1.07E-05 | 1.85E-05 | 5.87E-05 | 2.78E-05 | 0.00E+00 | 3.63E-05 | 1.26E-05 | 1.22E-05 | 0.00E+00 | 1.55E-05 | 0.00E+00 | 2.56E-05 | 0.00E+00 | 0.00E+00 | 3.18E-05 | 1.26E-05 |
| Si, mol/l | 0.00E+00 | 0.00E+00 | 0.00E+00 | 0.00E+00 | 0.00E+00 | 0.00E+00 | 0.00E+00 | 0.00E+00 | 0.00E+00 | 0.00E+00 | 0.00E+00 | 0.00E+00 | 0.00E+00 | 0.00E+00 | 0.00E+00 | 0.00E+00 | 0.00E+00 | 0.00E+00 | 0.00E+00 | 0.00E+00 | 0.00E+00 | 0.00E+00 |
| K, mol/l | 2.48E-06 | 0.00E+00 | 0.00E+00 | 0.00E+00 | 0.00E+00 | 0.00E+00 | 0.00E+00 | 0.00E+00 | 0.00E+00 | 0.00E+00 | 0.00E+00 | 0.00E+00 | 0.00E+00 | 0.00E+00 | 0.00E+00 | 0.00E+00 | 0.00E+00 | 0.00E+00 | 0.00E+00 | 0.00E+00 | 0.00E+00 | 0.00E+00 |
| Ca, mol/l (±6%) | 2.30E-06 | 1.43E-03 | 1.51E-03 | 2.24E-03 | 5.22E-03 | 7.54E-03 | 1.00E-02 | 1.10E-02 | 1.26E-02 | 1.24E-02 | 1.25E-02 | 1.29E-02 | 1.23E-02 | 1.28E-02 | 1.29E-02 | 1.14E-02 | 1.16E-02 | 1.23E-02 | 1.21E-02 | 1.23E-02 | 1.26E-02 | 1.25E-02 |
| Mn, mol/l | 3.09E-06 | 2.11E-05 | 1.66E-05 | 1.12E-05 | 1.15E-05 | 5.87E-06 | 6.51E-06 | 4.99E-06 | 4.60E-06 | 3.93E-06 | 3.66E-06 | 4.71E-06 | 4.32E-06 | 3.79E-06 | 4.32E-06 | 3.84E-06 | 4.34E-06 | 4.90E-06 | 4.40E-06 | 4.01E-06 | 4.64E-06 | 4.29E-06 |
| Fe, mol/l | 0.00E+00 | 0.00E+00 | 0.00E+00 | 0.00E+00 | 0.00E+00 | 0.00E+00 | 0.00E+00 | 0.00E+00 | 0.00E+00 | 0.00E+00 | 0.00E+00 | 0.00E+00 | 0.00E+00 | 0.00E+00 | 0.00E+00 | 0.00E+00 | 0.00E+00 | 0.00E+00 | 0.00E+00 | 0.00E+00 | 0.00E+00 | 0.00E+00 |
| Sr, mol/l | 0.00E+00 | 7.99E-07 | 8.19E-07 | 1.14E-06 | 2.09E-06 | 2.60E-06 | 3.23E-06 | 3.56E-06 | 3.72E-06 | 3.86E-06 | 3.95E-06 | 3.98E-06 | 3.99E-06 | 3.94E-06 | 3.86E-06 | 3.83E-06 | 3.84E-06 | 4.18E-06 | 4.15E-06 | 4.11E-06 | 4.25E-06 | 4.24E-06 |
| Ba, mol/l | 1.06E-05 | 0.00E+00 | 0.00E+00 | 0.00E+00 | 0.00E+00 | 0.00E+00 | 0.00E+00 | 0.00E+00 | 0.00E+00 | 0.00E+00 | 0.00E+00 | 0.00E+00 | 0.00E+00 | 0.00E+00 | 0.00E+00 | 0.00E+00 | 0.00E+00 | 0.00E+00 | 0.00E+00 | 0.00E+00 | 0.00E+00 | 0.00E+00 |
| Na (est), mol/l | | 0.00E+00 | 0.00E+00 | 0.00E+00 | 0.00E+00 | 0.00E+00 | 0.00E+00 | 0.00E+00 | 0.00E+00 | 0.00E+00 | 0.00E+00 | 0.00E+00 | 0.00E+00 | 0.00E+00 | 0.00E+00 | 0.00E+00 | 0.00E+00 | 0.00E+00 | 0.00E+00 | 0.00E+00 | 0.00E+00 | 0.00E+00 |
| Alkalinity(est), mol/l | | 1.43E-03 | 1.51E-03 | 2.24E-03 | 5.22E-03 | 7.54E-03 | 1.00E-02 | 1.10E-02 | 1.26E-02 | 1.24E-02 | 1.25E-02 | 1.29E-02 | 1.23E-02 | 1.28E-02 | 1.29E-02 | 1.14E-02 | 1.16E-02 | 1.23E-02 | 1.21E-02 | 1.23E-02 | 1.26E-02 | 1.25E-02 |
| Fluid in exp. (kg) | | 0.105 | 0.104 | 0.100 | 0.098 | 0.096 | 0.094 | 0.092 | 0.091 | 0.089 | 0.086 | 0.084 | 0.082 | 0.081 | 0.080 | 0.079 | 0.077 | 0.076 | 0.074 | 0.073 | 0.071 | 0.070 |

| 195 cont.: DI, 31bar pCO2, 70C | | | | | | | | | | | | | | | | | | | | |
|---|---|---|---|---|---|---|---|---|---|---|---|---|---|---|---|---|---|---|---|---|
| Time, hours | Std. Dev. Mol/l | 190.93 | 198.03 | 212.65 | 221.37 | 221.37 | 239.35 | 247.30 | 263.02 | 288.37 | 312.45 | 335.45 | 359.47 | 387.58 | 437.08 | 485.93 | 530.32 | 558.45 | 679.48 | 679.48 |
| VCT, hours | | 249.59 | 260.68 | 284.06 | 298.34 | 298.34 | 328.84 | 342.72 | 370.93 | 417.69 | 463.73 | 509.26 | 558.41 | 618.07 | 727.20 | 839.53 | 945.39 | 1015.42 | 1327.65 | 1327.65 |
| Mg, mol/l | 4.75E-06 | 9.50E-05 | 1.04E-04 | 9.20E-05 | 9.94E-05 | 1.01E-04 | 1.03E-04 | 9.95E-05 | 9.02E-05 | 8.77E-05 | 9.51E-05 | 9.32E-05 | 9.93E-05 | 9.18E-05 | 9.59E-05 | 1.05E-04 | 2.98E-04 | 1.03E-04 | 1.04E-04 | 1.04E-04 |
| Al, mol/l | 1.29E-05 | 0.00E+00 | 1.09E-05 | 1.45E-05 | 0.00E+00 | 0.00E+00 | 1.79E-05 | 0.00E+00 | 0.00E+00 | 1.84E-05 | 0.00E+00 | 0.00E+00 | 0.00E+00 | 2.33E-05 | 0.00E+00 | 0.00E+00 | 6.70E-05 | 2.01E-05 | 0.00E+00 | 0.00E+00 |
| Si, mol/l | 0.00E+00 | 0.00E+00 | 0.00E+00 | 0.00E+00 | 0.00E+00 | 0.00E+00 | 0.00E+00 | 0.00E+00 | 0.00E+00 | 0.00E+00 | 0.00E+00 | 0.00E+00 | 0.00E+00 | 0.00E+00 | 0.00E+00 | 0.00E+00 | 0.00E+00 | 0.00E+00 | 0.00E+00 | 0.00E+00 |
| K, mol/l | 2.48E-06 | 0.00E+00 | 0.00E+00 | 0.00E+00 | 0.00E+00 | 0.00E+00 | 0.00E+00 | 0.00E+00 | 0.00E+00 | 0.00E+00 | 0.00E+00 | 0.00E+00 | 0.00E+00 | 0.00E+00 | 0.00E+00 | 0.00E+00 | 0.00E+00 | 0.00E+00 | 0.00E+00 | 0.00E+00 |
| Ca, mol/l (±6%) | 2.30E-06 | 1.26E-02 | 1.24E-02 | 1.22E-02 | 1.25E-02 | 1.15E-02 | 1.31E-02 | 1.17E-02 | 1.21E-02 | 1.21E-02 | 1.21E-02 | 1.16E-02 | 1.18E-02 | 1.23E-02 | 1.21E-02 | 1.31E-02 | 1.32E-02 | 1.25E-02 | 1.27E-02 | 1.33E-02 |
| Mn, mol/l | 3.09E-06 | 4.32E-06 | 3.97E-06 | 4.00E-06 | 3.81E-06 | 3.94E-06 | 4.11E-06 | 3.94E-06 | 3.98E-06 | 4.06E-06 | 4.34E-06 | 3.94E-06 | 4.15E-06 | 4.57E-06 | 4.34E-06 | 4.87E-06 | 4.83E-06 | 4.78E-06 | 4.23E-06 | 4.46E-06 |
| Fe, mol/l | 0.00E+00 | 0.00E+00 | 0.00E+00 | 0.00E+00 | 0.00E+00 | 0.00E+00 | 0.00E+00 | 1.41E-04 | 0.00E+00 | 0.00E+00 | 0.00E+00 | 0.00E+00 | 0.00E+00 | 0.00E+00 | 0.00E+00 | 2.85E-05 | 5.62E-05 | 3.92E-05 | 3.02E-05 | 0.00E+00 |
| Sr, mol/l | 0.00E+00 | 4.21E-06 | 4.12E-06 | 4.21E-06 | 4.08E-06 | 3.96E-06 | 4.04E-06 | 4.00E-06 | 4.02E-06 | 3.85E-06 | 3.83E-06 | 3.73E-06 | 3.78E-06 | 4.39E-06 | 3.81E-06 | 4.05E-06 | 4.10E-06 | 4.11E-06 | 3.95E-06 | 4.05E-06 |
| Ba, mol/l | 1.06E-05 | 0.00E+00 | 0.00E+00 | 0.00E+00 | 0.00E+00 | 0.00E+00 | 0.00E+00 | 0.00E+00 | 0.00E+00 | 0.00E+00 | 0.00E+00 | 0.00E+00 | 0.00E+00 | 0.00E+00 | 0.00E+00 | 0.00E+00 | 0.00E+00 | 0.00E+00 | 0.00E+00 | 0.00E+00 |
| Na (est), mol/l | | 0.00E+00 | 0.00E+00 | 0.00E+00 | 0.00E+00 | 0.00E+00 | 0.00E+00 | 0.00E+00 | 0.00E+00 | 0.00E+00 | 0.00E+00 | 0.00E+00 | 0.00E+00 | 0.00E+00 | 0.00E+00 | 0.00E+00 | 0.00E+00 | 0.00E+00 | 0.00E+00 | 0.00E+00 |
| Alkalinity(est), mol/l | | 1.26E-02 | 1.24E-02 | 1.22E-02 | 1.25E-02 | 1.15E-02 | 1.31E-02 | 1.17E-02 | 1.21E-02 | 1.21E-02 | 1.21E-02 | 1.16E-02 | 1.18E-02 | 1.23E-02 | 1.21E-02 | 1.31E-02 | 1.32E-02 | 1.25E-02 | 1.27E-02 | 1.33E-02 |
| Fluid in exp. (kg) | | 0.068 | 0.066 | 0.065 | 0.063 | 0.062 | 0.061 | 0.059 | 0.058 | 0.056 | 0.054 | 0.052 | 0.051 | 0.049 | 0.047 | 0.045 | 0.043 | 0.042 | 0.040 | 0.037 |

| 196: 1.36M NaCl, 4bar pCO2, 70C |
|---|

| Time, hours | Std. Dev. Mol/l | -0.10 | 0.03 | 1.22 | 3.42 | 6.35 | 19.85 | 22.57 | 24.67 | 43.47 | 51.57 | 67.70 | 73.82 | 97.48 | 97.48 | 120.68 | 146.32 | 170.90 | 194.48 | 261.32 | 333.82 | 362.73 | 404.45 | 434.10 |
|---|---|---|---|---|---|---|---|---|---|---|---|---|---|---|---|---|---|---|---|---|---|---|---|---|
| VCT, hours | | 0.00 | 0.03 | 1.45 | 4.16 | 7.92 | 26.07 | 29.90 | 32.99 | 62.01 | 75.17 | 102.72 | 113.75 | 159.54 | 159.54 | 206.17 | 263.36 | 322.13 | 385.37 | 580.05 | 815.41 | 918.90 | 1090.50 | 1227.61 |
| Mg, mol/l | 3.32E-06 | 4.07E-06 | 5.29E-06 | 1.89E-05 | 2.87E-05 | 3.60E-05 | 3.36E-05 | 3.68E-05 | | 3.74E-05 | 3.93E-05 | 3.90E-05 | | 4.61E-05 | | 4.24E-05 | 4.26E-05 | 4.85E-05 | | 4.42E-05 | 4.25E-05 | | 4.04E-05 | 3.90E-05 |
| Al, mol/l | 2.94E-06 | 0.00E+00 | 1.65E-07 | 0.00E+00 | 0.00E+00 | 0.00E+00 | 0.00E+00 | 0.00E+00 | | 0.00E+00 | 0.00E+00 | 0.00E+00 | | 0.00E+00 | | 0.00E+00 | 0.00E+00 | 0.00E+00 | | 0.00E+00 | 0.00E+00 | | 0.00E+00 | 0.00E+00 |
| Si, mol/l | 7.55E-06 | 0.00E+00 | 0.00E+00 | 0.00E+00 | 0.00E+00 | 0.00E+00 | 0.00E+00 | 0.00E+00 | | 0.00E+00 | 0.00E+00 | 0.00E+00 | | 0.00E+00 | | 0.00E+00 | 0.00E+00 | 0.00E+00 | | 0.00E+00 | 0.00E+00 | | 0.00E+00 | 0.00E+00 |
| K, mol/l | 3.89E-05 | 2.58E-05 | 4.51E-05 | 4.57E-05 | 1.08E-04 | 1.38E-04 | 3.78E-05 | 6.34E-05 | | 1.08E-04 | 6.60E-05 | 2.21E-05 | | 1.21E-04 | | 3.10E-05 | 2.01E-05 | 7.64E-05 | | 1.91E-05 | 0.00E+00 | | 0.00E+00 | 0.00E+00 |
| Ca, mol/l (±25%) | 1.36E-05 | 2.62E-04 | 3.61E-04 | 2.78E-03 | 4.20E-03 | 5.10E-03 | 5.56E-03 | 6.03E-03 | | 6.05E-03 | 6.53E-03 | 6.67E-03 | | 7.31E-03 | | 7.19E-03 | 7.32E-03 | 7.77E-03 | | 7.23E-03 | 7.09E-03 | | 6.47E-03 | 6.22E-03 |
| Mn, mol/l | 0.00E+00 | 0.00E+00 | 0.00E+00 | 0.00E+00 | 0.00E+00 | 0.00E+00 | 0.00E+00 | 0.00E+00 | | 0.00E+00 | 0.00E+00 | 0.00E+00 | | 0.00E+00 | | 0.00E+00 | 0.00E+00 | 0.00E+00 | | 0.00E+00 | 0.00E+00 | | 0.00E+00 | 0.00E+00 |
| Fe, mol/l | 0.00E+00 | 0.00E+00 | 0.00E+00 | 0.00E+00 | 1.41E-05 | 2.06E-07 | 3.61E-06 | 0.00E+00 | | 0.00E+00 | 0.00E+00 | 0.00E+00 | | 0.00E+00 | | 0.00E+00 | 0.00E+00 | 0.00E+00 | | 4.34E-05 | 3.00E-05 | | 2.82E-05 | 1.57E-04 |
| Sr, mol/l | 6.42E-08 | 2.26E-08 | 4.03E-08 | 6.32E-07 | 1.06E-06 | 1.34E-06 | 1.38E-06 | 1.50E-06 | | 1.52E-06 | 1.62E-06 | 1.65E-06 | | 1.87E-06 | | 1.80E-06 | 1.83E-06 | 2.00E-06 | | 1.85E-06 | 1.81E-06 | | 1.70E-06 | 1.66E-06 |
| Ba, mol/l | 2.98E-08 | 8.06E-07 | 2.80E-07 | 3.18E-07 | 0.00E+00 | 3.23E-08 | 0.00E+00 | 0.00E+00 | | 0.00E+00 | 1.13E-07 | 0.00E+00 | | 5.48E-08 | | 7.70E-09 | 0.00E+00 | 1.81E-07 | | 9.18E-09 | 0.00E+00 | | 0.00E+00 | 2.32E-07 |
| Na (est), mol/l | | 1.36E+00 | 1.36E+00 | 1.36E+00 | 1.36E+00 | 1.36E+00 | 1.36E+00 | 1.36E+00 | | 1.36E+00 | 1.36E+00 | 1.36E+00 | | 1.36E+00 | | 1.36E+00 | 1.36E+00 | 1.36E+00 | | 1.36E+00 | 1.36E+00 | | 1.36E+00 | 1.36E+00 |
| Alkalinity(est), mol/l | | 2.62E-04 | 3.61E-04 | 2.78E-03 | 4.20E-03 | 5.10E-03 | 5.56E-03 | 6.03E-03 | | 6.05E-03 | 6.53E-03 | 6.67E-03 | | 7.31E-03 | | 7.19E-03 | 7.32E-03 | 7.77E-03 | | 7.23E-03 | 7.09E-03 | | 6.47E-03 | 6.22E-03 |
| Fluid in exp. (kg) | | 0.098 | 0.097 | 0.081 | 0.078 | 0.075 | 0.072 | 0.069 | | 0.063 | 0.059 | 0.057 | | 0.050 | | 0.048 | 0.043 | 0.040 | | 0.033 | 0.030 | | 0.023 | 0.021 |

# A.5 Dolomite Fluid Chemistry Data

| 131: 1.36M NaCl, 4bar pCO2, 22C | | | | | | | | | | | | | | | | |
|---|---|---|---|---|---|---|---|---|---|---|---|---|---|---|---|---|
| Time, hours | Std. Dev. Mol/l | -0.67 | 0.05 | 2.92 | 22.50 | 25.37 | 45.03 | 49.67 | 71.35 | 189.13 | 238.15 | 311.38 | 359.57 | 476.55 | 557.27 | 557.27 |
| VCT, hours | | 0.00 | 0.05 | 2.92 | 23.15 | 26.21 | 47.91 | 53.16 | 78.65 | 221.44 | 282.56 | 377.34 | 441.78 | 604.37 | 720.96 | 720.96 |
| Mg, mol/l | 6.47E-06 | 3.05E-04 | 3.65E-04 | 4.17E-04 | 6.87E-04 | 7.55E-04 | 8.27E-04 | 8.96E-04 | 1.23E-03 | 2.28E-03 | 2.64E-03 | 2.90E-03 | 2.79E-03 | 3.54E-03 | 3.82E-03 | 3.70E-03 |
| Al, mol/l | 5.09E-08 | 5.36E-07 | 1.89E-06 | 1.39E-06 | 2.30E-06 | 1.08E-06 | 1.73E-06 | 1.42E-06 | 1.65E-06 | 4.93E-06 | 3.37E-06 | 5.27E-06 | 3.77E-06 | 4.34E-06 | 1.97E-06 | 3.25E-06 |
| Si, mol/l | 2.64E-07 | 6.75E-06 | 5.98E-06 | 9.91E-06 | 1.54E-05 | 1.70E-05 | 1.70E-05 | 1.98E-05 | 2.76E-05 | 2.92E-05 | 3.18E-05 | 3.51E-05 | 3.58E-05 | 3.63E-05 | 3.93E-05 | 3.65E-05 |
| K, mol/l | 2.33E-06 | 2.81E-05 | 4.44E-05 | 3.81E-05 | 3.21E-05 | 3.88E-05 | 3.72E-05 | 3.84E-05 | 3.42E-05 | 4.57E-05 | 4.62E-05 | 4.61E-05 | 3.76E-05 | 4.47E-05 | 4.89E-05 | 5.01E-05 |
| Ca, mol/l (±5%) | 7.19E-06 | 3.94E-04 | 3.52E-04 | 5.18E-04 | 8.94E-04 | 9.26E-04 | 1.11E-03 | 1.23E-03 | 1.95E-03 | 2.64E-03 | 2.93E-03 | 3.28E-03 | 3.50E-03 | 3.87E-03 | 4.05E-03 | 4.36E-03 |
| Mn, mol/l | 1.65E-09 | 4.98E-07 | 8.09E-07 | 3.11E-06 | 1.35E-05 | 1.56E-05 | 1.95E-05 | 2.17E-05 | 3.30E-05 | 6.01E-05 | 6.34E-05 | 7.62E-05 | 6.85E-05 | 9.18E-05 | 8.93E-05 | 8.36E-05 |
| Fe, mol/l | 9.78E-09 | 2.71E-07 | 3.64E-06 | 3.47E-06 | 5.68E-06 | 5.16E-06 | 1.12E-05 | 4.99E-06 | 1.56E-05 | 9.03E-05 | 4.04E-05 | 3.22E-04 | 2.04E-04 | 3.54E-04 | 9.94E-05 | 4.88E-06 |
| Sr, mol/l | 8.95E-09 | 4.53E-07 | 5.88E-07 | 5.32E-07 | 5.67E-07 | 6.14E-07 | 6.13E-07 | 6.51E-07 | 6.79E-07 | 8.61E-07 | 8.76E-07 | 8.97E-07 | 8.15E-07 | 9.84E-07 | 1.01E-06 | 1.00E-06 |
| Ba, mol/l | 1.96E-09 | 1.00E-07 | 6.90E-08 | 3.64E-08 | 8.58E-08 | 5.04E-08 | 4.37E-08 | 5.66E-08 | 1.27E-07 | 1.83E-07 | 7.63E-08 | 8.90E-08 | 4.34E-07 | 1.42E-07 | 6.81E-08 | 8.90E-08 |
| Na (est), mol/l | - | 1.36E+00 | 1.36E+00 | 1.36E+00 | 1.36E+00 | 1.36E+00 | 1.36E+00 | 1.36E+00 | 1.36E+00 | 1.36E+00 | 1.36E+00 | 1.36E+00 | 1.36E+00 | 1.36E+00 | 1.36E+00 | 1.36E+00 |
| Alkalinity(est), mol/l | - | 6.99E-04 | 7.17E-04 | 9.34E-04 | 1.58E-03 | 1.68E-03 | 1.94E-03 | 2.12E-03 | 3.18E-03 | 4.93E-03 | 5.58E-03 | 6.18E-03 | 6.29E-03 | 7.41E-03 | 7.87E-03 | 8.06E-03 |
| Fluid in exp. (kg) | - | 0.100 | 0.099 | 0.094 | 0.091 | 0.088 | 0.085 | 0.083 | 0.080 | 0.077 | 0.075 | 0.072 | 0.070 | 0.067 | 0.065 | 0.062 |
| 132: 1.36M NaCl, 4bar pCO2, 22C | | | | | | | | | | | | | | | | |
| Time, hours | Std. Dev. Mol/l | -0.70 | 0.05 | 2.88 | 22.47 | 25.33 | 45.00 | 49.63 | 71.32 | 189.10 | 235.83 | 311.35 | 359.53 | 476.52 | 557.27 | 557.27 |
| VCT, hours | | 0.00 | 0.05 | 2.88 | 23.02 | 26.04 | 47.34 | 52.48 | 77.31 | 216.36 | 273.21 | 368.18 | 430.81 | 589.19 | 702.96 | 702.96 |
| Mg, mol/l | 6.47E-06 | 2.17E-04 | 2.33E-04 | 2.83E-04 | 6.93E-04 | 7.27E-04 | 1.13E-03 | 1.10E-03 | 1.34E-03 | 2.08E-03 | 2.16E-03 | 2.57E-03 | 3.40E-03 | 3.33E-03 | 3.58E-03 | 3.55E-03 |
| Al, mol/l | 5.09E-08 | 3.33E-08 | 4.53E-07 | 8.77E-07 | 1.08E-06 | 1.10E-06 | 1.25E-05 | 4.21E-07 | 6.10E-07 | 9.62E-07 | 9.41E-07 | 1.31E-06 | 7.13E-05 | 8.83E-07 | 1.32E-06 | 8.87E-07 |
| Si, mol/l | 2.64E-07 | 6.80E-06 | 9.44E-06 | 9.15E-06 | 1.09E-05 | 1.11E-05 | 1.49E-05 | 1.60E-05 | 1.22E-05 | 1.69E-05 | 1.78E-05 | 1.62E-05 | 1.84E-05 | 2.18E-05 | 2.39E-05 | 2.06E-05 |
| K, mol/l | 2.33E-06 | 2.07E-05 | 3.22E-05 | 3.35E-05 | 2.33E-05 | 2.19E-05 | 2.53E-05 | 2.63E-05 | 3.71E-05 | 3.34E-05 | 3.07E-05 | 2.92E-05 | 4.87E-05 | 2.86E-05 | 3.11E-05 | 3.28E-05 |
| Ca, mol/l (±6%) | 7.19E-06 | 2.89E-04 | 4.95E-04 | 3.94E-04 | 8.45E-04 | 8.83E-04 | 1.37E-03 | 1.37E-03 | 1.27E-03 | 2.25E-03 | 2.49E-03 | 2.65E-03 | 2.90E-03 | 3.61E-03 | 4.05E-03 | 3.71E-03 |
| Mn, mol/l | 1.65E-09 | 2.72E-07 | 3.25E-05 | 4.41E-06 | 1.71E-05 | 1.77E-05 | 2.92E-05 | 2.76E-05 | 3.44E-05 | 4.69E-05 | 4.79E-05 | 5.48E-05 | 7.20E-05 | 7.02E-05 | 7.39E-05 | 7.18E-05 |
| Fe, mol/l | 9.78E-09 | 0.00E+00 | 4.20E-05 | 2.04E-05 | 5.02E-06 | 2.78E-06 | 4.78E-06 | 2.09E-06 | 1.38E-05 | 3.71E-06 | 5.60E-07 | 1.39E-05 | 5.86E-06 | 4.24E-05 | 4.57E-05 | 3.72E-06 |
| Sr, mol/l | 8.95E-09 | 3.20E-07 | 5.36E-05 | 3.90E-07 | 4.22E-07 | 4.54E-07 | 5.21E-07 | 5.12E-07 | 6.00E-07 | 6.49E-07 | 6.21E-07 | 6.64E-07 | 8.77E-07 | 7.36E-07 | 7.78E-07 | 7.81E-07 |
| Ba, mol/l | 1.96E-09 | 6.46E-08 | 5.22E-08 | 1.56E-08 | 1.64E-08 | 4.63E-08 | 2.65E-08 | 7.19E-09 | 8.09E-08 | 4.52E-08 | 2.41E-08 | 5.92E-08 | 7.04E-08 | 3.89E-08 | 4.80E-08 | 7.24E-08 |
| Na (est), mol/l | - | 1.36E+00 | 1.36E+00 | 1.36E+00 | 1.36E+00 | 1.36E+00 | 1.36E+00 | 1.36E+00 | 1.36E+00 | 1.36E+00 | 1.36E+00 | 1.36E+00 | 1.36E+00 | 1.36E+00 | 1.36E+00 | 1.36E+00 |
| Alkalinity(est), mol/l | - | 5.06E-04 | 7.29E-04 | 6.77E-04 | 1.54E-03 | 1.61E-03 | 2.50E-03 | 2.47E-03 | 2.61E-03 | 4.33E-03 | 4.66E-03 | 5.22E-03 | 6.30E-03 | 6.94E-03 | 7.63E-03 | 7.26E-03 |
| Fluid in exp. (kg) | - | 0.100 | 0.099 | 0.094 | 0.091 | 0.089 | 0.087 | 0.084 | 0.082 | 0.079 | 0.077 | 0.075 | 0.072 | 0.069 | 0.067 | 0.064 |

| 133: DI, 4bar pCO2, 22C | | | | | | | | | | | | | | | | | | | |
|---|---|---|---|---|---|---|---|---|---|---|---|---|---|---|---|---|---|---|---|
| Time, hours | Std. Dev. Mol/l | -0.22 | 0.02 | 2.28 | 3.92 | 5.40 | 24.15 | 27.28 | 31.15 | 45.53 | 48.87 | 53.25 | 73.45 | 73.45 | 75.53 | 78.20 | 98.87 | 101.45 | 103.03 | 121.12 |
| VCT, hours | - | 0.00 | 0.02 | 2.28 | 3.97 | 5.54 | 26.11 | 29.66 | 34.17 | 51.52 | 55.66 | 61.27 | 88.01 | 88.01 | 90.91 | 94.80 | 126.17 | 130.23 | 132.83 | 163.62 |
| Mg, mol/l | 4.46E-06 | 4.17E-04 | 4.15E-04 | 4.71E-04 | 4.90E-04 | 5.24E-04 | 7.32E-04 | 7.72E-04 | 8.23E-04 | 9.74E-04 | 1.02E-03 | 1.03E-03 | 1.27E-03 | 1.26E-03 | 1.30E-03 | 1.26E-03 | 1.61E-03 | 1.55E-03 | 1.57E-03 | 1.88E-03 |
| Al, mol/l | 3.05E-06 | 0.00E+00 | 2.37E-08 | 0.00E+00 | 0.00E+00 | 1.44E-07 | 0.00E+00 | 0.00E+00 | 0.00E+00 | 3.00E-07 | 0.00E+00 | 0.00E+00 | 0.00E+00 | 2.30E-07 | 5.65E-08 | 0.00E+00 | 8.39E-08 | 2.56E-07 | 0.00E+00 | 2.00E-07 |
| Si, mol/l | 7.67E-06 | 1.24E-05 | 1.23E-05 | 1.31E-05 | 1.33E-05 | 1.37E-05 | 1.58E-05 | 1.57E-05 | 1.63E-05 | 1.69E-05 | 1.70E-05 | 1.73E-05 | 1.85E-05 | 1.84E-05 | 1.80E-05 | 1.85E-05 | 2.01E-05 | 1.96E-05 | 2.00E-05 | 2.07E-05 |
| K, mol/l | 3.15E-06 | 1.01E-05 | 1.08E-05 | 1.09E-05 | 1.07E-05 | 1.18E-05 | 1.22E-05 | 1.45E-05 | 1.25E-05 | 1.30E-05 | 1.28E-05 | 1.28E-05 | 1.37E-05 | 1.40E-05 | 1.43E-05 | 1.34E-05 | 1.45E-05 | 1.47E-05 | 1.36E-05 | 1.48E-05 |
| Ca, mol/l (±1%) | 6.88E-05 | 4.79E-04 | 4.80E-04 | 5.36E-04 | 5.85E-04 | 6.04E-04 | 8.92E-04 | 9.20E-04 | 9.97E-04 | 1.15E-03 | 1.17E-03 | 1.21E-03 | 1.46E-03 | 1.43E-03 | 1.44E-03 | 1.48E-03 | 1.76E-03 | 1.72E-03 | 1.76E-03 | 2.02E-03 |
| Mn, mol/l | 3.59E-08 | 1.99E-06 | 2.04E-06 | 4.57E-06 | 5.65E-06 | 6.64E-06 | 1.55E-05 | 1.70E-05 | 1.85E-05 | 2.32E-05 | 2.46E-05 | 2.57E-05 | 3.19E-05 | 3.18E-05 | 3.29E-05 | 3.19E-05 | 4.09E-05 | 3.98E-05 | 4.07E-05 | 4.77E-05 |
| Fe, mol/l | 2.62E-07 | 9.22E-08 | 3.00E-07 | 5.10E-07 | 7.50E-07 | 1.65E-06 | 1.47E-06 | 2.12E-06 | 2.32E-06 | 3.07E-06 | 3.12E-06 | 3.21E-06 | 4.27E-06 | 3.97E-06 | 4.34E-06 | 4.25E-06 | 5.85E-06 | 6.20E-06 | 5.91E-06 | 8.11E-06 |
| Sr, mol/l | 3.17E-08 | 3.59E-07 | 3.53E-07 | 3.58E-07 | 3.89E-07 | 3.86E-07 | 4.78E-07 | 4.82E-07 | 4.90E-07 | 5.20E-07 | 5.14E-07 | 5.14E-07 | 5.37E-07 | 5.47E-07 | 5.56E-07 | 5.22E-07 | 5.82E-07 | 5.76E-07 | 5.78E-07 | 5.95E-07 |
| Ba, mol/l | 2.02E-08 | 3.37E-07 | 1.42E-07 | 5.71E-08 | 4.38E-08 | 4.93E-08 | 4.62E-08 | 7.97E-08 | 3.65E-08 | 8.68E-08 | 5.43E-08 | 4.18E-08 | 6.82E-08 | 7.31E-08 | 5.40E-08 | 5.29E-08 | 8.24E-08 | 1.55E-07 | 7.91E-08 | 1.12E-07 |
| Na (est), mol/l | - | 0.00E+00 | 0.00E+00 | 0.00E+00 | 0.00E+00 | 0.00E+00 | 0.00E+00 | 0.00E+00 | 0.00E+00 | 0.00E+00 | 0.00E+00 | 0.00E+00 | 0.00E+00 | 0.00E+00 | 0.00E+00 | 0.00E+00 | 0.00E+00 | 0.00E+00 | 0.00E+00 | 0.00E+00 |
| Alkalinity(est), mol/l | - | 8.96E-04 | 8.95E-04 | 1.01E-03 | 1.08E-03 | 1.13E-03 | 1.62E-03 | 1.69E-03 | 1.82E-03 | 2.13E-03 | 2.19E-03 | 2.24E-03 | 2.73E-03 | 2.69E-03 | 2.73E-03 | 2.74E-03 | 3.37E-03 | 3.28E-03 | 3.33E-03 | 3.90E-03 |
| Fluid in exp. (kg) | | 0.099 | 0.097 | 0.094 | 0.091 | 0.088 | 0.085 | 0.083 | 0.080 | 0.078 | 0.075 | 0.073 | 0.071 | 0.068 | 0.067 | 0.064 | 0.062 | 0.059 | 0.057 | 0.055 |

| 133 cont.: DI, 4bar pCO2, 22C | | | | | | | | | | | | | | | |
|---|---|---|---|---|---|---|---|---|---|---|---|---|---|---|---|
| Time, hours | Std. Dev. Mol/l | 126.03 | 139.92 | 150.65 | 168.98 | 168.98 | 172.48 | 190.38 | 193.37 | 290.00 | 311.08 | 332.50 | 382.12 | 531.05 | 531.05 |
| VCT, hours | - | 172.33 | 197.91 | 218.54 | 255.11 | 255.11 | 262.52 | 302.23 | 309.22 | 547.61 | 602.56 | 662.10 | 809.88 | 1289.73 | 1289.73 |
| Mg, mol/l | 4.46E-06 | 1.97E-03 | 2.17E-03 | 2.40E-03 | 2.64E-03 | 2.60E-03 | 2.65E-03 | 2.87E-03 | 2.40E-03 | 0.00E+00 | 3.82E-03 | 3.86E-03 | 4.08E-03 | 4.65E-03 | 4.58E-03 |
| Al, mol/l | 3.05E-06 | 2.14E-07 | 1.97E-07 | 5.83E-07 | 8.66E-07 | 3.89E-07 | 4.60E-07 | 5.52E-07 | 2.00E-07 | 0.00E+00 | 2.89E-07 | 2.75E-07 | 4.62E-07 | 2.52E-07 | 4.25E-06 |
| Si, mol/l | 7.67E-06 | 2.15E-05 | 2.25E-05 | 2.22E-05 | 2.34E-05 | 2.33E-05 | 2.31E-05 | 2.46E-05 | 2.41E-05 | 4.60E-07 | 3.13E-05 | 3.17E-05 | 3.44E-05 | 4.15E-05 | 5.02E-05 |
| K, mol/l | 3.15E-06 | 1.42E-05 | 1.42E-05 | 1.38E-05 | 1.41E-05 | 1.48E-05 | 1.60E-05 | 1.65E-05 | 4.52E-05 | 3.33E-05 | 1.73E-05 | 1.81E-05 | 1.84E-05 | 1.99E-05 | 1.95E-05 |
| Ca, mol/l (±1%) | 6.88E-05 | 2.10E-03 | 2.35E-03 | 2.37E-03 | 2.64E-03 | 2.62E-03 | 2.65E-03 | 2.90E-03 | 3.16E-03 | 7.87E-06 | 3.77E-03 | 3.80E-03 | 4.05E-03 | 4.47E-03 | 4.49E-03 |

| | | | | | | | | | | | | | | |
|---|---|---|---|---|---|---|---|---|---|---|---|---|---|---|
| Mn, mol/l | 3.59E-08 | 4.98E-05 | 5.46E-05 | 6.04E-05 | 6.61E-05 | 6.44E-05 | 6.56E-05 | 6.99E-05 | 6.41E-05 | 3.55E-08 | 8.95E-05 | 9.14E-05 | 9.36E-05 | 1.02E-04 | 1.03E-04 |
| Fe, mol/l | 2.62E-07 | 9.18E-06 | 1.12E-05 | 1.33E-05 | 1.48E-05 | 1.95E-05 | 1.47E-05 | 1.52E-05 | 1.33E-05 | 5.83E-06 | 6.84E-06 | 5.15E-06 | 3.88E-06 | 2.08E-06 | 2.20E-06 |
| Sr, mol/l | 3.17E-08 | 6.03E-07 | 6.15E-07 | 6.82E-07 | 6.92E-07 | 6.85E-07 | 6.66E-07 | 6.97E-07 | 7.00E-07 | 1.35E-08 | 8.08E-07 | 7.98E-07 | 8.05E-07 | 8.95E-07 | 8.88E-07 |
| Ba, mol/l | 2.02E-08 | 9.40E-08 | 1.30E-07 | 7.69E-08 | 1.20E-07 | 9.76E-08 | 7.02E-08 | 7.79E-08 | 3.18E-08 | 0.00E+00 | 9.93E-08 | 5.30E-08 | 1.07E-07 | 9.22E-08 | 1.72E-07 |
| Na (est), mol/l | - | 0.00E+00 | 0.00E+00 | 0.00E+00 | 0.00E+00 | 0.00E+00 | 0.00E+00 | 0.00E+00 | 0.00E+00 | 0.00E+00 | 0.00E+00 | 0.00E+00 | 0.00E+00 | 0.00E+00 | 0.00E+00 |
| Alkalinity(est), mol/l | - | 4.07E-03 | 4.52E-03 | 4.77E-03 | 5.28E-03 | 5.23E-03 | 5.30E-03 | 5.77E-03 | 5.57E-03 | 7.87E-06 | 7.59E-03 | 7.66E-03 | 8.13E-03 | 9.12E-03 | 9.07E-03 |
| Fluid in exp. (kg) | | 0.053 | 0.051 | 0.049 | 0.047 | 0.045 | 0.044 | 0.042 | 0.040 | 0.038 | 0.036 | 0.034 | 0.031 | 0.029 | 0.027 |

| 134: DI, 31bar pCO2, 70C | | | | | | | | | | | | | | | | | | | | |
|---|---|---|---|---|---|---|---|---|---|---|---|---|---|---|---|---|---|---|---|---|
| Time, hours | Std. Dev. Mol/l | -0.93 | 0.02 | 0.77 | 3.57 | 10.40 | 21.90 | 26.87 | 31.23 | 50.60 | 53.45 | 55.65 | 71.57 | 71.57 | 73.73 | 148.08 | 152.22 | 166.92 | 175.18 | 190.87 |
| VCT, hours | | 0.00 | 0.02 | 0.77 | 3.63 | 10.75 | 23.03 | 28.41 | 33.22 | 54.93 | 58.17 | 60.72 | 79.49 | 79.49 | 82.11 | 173.76 | 178.95 | 197.73 | 208.50 | 229.33 |
| Mg, mol/l | 4.81E-06 | 1.93E-04 | 2.00E-04 | 2.53E-04 | 4.82E-04 | 1.02E-03 | 1.42E-03 | 1.90E-03 | 2.36E-03 | 2.62E-03 | 3.10E-03 | 3.37E-03 | 3.57E-03 | 3.73E-03 | 4.24E-03 | 3.67E-03 | 4.32E-03 | 4.59E-03 | 4.68E-03 | 4.76E-03 |
| Al, mol/l | 1.72E-06 | 0.00E+00 | 0.00E+00 | 0.00E+00 | 0.00E+00 | 0.00E+00 | 0.00E+00 | 0.00E+00 | 0.00E+00 | 0.00E+00 | 0.00E+00 | 0.00E+00 | 0.00E+00 | 0.00E+00 | 0.00E+00 | 0.00E+00 | 0.00E+00 | 0.00E+00 | 0.00E+00 | 0.00E+00 |
| Si, mol/l | 1.76E-06 | 3.61E-05 | 4.10E-05 | 5.99E-05 | 8.80E-05 | 8.72E-05 | 8.52E-05 | 7.79E-05 | 7.26E-05 | 8.13E-05 | 7.71E-05 | 7.15E-05 | 7.84E-05 | 7.83E-05 | 8.18E-05 | 9.77E-05 | 9.53E-05 | 9.08E-05 | 8.94E-05 | 9.36E-05 |
| K, mol/l | 7.99E-06 | 1.93E-05 | 1.97E-05 | 1.88E-05 | 2.03E-05 | 2.23E-05 | 2.35E-05 | 2.50E-05 | 2.72E-05 | 2.94E-05 | 2.93E-05 | 3.06E-05 | 3.08E-05 | 3.15E-05 | 3.44E-05 | 2.95E-05 | 3.30E-05 | 3.79E-05 | 3.61E-05 | 3.61E-05 |
| Ca, mol/l (±20%) | 1.75E-05 | 2.52E-04 | 2.85E-04 | 3.89E-04 | 5.85E-04 | 1.07E-03 | 1.47E-03 | 1.88E-03 | 2.34E-03 | 2.56E-03 | 3.00E-03 | 3.21E-03 | 3.42E-03 | 3.55E-03 | 3.99E-03 | 3.60E-03 | 3.98E-03 | 4.16E-03 | 4.28E-03 | 4.32E-03 |
| Mn, mol/l | 3.76E-08 | 6.67E-07 | 2.04E-05 | 2.50E-05 | 4.79E-05 | 4.20E-05 | 4.39E-05 | 4.81E-05 | 5.52E-05 | 6.27E-05 | 6.97E-05 | 7.52E-05 | 8.02E-05 | 8.29E-05 | 9.27E-05 | 8.57E-05 | 9.49E-05 | 9.69E-05 | 9.85E-05 | 1.01E-04 |
| Fe, mol/l | 4.79E-07 | 1.84E-07 | 1.69E-05 | 4.86E-06 | 6.50E-05 | 2.08E-04 | 4.33E-04 | 2.82E-04 | 1.61E-04 | 2.58E-04 | 1.40E-04 | 7.00E-05 | 1.14E-04 | 8.28E-05 | 5.40E-05 | 1.21E-04 | 5.79E-05 | 3.30E-05 | 2.32E-05 | 2.19E-05 |
| Sr, mol/l | 3.15E-08 | 3.25E-07 | 3.09E-07 | 3.56E-07 | 4.25E-07 | 5.03E-07 | 5.61E-07 | 5.88E-07 | 6.31E-07 | 6.57E-07 | 6.95E-07 | 7.38E-07 | 7.32E-07 | 7.48E-07 | 8.42E-07 | 7.23E-07 | 8.02E-07 | 8.39E-07 | 8.61E-07 | 8.63E-07 |
| Ba, mol/l | 2.72E-08 | 6.92E-07 | 1.86E-07 | 6.71E-08 | 8.79E-08 | 1.80E-07 | 0.00E+00 | 0.00E+00 | 2.47E-08 | 0.00E+00 | 4.01E-08 | 1.65E-07 | 1.85E-08 | 1.97E-08 | 3.32E-08 | 8.53E-09 | 7.38E-08 | 3.26E-08 | 5.64E-08 | 1.80E-08 |
| Na (est), mol/l | | 0.00E+00 | 0.00E+00 | 0.00E+00 | 0.00E+00 | 0.00E+00 | 0.00E+00 | 0.00E+00 | 0.00E+00 | 0.00E+00 | 0.00E+00 | 0.00E+00 | 0.00E+00 | 0.00E+00 | 0.00E+00 | 0.00E+00 | 0.00E+00 | 0.00E+00 | 0.00E+00 | 0.00E+00 |
| Alkalinity(est), mol/l | | 4.46E-04 | 4.85E-04 | 6.42E-04 | 1.07E-03 | 2.09E-03 | 2.89E-03 | 3.78E-03 | 4.70E-03 | 5.18E-03 | 6.10E-03 | 6.58E-03 | 6.99E-03 | 7.29E-03 | 8.23E-03 | 7.28E-03 | 8.30E-03 | 8.74E-03 | 8.96E-03 | 9.07E-03 |
| Fluid in exp. (kg) | | 0.151 | 0.150 | 0.146 | 0.143 | 0.140 | 0.137 | 0.135 | 0.133 | 0.131 | 0.128 | 0.126 | 0.124 | 0.122 | 0.121 | 0.119 | 0.117 | 0.114 | 0.112 | 0.110 |

| 134 cont.: DI, 31bar pCO2, 70C | | | | | | | | | | | | | | | | | |
|---|---|---|---|---|---|---|---|---|---|---|---|---|---|---|---|---|---|
| Time, hours | Std. Dev. Mol/l | 198.18 | 215.48 | 223.07 | 239.98 | 239.98 | 248.07 | 313.07 | 322.23 | 335.00 | 366.42 | 389.98 | 409.73 | 487.15 | 502.98 | 581.13 | 581.13 |
| VCT, hours | | 239.24 | 263.15 | 273.87 | 298.29 | 298.29 | 310.26 | 408.62 | 422.78 | 442.94 | 493.71 | 532.75 | 566.22 | 700.55 | 728.73 | 871.12 | 871.12 |
| Mg, mol/l | 4.81E-06 | 4.80E-03 | 4.82E-03 | 4.76E-03 | 4.87E-03 | 4.85E-03 | 4.84E-03 | 4.86E-03 | 4.74E-03 | 5.02E-03 | 5.06E-03 | 5.12E-03 | 5.02E-03 | 5.18E-03 | 6.06E-03 | 5.30E-03 | 5.28E-03 |
| Al, mol/l | 1.72E-06 | 0.00E+00 | 6.25E-07 | 0.00E+00 | 0.00E+00 | 0.00E+00 | 0.00E+00 | 0.00E+00 | 0.00E+00 | 0.00E+00 | 0.00E+00 | 0.00E+00 | 0.00E+00 | 3.56E-06 | 0.00E+00 | 0.00E+00 | 0.00E+00 |
| Si, mol/l | 1.76E-06 | 9.26E-05 | 9.74E-05 | 9.61E-05 | 9.48E-05 | 9.77E-05 | 9.76E-05 | 9.78E-05 | 1.09E-04 | 9.94E-05 | 1.05E-04 | 1.52E-04 | 1.13E-04 | 1.11E-04 | 1.46E-04 | 1.24E-04 | 8.64E-05 |
| K, mol/l | 7.99E-06 | 3.68E-05 | 3.83E-05 | 3.63E-05 | 3.73E-05 | 3.82E-05 | 4.15E-05 | 3.09E-05 | 3.19E-05 | 3.64E-05 | 3.63E-05 | 4.32E-05 | 3.40E-05 | 3.60E-05 | 4.58E-05 | 3.85E-05 | 3.72E-05 |
| Ca, mol/l (±20%) | 1.75E-05 | 4.28E-03 | 4.39E-03 | 4.39E-03 | 4.29E-03 | 4.54E-03 | 4.51E-03 | 3.71E-03 | 3.98E-03 | 3.82E-03 | 3.78E-03 | 5.51E-03 | 4.05E-03 | 3.87E-03 | 5.10E-03 | 4.14E-03 | 2.95E-03 |
| Mn, mol/l | 3.76E-08 | 1.02E-04 | 1.01E-04 | 9.90E-05 | 1.01E-04 | 9.99E-05 | 1.00E-04 | 1.07E-04 | 1.02E-04 | 1.01E-04 | 1.06E-04 | 1.05E-04 | 1.03E-04 | 1.06E-04 | 1.28E-04 | 1.06E-04 | 1.05E-04 |
| Fe, mol/l | 4.79E-07 | 1.63E-05 | 1.76E-05 | 1.42E-05 | 1.81E-05 | 1.08E-05 | 1.26E-05 | 1.87E-05 | 1.14E-05 | 9.40E-06 | 8.37E-06 | 9.84E-06 | 7.85E-06 | 8.37E-06 | 1.02E-05 | 1.11E-05 | 6.39E-06 |
| Sr, mol/l | 3.15E-08 | 8.78E-07 | 8.77E-07 | 8.73E-07 | 8.84E-07 | 9.10E-07 | 8.98E-07 | 9.12E-07 | 9.01E-07 | 9.64E-07 | 9.52E-07 | 9.84E-07 | 9.49E-07 | 9.85E-07 | 1.14E-06 | 1.00E-06 | 1.00E-06 |
| Ba, mol/l | 2.72E-08 | 1.17E-07 | 2.92E-08 | 6.23E-08 | 7.16E-08 | 1.71E-07 | 1.06E-08 | 0.00E+00 | 0.00E+00 | 0.00E+00 | 0.00E+00 | 0.00E+00 | 0.00E+00 | 0.00E+00 | 0.00E+00 | 0.00E+00 | 0.00E+00 |
| Na (est), mol/l | | 0.00E+00 | 0.00E+00 | 0.00E+00 | 0.00E+00 | 0.00E+00 | 0.00E+00 | 0.00E+00 | 0.00E+00 | 0.00E+00 | 0.00E+00 | 0.00E+00 | 0.00E+00 | 0.00E+00 | 0.00E+00 | 0.00E+00 | 0.00E+00 |
| Alkalinity(est), mol/l | | 9.08E-03 | 9.21E-03 | 9.15E-03 | 9.17E-03 | 9.39E-03 | 9.35E-03 | 8.57E-03 | 8.73E-03 | 8.85E-03 | 8.84E-03 | 1.06E-02 | 9.07E-03 | 9.06E-03 | 1.12E-02 | 9.45E-03 | 8.23E-03 |
| Fluid in exp. (kg) | | 0.108 | 0.106 | 0.104 | 0.101 | 0.099 | 0.099 | 0.097 | 0.095 | 0.093 | 0.091 | 0.088 | 0.086 | 0.084 | 0.082 | 0.080 | 0.079 |

| 135: DI, 31bar pCO2, 70C | | | | | | | | | | | | | | | | | | |
|---|---|---|---|---|---|---|---|---|---|---|---|---|---|---|---|---|---|---|
| Time, hours | Std. Dev. Mol/l | -0.98 | 0.02 | 0.72 | 3.52 | 10.35 | 21.85 | 26.82 | 31.18 | 50.55 | 53.40 | 55.60 | 71.52 | 71.52 | 73.68 | 148.03 | 152.17 | 166.87 |
| VCT, hours | | 0.00 | 0.02 | 0.74 | 3.68 | 10.98 | 23.46 | 28.95 | 33.86 | 55.97 | 59.28 | 61.88 | 81.05 | 81.05 | 83.73 | 177.83 | 183.15 | 202.47 |
| Mg, mol/l | 4.81E-06 | 1.03E-03 | 1.00E-03 | 1.03E-03 | 1.13E-03 | 1.43E-03 | 1.91E-03 | 2.57E-03 | 2.93E-03 | 3.27E-03 | 3.69E-03 | 3.98E-03 | 4.15E-03 | 4.21E-03 | 4.41E-03 | 4.25E-03 | 4.85E-03 | 4.93E-03 |
| Al, mol/l | 1.72E-06 | 0.00E+00 | 5.05E-07 | 0.00E+00 | 2.57E-06 | 2.07E-06 | 2.16E-06 | 1.99E-06 | 2.46E-06 | 2.61E-06 | 3.78E-06 | 3.69E-06 | 4.42E-06 | 4.23E-06 | 4.35E-06 | 5.43E-06 | 3.97E-06 | 3.66E-06 |
| Si, mol/l | 1.76E-06 | 3.27E-05 | 4.50E-05 | 5.20E-05 | 6.29E-05 | 7.79E-05 | 9.78E-05 | 6.96E-05 | 6.24E-05 | 7.01E-05 | 6.21E-05 | 5.53E-05 | 6.84E-05 | 6.46E-05 | 5.87E-05 | 1.15E-04 | 8.47E-05 | 8.05E-05 |
| K, mol/l | 7.99E-06 | 2.48E-05 | 1.73E-03 | 1.16E-03 | 8.48E-04 | 5.21E-04 | 3.50E-04 | 2.75E-04 | 2.43E-04 | 2.32E-04 | 2.22E-04 | 2.27E-04 | 2.28E-04 | 2.24E-04 | 2.28E-04 | 2.13E-04 | 2.30E-04 | 2.30E-04 |
| Ca, mol/l (±5%) | 1.75E-05 | 9.94E-04 | 9.36E-04 | 9.75E-04 | 1.08E-03 | 1.34E-03 | 1.69E-03 | 2.27E-03 | 2.70E-03 | 2.89E-03 | 3.24E-03 | 3.54E-03 | 3.77E-03 | 3.92E-03 | 3.92E-03 | 3.96E-03 | 4.34E-03 | 4.41E-03 |
| Mn, mol/l | 3.76E-08 | 1.44E-05 | 2.77E-05 | 3.68E-05 | 4.98E-05 | 5.34E-05 | 5.75E-05 | 5.98E-05 | 6.31E-05 | 6.92E-05 | 7.49E-05 | 7.89E-05 | 8.36E-05 | 8.45E-05 | 8.63E-05 | 9.13E-05 | 9.58E-05 | 9.58E-05 |
| Fe, mol/l | 4.79E-07 | 6.46E-07 | 2.47E-05 | 9.36E-05 | 2.06E-04 | 2.88E-04 | 3.57E-04 | 1.71E-04 | 1.15E-04 | 1.44E-04 | 8.64E-05 | 4.45E-05 | 1.96E-05 | 1.31E-05 | 1.22E-05 | 3.71E-05 | 2.60E-05 | 1.38E-05 |
| Sr, mol/l | 3.15E-08 | 4.43E-07 | 4.30E-07 | 4.50E-07 | 4.75E-07 | 5.20E-07 | 5.23E-07 | 5.92E-07 | 6.14E-07 | 6.59E-07 | 6.72E-07 | 7.06E-07 | 7.13E-07 | 7.22E-07 | 7.34E-07 | 7.01E-07 | 7.71E-07 | 7.84E-07 |
| Ba, mol/l | 2.72E-08 | 7.84E-07 | 9.73E-08 | 1.41E-07 | 1.19E-07 | 1.33E-07 | 6.76E-08 | 4.05E-08 | 9.41E-08 | 7.71E-08 | 5.38E-08 | 1.05E-07 | 2.34E-07 | 1.11E-07 | 3.25E-08 | 5.41E-08 | 7.44E-08 | 5.10E-08 |
| Na (est), mol/l | | 0.00E+00 | 0.00E+00 | 0.00E+00 | 0.00E+00 | 0.00E+00 | 0.00E+00 | 0.00E+00 | 0.00E+00 | 0.00E+00 | 0.00E+00 | 0.00E+00 | 0.00E+00 | 0.00E+00 | 0.00E+00 | 0.00E+00 | 0.00E+00 | 0.00E+00 |
| Alkalinity(est), mol/l | | 2.03E-03 | 1.94E-03 | 2.00E-03 | 2.21E-03 | 2.77E-03 | 3.59E-03 | 4.84E-03 | 5.64E-03 | 6.16E-03 | 6.93E-03 | 7.52E-03 | 7.91E-03 | 8.14E-03 | 8.33E-03 | 8.21E-03 | 9.19E-03 | 9.34E-03 |
| Fluid in exp. (kg) | | 0.151 | 0.149 | 0.145 | 0.142 | 0.139 | 0.137 | 0.135 | 0.133 | 0.130 | 0.128 | 0.126 | 0.124 | 0.121 | 0.120 | 0.118 | 0.116 | 0.113 |

| 135 cont.: DI, 31bar pCO2, 70C | | | | | | | | | | | | | | | | |
|---|---|---|---|---|---|---|---|---|---|---|---|---|---|---|---|---|
| Time, hours | Std. Dev. Mol/l | 175.13 | 190.82 | 198.13 | 215.43 | 223.02 | 239.93 | 239.93 | 248.02 | 313.02 | 322.18 | 334.95 | 366.37 | 389.93 | 409.68 | 487.10 |
| VCT, hours | | 213.55 | 235.01 | 245.24 | 269.94 | 281.01 | 306.27 | 306.27 | 318.74 | 421.30 | 436.09 | 457.18 | 510.55 | 551.54 | 586.79 | 728.45 |
| Mg, mol/l | 4.81E-06 | 5.18E-03 | 5.07E-03 | 5.25E-03 | 5.18E-03 | 5.19E-03 | 5.22E-03 | 5.27E-03 | 5.33E-03 | 5.20E-03 | 4.90E-03 | 5.38E-03 | 5.21E-03 | 5.29E-03 | 5.35E-03 | 5.51E-03 |
| Al, mol/l | 1.72E-06 | 3.98E-06 | 4.00E-06 | 5.16E-06 | 4.14E-06 | 4.64E-06 | 4.28E-06 | 4.69E-06 | 8.40E-06 | 0.00E+00 | 0.00E+00 | 1.77E-07 | 0.00E+00 | 1.26E-07 | 0.00E+00 | 2.51E-06 |
| Si, mol/l | 1.76E-06 | 8.04E-05 | 8.35E-05 | 7.91E-05 | 8.78E-05 | 8.69E-05 | 9.02E-05 | 9.11E-05 | 8.26E-05 | 1.19E-04 | 1.17E-04 | 9.78E-05 | 9.14E-05 | 8.63E-05 | 8.74E-05 | 1.12E-04 |
| K, mol/l | 7.99E-06 | 2.35E-04 | 2.28E-04 | 2.36E-04 | 2.45E-04 | 2.28E-04 | 2.32E-04 | 2.31E-04 | 2.39E-04 | 2.08E-04 | 1.92E-04 | 2.11E-04 | 2.02E-04 | 2.07E-04 | 2.08E-04 | 2.16E-04 |

| | | | | | | | | | | | | | | | | |
|---|---|---|---|---|---|---|---|---|---|---|---|---|---|---|---|---|
| Ca, mol/l (±5%) | 1.75E-05 | 4.53E-03 | 4.54E-03 | 4.59E-03 | 4.82E-03 | 4.71E-03 | 4.60E-03 | 4.90E-03 | 4.85E-03 | 4.30E-03 | 4.60E-03 | 4.20E-03 | 3.77E-03 | 3.36E-03 | 3.42E-03 | 3.62E-03 |
| Mn, mol/l | 3.76E-08 | 9.93E-05 | 9.72E-05 | 9.87E-05 | 9.79E-05 | 9.79E-05 | 9.92E-05 | 9.82E-05 | 9.88E-05 | 9.71E-05 | 9.11E-05 | 9.67E-05 | 9.69E-05 | 9.52E-05 | 9.74E-05 | 9.83E-05 |
| Fe, mol/l | 4.79E-07 | 1.00E-05 | 9.43E-06 | 7.14E-06 | 6.96E-06 | 5.60E-06 | 5.78E-06 | 4.46E-06 | 4.95E-06 | 8.80E-06 | 3.64E-06 | 4.79E-06 | 3.98E-06 | 4.29E-06 | 3.78E-06 | 3.88E-06 |
| Sr, mol/l | 3.15E-08 | 8.11E-07 | 7.95E-07 | 8.29E-07 | 8.16E-07 | 8.12E-07 | 8.15E-07 | 8.21E-07 | 8.29E-07 | 8.54E-07 | 7.86E-07 | 8.70E-07 | 8.53E-07 | 8.70E-07 | 8.74E-07 | 8.86E-07 |
| Ba, mol/l | 2.72E-08 | 2.57E-08 | 1.00E-07 | 3.94E-08 | 5.94E-08 | 1.67E-07 | 2.52E-08 | 5.78E-08 | 9.78E-09 | 0.00E+00 | 0.00E+00 | 0.00E+00 | 0.00E+00 | 0.00E+00 | 0.00E+00 | 0.00E+00 |
| Na (est), mol/l | | 0.00E+00 | 0.00E+00 | 0.00E+00 | 0.00E+00 | 0.00E+00 | 0.00E+00 | 0.00E+00 | 0.00E+00 | 0.00E+00 | 0.00E+00 | 0.00E+00 | 0.00E+00 | 0.00E+00 | 0.00E+00 | 0.00E+00 |
| Alkalinity(est), mol/l | | 9.70E-03 | 9.62E-03 | 9.84E-03 | 1.00E-02 | 9.90E-03 | 9.83E-03 | 1.02E-02 | 1.02E-02 | 9.50E-03 | 9.50E-03 | 9.58E-03 | 8.98E-03 | 8.65E-03 | 8.76E-03 | 9.14E-03 |
| Fluid in exp. (kg) | | 0.111 | 0.109 | 0.107 | 0.104 | 0.102 | 0.100 | 0.098 | 0.097 | 0.094 | 0.092 | 0.090 | 0.088 | 0.086 | 0.083 | 0.081 |

| 143: 1.36M NaCl, 31bar pCO2, 70C | | | | | | | | | | | | | | | | | | |
|---|---|---|---|---|---|---|---|---|---|---|---|---|---|---|---|---|---|---|
| Time, hours | Std. Dev. Mol/l | -16.58 | 0.03 | 2.08 | 4.25 | 6.32 | 24.72 | 27.83 | 30.62 | 47.70 | 51.20 | 53.92 | 73.75 | 73.75 | 78.68 | 98.27 | 101.95 | 119.68 | 125.28 |
| VCT, hours | | 0.00 | 0.03 | 2.12 | 4.36 | 6.53 | 26.03 | 29.36 | 32.37 | 51.05 | 54.93 | 57.98 | 80.54 | 80.54 | 86.27 | 109.26 | 113.64 | 135.01 | 141.85 |
| Mg, mol/l | 4.75E-06 | 2.59E-04 | 2.73E-04 | 3.64E-04 | 5.50E-04 | 1.23E-03 | 9.38E-04 | 2.71E-03 | 2.35E-03 | 3.96E-03 | 3.27E-03 | 3.52E-03 | 3.94E-03 | 4.09E-03 | 4.38E-03 | 4.56E-03 | 4.95E-03 | 5.53E-03 | 5.97E-03 |
| Al, mol/l | 1.29E-05 | 0.00E+00 | 0.00E+00 | 0.00E+00 | 0.00E+00 | 0.00E+00 | 0.00E+00 | 0.00E+00 | 0.00E+00 | 0.00E+00 | 4.91E-07 | 3.44E-07 | 0.00E+00 | 0.00E+00 | 0.00E+00 | 0.00E+00 | 0.00E+00 | 2.47E-06 | 0.00E+00 |
| Si, mol/l | 0.00E+00 | 8.62E-05 | 1.25E-04 | 1.40E-04 | 1.52E-04 | 5.41E-04 | 1.79E-04 | 3.67E-04 | 1.99E-04 | 3.09E-04 | 2.23E-04 | 2.11E-04 | 2.30E-04 | 2.29E-04 | 2.23E-04 | 2.35E-04 | 2.35E-04 | 2.45E-04 | 2.53E-04 |
| K, mol/l | 2.48E-06 | 1.12E-04 | 1.23E-04 | 1.46E-04 | 1.20E-04 | 7.56E-05 | 1.13E-04 | 2.44E-04 | 1.44E-04 | 2.10E-04 | 1.61E-04 | 1.63E-04 | 1.73E-04 | 1.66E-04 | 1.71E-04 | 1.67E-04 | 1.96E-04 | 1.83E-04 | 1.98E-04 |
| Ca, mol/l (±3%) | 2.30E-06 | 4.55E-04 | 4.97E-04 | 6.34E-04 | 8.31E-04 | 1.89E-05 | 1.29E-03 | 3.56E-03 | 2.97E-03 | 4.81E-03 | 4.14E-03 | 4.29E-03 | 4.72E-03 | 4.90E-03 | 5.34E-03 | 5.35E-03 | 5.90E-03 | 6.54E-03 | 7.12E-03 |
| Mn, mol/l | 3.09E-06 | 5.22E-05 | 6.96E-05 | 4.23E-05 | 4.48E-05 | 2.49E-05 | 7.93E-05 | 1.94E-04 | 1.15E-04 | 2.05E-04 | 1.44E-04 | 1.42E-04 | 1.66E-04 | 1.65E-04 | 1.64E-04 | 1.77E-04 | 1.79E-04 | 1.97E-04 | 2.03E-04 |
| Fe, mol/l | 0.00E+00 | 1.16E-03 | 2.08E-03 | 9.60E-04 | 7.91E-04 | 4.25E-04 | 1.44E-03 | 3.57E-03 | 8.38E-04 | 2.20E-03 | 9.19E-04 | 5.33E-04 | 9.46E-04 | 9.16E-04 | 4.89E-04 | 8.50E-04 | 6.09E-04 | 7.71E-04 | 5.55E-04 |
| Sr, mol/l | 0.00E+00 | 3.69E-07 | 4.16E-07 | 5.56E-07 | 5.79E-07 | 3.94E-06 | 5.48E-07 | 9.98E-07 | 7.49E-07 | 1.10E-06 | 8.72E-07 | 8.76E-07 | 9.41E-07 | 8.85E-07 | 9.58E-07 | 9.15E-07 | 1.00E-06 | 1.03E-06 | 1.09E-06 |
| Ba, mol/l | 1.06E-05 | 7.16E-07 | 2.77E-06 | 5.58E-06 | 6.87E-06 | 3.02E-06 | 2.79E-07 | 2.68E-06 | 4.05E-06 | 6.85E-06 | 8.02E-06 | 4.84E-06 | 7.79E-06 | 1.23E-06 | 2.92E-06 | 1.54E-06 | 3.79E-06 | 5.07E-07 | 3.80E-06 |
| Na (est), mol/l | | 1.36E+00 | 1.36E+00 | 1.36E+00 | 1.36E+00 | 1.36E+00 | 1.36E+00 | 1.36E+00 | 1.36E+00 | 1.36E+00 | 1.36E+00 | 1.36E+00 | 1.36E+00 | 1.36E+00 | 1.36E+00 | 1.36E+00 | 1.36E+00 | 1.36E+00 | 1.36E+00 |
| Alkalinity(est), mol/l | | 7.14E-04 | 7.70E-04 | 9.98E-04 | 1.38E-03 | 1.25E-03 | 2.23E-03 | 6.27E-03 | 5.31E-03 | 8.76E-03 | 7.41E-03 | 7.81E-03 | 8.66E-03 | 8.99E-03 | 9.72E-03 | 9.91E-03 | 1.09E-02 | 1.21E-02 | 1.31E-02 |
| Fluid in exp. (kg) | | 0.200 | 0.196 | 0.192 | 0.190 | 0.187 | 0.185 | 0.184 | 0.182 | 0.179 | 0.177 | 0.175 | 0.173 | 0.170 | 0.169 | 0.167 | 0.165 | 0.163 | 0.161 |

| 143 cont.: 1.36M NaCl, 31bar pCO2, 70C | | | | | | | | | | | | | | | | | |
|---|---|---|---|---|---|---|---|---|---|---|---|---|---|---|---|---|---|
| Time, hours | Std. Dev. Mol/l | 144.22 | 149.85 | 168.00 | 173.50 | 191.00 | 214.92 | 268.33 | 285.42 | 309.18 | 365.25 | 365.25 | 387.18 | 434.42 | 480.42 | 525.55 | 525.55 |
| VCT, hours | | 165.36 | 172.47 | 195.68 | 202.83 | 225.90 | 257.89 | 330.44 | 354.00 | 387.34 | 467.40 | 467.40 | 499.47 | 569.69 | 639.25 | 708.72 | 708.72 |
| Mg, mol/l | 4.75E-06 | 5.98E-03 | 6.57E-03 | 7.26E-03 | 6.49E-03 | 6.94E-03 | 6.86E-03 | 7.86E-03 | 8.25E-03 | 8.48E-03 | 8.19E-03 | 8.50E-03 | 8.70E-03 | 8.72E-03 | 8.30E-03 | 8.87E-03 | 7.65E-03 |
| Al, mol/l | 1.29E-05 | 0.00E+00 | 0.00E+00 | 0.00E+00 | 0.00E+00 | 0.00E+00 | 1.98E-06 | 1.23E-06 | 8.94E-07 | 0.00E+00 | 0.00E+00 | 2.94E-07 | 0.00E+00 | 0.00E+00 | 0.00E+00 | 0.00E+00 | 8.62E-08 |

| | | | | | | | | | | | | | | | | | |
|---|---|---|---|---|---|---|---|---|---|---|---|---|---|---|---|---|---|
| Si, mol/l | 0.00E+00 | 2.48E-04 | 2.56E-04 | 2.49E-04 | 2.41E-04 | 2.61E-04 | 2.57E-04 | 2.85E-04 | 2.72E-04 | 2.70E-04 | 2.77E-04 | 2.89E-04 | 2.80E-04 | 2.88E-04 | 2.84E-04 | 2.79E-04 | 2.80E-04 |
| K, mol/l | 2.48E-06 | 1.96E-04 | 2.08E-04 | 1.88E-04 | 2.04E-04 | 2.11E-04 | 2.13E-04 | 2.08E-04 | 2.20E-04 | 2.15E-04 | 2.26E-04 | 2.17E-04 | 2.48E-04 | 2.50E-04 | 2.38E-04 | 2.40E-04 | 2.56E-04 |
| Ca, mol/l (±3%) | 2.30E-06 | 7.10E-03 | 7.69E-03 | 7.49E-03 | 7.61E-03 | 8.16E-03 | 8.09E-03 | 8.14E-03 | 8.38E-03 | 8.55E-03 | 8.61E-03 | 8.85E-03 | 8.98E-03 | 9.10E-03 | 8.83E-03 | 8.88E-03 | 8.91E-03 |
| Mn, mol/l | 3.09E-06 | 2.07E-04 | 2.11E-04 | 2.12E-04 | 2.11E-04 | 2.28E-04 | 2.33E-04 | 2.54E-04 | 2.47E-04 | 2.41E-04 | 2.44E-04 | 2.55E-04 | 2.43E-04 | 2.51E-04 | 2.45E-04 | 2.42E-04 | 2.40E-04 |
| Fe, mol/l | 0.00E+00 | 7.40E-04 | 6.16E-04 | 6.78E-04 | 5.00E-04 | 6.13E-04 | 8.10E-04 | 1.53E-03 | 1.13E-03 | 8.67E-04 | 1.03E-03 | 1.27E-03 | 6.65E-04 | 8.96E-04 | 8.24E-04 | 7.41E-04 | 6.85E-04 |
| Sr, mol/l | 0.00E+00 | 1.15E-06 | 1.14E-06 | 1.04E-06 | 1.15E-06 | 1.18E-06 | 1.29E-06 | 1.15E-06 | 1.16E-06 | 1.34E-06 | 1.25E-06 | 1.23E-06 | 1.26E-06 | 1.30E-06 | 1.29E-06 | 1.24E-06 | 1.51E-06 |
| Ba, mol/l | 1.06E-05 | 6.00E-07 | 3.40E-06 | 3.69E-07 | 3.79E-06 | 6.99E-07 | 8.26E-07 | 3.23E-07 | 4.21E-07 | 1.00E-05 | 2.30E-06 | 2.24E-06 | 6.76E-07 | 1.83E-06 | 8.33E-06 | 4.75E-06 | 2.49E-05 |
| Na (est), mol/l | | 1.36E+00 | 1.36E+00 | 1.36E+00 | 1.36E+00 | 1.36E+00 | 1.36E+00 | 1.36E+00 | 1.36E+00 | 1.36E+00 | 1.36E+00 | 1.36E+00 | 1.36E+00 | 1.36E+00 | 1.36E+00 | 1.36E+00 | 1.36E+00 |
| Alkalinity(est), mol/l | | 1.31E-02 | 1.43E-02 | 1.48E-02 | 1.41E-02 | 1.51E-02 | 1.49E-02 | 1.60E-02 | 1.66E-02 | 1.70E-02 | 1.68E-02 | 1.74E-02 | 1.77E-02 | 1.78E-02 | 1.71E-02 | 1.78E-02 | 1.66E-02 |
| Fluid in exp. (kg) | | 0.158 | 0.156 | 0.153 | 0.151 | 0.149 | 0.147 | 0.144 | 0.142 | 0.140 | 0.137 | 0.135 | 0.134 | 0.132 | 0.130 | 0.127 | 0.125 |

| 136: 1.36M NaCl, 4bar pCO2, 70C | | | | | | | | | | | | | | | | | |
|---|---|---|---|---|---|---|---|---|---|---|---|---|---|---|---|---|---|
| Time, hours | Std. Dev. Mol/l | -0.17 | 0.00 | 1.65 | 4.47 | 9.10 | 19.33 | 22.80 | 27.12 | 44.50 | 48.75 | 52.75 | 68.10 | 75.17 | 89.78 | 98.55 | 98.55 | 116.52 |
| VCT, hours | | 0.00 | 0.02 | 1.69 | 4.66 | 9.66 | 20.92 | 24.83 | 29.82 | 50.48 | 55.67 | 60.69 | 80.58 | 90.02 | 110.18 | 122.71 | 122.71 | 149.57 |
| Mg, mol/l | 1.92E-05 | 1.31E-03 | 7.54E-04 | 1.56E-03 | 2.01E-03 | 2.49E-03 | 3.07E-03 | 3.35E-03 | 3.81E-03 | 4.62E-03 | 3.03E-03 | 3.60E-03 | 4.01E-03 | 3.40E-03 | 4.53E-03 | 4.71E-03 | 4.64E-03 | 4.83E-03 |
| Al, mol/l | 2.05E-06 | 0.00E+00 | 0.00E+00 | 0.00E+00 | 0.00E+00 | 0.00E+00 | 0.00E+00 | 0.00E+00 | 0.00E+00 | 0.00E+00 | 0.00E+00 | 0.00E+00 | 0.00E+00 | 0.00E+00 | 0.00E+00 | 0.00E+00 | 0.00E+00 | 0.00E+00 |
| Si, mol/l | 1.80E-05 | 0.00E+00 | 0.00E+00 | 0.00E+00 | 0.00E+00 | 0.00E+00 | 0.00E+00 | 0.00E+00 | 0.00E+00 | 0.00E+00 | 0.00E+00 | 0.00E+00 | 0.00E+00 | 0.00E+00 | 0.00E+00 | 0.00E+00 | 0.00E+00 | 0.00E+00 |
| K, mol/l | 3.94E-04 | 1.70E-04 | 0.00E+00 | 1.30E-04 | 1.40E-04 | 1.66E-04 | 1.42E-04 | 1.41E-04 | 1.38E-04 | 1.44E-04 | 1.03E-04 | 1.17E-04 | 1.35E-04 | 0.00E+00 | 1.24E-04 | 1.60E-04 | 1.21E-04 | 1.17E-04 |
| Ca, mol/l (±22%) | 1.43E-04 | 3.09E-03 | 0.00E+00 | 2.79E-03 | 3.50E-03 | 4.49E-03 | 4.62E-03 | 4.80E-03 | 5.23E-03 | 6.15E-03 | 4.22E-03 | 5.07E-03 | 5.65E-03 | 4.12E-03 | 6.29E-03 | 6.52E-03 | 6.61E-03 | 6.67E-03 |
| Mn, mol/l | 2.28E-07 | 3.44E-06 | 2.70E-06 | 1.37E-05 | 2.78E-05 | 4.15E-05 | 5.82E-05 | 6.82E-05 | 7.52E-05 | 9.12E-05 | 6.28E-05 | 7.56E-05 | 8.50E-05 | 7.33E-05 | 9.50E-05 | 9.79E-05 | 9.73E-05 | 1.01E-04 |
| Fe, mol/l | 1.75E-05 | 6.70E-05 | 0.00E+00 | 0.00E+00 | 0.00E+00 | 0.00E+00 | 0.00E+00 | 2.26E-05 | 1.54E-05 | 2.42E-05 | 0.00E+00 | 0.00E+00 | 0.00E+00 | 0.00E+00 | 0.00E+00 | 0.00E+00 | 0.00E+00 | 0.00E+00 |
| Sr, mol/l | 4.05E-07 | 4.71E-07 | 0.00E+00 | 3.31E-07 | 3.11E-07 | 5.06E-08 | 4.41E-07 | 5.32E-07 | 5.19E-07 | 5.58E-07 | 3.34E-07 | 3.62E-07 | 4.24E-07 | 0.00E+00 | 5.13E-07 | 4.51E-07 | 4.49E-07 | 5.06E-07 |
| Ba, mol/l | 4.84E-07 | 2.21E-06 | 4.16E-07 | 2.28E-07 | 2.58E-07 | 5.45E-07 | 2.06E-07 | 2.92E-07 | 1.18E-07 | 2.77E-07 | 2.89E-07 | 7.86E-07 | 2.81E-07 | 3.44E-07 | 6.66E-07 | 4.02E-07 | 8.08E-07 | 6.54E-07 |
| Na (est), mol/l | | 1.36E+00 | 1.36E+00 | 1.36E+00 | 1.36E+00 | 1.36E+00 | 1.36E+00 | 1.36E+00 | 1.36E+00 | 1.36E+00 | 1.36E+00 | 1.36E+00 | 1.36E+00 | 1.36E+00 | 1.36E+00 | 1.36E+00 | 1.36E+00 | 1.36E+00 |
| Alkalinity(est), mol/l | | 4.40E-03 | 7.54E-04 | 4.35E-03 | 5.51E-03 | 6.98E-03 | 7.70E-03 | 8.15E-03 | 9.04E-03 | 1.08E-02 | 7.25E-03 | 8.67E-03 | 9.66E-03 | 7.52E-03 | 1.08E-02 | 1.12E-02 | 1.12E-02 | 1.15E-02 |
| Fluid in exp. (kg) | | 0.105 | 0.104 | 0.101 | 0.099 | 0.097 | 0.095 | 0.092 | 0.090 | 0.088 | 0.085 | 0.083 | 0.080 | 0.078 | 0.076 | 0.073 | 0.071 | 0.070 |

| 136 cont.: 1.36M NaCl, 4bar pCO2, 70C | | | | | | | | | | | | | | | |
|---|---|---|---|---|---|---|---|---|---|---|---|---|---|---|---|
| Time, hours | Std. Dev. Mol/l | 124.47 | 140.18 | 145.47 | 165.50 | 189.60 | 212.57 | 212.57 | 236.62 | 264.72 | 314.22 | 363.10 | 407.45 | 435.58 | 556.62 |
| VCT, hours | | 161.89 | 187.01 | 195.77 | 230.31 | 273.67 | 316.91 | 316.91 | 364.83 | 423.40 | 531.47 | 642.93 | 749.47 | 820.84 | 1150.00 |
| Mg, mol/l | 1.92E-05 | 4.91E-03 | 4.99E-03 | 4.91E-03 | 5.14E-03 | 5.20E-03 | 5.27E-03 | 4.20E-03 | 5.47E-03 | 6.27E-03 | 7.07E-03 | 7.86E-03 | 9.32E-03 | 1.00E-02 | 1.25E-02 |
| Al, mol/l | 2.05E-06 | 0.00E+00 | 0.00E+00 | 0.00E+00 | 0.00E+00 | 0.00E+00 | 0.00E+00 | 0.00E+00 | 0.00E+00 | 0.00E+00 | 0.00E+00 | 0.00E+00 | 0.00E+00 | 0.00E+00 | 0.00E+00 |

| | | | | | | | | | | | | | | | |
|---|---|---|---|---|---|---|---|---|---|---|---|---|---|---|---|
| Si, mol/l | 1.80E-05 | 0.00E+00 | 0.00E+00 | 0.00E+00 | 0.00E+00 | 0.00E+00 | 0.00E+00 | 0.00E+00 | 0.00E+00 | 0.00E+00 | 0.00E+00 | 0.00E+00 | 0.00E+00 | 0.00E+00 | 0.00E+00 |
| K, mol/l | 3.94E-04 | 1.22E-04 | 1.26E-04 | 1.18E-04 | 1.22E-04 | 1.25E-04 | 1.29E-04 | 0.00E+00 | 1.21E-04 | 1.37E-04 | 1.59E-04 | 1.77E-04 | 2.16E-04 | 2.48E-04 | 3.78E-04 |
| Ca, mol/l (±22%) | 1.43E-04 | 6.91E-03 | 6.89E-03 | 6.83E-03 | 7.15E-03 | 7.24E-03 | 7.27E-03 | 4.97E-03 | 6.94E-03 | 7.98E-03 | 9.03E-03 | 1.01E-02 | 1.20E-02 | 1.27E-02 | 9.77E-03 |
| Mn, mol/l | 2.28E-07 | 1.02E-04 | 1.03E-04 | 1.01E-04 | 1.04E-04 | 1.03E-04 | 1.04E-04 | 8.35E-05 | 1.00E-04 | 1.12E-04 | 1.13E-04 | 9.25E-05 | 5.27E-05 | 1.92E-05 | 3.46E-06 |
| Fe, mol/l | 1.75E-05 | 0.00E+00 | 0.00E+00 | 0.00E+00 | 0.00E+00 | 0.00E+00 | 7.96E-05 | 0.00E+00 | 0.00E+00 | 2.75E-05 | 5.41E-05 | 1.71E-05 | 0.00E+00 | 0.00E+00 | 1.70E-05 |
| Sr, mol/l | 4.05E-07 | 4.41E-07 | 5.09E-07 | 4.74E-07 | 5.66E-07 | 5.08E-07 | 5.33E-07 | 3.61E-08 | 7.11E-07 | 8.46E-07 | 8.82E-07 | 1.02E-06 | 1.20E-06 | 1.37E-06 | 2.33E-06 |
| Ba, mol/l | 4.84E-07 | 3.93E-07 | 3.26E-08 | 0.00E+00 | 0.00E+00 | 2.78E-08 | 9.36E-08 | 8.92E-08 | 5.25E-08 | 5.31E-08 | 1.40E-07 | 0.00E+00 | 1.55E-07 | 2.13E-08 | 4.89E-07 |
| Na (est), mol/l | | 1.36E+00 | 1.36E+00 | 1.36E+00 | 1.36E+00 | 1.36E+00 | 1.36E+00 | 1.36E+00 | 1.36E+00 | 1.36E+00 | 1.36E+00 | 1.36E+00 | 1.36E+00 | 1.36E+00 | 1.36E+00 |
| Alkalinity(est), mol/l | | 1.18E-02 | 1.19E-02 | 1.17E-02 | 1.23E-02 | 1.24E-02 | 1.25E-02 | 9.17E-03 | 1.24E-02 | 1.43E-02 | 1.61E-02 | 1.80E-02 | 2.13E-02 | 2.27E-02 | 2.23E-02 |
| Fluid in exp. (kg) | | 0.067 | 0.065 | 0.063 | 0.060 | 0.058 | 0.055 | 0.053 | 0.052 | 0.050 | 0.048 | 0.046 | 0.043 | 0.041 | 0.038 |

## A.6 Sandstone Fluid Chemistry Data

| 141: 1.36M NaCl, 4bar pCO2, 22C | | | | | | | | | | | | | | | | | |
|---|---|---|---|---|---|---|---|---|---|---|---|---|---|---|---|---|---|
| Time, hours | Std. Dev. Mol/l | -0.37 | 0.05 | 2.58 | 4.42 | 20.50 | 25.33 | 27.83 | 27.83 | 48.35 | 54.18 | 68.75 | 77.38 | 77.40 | 97.17 | 100.32 | 170.20 |
| VCT, hours | | 0.00 | 0.05 | 2.67 | 4.63 | 22.25 | 27.67 | 30.54 | 30.54 | 54.91 | 62.05 | 80.31 | 91.44 | 91.46 | 118.08 | 122.46 | 222.71 |
| Mg, mol/l | 4.31E-06 | 1.99E-04 | 2.08E-04 | 2.44E-04 | 2.97E-04 | 7.02E-04 | 7.74E-04 | 8.27E-04 | 8.43E-04 | 1.28E-03 | 1.41E-03 | 1.69E-03 | 1.80E-03 | 1.83E-03 | 2.08E-03 | 2.10E-03 | 2.76E-03 |
| Al, mol/l | 3.51E-08 | 2.36E-07 | 9.18E-06 | 1.43E-06 | 3.34E-06 | 4.55E-06 | 5.29E-06 | 5.15E-06 | 5.78E-06 | 7.70E-06 | 9.42E-06 | 9.03E-06 | 9.47E-06 | 9.26E-06 | 9.59E-06 | 1.02E-05 | 1.17E-05 |
| Si, mol/l | 7.77E-08 | 1.79E-05 | 2.43E-05 | 1.76E-05 | 1.80E-05 | 2.81E-05 | 2.56E-05 | 2.59E-05 | 2.63E-05 | 3.29E-05 | 3.05E-05 | 4.08E-05 | 3.56E-05 | 3.50E-05 | 3.93E-05 | 3.84E-05 | 4.53E-05 |
| K, mol/l (±12%) | 1.8E-06 | 1.04E-04 | 1.31E-04 | 1.31E-04 | 1.33E-04 | 1.13E-04 | 1.05E-04 | 1.15E-04 | 1.34E-04 | 1.33E-04 | 1.29E-04 | 1.43E-04 | 1.29E-04 | 1.45E-04 | 1.62E-04 | 1.21E-04 | 1.41E-04 |
| Ca, mol/l (±1%) | 1.04E-05 | 1.30E-03 | 1.36E-03 | 1.36E-03 | 1.40E-03 | 1.81E-03 | 1.77E-03 | 1.84E-03 | 1.82E-03 | 2.22E-03 | 2.24E-03 | 2.78E-03 | 2.70E-03 | 2.62E-03 | 2.94E-03 | 2.98E-03 | 3.52E-03 |
| Mn, mol/l | 5.78E-09 | 8.01E-07 | 1.61E-05 | 5.82E-06 | 2.72E-06 | 6.03E-06 | 6.45E-06 | 6.96E-06 | 6.81E-06 | 1.14E-05 | 1.15E-05 | 1.43E-05 | 1.44E-05 | 1.47E-05 | 1.74E-05 | 1.70E-05 | 2.36E-05 |
| Fe, mol/l | 6.99E-08 | 0.00E+00 | 1.78E-04 | 3.98E-05 | 8.92E-06 | 8.74E-06 | 4.82E-06 | 4.46E-06 | 2.92E-06 | 1.06E-05 | 2.05E-05 | 1.31E-05 | 5.84E-06 | 4.78E-06 | 1.61E-05 | 7.20E-06 | 1.97E-05 |
| Sr, mol/l | 5.03E-09 | 2.34E-06 | 2.42E-06 | 2.34E-06 | 2.48E-06 | 2.36E-06 | 2.39E-06 | 2.36E-06 | 2.43E-06 | 2.50E-06 | 2.45E-06 | 2.52E-06 | 2.50E-06 | 2.54E-06 | 2.55E-06 | 2.51E-06 | 2.59E-06 |
| Ba, mol/l | | 6.09E-07 | 7.01E-07 | 6.82E-07 | 1.08E-06 | 7.00E-07 | 7.47E-07 | 7.53E-07 | 8.06E-07 | 7.93E-07 | 1.54E-06 | 8.99E-07 | 2.82E-06 | 2.08E-06 | 8.86E-07 | 1.56E-06 | 1.12E-06 |
| Na (est), mol/l | | 1.36E+00 | 1.36E+00 | 1.36E+00 | 1.36E+00 | 1.36E+00 | 1.36E+00 | 1.36E+00 | 1.36E+00 | 1.36E+00 | 1.36E+00 | 1.36E+00 | 1.36E+00 | 1.36E+00 | 1.36E+00 | 1.36E+00 | 1.36E+00 |
| Alkalinity(est), mol/l | | 2.59E-03 | 2.73E-03 | 2.71E-03 | 2.80E-03 | 3.62E-03 | 3.54E-03 | 3.68E-03 | 3.65E-03 | 4.44E-03 | 4.48E-03 | 5.56E-03 | 5.39E-03 | 5.24E-03 | 5.89E-03 | 5.96E-03 | 7.03E-03 |
| Fluid in exp. (kg) | | 0.104 | 0.103 | 0.100 | 0.096 | 0.094 | 0.092 | 0.090 | 0.088 | 0.087 | 0.084 | 0.082 | 0.080 | 0.078 | 0.077 | 0.074 | 0.072 |

| 141 cont.: 1.36M NaCl, 4bar pCO2, 22C | | | | | | | | | | | | | | | | |
|---|---|---|---|---|---|---|---|---|---|---|---|---|---|---|---|---|
| Time, hours | Std. Dev. Mol/l | 192.93 | 218.52 | 240.00 | 266.65 | 363.17 | 412.23 | 412.23 | 532.57 | 602.73 | 724.57 | 844.73 | 938.73 | 1036.72 | 1036.72 | 1083.37 |
| VCT, hours | | 256.62 | 296.07 | 330.87 | 376.15 | 546.70 | 636.69 | 636.69 | 876.51 | 1022.36 | 1289.13 | 1562.00 | 1791.02 | 2046.14 | 2046.14 | 2176.87 |
| Mg, mol/l | 4.31E-06 | 2.93E-03 | 3.15E-03 | 2.85E-03 | 3.21E-03 | 3.52E-03 | 3.61E-03 | 3.65E-03 | 4.25E-03 | 3.79E-03 | 3.89E-03 | 4.94E-03 | 2.77E-04 | 4.06E-03 | 4.02E-03 | 4.13E-03 |
| Al, mol/l | 3.51E-08 | 1.22E-05 | 1.46E-05 | 1.03E-05 | 1.88E-05 | 1.34E-05 | 1.36E-05 | 1.39E-05 | 1.51E-05 | 1.30E-05 | 1.43E-05 | 1.90E-05 | 9.11E-05 | 1.28E-05 | 1.28E-05 | 1.21E-05 |

| | | | | | | | | | | | | | | | | |
|---|---|---|---|---|---|---|---|---|---|---|---|---|---|---|---|---|
| Si, mol/l | 7.77E-08 | 4.40E-05 | 5.10E-05 | 4.54E-05 | 4.95E-05 | 5.27E-05 | 6.72E-05 | 6.67E-05 | 8.19E-05 | 8.40E-05 | 6.78E-05 | 9.37E-05 | 9.37E-05 | 7.65E-05 | 7.68E-05 | 8.38E-05 |
| K, mol/l (±12%) | 1.8E-06 | 1.56E-04 | 1.58E-04 | 1.12E-04 | 1.65E-04 | 1.60E-04 | 1.71E-04 | 1.75E-04 | 2.00E-04 | 1.72E-04 | 2.21E-04 | 2.58E-04 | 7.51E-04 | 1.93E-04 | 1.98E-04 | 2.18E-04 |
| Ca, mol/l (±1%) | 1.04E-05 | 3.50E-03 | 4.00E-03 | 3.65E-03 | 3.78E-03 | 3.92E-03 | 4.03E-03 | 4.05E-03 | 4.88E-03 | 4.22E-03 | 4.26E-03 | 5.51E-03 | 5.51E-03 | 4.38E-03 | 4.38E-03 | 4.50E-03 |
| Mn, mol/l | 5.78E-09 | 2.30E-05 | 2.47E-05 | 2.22E-05 | 2.46E-05 | 2.68E-05 | 2.75E-05 | 2.78E-05 | 3.24E-05 | 3.17E-05 | 2.91E-05 | 3.88E-05 | 1.20E-05 | 3.11E-05 | 3.13E-05 | 3.18E-05 |
| Fe, mol/l | 6.99E-08 | 1.87E-05 | 2.27E-05 | 1.42E-05 | 2.06E-05 | 2.07E-05 | 1.16E-05 | 9.59E-06 | 3.79E-05 | 6.48E-05 | 1.53E-05 | 1.19E-05 | 1.19E-05 | 1.24E-05 | 9.89E-06 | 1.24E-05 |
| Sr, mol/l | 5.03E-09 | 2.58E-06 | 2.67E-06 | 2.36E-06 | 2.59E-06 | 2.61E-06 | 2.67E-06 | 2.68E-06 | 3.02E-06 | 2.72E-06 | 2.73E-06 | 3.45E-06 | 2.09E-07 | 2.75E-06 | 2.78E-06 | 2.81E-06 |
| Ba, mol/l | | 1.15E-06 | 1.06E-06 | 1.04E-06 | 1.10E-06 | 1.16E-06 | 1.37E-06 | 1.61E-06 | 2.83E-06 | 1.94E-06 | 1.66E-06 | 4.04E-06 | 2.57E-06 | 1.86E-06 | 1.88E-06 | 1.75E-06 |
| Na (est), mol/l | | 1.36E+00 | 1.36E+00 | 1.36E+00 | 1.36E+00 | 1.36E+00 | 1.36E+00 | 1.36E+00 | 1.36E+00 | 1.36E+00 | 1.36E+00 | 1.36E+00 | 1.36E+00 | 1.36E+00 | 1.36E+00 | 1.36E+00 |
| Alkalinity(est), mol/l | | 7.00E-03 | 7.99E-03 | 7.30E-03 | 7.56E-03 | 7.85E-03 | 8.05E-03 | 8.09E-03 | 9.75E-03 | 8.43E-03 | 8.51E-03 | 1.10E-02 | 1.10E-02 | 8.76E-03 | 8.77E-03 | 9.01E-03 |
| Fluid in exp. (kg) | | 0.069 | 0.067 | 0.064 | 0.061 | 0.058 | 0.056 | 0.054 | 0.052 | 0.050 | 0.047 | 0.046 | 0.042 | 0.040 | 0.038 | 0.037 |

| 142: 1.36M NaCl, 4bar pCO2, 22C | | | | | | | | | | | | | | | | | |
|---|---|---|---|---|---|---|---|---|---|---|---|---|---|---|---|---|---|
| Time, hours | Std. Dev. Mol/l | -0.33 | 0.07 | 2.62 | 4.52 | 20.50 | 25.33 | 27.95 | 27.95 | 48.38 | 54.22 | 68.78 | 77.33 | 77.43 | 97.20 | 100.35 | 170.23 |
| VCT, hours | | 0.00 | 0.07 | 2.68 | 4.68 | 21.85 | 27.15 | 30.09 | 30.09 | 53.90 | 60.85 | 78.60 | 89.27 | 89.40 | 115.09 | 119.30 | 215.19 |
| Mg, mol/l | 4.31E-06 | 2.01E-04 | 2.00E-04 | 2.23E-04 | 2.78E-04 | 7.78E-04 | 9.77E-04 | 1.05E-03 | 1.02E-03 | 1.68E-03 | 1.83E-03 | 2.12E-03 | 2.60E-03 | 2.22E-03 | 2.45E-03 | 2.52E-03 | 3.43E-03 |
| Al, mol/l | 3.51E-08 | 0.00E+00 | 0.00E+00 | 0.00E+00 | 1.96E-07 | 1.33E-06 | 1.17E-06 | 2.21E-06 | 1.82E-06 | 1.04E-06 | 5.07E-06 | 6.24E-06 | 2.38E-06 | 2.46E-05 | 2.62E-06 | 1.36E-06 | 1.90E-06 |
| Si, mol/l | 7.77E-08 | 1.02E-05 | 9.56E-06 | 1.11E-05 | 1.38E-05 | 1.15E-05 | 1.17E-05 | 1.51E-05 | 2.08E-05 | 1.61E-05 | 1.71E-05 | 1.89E-05 | 1.33E-05 | 1.59E-05 | 1.60E-05 | 1.56E-05 | 1.58E-05 |
| K, mol/l (±5%) | 1.8E-06 | 2.31E-04 | 2.11E-04 | 1.95E-04 | 2.07E-04 | 2.03E-04 | 2.10E-04 | 2.19E-04 | 2.02E-04 | 2.04E-02 | 2.10E-04 | 2.18E-04 | 2.63E-04 | 1.98E-04 | 2.51E-04 | 2.13E-04 | 2.41E-04 |
| Ca, mol/l (±23%) | 1.04E-05 | 1.00E-03 | 8.72E-04 | 8.79E-04 | 1.18E-03 | 1.28E-03 | 1.51E-03 | 1.77E-03 | 1.58E-03 | 2.28E-03 | 2.57E-03 | 2.89E-03 | 2.32E-03 | 2.72E-03 | 2.74E-03 | 2.92E-03 | 3.40E-03 |
| Mn, mol/l | 5.78E-09 | 1.10E-06 | 1.40E-05 | 3.85E-06 | 2.78E-06 | 8.40E-06 | 1.01E-05 | 1.07E-05 | 1.05E-05 | 1.66E-05 | 1.76E-05 | 2.06E-05 | 2.44E-05 | 2.11E-05 | 2.36E-05 | 2.39E-05 | 3.08E-05 |
| Fe, mol/l | 6.99E-08 | 0.00E+00 | 2.68E-04 | 7.73E-05 | 1.27E-05 | 6.25E-06 | 3.69E-06 | 6.58E-06 | 4.26E-06 | 8.32E-06 | 8.15E-06 | 1.07E-05 | 7.15E-06 | 7.99E-06 | 1.14E-05 | 8.75E-06 | 1.31E-05 |
| Sr, mol/l | 5.03E-09 | 1.53E-06 | 1.41E-06 | 1.39E-06 | 1.44E-06 | 1.44E-06 | 1.49E-06 | 1.48E-06 | 1.44E-06 | 1.53E-06 | 1.56E-06 | 1.58E-06 | 1.84E-06 | 1.55E-06 | 1.59E-06 | 1.58E-06 | 1.72E-06 |
| Ba, mol/l | | 4.83E-07 | 4.60E-07 | 4.87E-07 | 7.98E-07 | 5.73E-07 | 5.47E-07 | 5.99E-07 | 7.65E-07 | 8.54E-07 | 1.34E-06 | 6.27E-07 | 1.62E-06 | 2.31E-06 | 7.43E-07 | 1.51E-06 | 8.79E-07 |
| Na (est), mol/l | | 1.36E+00 | 1.36E+00 | 1.36E+00 | 1.36E+00 | 1.36E+00 | 1.36E+00 | 1.36E+00 | 1.36E+00 | 1.36E+00 | 1.36E+00 | 1.36E+00 | 1.36E+00 | 1.36E+00 | 1.36E+00 | 1.36E+00 | 1.36E+00 |
| Alkalinity(est), mol/l | | 2.00E-03 | 1.74E-03 | 1.76E-03 | 2.37E-03 | 2.56E-03 | 3.02E-03 | 3.55E-03 | 3.16E-03 | 4.56E-03 | 5.15E-03 | 5.78E-03 | 4.64E-03 | 5.45E-03 | 5.48E-03 | 5.85E-03 | 6.79E-03 |
| Fluid in exp. (kg) | | 0.104 | 0.103 | 0.100 | 0.098 | 0.096 | 0.094 | 0.092 | 0.089 | 0.088 | 0.086 | 0.085 | 0.082 | 0.080 | 0.075 | 0.079 | 0.077 |

| 142 cont.: 1.36M NaCl, 4bar pCO2, 22C | | | | | | | | | | | | | | | | |
|---|---|---|---|---|---|---|---|---|---|---|---|---|---|---|---|---|
| Time, hours | Std. Dev. Mol/l | 192.97 | 218.55 | 240.03 | 266.68 | 363.20 | 414.30 | 414.30 | 532.60 | 602.77 | 724.60 | 844.77 | 938.77 | 1036.75 | 1036.75 | 1083.40 |
| VCT, hours | | 247.48 | 284.99 | 317.63 | 359.15 | 514.71 | 600.34 | 600.34 | 810.16 | 939.43 | 1173.58 | 1411.74 | 1606.52 | 1822.46 | 1822.46 | 1932.55 |

| | | | | | | | | | | | | | | | | | | | |
|---|---|---|---|---|---|---|---|---|---|---|---|---|---|---|---|---|---|---|---|
| Mg, mol/l | 4.31E-06 | 3.68E-03 | 3.91E-03 | 3.80E-03 | 4.00E-03 | 4.52E-03 | 4.51E-03 | 4.60E-03 | 4.81E-03 | 4.74E-03 | 4.91E-03 | 5.11E-03 | 5.13E-03 | 5.30E-03 | 5.34E-03 | 5.36E-03 | | | |
| Al, mol/l | 3.51E-08 | 1.75E-06 | 2.67E-06 | 1.85E-05 | 1.62E-06 | 2.05E-06 | 2.05E-06 | 1.43E-06 | 1.06E-06 | 9.48E-07 | 3.21E-06 | 2.29E-06 | 1.62E-06 | 2.54E-06 | 1.69E-06 | 1.53E-06 | | | |
| Si, mol/l | 7.77E-08 | 2.39E-05 | 1.92E-05 | 1.41E-05 | 1.67E-05 | 2.08E-05 | 3.23E-05 | 4.53E-05 | 2.77E-05 | 4.90E-05 | 2.11E-05 | 3.19E-05 | 2.00E-05 | 2.73E-05 | 2.58E-05 | 2.47E-05 | | | |
| K, mol/l (±5%) | 1.8E-06 | 2.40E-04 | 2.41E-04 | 1.90E-04 | 2.08E-04 | 2.39E-04 | 2.22E-04 | 2.39E-04 | 2.35E-04 | 2.11E-04 | 2.43E-04 | 2.57E-04 | 2.64E-04 | 2.61E-04 | 2.70E-04 | 2.78E-04 | | | |
| Ca, mol/l (±23%) | 1.04E-05 | 3.97E-03 | 4.00E-03 | 3.81E-03 | 3.98E-03 | 4.43E-03 | 4.68E-03 | 6.18E-03 | 4.80E-03 | 6.44E-03 | 4.70E-03 | 5.37E-03 | 4.45E-03 | 5.51E-03 | 5.38E-03 | 5.07E-03 | | | |
| Mn, mol/l | 5.78E-09 | 3.30E-05 | 3.44E-05 | 3.43E-05 | 3.59E-05 | 3.93E-05 | 3.98E-05 | 4.00E-05 | 4.04E-05 | 4.25E-05 | 4.15E-05 | 4.37E-05 | 4.43E-05 | 4.37E-05 | 4.47E-05 | 4.52E-05 | | | |
| Fe, mol/l | 6.99E-08 | 1.48E-05 | 2.88E-05 | 3.49E-05 | 4.31E-05 | 3.26E-05 | 3.45E-05 | 2.67E-05 | 2.17E-05 | 4.94E-05 | 2.70E-05 | 1.54E-05 | 9.18E-06 | 1.01E-05 | 9.20E-06 | 7.85E-06 | | | |
| Sr, mol/l | 5.03E-09 | 1.75E-06 | 1.77E-06 | 1.63E-06 | 1.71E-06 | 1.88E-06 | 1.83E-06 | 1.86E-06 | 1.92E-06 | 1.92E-06 | 2.00E-06 | 2.19E-06 | 2.21E-06 | 2.18E-06 | 2.21E-06 | 2.29E-06 | | | |
| Ba, mol/l | | 9.34E-07 | 9.81E-07 | 1.14E-06 | 1.11E-06 | 1.24E-06 | 1.66E-06 | 1.81E-06 | 2.22E-06 | 1.83E-06 | 1.94E-06 | 3.86E-06 | 2.48E-06 | 2.37E-06 | 2.41E-06 | 2.38E-06 | | | |
| Na (est), mol/l | | 1.36E+00 | 1.36E+00 | 1.36E+00 | 1.36E+00 | 1.36E+00 | 1.36E+00 | 1.36E+00 | 1.36E+00 | 1.36E+00 | 1.36E+00 | 1.36E+00 | 1.36E+00 | 1.36E+00 | 1.36E+00 | 1.36E+00 | | | |
| Alkalinity(est), mol/l | | 7.93E-03 | 8.00E-03 | 7.62E-03 | 7.97E-03 | 8.85E-03 | 9.35E-03 | 1.24E-02 | 9.59E-03 | 1.29E-02 | 9.39E-03 | 1.07E-02 | 8.91E-03 | 1.10E-02 | 1.08E-02 | 1.01E-02 | | | |
| Fluid in exp. (kg) | | 0.075 | 0.073 | 0.070 | 0.068 | 0.066 | 0.064 | 0.061 | 0.059 | 0.058 | 0.056 | 0.054 | 0.052 | 0.050 | 0.047 | 0.045 | | | |
| 146: 1.36M NaCl, 31bar pCO2, 70C | | | | | | | | | | | | | | | | | | | |
| Time, hours | Std. Dev. Mol/l | -0.08 | 0.08 | 2.33 | 4.37 | 6.30 | 21.42 | 25.95 | 29.13 | 29.13 | 45.38 | 49.03 | 52.45 | 69.60 | 69.60 | 73.75 | 77.03 | 122.83 | 125.02 | 143.88 |
| VCT, hours | | 0.00 | 0.08 | 2.37 | 4.48 | 6.52 | 22.75 | 27.68 | 31.19 | 31.19 | 49.49 | 53.67 | 57.65 | 77.92 | 77.92 | 82.94 | 86.98 | 144.32 | 147.10 | 171.62 |
| Mg, mol/l | 1.92E-05 | 1.08E-03 | 7.72E-04 | 8.53E-04 | 1.01E-03 | 1.28E-03 | 2.21E-03 | 1.44E-03 | 2.81E-03 | 2.95E-03 | 3.04E-03 | 3.21E-03 | 3.78E-03 | 3.78E-03 | 4.32E-03 | 4.68E-03 | 4.84E-03 | 4.94E-03 | 5.14E-03 | 5.39E-03 |
| Al, mol/l | 2.05E-06 | 2.11E-06 | 1.73E-06 | 9.32E-07 | 0.00E+00 | 3.91E-06 | 1.48E-06 | 1.26E-05 | 4.52E-06 | 4.89E-07 | 0.00E+00 | 0.00E+00 | 0.00E+00 | 2.88E-06 | 0.00E+00 | 1.19E-05 | 3.90E-06 | 6.82E-05 | 1.08E-06 | 0.00E+00 |
| Si, mol/l | 1.80E-05 | 2.25E-04 | 9.35E-05 | 1.16E-04 | 1.25E-04 | 1.21E-04 | 3.22E-04 | 1.81E-04 | 1.86E-04 | 1.89E-04 | 1.44E-04 | 1.60E-04 | 1.51E-04 | 1.51E-04 | 1.56E-04 | 1.57E-04 | 1.36E-04 | 1.93E-04 | 1.92E-04 | 1.79E-04 |
| K, mol/l (±9%) | 3.94E-04 | 0.00E+00 | 0.00E+00 | 0.00E+00 | 0.00E+00 | 1.15E-06 | 0.00E+00 | 0.00E+00 | 0.00E+00 | 0.00E+00 | 0.00E+00 | 0.00E+00 | 1.58E-05 | 0.00E+00 | 0.00E+00 | 0.00E+00 | 0.00E+00 | 0.00E+00 | 0.00E+00 | 0.00E+00 |
| Ca, mol/l (±8%) | 1.43E-04 | 1.30E-03 | 1.54E-03 | 1.62E-03 | 1.88E-03 | 2.21E-03 | 3.68E-03 | 2.91E-03 | 4.06E-03 | 3.65E-03 | 4.20E-03 | 4.56E-03 | 4.93E-03 | 5.31E-03 | 5.21E-03 | 5.66E-03 | 5.73E-03 | 5.87E-03 | 6.07E-03 | 6.45E-03 |
| Mn, mol/l | 2.28E-07 | 2.22E-04 | 5.04E-05 | 5.53E-05 | 5.03E-05 | 4.55E-05 | 9.33E-05 | 5.30E-05 | 7.89E-05 | 6.79E-05 | 8.31E-05 | 9.05E-05 | 8.36E-05 | 9.32E-05 | 9.90E-05 | 9.48E-05 | 8.92E-05 | 1.07E-04 | 1.12E-04 | 1.12E-04 |
| Fe, mol/l | 1.75E-05 | 6.66E-03 | 5.26E-04 | 8.30E-05 | 1.13E-04 | 1.03E-04 | 9.59E-04 | 6.21E-04 | 6.76E-04 | 5.59E-04 | 8.21E-04 | 1.02E-03 | 6.65E-04 | 7.72E-04 | 1.06E-03 | 6.64E-04 | 3.59E-04 | 1.06E-03 | 1.12E-03 | 9.26E-04 |
| Sr, mol/l | 4.05E-07 | 1.55E-06 | 1.63E-06 | 1.74E-06 | 1.60E-06 | 1.60E-06 | 2.44E-06 | 2.00E-06 | 2.57E-06 | 1.70E-06 | 1.72E-06 | 1.79E-06 | 1.84E-06 | 1.88E-06 | 1.82E-06 | 2.45E-06 | 2.85E-06 | 2.03E-06 | 2.26E-06 | 2.01E-06 |
| Ba, mol/l | 4.84E-07 | 1.32E-05 | 1.31E-05 | 1.89E-05 | 4.88E-06 | 4.17E-06 | 9.40E-06 | 6.61E-06 | 4.11E-05 | 5.58E-06 | 2.05E-06 | 4.21E-06 | 5.37E-06 | 3.80E-06 | 4.02E-06 | 3.88E-05 | 6.68E-05 | 1.27E-05 | 2.74E-05 | 6.17E-06 |
| Na (est), mol/l | | 1.36E+00 | 1.36E+00 | 1.36E+00 | 1.36E+00 | 1.36E+00 | 1.36E+00 | 1.36E+00 | 1.36E+00 | 1.36E+00 | 1.36E+00 | 1.36E+00 | 1.36E+00 | 1.36E+00 | 1.36E+00 | 1.36E+00 | 1.36E+00 | 1.36E+00 | 1.36E+00 | 1.36E+00 |
| Alkalinity(est), mol/l | | 2.60E-03 | 3.08E-03 | 3.23E-03 | 3.76E-03 | 4.42E-03 | 7.37E-03 | 5.83E-03 | 8.12E-03 | 7.29E-03 | 8.40E-03 | 9.12E-03 | 9.85E-03 | 1.06E-02 | 1.04E-02 | 1.13E-02 | 1.15E-02 | 1.17E-02 | 1.21E-02 | 1.29E-02 |
| Fluid in exp. (kg) | | 0.157 | 0.153 | 0.151 | 0.148 | 0.145 | 0.143 | 0.141 | 0.139 | 0.137 | 0.136 | 0.134 | 0.132 | 0.130 | 0.128 | 0.127 | 0.125 | 0.123 | 0.120 | 0.118 |

| 146 cont.: 1.36M NaCl, 31bar pCO2, 70C | | | | | | | | | | | | | | | | | | | |
|---|---|---|---|---|---|---|---|---|---|---|---|---|---|---|---|---|---|---|---|
| Time, hours | Std. Dev. Mol/l | 151.53 | 165.13 | 173.92 | 187.78 | 197.08 | 213.25 | 213.25 | 220.67 | 238.70 | 244.37 | 297.47 | 337.50 | 357.07 | 380.90 | 406.33 | 456.12 | 509.42 | 652.83 |
| VCT, hours | | 181.76 | 200.12 | 212.24 | 231.77 | 245.14 | 268.87 | 268.87 | 280.09 | 307.95 | 316.90 | 402.72 | 469.27 | 502.65 | 544.33 | 590.03 | 681.97 | 783.25 | 1064.25 |
| Mg, mol/l | 1.92E-05 | 5.45E-03 | 5.46E-03 | 5.78E-03 | 5.73E-03 | 2.94E-03 | 6.07E-03 | 6.87E-03 | 6.65E-03 | 7.01E-03 | 6.64E-03 | 6.57E-03 | 6.13E-03 | 6.03E-03 | 6.26E-03 | 6.35E-03 | 6.39E-03 | 6.25E-03 | 4.86E-03 |
| Al, mol/l | 2.05E-06 | 3.17E-06 | 2.03E-05 | 6.87E-08 | 0.00E+00 | 6.17E-06 | 0.00E+00 | 0.00E+00 | 3.27E-06 | 1.64E-06 | 5.54E-06 | 8.72E-06 | 2.62E-06 | 0.00E+00 | 6.93E-08 | 0.00E+00 | 0.00E+00 | 2.94E-06 | 0.00E+00 |
| Si, mol/l | 1.80E-05 | 1.82E-04 | 1.70E-04 | 1.65E-04 | 1.55E-04 | 1.67E-04 | 1.76E-04 | 1.90E-04 | 1.79E-04 | 1.84E-04 | 1.93E-04 | 2.99E-04 | 3.40E-04 | 2.00E-04 | 2.05E-04 | 1.92E-04 | 2.58E-04 | 2.82E-04 | 7.76E-04 |
| K, mol/l (±9%) | 3.94E-04 | 0.00E+00 | 4.41E-06 | 8.01E-05 | 0.00E+00 | 2.33E-06 | 4.52E-05 | 3.93E-05 | 8.58E-05 | 1.11E-04 | 2.89E-04 | 1.10E-04 | 1.57E-05 | 6.22E-06 | 3.26E-05 | 6.63E-05 | 3.64E-05 | 7.17E-05 | 0.00E+00 |
| Ca, mol/l (±8%) | 1.43E-04 | 6.42E-03 | 6.71E-03 | 6.85E-03 | 6.64E-03 | 4.57E-03 | 7.16E-03 | 7.93E-03 | 7.77E-03 | 8.37E-03 | 7.79E-03 | 7.37E-03 | 6.80E-03 | 6.84E-03 | 6.95E-03 | 7.09E-03 | 7.38E-03 | 7.07E-03 | 6.31E-03 |
| Mn, mol/l | 2.28E-07 | 1.08E-04 | 1.09E-04 | 1.08E-04 | 1.08E-04 | 7.74E-05 | 1.13E-04 | 1.30E-04 | 1.16E-04 | 1.24E-04 | 1.18E-04 | 1.19E-04 | 1.12E-04 | 1.07E-04 | 1.10E-04 | 1.09E-04 | 1.16E-04 | 1.13E-04 | 1.08E-04 |
| Fe, mol/l | 1.75E-05 | 8.01E-04 | 7.72E-04 | 5.95E-04 | 5.90E-04 | 9.74E-04 | 6.20E-04 | 6.98E-04 | 3.92E-04 | 4.47E-04 | 4.04E-04 | 5.43E-04 | 5.21E-04 | 4.52E-04 | 4.85E-04 | 3.79E-04 | 5.59E-04 | 5.68E-04 | 7.32E-04 |
| Sr, mol/l | 4.05E-07 | 2.74E-06 | 2.03E-06 | 2.23E-06 | 2.01E-06 | 3.62E-06 | 2.21E-06 | 2.46E-06 | 3.24E-06 | 2.57E-06 | 3.15E-06 | 3.40E-06 | 2.62E-06 | 2.05E-06 | 2.09E-06 | 2.11E-06 | 2.18E-06 | 3.11E-06 | 1.88E-06 |
| Ba, mol/l | 4.84E-07 | 5.45E-05 | 7.13E-06 | 2.02E-05 | 4.62E-06 | 5.92E-05 | 1.21E-05 | 1.00E-05 | 6.92E-05 | 1.66E-05 | 5.60E-05 | 8.07E-05 | 4.55E-05 | 4.27E-06 | 5.65E-06 | 5.86E-06 | 7.80E-06 | 8.28E-05 | 4.43E-06 |
| Na (est), mol/l | | 1.36E+00 | 1.36E+00 | 1.36E+00 | 1.36E+00 | 1.36E+00 | 1.36E+00 | 1.36E+00 | 1.36E+00 | 1.36E+00 | 1.36E+00 | 1.36E+00 | 1.36E+00 | 1.36E+00 | 1.36E+00 | 1.36E+00 | 1.36E+00 | 1.36E+00 | 1.36E+00 |
| Alkalinity(est), mol/l | | 1.28E-02 | 1.34E-02 | 1.37E-02 | 1.33E-02 | 9.14E-03 | 1.43E-02 | 1.59E-02 | 1.55E-02 | 1.67E-02 | 1.56E-02 | 1.47E-02 | 1.36E-02 | 1.37E-02 | 1.39E-02 | 1.42E-02 | 1.48E-02 | 1.41E-02 | 1.26E-02 |
| Fluid in exp. (kg) | | 0.116 | 0.114 | 0.111 | 0.109 | 0.107 | 0.104 | 0.102 | 0.101 | 0.099 | 0.097 | 0.095 | 0.092 | 0.090 | 0.088 | 0.085 | 0.083 | 0.081 | 0.078 |

| 147: 1.36M NaCl, 31bar pCO2, 70C | | | | | | | | | | | | | | | | | | | | |
|---|---|---|---|---|---|---|---|---|---|---|---|---|---|---|---|---|---|---|---|---|
| Time, hours | Std. Dev. Mol/l | -144.03 | -0.07 | 0.08 | 2.02 | 3.58 | 7.58 | 21.18 | 24.07 | 29.97 | 43.83 | 47.47 | 53.13 | 69.30 | 69.35 | 72.93 | 76.72 | 94.75 | 97.43 | 100.65 |
| VCT, hours | | #REF! | 0.00 | 0.08 | 2.08 | 3.74 | 8.05 | 23.00 | 26.23 | 32.93 | 48.94 | 53.21 | 60.00 | 79.70 | 79.76 | 84.24 | 89.06 | 112.48 | 116.05 | 120.40 |
| Mg, mol/l | 1.92E-05 | 8.39E-04 | 2.15E-04 | 2.08E-04 | 2.81E-04 | 4.20E-04 | 8.52E-04 | 9.55E-04 | 1.24E-03 | 1.78E-03 | 2.11E-03 | 2.43E-03 | 5.46E-03 | 2.84E-03 | 2.92E-03 | 3.05E-03 | 3.15E-03 | 3.21E-03 | 3.29E-03 | 3.42E-03 |
| Al, mol/l | 2.05E-06 | 2.46E-07 | 8.07E-07 | 4.09E-06 | 9.87E-07 | 2.51E-06 | 4.36E-06 | 1.22E-07 | 2.43E-06 | 3.58E-06 | 1.53E-06 | 2.55E-06 | 0.00E+00 | 0.00E+00 | 2.11E-07 | 6.39E-07 | 6.05E-07 | 0.00E+00 | 5.05E-07 | 2.76E-06 |
| Si, mol/l | 1.80E-05 | 1.08E-04 | 7.81E-05 | 8.28E-05 | 1.02E-04 | 1.23E-04 | 1.71E-04 | 1.32E-04 | 1.28E-04 | 1.56E-04 | 1.31E-04 | 1.33E-04 | 1.65E-04 | 1.26E-04 | 1.22E-04 | 1.29E-04 | 1.34E-04 | 1.28E-04 | 1.32E-04 | 1.36E-04 |
| K, mol/l (±16%) | 3.94E-04 | 1.43E-04 | 1.24E-04 | 1.06E-04 | 1.11E-04 | 4.28E-05 | 1.31E-04 | 4.11E-05 | 0.00E+00 | 5.18E-05 | 8.99E-05 | 9.65E-05 | 1.34E-04 | 9.15E-05 | 1.12E-04 | 8.77E-05 | 1.26E-04 | 1.45E-04 | 1.30E-04 | 1.75E-04 |
| Ca, mol/l (±1%) | 1.43E-04 | 1.89E-03 | 1.25E-03 | 1.25E-03 | 1.31E-03 | 1.37E-03 | 2.14E-03 | 2.00E-03 | 2.31E-03 | 2.98E-03 | 3.36E-03 | 3.63E-03 | 6.19E-03 | 4.15E-03 | 4.12E-03 | 4.46E-03 | 4.50E-03 | 4.53E-03 | 4.68E-03 | 4.80E-03 |
| Mn, mol/l | 2.28E-07 | 4.77E-05 | 2.49E-04 | 3.96E-05 | 6.78E-05 | 5.78E-05 | 7.90E-05 | 8.71E-05 | 7.75E-05 | 7.69E-05 | 8.13E-05 | 7.73E-05 | 1.06E-04 | 8.02E-05 | 8.53E-05 | 7.54E-05 | 7.02E-05 | 8.29E-05 | 8.07E-05 | 7.22E-05 |
| Fe, mol/l | 1.75E-05 | 2.44E-04 | 8.92E-04 | 2.53E-04 | 5.45E-04 | 7.56E-04 | 1.16E-03 | 1.51E-03 | 1.44E-03 | 1.29E-03 | 1.32E-03 | 1.16E-03 | 6.35E-04 | 1.09E-03 | 1.25E-03 | 8.83E-04 | 6.95E-04 | 1.01E-03 | 9.82E-04 | 6.89E-04 |
| Sr, mol/l | 4.05E-07 | 2.42E-06 | 2.30E-06 | 2.25E-06 | 2.60E-06 | 2.79E-06 | 3.52E-06 | 2.50E-06 | 3.05E-06 | 3.34E-06 | 2.57E-06 | 3.21E-06 | 2.19E-06 | 2.61E-06 | 2.69E-06 | 2.86E-06 | 2.78E-06 | 2.72E-06 | 2.94E-06 | 3.47E-06 |
| Ba, mol/l | 4.84E-07 | 7.10E-06 | 4.79E-06 | 8.77E-06 | 1.70E-05 | 4.76E-05 | 4.24E-05 | 8.78E-06 | 6.37E-05 | 6.74E-05 | 7.88E-06 | 5.91E-05 | 2.57E-05 | 6.79E-06 | 1.23E-05 | 2.44E-05 | 1.53E-05 | 1.31E-05 | 3.13E-05 | 6.67E-05 |
| Na (est), mol/l | | 1.36E+00 | 1.36E+00 | 1.36E+00 | 1.36E+00 | 1.36E+00 | 1.36E+00 | 1.36E+00 | 1.36E+00 | 1.36E+00 | 1.36E+00 | 1.36E+00 | 1.36E+00 | 1.36E+00 | 1.36E+00 | 1.36E+00 | 1.36E+00 | 1.36E+00 | 1.36E+00 | 1.36E+00 |
| Alkalinity(est), mol/l | | 3.77E-03 | 2.51E-03 | 2.50E-03 | 2.61E-03 | 2.75E-03 | 4.28E-03 | 4.00E-03 | 4.62E-03 | 5.96E-03 | 6.72E-03 | 7.25E-03 | 1.24E-02 | 8.29E-03 | 8.24E-03 | 8.92E-03 | 8.99E-03 | 9.06E-03 | 9.36E-03 | 9.61E-03 |
| Fluid in exp. (kg) | | 0.156 | 0.152 | 0.147 | 0.143 | 0.141 | 0.138 | 0.135 | 0.133 | 0.131 | 0.129 | 0.127 | 0.124 | 0.122 | 0.121 | 0.119 | 0.117 | 0.114 | 0.112 | 0.110 |

| 147 cont.: 1.36M NaCl, 31bar pCO2, 70C | | | | | | | | | | | | | | | | | | |
|---|---|---|---|---|---|---|---|---|---|---|---|---|---|---|---|---|---|---|
| Time, hours | Std. Dev. Mol/l | 153.62 | 193.55 | 197.00 | 213.12 | 221.40 | 236.95 | 236.95 | 245.02 | 262.38 | 268.43 | 291.03 | 312.17 | 320.90 | 336.67 | 365.47 | 389.97 | 508.88 |

| VCT, hours | | 193.69 | 250.05 | 255.05 | 278.90 | 291.47 | 315.60 | 315.60 | 328.54 | 357.08 | 367.30 | 406.55 | 444.23 | 460.24 | 489.97 | 545.86 | 594.88 | 839.22 |
|---|---|---|---|---|---|---|---|---|---|---|---|---|---|---|---|---|---|---|
| Mg, mol/l | 1.92E-05 | 3.45E-03 | 3.62E-03 | 7.42E-03 | 3.66E-03 | 3.76E-03 | 3.71E-03 | 3.66E-03 | 3.74E-03 | 3.79E-03 | 3.88E-03 | 3.86E-03 | 3.81E-03 | 3.87E-03 | 3.88E-03 | 3.96E-03 | 3.96E-03 | 4.17E-03 |
| Al, mol/l | 2.05E-06 | 4.06E-06 | 8.05E-06 | 2.58E-05 | 2.85E-07 | 3.14E-06 | 0.00E+00 | 6.56E-07 | 0.00E+00 | 0.00E+00 | 2.41E-06 | 9.34E-07 | 0.00E+00 | 1.38E-06 | 2.86E-06 | 8.84E-06 | 1.09E-06 | 2.80E-07 |
| Si, mol/l | 1.80E-05 | 1.74E-04 | 1.93E-04 | 3.85E-04 | 1.32E-04 | 1.52E-04 | 1.35E-04 | 1.33E-04 | 1.53E-04 | 1.39E-04 | 1.38E-04 | 1.37E-04 | 1.35E-04 | 1.59E-04 | 1.53E-04 | 1.60E-04 | 1.67E-04 | 4.39E-04 |
| K, mol/l (±16%) | 3.94E-04 | 1.77E-04 | 1.97E-04 | 3.74E-04 | 1.49E-04 | 1.35E-04 | 1.68E-04 | 1.69E-04 | 1.73E-04 | 1.83E-04 | 2.21E-04 | 1.92E-04 | 1.87E-04 | 2.16E-04 | 2.13E-04 | 2.28E-04 | 2.40E-04 | 2.57E-04 |
| Ca, mol/l (±1%) | 1.43E-04 | 4.78E-03 | 4.74E-03 | 1.03E-02 | 4.91E-03 | 4.90E-03 | 5.06E-03 | 5.04E-03 | 5.13E-03 | 5.38E-03 | 5.01E-03 | 5.15E-03 | 5.13E-03 | 5.49E-03 | 5.26E-03 | 5.30E-03 | 5.40E-03 | 5.52E-03 |
| Mn, mol/l | 2.28E-07 | 9.68E-05 | 1.40E-04 | 2.10E-04 | 9.27E-05 | 8.80E-05 | 8.80E-05 | 8.48E-05 | 8.06E-05 | 8.69E-05 | 8.46E-05 | 9.72E-05 | 9.40E-05 | 9.76E-05 | 1.01E-04 | 1.08E-04 | 1.09E-04 | 1.78E-04 |
| Fe, mol/l | 1.75E-05 | 1.27E-03 | 2.60E-03 | 3.25E-03 | 1.24E-03 | 9.99E-04 | 9.88E-04 | 9.56E-04 | 7.66E-04 | 8.90E-04 | 7.98E-04 | 1.20E-03 | 1.07E-03 | 1.23E-03 | 1.31E-03 | 1.49E-03 | 1.49E-03 | 3.49E-03 |
| Sr, mol/l | 4.05E-07 | 3.20E-06 | 3.60E-06 | 7.55E-06 | 2.72E-06 | 3.82E-06 | 2.80E-06 | 2.77E-06 | 3.02E-06 | 2.87E-06 | 3.41E-06 | 3.09E-06 | 2.90E-06 | 3.30E-06 | 3.77E-06 | 3.58E-06 | 3.21E-06 | 2.92E-06 |
| Ba, mol/l | 4.84E-07 | 4.16E-05 | 7.01E-05 | 1.49E-04 | 7.76E-06 | 8.68E-05 | 9.53E-06 | 9.59E-06 | 2.31E-05 | 1.16E-05 | 5.17E-05 | 2.78E-05 | 1.59E-05 | 4.50E-05 | 7.21E-05 | 6.20E-05 | 3.70E-05 | 4.74E-06 |
| Na (est), mol/l | | 1.36E+00 | 1.36E+00 | 1.36E+00 | 1.36E+00 | 1.36E+00 | 1.36E+00 | 1.36E+00 | 1.36E+00 | 1.36E+00 | 1.36E+00 | 1.36E+00 | 1.36E+00 | 1.36E+00 | 1.36E+00 | 1.36E+00 | 1.36E+00 | 1.36E+00 |
| Alkalinity(est), mol/l | | 9.56E-03 | 9.49E-03 | 2.05E-02 | 9.82E-03 | 9.80E-03 | 1.01E-02 | 1.01E-02 | 1.03E-02 | 1.08E-02 | 1.00E-02 | 1.03E-02 | 1.03E-02 | 1.10E-02 | 1.05E-02 | 1.06E-02 | 1.08E-02 | 1.10E-02 |
| Fluid in exp. (kg) | | 0.107 | 0.105 | 0.102 | 0.100 | 0.098 | 0.095 | 0.094 | 0.092 | 0.090 | 0.087 | 0.085 | 0.083 | 0.080 | | | | |

| 144: DI, 4bar pCO2, 22C | | | | | | | | | | | | | | | | | | |
|---|---|---|---|---|---|---|---|---|---|---|---|---|---|---|---|---|---|---|
| Time, hours | Std. Dev. Mol/l | -23.05 | 0.02 | 1.62 | 3.65 | 5.48 | 22.78 | 25.95 | 30.28 | 30.28 | 45.53 | 50.15 | 53.37 | 67.87 | 67.87 | 77.95 | 94.30 | 98.53 |
| VCT, hours | - | 0.00 | 0.02 | 1.68 | 3.86 | 5.87 | 25.50 | 29.22 | 34.45 | 34.45 | 53.62 | 59.66 | 64.00 | 84.27 | 84.27 | 99.15 | 124.25 | 130.97 |
| Mg, mol/l | 4.46E-06 | 8.68E-05 | 9.07E-05 | 1.00E-04 | 1.33E-04 | 1.50E-04 | 3.58E-04 | 3.93E-04 | 4.31E-04 | 4.22E-04 | 5.38E-04 | 8.23E-04 | 4.73E-04 | 7.77E-04 | 7.67E-04 | 9.32E-04 | 1.13E-03 | 1.18E-03 |
| Al, mol/l | 3.05E-06 | 2.23E-06 | 1.84E-06 | 2.93E-06 | 2.88E-06 | 2.71E-06 | 3.09E-06 | 4.20E-06 | 3.70E-06 | 4.97E-06 | 3.24E-06 | 6.13E-06 | 3.92E-06 | 3.20E-06 | 3.18E-06 | 4.66E-06 | 3.90E-06 | 3.88E-06 |
| Si, mol/l | 7.67E-06 | 3.07E-05 | 3.22E-05 | 3.70E-05 | 4.17E-05 | 4.48E-05 | 4.34E-05 | 4.82E-05 | 5.48E-05 | 5.54E-05 | 4.62E-05 | 7.58E-05 | 4.54E-05 | 5.12E-05 | 5.00E-05 | 6.57E-05 | 5.86E-05 | 6.44E-05 |
| K, mol/l (±4%) | 3.15E-06 | 6.30E-05 | 6.36E-05 | 6.18E-05 | 6.85E-05 | 7.11E-05 | 6.85E-05 | 6.71E-05 | 6.63E-05 | 6.59E-05 | 6.88E-05 | 9.36E-05 | 5.00E-05 | 7.05E-05 | 6.70E-05 | 7.71E-05 | 7.08E-05 | 7.17E-05 |
| Ca, mol/l (±2%) | 6.88E-05 | 1.07E-03 | 1.06E-03 | 1.10E-03 | 1.14E-03 | 1.17E-03 | 1.41E-03 | 1.47E-03 | 1.50E-03 | 1.46E-03 | 1.58E-03 | 2.33E-03 | 1.26E-03 | 1.79E-03 | 1.77E-03 | 1.96E-03 | 2.11E-03 | 2.13E-03 |
| Mn, mol/l | 3.59E-08 | 3.64E-07 | 4.01E-06 | 4.34E-06 | 1.25E-06 | 1.69E-06 | 3.92E-06 | 3.93E-06 | 4.44E-06 | 4.22E-06 | 5.52E-06 | 8.35E-06 | 4.80E-06 | 8.32E-06 | 7.89E-06 | 1.00E-05 | 1.16E-05 | 1.25E-05 |
| Fe, mol/l | 2.62E-07 | 1.24E-06 | 1.83E-05 | 1.62E-05 | 3.84E-06 | 4.32E-06 | 7.30E-06 | 4.96E-06 | 5.91E-06 | 3.43E-06 | 3.18E-06 | 4.57E-06 | 2.51E-06 | 3.56E-06 | 3.49E-06 | 3.43E-06 | 7.30E-06 | 4.59E-06 |
| Sr, mol/l | 3.17E-08 | 2.21E-06 | 2.28E-06 | 2.28E-06 | 2.45E-06 | 2.43E-06 | 2.73E-06 | 3.08E-06 | 2.91E-06 | 3.18E-06 | 2.81E-06 | 4.49E-06 | 2.41E-06 | 2.84E-06 | 2.80E-06 | 3.03E-06 | 2.90E-06 | 2.85E-06 |
| Ba, mol/l | 2.02E-08 | 3.31E-07 | 7.61E-07 | 5.52E-07 | 1.13E-06 | 1.20E-06 | 2.20E-06 | 1.86E-05 | 9.73E-06 | 2.59E-05 | 3.13E-06 | 3.35E-05 | 2.01E-05 | 7.26E-07 | 2.77E-06 | 7.49E-06 | 6.90E-07 | 1.06E-06 |
| Na (est), mol/l | - | 0.00E+00 | 0.00E+00 | 0.00E+00 | 0.00E+00 | 0.00E+00 | 0.00E+00 | 0.00E+00 | 0.00E+00 | 0.00E+00 | 0.00E+00 | 0.00E+00 | 0.00E+00 | 0.00E+00 | 0.00E+00 | 0.00E+00 | 0.00E+00 | 0.00E+00 |
| Alkalinity(est), mol/l | - | 2.13E-03 | 2.12E-03 | 2.20E-03 | 2.29E-03 | 2.34E-03 | 2.82E-03 | 2.94E-03 | 3.00E-03 | 2.92E-03 | 3.16E-03 | 4.65E-03 | 2.53E-03 | 3.57E-03 | 3.53E-03 | 3.93E-03 | 4.22E-03 | 4.26E-03 |
| Fluid in exp. (kg) | | 0.098 | 0.097 | 0.093 | 0.090 | 0.088 | 0.085 | 0.082 | 0.080 | 0.078 | 0.077 | 0.074 | 0.072 | 0.069 | 0.067 | 0.065 | 0.063 | 0.061 |

| 144 cont.: DI, 4bar pCO2, 22C | | | | | | | | | | | | | | | | |
|---|---|---|---|---|---|---|---|---|---|---|---|---|---|---|---|---|
| Time, hours | Std. Dev. Mol/l | 164.53 | 188.00 | 216.40 | 235.33 | 265.83 | 335.43 | 404.33 | 409.78 | 532.92 | 597.70 | 597.72 | 696.45 | 765.37 | 793.70 | 793.70 |
| VCT, hours | - | 239.73 | 279.70 | 330.11 | 365.24 | 424.61 | 566.87 | 714.16 | 726.47 | 1023.03 | 1190.38 | 1190.42 | 1472.76 | 1685.87 | 1780.71 | 1780.71 |

| | | | | | | | | | | | | | | | | |
|---|---|---|---|---|---|---|---|---|---|---|---|---|---|---|---|---|
| Mg, mol/l | 4.46E-06 | 1.87E-03 | 2.03E-03 | 2.22E-03 | 2.28E-03 | 2.44E-03 | 2.55E-03 | 2.67E-03 | 2.74E-03 | 2.76E-03 | 2.92E-03 | 2.86E-03 | 2.93E-03 | 2.95E-03 | 2.94E-03 | 2.96E-03 |
| Al, mol/l | 3.05E-06 | 4.83E-06 | 4.59E-06 | 5.55E-06 | 5.09E-06 | 5.12E-06 | 4.67E-06 | 4.54E-06 | 5.58E-06 | 7.21E-06 | 5.83E-06 | 5.40E-06 | 5.03E-06 | 5.02E-06 | 5.71E-06 | 5.28E-06 |
| Si, mol/l | 7.67E-06 | 7.34E-05 | 6.70E-05 | 6.99E-05 | 7.41E-05 | 7.56E-05 | 7.71E-05 | 8.44E-05 | 8.54E-05 | 1.04E-04 | 9.97E-05 | 9.64E-05 | 2.28E-04 | 1.04E-04 | 1.07E-04 | 1.09E-04 |
| K, mol/l (±4%) | 3.15E-06 | 7.50E-05 | 8.05E-05 | 8.22E-05 | 7.95E-05 | 8.18E-05 | 8.00E-05 | 8.39E-05 | 8.42E-05 | 8.63E-05 | 8.88E-05 | 8.93E-05 | 8.85E-05 | 9.30E-05 | 9.19E-05 | 9.30E-05 |
| Ca, mol/l (±2%) | 6.88E-05 | 2.76E-03 | 2.87E-03 | 3.12E-03 | 3.17E-03 | 3.22E-03 | 3.32E-03 | 3.41E-03 | 3.42E-03 | 3.53E-03 | 3.64E-03 | 3.62E-03 | 3.60E-03 | 3.63E-03 | 3.69E-03 | 3.79E-03 |
| Mn, mol/l | 3.59E-08 | 1.85E-05 | 2.13E-05 | 2.26E-05 | 2.32E-05 | 2.52E-05 | 2.62E-05 | 2.77E-05 | 2.75E-05 | 2.90E-05 | 3.05E-05 | 2.92E-05 | 2.97E-05 | 3.20E-05 | 3.12E-05 | 3.03E-05 |
| Fe, mol/l | 2.62E-07 | 7.51E-06 | 7.22E-06 | 7.37E-06 | 7.52E-06 | 8.22E-06 | 8.42E-06 | 8.83E-06 | 8.41E-06 | 8.22E-06 | 8.41E-06 | 8.68E-06 | 8.37E-06 | 8.30E-06 | 8.46E-06 | 8.21E-06 |
| Sr, mol/l | 3.17E-08 | 2.95E-06 | 2.98E-06 | 3.04E-06 | 3.03E-06 | 3.07E-06 | 3.04E-06 | 3.06E-06 | 3.07E-06 | 3.57E-06 | 3.29E-06 | 3.18E-06 | 3.09E-06 | 3.22E-06 | 3.34E-06 | 3.24E-06 |
| Ba, mol/l | 2.02E-08 | 5.89E-07 | 4.07E-07 | 7.41E-07 | 8.85E-07 | 3.74E-07 | 5.61E-07 | 5.17E-07 | 3.19E-06 | 3.08E-05 | 8.67E-06 | 5.22E-06 | 2.11E-06 | 1.76E-06 | 1.17E-05 | 5.42E-06 |
| Na (est), mol/l | - | 0.00E+00 | 0.00E+00 | 0.00E+00 | 0.00E+00 | 0.00E+00 | 0.00E+00 | 0.00E+00 | 0.00E+00 | 0.00E+00 | 0.00E+00 | 0.00E+00 | 0.00E+00 | 0.00E+00 | 0.00E+00 | 0.00E+00 |
| Alkalinity(est), mol/l | - | 5.52E-03 | 5.74E-03 | 6.24E-03 | 6.33E-03 | 6.45E-03 | 6.63E-03 | 6.82E-03 | 6.83E-03 | 7.06E-03 | 7.28E-03 | 7.25E-03 | 7.20E-03 | 7.26E-03 | 7.38E-03 | 7.58E-03 |
| Fluid in exp. (kg) | | 0.059 | 0.057 | 0.054 | 0.052 | 0.050 | 0.047 | 0.045 | 0.043 | 0.040 | 0.037 | 0.035 | 0.034 | 0.031 | 0.029 | 0.027 |

| 148: DI, 31bar pCO2, 70C | | | | | | | | | | | | | | | | | | | | | |
|---|---|---|---|---|---|---|---|---|---|---|---|---|---|---|---|---|---|---|---|---|---|
| Time, hours | Std. Dev. Mol/l | -0.18 | 0.08 | 2.58 | 5.45 | 8.12 | 21.42 | 25.77 | 32.17 | 48.22 | 53.28 | 70.32 | 76.28 | 76.28 | 94.30 | 99.38 | 120.88 | 131.87 | 141.98 | 149.98 | 167.37 |
| VCT, hours | | 0.00 | 0.08 | 2.64 | 5.63 | 8.44 | 22.66 | 27.37 | 34.38 | 52.19 | 57.88 | 77.27 | 84.13 | 84.13 | 105.18 | 111.19 | 136.92 | 150.23 | 162.66 | 172.62 | 194.56 |
| Mg, mol/l | 4.75E-06 | 3.93E-04 | 4.20E-04 | 4.53E-04 | 6.23E-04 | 8.73E-04 | 1.11E-03 | 1.74E-03 | 2.02E-03 | 2.30E-03 | 2.53E-03 | 2.76E-03 | 2.99E-03 | 3.01E-03 | 3.03E-03 | 3.27E-03 | 3.30E-03 | 3.32E-03 | 3.50E-03 | 3.60E-03 | 3.73E-03 |
| Al, mol/l | 1.29E-05 | 7.92E-06 | 0.00E+00 | 0.00E+00 | 1.31E-05 | 1.65E-05 | 0.00E+00 | 3.39E-05 | 0.00E+00 | 0.00E+00 | 0.00E+00 | 5.88E-05 | 0.00E+00 | 0.00E+00 | 0.00E+00 | 5.31E-05 | 5.72E-05 | 1.27E-05 | 0.00E+00 | 0.00E+00 | 0.00E+00 |
| Si, mol/l | 0.00E+00 | 0.00E+00 | 0.00E+00 | 0.00E+00 | 0.00E+00 | 0.00E+00 | 0.00E+00 | 0.00E+00 | 0.00E+00 | 0.00E+00 | 0.00E+00 | 0.00E+00 | 0.00E+00 | 0.00E+00 | 0.00E+00 | 0.00E+00 | 0.00E+00 | 0.00E+00 | 0.00E+00 | 0.00E+00 | 0.00E+00 |
| K, mol/l (±20%) | 2.48E-06 | 8.90E-05 | 9.48E-05 | 9.61E-05 | 0.00E+00 | 0.00E+00 | 0.00E+00 | 0.00E+00 | 0.00E+00 | 0.00E+00 | 0.00E+00 | 0.00E+00 | 0.00E+00 | 0.00E+00 | 0.00E+00 | 1.67E-04 | 0.00E+00 | 1.40E-04 | 0.00E+00 | 0.00E+00 | 0.00E+00 |
| Ca, mol/l (±4%) | 2.30E-06 | 1.43E-03 | 1.47E-03 | 1.52E-03 | 1.79E-03 | 0.00E+00 | 2.22E-03 | 2.72E-03 | 2.96E-03 | 3.11E-03 | 3.41E-03 | 0.00E+00 | 3.91E-03 | 4.05E-03 | 3.98E-03 | 4.07E-03 | 3.94E-03 | 4.28E-03 | 4.30E-03 | 4.36E-03 | 4.52E-03 |
| Mn, mol/l | 3.09E-06 | 3.06E-04 | 3.37E-04 | 2.52E-04 | 2.76E-04 | 2.96E-04 | 2.92E-04 | 2.28E-04 | 1.44E-04 | 1.41E-04 | 9.80E-05 | 9.00E-05 | 7.10E-05 | 6.39E-05 | 5.99E-05 | 5.30E-05 | 5.45E-05 | 5.06E-05 | 4.65E-05 | 4.50E-05 | 4.62E-05 |
| Fe, mol/l | 0.00E+00 | 0.00E+00 | 0.00E+00 | 0.00E+00 | 0.00E+00 | 0.00E+00 | 2.80E-05 | 3.17E-05 | 2.93E-05 | 4.90E-05 | 3.38E-05 | 0.00E+00 | 3.23E-05 | 0.00E+00 | 3.28E-05 | 4.07E-05 | 5.81E-05 | 3.52E-05 | 3.06E-05 | 0.00E+00 | 2.89E-05 |
| Sr, mol/l | 0.00E+00 | 1.92E-06 | 1.96E-06 | 1.97E-06 | 2.27E-06 | 2.35E-06 | 2.28E-06 | 2.40E-06 | 2.36E-06 | 2.38E-06 | 2.44E-06 | 2.68E-06 | 2.61E-06 | 2.63E-06 | 2.59E-06 | 2.61E-06 | 2.59E-06 | 2.65E-06 | 2.58E-06 | 2.66E-06 | 2.64E-06 |
| Ba, mol/l | 1.06E-05 | 0.00E+00 | 0.00E+00 | 0.00E+00 | 0.00E+00 | 0.00E+00 | 0.00E+00 | 0.00E+00 | 0.00E+00 | 0.00E+00 | 0.00E+00 | 0.00E+00 | 0.00E+00 | 0.00E+00 | 0.00E+00 | 0.00E+00 | 0.00E+00 | 0.00E+00 | 0.00E+00 | 0.00E+00 | 0.00E+00 |
| Na (est), mol/l | | 0.00E+00 | 0.00E+00 | 0.00E+00 | 0.00E+00 | 0.00E+00 | 0.00E+00 | 0.00E+00 | 0.00E+00 | 0.00E+00 | 0.00E+00 | 0.00E+00 | 0.00E+00 | 0.00E+00 | 0.00E+00 | 0.00E+00 | 0.00E+00 | 0.00E+00 | 0.00E+00 | 0.00E+00 | 0.00E+00 |
| Alkalinity(est), mol/l | | 2.85E-03 | 2.94E-03 | 3.04E-03 | 3.59E-03 | 0.00E+00 | 4.43E-03 | 5.45E-03 | 5.92E-03 | 6.22E-03 | 6.82E-03 | 0.00E+00 | 7.82E-03 | 8.11E-03 | 7.96E-03 | 8.13E-03 | 7.88E-03 | 8.56E-03 | 8.60E-03 | 8.73E-03 | 9.04E-03 |
| Fluid in exp. (kg) | | 0.154 | 0.152 | 0.148 | 0.145 | 0.144 | 0.142 | 0.140 | 0.138 | 0.137 | 0.135 | 0.133 | 0.132 | 0.130 | 0.130 | 0.128 | 0.127 | 0.125 | 0.123 | 0.122 | 0.120 |

| 148 cont.: DI, 31bar pCO2, 70C | | | | | | | | | | | | | | | | | | | | | |
|---|---|---|---|---|---|---|---|---|---|---|---|---|---|---|---|---|---|---|---|---|---|
| Time, hours | Std. Dev. Mol/l | 175.58 | 190.93 | 198.03 | 212.65 | 221.37 | 221.37 | 239.35 | 247.30 | 263.02 | 288.37 | 312.45 | 335.45 | 359.47 | 387.58 | 437.08 | 485.93 | 530.32 | 558.45 | 679.48 | 679.48 |
| VCT, hours | | 205.05 | 224.93 | 234.24 | 253.69 | 265.46 | 265.46 | 290.35 | 301.54 | 324.00 | 360.78 | 396.32 | 430.85 | 467.54 | 511.26 | 589.75 | 668.63 | 741.65 | 788.78 | 995.49 | 995.49 |
| Mg, mol/l | 4.75E-06 | 3.60E-03 | 3.71E-03 | 3.81E-03 | 3.99E-03 | 3.74E-03 | 4.14E-03 | 4.15E-03 | 4.07E-03 | 3.39E-03 | 3.46E-03 | 3.51E-03 | 3.59E-03 | 3.61E-03 | 4.11E-03 | 3.88E-03 | 4.00E-03 | 4.12E-03 | 4.08E-03 | 4.24E-03 | 4.35E-03 |
| Al, mol/l | 1.29E-05 | 2.42E-05 | 0.00E+00 | 0.00E+00 | 0.00E+00 | 7.46E-05 | 0.00E+00 | 2.84E-05 | 0.00E+00 | 0.00E+00 | 0.00E+00 | 0.00E+00 | 0.00E+00 | 0.00E+00 | 1.64E-04 | 2.26E-05 | 0.00E+00 | 0.00E+00 | 0.00E+00 | 0.00E+00 | 1.94E-05 |
| Si, mol/l | 0.00E+00 | 0.00E+00 | 0.00E+00 | 0.00E+00 | 0.00E+00 | 0.00E+00 | 0.00E+00 | 0.00E+00 | 0.00E+00 | 0.00E+00 | 0.00E+00 | 0.00E+00 | 0.00E+00 | 0.00E+00 | 0.00E+00 | 0.00E+00 | 0.00E+00 | 0.00E+00 | 0.00E+00 | 0.00E+00 | 0.00E+00 |
| K, mol/l (±20%) | 2.48E-06 | 0.00E+00 | 0.00E+00 | 1.62E-04 | 0.00E+00 | 2.29E-04 | 1.66E-04 | 1.95E-04 | 1.67E-04 | 0.00E+00 | 0.00E+00 | 0.00E+00 | 1.43E-04 | 0.00E+00 | 2.42E-04 | 0.00E+00 | 0.00E+00 | 0.00E+00 | 0.00E+00 | 1.63E-04 | 1.84E-04 |
| Ca, mol/l (±4%) | 2.30E-06 | 4.31E-03 | 4.33E-03 | 4.57E-03 | 4.75E-03 | 4.69E-03 | 4.95E-03 | 4.94E-03 | 4.86E-03 | 4.63E-03 | 4.66E-03 | 4.53E-03 | 4.69E-03 | 4.60E-03 | 4.78E-03 | 5.01E-03 | 4.99E-03 | 5.25E-03 | 5.28E-03 | 5.24E-03 | 5.33E-03 |
| Mn, mol/l | 3.09E-06 | 4.29E-05 | 4.35E-05 | 4.29E-05 | 4.51E-05 | 4.50E-05 | 4.43E-05 | 4.58E-05 | 4.38E-05 | 4.19E-05 | 4.39E-05 | 4.31E-05 | 4.31E-05 | 4.19E-05 | 4.35E-05 | 4.72E-05 | 4.90E-05 | 4.90E-05 | 4.95E-05 | 5.23E-05 | 5.03E-05 |
| Fe, mol/l | 0.00E+00 | 0.00E+00 | 0.00E+00 | 0.00E+00 | 0.00E+00 | 3.33E-05 | 0.00E+00 | 0.00E+00 | 0.00E+00 | 0.00E+00 | 0.00E+00 | 0.00E+00 | 0.00E+00 | 0.00E+00 | 1.08E-04 | 0.00E+00 | 0.00E+00 | 0.00E+00 | 0.00E+00 | 0.00E+00 | 0.00E+00 |
| Sr, mol/l | 0.00E+00 | 2.61E-06 | 2.62E-06 | 2.63E-06 | 2.63E-06 | 3.01E-06 | 2.76E-06 | 2.77E-06 | 2.69E-06 | 2.69E-06 | 2.65E-06 | 2.64E-06 | 2.63E-06 | 2.48E-06 | 2.58E-06 | 2.64E-06 | 2.68E-06 | 2.78E-06 | 2.75E-06 | 2.69E-06 | 2.74E-06 |
| Ba, mol/l | 1.06E-05 | 0.00E+00 | 0.00E+00 | 0.00E+00 | 0.00E+00 | 0.00E+00 | 0.00E+00 | 0.00E+00 | 0.00E+00 | 0.00E+00 | 0.00E+00 | 0.00E+00 | 0.00E+00 | 0.00E+00 | 0.00E+00 | 0.00E+00 | 0.00E+00 | 0.00E+00 | 0.00E+00 | 0.00E+00 | 0.00E+00 |
| Na (est), mol/l | | 0.00E+00 | 0.00E+00 | 0.00E+00 | 0.00E+00 | 0.00E+00 | 0.00E+00 | 0.00E+00 | 0.00E+00 | 0.00E+00 | 0.00E+00 | 0.00E+00 | 0.00E+00 | 0.00E+00 | 0.00E+00 | 0.00E+00 | 0.00E+00 | 0.00E+00 | 0.00E+00 | 0.00E+00 | 0.00E+00 |
| Alkalinity(est), mol/l | | 8.62E-03 | 8.65E-03 | 9.15E-03 | 9.49E-03 | 9.37E-03 | 9.90E-03 | 9.89E-03 | 9.71E-03 | 9.25E-03 | 9.31E-03 | 9.05E-03 | 9.37E-03 | 9.20E-03 | 9.57E-03 | 1.00E-02 | 9.97E-03 | 1.05E-02 | 1.06E-02 | 1.05E-02 | 1.07E-02 |
| Fluid in exp. (kg) | | 0.119 | 0.117 | 0.116 | 0.114 | 0.112 | 0.110 | 0.109 | 0.108 | 0.106 | 0.104 | 0.103 | 0.101 | 0.099 | 0.097 | 0.096 | 0.094 | 0.092 | 0.090 | 0.089 | 0.087 |

| 149, 1.36M NaCl, 4bar pCO2, 70C | | | | | | | | | | | | | | | | | | |
|---|---|---|---|---|---|---|---|---|---|---|---|---|---|---|---|---|---|---|
| Time, hours | Std. Dev. Mol/l | -0.17 | 0.02 | 1.65 | 4.47 | 9.10 | 19.33 | 22.80 | 27.12 | 44.50 | 48.75 | 52.75 | 68.10 | 75.17 | 89.78 | 98.55 | 98.55 | 116.52 |
| VCT, hours | | 0.00 | 0.02 | 1.69 | 4.66 | 9.66 | 20.92 | 24.83 | 29.82 | 50.48 | 55.67 | 60.69 | 80.58 | 90.02 | 110.18 | 122.71 | 122.71 | 149.57 |
| Mg, mol/l | 1.34E-06 | 8.09E-04 | 6.16E-04 | 6.17E-04 | 7.36E-04 | 6.34E-04 | 8.57E-04 | 1.20E-03 | 1.31E-03 | 1.28E-03 | 1.66E-03 | 9.98E-04 | 1.68E-03 | 1.59E-03 | 1.26E-03 | 2.01E-03 | 1.70E-03 | 2.27E-03 |
| Al, mol/l | 1.29E-05 | 0.00E+00 | 0.00E+00 | 0.00E+00 | 0.00E+00 | 0.00E+00 | 0.00E+00 | 0.00E+00 | 0.00E+00 | 0.00E+00 | 0.00E+00 | 0.00E+00 | 0.00E+00 | 0.00E+00 | 0.00E+00 | 0.00E+00 | 0.00E+00 | 0.00E+00 |
| Si, mol/l | 0.00E+00 | 0.00E+00 | 0.00E+00 | 0.00E+00 | 0.00E+00 | 0.00E+00 | 0.00E+00 | 0.00E+00 | 0.00E+00 | 0.00E+00 | 0.00E+00 | 0.00E+00 | 0.00E+00 | 0.00E+00 | 0.00E+00 | 0.00E+00 | 0.00E+00 | 0.00E+00 |
| K, mol/l | 7.52E-07 | 1.86E-04 | 1.41E-04 | 1.33E-04 | 0.00E+00 | 0.00E+00 | 0.00E+00 | 0.00E+00 | 0.00E+00 | 0.00E+00 | 0.00E+00 | 0.00E+00 | 0.00E+00 | 0.00E+00 | 0.00E+00 | 1.04E-04 | 0.00E+00 | 9.61E-05 |
| Ca, mol/l (±14%) | 2.30E-06 | 2.98E-03 | 2.19E-03 | 2.11E-03 | 2.15E-03 | 0.00E+00 | 1.74E-03 | 1.90E-03 | 1.94E-03 | 1.74E-03 | 2.24E-03 | 0.00E+00 | 2.22E-03 | 2.16E-03 | 1.67E-03 | 2.52E-03 | 2.04E-03 | 2.94E-03 |
| Mn, mol/l | 5.40E-07 | 6.38E-04 | 5.03E-04 | 3.49E-04 | 3.31E-04 | 2.18E-04 | 2.29E-04 | 1.59E-04 | 9.43E-05 | 7.90E-05 | 6.44E-05 | 3.28E-05 | 4.02E-05 | 3.39E-05 | 2.51E-05 | 3.28E-05 | 2.81E-05 | 3.47E-05 |
| Fe, mol/l | 0.00E+00 | 0.00E+00 | 0.00E+00 | 0.00E+00 | 0.00E+00 | 0.00E+00 | 2.19E-05 | 2.21E-05 | 1.92E-05 | 2.75E-05 | 2.23E-05 | 0.00E+00 | 1.83E-05 | 0.00E+00 | 1.38E-05 | 2.52E-05 | 3.01E-05 | 2.42E-05 |
| Sr, mol/l | 0.00E+00 | 3.59E-06 | 2.53E-06 | 2.31E-06 | 2.28E-06 | 1.35E-06 | 1.43E-06 | 1.29E-06 | 1.20E-06 | 1.01E-06 | 1.24E-06 | 5.05E-07 | 1.12E-06 | 1.06E-06 | 7.93E-07 | 1.24E-06 | 9.83E-07 | 1.48E-06 |
| Ba, mol/l | 8.42E-07 | 6.10E-08 | 3.51E-08 | 6.15E-08 | 1.10E-08 | 0.00E+00 | 2.06E-09 | 0.00E+00 | 0.00E+00 | 0.00E+00 | 4.39E-08 | 0.00E+00 | 8.33E-08 | 3.78E-08 | 0.00E+00 | 4.45E-08 | 4.27E-07 | 5.26E-08 |
| Na (est), mol/l | | 1.36E+00 | 1.36E+00 | 1.36E+00 | 1.36E+00 | 1.36E+00 | 1.36E+00 | 1.36E+00 | 1.36E+00 | 1.36E+00 | 1.36E+00 | 1.36E+00 | 1.36E+00 | 1.36E+00 | 1.36E+00 | 1.36E+00 | 1.36E+00 | 1.36E+00 |
| Alkalinity(est), mol/l | | 5.95E-03 | 4.39E-03 | 4.21E-03 | 4.30E-03 | 0.00E+00 | 3.47E-03 | 3.79E-03 | 3.88E-03 | 3.49E-03 | 4.48E-03 | 0.00E+00 | 4.43E-03 | 4.31E-03 | 3.34E-03 | 5.03E-03 | 4.07E-03 | 5.89E-03 |
| Fluid in exp. (kg) | | 0.102 | 0.102 | 0.099 | 0.097 | 0.095 | 0.093 | 0.090 | 0.088 | 0.085 | 0.083 | 0.081 | 0.079 | 0.076 | 0.074 | 0.071 | 0.069 | 0.068 |

| 149 cont., 1.36M NaCl, 4bar pCO2, 70C | | | | | | | | | | | | | | | | |
|---|---|---|---|---|---|---|---|---|---|---|---|---|---|---|---|---|
| Time, hours | Std. Dev. Mol/l | 124.47 | 140.18 | 145.47 | 165.50 | 189.60 | 212.57 | 212.57 | 236.62 | 264.72 | 314.22 | 363.10 | 407.45 | 435.58 | 556.62 | 556.62 |
| VCT, hours | | 161.89 | 187.01 | 195.77 | 230.31 | 273.67 | 316.91 | 316.91 | 364.83 | 423.40 | 531.47 | 642.93 | 749.47 | 820.84 | 1150.00 | 1150.00 |
| Mg, mol/l | 1.34E-06 | 2.37E-03 | 1.76E-03 | 2.32E-03 | 1.83E-03 | 2.24E-03 | 2.84E-03 | 2.45E-03 | 2.12E-03 | 2.86E-03 | 2.66E-03 | 2.82E-03 | 2.58E-03 | 4.88E-03 | 2.31E-03 | 2.97E-03 |
| Al, mol/l | 1.29E-05 | 0.00E+00 | 0.00E+00 | 0.00E+00 | 0.00E+00 | 0.00E+00 | 0.00E+00 | 0.00E+00 | 0.00E+00 | 0.00E+00 | 0.00E+00 | 0.00E+00 | 0.00E+00 | 0.00E+00 | 0.00E+00 | 0.00E+00 |

| | | | | | | | | | | | | | | | | |
|---|---|---|---|---|---|---|---|---|---|---|---|---|---|---|---|---|
| Si, mol/l | 0.00E+00 | 0.00E+00 | 0.00E+00 | 0.00E+00 | 0.00E+00 | 0.00E+00 | 0.00E+00 | 0.00E+00 | 0.00E+00 | 0.00E+00 | 0.00E+00 | 0.00E+00 | 0.00E+00 | 0.00E+00 | 0.00E+00 | 0.00E+00 |
| K, mol/l | 7.52E-07 | 0.00E+00 | 0.00E+00 | 0.00E+00 | 0.00E+00 | 0.00E+00 | 1.21E-04 | 0.00E+00 | 1.30E-04 | 1.15E-04 | 1.26E-04 | 1.16E-04 | 0.00E+00 | 0.00E+00 | 0.00E+00 | 1.19E-04 |
| Ca, mol/l (±14%) | 2.30E-06 | 2.93E-03 | 2.15E-03 | 2.83E-03 | 2.20E-03 | 2.63E-03 | 3.41E-03 | 2.92E-03 | 2.67E-03 | 3.43E-03 | 3.18E-03 | 3.37E-03 | 3.53E-03 | 6.60E-03 | 2.99E-03 | 3.89E-03 |
| Mn, mol/l | 5.40E-07 | 3.16E-05 | 2.21E-05 | 2.88E-05 | 2.18E-05 | 2.64E-05 | 3.20E-05 | 2.77E-05 | 2.56E-05 | 3.06E-05 | 2.94E-05 | 3.04E-05 | 3.19E-05 | 6.21E-05 | 2.85E-05 | 3.57E-05 |
| Fe, mol/l | 0.00E+00 | 2.08E-05 | 0.00E+00 | 1.81E-05 | 0.00E+00 | 0.00E+00 | 0.00E+00 | 0.00E+00 | 1.90E-05 | 0.00E+00 | 0.00E+00 | 0.00E+00 | 0.00E+00 | 0.00E+00 | 0.00E+00 | 0.00E+00 |
| Sr, mol/l | 0.00E+00 | 1.38E-06 | 9.66E-07 | 1.30E-06 | 9.90E-07 | 1.24E-06 | 1.56E-06 | 1.27E-06 | 1.35E-06 | 1.53E-06 | 1.41E-06 | 1.50E-06 | 1.64E-06 | 2.98E-06 | 1.36E-06 | 1.76E-06 |
| Ba, mol/l | 8.42E-07 | 4.45E-08 | 3.77E-08 | 0.00E+00 | 3.76E-08 | 5.87E-08 | 1.18E-07 | 4.79E-08 | 8.63E-08 | 1.77E-07 | 1.57E-07 | 1.59E-07 | 8.89E-08 | 3.29E-07 | 7.28E-08 | 1.06E-07 |
| Na (est), mol/l | | 1.36E+00 | 1.36E+00 | 1.36E+00 | 1.36E+00 | 1.36E+00 | 1.36E+00 | 1.36E+00 | 1.36E+00 | 1.36E+00 | 1.36E+00 | 1.36E+00 | 1.36E+00 | 1.36E+00 | 1.36E+00 | 1.36E+00 |
| Alkalinity(est), mol/l | | 5.85E-03 | 4.30E-03 | 5.65E-03 | 4.40E-03 | 5.26E-03 | 6.83E-03 | 5.84E-03 | 5.34E-03 | 6.86E-03 | 6.36E-03 | 6.74E-03 | 7.06E-03 | 1.32E-02 | 5.98E-03 | 7.78E-03 |
| Fluid in exp. (kg) | | 0.065 | 0.063 | 0.060 | 0.058 | 0.055 | 0.053 | 0.050 | 0.049 | 0.047 | 0.044 | 0.042 | 0.040 | 0.038 | 0.036 | 0.034 |

| SCORE: 1.36M NaCl, 31bar pCO2, 70C | | | | | | | | | | | | | | | | | | | |
|---|---|---|---|---|---|---|---|---|---|---|---|---|---|---|---|---|---|---|---|
| Time, hours | Std. Dev. Mol/l | 4.08 | 5.95 | 8.45 | 24.37 | 28.35 | 31.88 | 49.52 | 52.33 | 56.82 | 75.27 | 75.27 | 79.25 | 84.48 | 95.22 | 101.90 | 108.50 | 119.23 | 145.47 | 154.47 |
| VCT, hours | | | | | | | | | | | | | | | | | | | | |
| Mg, mol/l | 1.34E-06 | 1.81E-02 | 1.41E-02 | 1.03E-02 | 8.21E-03 | 5.50E-03 | 5.63E-03 | 5.62E-03 | 5.57E-03 | 5.49E-03 | 5.41E-03 | 5.33E-03 | 5.29E-03 | 5.81E-03 | 6.26E-03 | 6.21E-03 | 6.33E-03 | 6.32E-03 | 6.27E-03 | 6.16E-03 |
| Al, mol/l | 1.29E-05 | 6.63E-05 | 6.63E-05 | 6.63E-05 | 6.63E-05 | 6.63E-05 | 6.63E-05 | 6.63E-05 | 6.63E-05 | 6.63E-05 | 6.63E-05 | 6.63E-05 | 6.63E-05 | 6.63E-05 | 6.63E-05 | 6.63E-05 | 6.63E-05 | 6.63E-05 | 6.63E-05 | 6.63E-05 |
| Si, mol/l | 0.00E+00 | 2.50E-03 | 1.87E-03 | 1.17E-03 | 1.00E-03 | 1.00E-03 | 1.00E-03 | 1.00E-03 | 1.00E-03 | 1.00E-03 | 1.00E-03 | 1.00E-03 | 1.00E-03 | 1.00E-03 | 1.00E-03 | 1.00E-03 | 1.00E-03 | 1.00E-03 | 1.00E-03 | 1.00E-03 |
| K, mol/l (±5%) | 7.52E-07 | 2.17E-02 | 1.26E-02 | 3.54E-03 | 8.05E-04 | 4.78E-04 | 4.48E-04 | 3.55E-04 | 3.45E-04 | 3.16E-04 | 2.79E-04 | 2.76E-04 | 2.75E-04 | 2.58E-04 | 2.51E-04 | 2.43E-04 | 2.42E-04 | 2.82E-04 | 2.23E-04 | 1.97E-04 |
| Ca, mol/l (±2%) | 2.30E-06 | 7.03E-02 | 4.28E-02 | 2.36E-02 | 1.40E-02 | 9.81E-03 | 1.01E-02 | 9.98E-03 | 1.01E-02 | 9.68E-03 | 8.99E-03 | 9.12E-03 | 9.26E-03 | 9.41E-03 | 9.79E-03 | 9.33E-03 | 9.62E-03 | 9.41E-03 | 9.26E-03 | 9.63E-03 |
| Mn, mol/l | 5.40E-07 | 2.82E-04 | 2.20E-04 | 2.23E-04 | 1.10E-04 | 7.34E-05 | 7.38E-05 | 6.67E-05 | 6.54E-05 | 6.38E-05 | 5.75E-05 | 6.16E-05 | 6.11E-05 | 5.82E-05 | 6.02E-05 | 6.14E-05 | 6.69E-05 | 6.41E-05 | 5.02E-05 | 5.78E-05 |
| Fe, mol/l | 0.00E+00 | 2.40E-04 | 3.05E-04 | 2.90E-04 | 1.58E-04 | 1.15E-04 | 1.35E-04 | 2.82E-04 | 2.92E-04 | 3.00E-04 | 3.01E-04 | 3.95E-04 | 3.07E-04 | 3.63E-04 | 2.74E-04 | 2.46E-04 | 2.26E-04 | 1.87E-04 | 1.55E-04 | 1.62E-04 |
| Sr, mol/l | 0.00E+00 | 1.17E-04 | 6.25E-05 | 2.68E-05 | 1.30E-05 | 9.03E-06 | 8.97E-06 | 7.92E-06 | 7.72E-06 | 7.39E-06 | 6.16E-06 | 6.48E-06 | 6.76E-06 | 6.21E-06 | 5.85E-06 | 5.03E-06 | 5.18E-06 | 5.10E-06 | 5.07E-06 | 5.09E-06 |
| Ba, mol/l | 8.42E-07 | 1.88E-05 | 1.35E-05 | 1.04E-05 | 4.91E-06 | 4.50E-06 | 3.95E-06 | 2.86E-06 | 2.66E-06 | 2.54E-06 | 2.20E-06 | 2.29E-06 | 2.24E-06 | 2.24E-06 | 1.82E-06 | 1.53E-06 | 1.65E-06 | 1.57E-06 | 1.35E-06 | 1.21E-06 |
| Na (est), mol/l | | 1.36E+00 | 1.36E+00 | 1.36E+00 | 1.36E+00 | 1.36E+00 | 1.36E+00 | 1.36E+00 | 1.36E+00 | 1.36E+00 | 1.36E+00 | 1.36E+00 | 1.36E+00 | 1.36E+00 | 1.36E+00 | 1.36E+00 | 1.36E+00 | 1.36E+00 | 1.36E+00 | 1.36E+00 |
| Alkalinity(est), mol/l | | 1.41E-01 | 8.55E-02 | 4.72E-02 | 2.80E-02 | 1.96E-02 | 2.03E-02 | 2.00E-02 | 2.01E-02 | 1.94E-02 | 1.80E-02 | 1.82E-02 | 1.85E-02 | 1.88E-02 | 1.96E-02 | 1.87E-02 | 1.92E-02 | 1.88E-02 | 1.85E-02 | 1.93E-02 |
| Fluid in exp. (kg) | | 0.010 | 0.010 | 0.010 | 0.010 | 0.010 | 0.010 | 0.010 | 0.010 | 0.010 | 0.010 | 0.010 | 0.010 | 0.010 | 0.010 | 0.010 | 0.010 | 0.010 | 0.010 | 0.010 |

| SCORE cont.: 1.36M NaCl, 31bar pCO2, 70C | | | | | | | | | | | | | | | | | | | | |
|---|---|---|---|---|---|---|---|---|---|---|---|---|---|---|---|---|---|---|---|---|
| Time, hours | Std. Dev. Mol/l | 167.37 | 174.38 | 174.38 | 192.10 | 200.55 | 216.47 | 223.87 | 239.72 | 246.77 | 269.05 | 293.97 | 318.63 | 340.77 | 366.40 | 389.38 | 481.25 | 529.38 | 578.97 | 578.97 |
| VCT, hours | | | | | | | | | | | | | | | | | | | | |
| Mg, mol/l | 1.34E-06 | 5.58E-03 | 5.34E-03 | 5.37E-03 | 5.30E-03 | 5.65E-03 | 6.13E-03 | 5.83E-03 | 6.19E-03 | 6.31E-03 | 5.55E-03 | 4.98E-03 | 5.60E-03 | 5.40E-03 | 5.84E-03 | 6.52E-03 | 5.41E-03 | 6.04E-03 | 5.85E-03 | 5.98E-03 |
| Al, mol/l | 1.29E-05 | 6.63E-05 | 6.63E-05 | 6.63E-05 | 6.63E-05 | 6.63E-05 | 6.63E-05 | 6.63E-05 | 6.63E-05 | 6.63E-05 | 6.63E-05 | 6.63E-05 | 6.63E-05 | 6.63E-05 | 6.63E-05 | 6.63E-05 | 6.63E-05 | 6.63E-05 | 6.63E-05 | 6.63E-05 |
| Si, mol/l | 0.00E+00 | 1.00E-03 | 1.00E-03 | 1.00E-03 | 1.00E-03 | 1.00E-03 | 1.00E-03 | 1.00E-03 | 1.00E-03 | 1.00E-03 | 1.00E-03 | 1.00E-03 | 1.00E-03 | 1.00E-03 | 1.00E-03 | 1.00E-03 | 1.00E-03 | 1.00E-03 | 1.00E-03 | 1.00E-03 |
| K, mol/l (±5%) | 7.52E-07 | 1.58E-04 | 1.30E-04 | 1.40E-04 | 1.38E-04 | 1.40E-04 | 1.55E-04 | 1.48E-04 | 1.48E-04 | 1.50E-04 | 1.37E-04 | 1.38E-04 | 1.98E-04 | 1.08E-04 | 1.16E-04 | 1.29E-04 | 1.10E-04 | 1.24E-04 | 1.16E-04 | 3.41E-04 |
| Ca, mol/l (±2%) | 2.30E-06 | 7.59E-03 | 7.17E-03 | 7.09E-03 | 7.00E-03 | 7.66E-03 | 8.15E-03 | 7.69E-03 | 8.09E-03 | 7.27E-03 | 7.28E-03 | 6.67E-03 | 7.19E-03 | 6.22E-03 | 6.71E-03 | 7.29E-03 | 5.56E-03 | 6.03E-03 | 5.82E-03 | 5.99E-03 |
| Mn, mol/l | 5.40E-07 | 5.51E-05 | 5.33E-05 | 5.24E-05 | 5.14E-05 | 5.43E-05 | 5.73E-05 | 5.65E-05 | 5.65E-05 | 6.54E-05 | 5.11E-05 | 4.52E-05 | 8.59E-05 | 4.77E-05 | 5.02E-05 | 5.67E-05 | 6.51E-05 | 7.13E-05 | 7.41E-05 | 7.76E-05 |
| Fe, mol/l | 0.00E+00 | 1.58E-04 | 1.48E-04 | 1.50E-04 | 1.57E-04 | 1.77E-04 | 2.08E-04 | 2.07E-04 | 1.44E-04 | 2.60E-04 | 1.70E-04 | 1.47E-04 | 7.24E-04 | 1.63E-04 | 1.68E-04 | 2.08E-04 | 1.09E-03 | 1.23E-03 | 1.40E-03 | 1.44E-03 |
| Sr, mol/l | 0.00E+00 | 4.59E-06 | 4.32E-06 | 4.34E-06 | 4.29E-06 | 4.35E-06 | 4.22E-06 | 3.95E-06 | 3.86E-06 | 2.51E-06 | 3.57E-06 | 3.14E-06 | 3.90E-06 | 2.06E-06 | 1.90E-06 | 1.63E-06 | 5.73E-07 | 2.59E-07 | 1.56E-07 | 0.00E+00 |
| Ba, mol/l | 8.42E-07 | 1.15E-06 | 1.16E-06 | 1.13E-06 | 1.08E-06 | 1.13E-06 | 1.13E-06 | 1.13E-06 | 1.05E-06 | 9.73E-07 | 9.76E-07 | 1.61E-06 | 1.63E-06 | 8.37E-07 | 7.67E-07 | 7.99E-07 | 7.46E-07 | 6.44E-07 | 5.67E-07 | 5.65E-07 |
| Na (est), mol/l | | 1.36E+00 | 1.36E+00 | 1.36E+00 | 1.36E+00 | 1.36E+00 | 1.36E+00 | 1.36E+00 | 1.36E+00 | 1.36E+00 | 1.36E+00 | 1.36E+00 | 1.36E+00 | 1.36E+00 | 1.36E+00 | 1.36E+00 | 1.36E+00 | 1.36E+00 | 1.36E+00 | 1.36E+00 |
| Alkalinity(est), mol/l | | 1.52E-02 | 1.43E-02 | 1.42E-02 | 1.40E-02 | 1.53E-02 | 1.63E-02 | 1.54E-02 | 1.62E-02 | 1.45E-02 | 1.46E-02 | 1.33E-02 | 1.44E-02 | 1.24E-02 | 1.34E-02 | 1.46E-02 | 1.11E-02 | 1.21E-02 | 1.16E-02 | 1.20E-02 |
| Fluid in exp. (kg) | | 0.010 | 0.010 | 0.010 | 0.010 | 0.010 | 0.010 | 0.010 | 0.010 | 0.010 | 0.010 | 0.010 | 0.010 | 0.010 | 0.010 | 0.010 | 0.010 | 0.010 | 0.010 | 0.010 |

| STATIC: 1.36M NaCl, 31bar pCO2, 70C | | |
|---|---|---|
| Time, hours | Std. Dev. Mol/l | 1103.7 |
| VCT, hours | | |
| Mg, mol/l | 1.34E-06 | 3.98E-03 |
| Al, mol/l | 1.29E-05 | 0.00E+00 |
| Si, mol/l | 0.00E+00 | 1.12E-03 |

| | | |
|---|---|---|
| K, mol/l (±25%) | 7.52E-07 | 1.16E-02 |
| Ca, mol/l (±25%) | 2.30E-06 | 2.14E-02 |
| Mn, mol/l | 5.40E-07 | 8.41E-05 |
| Fe, mol/l | 0.00E+00 | 2.38E-03 |
| Sr, mol/l | 0.00E+00 | 4.18E-05 |
| Ba, mol/l | 8.42E-07 | 1.92E-06 |
| Na (est), mol/l | | 1.36E+00 |
| Alkalinity(est), mol/l | | 4.27E-02 |
| Fluid in exp. (kg) | | 0.010 |

| SC2: 1.36M NaCl, 31bar pCO2, 70C | | | | | |
|---|---|---|---|---|---|
| Time, hours | Std. Dev. Mol/l | | | | |
| VCT, hours | | 0 | 2185.812 | 2587.753 | 2743.553 |
| Mg, mol/l | 6.47E-06 | 8.87E-05 | 4.89E-03 | 6.42E-03 | 6.05E-03 |
| Al, mol/l | 5.09E-08 | 1.48E-06 | 1.07E-06 | 0.00E+00 | 5.86E-08 |
| Si, mol/l (±25%) | 2.64E-07 | 7.55E-05 | 3.79E-04 | 4.81E-04 | 4.29E-04 |
| K, mol/l (±25%) | 2.33E-06 | 2.32E-04 | 2.14E-04 | 3.40E-04 | 2.93E-04 |
| Ca, mol/l | 7.19E-06 | 8.14E-04 | 5.50E-03 | 7.39E-03 | 6.85E-03 |
| Mn, mol/l | 1.65E-09 | 2.85E-04 | 3.53E-04 | 5.16E-04 | 3.75E-04 |
| Fe, mol/l | 9.78E-09 | 3.21E-03 | 5.53E-03 | 6.26E-03 | 3.33E-03 |
| Sr, mol/l | 8.95E-09 | 1.44E-06 | 1.26E-06 | 1.60E-06 | 2.06E-06 |
| Ba, mol/l | 1.96E-09 | 1.50E-07 | 8.13E-07 | 8.56E-07 | 4.61E-07 |
| Na (est), mol/l | - | 1.36E+00 | 1.36E+00 | 1.36E+00 | 1.36E+00 |
| Alkalinity(est), mol/l | - | 1.63E-03 | 1.10E-02 | 1.48E-02 | 1.37E-02 |
| Fluid in exp. (kg) | - | 0.010 | 0.010 | 0.010 | 0.010 |

# Appendix B Selected Modelling Outputs

The following appendix will present selected output from the various pieces of modelling carried out using PHREEQC3 discussed elsewhere in this work.

## B.1 pH Calculations

pH during the dissolution experiments, described in Sections 4, 5 & 6, was calculated using PHREEQC3. Analysed solution compositions, corrected for dilution etc., were formatted into an input file designed to back calculate pH speciation and mineral saturation indices of the samples fluids. The figures below were constructed for each experiment to illustrate estimated pH behaviour during the experiments. Details on experimental conditions and set-up can be found in the main text (Chapters 3 – 5).

## B.1.1 Quartz Experiments

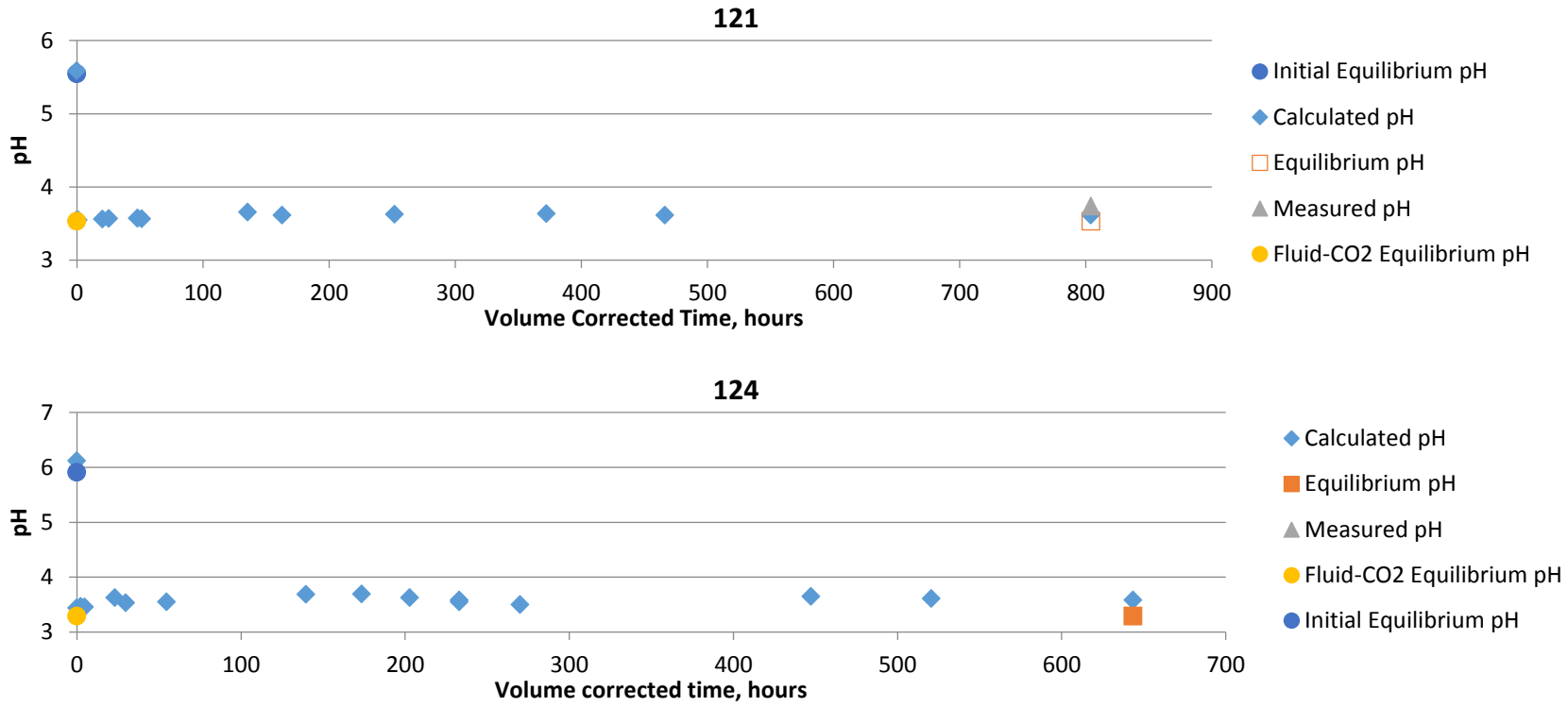

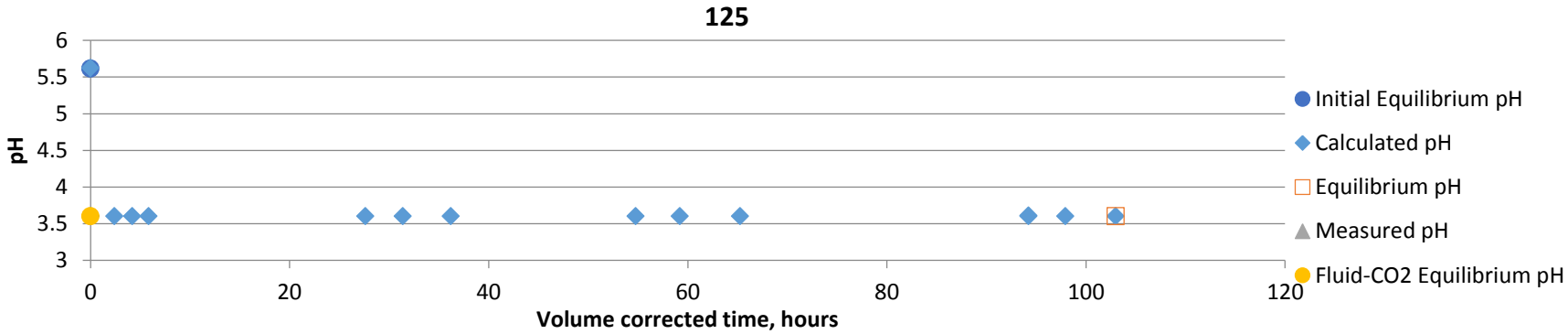
125
pH
6
5.5
5
4.5
4
3.5
3
0
20
40
60
80
100
120
Volume corrected time, hours
Initial Equilibrium pH
Calculated pH
Equilibrium pH
Measured pH
Fluid-CO2 Equilibrium pH

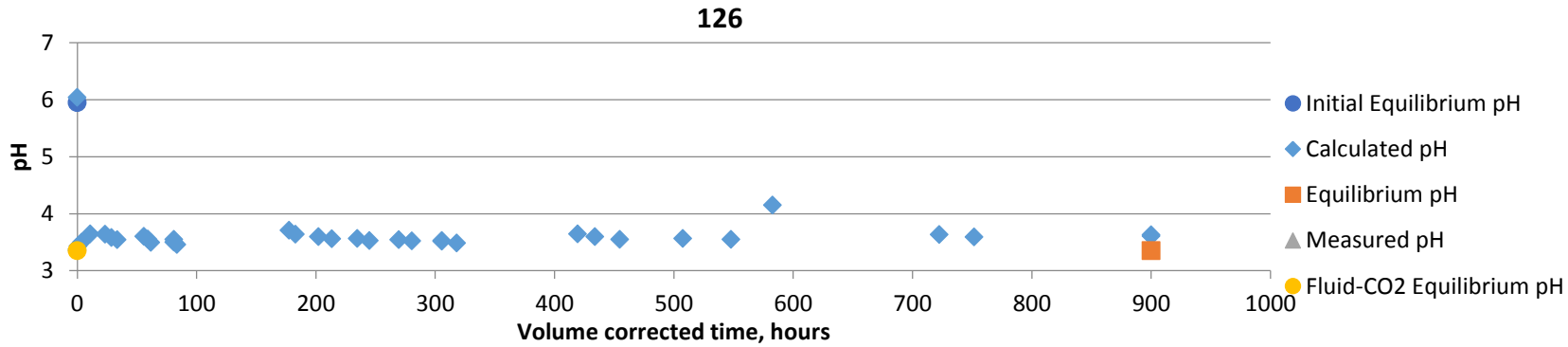
126
pH
7
6
5
4
3
0
100
200
300
400
500
600
700
800
900
1000
Volume corrected time, hours
Initial Equilibrium pH
Calculated pH
Equilibrium pH
Measured pH
Fluid-CO2 Equilibrium pH

## B.1.2 K-Feldspar Experiments

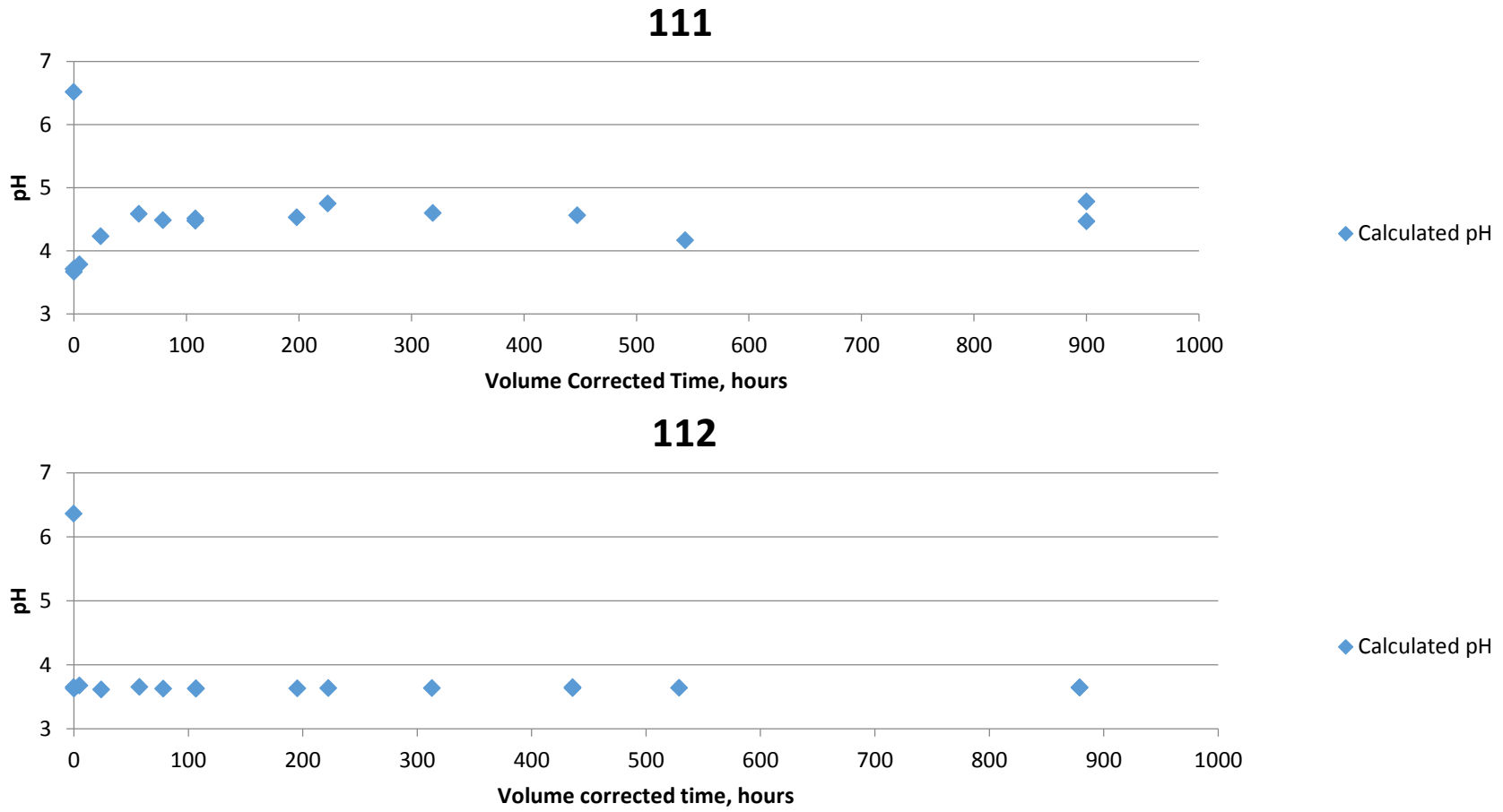

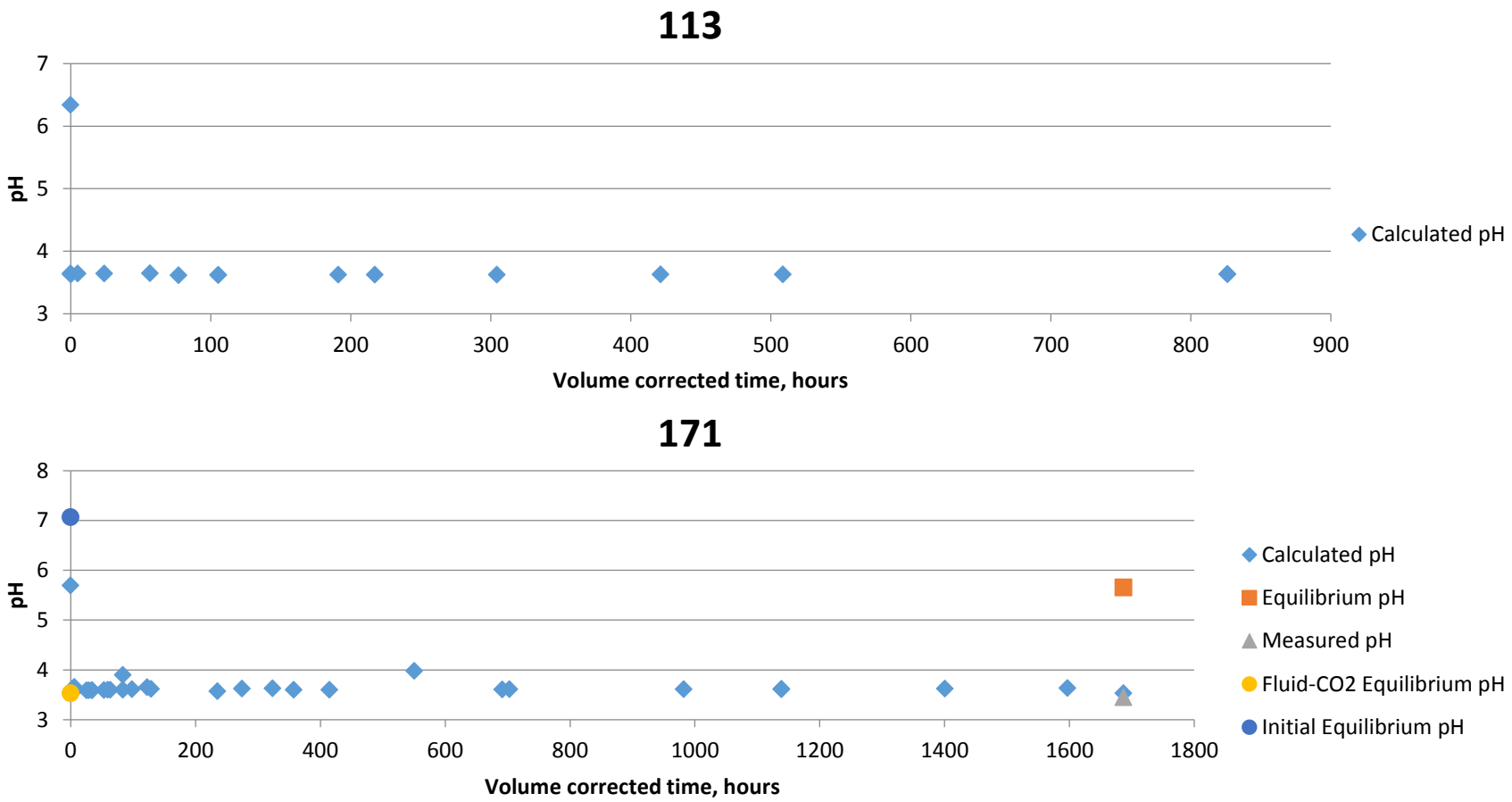
113
pH
7
6
5
4
3
0
100
200
300
400
500
600
700
800
900
Volume corrected time, hours
Calculated pH
171
pH
8
7
6
5
4
3
0
200
400
600
800
1000
1200
1400
1600
1800
Volume corrected time, hours
Calculated pH
Equilibrium pH
Measured pH
Fluid-CO2 Equilibrium pH
Initial Equilibrium pH

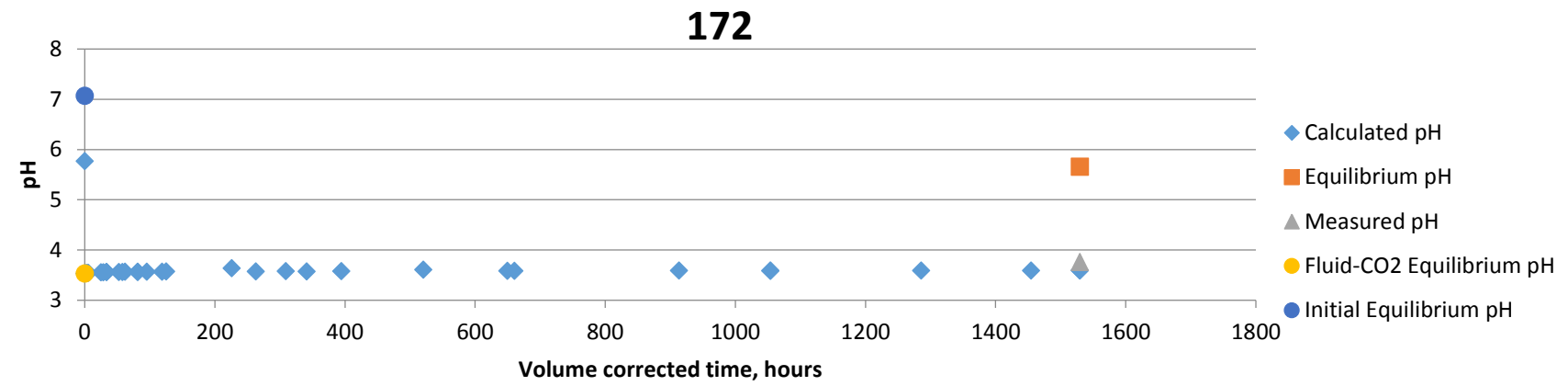
172
8
7
6
5
4
3
pH
0
200
400
600
800
1000
1200
1400
1600
1800
Volume corrected time, hours
Calculated pH
Equilibrium pH
Measured pH
Fluid-CO2 Equilibrium pH
Initial Equilibrium pH

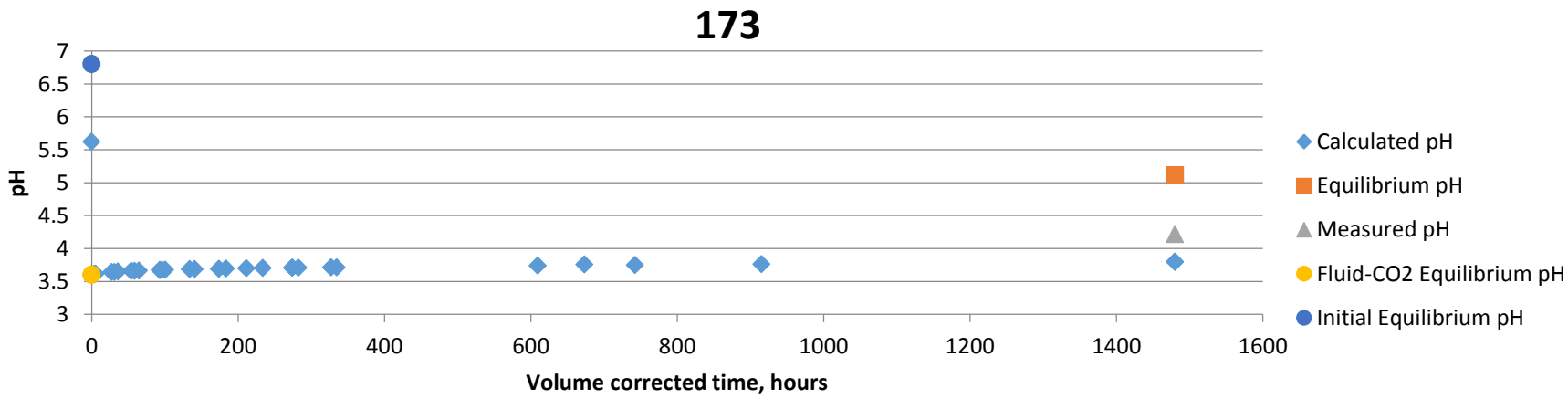
173
7
6.5
6
5.5
5
4.5
4
3.5
3
pH
0
200
400
600
800
1000
1200
1400
1600
Volume corrected time, hours
Calculated pH
Equilibrium pH
Measured pH
Fluid-CO2 Equilibrium pH
Initial Equilibrium pH

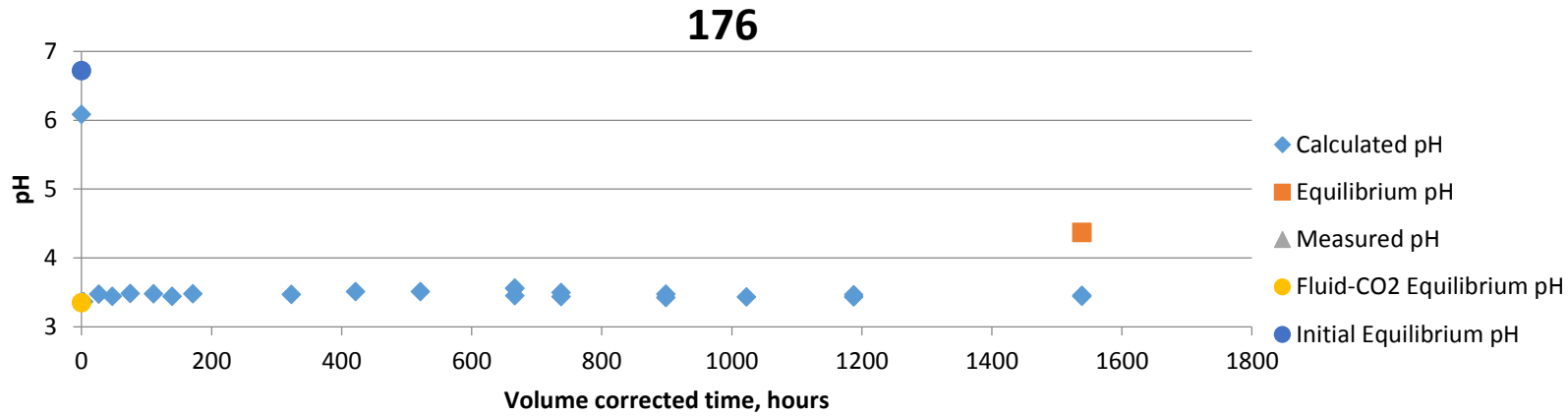
176
pH
7
6
5
4
3
0
200
400
600
800
1000
1200
1400
1600
1800
Volume corrected time, hours
Calculated pH
Equilibrium pH
Measured pH
Fluid-CO2 Equilibrium pH
Initial Equilibrium pH

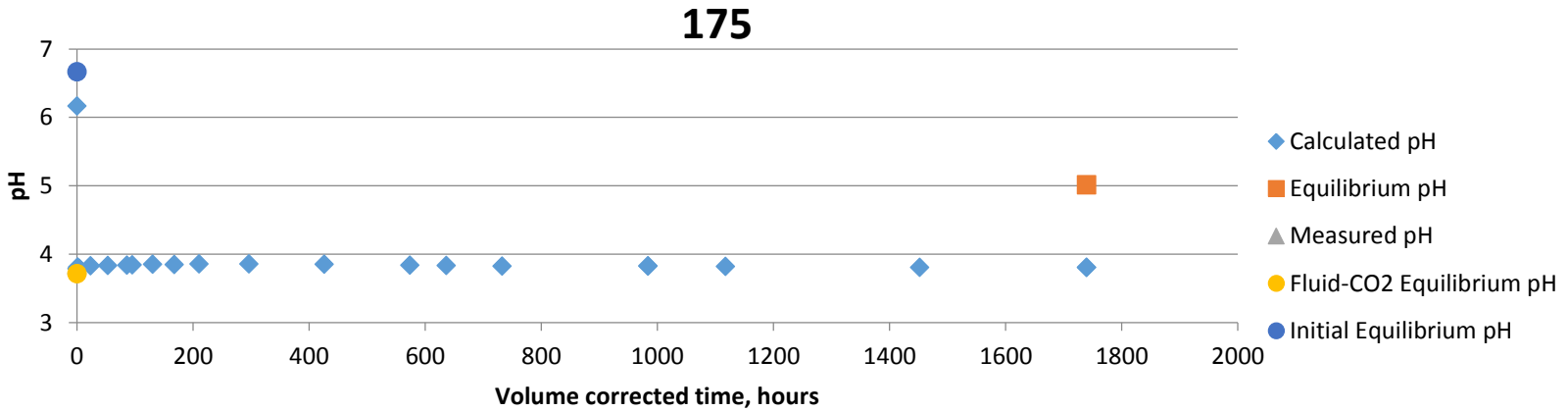
175
pH
7
6
5
4
3
0
200
400
600
800
1000
1200
1400
1600
1800
2000
Volume corrected time, hours
Calculated pH
Equilibrium pH
Measured pH
Fluid-CO2 Equilibrium pH
Initial Equilibrium pH

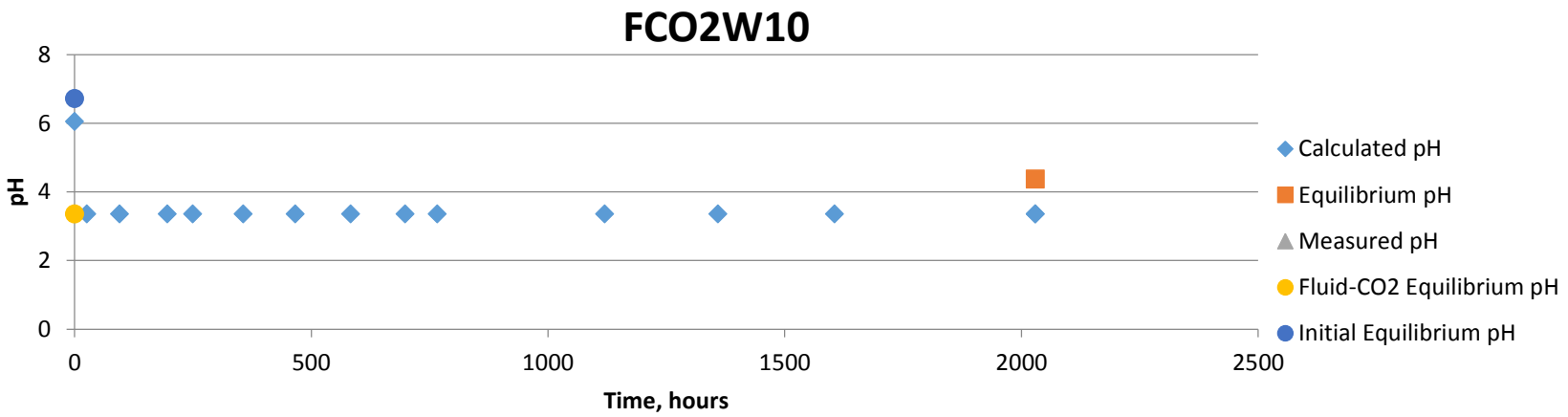
FCO2W10
8
6
4
2
0
pH
0
500
1000
1500
2000
2500
Time, hours
Calculated pH
Equilibrium pH
Measured pH
Fluid-CO2 Equilibrium pH
Initial Equilibrium pH

## B.1.3 Albite Experiments

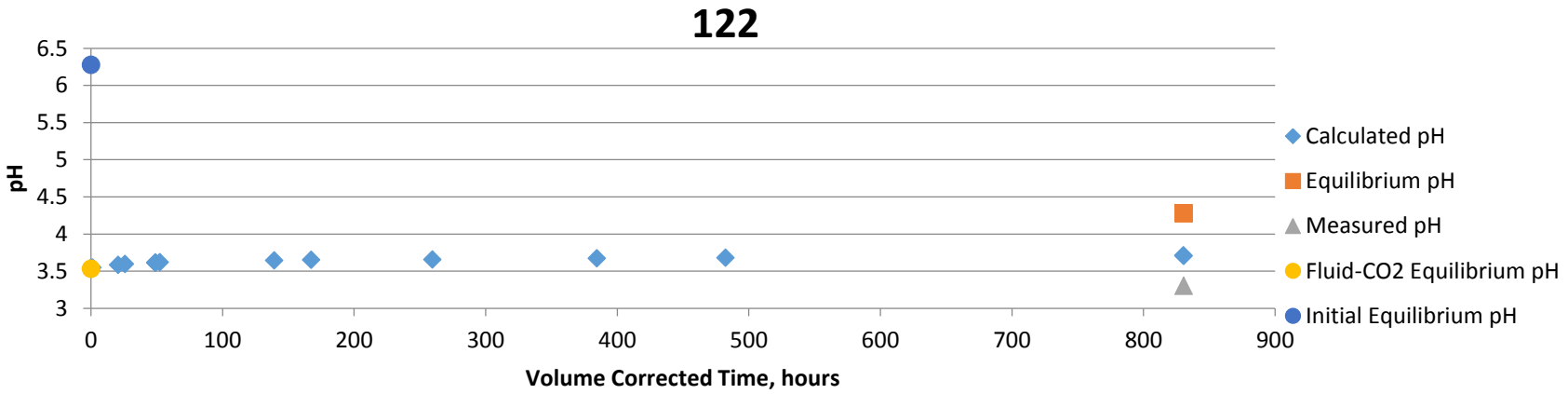


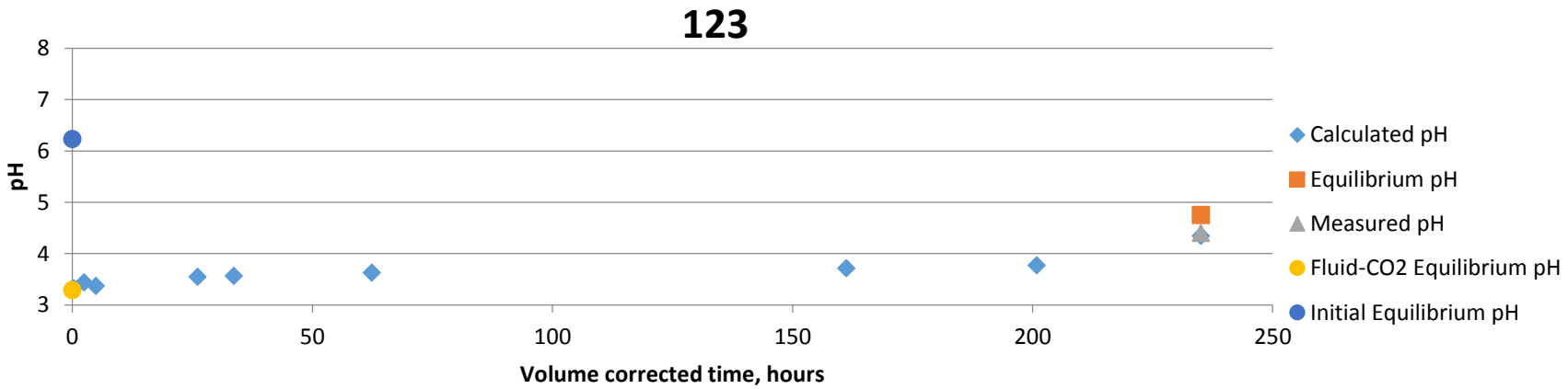

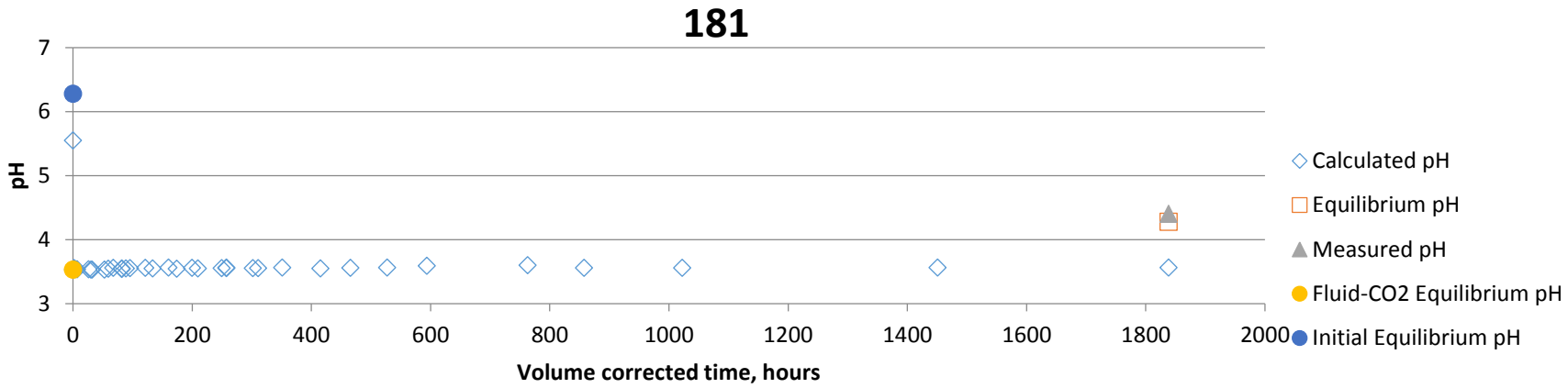
181
pH
7
6
5
4
3
0
200
400
600
800
1000
1200
1400
1600
1800
2000
Volume corrected time, hours
Calculated pH
Equilibrium pH
Measured pH
Fluid-CO2 Equilibrium pH
Initial Equilibrium pH

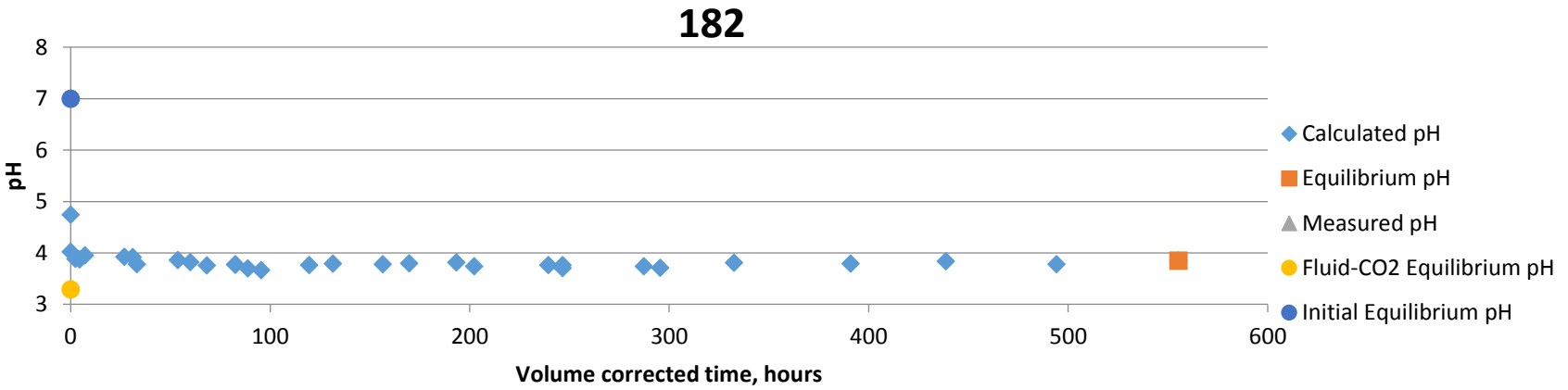
182
pH
8
7
6
5
4
3
0
100
200
300
400
500
600
Volume corrected time, hours
Calculated pH
Equilibrium pH
Measured pH
Fluid-CO2 Equilibrium pH
Initial Equilibrium pH

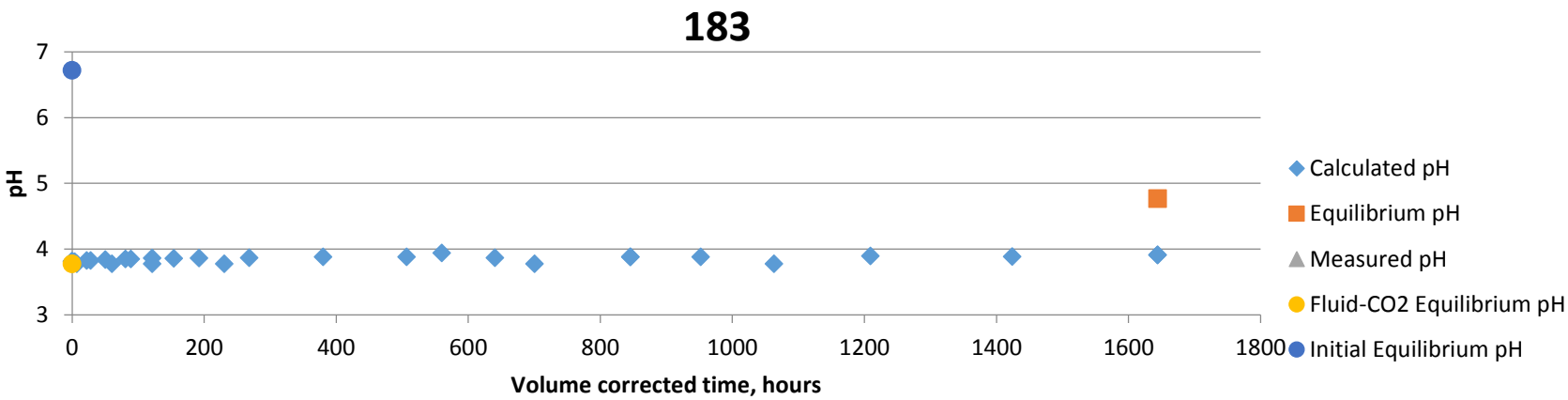
183
pH
7
6
5
4
3
0
200
400
600
800
1000
1200
1400
1600
1800
Volume corrected time, hours
Calculated pH
Equilibrium pH
Measured pH
Fluid-CO2 Equilibrium pH
Initial Equilibrium pH

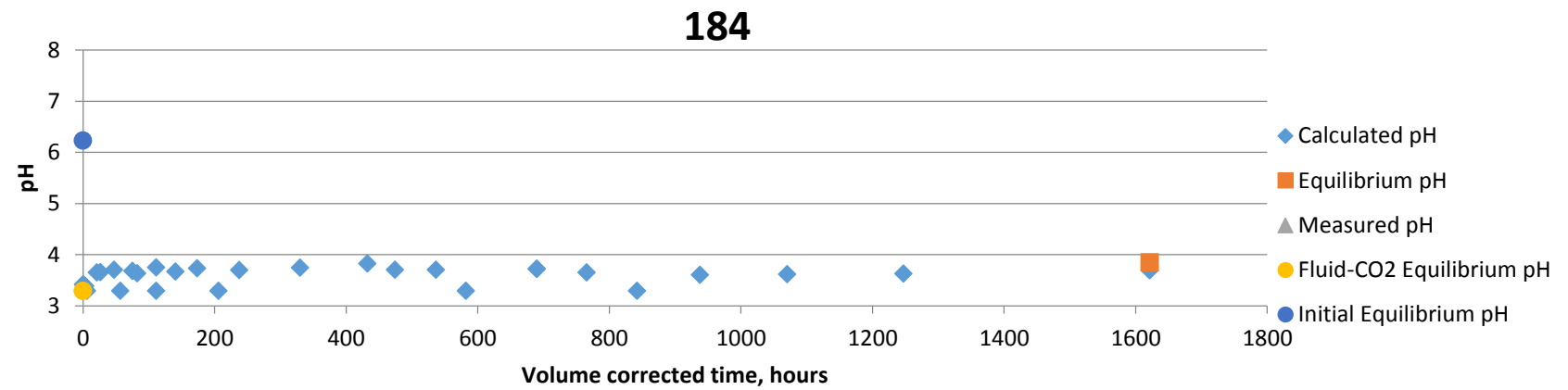
184
8
7
6
5
4
3
pH
0
200
400
600
800
1000
1200
1400
1600
1800
Volume corrected time, hours
Calculated pH
Equilibrium pH
Measured pH
Fluid-CO2 Equilibrium pH
Initial Equilibrium pH

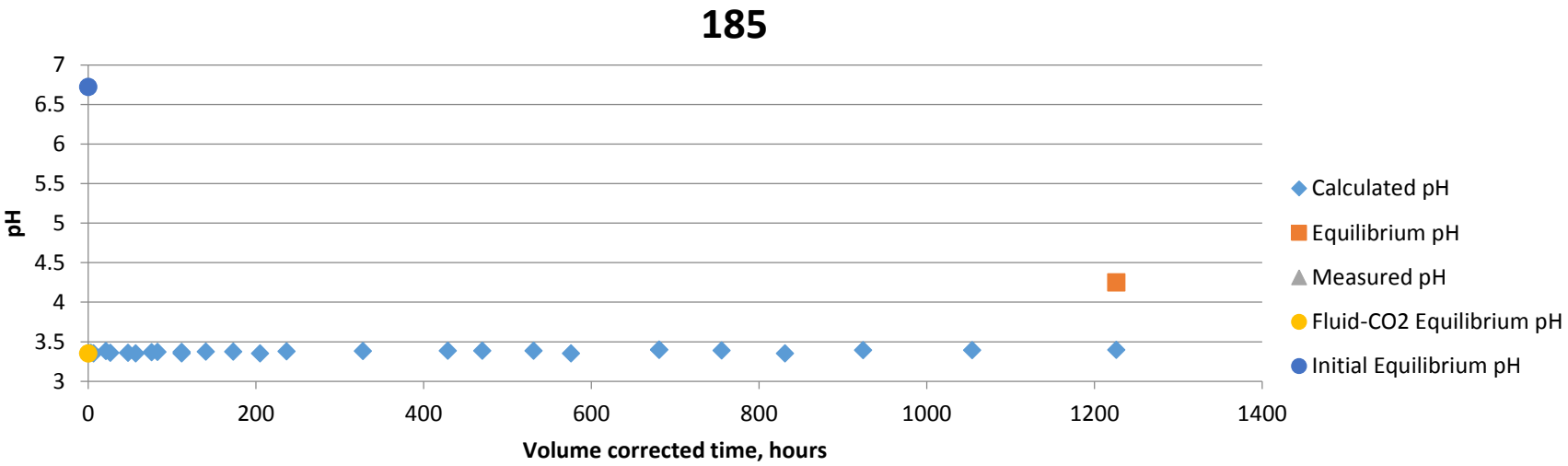
185
7
6.5
6
5.5
5
4.5
4
3.5
3
pH
0
200
400
600
800
1000
1200
1400
Volume corrected time, hours
Calculated pH
Equilibrium pH
Measured pH
Fluid-CO2 Equilibrium pH
Initial Equilibrium pH

## B.1.4 Calcite Experiments

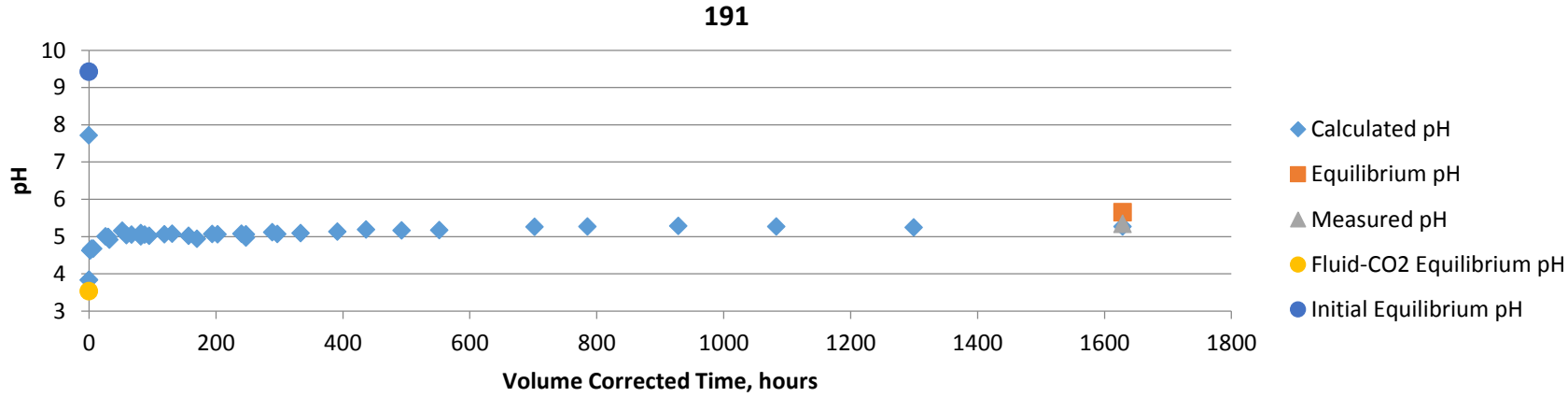


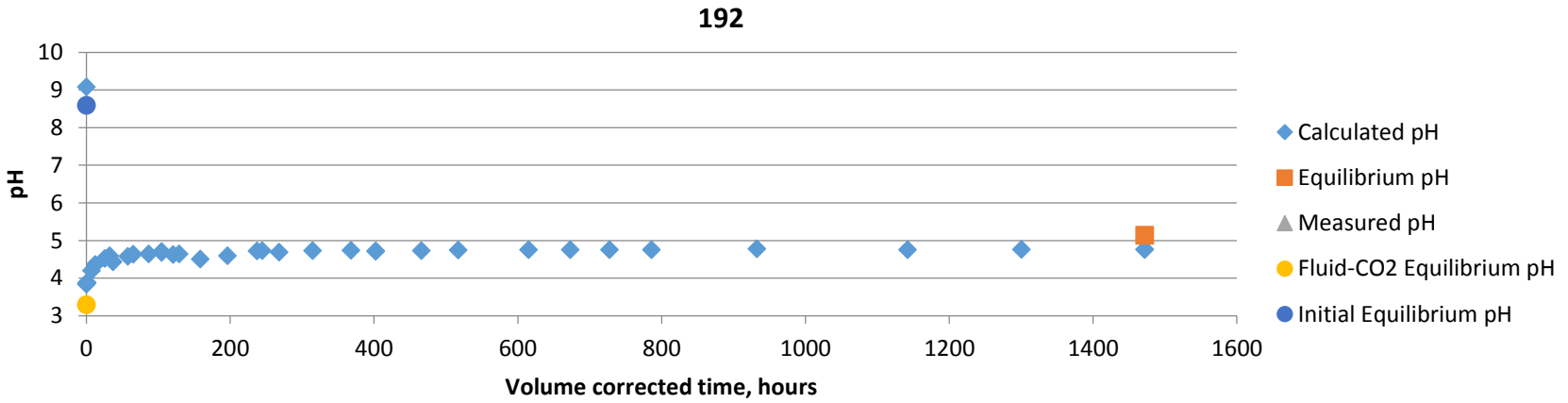

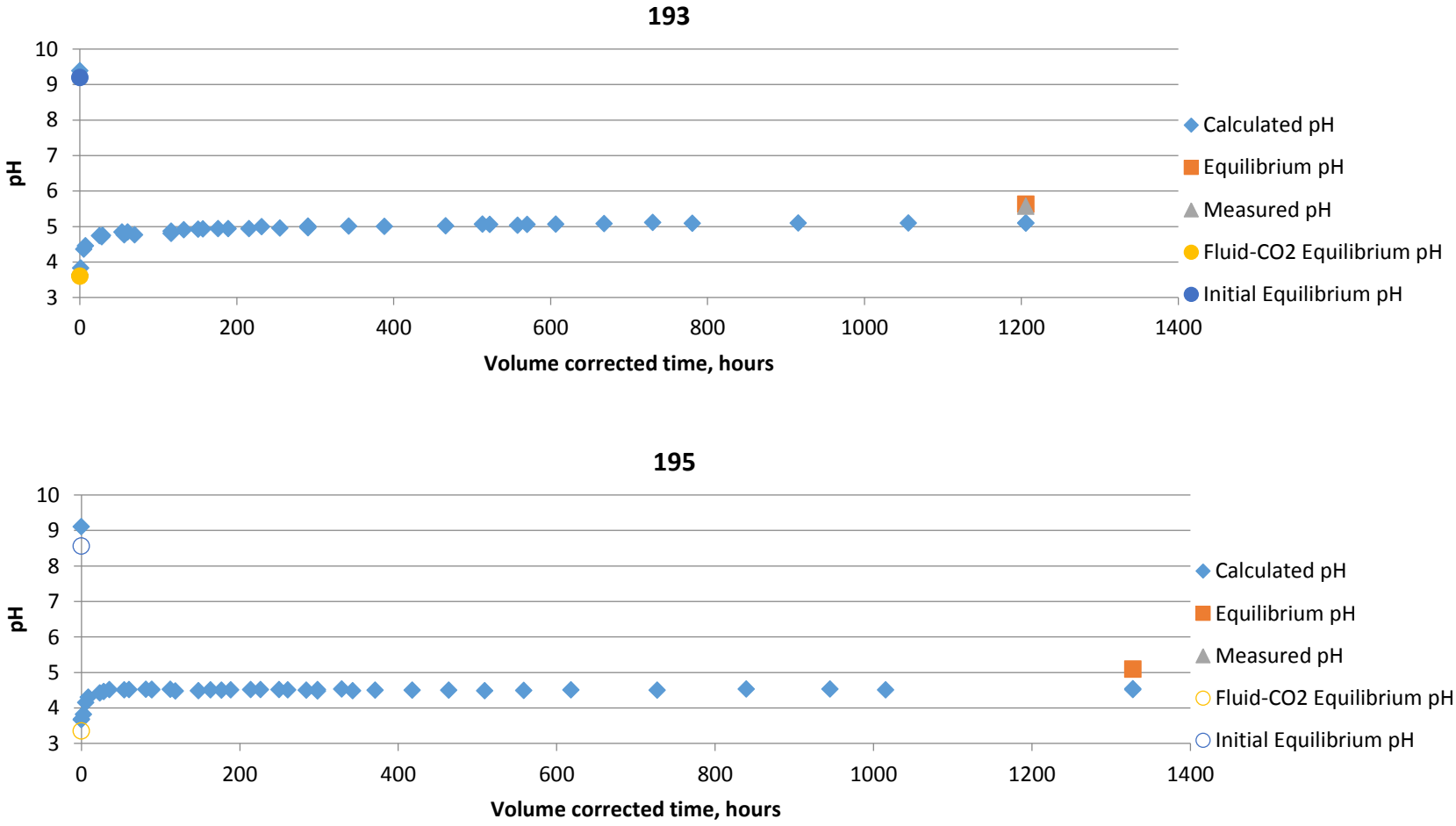
193
pH
Volume corrected time, hours
Calculated pH
Equilibrium pH
Measured pH
Fluid-CO2 Equilibrium pH
Initial Equilibrium pH
195
pH
Volume corrected time, hours
Calculated pH
Equilibrium pH
Measured pH
Fluid-CO2 Equilibrium pH
Initial Equilibrium pH

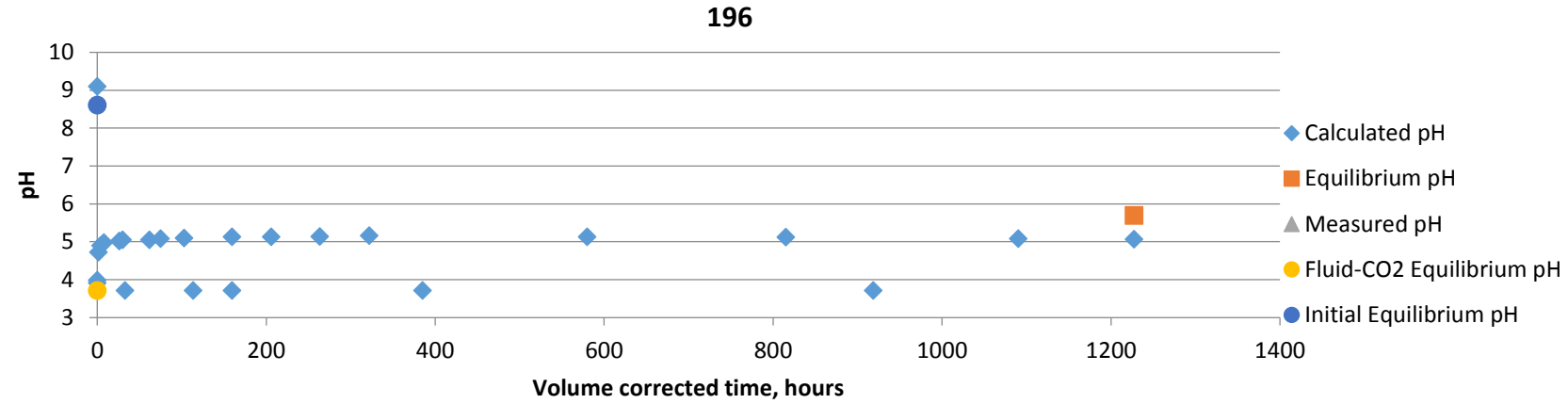
196
10
9
8
7
6
5
4
3
pH
0
200
400
600
800
1000
1200
1400
Volume corrected time, hours
Calculated pH
Equilibrium pH
Measured pH
Fluid-CO2 Equilibrium pH
Initial Equilibrium pH

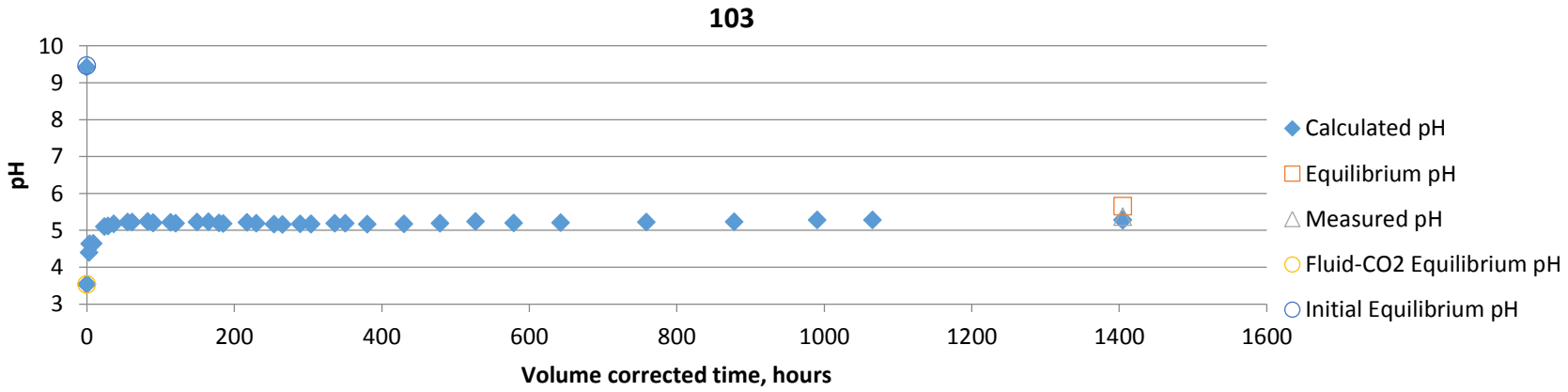
103
10
9
8
7
6
5
4
3
pH
0
200
400
600
800
1000
1200
1400
1600
Volume corrected time, hours
Calculated pH
Equilibrium pH
Measured pH
Fluid-CO2 Equilibrium pH
Initial Equilibrium pH

## B.1.5 Dolomite Experiments

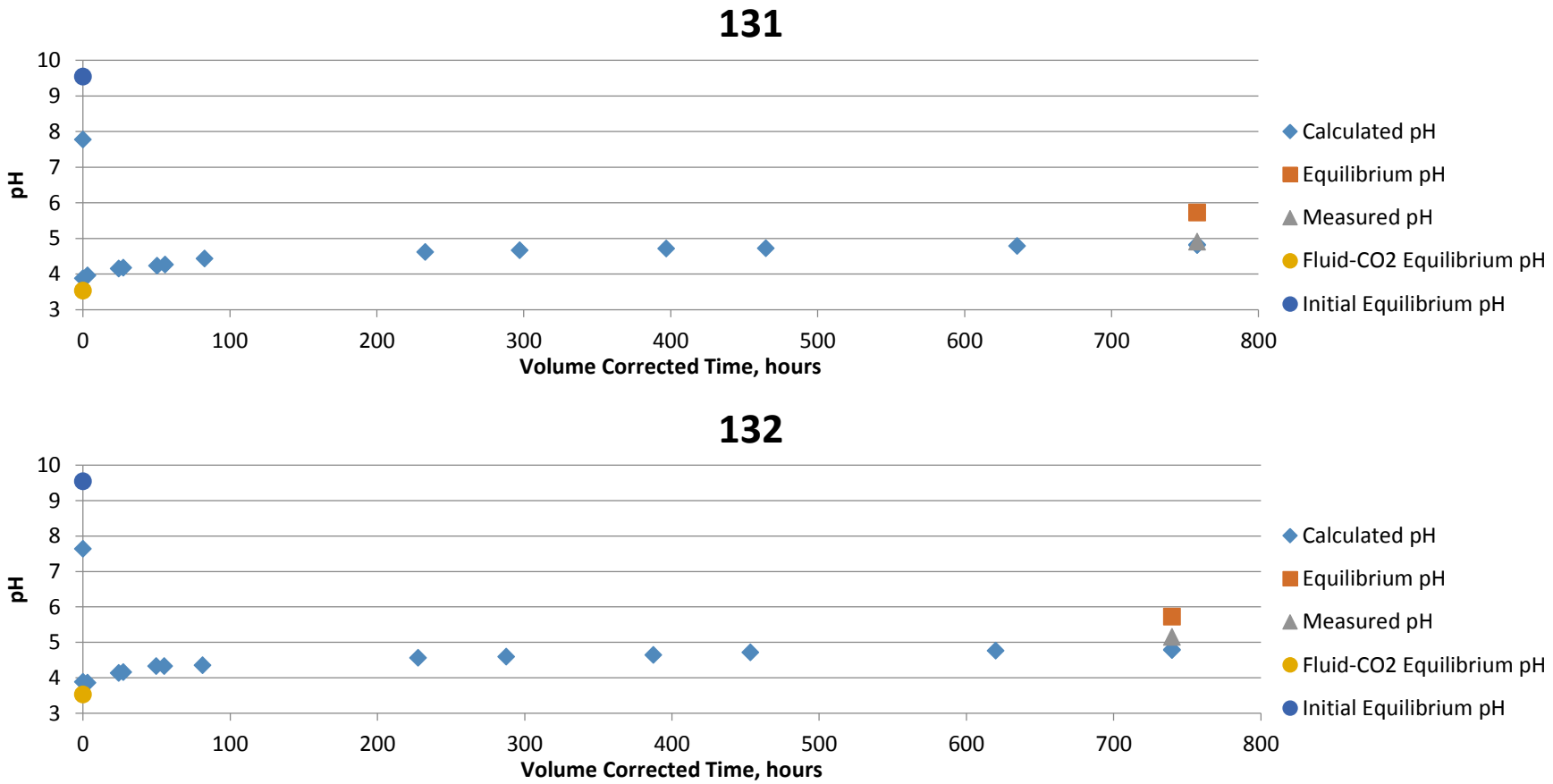

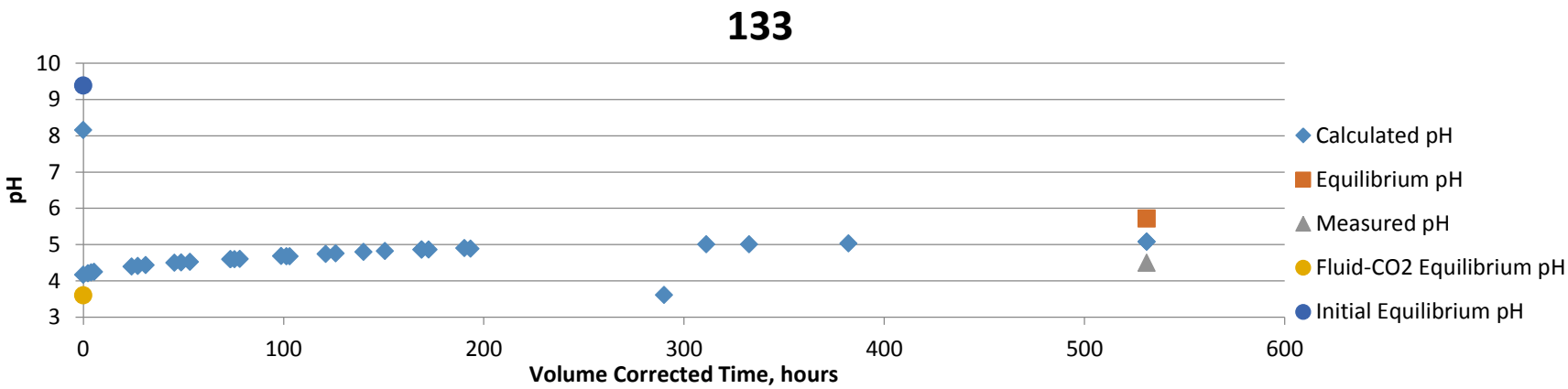
133
pH
Volume Corrected Time, hours
Calculated pH
Equilibrium pH
Measured pH
Fluid-CO2 Equilibrium pH
Initial Equilibrium pH

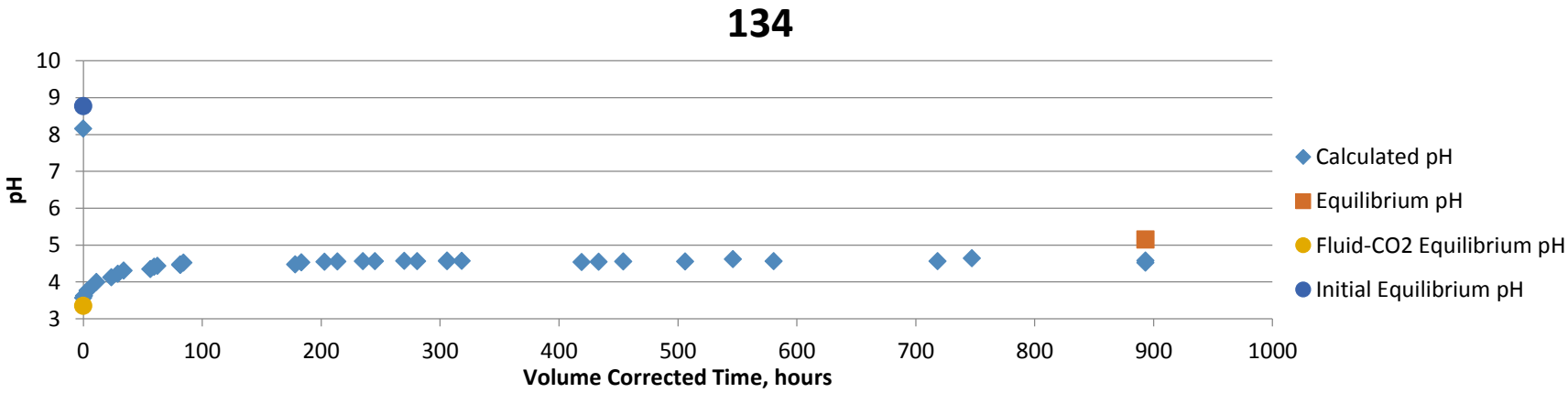
134
pH
Volume Corrected Time, hours
Calculated pH
Equilibrium pH
Fluid-CO2 Equilibrium pH
Initial Equilibrium pH

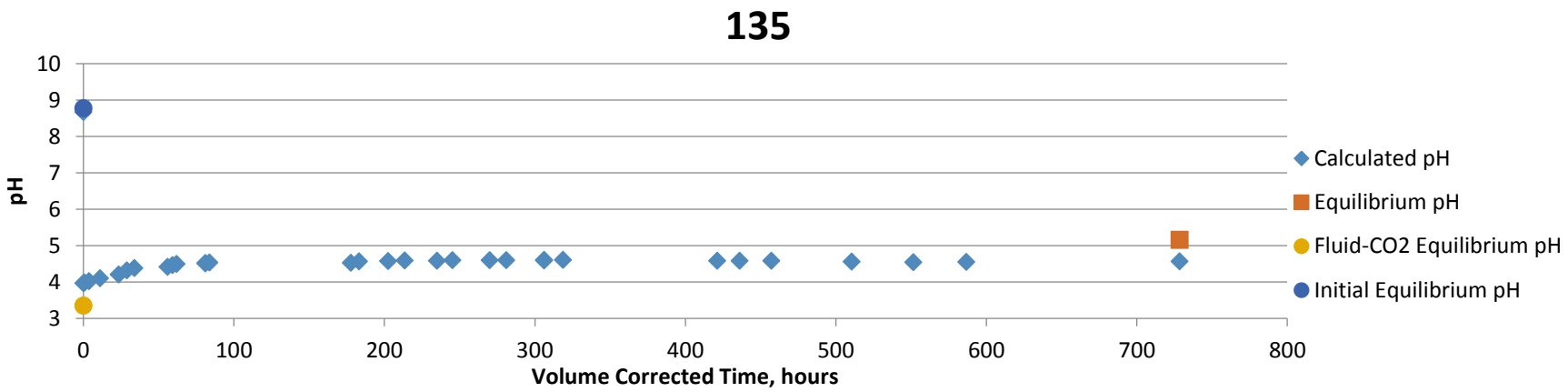
135
pH
10
9
8
7
6
5
4
3
0
100
200
300
400
500
600
700
800
Volume Corrected Time, hours
Calculated pH
Equilibrium pH
Fluid-CO2 Equilibrium pH
Initial Equilibrium pH

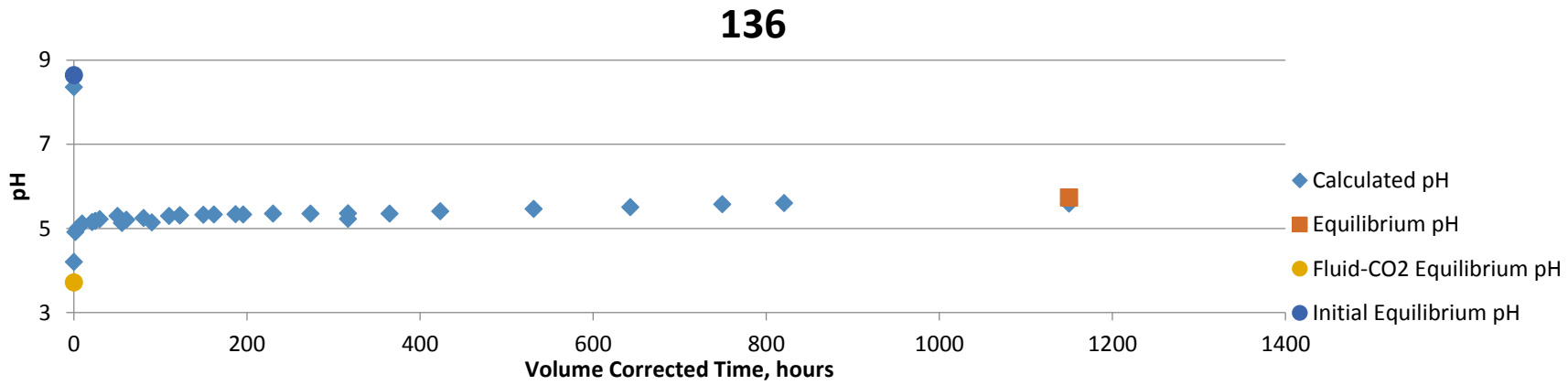
136
pH
9
7
5
3
0
200
400
600
800
1000
1200
1400
Volume Corrected Time, hours
Calculated pH
Equilibrium pH
Fluid-CO2 Equilibrium pH
Initial Equilibrium pH

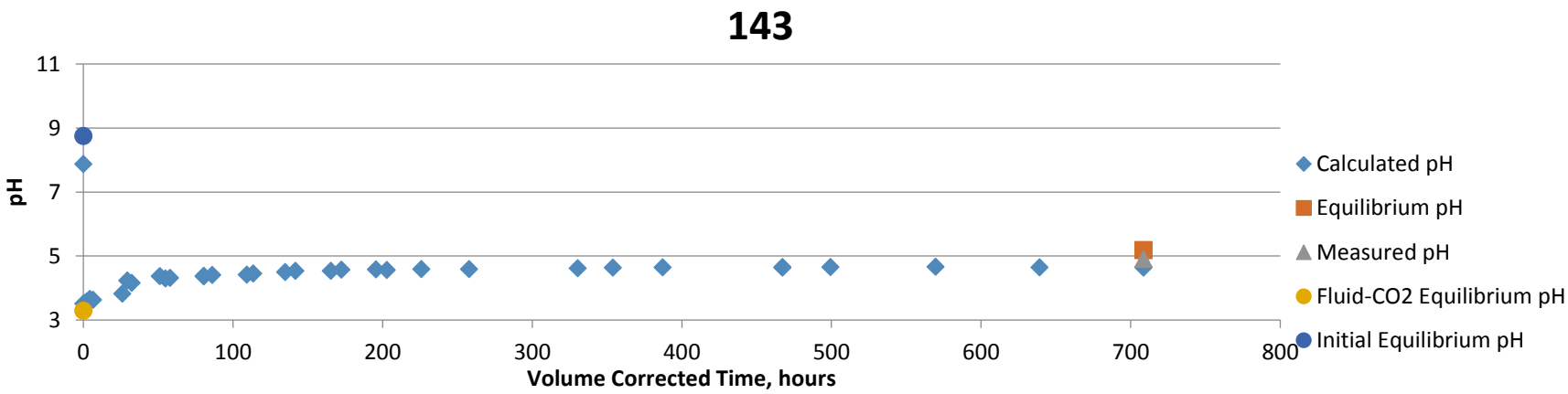
143
11
9
7
5
3
pH
0
100
200
300
400
500
600
700
800
Volume Corrected Time, hours
Calculated pH
Equilibrium pH
Measured pH
Fluid-CO2 Equilibrium pH
Initial Equilibrium pH

## B.1.6 Sandstone Experiments

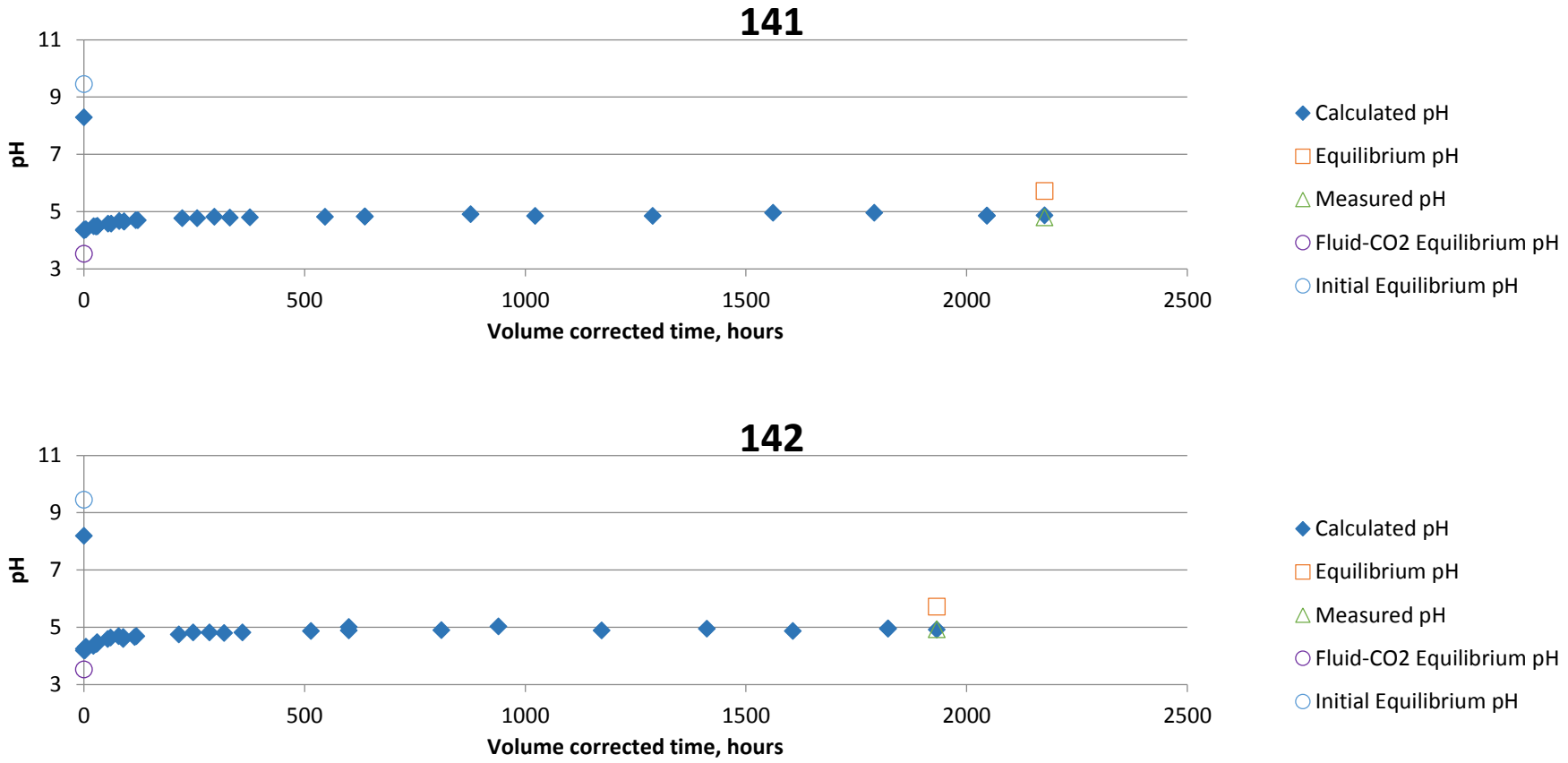

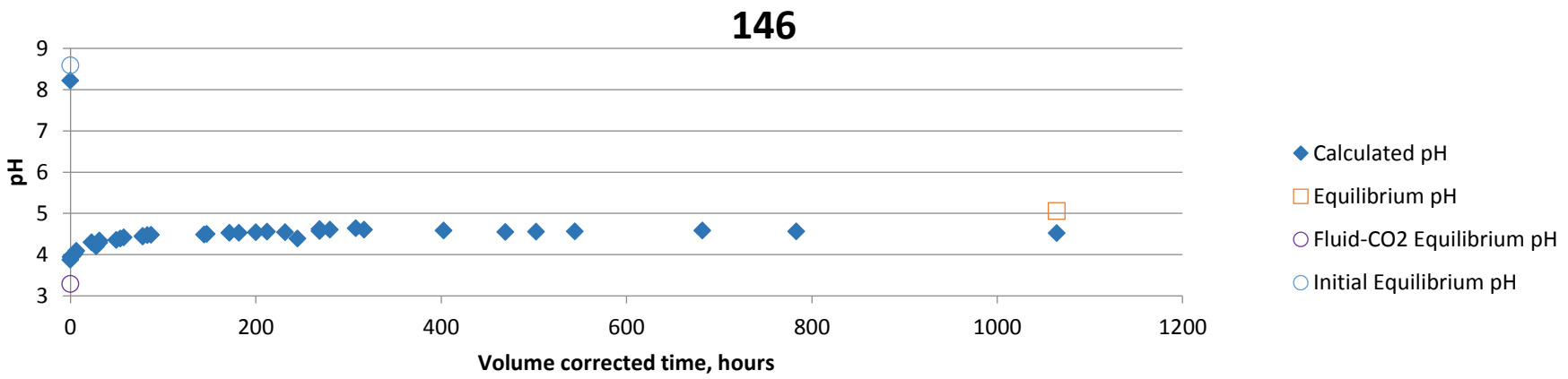
146
pH
9
8
7
6
5
4
3
0
200
400
600
800
1000
1200
Volume corrected time, hours
Calculated pH
Equilibrium pH
Fluid-CO2 Equilibrium pH
Initial Equilibrium pH

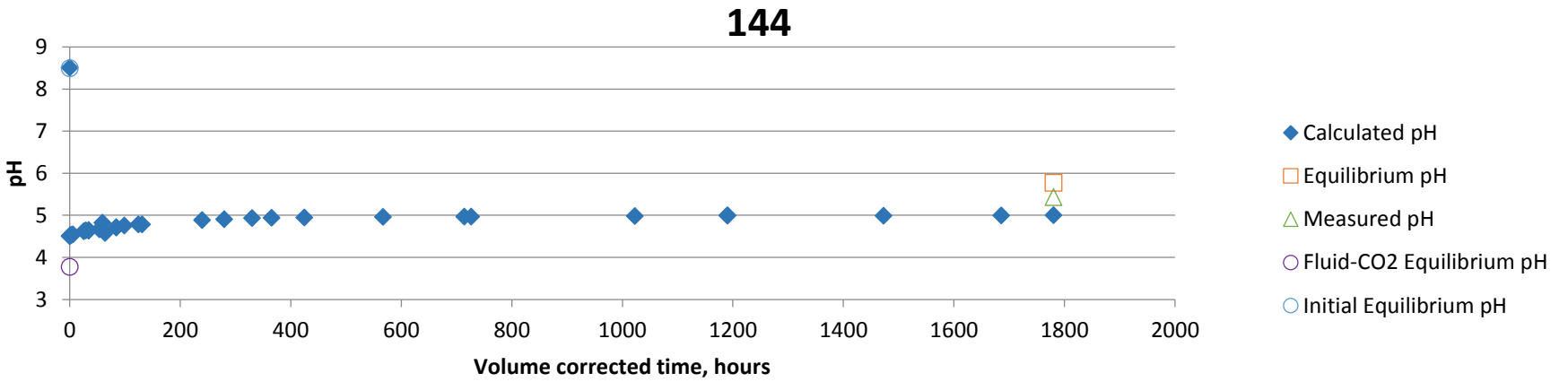
144
pH
9
8
7
6
5
4
3
0
200
400
600
800
1000
1200
1400
1600
1800
2000
Volume corrected time, hours
Calculated pH
Equilibrium pH
Measured pH
Fluid-CO2 Equilibrium pH
Initial Equilibrium pH

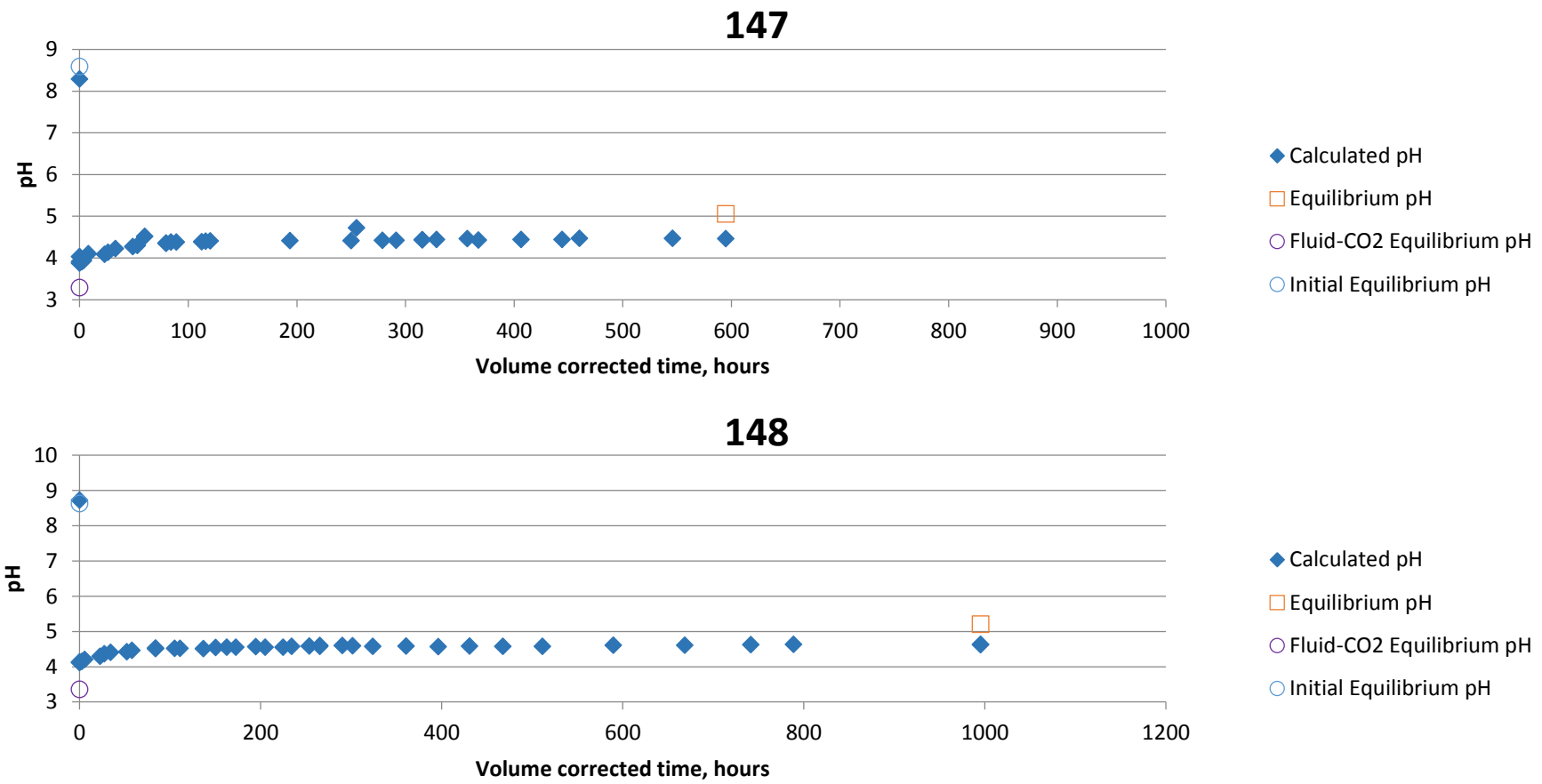
147
pH
Volume corrected time, hours
Calculated pH
Equilibrium pH
Fluid-CO2 Equilibrium pH
Initial Equilibrium pH
148
pH
Volume corrected time, hours
Calculated pH
Equilibrium pH
Fluid-CO2 Equilibrium pH
Initial Equilibrium pH

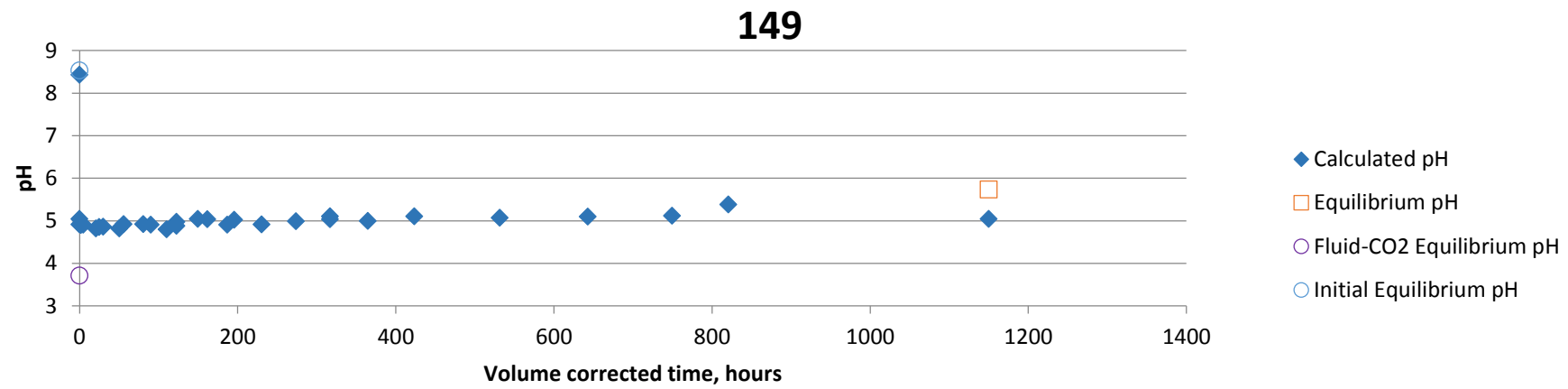
149
pH
9
8
7
6
5
4
3
0
200
400
600
800
1000
1200
1400
Volume corrected time, hours
Calculated pH
Equilibrium pH
Fluid-CO2 Equilibrium pH
Initial Equilibrium pH

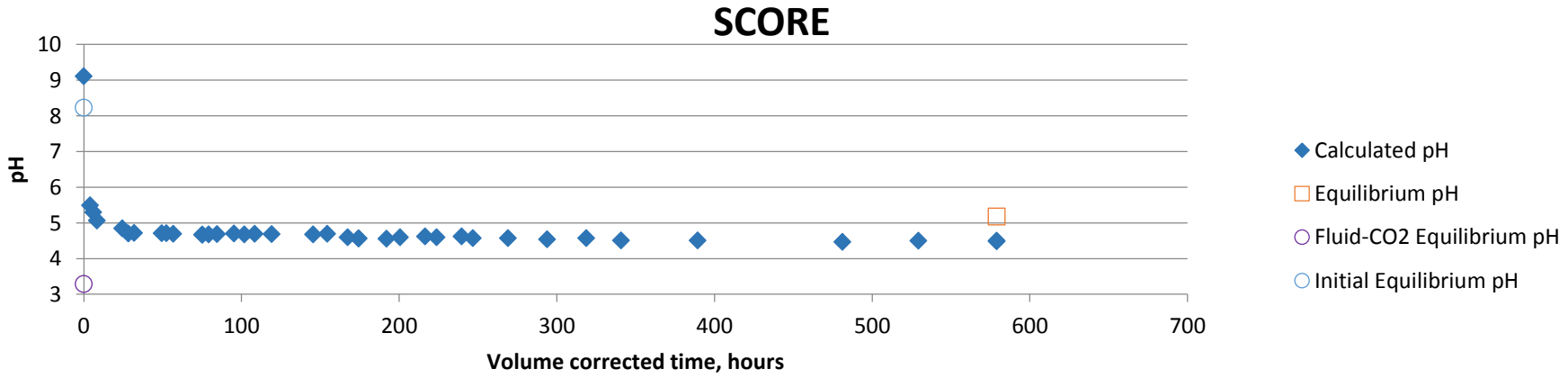
SCORE
pH
10
9
8
7
6
5
4
3
0
100
200
300
400
500
600
700
Volume corrected time, hours
Calculated pH
Equilibrium pH
Fluid-CO2 Equilibrium pH
Initial Equilibrium pH

## B.2 Kinetic Model Outputs

A kinetic model was built in order to simulate the dissolution of the Sherwood Sandstone material in each of the batch experiments. Details can be found in Section 5.1.5. Results of the modelling, showing selected elemental output, compared with measured elemental concentrations (where available), are shown in the following pages for each batch sandstone experiment carried out.

## B.2.1 Experiment 141

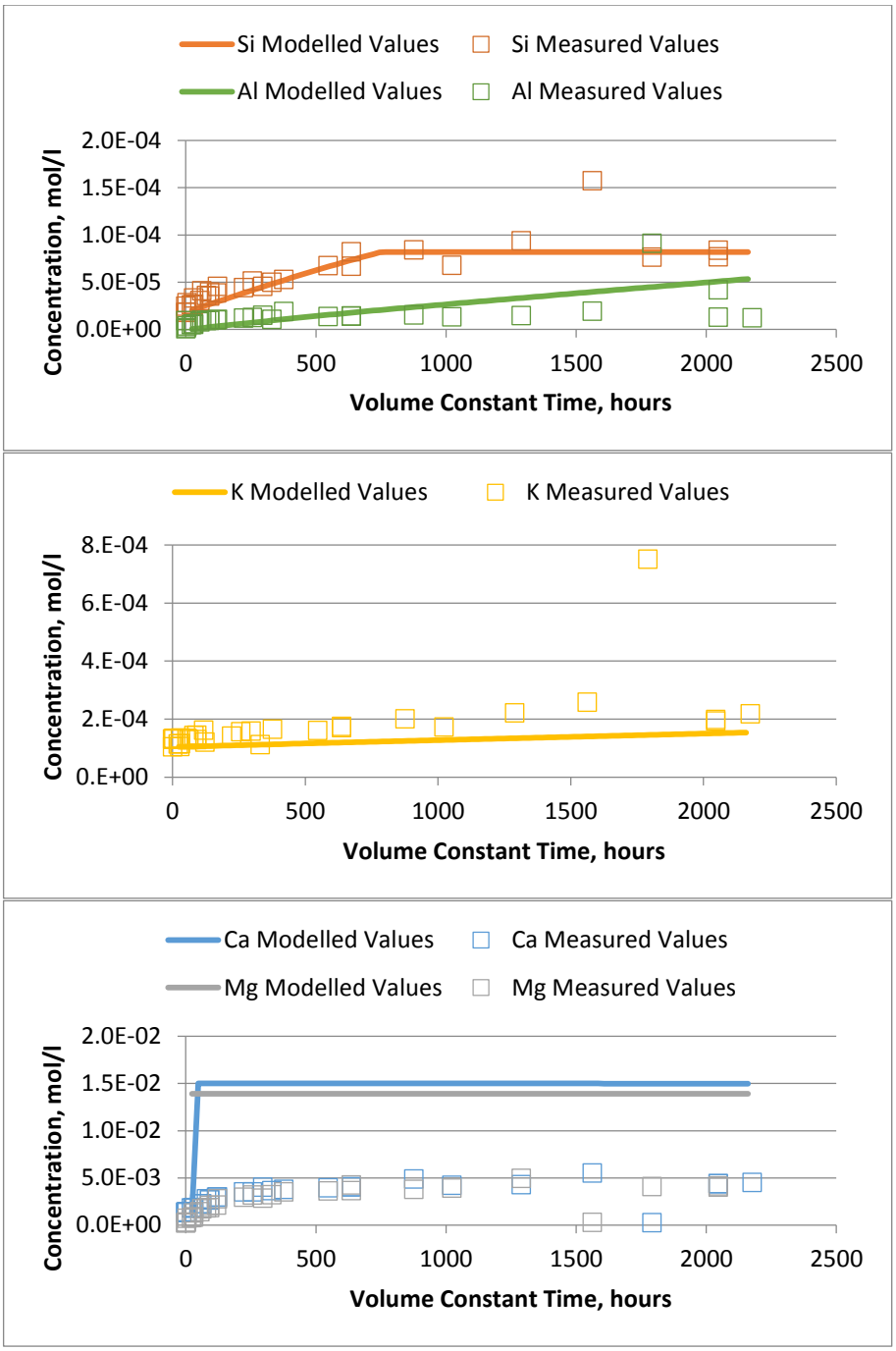

## B.2.2 Experiment 142

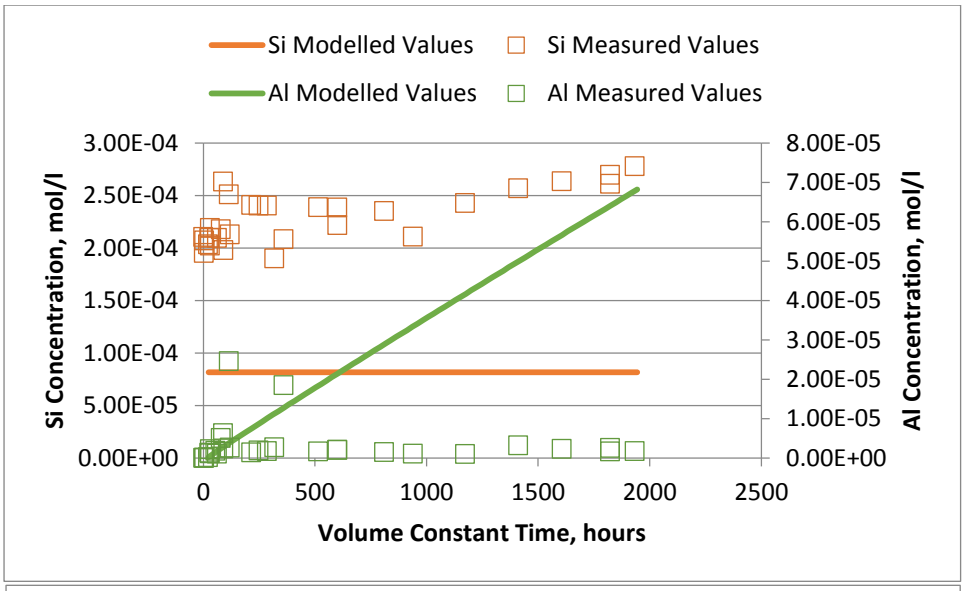


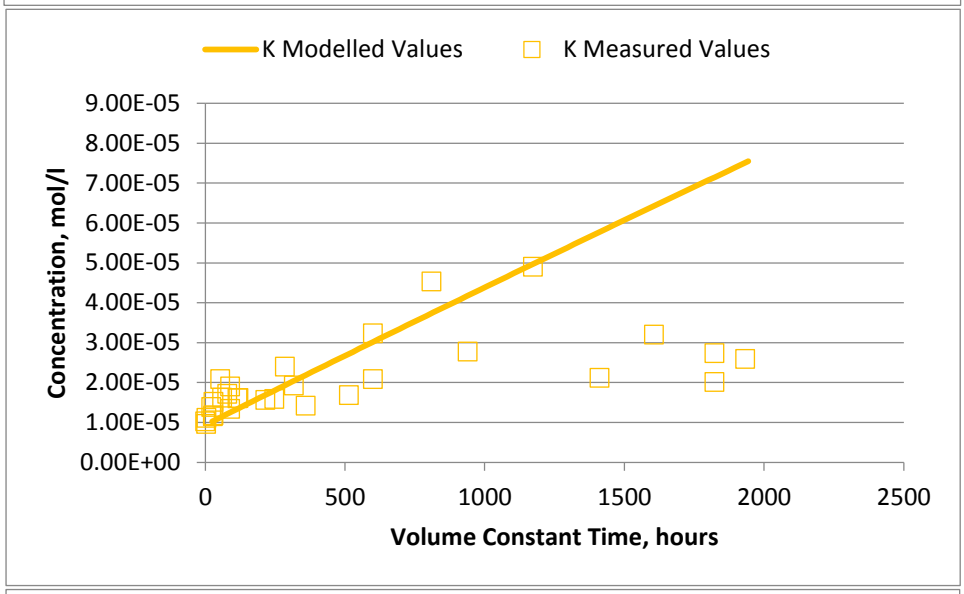


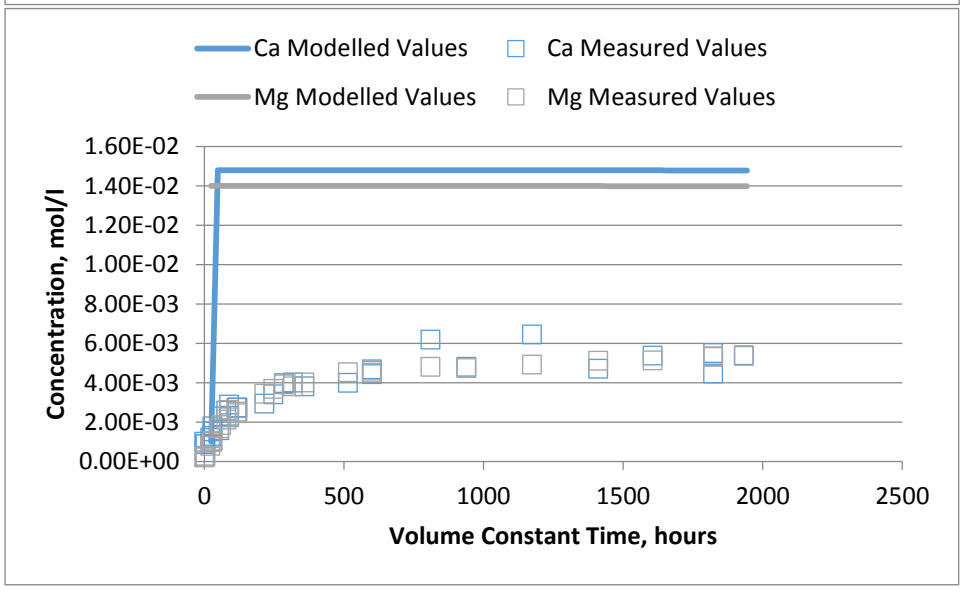

## B.2.3 Experiment 144

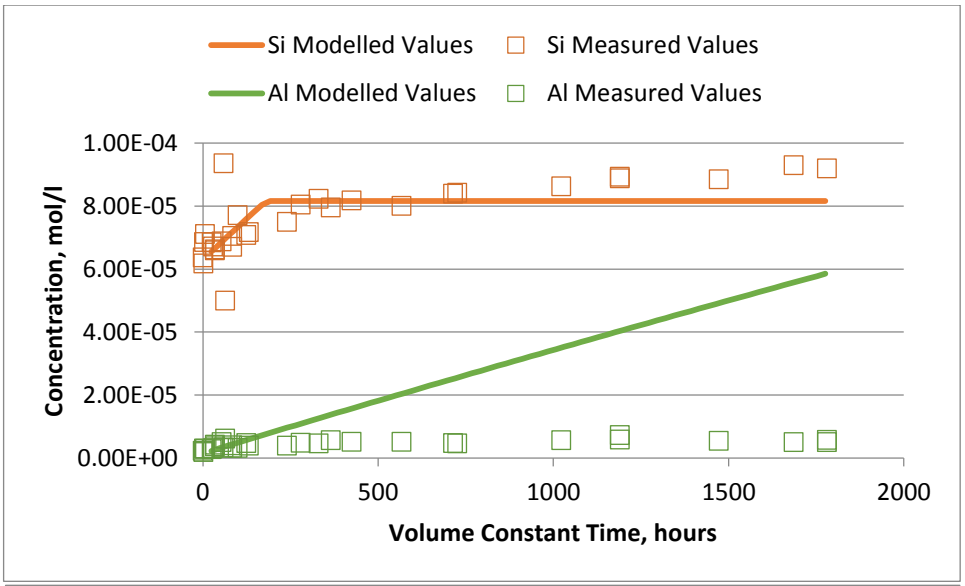


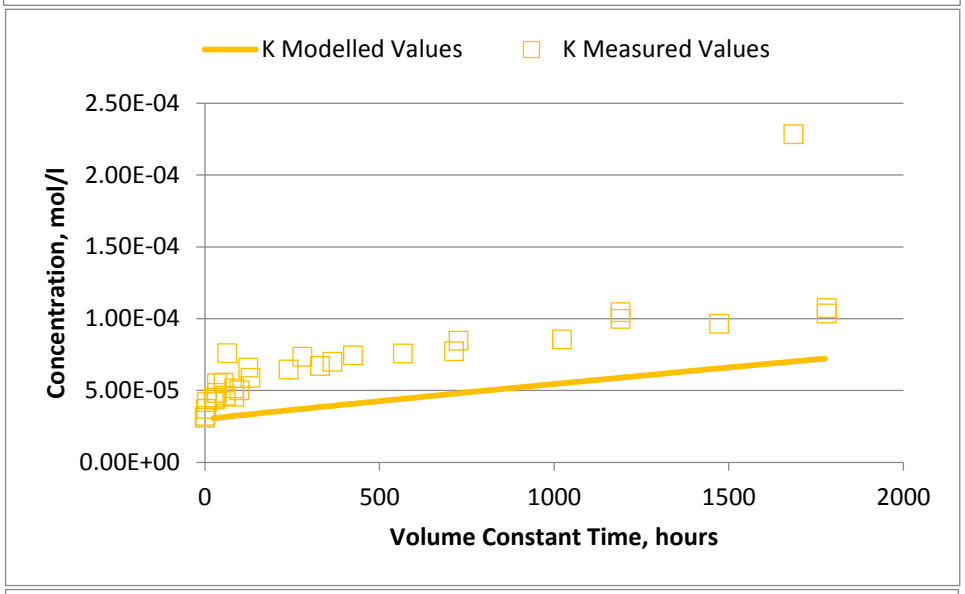


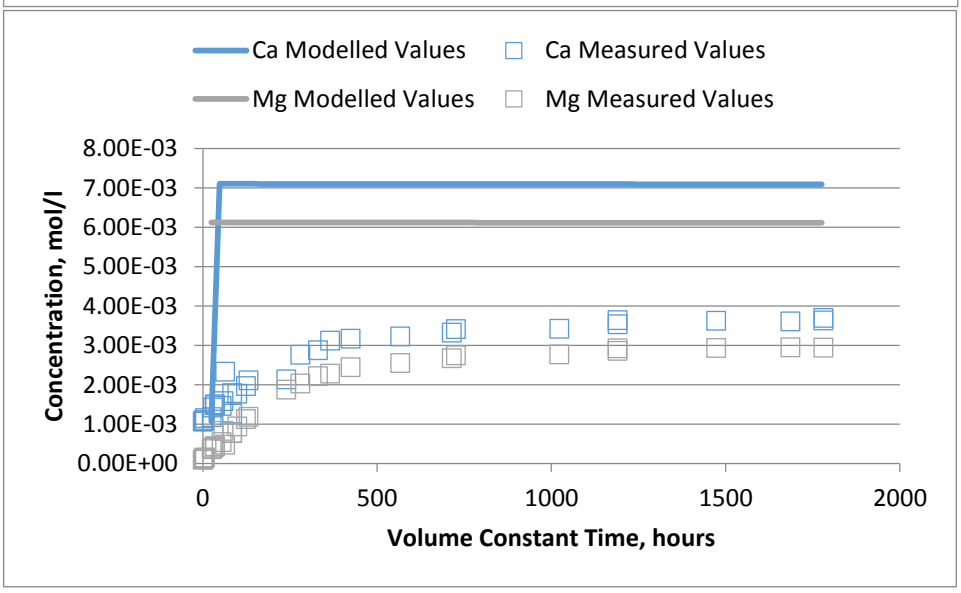

## B.2.4 Experiment 146

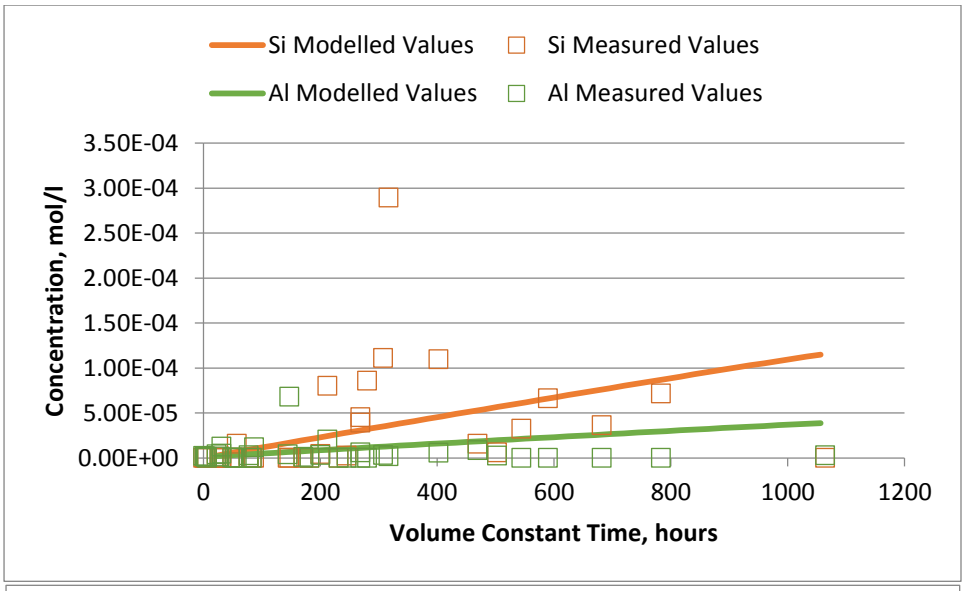


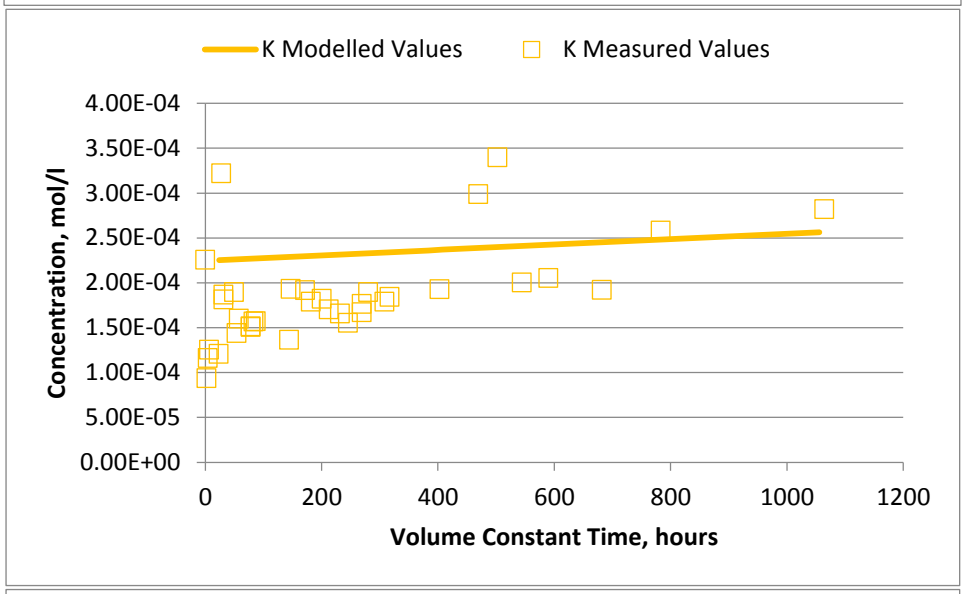


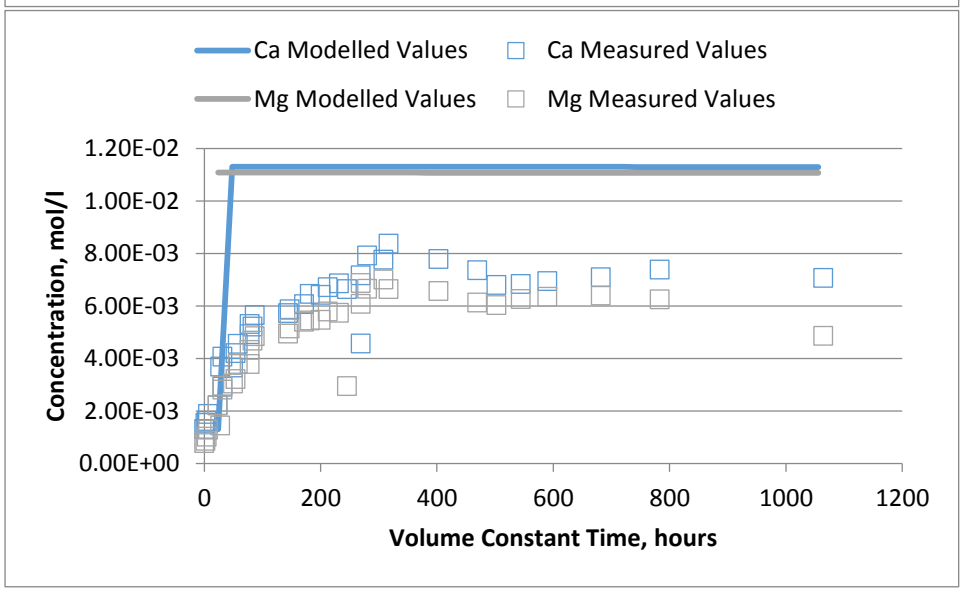

## B.2.5 Experiment 147

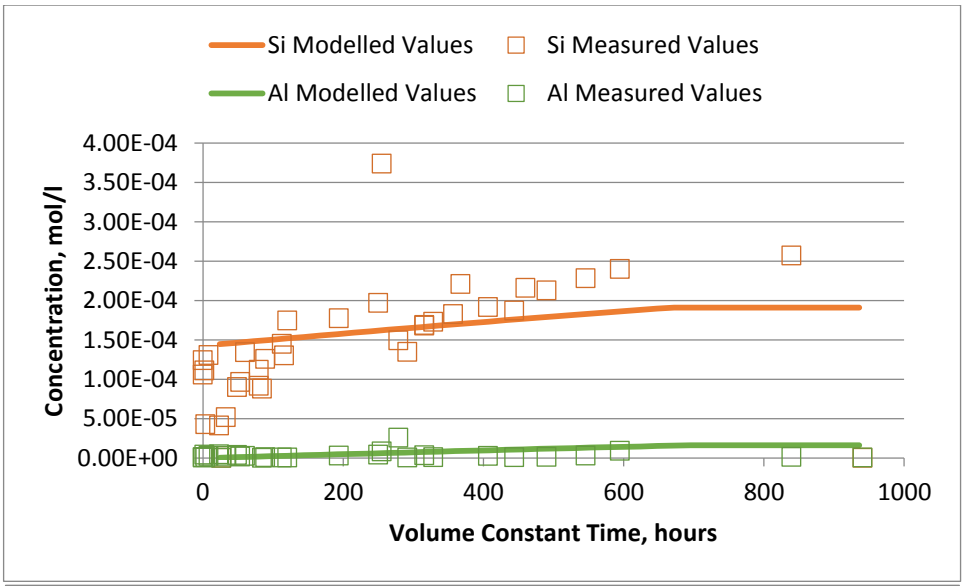


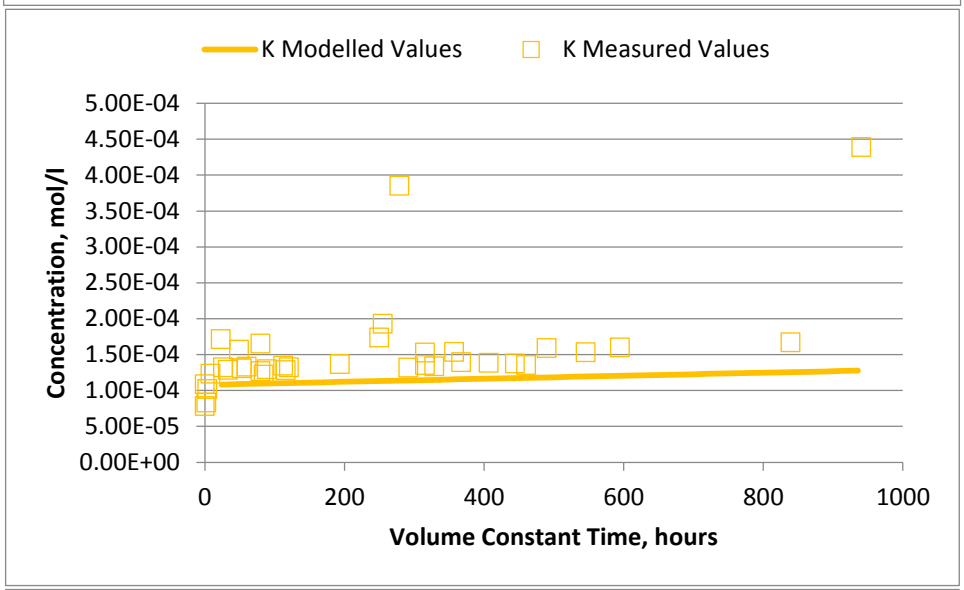


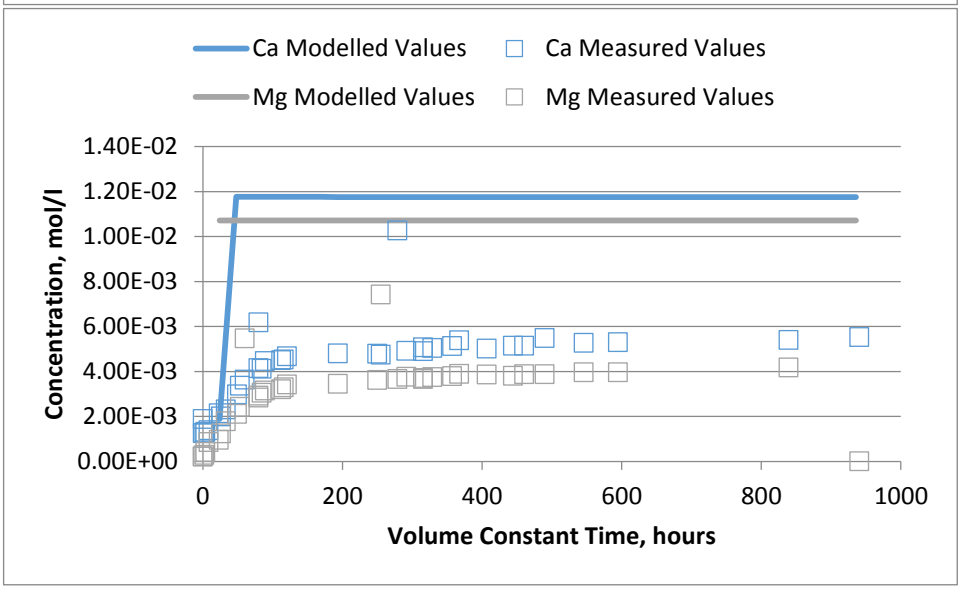

## B.2.6 Experiment 148

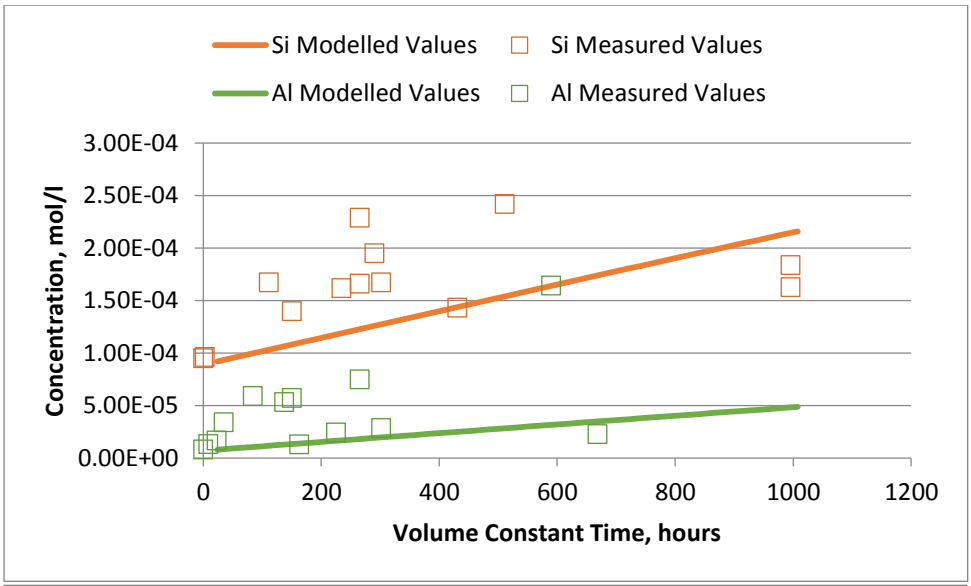


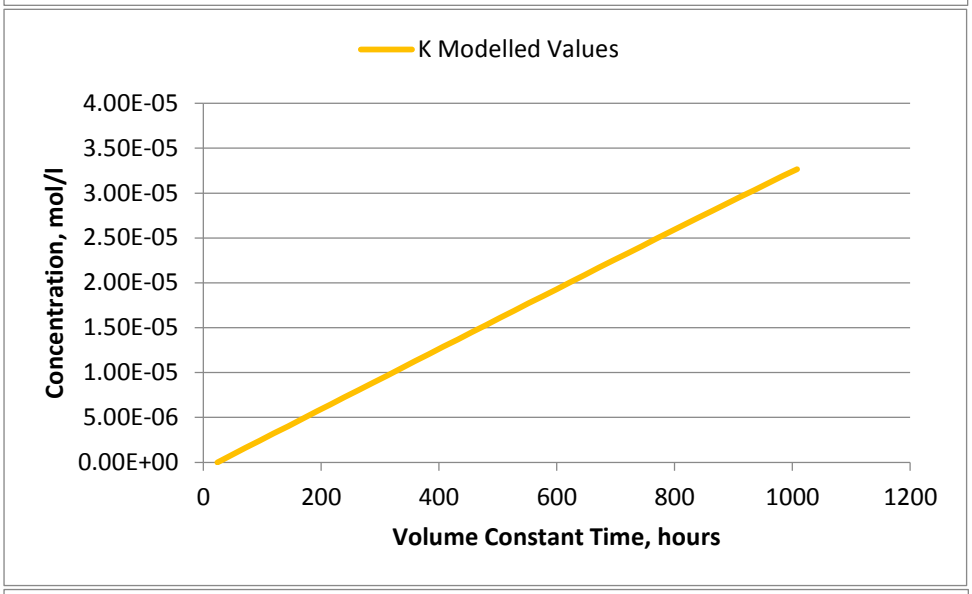


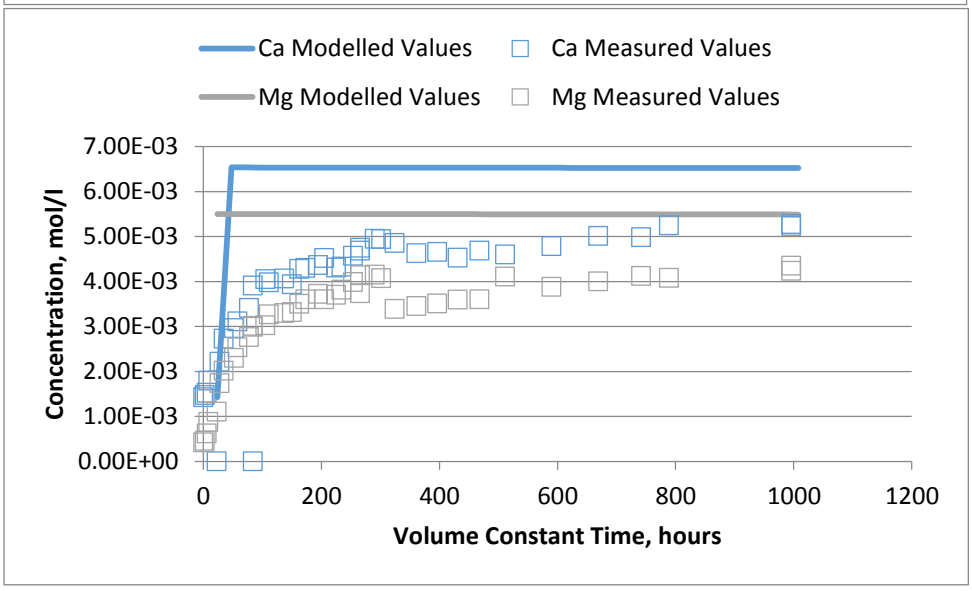

## B.2.7 Experiment 149